

Ph.D. programme: Cell and molecular biology, genetics and virology

Mgr. Jitka Stančíková

Molecular mechanisms of physiological renewal and cancer transformation of mammalian gastrointestinal tissues

Dissertation thesis

Supervisor of thesis: RNDr. Vladimír Kořínek, CSc.

Laboratory of Cell and Developmental Biology

Institute of Molecular Genetics, Academy of Science of the Czech Republic

Prague, 2016



Declaration

I hereby declare that this thesis is a presentation of my original research work. Wherever contributions of others are involved, every effort is made to indicate this clearly, with due reference to the literature and acknowledgement of collaborative research and discussions. This thesis contains no material that has been submitted previously, in whole or in part, for the award of any other academic degree or diploma.

Prague, …….. 2016

Signature:

Acknowledgements

I would like to thank all the people that contributed to this thesis. Most of the gratitude goes to my laboratory with great colleagues and friends always ready to give a helping hand (especially Bobeš, but also Lucka, Míša, Vendy, Vítek, Katka, Eva and Adél) and the best supervisor I have ever met. Special thanks goes to my family. Finally, I would like to thank my husband Ondra for all his eternal support on the long way and our good daughter Eva.

Motto: Deal with it.

Sigismund of Luxemburg

Contents

List of abbreviations 8
Abstract 16
Abstrakt 18
List of publications 20
Introduction 22
The canonical Wnt signaling pathway 23
The Wnt signaling pathway in OFF state 24
The Wnt signaling pathway in ON state 25
Switching off Wnt signaling 27
Regulation of the Wnt signaling pathway 29
Wnt target genes 33
GIT 33
The gut – small intestine and colon anatomy 33
Stomach anatomy 34
Common histology of GIT 34
Intestinal epithelium architecture and cell types 34
Stomach epithelium architecture and cell types 39
Signaling pathways in the intestinal and gastric epithelium 43
CRC 51
Gastric cancer 56
Gut microbiota 59
The liver 61
Working aims 65
Methods 66
Results and discussion 67
Troy, a tumor necrosis factor receptor family member, interacts with Lgr5 to inhibit Wnt signaling in intestinal stem cells 67
Mist1 expressing gastric stem cells maintain the normal and neoplastic gastric epithelium and are supported by a perivascular stem cell niche 112
NKD1 marks intestinal and liver tumors linked to aberrant Wnt signaling 157
HIC1 tumor suppressor loss potentiates TLR2/NF-kappaB signaling and promotes tissue damage-associated tumorigenesis 191
Monensin inhibits canonical Wnt signaling in human colorectal cancer cells and suppresses tumor growth in multiple intestinal neoplasia mice 219
Unique gene expression signatures in the intestinal mucosa of germ-free and monoassociated gnotobiotic mice 259
Conclusions 312
List of figures 313
References 314

List of abbreviations

ADAM10	A disintegrin and metalloproteinase domain-containing protein 10
AFAP	attenuated FAP
ALDH	aldehyde dehydrogenase
APC	adenomatous polyposis coli
ARM	armadillo
ASCL2	achaete-scute complex homolog 2
ATOH1	atonal homolog 1
AXIN	axis inhibition protein
BAC	bacterial artificial chromosome
BAD	Bcl-2 associated death promoter
BAX	Bcl-2 associated X protein
bHLH	basic helix-loop-helix
BIM	Bcl-2-interacting mediator of cell death
BMDC	bone marrow-derived cell
BMI1	B-cell specific Moloney murine leukemia virus integration site 1
BMP	bone morphogenetic protein
βTrCP	F-box-containing beta transducing repeat containing
cagA	cytotoxin-associated gene product
CALB2	calbindin 2
CBC	crypt base columnar
CBP	CREB-binding protein
Cby	Chibby
CCK	cholecystokinin
CCKBR	cholecystokinin type B receptor
CCKR	cholecystokinin receptor
CDCP1	CUB domain-containing protein 1
CDK	cyclin-dependent kinase
CDX2	caudal type homeobox 2
ChIP	chromatin immunoprecipitation
CIN	chromosomal instability
CIITA	class II transactivator
CK1	casein kinase 1

CR	conventionally reared
CRC	colorectal cancer
CRCSC	colorectal cancer stem cell
CREB	cyclic AMP-responsive element-binding protein
CRM1	chromosomal region maintenance 1
CTD	cysteine-rich transmembrane domain
CXCR4	scavenger chemokine receptor 4
DCC	deleted in colorectal carcinoma
DCLK	doublecortin-like kinase
ddPCR	droplet digital PCR
DEN	diethylnitrosamine
DEP	Dvl, Egl10, pleckstrin
DGC	diffuse type gastric cancer
Dhh	desert hedgehog
DISP	Dispatched
DKK	Dickkopf
DLL1	delta-like 1
dn	dominant negative
DOT1L	DOT1-like protein
DPYSL2	dihydropyrimidinase-like 2
DSS	dextran sulfate sodium
DVL	Disheveled
ECD	extracellular domain
ECL	enterochromaffin-like
EDAR	Ectodysplasin A receptor
EDN1	endothelin 1
EGF	epidermal growth factor
EGFP	enhanced green fluorescent protein
EGFR	epidermal growth factor receptor
EMT	epithelial mesenchymal transition
EPCAM	epithelial cell adhesion molecule
EPHB	ephrin receptor
ER	endoplasmatic reticulum

FACS	fluorescence activated cell sorting
FAP	familial adenomatous polyposis coli
FKBP5	FK506 binding protein 5
FOX	fork-head box
FRAT/GBP	frequently rearranged in advanced T-cell lymphomas / guanylate binding protein
FRET	Förster resonance energy transfer
FZD	frizzled
GATA6	GATA-binding factor 6
GC	gastric cancer
GCSC	gastric cancer stem cell
GF	germ-free
GIF	gastric intrinsic factor
GIT	gastrointestinal tract
GLI	glioma-associated oncogene
GLT-1	glutamate transporter 1
GO BP	gene ontology biological process
GRB2	growth factor receptor-bound protein 2
GS	glutamine synthetase
GSEA	gene enrichment analysis
GSK3	glycogen synthase kinase 3
H2-Ab1	histocompatibility 2, class II antigen A, beta 1
HAT	histone acetyl transferase
HCC	hepatocellular cancer
HDAC	histone deacetylase
HES	hairy and enhancer of split
HGF	hepatocyte growth factor
Hh	hedgehog
HIC1	hypermethylated in cancer 1
HiRE	Hic1 responsive element
HMG	high-mobility group
hMSC	human mesenchymal stem cell
HNFα	hepatocyte nuclear factor alpha

HOPX	HOP homeobox
HTS	high throughput screening
IBD	inflammatory bowel disease
ICD	intracellular domain
ID1	inhibitor of DNA binding
IGC	intestinal type gastric cancer
IGF	insulin-like growth factor
Ihh	indian hedgehog
IKK	inhibitor of nuclear factor κ-B kinase
IL	interleukin
ILC	innate lymphoid cells
INT1	integrator complex subunit 1
IRS2	insulin receptor substrate 2
ISW1	imitation switch subfamily 1
JNK	c-Jun N-terminal kinase
KDM6B	lysine-specific demethylase 6 B
KLHL12	kelch-like protein 12
KO	knock-out
KRAS	Kirsten rat sarcoma viral oncogene homolog
KRM	kremen
KRT19	keratin 19
LECT2	leukocyte cell-derived chemotaxin 2
LEF/TCF	lymphoid enhancer-binding factor/T-cell factor
LGR	leucine-rich repeat containing G-protein coupled receptor
LGS/BCL9	legless/B-cell CLL/lymphoma 9
LIMMA	Linear Models for Microarray Data
LOH	loss of heterozygosity
LRC	label-retaining cell
LRIG1	leucine-rich repeats and immunoglobulin-like domains protein 1
LRP	lipoprotein receptor-related protein
LS/MS-MS	liquid chromatography / tandem mass spectrometry
MAP	MUTYH-associated polyposis

MAPK/ERK	mitogen-activated protein kinase / extracellular signal-regulated kinase
MCR	mutation cluster region
MEF	mouse embryonic fibroblast
MESD	mesoderm development
MIST1	muscle, intestine and stomach expression 1
MLH	MutL homologous
MMR	mismatch repair
MSH	MutS homologous
MSI	microsatellite instability
mTERT	mouse telomerase reverse transcriptase
MTGR-1	myeloid translocation gene related-1
MUC	mucin
MUTYH	mutY homolog
MyD88	myeloid differentiation primary response 88
NCOR1	nuclear receptor co-repressor 1
NEDL1	NEDD4-like ubiquitin protein ligase 1
NES	nuclear export signal
NF-κB	nuclear factor kappa-light-chain-enhancer of activated B cells
NKD1	naked cuticle homolog 1
NKX2-3	NK2 transcription factor related, locus 3
NLR	Nod-like receptor
NLS	nuclear localization signal
NPC	nuclear pore complex component
OAT	ornithine aminotransferase
OLFM4	olfactomedin 4
OPN	osteopontin
ORF	open reading frame
PAS	periodic acid-Schiff
PC	pericentral
PCP	planar cell polarity
PCR	polymerase chain reaction
PDGF	platelet derived growth factor

PDZ	postsynaptic density 95, disc large, zonula occludens-1
PI3K/AKT	phosphatidylinositol 3-kinase / Akt kinase
PIASy	protein inhibitor of activated STAT protein gamma
PIK3CA	phosphatidylinositol-4,5-bisphosphate 3-kinase, catalytic subunit alpha
PH	pleckstrin-homology
PIP2	phosphatidylinositol bisphosphate
PIP3	phosphatidylinositol trisphosphate
PKB	protein kinase B
PKC	protein kinase C
PLC	phospholipase C
PP	periportal
PP	protein phosphatase
PTCH	patched
PTEN	phosphatase and tensin homolog
PYGO	pygopus
qRT-PCR	quantitative reverse transcriptase PCR
RB	retinoblastoma
REG4	regenerating islet-derived family, member 4
RHOA	Ras homolog gene family member A
RNAi	RNA interference
RNF43	ring finger protein 43
RSPO	roof palate-specific spondin
RUNX3	runt-related transcription factor 3
SC	stem cell
SDF1	stromal cell-derived factor 1
SFRP	secreted frizzled related protein
SH2	Src homology 2
Shh	Sonic hedgehog
SHP2	tyrosine phosphatase containing SH2 domain
SIRT1	sirtulin 1
SLPI	secretory leukocyte peptidase inhibitor
SMAD	mothers against decapentaplegic

SMARCA4	SWI / SNF-related, matrix associated, actin dependent regulator of chromatin, subfamily A, member 4
SMO	smoothened
SMOC2	SPARC-related modular calcium-binding protein 2
SMRT	silencing mediator of retinoic acid and thyroid hormone receptor
SOS	son of sevenless
SOST	sclerostin
SOX	SRY-box
SPDEF	SAM pointed domain containing ETS transcription factor
SPEM	spasmolytic polypeptide-expressing metaplasia
STF	superTOPFLASH
SWI/SNF	Switch / sucrose non-fermentable
TA	transit-amplifying
TAZ	transcriptional coactivator with PDZ-binding motif
TCGA	The Cancer Genome Atlas
TEAD	tea domain family member 1
TFF2	trefoil factor 2
TGF-β	transforming growth factor beta
TGFBR2	transforming growth factor, beta receptor II
TLE	transducing-like enhancer of split
TLR	toll-like receptor
TNFR	tumor necrosis factor receptor
TNFRSF19	tumor necrosis factor receptor superfamily 19
TNIK	TNF1 and NCK-interacting kinase
Treg	T regulatory cells
USP14	ubiquitin specific peptidase 14
vacA	vacuolating cytotoxin A
VEGF-A	vascular endothelial growth factor A
VIP	vasoactive intestinal polypeptide
Wg	wingless
WIF	Wnt inhibitory factor
WISE	Wnt modulator in surface ectoderm
Wls	wintless

WRE	Wnt responsive element
wt	wild-type
XEDAR	X-linked ectodysplasin A receptor
YAP	Yes-associated protein
ZNRF3	zinc and ring finger 3

Abstract

The plot of this PhD thesis is dedicated to investigation of the molecular pathways and events and their disruptions in the gastrointestinal tract (further abbreviated as GIT). The major role in this part plays the Wnt signaling pathway. This marvelous multipurpose machinery is responsible for epithelia renewal from stem cells (SCs) in the stomach and intestine, and for correct zonation and function of hepatic units. Of note, the Wnt pathway directs also development of embryo as well as homeostasis of many tissues apart from GIT in all metazoans, thus its flawless function is indispensable from one´s origin to death. The main part of the thesis follows canonical Wnt signaling in its physiological condition and, in contrast, with pathological disturbances. This issue can be taken by variety of means as it is described in attached publications.

The first publication deals with searching for new participants of Wnt signaling and their functions and describing unique markers of SCs in the intestine. *Troy*, the member of tumor necrosis factor receptor (TNFR) superfamily, was identified as a novel marker of intestinal SCs by probing microarray data from chromatin immunoprecipitation obtained in cultured colorectal cancer cell lines. Moreover, we found that *Troy* is a Wnt target gene inhibiting the signaling pathway in the feedback loop. From the same microarray data we also chose a gene encoding *naked cuticle homolog 1* (*Nkd1*) for further analysis. This gene was already determined as a Wnt-regulated inhibitor of the pathway, but a little was known about its role in intestinal homeostasis and tumorigenesis. Our published results depict *Nkd1* expression in Wnt-responsive cells of the small intestine and liver. Additionally, we found *Nkd1* highly expressed in intestinal lesions of mice. In human patient samples NKD1 was described as a potential marker of intestinal and liver tumors. The next publication describes identification of the unique marker of SCs in the stomach corpus: muscle, intestine and stomach expression 1 (Mist1). This particular protein was previously described as a marker of short-living gastric epithelial progenitors. Our recent study uncovered its novel expression site – quiescent stem cells in the corpus isthmus. The last publication from this group relates to *hypermethylated in cancer (Hic1)*, a tumor suppressor inactivated in many types of tumors. We used a genetically modified mouse strain to identify genes influenced by Hic1 loss. As the most interesting we described Hic1-mediated regulation of *toll-like receptor 2 (Tlr2*) expression. Tlr2 upregulation upon Hic1 depletion leads to switching on proinflammatory pathways [e. g. nuclear factor

kappa-light-chain-enhancer of activated B cells (NF-κB)], that have the potential to initiate tumor growth.

Another approach to investigate molecular relations in the gut is to search for therapeutics, which affect the Wnt signaling pathway leading to tumor growth reduction. We published that monensin, a small compound already used in dairy industry, is able to reduce size of intestinal lesions in mice via decreased Wnt signaling. The particular effect of monensin has not been disclosed yet.

The final publication encompasses the microarray data gained from germ-free (GF) mice compared to conventionally reared (CR) and monoassociated animals populated with a particular bacterial strain. Results confirmed previous data that in GF mice the immune system development is the most impaired. Additionally, we presumed that monoassociation did not rescue immunity development. We described various genes with different expression in GF mice, which are linked to inflammation, intestinal development and cancer.

Abstrakt

Tématem této dizertační práce je výzkum molekulárních drah a mechanismů a jejich poruch v buňkách a tkáních trávicího traktu. Hlavní roli zde zaujímá signalizační dráha Wnt. Toto obdivuhodné víceúčelové „soustrojí“ je zodpovědné za obnovu epitelu z kmenových buněk v žaludku a střevu a za správnou zonaci a funkci jaterní tkáně. Signalizace Wnt řídí také embryonální vývoj a homeostázi mnoha tkání mimo trávicí soustavu, a to u všech metazoálních organismů, její bezchybné fungování je tudíž nezbytné v životě každého jedince od jeho vzniku až po zánik. Hlavní část práce popisuje kanonickou signalizaci Wnt v její fyziologické podobě a dále pak její patologická narušení. Toto téma je nahlíženo z mnoha hledisek, jak je možné vidět z uvedených publikací.

První publikace se zabývá hledáním nových účastníků signalizace Wnt a jejich funkce, a to prostřednictvím popisu unikátních markerů střevních kmenových buněk. *Troy*, člen velké skupiny tumor necrosis factor receptorů (TNFR), byl popsán pomocí dat získaných z čipových analýz a chromatinové imunoprecipitace jako nový marker střevních kmenových buněk. K uvedeným analýzám byly použity buňky kolorektálního karcinomu pěstované v buněčných kulturách. Zjistili jsme, že *Troy* je cílovým genem signalizace Wnt a sám tuto dráhu inhibuje. Ze zmíněných čipových analýz jsme též vybrali gen *naked cuticle homolog 1* (*Nkd1)*. Tento gen byl již dříve popsán jako cílový gen a zároveň inhibitor signalizace Wnt, ale znalosti o jeho působení v homeostázi a nádorovém bujení střeva byly minimální. Data, která jsme zveřejnili v dalším článku, pak charakterizují expresi *Nkd1* ve střevních a jaterních buňkách. Dále jsme zjistili, že *Nkd1* je také vysoce exprimován v myších střevních nádorech. Ve vzorcích získaných od lidských pacientů jsme popsali NKD1 jako potenciální marker střevních a jaterních nádorů. Další publikace popisuje identifikaci jedinečného markeru kmenových buněk v těle žaludku, kterým je gen *muscle, intestine and stomach expression 1 (Mist1)*. Mist1 byl dříve znám jako marker krátce žijících progenitorů žaludečního epitelu. Naše studie popisuje expresi Mist1 ve zřídka se dělících kmenových buňkách v isthmální části žláz žaludečního těla. Poslední publikace z této skupiny článků je věnována genu *hypermethylated in cancer (Hic1)*, nádorovému supresoru inaktivovanému v mnoha typech nádorů. Pro určení genů, které jsou ztrátou transkripčního represoru Hic1 ovlivněny, jsme použili geneticky modifikovaný myší kmen umožňující inaktivaci tohoto genu. Z výsledných genů jsme určili jako nejvíce zajímavý *toll-like receptor 2 (Tlr2)*, který je regulován přímo

proteinem Hic1. Zvýšená exprese Tlr2 v důsledku ztráty Hic1 vede k „zapnutí“ prozánětlivých signalizačních drah, např. dráhy nuclear factor kappa-light-chain-enhancer of activated B cells (NF-κB), což následně může zvýšit riziko nádorového bujení.

Jiným přístupem pro výzkum molekulárních vztahů v trávicí soustavě je hledání látky, která působí na signalizaci Wnt s možným výsledkem potlačení nádorového bujení. V naší studii jsme objevili, že monensin, antibiotikum užívané v mlékárenském průmyslu, je schopno redukovat, a to snížením hladiny signalizace Wnt, velikost myších střevních nádorů. Podrobný mechanismus působení monensinu však nebyl doposud studován.

Poslední publikace zahrnuje data z expresních čipů získaná z bezmikrobních myší a jejich srovnáním s konvenčně chovanými myšmi a myšmi „osazenými“ jedním konkrétním bakteriálním kmenem. Výsledky potvrdily předchozí zjištění, že imunitní systém u bezmikrobních myší není plně vyvinut. Navíc jsme zjistili, že osazení střev jedním bakteriálním kmenem vývoj imunitního systému plnohodnotně nepodpoří. U bezmikrobních myší jsme také popsali rozdíl v expresi genů souvisejících se zánětem, vývojem střeva a rakovinou.

List of publications

Fafilek B, Krausova M, Vojtechova M, Pospichalova V, Tumova L, Sloncova E, Huranova M, **Stancikova J**, Hlavata A, Svec J, Sedlacek R, Luksan O, Oliverius M, Voska L, Jirsa M, Paces J, Kolar M, Krivjanska M, Klimesova K, Tlaskalova-Hogenova H, Korinek V. 2013. Troy, a tumor necrosis factor receptor family member, interacts with lgr5 to inhibit wnt signaling in intestinal stem cells. Gastroenterology 144(2):381-91
IF 16.716

Hayakawa Y, Ariyama H, **Stancikova J**, Sakitani K, Asfaha S, Renz BW, Dubeykovskaya ZA, Shibata W, Wang H, Westphalen CB, Chen X, Takemoto Y, Kim W, Khurana SS, Tailor Y, Nagar K, Tomita H, Hara A, Sepulveda AR, Setlik W, Gershon MD, Saha S, Ding L, Shen Z, Fox JG, Friedman RA, Konieczny SF, Worthley DL, Korinek V, Wang TC. 2015. Mist1 Expressing Gastric Stem Cells Maintain the Normal and Neoplastic Gastric Epithelium and Are Supported by a Perivascular Stem Cell Niche. Cancer Cell 28: 1-15
IF 23.523

Stancikova J*, Krausova M*, Kolar M, Fafilek B, Svec J, Sedlacek R, Neroldova M, Dobes J, Horazna M, Janeckova L, Vojtechova M, Oliverius M, Jirsa M, Korinek V. 2015. NKD1 marks intestinal and liver tumors linked to aberrant Wnt signaling. Cellular Signalling 27(2): 245-56
IF 4.471

Janeckova L, Pospichalova V, Fafilek B, Vojtechova M, Tureckova J, Dobes J, Dubuissez M, Leprince D, Baloghova N, Horazna M, Hlavata A, **Stancikova J**, Sloncova E, Galuskova K, Strnad H, Korinek V. 2015. HIC1 Tumor Suppressor Loss Potentiates TLR2/NF-kappaB Signaling and Promotes Tissue Damage-associated Tumorigenesis. Molecular Cancer Research 13(7): 1139-48
IF 4.502

Tumova L, Pombinho AR, Vojtechova M, **Stancikova J**, Gradl D, Krausova M, Sloncova E, Horazna M, Kriz V, Machonova O, Jindrich J, Zdrahal Z, Bartunek P, Korinek V. 2014. Monensin inhibits canonical Wnt signaling in human colorectal cancer cells and suppresses tumor growth in multiple intestinal neoplasia mice. Molecular Cancer Therapeutics 13(4):812-22

IF 6.107

Janeckova L*,Stancikova J*,Strnad H, Hudcovic T, Tureckova J, Horazna M, Baloghova N, Sloncova E, Galuskova K, Tlaskalova-Hogenova H, Korinek V. 2016. Unique gene expression signatures in the intestinal mucosa of germ-free and monoassociated gnotobiotic mice. Submitted publication.

*equal contribution

Introduction

The digestive system functions as a multiorgan complex in human body. Its anatomical regions have an ability not only to gain nutrients but, simultaneously, to cover a negligible role of the immune system or produce hormones. Mentioning the core of the system, GIT shields cell layer facing the lumen being extremely strained and confronted to harming substances in the passing nutrients, therefore the cell turnover is the fastest across all tissues. Unsurprisingly, components of GIT are very prone to develop tumor growth, which, progressed to malignancy, has alarming incidence in developed countries (el-Serag 2001; Ferlay et al. 2010; Jemal et al. 2011; Stracci et al. 2014). Cancer of this organ arises from various disfunctionings in signaling pathways in SCs of GIT. One of the most crucial signaling pathways connected to the maintenance and function of gastrointestinal epithelia and hepatic tissue is the Wnt signaling pathway (Benhamouche et al. 2006; Crosnier et al. 2006; Giannakis et al. 2006). Apart from its substantial importance in the adult organism, Wnt signaling directs many aspects of embryonic development in all metazoans (Herr et al. 2012).

In this study we mainly deal with Wnt / β-catenin signaling (so called canonical Wnt signaling). The core of the pathway is occupied by β-catenin protein residing on cell scaffold and in soluble form in the cytoplasm. The cytoplasmic form of β-catenin functions as the second messenger for the Wnt signal, subsequently entering the nucleus where it activates expression of Wnt-responsive genes (Behrens et al. 1996). These genes very often figurate as the basic and universal elements in cellular pathways linked to cell proliferation [e. g. *v-myc avian myelocytomatosis viral oncogene homolog (c-myc), cyclin D* or some of the *fibroblast growth factors*], moreover, some of the genes encode modulators of the Wnt signaling themselves [e. g. *Troy, Nkd1, axis inhibitor protein 2* (*Axin 2*)]. Wnt signaling cares of the maintenance of the intestinal and stomach epithelia via the stem cell support (Crosnier et al. 2006; Barker et al. 2010b). Additionally, it establishes the proper zonation of the hepatic units, necessary for detoxification, glycolysis and many more metabolic processes (Monga et al. 2002; Zeng et al. 2006; Zeng et al. 2007). The Wnt pathway cooperates with other pathways crucial in GIT tissues maintenance (Solanas et al. 2011; Voon et al. 2012; Heuberger et al. 2014). In conclusion, Wnt signaling is absolutely indispensable for vital functions of GIT with fatal consequences being aberrantly influenced.

The canonical Wnt signaling pathway

The Wnt signaling pathway has a fundamental role in embryonic development in metazoans controlling cell proliferation, differentiation, migration and cell polarity (Nusse and Varmus 1992). Additionally, in adult organism, it is responsible for somatic stem cell maintenance and homeostasis in various types of tissues from central nervous system through skin to gastrointestinal epithelium (Kalani et al. 2008; Lim and Nusse 2013; Kinzel et al. 2014; Lerner and Ohlsson 2015). Although there are more studied types of the Wnt signaling cascades, namely the β-catenin-independent pathway involved in planar cell polarity (PCP) signaling and the Wnt-dependent calcium / protein kinase C (PKC)-dependent pathway (Kohn and Moon 2005), in this thesis we are mainly focused on the β-catenin-dependent, so called the canonical Wnt signaling pathway. The core of the pathway, β-catenin, is a multi-purpose protein with cytosolic and cadherin-based adherens junctions attached localization (Ozawa et al. 1989). It preserves tightly conserved molecule during metazoan evolution. As a member of the Armadillo (ARM) repeat protein superfamily, it contains 12 imperfect ARM repeats, R1-R12. The repeats build structurally rigid central region, functioning as a scaffold for several binding partners. The region is flanked by two distinct N- and C-terminal domains, NTD and CTD (Fig. 1). The central region as well as the terminal domains have potential to be regulated by phosphorylation “tunning” the β-catenin effector function (Huber et al. 1997; Xing et al. 2008).

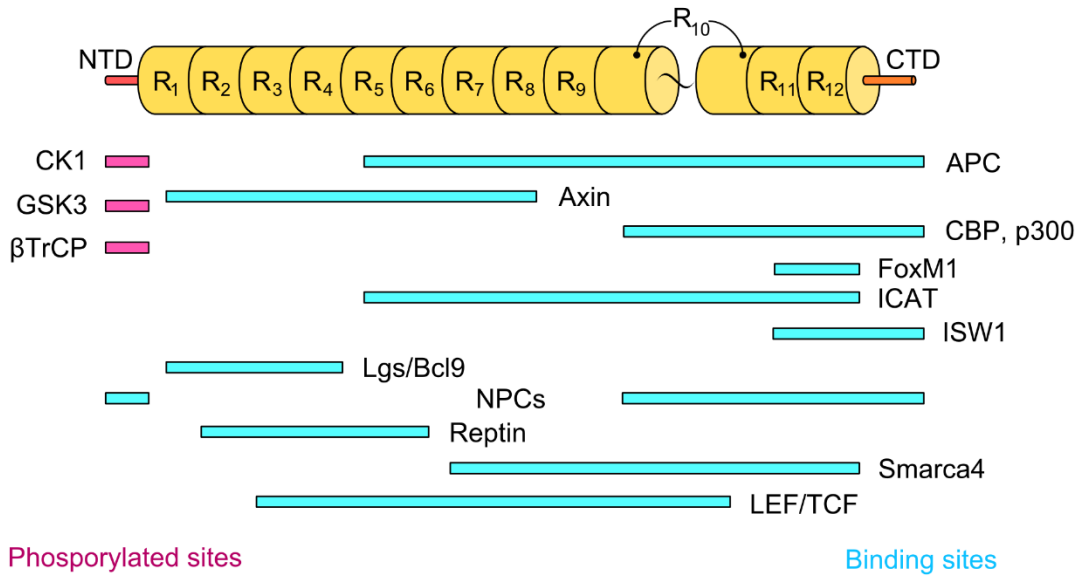


Figure 1: Scheme of β-catenin with phosphorylated and binding sites. Two terminal domains, NTD and CTD, flank 12 Armadillo repeats. Some of the kinases phosphorylating the NTD domain and molecules associating the various sites are depicted. With contribution of (Jessen et al. 2008; Mosimann et al. 2009).

The Wnt signaling pathway in OFF state

In the absence of a Wnt ligand the pathway is switched off (Fig. 2). Free cytosolic β-catenin is short living, targeted promptly to degradation by the F-box-containing beta-transducin repeat containing (βTrCP) E3 ubiquitin protein ligase complex and then cleaved in the proteasome (Kim et al. 2007). First, the central domain of β-catenin is attached by key units of so called destruction complex, Axin and adenomatous polyposis coli (APC). These two proteins make an indispensable scaffold for casein kinase 1 alpha (CK1α) and glycogen synthase kinase 3 (GSK3) to phosphorylate serine / threonine residues of β-catenin on the N-terminal domain (Liu et al. 2002). Subsequently, phosphorylated β-catenin is marked by βTrCP and destroyed. If N-terminally phosphorylated β-catenin is not joined to APC, it is dephosphorylated by protein phosphatase 2A (PP2A) after leaving the destruction complex (Zhang et al. 2009). Apart from Axin, APC, CK1α, GSK3 and βTrCP additional member of the destruction complex was discovered recently (Azzolin et al. 2014). Yes-associated protein (YAP) and transcriptional coactivator with PDZ-binding motif (TAZ), nuclear effectors of tea

domain family member 1 (TEAD)-dependent transcription (Wang et al. 2009; Pan 2010), link the Wnt and Hippo signaling pathways through βTrCP. It has been shown that YAP/TAZ essentially recruits βTrCP to the destruction complex, where it is associated with Axin. In case that Wnt signaling is switched on, YAP/TAZ is released from the destruction complex and relocates to the nucleus, where it activates transcription of Hippo target genes connected to proliferation and organ growth regulation (Azzolin et al. 2014).

The Wnt signaling pathway in ON state

The activation of the Wnt signaling pathway (Fig. 2) starts on the plasma membrane by binding Wnt ligands to the receptors. The proto-oncogene encoding Wnt protein, originally named *integrator complex subunit 1* (*Int1)*, was identified as preferential integration site for the Mouse Mammary Tumor Virus (Nusse and Varmus 1982). Six years earlier, *Int1* analog *wingless (Wg)* was described in *D. melanogaster* (Sharma and Chopra 1976). There are 19 *Wnt* genes encoded by mammalian genome identified in total, all forming a similar three-dimensional structure (Cadigan and Nusse 1997). Posttranslational modifications preceding Wnt secretion include glycosylation, lipidation and acylation (Willert et al. 2003; Komekado et al. 2007; Kurayoshi et al. 2007).

Wnt ligands in the canonical pathway bind the extracellular N-terminal cysteine rich domain of seven times-spanning G protein-coupled receptor Frizzled (Fzd) (Schulte and Bryja 2007) and, additionally, the long extracellular domain of the co-receptor low density lipoprotein receptor-related protein 5 or 6 (LRP5/6) (Schweizer and Varmus 2003). Subsequently, the adaptor protein Dishveled (Dvl) is recruited to the plasma membrane and phosphorylated by CK1ε. Intracellular domain of LRP5/6 is phosphorylated by kinases CK1γ and GSK3, leading to recruitment of Axin to the ribosome-sized multiprotein signalosome complex containing GSK3, Axin, Fzd, Dvl and phosphorylated LRP5/6 (Wong et al. 2003; Cong et al. 2004; Mi et al. 2006; Piao et al. 2008). Axin is expressed at very low level, therefore it is a limiting factor for the signaling (Lee et al. 2003; Tolwinski et al. 2003). The phosphate residue of Axin is removed by protein phosphatase 1 (PP1) or PP2A to block the protein from connecting the destruction complex (Luo et al. 2007). In the absence of the preformed destruction complex, β-catenin accumulates in the cytoplasm and consequently enters the nucleus. Moreover, Wnt

stimulation suppresses GSK3 phosphorylation of β-catenin by reducing its enzymatic activity (Ding et al. 2000; Liu et al. 2002).

Transport of β-catenin through the nuclear envelope is still not fully understood. Although β-catenin lacks typical nuclear localization signal (NLS) or nuclear export signal (NES), it can easily drift between the cytoplasm and nucleus. This ability could be caused by its interaction with nuclear pore complex components (NPCs) (Shitashige et al. 2008) mediated by the Armadillo repeats R10-12 (Sharma et al. 2012) or NTD and CTD (Sharma et al. 2014). It has been also shown that the transcription factor forkhead-box M1 (FoxM1) creates complex with β-catenin, and together they pass the nuclear envelope (Zhang et al. 2011a). In the nucleus, β-catenin displaces the groucho/transducin-like enhancer of split (groucho/TLE) repressor from transcription factors of the lymphoid enhancer-binding factor/T-cell factor (LEF/TCF). Beta-catenin interacts with TCF binding DNA on the Wnt responsive elements (WREs) by ARM repeats R3-R10 (Graham et al. 2000), thus coactivates transcription of Wnt target genes. Interestingly, the transcription is enhanced by the β-catenin ability to associate with histone acetyltransferases (HATs) CREB-binding protein (CBP) and p300, which release tight winding between individual nucleosomes (Hecht et al. 2000; Takemaru and Moon 2000). Moreover, β-catenin can also perform histone rearrangement by association with switch/sucrose non-fermentable (SWI/SNF)-related, matrix associated, actin-dependent regulator of chromatin, subfamily A, member 4 (SMARCA4) (Griffin et al. 2011) or imitation switch subfamily 1 (ISW1) (Deuring et al. 2000). These ATPases have potential to shift nucleosomes on the Wnt target genes to open DNA conformation for transcription complexes.

The LEF/TCF family of transcription factors includes four members in mammals – LEF1, TCF1, TCF3 and TCF4. These high-mobility group (HMG) box containing proteins recognize a uniform consensus sequence called LEF/TCF DNA-binding motif [CCTTTGAT(G/C)] (van de Wetering et al. 1997), which is present in WRE of Wnt target genes. Incidentally, the consensus is degenerated, therefore some single-nucleotide substitutions increase the transcriptional effect, whereas another provide an opposite result (Wright et al. 2010). Surprisingly, in Wnt signaling "off" state LEF/TCF tether the DNA strand as transcriptional repressors together with corepressor groucho/TLE. Furthermore, invertebrate and some of the vertebrate TCFs have the special cysteine-rich domain called C-clamp. This structure is able to attach the helper site in target DNA,

augmenting potential of TCF to bind the sequence (Ravindranath and Cadigan 2014). The corepressor complex induces formation of the repressive chromatin structure by recruiting histone deacetylases (HDACs) (Arce et al. 2009). Interestingly, some of TCFs behave more like transcription repressors (e.g. TCF3), although others have activating characteristics (Lef1). TCF4 and TCF1 have duplicitous role depending on the cellular context (Mao and Byers 2011; Watanabe and Dai 2011).

Switching off Wnt signaling

Finally, the pathway directing such important event as cell proliferation has to be strictly regulated or switched off. This can be performed by exchange of activating binding partners to pathway repressors. Some of the repressors of Wnt signaling are mentioned in the next chapter. Beside them, another interesting repressing protein is Reptin (Rashid et al. 2009), which forms a complex with β-catenin, LEF/TCF and already mentioned HDACs (Bauer et al. 2000). Histone deacetylases tie the chromatin loops to make them less accessible for transcription (Sekiya and Zaret 2007). Nuclear receptor co-repressor 1 (NCOR1) and silencing mediator of retinoic acid and thyroid hormone receptor (NCOR2/SMRT) work in a similar manner by interaction with HDACs and prevention of β-catenin binding to LEF/TCF (Battaglia et al. 2010). Myeloid translocation gene related 1 (Mtgr-1) can replace β-catenin in the complex with LEF/TCF imposing transcriptional repression (Moore et al. 2008). Interestingly, MTGR-1 inactivation leads to increased sensitivity to chemical injury in the intestinal epithelium, therefore its expression is probably effective in intestinal progenitors (Martinez et al. 2006). Small protein chibby (Cby) suppresses β-catenin-mediated signaling by two mechanisms. It competes with LEF/TCF in binding to β-catenin in the nucleus and, simultaneously, can facilitate the β-catenin nuclear export by its incorporation to the β-catenin/14-3-3 protein/chromosomal region maintenance 1 (CRM1) complex (Li et al. 2008; Li et al. 2010a; Killoran et al. 2015). Moreover, β-catenin can be also sequestrated or exported by members of the destruction complex residing in the nucleus. APC protein lacks NLS, but harbors NES in its sequence, thus it can shuttle from and to the cytoplasm (Neufeld et al. 2000a). Apart from APC, Axin lacks NES and interacts with CRM1 in order to be transported to the nucleus (Cong and Varmus 2004). Function of both APC and Axin in the nucleus is not fully elucidated, but it seems that they putatively retain β-catenin in the

location, where it is temporarily required (Krieghoff et al. 2006). Interestingly, the Axin2 role in transcription of the Wnt-responsive gene *myc* has been uncovered. The *myc* promoter is occupied by a complex of β-catenin/TCF/Axin2, which suppresses its transcription (Rennoll et al. 2014). Additionally, it has been shown, that both nuclear APC and Axin perform the nuclear β-catenin export (Neufeld et al. 2000b; Cong and Varmus 2004). Kinase GSK3β contains NLS, but due to missing NES has to be exported from nucleus by binding protein frequently rearranged in advanced T-cell lymphomas/guanylate binding protein (FRAT/GBP) (Franca-Koh et al. 2002). The kinase also represses the β-catenin nuclear activity by forming a complex with this protein. Nevertheless, the repression is unexpectedly independent on β-catenin phosphorylation (Caspi et al. 2008).

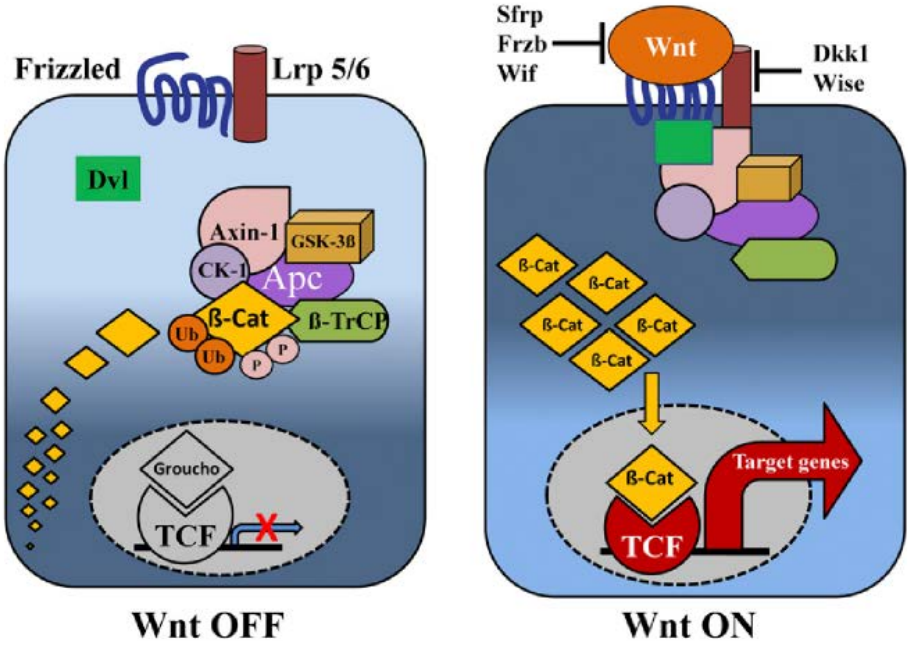


Figure 2: The canonical Wnt signaling pathway. In the OFF state, the destruction complex subunits APC and Axin serve as a scaffold binding β-catenin for subsequent phosphorylation performed by kinases GSK-3β and CK-1. Phosphorylated β-catenin is marked by ubiquitin E3 ligase β-TrCP and finally degraded. In the nucleus, groucho forces TCF to behave as repressor inhibiting transcription of Wnt target genes. In case Wnt ligand is bound to the Fzd-Lrp5/6 complex, the destruction complex is "out of order" via formation of the Axin-Lrp5/6 complex and adaptor protein Dvl phosphorylation. Due to elimination of the destruction complex, β-catenin accumulates in the cytoplasm, enters the nucleus and converts TCF to transcription activators. Extracellular inhibitors of Wnt signaling are also depicted in the right image. Adopted from (de Lau et al. 2014).

Regulation of the Wnt signaling pathway

Wnt ligand secretion, modification and inhibition of its binding

The Wnt signaling pathway is regulated at many levels. First, Wnt ligands are effectively regulated in secreting cell. Some posttranslational modifications, particularly lipidation and sequential glycosylations, affect mainly Wnt secretion (Doubravska et al. 2011). The effect of mutation in lipidated residues varies between retention of the ligand in the endoplasmatic reticulum (ER) in producing cell to secretion with decreased signaling ability (Harterink and Korswagen 2012). Porcupine (Pcn), acyltransferase anchored in the ER membrane, is responsible for lipid addition to Wnt proteins (Galli et al. 2007). Wnt exocytosis depends also on the activity of Wintless (Wls), transmembrane protein requiring Wnt lipidation on Ser209. Correctly modified Wnt is then bound directly to Wls, serving as a cargo receptor, and transmitted through the plasma membrane (Herr and Basler 2012). The turnover of Wls is ensured by a multiprotein retromer complex, which retrieves Wls from endosomes to the Golgi network (Port and Basler 2010).

Second, there are many extracellular inhibitors of Wnt signaling. From them, the Dickkopf protein family (Dkk), secreted frizzled related protein family (sFRP), Wnt inhibitory factor (WIF) and Wnt modulator in surface ectoderm (WISE) and sclerostin (Sost), both members of the cysteine knot family, could be mentioned. Dkk has higher affinity to the Lrp5/6 receptor than Wnt (Bafico et al. 2001), thus it is able to block effectively Wnt signaling via impeded formation of the ternary complex built by Lrp5/6, Fzd and Wnt (Semenov et al. 2001). Moreover, Dkk is a ligand also for the transmembrane receptors Kremen (Krm) 1 and Krm2. Krm2 with Dkk1 can bind Lrp6 and subsequently induces its rapid endocytosis (Mao et al. 2002). Members of the family of extracellular proteins sFRPs contain the cysteine-rich transmembrane domain (CTD), which resembles the extracellular domain of Fzd proteins. Accordingly, sFRPs can bind Wnt ligands in competition with Fzd (Lin et al. 1997; Rattner et al. 1997). As Wnt antagonists, sFRPs are related to many types of neoplasia, including colorectal and gastric cancer (Qi et al. 2006; Cheng et al. 2007). Although sFRPs are thought to be mainly tumor suppressors, their depletion could affect the correct distribution of particular Wnt ligand and thus tissue development (Esteve et al. 2011). Similarly to sFRPs, WIF is also potent suppressor of malignancy in various types of tissues (Silva et al. 2014; Paluszczak et al. 2015; Wei et al. 2015). The mechanism of Wnt binding by WIF is different from sFRPs as the protein lacks the CTD. It was proposed that the association is performed by protein

lipid-binding cavity sequestration (Malinauskas and Jones 2014). Proteins from the cysteine knot family, Wise and Sost, inhibit the Wnt signaling pathway by binding Lrp6 and Lrp5 (Itasaki et al. 2003; Krause et al. 2010). Moreover, Wise can disable trafficking of Lrp6 from the ER to the cell surface (Guidato and Itasaki 2007). Both Wise and Sost are also able to block the bone morphogenetic protein (BMP) signaling pathway. Wise prevents BMP ligand binding by direct attachment (Itasaki et al. 2003), whereas Sost retains BMP7 in secreting cell and mediates its proteosomal degradation (Krause et al. 2010).

Cytoplasmic regulators of Wnt signaling

Transport of the Wnt coreceptor LRP5/6 to the membrane is dependent on the activity of chaperone mesoderm development (Mesd) (Hsieh et al. 2003), which is involved in LRP5/6 extracellular domain (ECD) folding (Culi and Mann 2003). The intracellular domain (ICD) of LRP5/6 harbors many phosphorylation sites indispensable for the signal relay to Dvl and Axin. GSK3 phosphorylates the PPSP motif of LRP5/6 to activate Wnt signaling, moreover, it adds phosphate groups to β-catenin in order to inhibit the pathway (Zeng et al. 2005). CK1 phosphorylates β-catenin, Dvl, APC, Axin and Lef/TCF and PPSPXS sites on ICD of LRP5/6 (Price 2006; Verheyen and Gottardi 2010). Subsequent link in Wnt signaling, Dvl, encompasses three domains. The DIX (Dvl-Axin) domain is necessary for association with Axin and attaches to the postsynaptic density95, disc large, zonula occludens-1 (PDZ) domain. DIX and PDZ domains are required in β-catenin-dependent Wnt signaling. The third domain, Dvl, Egl-10, pleckstrin (DEP) altogether with PDZ are commonly involved in non-canonical Wnt pathways (Pan et al. 2004; Kim and Han 2005). Human Dvl is expressed in 3 isoforms, Dvl1, Dvl2 and Dvl3, with both similar and unique functions (Lee et al. 2008). The regulation of Dvl protein could be performed by phosphorylating kinases CK1 and CK2 that "push" the cascade to the higher transcription output (Bernatik et al. 2014). From the group of Dvl negative regulators could be mentioned Kelch-like protein 12 (KLHL12), NEDD4-like ubiquitin protein ligase 1 (NEDL1), Dapper1 and Prickle1 acting in the process of Dvl polyubiquitination (Miyazaki et al. 2004; Angers et al. 2006; Chan et al. 2006; Zhang et al. 2006). On the other hand, deubiquitination is accomplished by ubiquitin specific peptidase 14 (Usp14) (Jung et al. 2013). Surprisingly, Dvl functions as a negative Wnt signaling regulator as

well. Jiang et al. recently found, that E3 ligases ring finger protein 43 (Rnf43) and zinc and ring finger 3 (Znrf3) induce Wnt receptor degradation by binding the DEP domain of Dvl functioning as an adaptor between the ligases and Fzd (Jiang et al. 2015). One of the commonly known Wnt signaling inhibitor is Nkd1 (McEwen and Peifer 2001). The *Nkd* gene was first described in *D. melanogaster* as a segment polarity gene (Zeng et al. 2000). In mammals, two orthologs were discovered so far, *Nkd1* and *Nkd2*. Similar to fly nkd, mammalian Nkd proteins contain the conservative EFX domain indispensable for binding to Dvl, which participates in signal transduction in the cytoplasm (Wharton et al. 2001). When Wnt ligand is present, Dvl is recruited to Lrp6 and consequently disconnects Nkd1. Free Nkd1 can sequestrate β-catenin and prevents its transfer to the nucleus, thus inhibiting transcription of Wnt target genes (Larraguibel et al. 2015).

The main "safety guard" controlling the activity of Wnt signaling is the β-catenin destruction complex. The *APC* gene encoding the largest unit of the complex, was discovered in 1991 as a gene mutated in the hereditary type of cancer familial adenomatous polyposis coli (FAP) (Kinzler et al. 1991; Nishisho et al. 1991). Two years later, APC protein interaction with β-catenin was discovered (Rubinfeld et al. 1993; Su et al. 1993). Consequently, the link between Wnt signaling and cancer was established. Axin, the second key protein in the destruction complex, is expressed in two isoforms, Axin 1 (Axin) and Axin 2 (Conductin). Both proteins can be regulated by ubiquitination (Kim and Jho 2010; Callow et al. 2011; Lui et al. 2011) and sumoylation, although the latter modification is rare and occurs mainly in the context of the non-canonical Wnt pathways (Kim et al. 2008). Kinases GSK3 and CK1 phosphorylate Axin to enhance β-catenin association to Axin leading to suppression of the Wnt signal (Jho et al. 1999; Yamamoto et al. 1999). The DIX domain at the C-terminus of Axin permits homopolymerization in head-to-tail fashion (Schwarz-Romond et al. 2007). The DIX domain was primarily described as an adaptor for association with Dvl, thus leading to heteropolymerization of these two proteins and amplification of the signal (Yokoyama et al. 2012). As the last mentioned, Axin has a potential of self-organizing to closed conformation by linking the N- and C-terminus together, consequently becoming incompetent to bind β-catenin or LRP5/6 (Kim et al. 2013).

Regulation of transcription in Wnt signaling

The LEF/TCF transcription factors have to be supported by various cofactors to augment their transcriptional activity. Among others, pygopus (Pygo) could be mentioned due to its assorted abilities of enhancing LEF/TCF transcription. Although in mammals Pygo lacks as much essential role in regulation of the signaling pathways as in *D. melanogaster*, where its depletion causes similar phenotype like ablation of Wg and β-catenin ortolog Armadillo (Perrimon 1994), its deletion in mammals generates defects in kidney or lens development (Schwab et al. 2007; Song et al. 2007). Pygo encompasses two domains, the N-terminal NHD domain associating with LEF/TCF and PHD finger, which is crucial for β-catenin binding via Legless/B-cell CLL/lymphoma 9 (Lgs/BCL9) (Kramps et al. 2002). Pygo can increase the local concentration of chromatin remodeling enzymes associated with β-catenin (Mosimann et al. 2006) and, consequently, boosts the efficiency of β-catenin mediated transcription. Moreover, it serves as an anchor for β-catenin in the nucleus multiplying its activating effect on LEF/TCF. Strikingly, the PHD finger domain is capable to associate with LEF/TCF in β-catenin independent manner implicating its role in additional signaling pathways (de la Roche and Bienz 2007). Another helpers of transcription activation Traf1 and Nck-Interacting Kinase (TNIK) phosphorylate serine 154 residue of β-catenin and increase its action (Mahmoudi et al. 2009; Shitashige et al. 2010). Interestingly, the cytoplasmic hub of Wnt signaling, Dvl, has a crucial role also directly in the transcription activation process. It has been shown, that Dvl is transported into the nucleus by Foxk transcription factors 1 and 2 (Wang et al. 2015) and there it facilitates assembly of the complex formed of β-catenin, TCF and protein product of proto-oncogene *c-Jun* (Gan et al. 2008). The complex subsequently augments the efficiency of Wnt target genes transcription. The upregulation of Foxk2 induces hyperproliferation of intestinal crypts in mice and has been found also in human intestinal tumors (Wang et al. 2015). Contrarily, the β-catenin association with LEF/TCF could be also modified in repressive way. Inhibitor of β-catenin and TCF (ICAT) prevents the association of these two proteins by repressive binding to R5 to R12 Armadillo repeats of β-catenin (Daniels and Weis 2002). Likewise TCFs have repressive and activating properties, SUMO E3 ligase protein inhibitor of activated STAT protein gamma (PIASy) modifies Lef1 to immobilize it in nuclear bodies. In contrast, PIASy sumoylates TCF4 promoting β-catenin tighter binding and transcription efficacy (Sachdev et al. 2001; Ihara et al. 2005).

Wnt target genes

The Wnt signaling pathway upregulates diverse group of genes employed in crucial cellular events as proliferation, cell growth, differentiation and metabolic processes (Ziegler et al. 2005). Activation of Wnt target genes is strictly regulated and it is temporarily and spatially modulated, inasmuch it is often connected to embryonic development. Although numerous genes transcribed according to cell cycle and surviving lack the direct activation by Wnt signaling, their transcription is related to pathways influenced by Wnt signaling, such as *c-myc* and *K-Ras* (He et al. 1998; Zhang et al. 2001). The regulation of Wnt signaling is, moreover, sophistically performed by its own feedback loops in a form of the Wnt target genes such as *Axin, Nkd, Tcf1, Lef1* or *Dkk* and others (up to date chart of Wnt target genes can be found in webpage http://web.stanford.edu/group/nusselab/cgi-bin/wnt/target_genes). The issue of Wnt targets with special role in GIT will be discussed in following chapters. In conclusion, the Wnt signaling pathway is evolutionary conserved and fine-tuned orchestra with well-studied, but yet uncovered members and events.

GIT

Although the logical order of chapters would be describing the stomach anatomy and morphology before the gut, the rank is opposite. The thesis deals with the intestinal epithelium as with the main theme included in five publications, whereas the stomach epithelium is a research subject in one publication only. In addition, the signaling mechanisms and molecules are frequently identical in the intestinal as well as in gastric epithelium, the main interest is placed on the intestine and the molecular concept of consistent events is explained within the framework of the gut.

The gut – small intestine and colon anatomy

The small intestine, inferior continuation of GIT, sustains of three main parts. First segment, duodenum, harbors orifices of the stomach, pancreatic and gall bladder ducts. Duodenal muscle walls are tight as this section is well resolvable by an eye. Apart from other common types of intestinal epithelial cells the duodenal epithelium contains special submucosal Brunner´s glands producing alkaline secretion to neutralize gastric acid

(Zamolodchikova et al. 2013). The middle part of the small intestine is called jejunum. This intestinal segment harbors a typical small intestinal epithelium. The caudal section of the small intestine is the ileum, which leads to the colonic cecum. The large intestine consists of the ascending, transverse and descending colon. The gastrointestinal tract is terminated by the sigmoid flexure, rectum and anal canal (Gray et al. 2005).

Stomach anatomy

Stomach is divided in three main sections (Fig. 4). The most superior curvature of the organ forms fundus. The largest middle part of the stomach creates corpus and the most distal section is pylorus alias antrum continuing to duodenum (Lee et al. 2015).

Common histology of GIT

Likewise other organs in the abdominal cavity, GIT is fixed to prevent the unwanted motions by mesenteria. The wall of GIT encompasses four distinct sheets of tissues, from outer sheet to the lumen: serosa, muscularis externa, submucosa and mucosa (Weiss 1984; Cherciu et al. 2014). Outer serosa resembles the loose connective tissue. Digestive and peristaltic motions are ensured by the longitudinal and circular muscle, muscularis externa, and innerved by so called Auerbach´s plexus. Submucosa tissue comprises nerves, blood vessels and elastic fibers. Finally, connective lamina propria with myofibroblasts, blood vessels, nerves, immune cells and muscularis mucosae, which causes the peristaltics, separates lower tissue layers of the gastric or intestinal epithelium (Weiss 1984).

Intestinal epithelium architecture and cell types

The lumen of the small intestine and colon is circumvented by the cell monolayer called the intestinal epithelium (Fig. 3). In the small intestine, the epithelium is corrugated to the appearance of the brush border with protrusions called villi and invaginations to the underlying connective tissue called the intestinal crypts (alias crypts of Lieberkühn). The epithelium contains various types of differentiated cells. Absorptive enterocytes care of nutriment digestion and water transmission, while Paneth cells defend the intestine

against infection by producing bacteriostatic compounds. Another cells from secretory line produce mucin to lubricate the intestinal surface (goblet cells), GIT hormones (enteroendocrine cells) or opioids (tuft cells). Moreover, there are rapidly dividing undifferentiated cells, so-called transit-amplifying (TA) cells, direct descendants of crypt base columnar (CBC) SCs. TA cells divide 4-6 times before reaching the border of the crypt where they differentiate as they ascend upwards the villus (Potten 1998). The only known differentiated cells residing at the bottom of the crypt are the Paneth cells, which nest interspersed between SCs. Intestinal cells have very rapid turnover lasting about 4-5 days. In this time interval, the differentiated cell migrates from the bottom of the crypt to the tip of the villus, where it is shed into the gut lumen. Paneth cells lack the rapid rate of proliferation, resting in the crypt for 6-8 weeks [reviewed in (Schepers and Clevers 2012)]. The longevity of Paneth cells is possible due to their ability to create autophagosomes sequestering the waste peptides, which they cannot rid off by proliferation. Paneth cells produce essential growth factors to form the epithelial niche for maintenance of CBC cells (Sato et al. 2011). Moreover, they secrete antimicrobial peptides such as α-defensins and lysozyme that protect the intestinal epithelium against bacterial infections, while also maintaining the balanced composition of the gut microbiota. The protein posttranslational modification and secretion from Paneth cells is responsive to the ER stress pathways [reviewed in detail in (Clevers and Bevins 2013)]. Apart from rapidly cycling CBC cells, there are quiescent SCs residing in the 4^{th} position, bordering the crypt bottom, thus named "+4 SCs" (Potten 1998). Epithelium of the colon differs with villi and Paneth cells absence. Additionally, the portion of goblet cells producing mucin is increased in comparison to the small intestine.

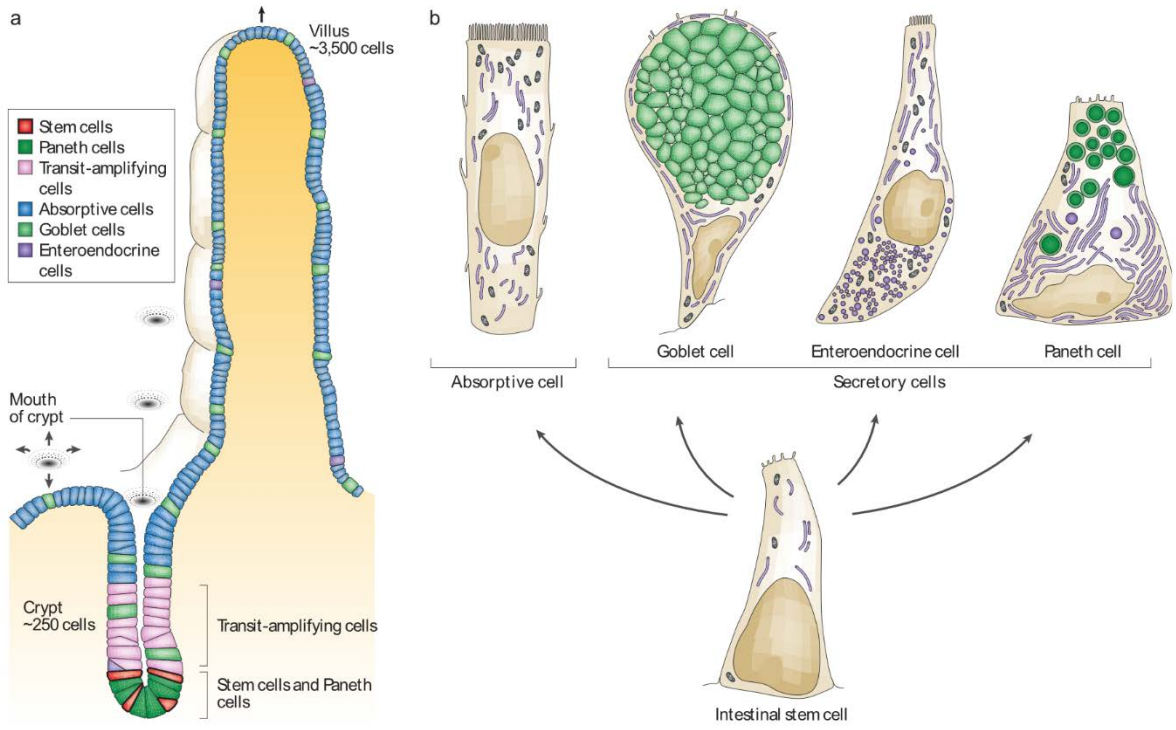


Figure 3: Architecture of the intestinal epithelium and types of intestinal cells. (a) The intestinal epithelium forms crypt invaginations and villi protrusions. In the bottom of the crypt resides rapidly cycling population of SCs. In common condition, SCs are precursors of all types of intestinal cells, namely absorptive, goblet, enteroendocrine, and Paneth (b). Mostly all of them migrate upward the villus with exception of the lattermost. Paneth cells establish themselves in the crypt bottom between SCs. Adopted from (Crosnier et al. 2006).

Intestinal SCs

SCs in adult tissue are responsible for its common regular renewal as well as repair after damage, for instance after exposure to chemicals or irradiation (Metcalfe et al. 2014; Zhang et al. 2014). Moreover, intestinal SCs were revealed as the originators of colorectal cancer (Barker et al. 2009). There is endless disputation about the description of "real" intestinal SCs. Actually, the intestinal epithelium contains more than one population of stem-like progenitors. Physiological regeneration of the epithelium is under control of fast cycling CBC cells. Additionally, the +4 cells are quiescent, slowly cycling SCs (Potten et al. 1974). These +4 cells are the reserve population in situations that the rapidly cycling CBC cells are diminished (Barker et al. 2007; Sangiorgi and Capecchi 2008), being uncovered by their ability to retain a radioactive label implicating their longevity (Cheng and Leblond 1974). An extensive effort is applied in search for marker proteins that are uniquely produced by intestinal SCs.

In 2007, Barker et al. established leucine-rich repeat-containing G-protein coupled receptor 5 (Lgr5) as a marker of CBC SCs in the gut (Barker et al. 2007). Previously, *Lgr5/Gpr49* gene was identified as a Wnt intestinal target gene in microarray analysis of colorectal cell lines, particularly LS174T and DLD1 stably expressing dominant-negative (dn)TCF1 or dnTCF4 (Van der Flier et al. 2007). Interestingly, Lgr5 protein marks SCs in various tissues, where the Wnt signaling pathway directs homeostasis including the eye, hair follicle or stomach. Lgr4, Lgr5 and Lgr6 proteins were identified in 1998 and 2000, respectively, as members of the G-protein-coupled, 7-transmembrane family of hormones (Hsu et al. 1998; Hsu et al. 2000). The ectodomain of Lgr proteins extending to the extracellular space harbors multiple leucine-rich repeats flanked by N- and C-terminal cysteine-rich sequences. The structure of the proteins is highly conserved in evolution, having also homologous proteins in invertebrates (Kudo et al. 2000; Nishi et al. 2000).

Lgr5 marks CBC cells, yet its conditional deletion has no effect on the adult intestinal epithelium (de Lau et al. 2011). In mouse embryos, *Lgr5* knock-out causes ankyloglossia, i. e. attachment of tongue to the lower jaw. The mice die of starving as they cannot suck milk (Morita et al. 2004). Interestingly, in developing intestine, Paneth cells maturation is accelerated (Garcia et al. 2009). *Lgr4* deletion causes reduction in intestinal crypt proliferation and disslocalization of cells – except Paneth cells - from the crypt bottom. Combination of *Lgr5* and *Lgr4* deletion affects the epithelium in a more destructive way, leading to the animal death (de Lau et al. 2011). In addition, *Lgr6* deletion has no phenotype in mice (Snippert et al. 2010). For a relatively long time, the Lgr proteins function remained unknown. The same was true for their ligands. In 2011, several research groups identified small molecules R(oof palate-specific) spondins secreted in the intestine by Paneth cells (Sato et al. 2011) as the ligands for Lgr4 and Lgr5 (Carmon et al. 2011; de Lau et al. 2011; Glinka et al. 2011; Ruffner et al. 2012). R-spondins (Rspos) are excreted proteins resembling the structure of epidermal growth factor (EGF) or insulin (de Lau et al. 2011). Overexpression of these ligands provokes massive proliferation of $Lgr5^+$ CBC cells (Kim et al. 2005; Ootani et al. 2009). Rspos are the synergists of the Wnt signaling pathway with potential to increase the signalization only if the Wnt ligand is bound to the receptor (Li et al. 2009). The mechanism of the augmentation is conducted by inhibition of E3 ligases Rnf43 and Znrf3, previously mentioned in connection to regulation of the Wnt pathway by Dvl binding (Jiang et al. 2015). In Lgr5-Rspo absence,

transmembrane domain of Frizzled is multiubiquitinated by these membrane ligases and subsequently endocyted and degraded in the lysosomes (Hao et al. 2012; Koo et al. 2012). Rspo associated with receptor Lgr5 binds Rnf43/Znrf3, which leads to sequestration of the Lgr5-Rspo-Rnf43/Znrf3 complex. Consequently, the signaling Wnt-LRP5/6-Fzd complex persists on the membrane (Hao et al. 2012).

$Lgr5^+$ cells behave as fast cycling intestinal SCs, thus they give rise to the functional intestinal organoid structure *ex vivo* (Sato et al. 2009), produce all specialized cell types (Barker et al. 2007) and form intestinal adenomas (Barker et al. 2009). In the experiment using in vivo live-imaging of $Lgr5^+$ dividing SCs was found, that the $Lgr5^+$ population has a spatially specific heterogeneity. SCs residing in the central position in the bottom of the crypt divide with three time higher probability than $Lgr5^+$ cells at the border of the crypt (Ritsma et al. 2014). It is therefore evident, that the position of the cells in the niche is determining beside the cell genomic program.

Since Barker et al. described CBC cells in intestine as intestinal SCs, this research field was accelerated. Many other markers of $Lgr5^+$ cells has been identified, such as achaete-scute complex homolog 2 (Ascl2) (van der Flier et al. 2009b), olfactomedin 4 (Olfm4) (van der Flier et al. 2009a), SPARC-related modular calcium-binding protein 2 (Smoc2) (Munoz et al. 2012), SRY-box 9 (Sox9) (Gracz et al. 2010), tumor necrosis factor receptor superfamily, member 19 (TNFRSF19) alias Troy (Fafilek et al. 2013). In addition, many more potential markers were unveiled by a screen performed by Munoz et al. in 2012 (Munoz et al. 2012). Although +4 cells have their putative "unique" markers, the specificity of these markers is controversial. B-cell specific Moloney murine leukemia virus integration site 1 (Bmi1), the possible marker of the quiescent stem cell population (Sangiorgi and Capecchi 2008), was shown as a suitable molecule for sorting cells that can form organoids (Yan et al. 2012). After diphtheria toxin ablation of $Lgr5^+$ cells, $Bmi1^+$ repopulate the epithelium by all differentiated cell types (Tian et al. 2011). Controversially, increased levels of *Bmi1* mRNA was found in fast cycling SCs (Itzkovitz et al. 2012) and lineage tracing of quiescent $Bmi1^+$ cells failed to be reproduced (Munoz et al. 2012). Moreover, leucine-rich repeats and immunoglobulin-like domains protein 1 (Lrig1), a previously defined marker of quiescent SCs (Powell et al. 2012), has been shown to be abundant in fast cycling SCs (Wong et al. 2012). The situation is very similar to another controversial quiescent stem cell markers mouse telomerase reverse transcriptase (mTert) or HOP homeobox (Hopx) (Itzkovitz et al. 2012). One of the

recently described marker of fast cycling or quiescent SCs as well as TA progenitors is inhibitor of DNA binding 1 (ID1), previously defined as an important player in embryonic stem cell renewal (Ying et al. 2003; Romero-Lanman et al. 2012). ID proteins in common facilitate cell cycle progression (Lasorella et al. 2014). ID1 marks all known progenitors in the small and large intestine and organoids derived from $ID1^+$ cell are long-lived containing all types of fully differentiated cells. Moreover, in the dextran sulfate sodium (DSS) treated large intestine ID1 ablation causes more severe phenotype than in wild-type (wt) tissue implicating high sensitization to the chemical injury (Zhang et al. 2014).

Recently, the stem cell "pool" was increased by cells that lack the Lgr5 marker. Delta-like 1 (Dll1) is the ligand for the Notch receptor crucial for directing intestinal epithelial cells to the secretory fate (Pellegrinet et al. 2011). It was shown that Dll^{high} cells are members of the TA compartment, generating short-lived clones of all secretory types of intestinal cells and have an ability to produce organoids. The $Dll1^+$ secretory progenitor can revert to the stem cell status after epithelial damage (van Es et al. 2012). In the small intestine, keratin 19 $(Krt19)^+/Lgr5^-$ cells were identified as long-lived, radioresistant and cancer initiating SCs (Asfaha et al. 2015). In the colon, this population probably substitutes $Bmi1^+$ cells, which are absent in the colonic epithelium. Striking evidence for existence of a specific progenitor secretory line came from Buczacki et al., who presented results using sophisticated strategy of labelling quiescent cells in the intestinal epithelium. Label-retaining cells (LRCs) display properties of $Lgr5^+$ cells during homeostasis, yet, surprisingly, LRCs are destined to become Paneth cells. However, LRCs regain stemness after epithelial damage (Buczacki et al. 2013). Finally, a striking notion was introduced by Zhu et al. His study uncovered negative coincidences of tamoxifen, a commonly used inductor of recombination in genetically manipulated animals and cells. Tamoxifen was identified as a pro-apoptotic agent affecting intestinal epithelium. Since the majority of the stem cell studies used tamoxifen-induced recombination, the fact rises some doubts about the credibility of the obtained results (Zhu et al. 2013).

Stomach epithelium architecture and cell types

In humans, the gastric epithelium renewing once every 2-7 days (Blanpain et al. 2007) represents a glandular type of tissue. In contrast to the human stomach, the mouse stomach contains the squamous epithelium in its first proximal third and the rest is

glandular (van den Brink 2007). Common glandular gastric epithelium is a component of gastric units, curvatures invaginating into deep pits, which continue deeper branching into gastric glands. There are various types of differentiated stomach cells and their precursors, gastric SCs. Specialized cells include parietal (oxyntic, delomorphous) cells secreting gastric acid and producing gastric intrinsic factor (GIF), chief (zymogenic) cells secreting pepsinogen and gastric lipase, pit (surface associated mucous) cells releasing mucus and hormone-secreting enteroendocrine cells, such as enterochromaffin-like (ECL) cells producing histamine for parietal cells stimulation (Li et al. 2014a). A special type of cells, the mucous neck cells secreting mucus, are the intermediate between SCs and chief cells (Fig. 5) [reviewed in (Schepers and Clevers 2012)]. In contrast to the intestinal crypt, the stomach gland is divided into 4 main parts – base at the bottom, neck, isthmus and surface foveolus facing the lumen of the organ. Interestingly, the gastric glands also differ in habitus and cell type composition regarding to the anatomic location. The corpus gland is formed by a base with chief cells, neck with parietal and interspersed mucous, isthmus with supposed SCs and faveolus with mucus secreting pit cells, the antral gland look unlike. On the surface, there are mucus secreting pit cells, however, neck and base fuse to one structure harboring cells with properties of parietal and mucous neck (Fig. 4) (Mills and Shivdasani 2011). Nevertheless, one fact concerning the gastric and intestinal epithelium can be applied to both: describing of SCs is controversial.

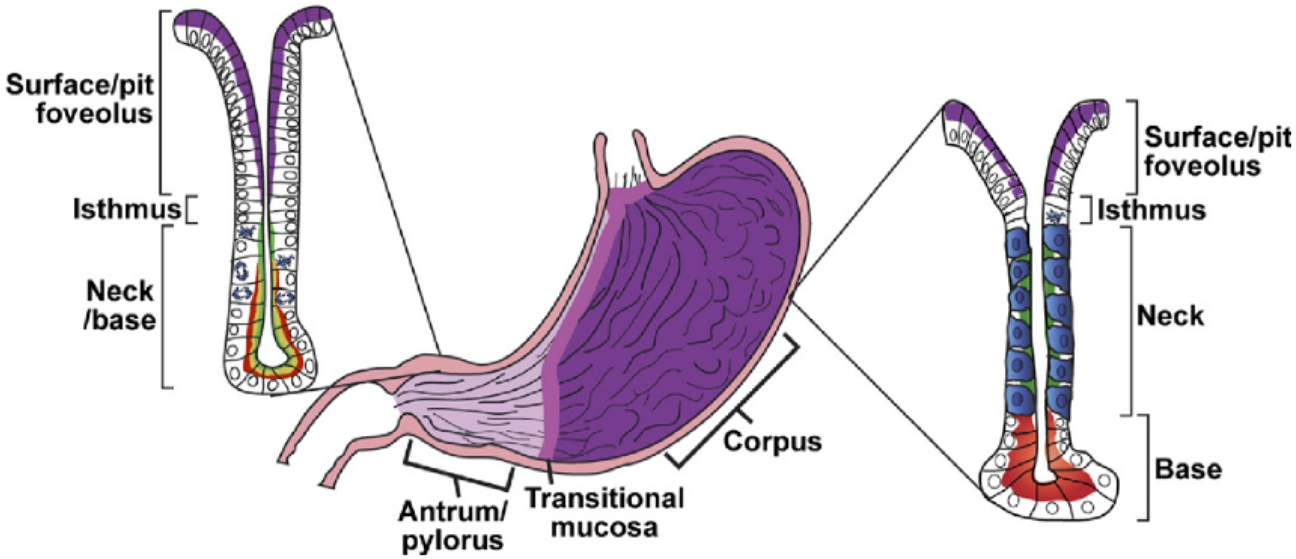


Figure 4: Stomach anatomy and epithelial architecture. Stomach sustains of three parts, from which the most superior, the fundus, is morphologically similar to the corpus. Depicting of cells in glands: acid secreting parietal (blue), digestive enzyme secreting chief (red), mucous neck (green), mucus secreting pit (purple). The antral glands differ from those in the corpus. Whereas in the corpus gland the functional and morphological proprieties of differentiated cells are rather pronounced, the antral gland base contains cells evocative to zymogenic (chief) as well as mucous neck cells in the corpus. Adopted from (Mills and Shivdasani 2011).

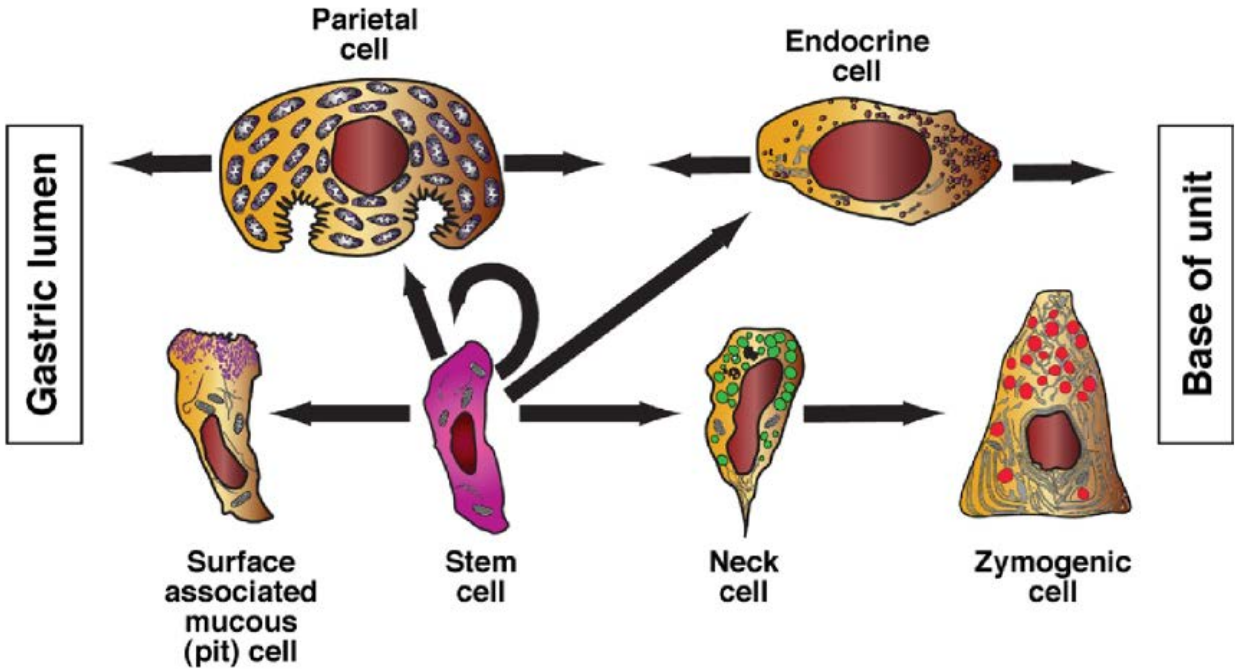


Figure 5: The stomach epithelial cell types, their origin and residence. "Common" gastric stem cell gives rise to 4 types of fully differentiated cells while retaining its stemness. Neck cells are secretory cells producing mucus and in addition they are an intermediate step in development of zymogenic cells. Adopted from (Mills and Shivdasani 2011).

Stomach SCs

As in the intestine, gastric SCs are crucial for self-renewing the epithelium as well as homeostasis of the gland. Moreover, they play a key role in process of tissue repair in case of injury (Hoffmann 2008). There has been plenty of studies describing markers of gastric SCs. There are differently marked stem cell populations in the corpus and antrum, although the populations share some characteristics. In the corpus, SCs are residing within the isthmus in the upper part of the gland (Karam and Leblond 1993). The putative marker of SCs in the gastric corpus is trefoil factor 2 (Tff2) expressed in short-lived progenitors (Quante et al. 2010). Sox2-positive cells are determined as SCs in the corpus as well as in antrum and, in contrary to $Tff2^+$ cells, are thought to be long-lived SCs (Arnold et al. 2011). The exception from the isthmus-residing progenitors are $Troy^+$ cells, nested at the bottom of the glands. Stange et al. proved, that $Troy^+$ cells take place of the reserve gastric stem-like chief cell population activated upon depletion of isthmus compartment in corpus due to damage (Stange et al. 2013).

In the antrum, apart from already mentioned $Sox2^+$ cells, another SC markers have been postulated. The common marker of intestinal epithelial cells villin has been surprisingly uncovered as protein specifically expressed by putative SCs in the pylorus. However, contribution of these cells to the differentiated cell pool occurs only in case of epithelial damage (Qiao et al. 2007). Rspo receptor Lgr5 was identified as a putative marker of antral SCs (Barker et al. 2010b). Lgr5 absence in the gastric corpus is connected to morphologic changes in the newborn stomach. Before this process, all cells in the epithelium originate from $Lgr5^+$ SCs. Afterwards, $Lgr5^+$ cells in the corpus disappear (Barker et al. 2010b). Very recently, the gastric stem cell biology field witnessed new development. Hayakawa et al. discovered gastrin/cholecystokinin type B receptor (CCKBR) as a marker for antral SCs in the +4 position in the gland. The ligands of CCKBR, gastrin and progastrin, stimulate secretion of gastric and pancreatic liquids, controlling motility of the stomach and intestine and having many other functions that include proliferative effects on gland cells (Walsh 1990). $CCKBR^+$ cells do not overlap with the $Lgr5^+$ high population, however, they produce very low or negligible amounts of Lgr5 (Hayakawa et al. 2015b). In case of ligand binding to CCKBR, $Lgr5^{low/-}/CCKBR^+$ cells undergo increased proliferation and become $Lgr5^{high}$. Interestingly, this proliferative potential promotes in carcinogenesis upon exposition to chemical carcinogens (Hayakawa et al. 2015b). Recently, $Mist1^+$ cells were identified as $Lgr5^-$ quiescent SCs

in the isthmus of the gastric corpus (Hayakawa et al. 2015a). In 2014, Simmini and colleagues came with striking evidences that knock-out of a single gene, encoding the transcription factor caudal type homeobox 2 (Cdx2), reprograms intestinal stem cell to gastric stem cell. The (re)specification results in cells creating growing organoid cultures without the need of mesenchyme-produced factors (Simmini et al. 2014).

Signaling pathways in the intestinal and gastric epithelium

Intestinal and gastric epithelia architecture resembles a sophisticated cellular system with multiple tasks performed by various cell types. This implies existence of a complex apparatus to orchestrate these tasks. The maintenance of the intestinal and gastric epithelium is the result of an interplay between signaling pathways directing cells to proliferation or differentiation [reviewed in (Giannakis et al. 2006; Krausova and Korinek 2012)]. Unsurprisingly, the impaired balance of the signaling may lead to colorectal cancer (CRC) and gastric cancer (GC) development (Iwao et al. 1998; Katoh et al. 2001; Sherman and Zavros 2011; Mundade et al. 2014).

Wnt signaling

The Wnt signaling pathway, in details described above, has a crucial role in stem and TA progenitor cell maintenance (Crosnier et al. 2006). Indispensable need of this pathway was elucidated by studies describing the intestinal epithelium damage after defective or null expression of the Wnt transcription effector TCF4 (Korinek et al. 1998; Muncan et al. 2007) or transcription co-activator β-catenin (Harada et al. 1999; Sangiorgi and Capecchi 2008). The maximum of the Wnt signal is produced in the crypt bottom and diminishes upwards the villus (van Es et al. 2005a). Paneth cells neighboring crypt SCs are the main producers of Wnt3 ligand, additional growth factors, and infection-protecting molecules, therefore their contribution to the CBC maintenance seems to be indispensable [reviewed in (Clevers and Bevins 2013)]. Interestingly, quiescent $Bmi1^{+}$ SCs are Wnt signaling independent (Yan et al. 2012). Despite the key role the Paneth cells play in the crypt, their ablation surprisingly does not destroy epithelial architecture (Farin et al. 2012). It has been shown, that Wnt2a is produced by underlying mesenchymal cells to support the stem cell proliferative activity (Gregorieff et al. 2005). In accordance,

epithelium in the large intestine lacks Paneth cells, although the colonic niche seems to support CBC cells in similar manner observed in the small intestine. Cells positive for cKit/CD117 lodged between $Lgr5^+$ cells are shown to produce molecules Dll1, Dll4, Egf, mucin 2 (Muc2), SAM pointed domain containing ETS transcription factor (Spdef) and defensins as Paneth cells. Unexpectedly, these cells do not produce any Wnt activators (Rothenberg et al. 2012).

In the stomach, the Wnt signaling pathway plays one of the main roles in stem cell maintenance. The $Lgr5^+$ population of SCs was discovered as being directed by Wnt signaling (Barker et al. 2010a), although the source of Wnt ligands is not known. Recent investigation described gastric organoids from the corpus growing independently on Wnt3a ligand, when $Lgr5^+$ cells are ablated. Quiescent $Mist1^+$ corpus SCs maintain the organoid growth with the support of non-canonical Wnt5a, produced in Scavenger Chemokine Receptor 4 $(Cxcr4)^+$ cells residing in the proximity of $Mist1^+$ cells in the isthmus (Hayakawa et al. 2015a). The major role of the Wnt pathway in gastric gland regulation has been confirmed by expression profiles of mouse stomach tissue, where β-catenin-dependent Wnt signaling target genes scored on the top place (Giannakis et al. 2006).

Notch signaling

Stemness of CBC cells is preserved by the Paneth cells-specific production of Dll1 ligand interacting with the Notch receptor on the CBC surface (Stamataki et al. 2011), thus Notch signaling is permanently "on" in crypt SCs (Pellegrinet et al. 2011). In brief description, the juxtacrine Notch signaling is initiated by Notch ligands (in mammals Dll1, Dll3, Dll4 and Jagged 1 and Jagged 2) bound to the Notch receptor extracellular domain, which is subsequently cleaved and endocyted together with the ligand. The intracellular domain is then cut from the transmembrane domain and relocated to the nucleus, where it associates with the transcription complex to start expression of target genes [details are reviewed in (Andersson et al. 2011)]. Active Notch signaling triggers transcription of *hairy and enhancer of split (Hes)* leading to expression of the basic helix-loop-helix (bHLH) transcription repressor Ascl2, the suppressor of atonal homolog 1 (Atoh1) (Ueo et al. 2012). Atoh1 acts as a main regulator of cell secretory fate, therefore its inhibition by Ascl2 causes CBC resting in undifferentiated state (Kim and Shivdasani

2011a). Since the cells leave the crypt bottom, they abandon the proximity of the Paneth cells and, consequently, Atoh1 blocking is slightly decreased, as well as Notch signaling is diminished. Finally, the stochastic ratio in the amount of Dll1 and Atoh1 proteins decides, whether the particular cell becomes secretory or absorptive (Philpott and Winton 2014). The absence of Notch signaling induces differentiation to secretory goblet cells (van Es et al. 2005b).

Gastric epithelium proliferation, apoptosis and differentiation is also directed by Notch signaling (Wu et al. 2010). As in the intestine, the increased number of endocrine cells is related to disrupted expression of Hes1 (Jensen et al. 2000). The mechanism has not been clarified yet, as Ascl2 expression in the stomach was not detected (Yang et al. 2001). The highest levels of Notch signaling is observed in the isthmus, where proliferation of progenitors occurs. Interestingly, in $Lgr5^{+}$ progenitor cells active Notch signaling supports their stemness, whereas differentiated gastric parietal cells can be reverted to the progenitor state by the Notch pathway. This de-differentiation consequently leads to adenoma formation (Kim and Shivdasani 2011b).

EphB/ephrin-B signaling

Wnt signaling functions not only in CBC cells, but even in Paneth cells themselves. The Paneth-maintained Wnt levels in the crypt bottom induce the expression of Wnt target genes, receptors *ephrin B2* (*EphB2*) and *B3*, and it also represses Eph ligand *ephrin-B1*. Eph receptors belong to the family of tyrosin kinases and contain two subclasses, EphA and EphB. Interestingly, both the receptors and ligands are transmembrane proteins (Himanen et al. 2004) that signal during cell to cell contact (Beauchamp et al. 2012). Moreover, the signal is reciprocal, hence both cells carrying receptor or ligand are influenced (Nievergall et al. 2012). As the progenitor descendants migrate from the crypt bottom, the effect of Wnt signaling decreases accompanied by decline in ephrin-B1 repression. The repulsion between EphB- and ephrin B-expressing cell is mediated by recruitment of A disintegrin and metalloproteinase domain-containing protein 10 (ADAM10) to the plasma membrane of EphB-positive cell. ADAM10 then cleaves E-cadherin in adherens junctions, which leads to sorting of cells in the epithelium (Solanas et al. 2011). Paneth cells producing EphB3 receptor as their unique marker escape this fate and stay nested in the crypt bottom (Batlle et al. 2002).

In the stomach, the principle of EphB and ephrin B repulsion ensures the highest level of the signaling in the isthmus of the gastric gland (Perez White and Getsios 2014; Uchiyama et al. 2015). The EphB/ephrin B signaling role in the gastric gland has not been described in detail, however, as in the intestine, the repulsion secures the proper stratification of the gastric glands and epithelial cells-sorting (Ishii et al. 2011). Upregulated EphB/ephrin B signaling is described as consequence of epithelium regeneration and tumor growth (Sugimura et al. 2010; Ogawa et al. 2011; Uchiyama et al. 2015).

BMP signaling

BMPs are members of the transforming growth factor β (TGF-β) superfamily. The canonical BMP pathway employs signalization through membrane BMP receptor I or II initiating phosphorylation of *D. melanogaster* homolog mothers against decapentaplegic and *C. elegans* sma (Smad) 1/5/8 transcription factors. This protein enters the nucleus in the form of a heterotrimeric complex (Miyazono 2000; Derynck and Zhang 2003). The complex with several other transcription factors regulates expression of target genes important for embryonic neural development, such as *dihydropyrimidinase-like 2* (*Dpysl2*) and *lysine-specific demethylase 6 b* (*Kdm6b*) (Fei et al. 2010). In the intestine, BMPs are highly expressed in the mesenchyme with maximum in the tip of the villi. Their expression decreases towards the crypts (Haramis et al. 2004; Hardwick et al. 2004). Intestinal myofibroblasts surrounding the crypt express BMP antagonists Noggin, Gremlins 1 and 2 and chordin-like 1 (He et al. 2004; Kosinski et al. 2007). BMP signaling creates the opposing pole to the Wnt pathway as it is restricted to the epithelial compartment containing differentiated cells. Additionally, by Wnt signaling suppression, it holds the cells in the non-proliferative status (He et al. 2004).

In the stomach, the mediator of the TGF-β pathway and antagonist of Wnt signaling, Runt-related transcription factor 3 (Runx3), guards the epithelium against uncontrolled proliferation (Voon et al. 2012). This tumor suppressor functions as a regulator of transcription of genes related to apoptosis, such as $p21^{WAF1}$ or *Bcl-2-interacting mediator of cell death (Bim)* (Chi et al. 2005; Yano et al. 2006). The Runx3 deficient mouse stomach epithelium hyperproliferates due to disabled apoptosis (Li et al. 2002). Runx3 can also directly affect Wnt signaling in a negative way by interaction with the TCF/β-catenin complex (Ito et al. 2008). Finally, Voon showed that loss of Runx3 increases a

tumorigenic stem cell-like population expressing Lgr5 and promotes spontaneous epithelial mesenchymal transition (EMT) of gastric epithelial cells, the event linked to invasiveness of gastric malignant tumors (Voon et al. 2012).

Hedgehog (Hh) signaling

Hh signaling is commenced by ligands Sonic hedgehog (Shh), Indian hedgehog (Ihh) and Desert hedgehog (Dhh) (McMahon 2000; Ingham and McMahon 2001). In case of Hh ligands absence, the receptor Patched (Ptch) inhibits function of Smoothened (Smo). Smo resides in the plasma membrane of the non-motile cilia in mammals and serves as the signal repressor (Taipale and Beachy 2001; Corbit et al. 2005). The zinc-finger transcription factors glioma-associated oncogene (Gli) 2 and Gli 3 are cleaved by the proteasome to variants repressing transcription of Hh target genes (Rubin and de Sauvage 2006). As the Hh ligands are released from secreting cell by transmembrane transporter Dispatched (Disp), Ptch repressive effect is terminated and Smo transduces the signal to the transcription-competent form of Gli proteins (Stamataki et al. 2005). Hereafter, Gli proteins induce expression of Hh signaling target genes, for instance *cyclin D*, *myc*, *Bmi1*, and *Bcl-2* (McMillan and Matsui 2012). The TA cell compartment in the intestinal epithelium produces Shh and Ihh, whereas the Ptch receptor resides on mesenchymal cells. The Hh pathway induces production of BMP from mesenchyme, thus inhibiting Wnt signaling and additional crypt formation and supporting enterocyte differentiation (Madison et al. 2005; van Dop et al. 2009).

Hh signaling is the crucial molecular cascade involved in gastric development. In mouse embryo, Shh inhibits the gland formation in the forestomach and supports squamous epithelium growth. In the glandular hindstomach, Shh expression is restricted by the Fgf10 mesenchymal production. Interestingly, Shh ablation has no effect on this tissue segment, as its function could be (probably) substituted by Ihh (van den Brink 2007). In the adult stomach, Hh signaling directs differentiation of gastric progenitor cells to mucous cells and parietal cells during the gastric ulcer repair process (Kang et al. 2009).

EGF signaling

Signalization through EGF employs several types of signaling pathways – mainly the mitogen-activated protein kinase/extracellular signal-regulated kinase (MAPK/ERK) pathway also known as Ras-Raf-MEK-ERK signaling, phosphatidylinositol 3-kinase/Akt kinase (PI3K/Akt) and phospholipase c (PLC) pathways (Krausova and Korinek 2012).

In the MAPK/ERK cascade, transmembrane tyrosine kinase EGF receptor (EGFR) binds EGF and its tyrosine residues get phosphorylated. This event primes growth factor receptor-bound protein GRB2 (Schulze et al. 2005) to activate son of sevenless (SOS) through GRB2 Src Homology 2 (SH2) domain (Zarich et al. 2006). The activated SOS SH3 domains transmit the signal to GTPase Ras by removing its GDP. Subsequently, Ras binds GTP and triggers the phosphorylating kinase cascade Raf-MEK-MAPK (Avruch et al. 2001). Active MAPK mobilizes transcription factors like c-myc, cyclic AMP-responsive element-binding protein (CREB) or c-fos (Cargnello and Roux 2011). These proto-oncogenes are linked to cell proliferation and differentiation. Heuberger and colleagues found, that Mek1/MAPK signaling controls the choice between the goblet and Paneth cell fate (Heuberger et al. 2014). Mediator of Mek1/MAPK, non-receptor tyrosine phosphatase containing SH2 domain (Shp2) ablation causes increase in the Paneth cell number and decrease in the goblet cell population. Moreover, it has been shown, that Shp2/Mek1/MAPK signaling attenuates canonical Wnt signaling. Thus, the resulting amount of Paneth and goblet cells reflects the balance between these two signaling pathways (Heuberger et al. 2014).

In the gastric epithelium, the MAPK/ERK cascade is linked functionally to the BMP pathway. Main producers of EGFR ligands and Shh are parietal cells (van den Brink et al. 2001; Stepan et al. 2005). Their main task is to work in process of differentiation and development of other cell lineages, e.g. zymogenic cells (Canfield et al. 1996; Li et al. 1996). Inhibition of the BMP pathway by Noggin leads to enhanced gastric epithelial cell proliferation due to restricted regulation of EGFR ligands production by parietal cells. Subsequently, this process can lead to epithelial hyperproliferation, which is considered to be one of the first steps to neoplasia development (Shinohara et al. 2010).

In the PI3K/Akt pathway phosphorylated intracellular domain of particular receptor recruits the SH2 domain of PI3K which then adds the phosphate group on the inositol ring 3´OH group in phosphatidylinositol bisphosphate (PIP2) (Hunter 2000). Created

phosphatidylinositol trisphosphate (PIP3) interacts with the pleckstrin-homology (PH) domain of Akt/protein kinase B (Akt/PKB) (Alessi et al. 1997). Akt kinase is an enzyme involved in the processes of apoptosis and cell death [e.g. Bcl-2 associated death promoter (Bad), procaspase-9, CREB and inhibitor of nuclear factor κ-B kinase (IKK)] (Du and Montminy 1998; Vanhaesebroeck and Alessi 2000; Kandasamy and Srivastava 2002; Manning and Cantley 2007). Moreover, Akt modulates cell cycle progression by phosphorylation of GSK3, cyclin-dependent kinase inhibitors p21 and p27, and β-catenin (Fang et al. 2000; Rossig et al. 2001; Liang et al. 2002; Fang et al. 2007b). Phosphatase and tensin homolog (PTEN) accomplishes phosphate group removal from PIP3. Therefore this tumor suppressor phosphatase inhibits the PI3K/Akt signaling and cell proliferation (Carracedo and Pandolfi 2008). In the intestinal epithelium, SCs produce EGFR on their surface receiving the EGF signals from adjacent fibroblasts in both the developing embryonic gut as well as in adult tissue (Suzuki et al. 2010). PI3K/AKT signaling forces immature cells in the intestinal crypt to proliferation. This event is regulated by PTEN, which inhibits overproducing of SCs and crypts (He et al. 2004; He et al. 2007). AKT kinase induces cell proliferation via phosphorylation of various substrates including β-catenin. Cellular junction-attached β-catenin is phosphorylated by AKT kinase and subsequently released to cytosol, where it can be included to signalization (Fang et al. 2007a). Phosphatase PTEN is regulated by BMP and Noggin (He et al. 2004; He et al. 2007). Cholecystokinin (CCK) and gastrin, both products of enteroendocrine cells in the gastric antrum and in duodenum (Rehfeld et al. 2007), stimulate various cell types in GIT. In the stomach, CCK and gastrin receptors (CCKRs) support the function, cellular composition and organization of the gastric mucosa by activating PI3K/Akt signaling (Dufresne et al. 2006). Transcription of common members of pathways employed in cell cycle such as *c-Jun* or *c-myc* is activated by CCKR signaling in the stomach. These events are crucial in the process of gastric acid secretion or parietal and ECL cells maintenance (Langhans et al. 1997; Chen et al. 2002).

The G-protein coupled tyrosine kinase receptor can activate also the PLC pathway. PLC is enzyme hydrolyzing PIP2 to inositol-1,4,5-trisphosphate and 1,2-diacylglacerol. The latter molecule induces increase of the intracellular Ca^{2+} level and activates the PKC signaling pathways. In various tissues including the intestine and stomach, the PKC pathways promote both cell differentiation and tumorigenesis (Yang et al. 2013). It has been shown that various subtypes of PLC influence colorectal tumor growth in the mouse

(Martins et al. 2014; Satow et al. 2014) implicating the key role of the enzyme in intestinal homeostasis maintenance. Moreover, the PLC subtype β isozymes enhance intestinal epithelial cell proliferation and migration in wound repair (Lee et al. 2013). The role of PLC signaling in the gastric epithelium is connected to CCK hormone. The CCK1 and CCK2 receptors activate stomach mucosal PLC subtype β and induce Ca^{2+} oscillations in target cells (Dufresne et al. 2006).

In summary, intestinal and gastric epithelium architecture is tightly dependent on the intensity of various signaling pathways (Fig. 6) influencing the tissues not only in embryonal development, but even in adulthood. Disturbances in the pathways may result in cancer growth, a theme described in the following chapters.

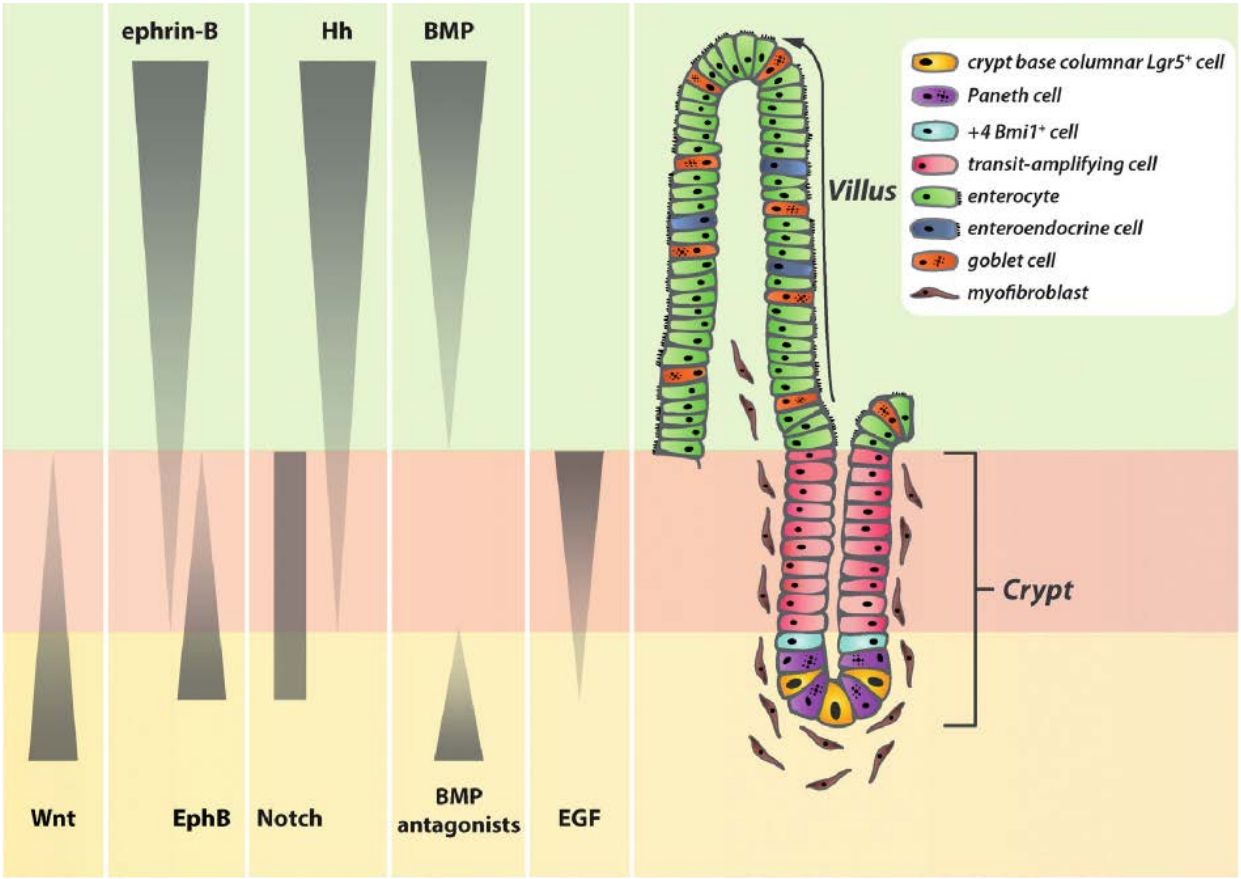


Figure 6: Architecture of the small intestinal epithelium and signaling pathways involved in its self-renewal. The intestinal crypt architecture is a result of opposing and cooperating actions of the signaling pathways. Wnt is produced in Paneth cells and in underlying mesenchymal cells and guards undifferentiated cells to preserve their stemness. Wnt signal intensity is decreasing toward the tip of the villus. EphB/ephrin-B repulsion results in the successful signaling in the transitional zone of the crypt. Notch signaling preserves stemness of SCs residing in the crypt, whereas the Hh pathway operates in the villus compartment and its effect diminishes downwards. The BMP pathway functions in the similar way driving cells to differentiation. EGF signaling presses undifferentiated TA cells to proliferation. Adopted from (Krausova and Korinek 2012).

CRC

Aberrant activation of Wnt signaling can lead to cancer development. Pathway dysregulation initiates cancer development in various organs such as the mammary gland, prostate, urinary bladder, skin, lungs, stomach, colon, and rectum (Brandt et al. 2009; Tanaka 2009; Nigam 2013; Li et al. 2014b; Liu et al. 2014; Ni et al. 2014; Xi and Chen 2014). According to epidemiology data in 2012, CRC was the 3rd most frequent cancer worldwide (in both sexes) even the most frequent in some Western countries. It is alarming that CRC is the 4th cause of cancer death worldwide (Stracci et al. 2014). Main risk factors for CRC development seem to be related to the lifestyle typical for developed countries – stress, nutrition poor for fiber and rich for fats, smoking, low physical activity and civilization-related diseases such as inflammatory bowel disease (IBD) (Deschner et al. 1983; Slattery 2000; Li et al. 2014c; Baccaro et al. 2015). The risk increases with elder age, usually over 65 years, and differs between sexes (Roncucci et al. 1988; Kim et al. 2015). All these aspects contribute to the first mutation as predisposition to CRC onset, usually in the *APC* gene.

While the first mutation occurs, prospective cancer cells start to proliferate to form a microadenoma, benign neoplasia with potential of malignancy (Del Vecchio Blanco et al. 2015). Although 70 – 85 % of CRCs are sporadic, the first mutation can be inherited (Taylor et al. 2010). In families with the FAP disease and its milder variant attenuated FAP (AFAP) probability of microadenoma formation is extremely high due to the germinal mutation in one copy of the *APC* gene. The second *APC* allele in somatic cell is disabled either by mutation or loss of heterozygosity (LOH) and this gives rise to APC-deficient lesions (Deschner and Lipkin 1975). Moreover, several extracolonic and extraintestinal manifestations occur in both diseases: the gastroduodenal polyps, fibromas, osteomas, desmoid tumors and many others (Leoz et al. 2015). The *APC* mutation occurs usually in the mutation cluster region (MCR) located approximately in the middle of the open reading frame (ORF) and it is represented by stop codons or frame-shifts. Interestingly, positions of the mutation in the *APC* gene is frequently linked to the number of developed polyps (Fearnhead et al. 2001). The protein product is usually truncated. Moreover, these truncated variants have limited functionality to participate in the β-catenin destruction complex (Elliott et al. 2013). Surprisingly, some truncated APC proteins are still able to modulate Wnt signaling as CRC cell lines with null APC cannot proliferate (Chandra et al. 2012). Besides mutations in the *APC* gene, other tumor

suppressor genes linked to cell cycle related pathways such as *TP53*, *PTEN* and *SMAD4* have to be impaired to start and progress CRC. The protein product of *TP53*, p53 is involved in apoptosis as the guardian preventing impaired DNA replication (Bates and Vousden 1996). *Kirsten rat sarcoma viral oncogene homolog* (*KRAS*) and *phosphatidylinositol-4,5-bisphosphate 3-kinase, catalytic subunit alpha* (*PIK3CA*), *c-myc* or *c-Src* kinase are also important for CRC. The corresponding genes are affected by missense mutations activating their proto-oncogenic potential (Krausova and Korinek 2014; Mundade et al. 2014). Furthermore, LOH of 18q clusters, which harbor tumor suppressor genes, such as *deleted in colorectal carcinoma* (*DCC*) occurs in 70 % of CRC (Takayama et al. 2006). The process described above is typical for CRC displaying chromosomal instability (CIN), that is typical for the majority of sporadic CRCs (Lengauer et al. 1998) (Fig. 7).

Ten to 15 % of CRCs show microsatellite instability (MSI) (Fig. 7). The phenotype results in the non-functional deregulated DNA mismatch repair (MMR) protein machinery, which normally corrects replication errors in DNA strands (Iyer et al. 2006). Impaired MMR mechanisms lead to accumulation of nucleotide insertions or deletions. Some MSI initiating mutations could result in APC loss. Furthermore, additional genes are "hit" in MSI tumors, e.g. *TGFβ receptor II* or proapoptotic *Bcl2-associated X protein* (*BAX*) (Mundade et al. 2014). Inheritable predisposition to hereditary non-polyposis colorectal cancer, the Lynch syndrome, is connected to the inactivation of the MMR genes, mainly *MutS homologous* (*MSH*) *2*, *MutL homologous* (*MLH*) *1* and *MSH6*. The afflicted patients have enormous risk for CRC as well as for development of endometrial, ovarian, gastric or small intestinal cancer (Bellizzi and Frankel 2009). MSH2 together with MSH6 form the MutSα complex that corrects DNA mispairs or short insertions and deletions (Drummond et al. 1995; Alani 1996; Matton et al. 2000). Similarly, the MutLα complex encompassing MLH1 protein and postmeiotic segregation increased (PMS) 2 mismatch repair endonuclease is also employed in DNA mismatch corrections (Leung et al. 2000).

In contrast to mentioned CIN and MSI CRC, neoplasia initiated by so-called serrated pathway (named after histological appearance of adenomas) does not affect the *APC* gene (Fig. 7) (Bettington et al. 2013). The process is initiated by activating mutation in protein kinase *B-Raf* (*BRAF*), a member of MAPK/ERK signaling controlling cell proliferation, growth and survival (McCain 2013). Deregulated BRAF signaling induces excessive cell division, angiogenesis and invasion leading to metastases (Ascierto et al. 2012).

Subsequent event as epigenetic silencing of *TP53* or *p16* genes is typical for onset of serrated CRC (Rustgi 2013).

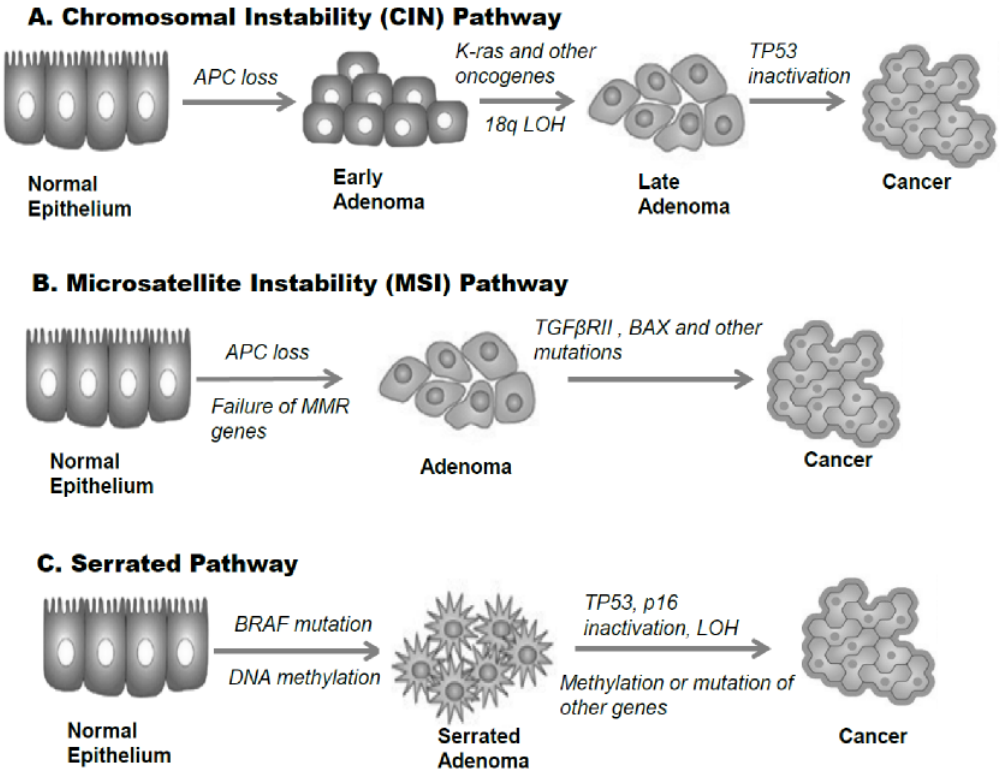


Figure 7: Genetic pathways involved in CRC pathogenesis. CRC usually follows one of these three routes. (A) The CIN pathway is initiated by APC loss, which leads to early benign adenoma. Activating mutation in K-ras and other oncogenes or 18q LOH continues to late adenoma. The process of progression to cancer is completed by TP53 inactivation. (B) The MSI pathway starts with APC loss and failure of MMR genes to repair mismatches in DNA. Adenoma progresses to carcinoma in case of mutations in genes related to apoptosis. Serrated adenoma rises as the result of growth factor-dependent kinase activation which causes deregulated cell division. Malignancy is afterwards achieved by elimination of tumor suppressors. Adopted from (Mundade et al. 2014).

It was shown, that nearly 85 % of sporadic CRCs harbor *APC* truncating mutation (Cancer Genome Atlas 2012). In the absence of *APC* mutations *β-catenin* is frequently mutated (Iwao et al. 1998). The character of the *β-catenin* gene *Ctnnb1* mutations is stabilizing, altering the APC-dependent exon 3-encoded serine/threonine phosphorylation residues participating in the CK1α and GSK3β interaction. The mutations prevent β-catenin sequestration and ubiquitination in the destruction complex, thus leading to β-catenin accumulation in the nucleus (Morin et al. 1997; Rubinfeld et al. 1997). Some other Wnt pathway genes are mutated or deleted, such as *Axin2*, *Sox9* or the Dkk family members (Cancer Genome Atlas 2012). Of note, the Wnt signaling level in CRC is variable and depends on the stage of tumor or its type (Vermeulen et al. 2010; Baker et al. 2015).

Moreover, additional signaling pathways are impaired in CRC. BMP receptor 1 deletion induces polyp development in mice. It was found that GATA-binding factor 6 (GATA6) regulates Wnt and BMP signaling in the neoplastic colon by repressive competition with the β-catenin/TCF4 complex in the regulatory region of the BMP4 gene (Whissell et al. 2014). Notch signaling is upregulated in neoplastic tissues preventing apoptosis and supporting the differentiated state of cells (Reedijk et al. 2008; Meng et al. 2009; Sikandar et al. 2010). In the study of Fender et al., increased Notch-1 was responsible for elevated production of proteins related to stemness and metastasizing such as CD44, Slug, Smad-3 and Jagged-1 (Fender et al. 2015). Furthermore, Notch-1 promotes infiltrating capability of tumor cells via decreasing cell junctional protein E-cadherin (Gao et al. 2012; Fender et al. 2015).

Besides the polyp-developing syndromes mentioned above, the MUTYH-associated polyposis (MAP), an autosomal recessive disease, has been described in 2002 (Al-Tassan et al. 2002). The *mutY homolog* (*MUTYH*) gene encodes a member of the base excision repair complex, which corrects the mispairs added to DNA due to guanine oxidation (Takao et al. 1999; Ohtsubo et al. 2000; Yamaguchi et al. 2014). Dysfunction of the complex leads to G:C to T:A transversion, frequently appearing in the *APC* or *KRAS* genes (Al-Tassan et al. 2002; Nielsen et al. 2011). In comparison to the FAP patients, the MAP affected persons with biallelic mutation have less polyps, lower risk of cancer and infrequent extracolonic phenotype (Jenkins et al. 2006; Grover et al. 2012).

Colorectal cancer SCs

The colorectal adenoma in closer view resembles the heterogenic mass of cells of the various tissue origin and usually more than one cell fueling tumor growth. The cell called colorectal cancer SC (CRCSC), was thought to be of the intestinal SC origin. Wide spectrum of studies describe, that the mutation initiating cancer has to occur in the stem cell compartment, inasmuch only SCs live long enough to gain additional mutation for adenoma progression. Therefore, intestinal SCs are possibly the cell type to initiate CRC (Sangiorgi and Capecchi 2008; Barker et al. 2009). Moreover, Barker and colleagues observed that mutations in TA cells induced microadenoma development, however the lesions rarely progress (Barker et al. 2009). In contrast to this conclusion, CRCSCs may not necessarily originate from normal SCs, as the subpopulation of differentiated

quiescent doublecortin-like kinase $(DCLK)^+$ tuft cells can promote the colorectal adenoma formation, provided that the *APC* gene is deleted and inflammation is present (Westphalen et al. 2014). Inflammatory signaling as the initiator of differentiation to tumorigenic cells was also indicated in the study of Schwitalla and colleagues (Schwitalla et al. 2013). Despite uncertainties about the CRCSCs origin, the cells can be described by increased self-renewal, resistance to chemotherapy, the ability to seed secondary tumors and expression of immature cell markers (O'Brien et al. 2007; Ricci-Vitiani et al. 2007; Todaro et al. 2007; Todaro et al. 2014). CRCSCs were isolated for the first time as $CD133^+$ cells which can induce tumor growth upon xenotransplantation (O'Brien et al. 2007; Ricci-Vitiani et al. 2007). Subsequently, many studies identified CRCSCs with using another markers such as $EphB2^{high}$ (Jung et al. 2011), epithelial cell adhesion molecule $(EpCAM)^{high}/CD44^+/CD166^+$ (Dalerba et al. 2007), aldehyde dehydrogenase $(ALDH)^+$ (Huang et al. 2009), $Lgr5^+$ (Kemper et al. 2012) and $CD44v6^+$ (Todaro et al. 2014). As mentioned above, any tumor is a very heterogenic entity showing enormous cell plasticity, thus various markers can be produced in relation to the tumor grade as well as according to cell distribution within a neoplastic lesion (Kreso and Dick 2014). That is the reason why is description of tumor tissue so variable. The markers frequently correlate with patient´s prognosis and survival as CRCSCs producing particular molecules are prone to seed metastases or hold resistance to chemotherapy (Horst et al. 2009; Chen et al. 2013). For instance, the subpopulations of $CD133^+$ CRCSCs marked by CD110 protein are prone to metastasize to the liver, whereas CUB domain-containing protein 1 $(CDCP1)^+$ cells infiltrate frequently to the lungs (Gao et al. 2013). Moreover, the CD133 marker tightly correlates with patient´s prognosis whilst Lgr5 expression is not suitable for prognosis (Ziskin et al. 2012; Chen et al. 2013). Interestingly, the presence of CD26 CRCSC marker implicates the potential of metastases, particularly to liver tissue (Pang et al. 2010).

The process of polyp growth progresses from high-grade dysplasia, to adenoma, and adenocarcinoma infiltrating local tissue and potentially metastasizing (Tanaka 2009). Latest research suggests that tumor maintenance and progression is intensively dependent on the microenvironment composed of endothelia, fibroblasts and immune cells as well as components of extracellular matrix – proteoglycans, hyaluronic acid and fibers (Zeuner et al. 2014). Like the stem cell niche in the healthy intestinal epithelium, the CRCSC niche supports tumor SCs and modulates tumor behavior due to environmental pressures

such as chemotherapy. Hepatocyte growth factor (HGF) produced by cancer associated fibroblasts (CAFs) activates β-catenin-dependent transcription and self-renewal of CRCSCs (Vermeulen et al. 2010). Another factors are produced by endothelia (Dll1) or mesenchyme (prostaglandin E_2, cytokines inducing β-catenin activation) (Li et al. 2012; Lu et al. 2013). Supportive $CD4^+$ T cells secrete interleukin 22 (IL-22) and activate histone H3 methyltransferase DOT1-like protein (DOT1l), leading to transcription of stem cell associated genes (Kryczek et al. 2014). In addition, some of the CRC niche secreted factors, for instance HGF, stromal cell-derived factor 1 (SDF1) and osteopontin (OPN), are capable to turn the non-invading tumor to the aggressive one (Ormanns et al. 2014). The process of cancer invasion is possible due to mechanisms of EMT, which includes events physiologically active usually during embryonic development (Yang and Weinberg 2008) potentiating cell motility, invasion and stem-like properties (Mani et al. 2008).

Gastric cancer

Gastric cancer is a multifactorial disease, the 5th in the rank of the most common cancers worldwide. Moreover, it occupies the 3rd place of cancer-related deaths (Ferlay et al. 2010; Jemal et al. 2011). In particular, the risk factors of the gastric cancer onset are genetic predisposition, *Helicobacter pylori* infection, dietary habits, increased salt intake, chemical carcinogens such as nitrates in food and smoking (Fox and Wang 2007; Katoh 2007a; Saikawa et al. 2010). The most common histological variant of gastric cancer is the intestinal type (IGC), which is initiated as chronic superficial gastritis continuing to chronic atrophic gastritis, intestinal metaplasia, dysplasia and leads to gastric adenocarcinoma (Correa 1988). Both IGC and diffuse gastric cancer type (DGC) can be caused by infection of *H. pylori*, which resides in the stomach of 50 % of adult individuals (McNamara and El-Omar 2008; Resende et al. 2011). The bacterium produces many cytotoxines interfering with cell homeostasis, such as cytotoxin-associated gene product (cagA), vacuolating cytotoxin A (vacA) and others (Shiota et al. 2013). CagA enters directly to gastric epithelial cell, where it interacts with Src homology 2 domain containing tyrosine phosphatase (Shp2) and impairs signal transduction in various cell processes (Tegtmeyer et al. 2011). VacA cytotoxin causes vacuolation of stomach epithelial cells leading to autophagy and apoptosis (Cover and Blanke 2005; Boquet and

Ricci 2012). Finally, *H. pylori* infection affects several pathways employed in gastric cancer development, such as NF-κB or canonical Wnt signaling (Ooi et al. 2009). Members of the latter pathway are impaired in 30-50 % of gastric adenomas. In the gastric corpus, activating *Kras* mutations together with chronic inflammation initiate the tumor onset (Okumura et al. 2010) whereas in the antral part of the stomach, APC deletion in $Lgr5^+$ cells as predisposition to gastric adenoma is more frequent (Barker et al. 2010b).

While well-differentiated IGC occurs with 60%-80% probability in the stomach antrum within aged patients, undifferentiated DGC is typical for younger patients (Hohenberger and Gretschel 2003). Many studies refer to increased expression of Wnt ligands in IGC and DGC, leading to cytoplasmic and nuclear β-catenin accumulation (Katoh et al. 2001; Cheng et al. 2005; Kurayoshi et al. 2006; Zhang and Xue 2008). Additionally, upregulated Fzd-3 or Pcn were described in relation to stomach tumorigenesis (To et al. 2001; Mo et al. 2013). As in colorectal cancer, the *CTNNB1* gene mutations affecting exon 3 encoding the phosphorylation consensus region are detected in 30 % of gastric tumors (Park et al. 1999; Woo et al. 2001). However, additional Wnt pathway genes are altered or display aberrant expression. The *Tcf7l2* gene encoding the β-catenin binding partner in the process of Wnt target genes transcription is impaired by frameshift mutation in a significant fraction of MSI gastric carcinoma (Saeki et al. 2001). Moreover, loss of Runx3 expression has been reported as an early event in gastric cancer leading to EMT (Li et al. 2002; Ito et al. 2011). About 25 % of human tumors harbor the mutated *APC* gene (Horii et al. 1992; Nakatsuru et al. 1993). The *APC* deletion appears during gastric cancer progression (Rhyu et al. 1994; Fang et al. 2012). Additionally, mutations in *AXIN2* and *βTRCP*, the members of the β-catenin destruction complex, have been reported in human gastric tumors (Kim et al. 2007; Kim et al. 2009). In DGC, the mutation in the *CDH1* gene encoding the β-catenin cytoskeletal binding partner E-cadherin is a predisposition for tumor growth (Guilford et al. 1998). Expectedly, E-cadherin loss is described as a direct cause of EMT in gastric cancer (Katoh 2005).

In gastric cancer, as well as in CRC, additional signaling pathways are affected. Hh signaling, decreased due to the *H. pylori* infection, loses therefore its ability to drive damage gastric tissue renewal (Sherman and Zavros 2011). Nevertheless, decreased Hh signaling alone is not capable to initiate gastric adenoma growth (Xiao et al. 2010). In contrast, the level of Hh signaling was found higher in gastric adenomas possibly due to repopulation of mucosa by bone marrow-derived mesenchymal SCs during inflammatory

response (Houghton et al. 2004; Sherman and Zavros 2011). Gastric cancer SCs (GCSCs) isolated using the surface markers CD44, CD24 and CD133 exhibit high expression levels of Hh target genes *Ptch* and *Gli1* (Song et al. 2011). The Notch signaling pathway is thought to regulate expression of the gastric mucin genes *MUC5AC* and *MUC6* via bHLH. Consequently, bHLH causes impaired cell differentiation and gastric cancer promotion (Sekine et al. 2006a). In the recent study by Piazzi et al., epigenetic silencing of Dll1 disrupts Notch signaling regulation and facilitates the gastric cancer onset (Piazzi et al. 2011).

Gastric cancer SCs

As in case of CRCSCs, GCSCs can proliferate to give rise to all cell types in stomach adenoma (Takaishi et al. 2008). They are thought to be altered gastric epithelial SCs, accumulating mutations promoting them to proliferate without control. This theory is in concordance with the hypothesis describing the origin of CRCSCs. Furthermore, gastric adenocarcinoma in mice model can also originate from bone marrow-derived cells (BMDCs) (Houghton et al. 2004). BMDCs have the capacity to derive blood elements and marrow stroma, however, they give rise to various different cell lineages in the locations where injury occurs (Jiang et al. 2002). It has been proposed that BMDCs migrate to the gastric mucosa, where they, due to *H. pylori* infection, undergo neoplastic transformation (Houghton et al. 2004; Kavanagh and Kalia 2011). The finding was confirmed by another study observing cancerous gastric cells derived from BMDCs in mice with *H. felis*-induced chronic gastritis (Varon et al. 2012).

There was an intensive effort undertaken to uncover markers of GCSCs. Expression of various GCSCs markers is related to the degree of malignancy and tumor grading, giving possibility to predict patient survival (Wen et al. 2013; Hashimoto et al. 2014). First isolation of GCSCs was performed according to the marker CD44. Isolated cells were able to form spherical colonies *in vitro* and generate tumors in immunosuppressed mice (Takaishi et al. 2009). In the mouse model harboring Cre recombinase under direction of the *Lgr5* promoter, Barker et al. induced *APC* deletion in $Lgr5^+$ cells. Gastric tissue afterwards developed microscopic adenomas in the antrum, indicating that $Lgr5^+$ cells are stomach tumor-initiating cells (Barker et al. 2010b). In cancer tissue, increased levels of Lgr5, CD26, CD44, CD133, Musashi-1 and others can be found in precancerous lesions

as well as in more progressed malignancies and drug-resistant cancer (Wang et al. 2011; Chen et al. 2012; Wu et al. 2013a). In the human gastric glands, CD133 is physiologically expressed in the stem cell zone. In addition, over 50 % of stomach tumors are positive for this surface protein (Zhao et al. 2010). Concerning correlation between CD133 and patients´ survival, high levels of CD133 implicate increased drug resistance, higher relapse rate and lower 5-year survival (Lee et al. 2012). Similarly, CD44 is also connected to drug resistance (Takaishi et al. 2009). Interestingly, CD44 functioning as the cell surface receptor for the extracellular matrix component hyaluronate (Aruffo et al. 1990; Almond 2007) is found in the majority of gastric adenocarcinomas, whereas in normal stomach tissue is absent (Ghaffarzadehgan et al. 2008).

Gut microbiota

The human body encompasses not only eukaryotic cells but also residential microorganisms such as bacteria, archaea, fungi and viruses, in overall called microbiota. Their impact in the organism can be negative (pathological). However, the cohabitation can be beneficial for both involved "participants". Specially in case of commensal bacteria living on the skin, in the oral cavity or GIT (Palm et al. 2015). GIT provides asylum for approximately 100 trillion of bacterial cells, whereas every human individual hosts 500 – 1000 species from which 100 – 150 are unique in each host (Hooper and Gordon 2001; Guarner and Malagelada 2003; Faith et al. 2013). Microbiome, the collection of microbiota genes, exceeds human genome in number of individual genes more than hundred times (Faith et al. 2013). The vital role of the intestine and colon would be inconceivable without participating of beneficial microbiota; their commensal "task" comprises processing of polysaccharides, anyway unused, production of essential vitamins and, moreover, formation of the intestinal epithelium and immune system (Sommer and Backhed 2013). On the other hand, the symbiosis between the host organism and microbiota could be impaired and dysbiosis might occur, in some cases leading to autoimmune disorders, IBD, obesity, metabolic syndromes or neurodevelopmental disorders (Littman and Pamer 2011).

Microbiota are introduced to the individual during the passage by the birth canal and reception of the mother´s milk. GF mice are risen in sterile conditions and after weaning from GF mother receive sterilized food, therefore their organism is free of any microbiota.

The mucus layer covering the intestinal epithelium, which normally preserves the cells against bacteria, is weakened in GF mice due to the reduced number of goblet cells (Johansson and Hansson 2011; Johansson et al. 2011). Moreover, the number of intra-epithelial lymphocytes is decreased as well as the size and quantity of Peyer´s patches and cryptopatches, lymphatic masses found in the intestine (Smith et al. 2007; Macpherson and McCoy 2015). GF animals are appreciably suitable for introducing individual bacteria species of interest.

Commensal bacteria presence in the organism is indispensable for proper maturation of the immune system (Round and Mazmanian 2010; Geuking et al. 2011) and *vice versa* – the innate and adaptive immunity control the composition of the intestinal microbiota (Palm et al. 2015). It was proved, that the potential of $CD4^+$ T regulatory cells (Treg) to maintain the homeostasis in the organism is modulated by intestinal bacteria (Kullberg et al. 2002; Ostman et al. 2006; Poutahidis et al. 2007). In western countries, cancer incidence is higher in comparison to developing countries. It was suggested, that exaggerated hygiene practices cause weakening of microbiome which can lead to improper modulation of immunity, and, consequently, to cancer development (Erdman and Poutahidis 2010; Rook and Dalgleish 2011). The relation between prolonged antibiotics consumption and breast cancer incidence was noted (Ness and Cauley 2004). Commensal intestinal bacteria inhibit and suppress cancer growth through decreasing the level of pro-inflammatory factors such as IL-6 and IL-17 (Niers et al. 2005; Lakritz et al. 2015). On the other side, the innate immunity regulates the microbiota composition mainly by the action of TLRs (Wen et al. 2008; Larsson et al. 2012), by Paneth cells products (Gallo and Hooper 2012), and Nod-like receptors (NLRs), whose ablation results in serious dysbiosis with tendency to develop intestinal inflammation (Elinav et al. 2011; Hu et al. 2013). The adaptive immunity, in particularly Treg and T helper cells Th17, influences also the composition of the microbiota populations (Kato et al. 2014; Kawamoto et al. 2014). Moreover, B cells produce IgAs primarily to the gut lumen where they bind the coat antigens of microbiota, thus restrict the potential inflammatory effect of commensals (Peterson et al. 2007; Corthesy 2013).

Interestingly, microbiota were considered in relevance to cancer development in recent years. It was shown that intestinal commensal dysbiosis can induce inflammation leading to colorectal, breast and prostate tumors in mice (Rao et al. 2006; Poutahidis et al. 2013).

This recognition possesses a possibilities in studying cancer in connection to seemingly unrelated events, just as microbiota dysbiosis.

The liver

The liver is a large complex organ with an exocrine and endocrine capability and regenerating capacity. Post-disease regeneration as well as renewal of liver tissue upon non-disease injury is directed by morphogens and growth factors such as HGF, EGF and TGF-α (Michalopoulos 2007). The liver cell structure seems to be uniform, the basic cell type called hepatocyte form hexagonal-shaped lobules which build the organ (Ekataksin and Kaneda 1999). The hepatic lobule encompasses terminal branches of the portal vein and hepatic artery which bring the blood through the hepatic sinusoid to the central vein. The hepatocytes surrounding each vein, i.e. periportal (PP) and pericentral (PC) cells, are separated by the transitional intermediate zone (Fig. 8) (Behari 2010). Each particular type of liver cells is responsible for a specific metabolic task. PP hepatocytes drive mainly gluconeogenesis, cholesterol biosynthesis, and urea synthesis. In contrast, perivenous hepatic cells conduce the metabolic pathways frequently acting in an opposite manner to PP such as glycolysis, bile acid biosynthesis, and glutamine synthesis and more (Katz 1992).

Wnt signaling in the liver

Wnt ligands are expressed in various hepatic cells like hepatocytes, Kupffer cells, stellate cells, sinusoidal endothelial cells, and biliary epithelial cells (Zeng et al. 2007). Interestingly, Wnt ligands in the liver are transported for shorter distances by lipoprotein particles and glypicans. Wnt signaling in the liver regulates expression of genes employed in various metabolic events, namely in ammonia and nitrogen metabolism, bile acid homeostasis, and drug detoxification, recovering from toxic and metabolic injury and oxidative stress or vitamin C biosynthesis (Gebhardt et al. 2007; Nejak-Bowen et al. 2009; Behari et al. 2010; Giera et al. 2010; Monga 2015). Aberrant activation of the Wnt pathway in the liver is one of the driving force of benign and malignant tumor growth (Nejak-Bowen and Monga 2008; Lemaigre 2009).

The core of the pathway, β-catenin, plays a key role in hepatocyte proliferation, particularly soon after liver injury (Tan et al. 2005; Nejak-Bowen et al. 2010). Beta-

catenin associates with the HGF receptor, c-Met, and it is displaced from the interaction by HGF that leads to β-catenin entering to nucleus where it activates transcription of liver-specific target genes (Monga et al. 2002; Zeng et al. 2006). It was shown that Wnt signaling is the master regulator of the liver zonation. The β-catenin level is highly increased in PC hepatocytes (Lee et al. 2014) and controls the zonation and expression of Wnt target genes (Benhamouche et al. 2006). Glutamine synthetase (GS), one of the Wnt target genes in the liver, is upregulated exclusively in the first row of the hepatocytes surrounding the central vein (Benhamouche et al. 2006). In contrast, APC, the major component of the destruction complex, is highly expressed in the PP zone (Sekine et al. 2006b; Tan et al. 2006). The zonation is established by an interplay between canonical Wnt signaling and hepatocyte nuclear factor α (HNFα) which converts the descendants of hepatic SCs, uniquely expressing genes typical for PP hepatocytes, to the PC fate. The transcription factor LEF1 is associated not only with WRE of the liver-specific Wnt target genes, but also with HNFα-bound elements and represses transcription of PP-specific genes. As the result, the PC fate definitely prevails in hepatocytes with active Wnt signaling near the central vein (Colletti et al. 2009). The most important Wnt target genes in PC hepatocytes are *Glul*, (the gene encoding GS), *cyclin-D1*, *leukocyte cell-derived chemotaxin 2* (*lect2*), *vascular endothelial growth factor A* (*VEGF-A*), *EpCAM*, *ornithine aminotransferase* (*OAT*), *glutamate transporter 1* (*GLT-1*) (Cadoret et al. 2002; Ovejero et al. 2004; Klein et al. 2008; Gedaly et al. 2014).

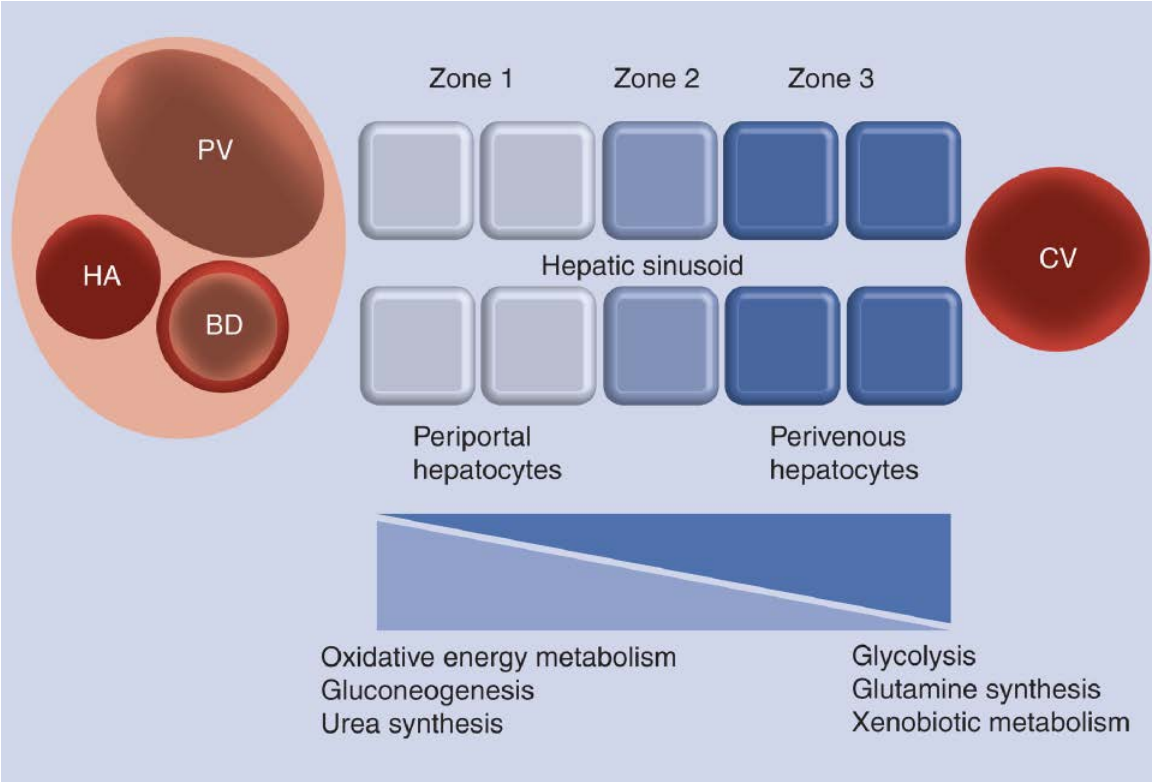


Figure 8: Liver lobule unit zonation. The hepatic lobule sustains of units polarized by extent of different metabolic pathways. Glycolysis, glutamine synthesis, and xenobiotic metabolism are established in perivenous hepatocytes in proximity to the central vein (CV). Oxidative energy metabolism, gluconeogenesis, and urea synthesis enzymes reside near the portal triad created by portal vein (PV), hepatic artery (HA) and bile duct (BD). Adopted from (Behari 2010).

Hepatocellular cancer

Hepatocellular cancer (HCC) is the 5th leading cause of cancer and 3rd in cancer-associated mortality worldwide (el-Serag 2001). The majority of the HCC cases rise as consequence of cirrhosis related to chronic hepatitis B and C infections (Bosch et al. 2005; Kawada et al. 2009). The HCC tumors frequently harbor mutations in the *TP53*, or *CTNNB1* gene (de La Coste et al. 1998; Gerlinger et al. 2012). Aberrant Wnt signaling is found in one third of HCCs. In these cases, 90 % of HCC tumors contain the *CTNNB1* mutation, frequently accompanied by additional alterations such as increased *Fzd* expression, or inactivating mutation in the *AXIN1/2* or *APC* gene (Kondo et al. 1999; Laurent-Puig et al. 2001; Wong et al. 2001; Taniguchi et al. 2002; Amaddeo et al. 2012). The situation in hepatic tumors of pediatric patients, hepatoblastomas, is different. The *CTNNB1* mutations are present in 50 – 90 % cases (Koch et al. 1999). Interestingly, correlation between the presence of the *CTNNB1* mutations and severity of the cancer was uncovered. The activating mutation in the β-catenin gene leads to upregulated expression of the liver-specific Wnt target genes such as *GLUL* (Loeppen et al. 2002),

development of low grade and well-differentiated tumors, chromosome stability and usually good prognosis. In contrast, HCC initiated by Wnt/β-catenin signaling dysregulation, but without the *CTNNB1* alterations, is linked to the high chromosomal instability and aggressive phenotype and is preferentially associated with hepatitis B infection (Suzuki et al. 2002; Hoshida et al. 2009; Lachenmayer et al. 2012b). Although mutated β-catenin occurs in numerous human tumors, experiments in mice revealed that the mutation in the *Ctnnb1* gene is not able to initiate HCC. Nevertheless, mice with serine/threonine substitution in exon 3 of the *Ctnnb1* gene are prone to develop several HCC tumors with more rapid progression after chemical sensitization by diethylnitrosamine (DEN) (Nejak-Bowen et al. 2010). Moreover, impact of the β-catenin activation on HCC development is "boosted" by additional activating mutations in *H-Ras* (Harada et al. 2004). In benign hepatic adenomas, β-catenin alterations are also frequent as well as biallelic inactivations of HNF4α (Bioulac-Sage et al. 2007). Finally, results of the study performed by Yuzugullu et al. showed the key role of the canonical Wnt pathway in HCC tumor initiation, whereas non-canonical Wnt drives tumor progression (Yuzugullu et al. 2009).

As in the process of CRC or stomach cancer expansion, HCCSCs originate from hepatic progenitor cells with impaired regulation of several signaling pathways (EpCAM, Hh, Notch, Hippo or Wnt) (Ishizaki et al. 2004; Katoh 2007b; Maetzel et al. 2009; Chan et al. 2011; Oishi and Wang 2011). Moreover, likewise GCSCs, HCCSCs could originate from extrahepatic tissues, particularly from the bone marrow (Alison 2005). Dysregulated signaling pathways in HCCSCs and high levels of insulin-like growth factor (IGF), EGF, platelet derived growth factor (PDGF), HGF and VEGF can be utilized as the predictive marker of hepatic tumor aggressiveness, EMT potential, angiogenesis and proliferation (Miura et al. 1997; Villavicencio et al. 2000; Lum and Beachy 2004; Tovar et al. 2010). Contrariwise, HNF4α suppresses tumorigenesis and tumor development by inducing differentiation of hepatic CSCs (Yin et al. 2008) implicating a possible usage in HCC treatment. HCCSCs were isolated using surface markers CD133, CD90, CD44, EpCAM, and CD13 (Kitisin et al. 2007; Yamashita et al. 2013).

In conclusion, broadening our knowledge about CSCs helps to develop new less harmful therapeutics for primary as well as metastatic carcinoma. Targeted therapy for tumor-initiating stem cells could be "tailored" individually for a given patient and tumor, therefore it can overcome the unintended side effects of conventional chemotherapy.

Working aims

The major objective of this thesis is to describe the molecular mechanisms involved in gastrointestinal tissues renewal and maintenance. The particular tissue of interest is the small intestine, colon, stomach and liver.

Specific aims of the thesis are:

1. To uncover novel markers of intestinal and gastric SCs, describe their role in tissue maintenance and cancer development and incorporate them to the signaling pathway networks.
2. To describe particular cell types, in which Wnt target genes are expressed, and consider these genes as markers of cancer development.
3. To find novel target genes of Hic1 and analyze their impact on tumor growth in the intestine.
4. To describe specific inhibitors of Wnt signaling, and test their activity in cellular and animal models of CRC.
5. To analyze the expression profile of the intestinal mucosa of GF and CR mice.

Methods

Animal manipulation: Mouse – intraperitoneal injections, gavage, AOM treatment, DSS treatment, tissue isolation, generation of transgenic mice strain with use of bacterial artificial chromosome (BAC) (without author´s contribution), intestinal crypts isolation and organoid culturing, gastric glands isolation and organoid culturing (without author´s contribution), *H. felis* infection (without author´s contribution), bone marrow transplantation (without author´s contribution), treatment with 5-fluorouracil, DMP-777, DBZ, AMD3100, dexamethasone and anti-CD90.2 antibody (without author´s contribution). Zebrafish – tailfin regeneration assay (without author´s contribution). Xenopus - doubleaxis formation assay (without author´s contribution)

Cell cultures: Mouse embryonic fibroblasts (MEFs) and intestinal and colonic crypts isolation and cultures, chemical treatment, transient transfections, RNA interference (RNAi), generation of stable cell lines, cell viability and apoptosis assays (without author´s contribution), cell proliferation and attachment assay (without author´s contribution)

Nucleic acid manipulation: RNA and DNA isolation and purification, mouse genotyping, cDNA synthesis, primer design, polymerase chain reaction (PCR), chromatin immunoprecipitation (ChIP) (without author´s contribution), droplet digital PCR (ddPCR) (without author´s contribution), quantitative real time PCR (qRT-PCR), microarray analysis, RNA probes construction, bisulfite analysis of cytosine methylation (without author´s contribution)

Transcriptional regulation: Luciferase reporter assay

Protein expression and characteristics: Fluorescence activated cell sorting (FACS), western blotting, recombinant Wnt3a isolation, Förster resonance energy transfer (FRET) (without author´s contribution), isolation of antibodies

Histology: Immunohistochemistry, X-gal staining, periodic acid-Schiff (PAS) staining, fixation and paraffin or O.C.T. embedding, tissue sectioning, in situ hybridization

Statistical analysis of data (without author´s contribution)**:** Student´s t-test, Linear Models for Microarray Data (LIMMA) package, Fisher exact test, Wilcoxon´s rank-sum test, gene enrichment analysis (GSEA)

Results and discussion

Troy, a tumor necrosis factor receptor family member, interacts with Lgr5 to inhibit Wnt signaling in intestinal stem cells

In recent years, many researchers identified novel intestinal stem cell markers. However, the results are frequently controversial. It seems that finding a unique marker of SCs is difficult or nearly impossible, as there is probably no single or unique intestinal SC population. Identification of intestinal SCs expressing canonical Wnt target genes as their markers seems to be crucial for recognizing the target cell population for treatment, as CRCSCs are derived possibly from intestinal SCs. To contribute to the SC marker field, we performed ChIP analysis of β-catenin/TCF binding sites, followed by DNA microarray analysis of precipitated genomic sequences. The experiment was performed using colorectal cell lines with aberrant Wnt activation due to the APC truncation (DLD1, SW480, Colo320) or oncogenic mutations in β-catenin (LS174T). In total, 960 promoter sequences were precipitated, that interacted with TCF, from which only 18 were common for all cell lines used in the analysis. As the most interesting genes for subsequent studies, we chose *Troy,* alias *TNFRSF19* or *TAJ,* and *Nkd1* (described in publication 3).

Troy was previously identified as the lymphotoxin A receptor (Hashimoto et al. 2008) with homology to Ectodysplasin A receptor (Edar) and X-linked ectodysplasin A receptor (Xedar), another members of the TNFRSF family. Troy interaction with the TRAF family members activates c-Jun N-terminal kinases (JNKs) and NF-κB pathways (Eby et al. 2000; Kojima et al. 2000). Overexpression of *Troy* caused apoptosis induction, although the receptor lacks the death domain (Eby et al. 2000; Wang et al. 2004). Expression of *Troy* was described during mouse somite development (Eby et al. 2000) and in the adult skin and hair follicles (Kojima et al. 2000). *Troy* expression in melanoma and glioblastoma is linked to poor patient prognosis (Spanjaard et al. 2007; Paulino et al. 2010). In addition, Troy functions in inhibition of axon regeneration in neurons (Shao et al. 2005) and in mouse brain development (Hisaoka et al. 2003).

In our article, we investigated expression of *Troy* in colorectal tumors. Increased levels of *Troy* mRNA were observed in the mouse intestinal tumors. Specifically, upregulated *Troy* mRNA was depicted in advanced tumors of $Apc^{min/+}$ mice, which harbor the *Apc* truncating mutation. Moreover, we also used animals with early microlesions, $Apc^{cko/cko}$/Lgr5-IRES-EGFP-$CreER^{T2}$ mice. These animals have a conditionally mutated

Apc gene controlled by tamoxifen-regulated Cre recombinase. The knock-out is present only in Lgr5-expressing cells, i.e. in intestinal SCs, which are the originators of intestinal tumors. These mice developed microadenomas positive for *Axin2* and *Troy* mRNA. Moreover, *Troy* was upregulated in the mouse colorectal tumors induced by azoxymethane/DSS treatment supporting the notion, that canonical Wnt signaling is upregulated in tumor cells and that *Troy* is a Wnt target gene (Buttitta et al. 2003; Baker et al. 2015). Nevertheless, human sporadic CRC lacked this Troy-Wnt connection, showing decreased levels of *Troy* mRNA in neoplastic tissue when compared to the healthy mucose. Levels of *Troy* mRNA neither in early, nor in advanced human polyps, did correlate with expressions of other canonical Wnt targets, *Lgr5* and *Axin2*. This result is in the conflict with the study of Schön and colleagues, who measured high levels of *Troy* mRNA in comparison with healthy tissue in 4 from 8 human colorectal tumors (Schon et al. 2014). The reason for the discrepancy may be found in low number of specimens in the study of Schön et al. versus our 35 human colorectal polyp samples. The fact that the trend of increased *Troy* expression in the mouse intestinal and colorectal tumors was not reproduced in human neoplasias could be caused by different "age" of human tumors and multiple and more complex regulatory mechanisms in human tumor cells maintenance and proliferation.

Human *Troy* transcript is spliced to isoforms 1 and 2, which were differently abundant in our specimens of intestinal epithelia. We found isoform 1 slightly more abundant than isoform 2. Two specimens of human CRC were outliners with extremely high *Troy* mRNA expression. These outliners depicted higher expression of *Troy* isoform 2 (unpublished observation of M. Krausova). However, in CRC cell lines, the abundance of *Troy* isoforms was equal. The study of Schön (Schon et al. 2014) presented a hypothesis, that *Troy* isoform 2 only is a target of canonical Wnt signaling. In another study, *Troy* isoform 2 was established as a target gene of canonical Wnt signaling in human mesenchymal SCs (hMSCs). Troy functions as a factor mediating signals that determine the hMSCs fate into osteoblasts and adipocytes (Qiu et al. 2010). The ambiguous results of two *Troy* isoforms expression indicate very complex mechanism of Troy expression (or function) in human intestinal epithelium.

Afterwards, we focused on physiological *Troy* expression in the intestinal epithelium. We found, that *Troy* is expressed exclusively in CBC SCs that express also *Lgr5*. By usage of BAC we introduced tamoxifen-regulated Cre recombinase under control of the *Troy*

promoter to mouse embryonic SCs to generate Troy-CreER^{T2} animals. Results from the lineage tracing experiments with R26/Troy-CreER^{T2} animals were in concordance with suspicion, that Troy represents a marker of the SC population in the small intestine and colon. In the study of Stange et al, the Troy^{+} cells in the stomach mucosa were investigated. It was found, that Troy^{+} cells serve as the reserve stem cell population located at the bottom of the gastric gland. This notion was confirmed by knock-in mouse harboring enhanced green fluorescent protein (EGFP) and tamoxifen-regulated Cre under control of the endogenous *Troy* promoter. Control lineage tracing of R26/Troy-IRES-EGFP-CreER^{T2} copied the same pattern of our R26/Troy-CreER^{T2} intestinal epithelium (Stange et al. 2013).

Additionally, we concentrated on the Troy function in the intestinal epithelium and also on its binding partners. We discovered the interaction with Lgr5, the receptor for Wnt agonist Rspo, using co-immunoprecipitations and FRET. By luciferase assay we found, that siRNA against *Troy* mRNA attenuates *Troy* expression and rises the Wnt pathway activity. This notion was confirmed by culturing of Troy knock-out (KO) organoids. When cultured in the medium without Rspo the Troy KO miniguts survive for 48 hours. The survival time of Troy KO organoids can be extended by adding Rspo in small amount, which is completely insufficient for surviving of wt organoids that are fully dependent on Rspo. Mechanism of Wnt signaling inhibition is putatively performed by Troy association with Lgr5 and attenuation of LRP6 phosphorylation. We assume that the ZNRF3/RNF43 transmembrane ubiquitin ligases (Hao et al. 2012) could be involved as well.

In conclusion, we identified Troy as a putative inhibitor of canonical Wnt signaling. All the more so, the missing phenotype of Troy KO mice is astounding at least. Discrepancy between organoid and mouse phenotype is therefore probably caused by complexity of the organism or putative Troy homology with Edar, which can substitute Troy in some functions (Pispa et al. 2003; Pispa et al. 2008). Although many questions about Troy as a marker of Wnt-dependent SCs in the intestinal epithelium stays unanswered, our study contributed to eliciting of some aspects in the field of SCs and CRC.

Author´s contribution: immunohistochemistry, qRT-PCR

Troy, a Tumor Necrosis Factor Receptor Family Member, Interacts With Lgr5 to Inhibit Wnt Signaling in Intestinal Stem Cells

BOHUMIL FAFILEK,[1] MICHAELA KRAUSOVA,[1] MARTINA VOJTECHOVA,[1] VENDULA POSPICHALOVA,[1] LUCIE TUMOVA,[1] EVA SLONCOVA,[1] MARTINA HURANOVA,[1] JITKA STANCIKOVA,[1] ADELA HLAVATA,[1] JIRI SVEC,[1,2] RADISLAV SEDLACEK,[1] ONDREJ LUKSAN,[3] MARTIN OLIVERIUS,[3] LUDEK VOSKA,[3] MILAN JIRSA,[3] JAN PACES,[1] MICHAL KOLAR,[1] MARIA KRIVJANSKA,[4] KLARA KLIMESOVA,[5] HELENA TLASKALOVA–HOGENOVA,[5] and VLADIMIR KORINEK[1]

[1]Institute of Molecular Genetics, Academy of Sciences of the Czech Republic, Prague; [2]Second Department of Internal Medicine, Third Faculty of Medicine, Charles University, Prague; [3]Institute for Clinical and Experimental Medicine, Prague; [4]Central European Biosystems Ltd, Vestec u Prahy; and [5]Institute of Microbiology, Academy of Sciences of the Czech Republic, Prague, Czech Republic

BACKGROUND & AIMS: The Wnt signaling pathway is required for maintenance of the intestinal epithelia; blocking this pathway reduces the proliferative capacity of the intestinal stem cells. However, aberrant Wnt signaling leads to intestinal cancer. We investigated the roles of the Wnt pathway in homeostasis of the intestinal epithelium and during malignant transformation in human cells and mice. **METHODS:** We performed chromatin immunoprecipitation (ChIP) with DNA microarray analysis (ChIP-on-chip) to identify genes regulated by Wnt signaling in human colorectal cancer cells Colo320, DLD1, LS174T, and SW480. Formation of intestinal tumor was induced in C57BL/6J mice using azoxymethane and dextran sulfate. Intestinal tissues from these mice, as well as $Apc^{+/Min}$ and $Apc^{CKO/CKO}$/Lgr5-EGFP-IRES-CreERT2 mice, were analyzed by immunohistochemistry and in situ hybridization. **RESULTS:** We identified promoter regions of 960 genes that interacted with the Wnt pathway nuclear effector T-cell factor 4 in 4 different human colorectal cancer–derived cell lines; 18 of these promoters were present in all chromatin precipitates. Wnt signaling up-regulated a member of the tumor necrosis factor receptor superfamily called TROY. Levels of TROY messenger RNA were increased in human cells with deficiencies in the adenomatous polyposis coli (*APC*) gene and in cells stimulated with the Wnt3a ligand. Expression of Troy was significantly up-regulated in neoplastic tissues from mice during intestinal tumorigenesis. Lineage tracing experiments revealed that Troy is produced specifically by fast-cycling intestinal stem cells. TROY associated with a unique marker of these cells, leucine-rich repeat-containing G-protein coupled receptor (LGR) 5. In organoids established from the intestinal crypts, Troy suppressed signaling mediated by R-spondin, a Wnt agonist. **CONCLUSIONS: TROY is up-regulated in human colorectal cancer cell lines and in intestinal tumors in mice. It functions as a negative modulator of the Wnt pathway in LGR5-positive stem cells.**

Keywords: Mouse Model of Colon Cancer; β-Catenin; TCF; Tnfrsf19.

Development of neoplasia is a multistep process requiring sequential acquisition of mutational events for its completion. In human colorectal cancer (CRC), the inheritance of a single mutation inactivating the *APC* gene can result in a significant predisposition to tumor formation and cancer. Moreover, mutations of the *APC* tumor suppressor are frequently found in sporadic CRC.[1] It has been well established that *APC*-deficient cells lose control over β-catenin turnover and display constitutive activation of the Wnt pathway.[2]

The central feature of the canonical Wnt pathway, also known as Wnt/β-catenin signaling, is the posttranscriptional control of the β-catenin protein stability (reviewed in Cadigan and Peifer[3]). In the absence of the Wnt ligand, the cytoplasmic level of free β-catenin is low due to the activity of a β-catenin degradation complex that includes Apc, axis inhibition protein (Axin), glycogen synthase kinase 3β, and casein kinase 1α. β-catenin is phosphorylated and subsequently destroyed in the ubiquitin-proteasome pathway. The binding of Wnt to the receptor Frizzled (Fz) and the Wnt coreceptor low-density lipoprotein receptor-related protein (Lrp) leads to disruption of the β-catenin degradation complex. Consequently, β-catenin accumulates in the cytoplasm and nucleus, where it associates with members of the lymphoid enhancer-binding factor/T-cell factor (Tcf) family of transcriptional factors (further referred to as Tcfs). Tcf/β-catenin heterocomplexes function as transcriptional activators of Wnt-responsive genes such as *Axin2*, *c-myc*, *Cyclin D1*, and *naked cuticle homolog* (*Nkd*) *1*.

Abbreviations used in this paper: AOM, azoxymethane; Axin, axis inhibition protein; CBC, crypt base columnar; ChIP, chromatin immunoprecipitation; CRC, colorectal cancer; DS, dextran sulfate; EDAR, ectodysplasin A receptor; EGFP, enhanced green fluorescent protein; FRET, fluorescence resonance energy transfer; GFP, green fluorescent protein; HIEC, human intestinal epithelial cell; ISH, in situ hybridization; LacZ, β-galactosidase; Lgr, leucine-rich repeat-containing G-protein coupled receptor; Lrp, low-density lipoprotein receptor-related protein; Min, multiple intestinal neoplasia; Rspo, R-spondin; RT-qPCR, reverse-transcription quantitative polymerase chain reaction; siRNA, small inhibitory RNA; Tcf, T-cell factor.

© 2013 by the AGA Institute
0016-5085/$36.00
http://dx.doi.org/10.1053/j.gastro.2012.10.048

The gastrointestinal epithelia represent the most rapidly self-renewing tissue in the adult mammalian body and completely renew approximately every 5 days (reviewed in Marshman et al[4]). The single-layer epithelium of the small intestine is ordered into invaginations called crypts and microscopic projections called villi. Each crypt contains several long-lived stem cells. The progenitors (transit-amplifying cells) generated from these stem cells frequently divide and move upward from the crypt. Transit-amplifying cells that have reached the edge of the crypts start to differentiate. When the differentiated cells arrive at the top of the villus (in the small intestine) or the luminal surface (in the colon), they undergo apoptosis and are shed to the intestinal lumen. Paneth cells of the small intestine are the only exception to this scheme. These antibacterial agent–producing cells stay at the crypt base, where they persist for approximately 3 to 6 weeks. Two types of intestinal stem cells have been described based on their markers, cycling rate, and location in the crypt. *Lgr5*-positive fast-cycling stem cells (also known as crypt base columnar [CBC] cells) are interspersed among the Paneth cells.[5] The second pool consists of *Bmi1*-expressing cells. These relatively slowly dividing cells represent the reserve stem population and reside several cell diameters from the bottom of the crypt.[6] The physiological role of Wnt signaling in the gut was revealed by gene targeting experiments in mice. Disruption of the Wnt signaling pathway components *Tcf4* or *β-catenin* resulted in the terminal differentiation of stem cells followed by complete loss of the intestinal proliferative compartments of the crypts.[7,8]

To investigate the role of the Wnt pathway in the intestine, we used chromatin immunoprecipitation (ChIP)-on-chip on chromatin isolated from human CRC cells. We identified TROY (alternative names *the tumor necrosis factor receptor superfamily, member 19* [TNFRSF19] or TAJ)[9] as a target of canonical Wnt signaling. In addition, we showed that Troy is produced in fast-cycling stem cells of the small intestine and interacts with leucine-rich repeat-containing G-protein coupled receptor (LGR) 5, a recently described receptor for the Wnt agonists R-spondins (Rspos).[10,11] Interestingly, multicellular structures called organoids established from the intestinal crypts of Troy-deficient mice could be propagated at remarkably lower concentrations of exogenous Rspo ligand than organoids derived from wild-type mice. This observation was in concordance with results showing that TROY inhibits signaling induced by Wnt and Rspo ligands. In conclusion, Troy represents a membrane modulator of the Wnt pathway that tunes the levels of the signaling in the signal-receiving cell.

Materials and Methods

Cell and Organoid Culture, ChIP-on-Chip, Biochemistry, and Microscopy

All cell lines were purchased from American Type Culture Collection (Manassas, VA). Isolated crypts were cultured according to Sato et al.[12] ChIP-on-chip on formaldehyde cross-linked chromatin isolated from approximately 2×10^9 Colo320, DLD1, SW480, and LS174T cells was processed as described previously[13] and immunoprecipitated using an anti-human TCF4 rabbit polyclonal antibody or anti–enhanced green fluorescent protein (EGFP) polyclonal antibody (negative control). Immunoprecipitated DNA was processed onto Human RefSeq Promoter Arrays (4226 HG18; Nimblegen, Madison, WI) covering 2000 base pairs upstream and 500 base pairs downstream of the putative transcription start sites of all known human genes. Complementary DNAs encoding human and mouse Troy, human LGR5, and ectodysplasin A receptor (EDAR) were purchased from Open Biosystems (Huntsville, AL). Two small inhibitory RNA (siRNA) targeting *β-CATENIN* (s437 and s438; Ambion, Austin, TX) and 2 *TROY*-specific siRNAs (Dharmacon siGENOME SMART pool; Ambion) were used and gave similar results. *LGR5*-specific (siGENOME SMART pool) and control nonsilencing siRNAs were purchased from Dharmacon (Lafayette, CO). Western blotting, coimmunoprecipitation, RNA purification, and reverse-transcription quantitative polymerase chain reaction (RT-qPCR) were performed as described previously.[13] Mouse Wnt3a ligand was isolated from the culture medium of Wnt3a-producing L cells according to the detailed protocol of Willert et al.[14] Wnt3a and/or mouse Rspo1 (R&D, Minneapolis, MN; final concentration, 250 ng/mL) stimulations lasted 18 hours. Control stimulations were performed by "empty" ligand buffers. Fluorescence resonance energy transfer (FRET) was measured by the acceptor photobleaching method[15] using a Leica SP5 confocal microscope (Leica Microsystems GmbH, Wetzlar, Germany). Additional information is given in Supplementary Materials and Methods. The primers are listed in Supplementary Table 1.

Animal Manipulations

$Apc^{+/Min}$, Lgr5-EGFP-IRES-CreERT2, and Rosa26 "reporter" (Rosa 26R) mice were purchased from the Jackson Laboratory (Bar Harbor, ME), $Apc^{CKO/CKO}$ mice were obtained from the Mouse Repository (National Cancer Institute, Frederick, MD), and $Troy^{-/-}$ mice[16] were obtained from Mutant Mouse Regional Resource Centers (University of California, Davis, CA). Animals were housed and handled according to guidelines approved by the institutional committee. Tamoxifen (Sigma-Aldrich, St. Louis, MO) was administered by a single intraperitoneal injection (1 mg dissolved in 0.1 mL of corn oil). β-galactosidase (LacZ) staining was performed as described elsewhere[5]; in situ hybridization (ISH) and immunohistochemistry were performed as described in detail previously.[17] Tumor induction, generation of transgenic mice, sequences of antisense RNA probes, and antibodies for immunohistochemistry are described in Supplementary Materials and Methods.

Human Tumor Analysis

Ethical approval was obtained from the Institute for Clinical and Experimental Medicine and the Thomayer University Hospital Research Ethics Committee and the Ethics Committee of the Third Faculty of Medicine, Charles University. A cohort of 35 patients with precancerous colorectal lesions and 20 nonconsecutive patients with primary CRC were enrolled in the study. Additional information is provided in Supplementary Materials and Methods.

Results

TROY *Is a Wnt/β-Catenin Target Gene in* APC*-Deficient Cancer Cells*

ChIP-on-chip was performed using chromatin isolated from human DLD1, SW480, Colo320, and LS174T

Table 1. List of the Genes Bound by TCF4 in Chromatin Isolated From All 4 CRC Cell Lines Tested

Cell line	Colo320		DLD1		LS174T		SW480			
Gene	Fold change	*P* value	Fold change	*P* value	Fold change	*P* value	Fold change	*P* value	Peak position	Gene identified by Hatzis et al[34]
LEF1	4.45	1.08E-09	3.73	1.57E-09	2.11	6.78E-10	3.62	9.87E-10	chr4: 109310227–109310282	+
TROY	4.03	1.08E-09	3.56	1.57E-09	2.69	6.78E-10	3.16	9.87E-10	chr13: 23042725–23042786	+
RPS27	3.91	7.58E-08	3.4	1.01E-07	2.75	5.25E-08	2.43	7.05E-08	chr1: 152229752–152229801	–
MOBKL3	3.37	1.08E-09	2.88	1.57E-09	2.24	6.78E-10	2.78	9.87E-10	chr2: 198088264–198088315	–
GGH	2.45	3.16E-07	3.36	1.57E-09	2.6	5.95E-09	2.84	9.87E-10	chr8: 64114840–64114890	–
C12orf35	3.45	7.58E-08	2.26	2.51E-06	2.33	2.24E-07	2.78	4.14E-07	chr12: 32002831–32002889	–
NT5C2	2.21	1.10E-06	3.98	1.57E-09	1.72	7.98E-07	2.21	3.51E-08	chr10: 104943406–104943455	–
SUPT4H1	2.9	1.08E-09	3.09	1.57E-09	1.59	2.56E-08	2.05	9.87E-10	chr17: 53785562–53785611	+
C9orf103	2.88	2.66E-06	2.26	3.34E-06	1.52	1.98E-06	2.87	7.05E-08	chr9: 85426185–85426234	–
SYMPK	2.65	7.58E-08	3.22	1.57E-09	1.7	2.24E-07	1.77	2.51E-06	chr19: 51057357–51057406	–
PCTK2	2.33	3.16E-07	2.58	4.14E-07	2.08	2.24E-07	2.32	8.48E-06	chr12: 95319254–95319303	–
CBWD3	2.46	6.42E-07	2	6.79E-06	2.67	4.23E-06	2.02	5.23E-06	chr9: 70047011–70047060	–
TOM1L1	1.69	1.08E-09	2.79	5.16E-08	2.22	7.98E-07	2.44	9.87E-10	chr17: 50332402–50332451	–
KLF5	2.94	1.08E-09	2.49	1.25E-08	1.77	2.24E-07	1.83	3.51E-08	chr13: 72530342–72530396	+
CBWD5	2.42	2.66E-06	1.83	6.79E-06	2.4	4.68E-07	2.05	6.03E-07	chr9: 69729627–69729676	–
DACH1	2.72	7.58E-08	2.53	3.34E-06	1.57	1.98E-06	1.87	2.51E-06	chr13: 71340031–71340087	+
CBWD2	2.59	5.51E-06	1.92	6.79E-06	2.37	4.23E-06	1.76	5.23E-06	chr2: 113912252–113912301	–
IFRD1	1.5	3.16E-07	2.73	3.16E-07	2.04	8.31E-09	1.65	4.14E-07	chr7: 111876650–111876702	–
AXIN2	3.52	6.42E-07	3.04	8.23E-07	1.49	4.68−07	2.17	8.31E-09	chr17: 60988928–60988982	+
LGR5	NA	NA	1.69	4.13E-07	1.59	5.94E-09	0.79	2.61E-02	chr12: 70119080–70119131	+
NKD1	2.22	7.57E-08	1.60	1.56E-09	0.83	4.16E-04	2.42	2.50E-06	chr16: 49137941–49137998	+
SP5	1.3	3.81E-03	2.72	1.75E-02	1.45	1.56E-08	1.08	2.18E-03	chr2: 171279606–171280055	+

NOTE. The columns on the left indicate the fold change of the signal obtained using the anti-TCF4 antibody vs negative control antibody. The statistical significance of the results (*P* value) was evaluated by χ^2 test (see Supplementary Materials and Methods for details). The genes are listed according to the signal intensity recorded in the ChIP-on-chip analysis of Colo320 cells. A region was scored as "TCF4 bound" if the ratio of the signal obtained by ChIP with the anti-TCF4 antibody vs control antibody was ≥1.5. The table includes previously identified TCF/β-catenin target genes *AXIN2*, *LGR5*, *NKD1*, and *SP5*, although none of these genes fulfilled completely the selection criterion. The base numbering of chromosomal DNA corresponds to the human genome annotation HG18. For comparison, genes identified by the screen of Hatzis et al[34] are shown in the column on the right.

cells. These CRC cells produce distinct truncated versions of the APC protein; LS174T cells are the only exception because they harbor wild-type *APC* but carry instead an oncogenic mutation in *β-catenin*.[18] Subsequent analysis revealed that promoter regions of 960 genes were retained on the anti-TCF4 antibody-coupled beads; promoters of only 18 genes were positive in all 4 cell lines tested (Table 1, Supplementary Figure 1, and Supplementary Table 8). Among these putative TCF target genes, we identified *TROY*. The gene encodes a type I transmembrane protein from the TNFRSF family that was described previously as a Wnt target in the dermomyotome of mouse embryos.[19] In contrast to some other putative Wnt/β-catenin–activated genes, the *TROY* promoter (containing multiple consensus TCF binding sites) was precipitated reproducibly with the TCF4-specific antibody (Figure 1*A*). A subsequent RT-qPCR analysis showed that *TROY* messenger RNA (mRNA) is abundant mainly in *APC*-deficient cells (Colo320, DLD1, SW480), although its expression in cells with intact *APC* (but harboring *β-CATENIN* activating mutation: LS174T, HCT116) was still detected (Figure 1*B*). In addition, we observed robust down-regulation of *TROY* mRNA on *β-CATENIN* knockdown (Figure 1*C*). Interestingly, when different mammalian cells were stimulated with recombinant Wnt3a, the *TROY* gene was, contrary to the "general" Wnt signaling target gene *Axin2*, up-regulated only in cells of human origin (HEK293, U2OS, primary human intestinal epithelial cells [HIECs]) and not in mouse cells (3T3, C57MG) (Figure 1*D*). Taken together, these results indicated that *TROY* is a tissue-specific target of canonical Wnt signaling.

Troy *Is a Tumor Marker in Mouse Intestinal Neoplasia*

Next, we analyzed expression of *Troy* in tumors in multiple intestinal neoplasia (Min) mice (further referred to as the $Apc^{+/Min}$ strain) and in neoplastic tissue generated in wild-type animals on treatment with azoxymethane (AOM) and dextran sulfate (DS). $Apc^{+/Min}$ animals carry a truncation mutation in one allele of the *Apc* gene, and all adults eventually develop large amounts of intestinal polyps and die of cancer.[20] Although treatment with AOM/DS induces tumors displaying aberrant Wnt signaling,[21] these tumors (in contrast to $Apc^{+/Min}$ animals, which mainly have neoplasia of the small intestine) are localized in the distal colon and rectum. We observed a substantial increase in *Troy* mRNA and protein in tumor tissue in both cancer models (Figure 2*A* and *B*). The same expression pattern was noted for another Wnt signaling target gene, *Nkd1*. The analysis of some additional genes regulated by the Wnt/β-catenin pathway was less conclusive. Whereas mRNAs encoding *Axin2* and *Lgr5* were more

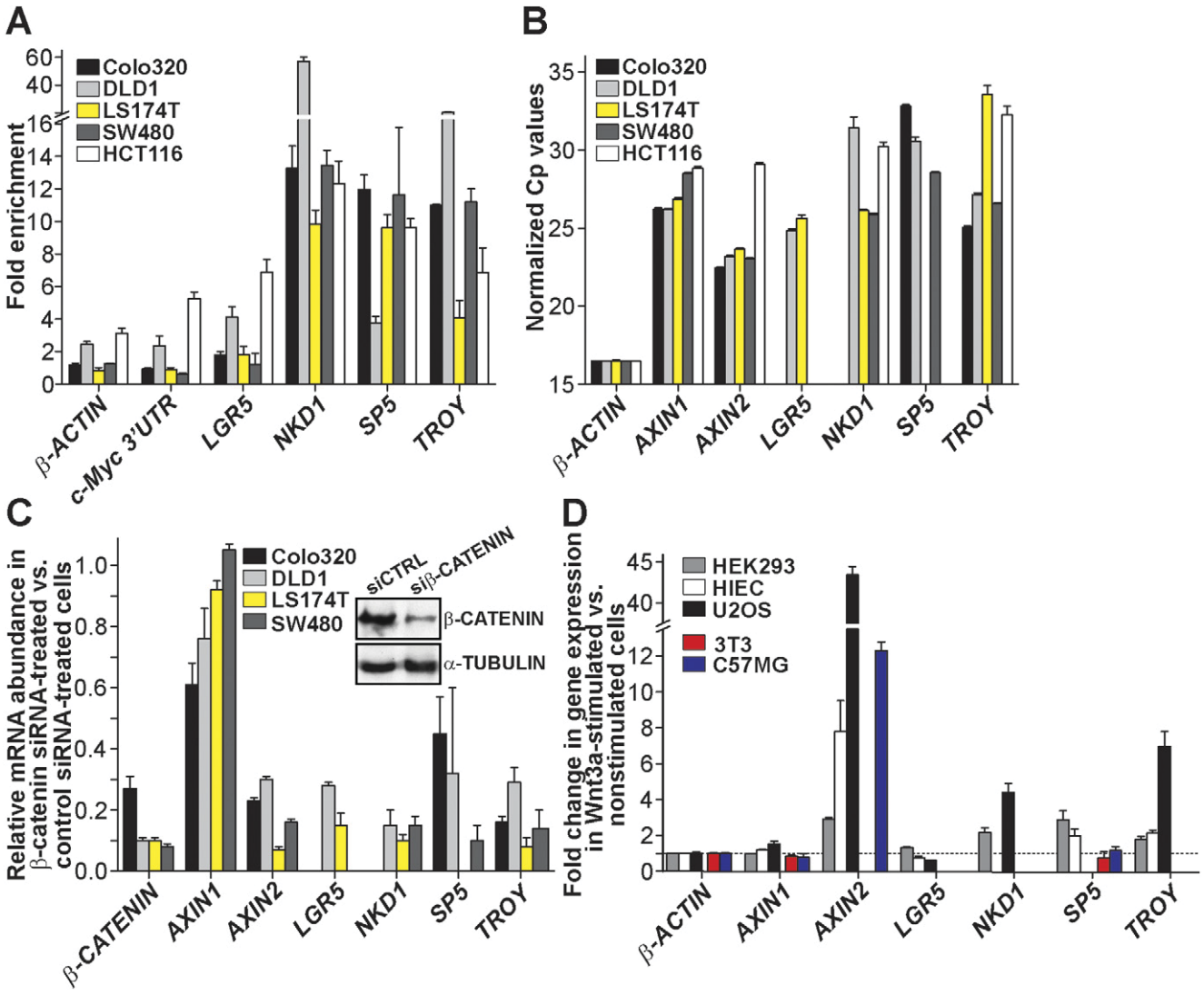


Figure 1. *TROY* is a Wnt/β-catenin target gene. (*A*) ChIP analysis in human CRC cells. Genomic DNA, including promoter regions of the presumptive Wnt signaling target genes *LGR5*, *NKD1*, *SP5*, and *TROY*, were immunoprecipitated from chromatin isolated from the indicated cells. The promoter sequences of the *β-ACTIN* gene and 3′ untranslated region (UTR) of *c-MYC* were used as negative controls. *Bars* represent enrichment of the tested DNA elements in precipitates obtained with the TCF4-specific vs control antibody. (*B*) Expression of *Troy* is abundant in *APC*-deficient cells. Results of the RT-qPCR analysis of mRNA were isolated from indicated CRC cells. Crossing point (Cp) values were normalized to the expression levels of *β-ACTIN* (Cp = 16.5). The Wnt/β-catenin nonresponsive gene *AXIN1* was also included in the test. (*C*) Knockdown of *β-CATENIN* reduces expression of *TROY*. (*D*) In human cells, *TROY* acts as a Wnt responsive gene. Cells of human (HEK293, HIEC, U2OS) or mouse (C57MG, 3T3) origin were stimulated using Wnt3a or Wnt storage buffer (vehicle) and assayed in RT-qPCR. All experiments were performed in triplicate and repeated 3 times. Histograms represent mean values of a representative experiment with the corresponding SDs. *Missing bars* represent unexpressed genes (normalized Cp ≥ 35).

abundant in the small intestinal lesions of $Apc^{+/Min}$ animals, another Wnt target gene, *Sp5*, was expressed predominantly in the large intestine tumors induced by AOM/DS (Figure 2*A*). Subsequently, we performed ISH using the *Troy*-specific antisense RNA probe. Similarly as *Axin2*, *Troy* expression was detected through the tumor mass, although the signal was less intense. Interestingly, the positive staining was detected not only in tumors but also in the crypts of healthy mucosa of the small intestine (Figure 2*C* and Supplementary Figure 4*A*).

Recently, Lgr5 was established as a specific marker of intestinal epithelium stem cells. Moreover, knock-in mice designated Lgr5-EGFP-IRES-CreERT2 expressing a tamoxifen-regulated variant of Cre recombinase from the *Lgr5* locus were produced.[5] To evaluate the expression of Troy at early stages of tumor development, we intercrossed Lgr5-EGFP-IRES-CreERT2 mice with animals carrying the conditional alleles (*CKO*) of the *Apc* gene. The Cre-mediated excision of the floxed exon 14 in the *CKO* allele results in production of the truncated nonfunctional Apc polypeptide.[22] Multiple β-catenin–positive dysplastic lesions were observed in $Apc^{CKO/CKO}$/Lgr5-EGFP-IRES-CreERT2 mice as early as 5 days after administration of tamoxifen. These microadenomas were also positive for *Axin2* and *Troy* mRNA (Figure 2*D*). To confirm our assumption that Troy possibly represents a reli-

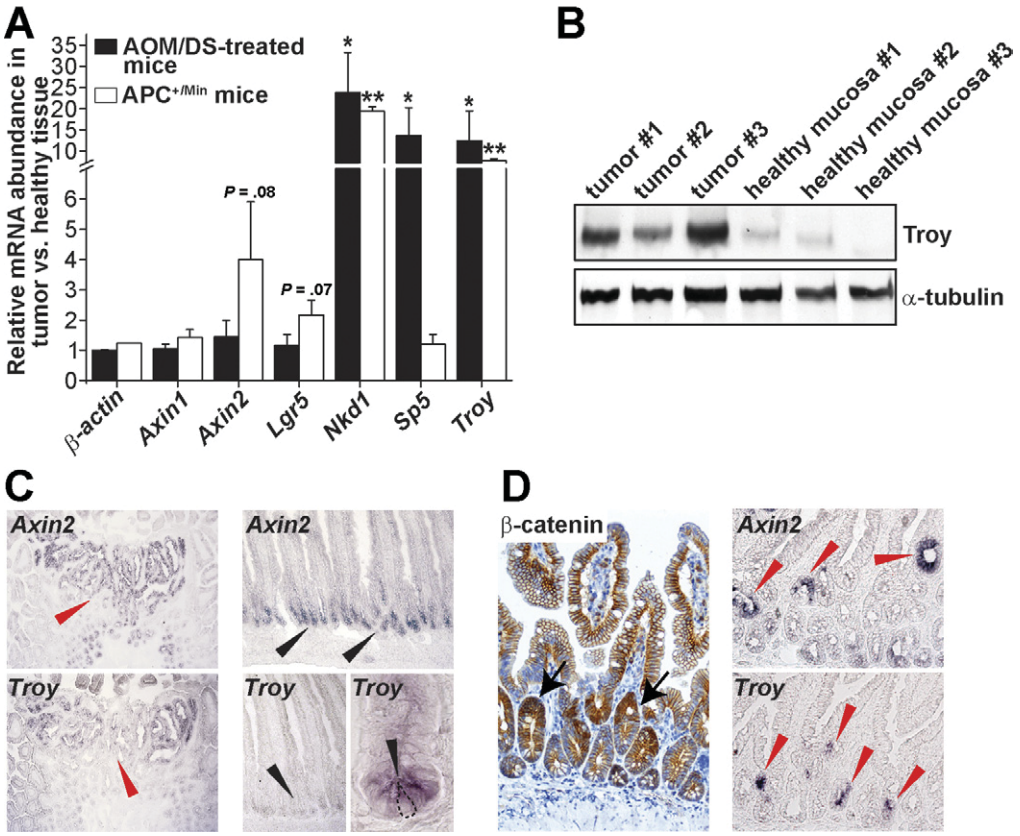


Figure 2. *Troy* mRNA is enriched in mouse intestinal tumors. (*A*) RT-qPCR analysis of 19 tumors dissected from colons of 12 AOM/DS-treated mice and 23 small intestinal tumors from 9 $Apc^{+/Min}$ animals. Control RNA samples were isolated from matched healthy tissue; $^{**}P < .01$, $^{*}P < .05$ (Student *t* test). (*B*) Western blot analysis of 3 tumors isolated from $Apc^{+/Min}$ mice. Intact mucosa adjacent to the corresponding neoplasia was used as a control; α-tubulin, loading control. (*C*) (*Left panel*) ISH of *Troy* and *Axin2* mRNAs in tumors (*red arrowheads*) developing in $Apc^{+/Min}$ mice. (*Right panel*) In the healthy intestinal tissue, both genes are expressed in the lower parts of the crypts (*black arrowheads*; the image was taken from the duodenum). The enlarged crypt base is shown in the *bottom right* of the image (one *Troy*-positive CBC cell is outlined by a *dashed line*). (*D*) Immunohistochemical detection of β-catenin (*left panel*; counterstained with hematoxylin) and ISH of *Axin2* and *Troy* (*right panels*) in the microadenomas developed 5 days after Cre-mediated ablation of the *Apc* gene in Lgr5-EGFP-IRES-CreERT2/$Apc^{CKO/CKO}$ animals. Notice that the neoplastic lesions (*black arrows* in the *left image*) produce increased amounts of β-catenin and are also positive for *Axin2* and *Troy* (*red arrowheads*). Original magnification: (*C*) 100× (*bottom right image*, 600×); (*D*) 200×.

able marker of the neoplastic growth related to nonphysiological Wnt signaling, we performed *TROY* expression analysis in sporadic human colorectal specimens. Both in early and advanced stages of tumor progression, the presence of the inactivating *APC* mutations was positively correlated with increased expression levels of *AXIN2* (Supplementary Figure 2 and Supplementary Table 6). In comparison, the increased expression of the intestinal stem cell marker *LGR5* was related to the *APC* mutation status only at the early, not the late, stages of tumorigenesis. Contrary to mouse tumors, *TROY* transcription in human carcinomas did not follow the expected pattern, and no correlation between the levels of *TROY* mRNA and the mutation status of *APC* was observed. In addition, the analysis of *TROY* expression in 35 polyps of the colon showed a decrease in *TROY* mRNA in the majority of these premalignant lesions (compared with healthy mucosa; Supplementary Figure 3 and Supplementary Table 7).

Taken together, these data indicate that in contrast to mouse neoplasia in human sporadic lesions, expression of TROY is governed possibly by a more complex regulatory mechanism.

Troy *Is Produced in Lgr5-Positive Intestinal Stem Cells*

Using ISH, we noted localization of *Troy* in the lower part of the crypt compartments (Figure 2*C*, *bottom right panels*, and Supplementary Figure 4*A*). Because the colocalization of *Troy* and EGFP (a surrogate marker of $Lgr5^{+}$ CBC cells) using a combination of ISH and immunohistochemistry was not conclusive (Supplementary Figure 4*A*), we prepared crypts from Lgr5-EGFP-IRES-CreERT2 knock-in mice and sorted the isolated cells according to the production of EGFP (Supplementary Figure 4*B*). *Troy* mRNA was detected mainly in cells with a high green fluorescent protein (GFP) signal (GFP^{high}) and not in cell populations with low or no GFP expression (GFP^{low} and $GFP^{negative}$, respectively). The same expression pattern was recorded for *Lgr5* but not for *Bmi1* (Figure 3*A*). In a complementary approach, neither *Troy* nor *Lgr5* was enriched in sorted Paneth cells (Supplementary Figure 4*C*). To study the identity of the Troy-producing cells in detail, we used a bacterial artificial chromosome carrying the mouse *Troy* locus to generate transgenic mice

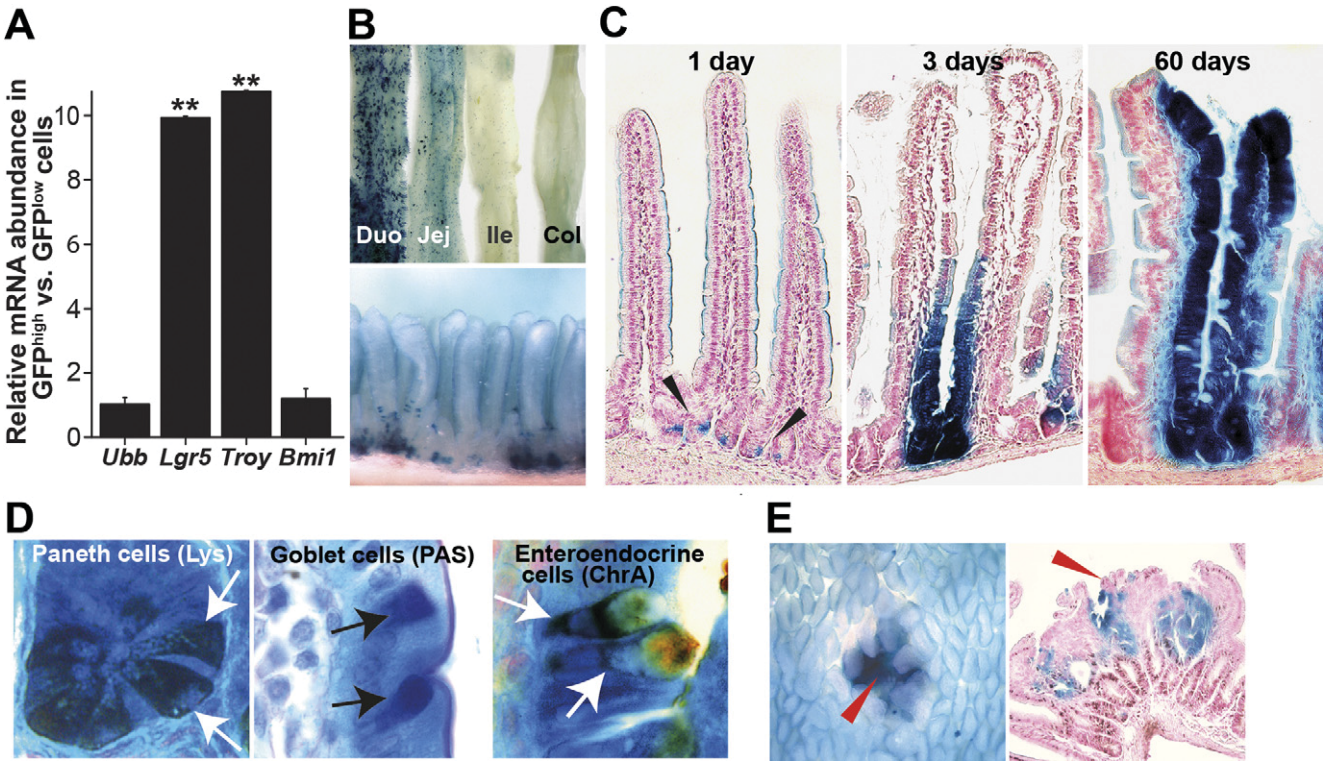


Figure 3. Expression of *Troy* is confined to the Lgr5-positive cells in the intestinal crypts. (*A*) Expression profiling of GFP^{high} and GFP^{low} cells isolated from the intestinal crypts of 10 Lgr5-EGFP-IRES-CreERT2 knock-in mice (details are given in Supplementary Figure 4*B*); $^{**}P < .01$ (Student *t* test). (*B–E*) Lineage tracing in the intestinal epithelium of Troy-$CreERT2^{+}$/Rosa26R mice. (*B*) (*Upper panel*) Whole-mount staining of LacZ in different parts of the intestine 1 day after administration of tamoxifen. (*Lower panel*) Whole-mount staining of the jejunum 3 days after administration of tamoxifen. Duo, duodenum; Jej, jejunum; Ile, ileum; Col, colon. (*C*) Histochemical detection of LacZ activity in the duodenum 1 day, 3 days, and 60 days after administration of tamoxifen. Notice that 1-day induction generates LacZ-positive cells located at the crypt base (*black arrowheads*). (*D*) Double labeling shows that LacZ-expressing ("blue") clones produce markers of differentiated cell lineages (*arrows*), including Paneth, goblet, and enteroendocrine cells. Lys, lysozyme; PAS, periodic acid–Schiff; ChrA, chromogranin A. (*E*) Tumor-associated LacZ activity (*red arrowhead*) developed in the small intestine of Troy-$CreERT2^{+}$/Rosa26R/$Apc^{+/Min}$ mice. The tissue was analyzed 1 day after administration of tamoxifen using whole-mount (*left panel*) or histochemical staining (*right panel*). Counterstain: nuclear red. Original magnification: (*B*) *upper panel* 1.5×, *lower panel* 7×; (*C*) 100×; (*D*) 600×; (*E*) *left panel* 7×, *right panel* 100×.

(designated Troy-CreERT2) expressing tamoxifen-inducible Cre enzyme inserted in frame at the translation initiation codon of the *Troy* gene (Supplementary Figure 5*A–C*). Then we performed the lineage tracing experiments in the intestinal tissue. We intercrossed Troy-CreERT2 with Rosa26R mice. Rosa26R animals produce bacterial *LacZ* mRNA from the ubiquitously active *Rosa26* allele.[23] The mRNA is not translated (and the enzyme produced) unless a transcriptional stop signal flanked by a pair of loxP sites is removed from the genome by Cre-mediated excision. Adult Troy-$CreERT2^{+}$/Rosa26R mice were injected with a single dose of tamoxifen and killed at several time points later. Interestingly, Cre-mediated recombination was most efficient in the proximal part of the small intestine (duodenum, jejunum) and much less effective in the ileum or colon (Figure 3*B* and Supplementary Figure 5*D*). As shown in Figure 3*C* and Supplementary Figure 5*F*, 1 day after the induction of Cre, LacZ-expressing cells were located at the crypt bottom of the small intestine. At later time points, "blue" cell clones were moving upward from the crypt and reached the top of the villus. The labeled cells persisted in the gut for more than 2 months (Figure 3*C* and Supplementary Figure 5*G*) and also descendants of *Troy*-expressing cells differentiated into all major cell lineages of the intestinal epithelium (Figure 3*D*). The labeling of Cre-expressing cells in the colon, although less efficient, displayed a similar pattern (see Supplementary Results for details). These data indicated that Troy-positive cells are capable of long-term renewal of the epithelium and correspond to CBC cells. Our conclusion that Troy is a novel marker of CBC stem cells was in concurrence with a recently published analysis of expression profiling of these cells.[24,25]

TROY Interacts With LGR5

Next, we visualized the cellular localization of TROY and LGR5 in HeLa cells transfected with TROY and LGR5 expression constructs using confocal microscopy. Interestingly, a clear colocalization of TROY with LGR5 was noted (Figure 4*A*). The possible interaction of TROY with LGR5 was further analyzed using coimmunoprecipitation. Experiments involving tagged variants of TROY and LGR5 showed that MYC-tagged LGR5 could be coisolated with FLAG-tagged TROY by an anti-FLAG

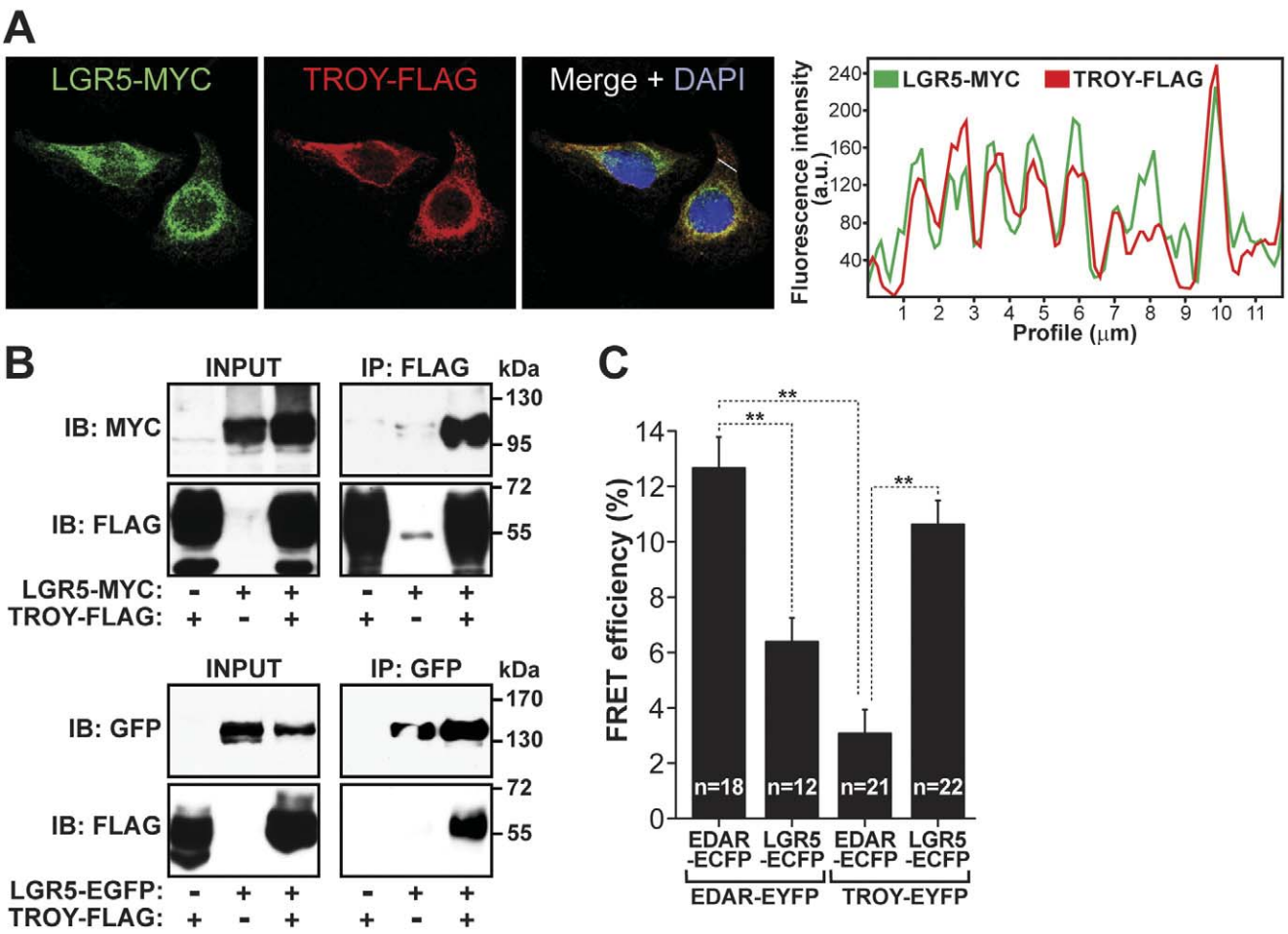


Figure 4. TROY interacts with LGR5, the marker of intestinal CBC cells. (*A*) Colocalization of ectopically expressed LGR5-MYC and TROY-FLAG in HeLa cells stained with rabbit anti-MYC and mouse anti-FLAG monoclonal antibodies. The *right panel* shows the overlap of fluorescence intensity peaks along the profile as indicated in the merged micrograph. (*B*) Coimmunoprecipitation of TROY and LGR5. IP, immunoprecipitation; IB, immunoblotting. (*C*) Detection of TROY binding to LGR5 using FRET microscopy. Fluorescently tagged LGR5, TROY, and EDAR proteins were coexpressed in HeLa cells and visualized as indicated under the histogram. EYFP was photobleached in a selected area of the cytoplasmic membrane, and FRET efficiency was measured as an increase of ECFP fluorescence on EYFP photo destruction. The *bars* indicate the relative FRET efficiency calculated from the given cell numbers (n); $^{**}P < .01$ (Student *t* test).

antibody. Conversely, TROY was present in the anti-GFP precipitates when TROY-FLAG and LGR5-EGFP were coproduced in the same cell (Figure 4*B*). To confirm the association of TROY with LGR5, we used the FRET acceptor photobleaching approach in HeLa cells expressing various combinations of TROY and LGR5 fused to fluorescent protein at their C-termini. EDAR, a TNFRSF member related to TROY known for its homodimerization, was used as a control.[26] Indeed, a high FRET signal was measured in cells coexpressing EDAR-EYFP (acceptor) and EDAR-ECFP (donor). Moreover, the signal was also detected in cells producing TROY-EYFP and LGR5-ECFP, confirming the results obtained by coimmunoprecipitation (Figure 4*C*). Virtually no energy transfer was recorded between EDAR and TROY; however, we noted FRET between EDAR and LGR5. This implied a possible association of these 2 molecules that was verified subsequently by coimmunoprecipitation of EDAR with LGR5 in HEK293 cells (Supplementary Figure 6).

TROY Functions as a Negative Regulator of Wnt Signaling

Recently, several studies have shown that Rspos, the secreted agonists of Wnt signaling, bind to Lgr5 and this interaction augments the action of Wnt ligands.[10,11,27] To examine whether TROY affects the function of Rspo, we performed a reporter gene assay and a RT-qPCR analysis in HEK293 cells treated with siRNA specific for TROY. We found that the *TROY* mRNA level was reduced to 15% to 20% on transfection with 2 different TROY siRNAs (Figure 5*A* and data not shown). Interestingly, TROY knockdown elevated the Wnt-dependent transcription not only in the cells treated with a combination of Wnt3 and Rspo1, but also in cells stimulated with the Wnt3a ligand only. In a parallel control experiment, cells were transfected with LGR5-specific siRNA and the potentiating effect of Rspo1 on Wnt signaling was partly abolished (Figure 5*A*). Of note, although the *LGR5* mRNA level was reduced to 16% on average (SD 1.1), the

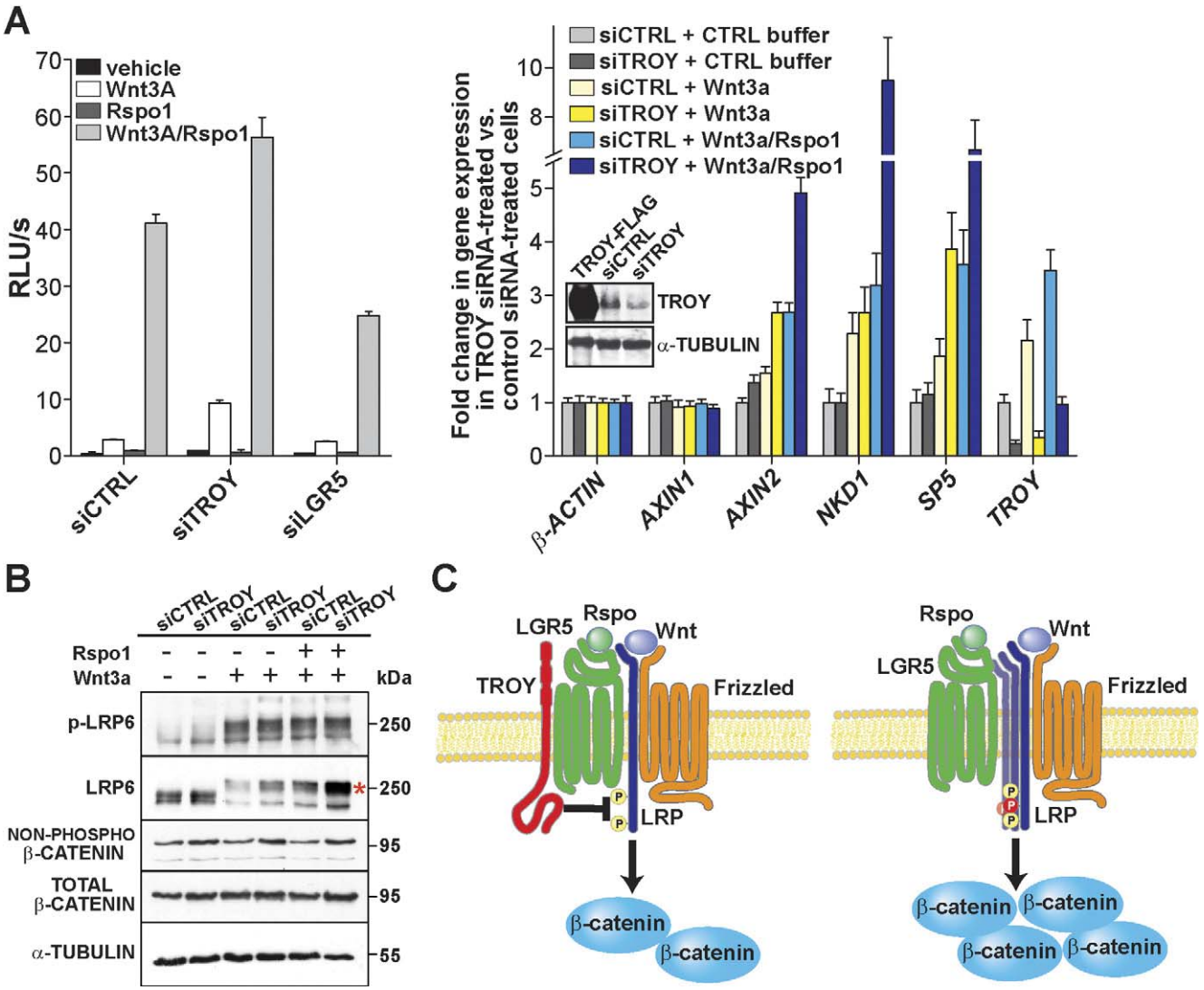


Figure 5. TROY inhibits Wnt signaling. (*A*) Down-regulation of TROY potentiates the responsiveness of HEK293 cells to Wnt3a and Rspo1 stimulation. (*Left panel*) Results of the reporter gene assay using the Wnt/β-catenin reporter pTOPFLASH. (*Right panel*) RT-qPCR analysis of HEK293 cells treated as indicated. The blot in the *inset* shows the efficiency of TROY knockdown. The reporter gene activity (*left panel*) or expression level of a given gene (*right panel*) in cells transfected with control nonsilencing siRNA and treated with vehicle (Wnt storage buffer) was arbitrarily set to 1. (*B*) TROY influences cellular levels and phosphorylation of LRP6. The Western blot of whole cell extracts was prepared from HEK293 cells treated with nonsilencing or TROY siRNA and further stimulated as indicated. Immunoblotting was performed with antibodies recognizing the total cellular pool of LRP6 (*lower panel*) or its form phosphorylated at Ser1490 (p-LRP; *upper panel*). Notice that TROY siRNA increased the amount and phosphorylation of LRP6 (the putative phosphoprotein with changed mobility is marked by a *red asterisk*) but other residue than Ser1490 is modified. Moreover, TROY siRNA induced stabilization of β-CATENIN, including the N-terminally nonphosphorylated form of the protein. (*C*) A possible model of TROY action. The absence of TROY increases levels and phosphorylation of LRP at specific residue (indicated by "P" in *red circle*). This potentiates the outcome of Wnt/Rspo signaling and leads to accumulation of β-catenin.

effect of the knockdown on the activity of pTOPFLASH reporter in cells stimulated with Wnt3a/Rspo1 was moderate (reduction to 59% in comparison to cells treated with nonsilencing siRNA). Nevertheless, because HEK293 cells produce an additional Rspo receptor, LGR4, this observation was in concordance with previously reported data indicating partial redundancy of LGR4 and LGR5 proteins.[27] Importantly, TROY knockdown had no effect on the transcription from the negative control reporter pFopFlash (not shown) and, furthermore, the TROY down-regulation did not potentiate TCF/β-catenin–mediated transcription in human CRC cells with aberrant Wnt signaling (Supplementary Figure 7*A*). The latter finding indicated that TROY functions at the level or upstream of the β-catenin degradation complex. In cells with inducible expression of TROY, only minor effects on transcription of Wnt signaling target genes were recorded (Supplementary Figure 7*B*). Nevertheless, we observed that binding of Rspo1 to LGR5 was not eradicated by the presence of TROY (Supplementary Figure 8). We further focused on the signaling downstream of Wnt and Rspo ligands. Interestingly, although Dvl phoshorylation was not changed by TROY knockdown, the treatment of HEK293 cells with TROY siRNA increased phosphorylation and cellular lev-

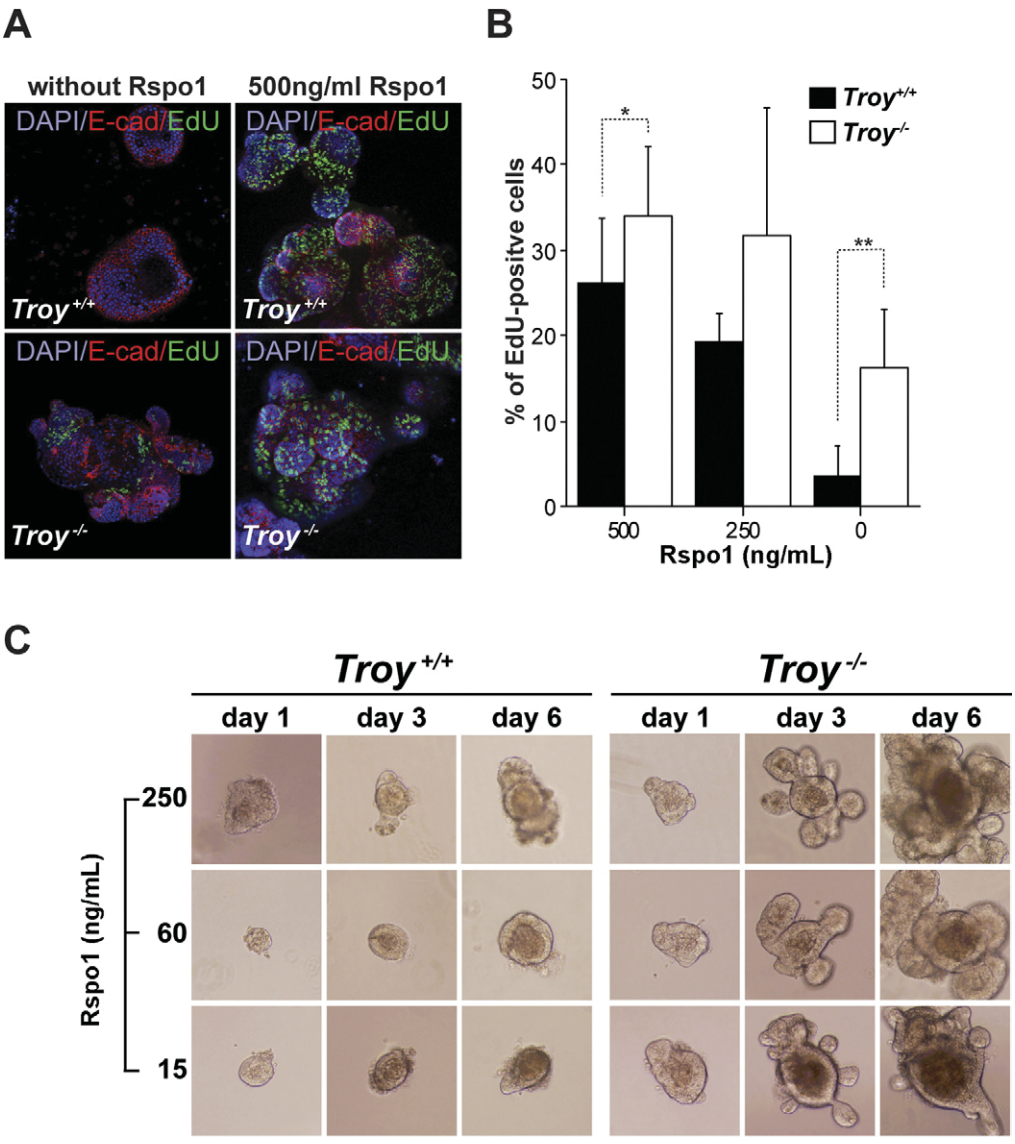


Figure 6. Proliferation of intestinal organoids derived from Troy$^{-/-}$ mice is less dependent on exogenous Rspo than the growth of organoids established from wild-type mice. (*A*) Confocal microscopy images of organoids derived from Troy$^{+/+}$ and Troy$^{-/-}$ small intestinal crypts. The organoids were grown for 2 days with or without Rspo1 and stained using an anti–E-cadherin (E-cad) antibody (*red*) and 4′,6-diamidino-2-phenylindole (DAPI) nuclear stain (*blue*); proliferating cells were visualized by incorporation of 5′-ethynyl-2′-deoxyuridine (EdU; *green*). (*B*) Proliferation assay of organoids. $^{*}P < .05$; $^{**}P < .01$. (*C*) Stereomicroscopic images of the intestinal organoids propagated at various concentrations of Rspo1. The images were taken for 6 consecutive days as indicated. Original magnification: (*A*) 400×; (*C*) 20×.

els of the Wnt coreceptor LRP6 (Supplementary Figure 8*B* and Figure 5*B*). We concluded that TROY might block specific modifications of LRP6, which in turn can change the stability and/or function of LRP6. However, Western blots with antibodies recognizing phospho-Ser1490 and phospo-Thr1572 of LRP6 protein did not show differential modification of these residues in control and TROY siRNA-treated cells (Figure 5*B* and data not shown). Thus, the putative phoshorylation site(s) remains to be determined. Finally, we functionally tested the role of Troy in defined primary cultures of the intestinal crypts. Troy$^{-/-}$ organoids, in contrast to organoids derived from wild-type mice, retained cell proliferation even in the absence of exogenous Rspo1 (Figure 6*A* and *B*). However, growth of these "mini-guts" ceased 48 hours after withdrawal of Rspo1 (Supplementary Figure 9). This prompted us to test the organoid culture at decreasing concentrations of Rspo1. Strikingly, *Troy*$^{-/-}$ organoids could be propagated for many weeks in culture medium supplemented with Rspo1 at a concentration of 15 ng/mL. Contrary to that, at the same Rspo1 concentration, the growth of intestinal organoids established from wild-type mice was arrested (Figure 6*C*). These results convincingly confirmed the possible inhibitory role of Troy on Wnt/Rspo signaling.

Discussion

In the present study, we identified TROY as the Wnt/β-catenin pathway target gene in human CRC cells and in mouse tumors. Using expression profiling, ISH, and lineage tracing experiments in the mouse, we showed that in the healthy small intestine, Troy marks the fast-cycling CBC stem cells. In addition, we showed that TROY interacts with LGR5 and inhibits canonical Wnt signaling.

In mouse neoplasia, Troy behaved as a reliable marker of tumors with active Wnt signaling. Of note, although expression analyses of mouse and human tissues or cell lines included several well-defined Wnt/β-catenin signaling target genes, we never observed a "100%" correlation between the expression of the analyzed genes and (hyper)

active Wnt signaling. Even *Axin2*, considered to be a "universal" target of the canonical Wnt pathway, was not (significantly) up-regulated in AOM/DS-induced neoplasia (Figures 1*B* and *D* and 2*A*). These data indicate that the transcription of the tested genes is regulated by complex mechanisms and cannot be solely related to the status of the Wnt pathway. Contrary to mouse tumors, *TROY* expression in human sporadic CRC did not correlate with the mutation status of *APC* (Supplementary Figure 2). Moreover, TROY mRNA was decreased in the majority of human premalignant lesions. These observations preclude the use of TROY as a marker of the Wnt pathway activity status in human CRC and/or TROY targeting in therapeutic applications.

ISH indicated that *Troy* mRNA is uniformly expressed throughout tumor tissues (Figure 2*B*). This result was somehow contradictory to the lineage tracing experiments in Troy-CreERT2^{+}/Rosa26R/Apc$^{+/Min}$ mice, which showed "patches" of the LacZ-positive cells in tumor tissues (Figure 3*E*). Because Cre-mediated recombination displayed different efficiency in distinct parts of the intestine, we suppose that the observed variability in LacZ staining was caused by the inefficient recombination of the "floxed" transcriptional stop signal rather than by the heterogeneous expression of *Troy* (or its surrogate marker Cre) in tumor tissue.

Expression of Troy was described in the adult central nervous system, the developing hair follicle, and embryonic skin.[26] In postnatal neurons, Troy interacts with the Nogo-66 receptor 1 (NgR1) and activates RhoA signaling.[28] Moreover, in glial tumor or HEK293 cells, TROY participates in the Rac1 and JNK pathways, respectively.[29,30] Recently, a study by Hashimoto et al revealed that the cytokine lymphotoxin α binds to Troy and triggers nuclear factor κB signaling.[31] All of these results suggest a complex and pleiotropic role of Troy in various cellular contexts.

According to our data, TROY interacts with LGR5 and limits the level of canonical Wnt signaling. Importantly, active Wnt/Rspo signaling could not be completely compensated by Troy deficiency and Troy$^{-/-}$ organoids arrested their growth on withdrawal of exogenous Rspo (Figure 6 and Supplementary Figure 9). This result indicated that Troy-mediated inhibition of the Wnt pathway is indirect. In agreement with this conclusion, we observed that Troy knockdown increased the levels and phosphorylation of LRP6 (Figure 5*B* and *C*). Recently, zinc and ring finger (ZNRF) 3 and ring finger (RNF) 43 transmembrane ubiquitin ligases were identified as negative regulators of Wnt signaling.[32] These related ligases decrease the stability of the Wnt receptor FZ through ubiquitin-mediated degradation. Interestingly, Rspo associates with both ZNRF3 and LGR and promotes removal of ZNRF3 from the plasma membrane. Consequently, the levels of FZ and also Wnt coreceptor LRP are increased, which leads to the enhanced Wnt response. However, the relationship between Troy and ZNRF3/RNF43 ligases and Troy involvement in LRP6 phosphorylation and stability remains to be determined.

Troy-deficient mice are viable and fertile with no apparent defects in the gut tissue.[16,31] This fact is rather unexpected considering the increased proliferation rate and decreased dependence on Rspo1 observed by the Troy-deficient organoids. Farin et al recently described a similar discrepancy between the requirement of Wnt3 for growth of intestinal organoids and dispensability of Wnt3 in living animals.[33] These data show that cultured crypt organoids do not entirely recapitulate the complex situation involving interaction of multiple cell types present in intestinal tissue. Alternatively, the absence of Troy results in a relatively subtle and survival-compatible phenotype that was not noted during the primary analysis of Troy$^{-/-}$ animals. Finally, Troy$^{-/-}$ mice must be "challenged" in some way to reveal any functional outcomes of the absence of Troy.

Supplementary Material

Note: To access the supplementary material accompanying this article, visit the online version of *Gastroenterology* at www.gastrojournal.org, and at http://dx.doi.org/10.1053/j.gastro.2012.10.048.

References

1. Kinzler KW, Vogelstein B. Lessons from hereditary colorectal cancer. Cell 1996;87:159–170.
2. Korinek V, Barker N, Morin PJ, et al. Constitutive transcriptional activation by a beta-catenin-Tcf complex in APC-/- colon carcinoma. Science 1997;275:1784–1787.
3. Cadigan KM, Peifer M. Wnt signaling from development to disease: insights from model systems. Cold Spring Harb Perspect Biol 2009;1:a002881.
4. Marshman E, Booth C, Potten CS. The intestinal epithelial stem cell. BioEssays 2002;24:91–98.
5. Barker N, van Es JH, Kuipers J, et al. Identification of stem cells in small intestine and colon by marker gene Lgr5. Nature 2007;449:1003–1007.
6. Tian H, Biehs B, Warming S, et al. A reserve stem cell population in small intestine renders Lgr5-positive cells dispensable. Nature 2011;478:255–259.
7. Fevr T, Robine S, Louvard D, et al. Wnt/beta-catenin is essential for intestinal homeostasis and maintenance of intestinal stem cells. Mol Cell Biol 2007;27:7551–7559.
8. Korinek V, Barker N, Moerer P, et al. Depletion of epithelial stem-cell compartments in the small intestine of mice lacking Tcf-4. Nat Genet 1998;19:379–383.
9. Hisaoka T, Morikawa Y, Kitamura T, et al. Expression of a member of tumor necrosis factor receptor superfamily, TROY, in the developing mouse brain. Brain Res Dev Brain Res 2003;143:105–109.
10. de Lau W, Barker N, Low TY, et al. Lgr5 homologues associate with Wnt receptors and mediate R-spondin signalling. Nature 2011;476:293–297.
11. Glinka A, Dolde C, Kirsch N, et al. LGR4 and LGR5 are R-spondin receptors mediating Wnt/beta-catenin and Wnt/PCP signalling. EMBO Rep 2011;12:1055–1061.
12. Sato T, Vries RG, Snippert HJ, et al. Single Lgr5 stem cells build crypt-villus structures in vitro without a mesenchymal niche. Nature 2009;459:262–265.
13. Lukas J, Mazna P, Valenta T, et al. Dazap2 modulates transcription driven by the Wnt effector TCF-4. Nucleic Acids Res 2009;37:3007–3020.

14. Willert K, Brown JD, Danenberg E, et al. Wnt proteins are lipid-modified and can act as stem cell growth factors. Nature 2003; 423:448–452.
15. Huranova M, Jablonski JA, Benda A, et al. In vivo detection of RNA-binding protein interactions with cognate RNA sequences by fluorescence resonance energy transfer. RNA 2009;15:2063–2071.
16. Pispa J, Pummila M, Barker PA, et al. Edar and Troy signalling pathways act redundantly to regulate initiation of hair follicle development. Hum Mol Genet 2008;17:3380–3391.
17. Pospichalova V, Tureckova J, Fafilek B, et al. Generation of two modified mouse alleles of the Hic1 tumor suppressor gene. Genesis 2011;49:142–151.
18. Rosin-Arbesfeld R, Cliffe A, Brabletz T, et al. Nuclear export of the APC tumour suppressor controls beta-catenin function in transcription. EMBO J 2003;22:1101–1113.
19. Buttitta L, Tanaka TS, Chen AE, et al. Microarray analysis of somitogenesis reveals novel targets of different WNT signaling pathways in the somitic mesoderm. Dev Biol 2003;258:91–104.
20. Su LK, Kinzler KW, Vogelstein B, et al. Multiple intestinal neoplasia caused by a mutation in the murine homolog of the APC gene. Science 1992;256:668–670.
21. Tanaka T, Kohno H, Suzuki R, et al. Dextran sodium sulfate strongly promotes colorectal carcinogenesis in Apc(Min/+) mice: inflammatory stimuli by dextran sodium sulfate results in development of multiple colonic neoplasms. Int J Cancer 2006;118: 25–34.
22. Kuraguchi M, Wang XP, Bronson RT, et al. Adenomatous polyposis coli (APC) is required for normal development of skin and thymus. PLoS Genet 2006;2:e146.
23. Soriano P. Generalized lacZ expression with the ROSA26 Cre reporter strain. Nat Genet 1999;21:70–71.
24. van der Flier LG, van Gijn ME, Hatzis P, et al. Transcription factor achaete scute-like 2 controls intestinal stem cell fate. Cell 2009; 136:903–912.
25. Sato T, van Es JH, Snippert HJ, et al. Paneth cells constitute the niche for Lgr5 stem cells in intestinal crypts. Nature 2011;469: 415–418.
26. Kojima T, Morikawa Y, Copeland NG, et al. TROY, a newly identified member of the tumor necrosis factor receptor superfamily, exhibits a homology with Edar and is expressed in embryonic skin and hair follicles. J Biol Chem 2000;275:20742–20747.
27. Carmon KS, Gong X, Lin Q, et al. R-spondins function as ligands of the orphan receptors LGR4 and LGR5 to regulate Wnt/beta-catenin signaling. Proc Natl Acad Sci U S A 2011;108:11452–11457.
28. Shao Z, Browning JL, Lee X, et al. TAJ/TROY, an orphan TNF receptor family member, binds Nogo-66 receptor 1 and regulates axonal regeneration. Neuron 2005;45:353–359.
29. Eby MT, Jasmin A, Kumar A, et al. TAJ, a novel member of the tumor necrosis factor receptor family, activates the c-Jun N-terminal kinase pathway and mediates caspase-independent cell death. J Biol Chem 2000;275:15336–15342.
30. Paulino VM, Yang Z, Kloss J, et al. TROY (TNFRSF19) is overexpressed in advanced glial tumors and promotes glioblastoma cell invasion via Pyk2-Rac1 signaling. Mol Cancer Res 2010;8:1558–1567.
31. Hashimoto T, Schlessinger D, Cui CY. Troy binding to lymphotoxin-alpha activates NF kappa B mediated transcription. Cell Cycle 2008;7:106–111.
32. Hao HX, Xie Y, Zhang Y, et al. ZNRF3 promotes Wnt receptor turnover in an R-spondin-sensitive manner. Nature 2012;485: 195–200.
33. Farin HF, Van Es JH, Clevers H. Redundant sources of Wnt regulate intestinal stem cells and promote formation of Paneth cells. Gastroenterology 2012;143:1518–1529.
34. Hatzis P, van der Flier LG, van Driel MA, et al. Genome-wide pattern of TCF7L2/TCF4 chromatin occupancy in colorectal cancer cells. Mol Cell Biol 2008;28:2732–2744.

Received December 23, 2011. Accepted October 28, 2012.

Reprint requests

Address requests for reprints to: Vladimir Korinek, PhD, Institute of Molecular Genetics AS CR, Videnska 1083, 142 20 Prague 4, Czech Republic. e-mail: korinek@img.cas.cz; fax: (420) 244472282.

Acknowledgements

The authors thank A. Abo, L. Andera, V. Bryja, and M. Klima for the constructs; J.F. Beaulieu for HIEC cells; Z. Kozmik for Rosa26R mice; the staff of the Transgenic Unit for generation of the transgenic mice; and S. Takacova and T. O'Hearn II for reading the manuscript.

Conflicts of interest

The authors disclose no conflicts.

Funding

Supported by the qChIP/chip06 project from the Ministry of Education, Youth and Sports of the Czech Republic (grant B06077); Grant Agency of the Czech Republic (P305/11/1780, P304/11/1252, and 204/09/H058); Grant Agency of Charles University in Prague (43-251452); and an institutional grant from the Academy of Sciences of the Czech Republic (RVO 68378050). J.S. was supported by the Third Faculty of Medicine, Charles University in Prague research project UNCE204010; R.S. by the project BIOCEV (CZ.1.05/1.1.00/02.0109) and Grant Agency of the Czech Republic (P305/10/2143); M.H. by the Academy of Sciences of the Czech Republic (KAN200520801); and O.L., M.O., and M.J. by the IKEM MZO 00023001 grant.

Supplemental Material

Supplemental Methods

Cell Lines and Transfections

Human HEK293, Colo320, DLD1, HCT116, HeLa, LS174T, SW480, U2OS cells and mouse 3T3, C57MG and Wnt3a-producing L cells were used for the experiments. All cell lines were maintained in Dulbecco's modified Eagle's medium [(DMEM); purchased from Sigma)] supplemented with 10% fetal bovine serum (Gibco), penicillin, streptomycin and gentamicin (Invitrogen). Transfections were performed using Lipofectamine RNAiMAX or Lipofectamine 2000 reagent (Invitrogen).

ChIP-on-chip Data Analysis

The results of hybridizations were obtained in a gff file format (Nimblegen). The fluorescent intensity peaks in corresponding areas of the microarray were identified by "triangle shape model" described by Kim and colleagues.[1] The peaks were used to define the threshold for "positive" probes. Enrichment of positive probes was then calculated using chi-square of the actual number compared to the expected number of positive probes in a given window.[2] The p-value listed in Table 1 and Supplementary Table S8 is the best (=smallest) p-value assigned to a probe located in the peak region.

Plasmids and Constructs

Proteins with a C-terminal FLAG or MYC tag were produced from pCMV-FLAG/MYC vector (Sigma). Fluorescently tagged proteins were generated in pECFP-N, pEGFP-N, pEYFP-N (Clontech) and pTaqBFP (Evrogen) vectors. The construct encoding the N-terminally truncated variant of human LRP6 protein (LRP6ΔN)[3] in the pCS2 vector was kindly provided by V. Bryja.

Coimmunoprecipitations and Western Blotting

The following antibodies were used: mouse anti-β-catenin, (clone E5; Santa Cruz); rabbit anti non-phospho-β-catenin/S33/S37/T41 (polyclonal; Santa Cruz); rabbit anti-Dvl2 (30D2; Cell Signaling); mouse anti-FLAG (M2; Sigma); mouse anti-GFP (JL-8; Clontech); goat anti-GFP (polyclonal; a gift of D. Stanek); mouse anti-MYC (9E10; Roche); rabbit anti-MYC (71D10; Cell Signaling); rabbit anti-LRP6 (C5C7; Cell Signaling); rabbit anti-phospho-LRP6/Ser1490 (polyclonal; Cell Signaling); rabbit anti-phospho-LRP6/T1572 (polyclonal; Millipore); mouse anti-TROY (ab55043, Abcam); mouse anti-α-tubulin (TU-01; Exbio CZ).

FRET

HeLa cells were transfected with the corresponding constructs. Twenty-four hours after transfection the cells were fixed in 4% (w/v) paraformaldehyde/PIPES buffer (10 min, at room temperature). After rinsing with PBS and distilled water, cells were embedded in glycerol containing DABCO (Sigma). Intensities of ECFP (excited by 405 nm laser set to 5-10% of maximum power) and EYFP (excited by 514 nm laser line set to 2-10% of maximum power) fluorescence were recorded. Subsequently, EYFP was bleached in the region of interest by four intensive (80% maximum power) pulses of 514 nm laser beam and ECFP- and EYFP-emitted fluorescence was measured again. The apparent FRET efficiency was calculated according to the equation: FRET efficiency {%} = (ECFP after -ECFP before) × 100/ECFP after. Unbleached regions of the same cell were used as negative control.

Rspo Binding Assay

Human U2OS or HeLa cells were transiently co-transfected with a combination of LGR5-EYFP and TROY-TagBFP or with LGR5-EYFP and "empty" pTagBFP vector. The next day, cells were incubated (1 hour, 37^{o}C) with conditioned medium containing recombinant mouse Rspo1 containing the constant region of the mouse immunoglobulin G2a heavy chain (IgG2a).[4] In control staining, the cells were incubated with recombinant IgG2a alone. Conditioned media were harvested from HEK293 cells transiently transfected with constructs encoding mouse Rspo1-IgG2a or IgG2a proteins (the constructs were kindly provided by V. Bryja; media were harvested 3 days upon transfection). The presence of recombinant proteins in culture media was verified by Western blotting using the goat anti mouse secondary antibodies (BIO-RAD). Cells were washed twice with PBS and fixed for 10 min in 4% (w/v) paraformaldehyde in PBS. Rspo1-IgG2a or IgG2a retained on the cell surface was visualized by a goat anti-mouse IgG2a Alexa Fluor 594 secondary antibody (Life Sciences; 1:900 dilution, 1 hour at room temperature). Nuclei were counterstained with Draq5 stain (Biostatus Limited).

Generation of Stable Cell Lines

To obtain cells with inducible expression of human TROY, the Lenti-X Tet-On Advanced Inducible Expression System (Clontech) was used. HEK293 cells were transduced with recombinant lentiviruses producing the tetracycline-controlled transcription activator (rtTA) and selected without subcloning using G418 (Enzo Life Sciences; 0.5 mg/ml). Resistant cells were further transduced with lentivirus pLVX-Tight-Puro encoding full-length human *TROY* with the C-terminal FLAG tag. HEK293/TROY cells were selected and maintained in puromycin (Alexis; 2 μg/ml) and G418 (0.2 mg/ml).

Reporter Gene Assays

To test the effect of TROY on the Wnt-dependent transcription, TROY expression was induced in HEK293/TROY by doxycycline (Sigma; 1μg/ml). The cells were stimulated simultaneously with doxycycline, Wnt3a and/or human Rspo1 and analyzed 18 hours later. Reporter gene assays in siRNA-treated HEK 293 cells were performed in an analogous manner. To ensure effective downregulation of TROY, two days after the first transfection with TROY or control non-silencing siRNA the cells were lipofected with the same siRNA together with pTOPFLASH/pFOPFLASH and *Renilla* luciferase expression plasmid. Twenty-four hours upon the second transfection, Wnt3a and Rspo1 ligands were added to culture medium (separately or in combination). The cells were stimulated for an additional 18 hours, then harvested and analyzed.

AOM/DS Treatment

Tumors of the colon and rectum were collected from adult C57BL/6J mice five weeks after a single subcutaneous injection of AOM (10 mg/kg; Sigma) followed by a 5-day DS treatment in drinking water [3% (w/v) DS; MW 36-50 kDa; MP Biomedicals].

Generation of Troy-CreERT2 Transgenic Mice

The TROY-CreERT2 bacterial artificial chromosome (BAC) transgenic construct was generated using homologous recombination in bacteria according to the previously published protocol.[5] A BAC clone RP23-166C22 was purchased from imaGenes (Berlin, Germany); a construct containing CreERT2 cDNA was kindly provided by M. Cepko via Addgene. The adapters "a" (5'-CCTCTCGTCTTTGACTTGCATCCTTCAGGAATAAACACGTTT GGTGAGAGCCatgtccaatttactgaccgtac - 3'; the *Troy*-specific sequence is highlighted in capital letters, the part complementary to the CreERT2 expression cassette is given in small caps) and "b" (5'-TGATAGGAGTTCTTTCCCCATATTCATATGAAAGAGAAGAGGCAACTTACgccgctctaga actagtggatc - 3') were derived from the sequence of the exon containing the translation start site or from the flanking intron, respectively (Supplemental Fig. S5*A*). The adapters were employed for the PCR amplification, the product was purified from agarose gel and electroporated into the *E. coli* strain EL250 harboring the BAC clone RP23-166C22. Bacterial clones containing correctly recombined BACs were verified by PCR. Isolated recombinant BAC DNA was linearized and used for pronuclear injection of fertilized eggs (C57Bl/6J background). Three TROY-CreERT2 transgenic founder lines were produced using the service of the Transgenic Unit of the Institute of Molecular Genetics. All three lines exhibited a virtually identical pattern of the Cre recombinase activity.

RNA Probes and IHC

Antisense RNA probes were derived from the following regions of the analyzed genes: *Axin2* (NM_015732.4), nucleotides 2069-2938; *Lgr5* (NM_010195.2), nucleotides 373-887, *Troy* (NM_013869.5), nucleotides 763-1924. Antibodies for IHC: mouse monoclonal anti-β-catenin antibody (E5; Santa Cruz); anti-Chromogranin A (Abcam) and anti-Lysozyme (DAKO) rabbit polyclonal antibodies.

Processing of Specimens of Human Sporadic Colorectal Carcinomas and Precancerous Colorectal Lesions

Samples of the following macroscopically distinguishable tissue segments were taken from fresh colectomy specimens: (1) the center (stroma) of the tumor without, if any present, ulcerated luminal portion and the least necrotic parts of the lesion were preferred, and, (2) healthy surrounding mucosa were collected in the distance of a maximum of 5 cm from the primary tumor site. Pathological and morphological criteria included tumor location, pTNM classification, histological subtype, grade of differentiation and presence of vessel invasion (a summary is given in Supplemental Table S2). RNA was isolated from biological replicates of distinct tumor segments and healthy mucosa. Sporadic precancerous colorectal lesions were obtained during colonoscopies carried out at the Second Department of Internal Medicine, Third Faculty of Medicine, Charles University in Prague. Collection of each polyp was accompanied by two biopsies of normal mucosa from the rectosigmoideum region.

Histopathology of the lesions was evaluated on hematoxylin and eosin stained sections by two pathologists (a summary is given in Supplemental Table S3). Tissue samples were homogenized in RNA Blue reagent (TopBio, Czech Republic) using a T8 Ultra Turrax disperser (IKA). Total RNAs were extracted according to the manufacturer's protocol and subjected to RNA integrity number (RIN) analysis (Agilent 2100 Bioanalyzer; samples with RIN > 8 were used). Reverse transcription was performed using the RevertAid H Minus reverse transcriptase (Fermentas) with1.5 μg of total RNA using random hexanucleotide primers (Invitrogen). Negative controls were represented by input RNA processed in the absence of reverse transcriptase. PCR reactions were run in parallel triplicates for each primer set in Light Cycler 480 (Roche Applied Science). Two housekeeping genes, *UBIQUITIN B* (*UBB*) and *β-ACTIN* were used as internal controls. Primer sequences are listed in Supplemental Table S1.

The APC Mutation Analysis

Genomic DNA was extracted from deep-frozen samples of tumor tissue and healthy surrounding mucosa using the DNeasy Blood & Tissue Kit (Qiagen). Seven PCR fragments partially

covering the sequence of human *APC* exon 18 and two fragments corresponding to *β-CATENIN* (*CTNNB1)* exons 3 and 4, including intron-exon boundaries, were amplified using gene-specific primers (Supplemental Table S4) containing overhangs recognized by T7 (5'-TAATACGACTCACTATAG - 3') and RP (5'-TGAAACAGCTATGACCATG - 3') universal sequencing primers. PCR was performed in 38 cycles with 30 second primer annealing at 60°C and 45 second extension at 71°C. Each fragment was directly sequenced from both sides using the BigDye® Terminator v3.1 cycle sequencing kit and ABI 3130 Genetic Analyzer (Applied Biosystems).

Statistical Analysis of RT-qPCR Data of Colorectal Cancer Samples

RNA isolated from each specimen (biological replicate) of tumor or healthy mucosa was subjected to the RT-qPCR analysis; the PCR reactions were performed in triplicates. In each technical replicate, Cp's were normalized using *β-ACTIN* as a reference gene to obtain ΔCp's and averaged. Principal component analysis (PCA) on ΔCp's of biological replicates identified one outlying patient. All samples of this patient were removed and the remaining 76 samples of 19 patients were used in downstream statistical analyses. To detect differences in expression, we applied Wilcoxon's rank-sum test. To account for different genetic background of the patients, we further fitted a linear model (REML) described by the formula ΔCp ~ patient + tissue/(stage * mutation), with biological replicates treated by a random effect and all healthy mucosa samples treated as a single group and validated the results. No correction of multiple testing was applied. Statistical significance was estimated at the level of 0.05 (or 0.01 and 0.001) and marked by asterisk (or ** and ***) in Supplemental Figure S2. All analyses were performed in R language/environment.

Statistical Analysis of RT-qPCR Data of Precancerous Lesions

Messenger RNA obtained from 35 samples of precancerous lesions of the colon and matching healthy mucosa was subjected to RT-qPCR analysis. Cp´s of individual technical triplicates were normalized by geometric average of internal control genes *β-ACTIN*, *AXIN1* and *UBB* and averaged (ΔCp). PCA revealed that specimens of one patient were deemed outlying and were consequently omitted from further statistical analyses. Differential expression was evaluated as described for colorectal cancer samples.

Bisulfite Analysis of Cytosine Methylation

Genomic DNA (0.5 μg) isolated from tumor center and matched healthy surrounding mucosa was subjected to bisulfite conversion using the EZ DNA Methylation™ Kit (Zymo Research). Bisulfite-treated DNA was amplified by nested PCR using the following primers: for primary amplification oligonucleotides 5´-ATTTTATTGGTGGAAAAGTATTTTAT-3´ [forward; priming on nucleotides (nt) -672 to -647 upstream from the *TROY* genes transcription start (according to sequence

NM_001204458.1)], and 5′-AACTTACTCTACAACTAAATTCTTTAA-3′ (reverse; nt -163 to -137). The PCR product was re-amplified using primers 5′-TTTTTTTAGTAAAATTGTTTAGTGAGTTTT -3′ (forward; nt -629 to -600) and 5′-AATAAATATAAAACTAACTAAAAACTTAAAAATA-3′ (reverse; nt -225 to -193). Cytosines (not included in CpG dinucleotides) were changed to T or A in forward and reverse primers, respectively. Amplification products were cloned into the pGEM-T-Easy vector (Promega) and sequenced. Nine to twelve independent PCR clones with at least 95% conversion of cytosine outside of CpG dinucleotides were analyzed.

Paneth Cells Sorting

Single cells from crypts were obtained as in reference[6]. Cells were stained with phycoerythrin (PE)-conjugated anti-CD24 antibody (eBioscience), allophycocyanin (APC)-conjugated anti-Epcam antibody (eBioscience) and FITC-conjugated anti-CD45 antibody (ExBio) for 30 min at 4°C, and sorted by Influx cell sorter (BD Biosciences).

Organoid Proliferation Assay

Freshly isolated crypts were cultured for 6 days in crypt culture medium containing Rspo1 (250 ng/ml). Crypt-derived multicellular organoids were removed from Matrigel (BD Biosciences), mechanically dissociated and then transferred to fresh Matrigel and medium (split ratio 1:4) containing various concentrations (0 to 500 ng/ml) of Rspo1. Cell proliferation was visualized by a Click-iT™ EdU Imaging Kit (10 μM EdU incorporation for 1 hour at 37°C) according to manufacturer's instructions (Invitrogen). Organoids were further stained with an anti-E-cadherin antibody (Zymed) and DAPI and imaged using a Leica Sp5 confocal microscope. The proliferation rate was determined by counting of EdU-positive vs. DAPI-positive cells; at least 10 organoids were evaluated per each genotype and Rspo1 concentration. The organoids prepared from 3 mice of corresponding genotype were grown in quadruplicates for each concentration of Rspo1. Statistical significance was estimated by the Student's t-test.

Supplemental Results

***Troy* expression in the mouse colon**

To detect Troy expression in the colon two experimental approaches were used. First, *in situ* hybridization was performed; however, our attempts to visualize *Troy* mRNA were not successful. Secondly, Troy-CreERT2^{+}/Rosa26R mice were used to detect Cre/LacZ-expressing cells in the colonic tissue. Recombined (i.e. blue) cells were observed – although at lower frequency than in the small intestine – at the bottom of the colonic crypts one day after the induction of Cre. Lately, the labeled cell clones spread to the luminal surface and persisted in the colon for several months (Supplemental Figure S5*G*). This result indicated that similarly to the small intestine epithelium, Troy-positive cells are self-renewing stem cells. The low frequency of the blue clones in the colon was rather unexpected as endogenous *Troy* expression (similar to the *CreERT2* production from the transgene) is abundant in the colon (Supplemental Figure 5*E*). A similar phenomenon was observed by Powel and colleagues in Lgr5-EGFP-IRES-CreERT2 mice.[7] Interestingly, in the same study induction of a remarkably greater number of labeled colonic crypts (compared to the Lgr5-CreERT2 mice) was observed in Leucine-rich repeats and immunoglobulin-like domains (Lrig) 1-CreERT2 reporter mice. Since Lrig1 marks noncycling, long-lived stem cells, these data indicate that the recombination of the transcription "roadblock" cassette is inefficient in highly proliferative Lgr5- or Troy-positive cells of the colon.

***TROY* expression profiling in sporadic colorectal carcinoma and premalignant lesions**

Two biological replicates of both tumor and healthy tissue were obtained from each individual and used for sequence analysis of the *APC* gene. The analyses encompassed the somatic mutation cluster region of *APC* as well as flanking regulatory sequences encoding elements required for the β-CATENIN interaction and downregulation [nucleotides 1959 to 4945 (numbering was taken from the sequence NM_000038.5)].[8] Putatively inactivating mutations of *APC* were found in 11 out of 20 patients (55%), which is in concordance with published data.[9] Of note, since the mutational analysis was covering only a "hot spot" of the *APC* gene, we cannot exclude that not all mutations in the *APC* sequence have been detected. No oncogenic mutations were detected in the somatic hotspot regions of exons 3 and 4 of *β-CATENIN* (summary of the *APC* mutations can be found in Supplemental Table S5).

To analyze differences in the expression of *AXIN2*, *LGR5* and *TROY* genes in tumor tissue versus healthy mucosa, we applied non-parametric Wilcoxon's test. In addition, to account for

histopathological variations in specimens obtained from different patients we used a linear model (REML). Both statistical analyses clearly showed significant correlation between the presence of the inactivating *APC* mutations and expression levels of the *AXIN2* gene (Supplemental Figure S2*A*; p- and other values are indicated in Supplemental Table S6). This result was in agreement with previously published data.[10] On the other hand, *LGR5* mRNA was increased in tumor tissues irrespective of the *APC* status. The *TROY* expression levels did not follow any conclusive expression pattern, moreover we detected a decrease in *TROY* expression in the majority of tumors. To study a molecular mechanism of possible *TROY* silencing in tumor tissue, genomic DNA isolated from specimens with elevated and decreased *TROY* expression was subjected to the cytosine methylation analysis. The analysis of the sequence containing 35 CpG doublets located in the proximity of the *TROY* transcription start (see Supplemental Methods for details) in two carcinomas with reduced *TROY* expression revealed that only 2 and 14% of analyzed CpG dinucleotides were methylated (Supplemental Fig. S2*B*). This implied that the observed reduction in *TROY* expression is not related to changes in the DNA methylation status. In addition, the analysis of *TROY* expression in thirty-five premalignant lesions of the colon was performed. In polyps, *AXIN2* and *LGR5* displayed a significant increase in mRNA levels (compared to healthy mucosa tissue). Expression of both genes strongly correlated with the grade of the neoplastic tissues showing elevated expression in more progressed lesions. These results were in good concordance with published data.[11] In contrast, *TROY* mRNA was decreased in the majority of premalignant lesions irrespective of their histological category (Supplemental Figure S3 and Supplemental Table S7).

Supplemental Acknowledgments

We thank J. Dobes and J. Tureckova for help with sorting and RT-qPCR analysis of Paneth cells. We also thank O. Sebesta for help with microscopy.

Supplemental Figure and Table Legends

Supplemental Figure S1. Summary of the ChIP-on-chip analysis. Venn diagram depicts the numbers of promoter regions bound by TCF4 in each cell line (the selection criterion is defined in the Table 1 legend). Of 960 genes identified, 18 genes scored positive in all four cell lines.

Supplemental Figure S2. *TROY* expression does not correlate with the *APC* status in human colorectal cancer. (*A*) Comparison of relative expression levels of *AXIN2*, *LGR5* and *TROY* genes in sporadic colorectal tumors (T) compared to surrounding healthy mucosa (HM) samples. Individual Cp values were normalized to the level of the housekeeping gene *β-ACTIN* to obtain a log of relative expression levels (-ΔCp) and averaged. Tumors were assigned to four distinct subgroups with respect to the *APC* mutation status (WT, wild-type *APC*; MUT, *APC* mutated) and disease stage. Stage grouping: the "early stage" encompasses tumors classified 0 to IIC according to the 7th Edition of the American Joint Committee on Cancer (AJCC) Cancer Staging Manual. Stages of advanced colorectal disease (IIIA-IV) constitute the subgroup designated as the "advanced stage". Median of ΔCp values for each respective subgroup is indicated by the red line. The differences in the expression levels of a selected gene in the given groups and their statistical significance were tested by Wilcoxon's rank-sum test (solid line) and a linear model (REML, dashed line), which accounted for tissue type, *APC* status, stage and biological background of the patients. *, $p < 0.05$; **, $p < 0.01$; ***, $p < 0.001$. Data accompanying this figure can be found in Supplemental Table S6. (*B*) Cytosine methylation analysis of the CpG island located upstream of the *TROY* promoter. The analysis was performed on genomic DNA isolated from tumors with "high" (normalized Cp<25.5) or "low" (Cp> 31) *TROY* expression. Both early and advanced stage tumors were assayed as indicated. Open circles mark unmethylated CpG dinucleotides, while closed circles indicate methylated CpGs. Tumor samples (T) are depicted in red, matched healthy surrounding mucosa (HM) in black.

Supplemental Figure S3. *TROY* expression is decreased in precancerous lesions of the human colon. Comparison of relative expression levels of *AXIN2*, *LGR5* and *TROY* genes in sporadic premalignant lesions (P) of human colon and matching healthy mucosa (HM) samples. Based on prevailing microscopic appearance, lesions were subdivided to three histological categories: hyperplasia (H), low grade dysplasia (LGD) and high grade dysplasia (HGD). Median of ΔCp values in individual subgroups is indicated by the red line. Statistical significance of differences in expression levels was examined by nonparametric Wilcoxon´s rank-sum test (solid line). Moreover, a linear model (REML; dashed line) encompassing tissue type, histology and individual biological background

of the patients was applied. *, $p < 0.05$; **, $p < 0.01$; ***, $p < 0.001$. Data accompanying this figure can be found in Supplemental Table S7.

Supplemental Figure S4. Analysis of Troy expression in the small intestine using ISH and fluorescence-activated cell sorting (FACS). (*A*) Left, ISH of *Troy* mRNAs in jejunum showing expression in the lower parts of the crypts (black arrowheads). Right, colocalization of Troy-expressing and CBC cells in the intestine. Frozen sections prepared from Lgr5-EGFP-IRES-CreERT2 mice were stained using ISH for *Troy* mRNA (black arrowhead). The slides were mounted in glycerol and the results recorded. Next, the cover slips were removed and the CBC cells were visualized in the same specimen using IHC detection of GFP protein (brown arrowheads). (*B*) FACS of $Lgr5^{+}$ cells. Left, fresh isolates of the crypts from the small intestine of Lgr5-EGFP-IRES-CreERT2 mice. A detailed confocal image of one crypt stained with DAPI nuclear stain is shown in bottom panel. The putative CBC stem cells located at the base of each crypt are marked by EGFP expression. Right, diagrams of the cell-sorting procedure. Three cell populations (GFP^{high}, GFP^{low}, $GFP^{negative}$) were obtained from the crypts of Lgr5-EGFP-IRES-CreERT2 mice. GFP^{high} and GFP^{low} cells, which are not present in the intestine of control wild-type (WT) mice, were used for the subsequent RT-qPCR analysis. The crypt isolations were performed as described in the reference.[12] (*C*) Cell sorting of Paneth cells. Left, FACS plots of dissociated single cells from small intestinal crypts of wild-type mice. Viable single cells were gated by forward scatter, side scatter, pulse-width parameter and negative staining for Hoechst 33258. Epithelial cells ($CD45^{-}Epcam^{+}$) were sorted in three gates. Two CD24 bright populations differed by side-scatter (SSC) pattern. Sorted $CD24^{high}SSC^{low}$ population (Gate 1) corresponds to enteroendocrine cells and $CD24^{high}SSC^{high}$ cells are Paneth cells (Sort 2 gate). Right, RT-qPCR from sorted cells, Sort 2 vs. Sort 3 gate ($CD24^{low}$) illustrates that *Troy* (and *Lgr5*), unlike the Paneth cell markers *Lysozyme (Lys)* and *Defensin α 20 (Defa20)*, is not enriched in Paneth cells. Original magnification: (*A*) left panel 100 ×, right panel 400 ×; (*B*) upper panel 200 ×, lower panel 400 ×.

Supplemental Figure S5. Tracking the Troy expression using the *Troy-CreERT2* BAC transgenic allele. (*A*) CreERT2 was inserted in frame into the first coding exon of the mouse *Troy* gene. The non-coding or translated regions are depicted by empty and black boxes, respectively. *a,b*, Troy sequences employed for the homologous recombination into the BAC clone RP23-166C22. *RGB poly A*, a poly A signal derived from the rabbit *β-globulin* gene; Kan^{r}, the *kanamycin* resistance gene; *pBla*, *β-lactamase* promoter. Prior to pronuclear injection, the bacterial resistance cassette was excised from recombinant BAC using Flp recombinase and FRT sites (black semicircles) flanking the cassette. (*B*) The whole-mount hybridization of wild-type mouse embryo at embryonic day (E) 14.5 using an antisense probe against *Troy*. (*C*) The activity of CreERT2 recombinase produced from the Troy-CreERT2 BAC transgene was visualized at E 14.5 in embryos derived from crossing of Troy-

CreERT2 and Rosa26R mice. Tamoxifen was injected intraperitoneally into pregnant females. The animals were sacrificed one day later; embryos were removed and used to stain the LacZ-expressing tissues. The CreERT2 expression pattern visualized by the X-gal substrate phenocopies the sites of expression of endogenous *Troy* mRNA and its localization is also in concordance with the *Troy* expression pattern described previously.[13, 14] cb, cerebral plate; drg, dorsal root ganglion; e, ear; ma, maxilla; mg, mammary gland primordium; v, vibrissae. (*D*) Frequency of Cre-mediated recombination in different anatomical parts of the intestine of Troy-CreERT2^{+}/Rosa26R mice. Three mice were injected with tamoxifen and sacrificed 60 days later. Percentage of positive (i.e. blue) crypts in duodenum (Duo), jejunum (Jej), ileum (Ile) and colon (Col) is indicated with given SD in parentheses. Notice that the image was taken from Figure 3*B*. (*E*) RT-qPCR profiling of the *CreERT2* and *Troy* genes in intestinal mucosa dissected from different parts of the gastrointestinal system. The tissues were obtained from four Troy-CreERT2 transgenic mice or from their wild-type littermates (n=4). (*F*) Localization of LacZ-positive cells in the crypts of Troy-CreERT2^{+}/Rosa26R mice 1 day after tamoxifen administration. The diagram depicts frequency of occurrence of blue cells at specific positions in the crypt; the positions are indicated in the scheme in the inset. Four hundred crypts from the proximal part of the small intestine of two mice were counted. Results are depicted as means with SDs. Most of the LacZ-expressing cells occurred in the bottom part of the crypt, whereas less than 6% of these cells were observed at the +5 position or higher. (*G*) Cell lineage tracing in the colon of Troy-CreERT2^{+}/Rosa26R mice 1 day and 60 days after tamoxifen administration. Black arrowheads indicate LacZ-positive cells emerging 1 day upon induction. Original magnification: 100 ×.

Supplemental Figure S6. LGR5 interacts with the TROY-related receptor EDAR. Co-immunoprecipitation of MYC-tagged EDAR or MYC-tagged TROY with LGR5-FLAG. In panels indicated as ”INPUT”, 20% of the total lysate used for one immunoprecipitation was loaded. AB, the precipitation was performed without cell lysates; NT, lysate from non-transfected cells was precipitated; IP, immunoprecipitation; IB, immunoblotting.

Supplemental Figure S7. (*A*) Downregulation of TROY does not potentiate TCF/β-catenin-mediated transcription in human CRC cells. Results of the RT-qPCR analysis of indicated genes in TROY siRNA-treated vs. control siRNA-treated cells. The Wnt/β-catenin non-responsive gene *AXIN1* was also included in the test. Cp values were normalized to the *β-ACTIN* expression levels (Cp=16.5). The histogram represents mean Cp values of a representative experiment performed in triplicates (repeated twice). The expression level of a given gene in cells transfected with control non-silencing siRNA and treated with vehicle was arbitrarily set to 1. Missing bars stand for unexpressed gene (normalized Cp>35). (*B*) The effect of ectopic TROY was tested in HEK293/TROY cells with doxycycline-

inducible expression of TROY transgene. RT-qPCR analysis of cells grown with or without doxycycline (DOX) and stimulated with Wnt3a and/or Rspo1 ligands.

Supplemental Figure S8. The most proximal events triggered by Wnt or Rspo ligand are not influenced by TROY. (*A*) TROY does not interfere with binding of Rspo1 to LGR5. Laser scanning confocal microscopy images of U2OS cells transfected with equimolar amounts of constructs expressing LGR5-EYFP (green) and TagBFP (pseudocolored in red; upper panels) or LGR5-EYFP and TROY-TagBFP (lower panels). Cells grown on cover slips were incubated with conditioned medium containing Rspo1-IgG2a fusion protein. The cell surface binding of Rspo1-IgG2a to its receptor LGR5 was detected using Alexa Fluor 594 anti-IgG2a antibody (gray). Recombinant IgG2a alone did not display any nonspecific binding to the cells (not shown). Nuclear counterstain Draq5 (gray) is omitted from the overlay images for clarity. (*B*) Colocalization analysis of LGR5 with its ligand Rspo1 in the presence of TagBFP (left panel) or TROY-TagBFP (right), respectively. The analysis was performed using the intensity correlation analysis (ICA) plug-in for ImageJ image processing program.[15] Areas displaying colocalization of the proteins were pseudocolored in white; the areas with non-overlapping localization are shown in black. Original magnification: 1000 ×. (*C*) Dvl phosphorylation is not affected by *TROY* knockdown. The western blot of whole-cell extracts prepared from HEK293 cells treated with non-silencing or TROY siRNA and further stimulated as indicated. The putative phosphorylated form of Dvl with changed mobility in the gel is marked by arrow.

Supplemental Figure S9. Stereomicroscopic images of the intestinal organoids derived from wild-type or *Troy*$^{-/-}$ mice. Organoids grown for 6 days in complete crypt culture medium were mechanically dissociated and then transferred to Matrigel and fresh medium with or without Rspo1 ligand. The images of the same organoids were taken for 5 consecutive days as indicated. Original magnification: 20 ×.

Supplemental Table S1. Sequences of primers used for ChIP and RT-qPCR analyses. The sequence of the forward primer is given in the upper line with the corresponding reverse primer in the lower line, respectively.

Supplemental Table S2. Clinical and histopathological features of colorectal cancer patients. Tumors were classified according to the 7th edition of AJCC Cancer Staging Manual.

Supplemental Table S3. Clinical and histopathological characteristics of patients with precancerous lesions of the colon. Polyps were classified according to the Vienna Classification of gastrointestinal epithelial neoplasia.[16]

Supplemental Table S4. Sequences of primers utilized to amplify selected *APC* and *β-CATENIN* exons. The sequence-specific portion of the primer is highlighted in capital letters; the T7 and RP adaptor primers are in small caps. [1)] Exon and nucleotide numbering according to NM_000038.5; [2)] primer sequence situated in intron 55 bps upstream of exon 18; [3)] primer sequence situated in intron 134 bps upstream of exon 3; [4)] primer sequence situated in intron 172 bps downstream of exon 3; [5)] primer sequence situated in intron 111 bps upstream of exon 4; [6)] primer sequence situated in intron 84 bps downstream of exon 4.

Supplemental Table S5. Summary of detected *APC* mutations in samples of sporadic human colorectal carcinomas. The sequenced region of the *APC* exon 18 encompasses c.1959-c.4945 (NM_000038.5) including the exon 18´s 5´ intron-exon boundary. [1)] Mutation identifiers: "c" syntax indicates the type and localization of the mutation in the *APC* cDNA coding sequence (CDS; NM_000038.5); "p" syntax indicates the position and change in the protein; see the reference Forbes et al., 2010 for details[17]; [2)] according to PolyPhen prediction analysis[18] this substitution is scored as possibly damaging (it is supposed to affect the protein function or structure; PSIC score difference: 1.773); [3)] according to PolyPhen prediction analysis, this substitution is considered benign (no evidence for damaging effect is seen; PSIC score difference: 1.386); [4)]the presence of single nucleotide polymorphism (SNP) at *APC* c.4479 (G/A; rs41115) indicated that heterozygosity status in a tumor sample was preserved (wt; patients #20 and #14) or lost (LOH; patients #1, #2 and #18). In the absence of *APC* c.4479 polymorphism (c.4479 A/A; patients #15 and #6), the information concerning zygosity status of the *APC* locus is not available (n.a.). [5)] In cases of carcinomas that display a reduction to homozygosity at c.4479 (patients #2 and #18), the presence of the *APC* inactivating mutations is presumed although it was not detected (n.d.) in the analyzed region (see reference[19] for additional information). All tumors listed in Supplemental Table S5 constitute the subgroup of the APC-deficient tumors [designated as "APC mut" in downstream statistical analyses (Supplemental Figure S2 and Supplemental Table S6)].

Supplemental Table S6. Statistical analysis of tumor expression profiles (data accompanying Supplemental Figure S2). Individual Cp values were normalized to the expression level of the *β-ACTIN* housekeeping gene to obtain relative expression levels (-ΔCp) and averaged. Biological replicates were further treated by a random effect and all HM treated as a single group (ΔΔCp). FC, fold change.

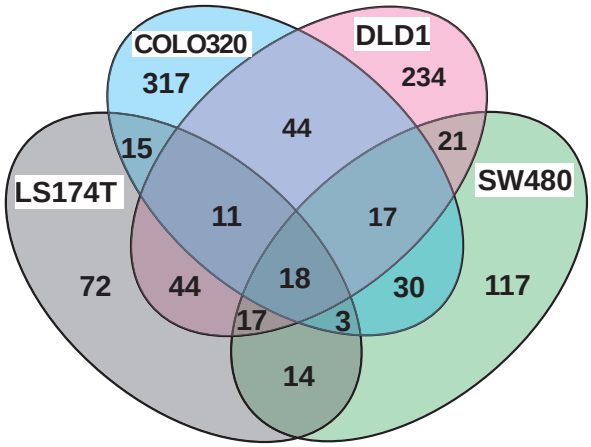
Supplemental Table S7. Statistical analysis of expression profiles of precancerous lesions of human colon (data accompanying Supplemental Figure S3). Individual Cp values were normalized using geometric average of three housekeeping genes (*β-ACTIN*, *AXIN1* and *UBB*) to obtain relative expression levels (-ΔCp) and averaged. All healthy mucosae were treated as a single group (ΔΔCp). FC, fold change.

Supplemental Table S8. A complete list of genes identified by Chip-on-chip using the TCF4-specific antibody and chromatin isolated from Colo320, DLD1, LS174T and SW480 CRC cells.

Supplemental References

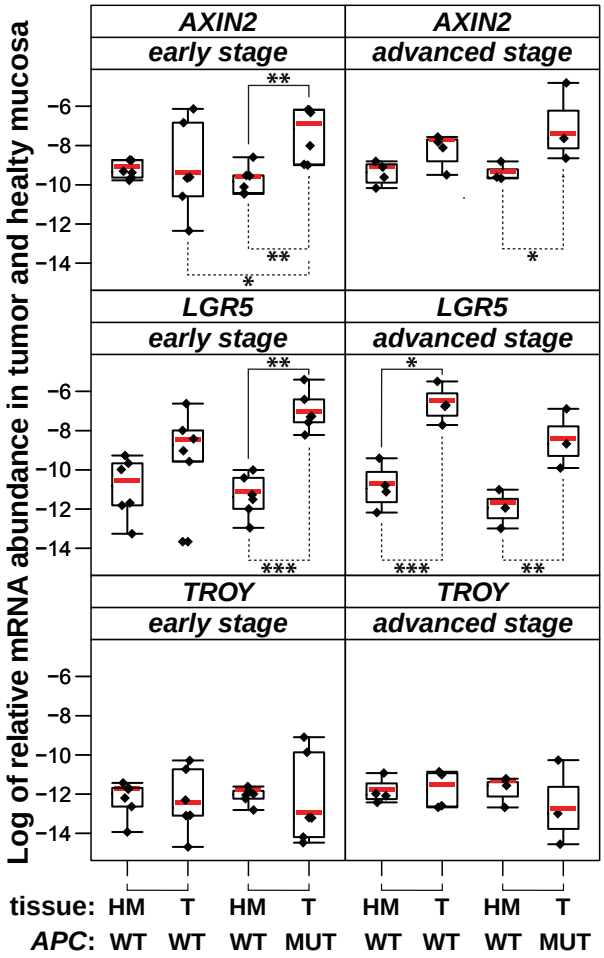
1. Kim TH, Barrera LO, Zheng M, et al. A high-resolution map of active promoters in the human genome. Nature 2005;436:876-80.
2. Scacheri PC, Crawford GE, Davis S. Statistics for ChIP-chip and DNase hypersensitivity experiments on NimbleGen arrays. Methods Enzymol 2006;411:270-82.
3. Tamai K, Zeng X, Liu C, et al. A mechanism for Wnt coreceptor activation. Mol Cell 2004;13:149-56.
4. Ootani A, Li X, Sangiorgi E, et al. Sustained in vitro intestinal epithelial culture within a Wnt-dependent stem cell niche. Nature medicine 2009;15:701-6.
5. Yang XW, Model P, Heintz N. Homologous recombination based modification in Escherichia coli and germline transmission in transgenic mice of a bacterial artificial chromosome. Nature biotechnology 1997;15:859-65.
6. Sato T, van Es JH, Snippert HJ, et al. Paneth cells constitute the niche for Lgr5 stem cells in intestinal crypts. Nature 2011;469:415-8.
7. Powell AE, Wang Y, Li Y, et al. The pan-ErbB negative regulator Lrig1 is an intestinal stem cell marker that functions as a tumor suppressor. Cell 2012;149:146-58.
8. Miyoshi Y, Nagase H, Ando H, et al. Somatic mutations of the APC gene in colorectal tumors: mutation cluster region in the APC gene. Human molecular genetics 1992;1:229-33.
9. Smith G, Carey FA, Beattie J, et al. Mutations in APC, Kirsten-ras, and p53--alternative genetic pathways to colorectal cancer. Proc Natl Acad Sci U S A 2002;99:9433-8.
10. Lustig B, Jerchow B, Sachs M, et al. Negative feedback loop of Wnt signaling through upregulation of conductin/axin2 in colorectal and liver tumors. Mol Cell Biol 2002;22:1184-93.
11. Cattaneo E, Laczko E, Buffoli F, et al. Preinvasive colorectal lesion transcriptomes correlate with endoscopic morphology (polypoid vs. nonpolypoid). EMBO Mol Med 2011;3:334-47.
12. Sato T, Vries RG, Snippert HJ, et al. Single Lgr5 stem cells build crypt-villus structures in vitro without a mesenchymal niche. Nature 2009;459:262-5.
13. Kojima T, Morikawa Y, Copeland NG, et al. TROY, a newly identified member of the tumor necrosis factor receptor superfamily, exhibits a homology with Edar and is expressed in embryonic skin and hair follicles. The Journal of biological chemistry 2000;275:20742-7.
14. Pispa J, Mikkola ML, Mustonen T, et al. Ectodysplasin, Edar and TNFRSF19 are expressed in complementary and overlapping patterns during mouse embryogenesis. Gene expression patterns 2003;3:675-9.
15. Li Q, Lau A, Morris TJ, et al. A syntaxin 1, Galpha(o), and N-type calcium channel complex at a presynaptic nerve terminal: analysis by quantitative immunocolocalization. The Journal of neuroscience : the official journal of the Society for Neuroscience 2004;24:4070-81.
16. Schlemper RJ, Riddell RH, Kato Y, et al. The Vienna classification of gastrointestinal epithelial neoplasia. Gut 2000;47:251-5.
17. Forbes SA, Tang G, Bindal N, et al. COSMIC (the Catalogue of Somatic Mutations in Cancer): a resource to investigate acquired mutations in human cancer. Nucleic acids research 2010;38:D652-7.
18. Ramensky V, Bork P, Sunyaev S. Human non-synonymous SNPs: server and survey. Nucleic acids research 2002;30:3894-900.
19. Segditsas S, Rowan AJ, Howarth K, et al. APC and the three-hit hypothesis. Oncogene 2009;28:146-55.

Supplemental Figure S1

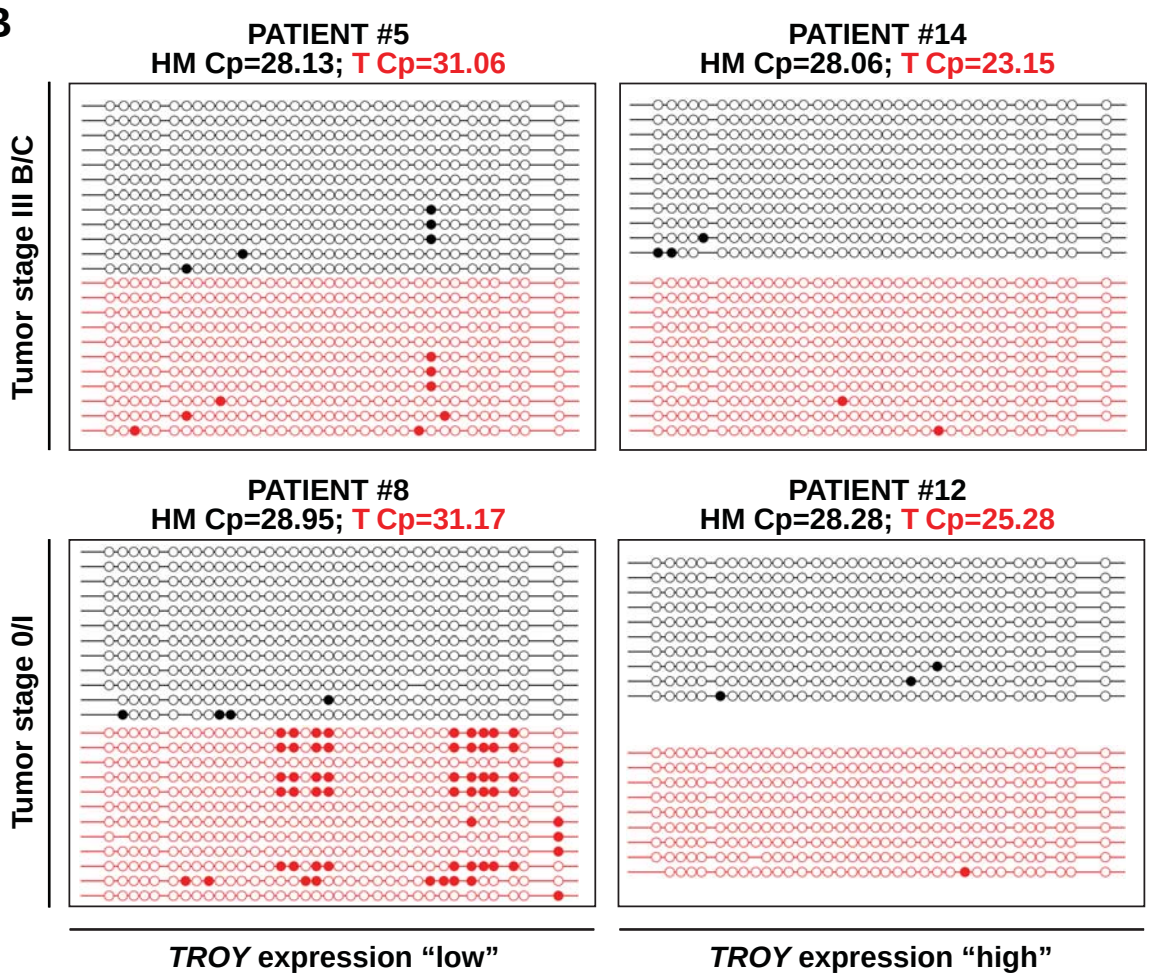


Supplemental Figure S2

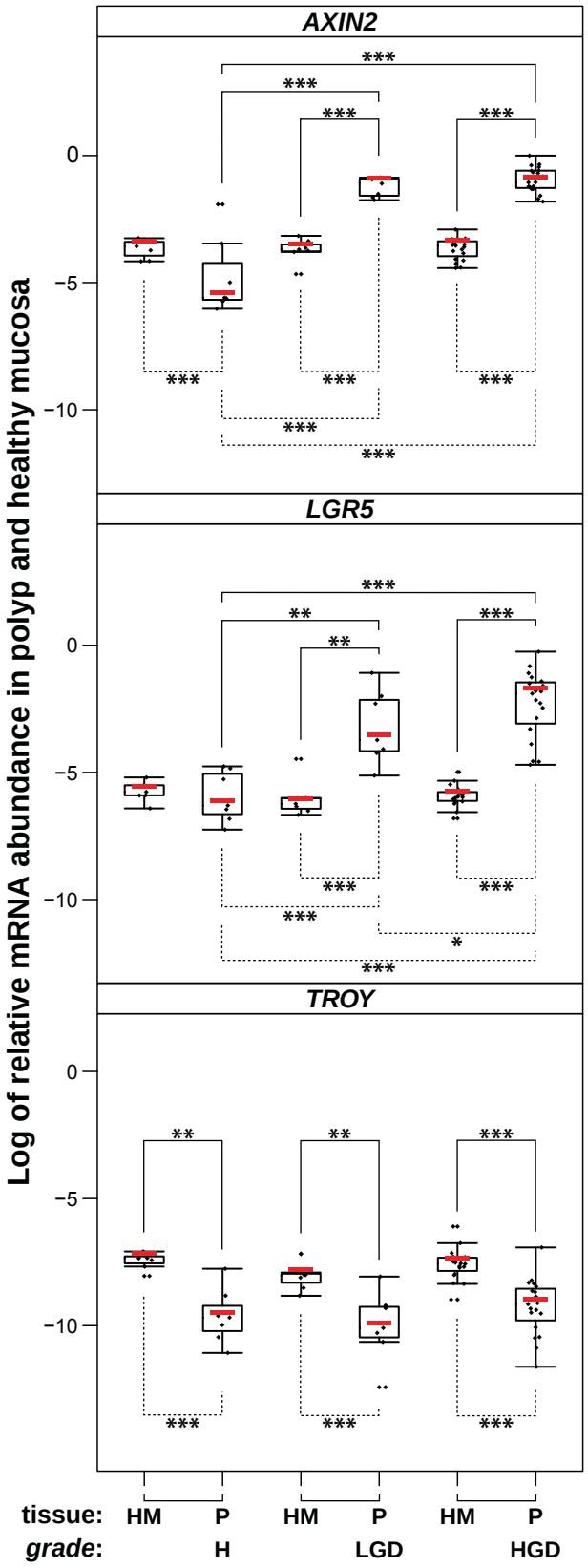
A



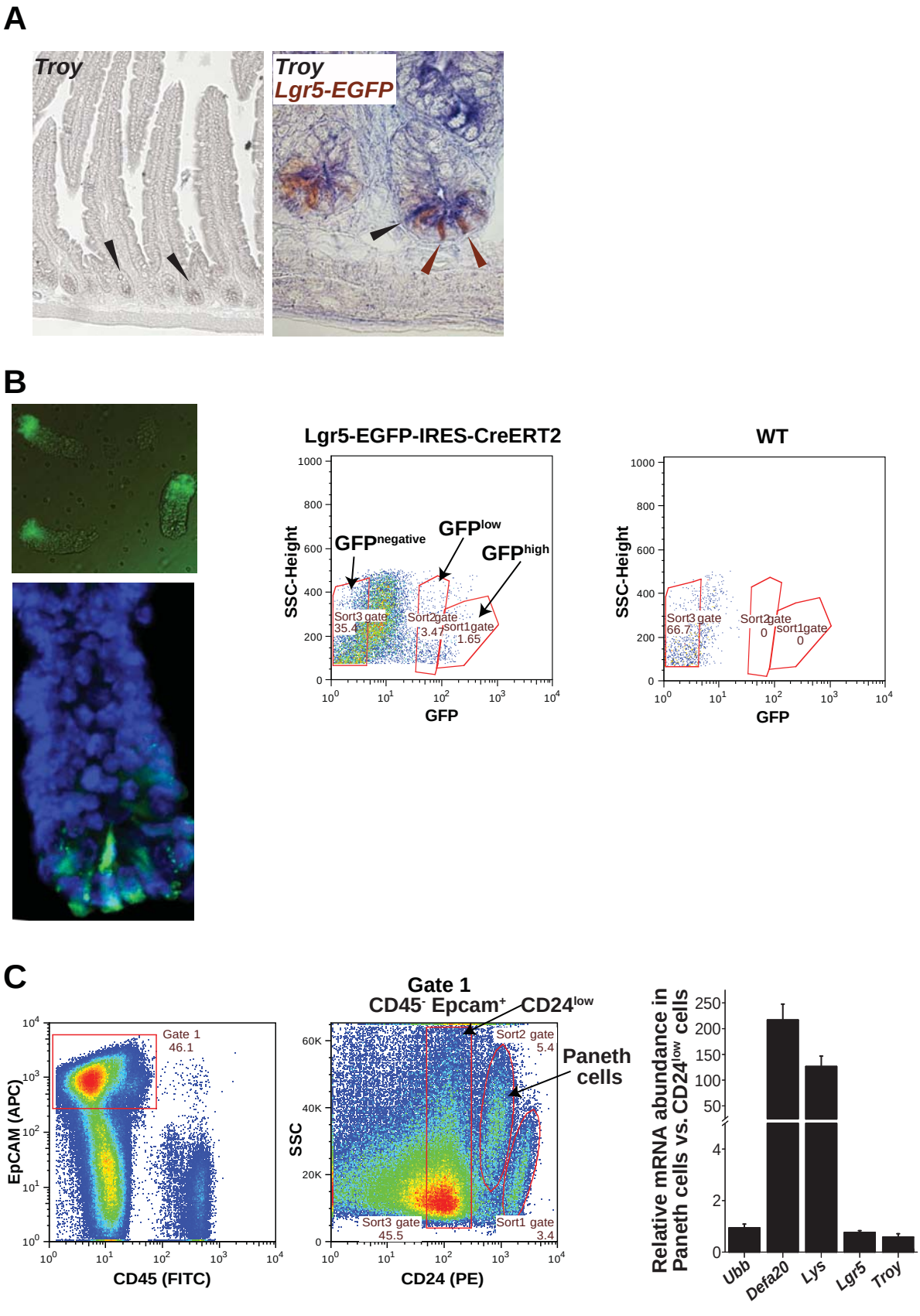
B



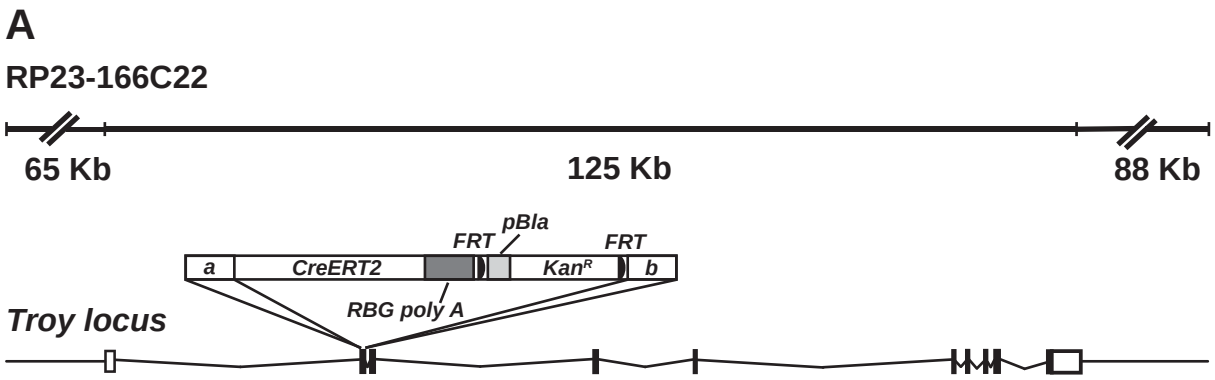
Supplemental Figure S3

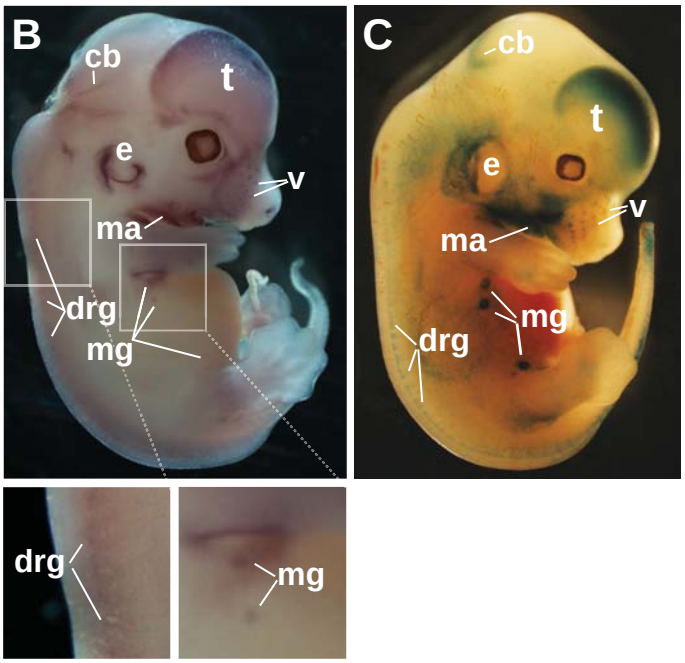


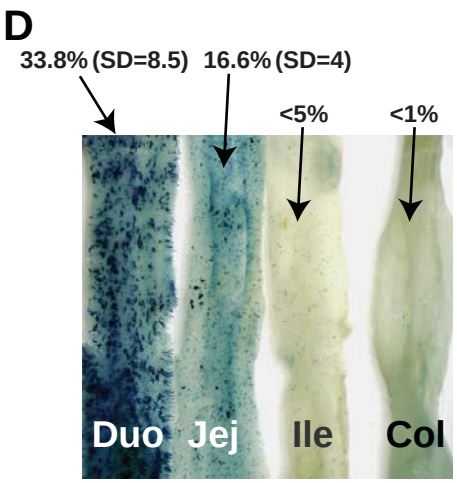
Supplemental Figure S4

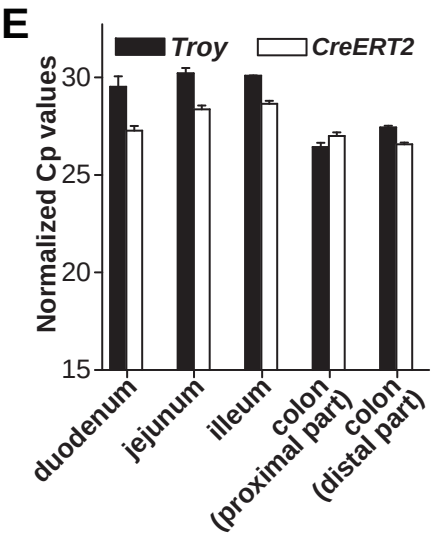


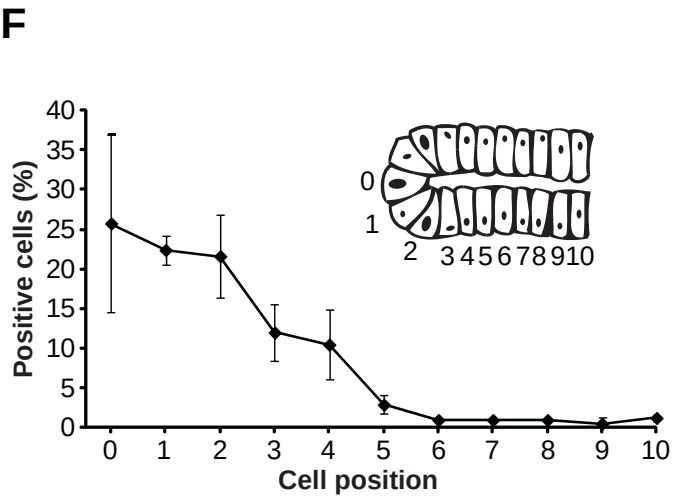
Supplemental Figure S5

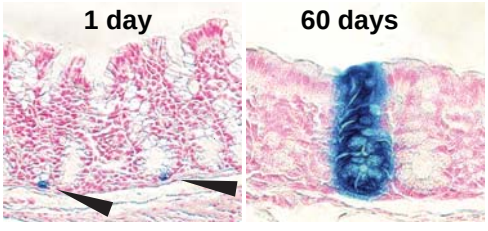




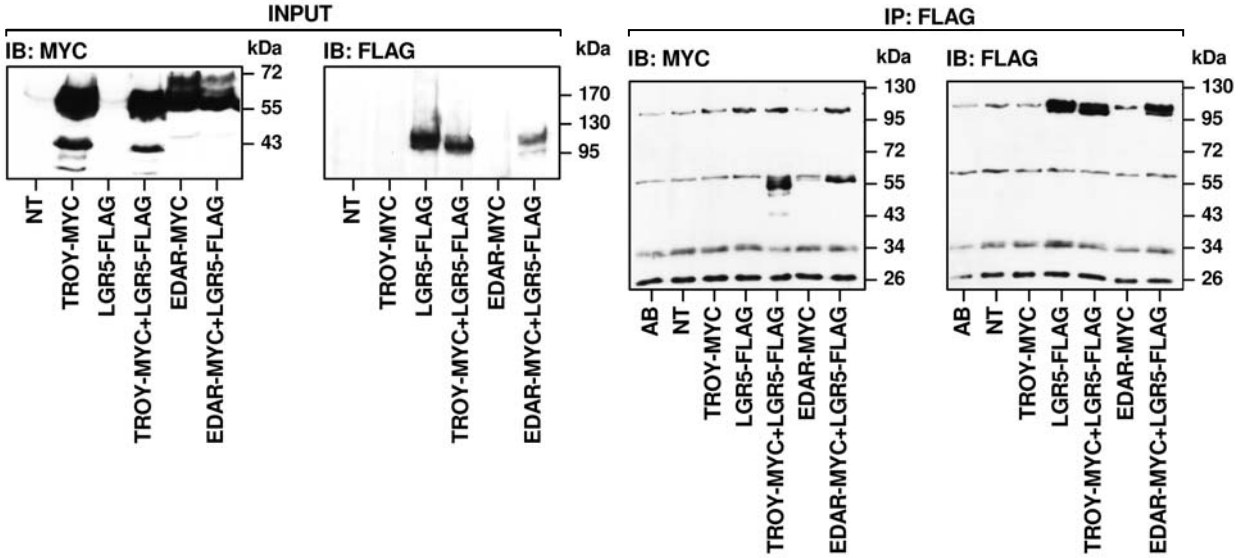




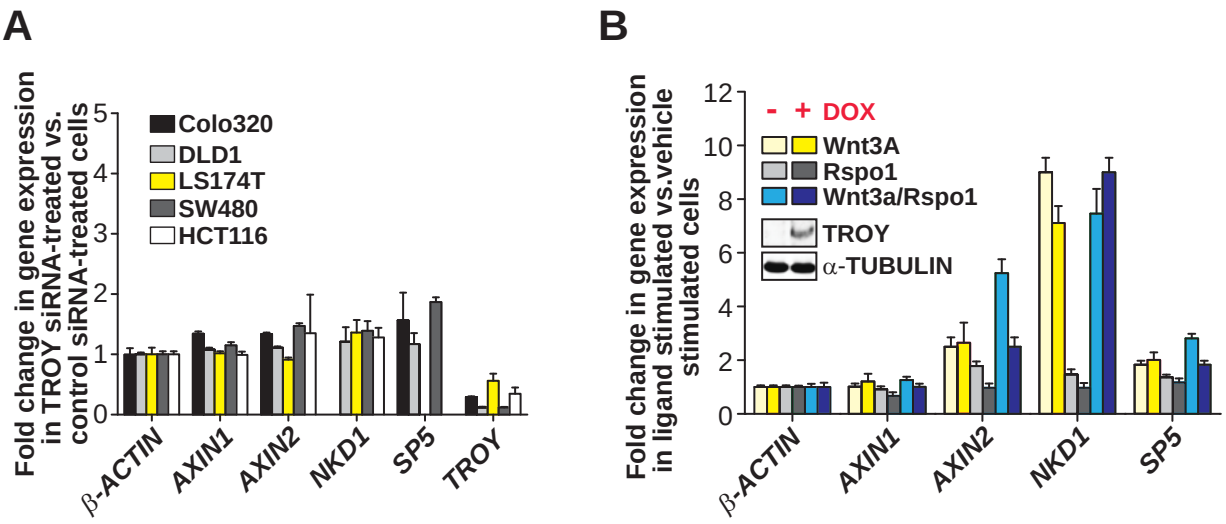




Supplemental Figure S6

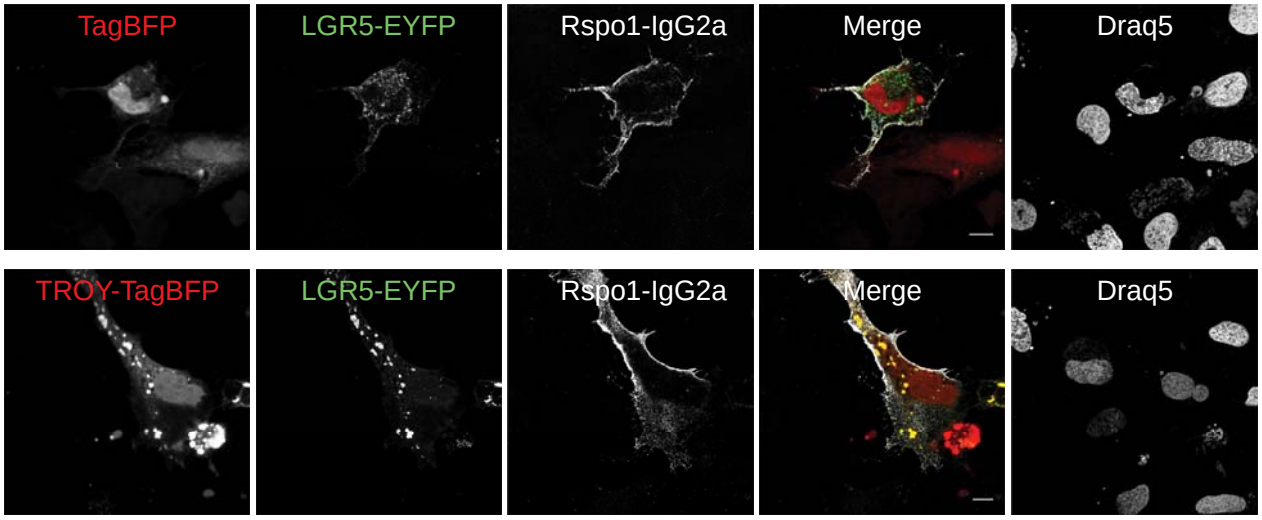


Supplemental Figure S7

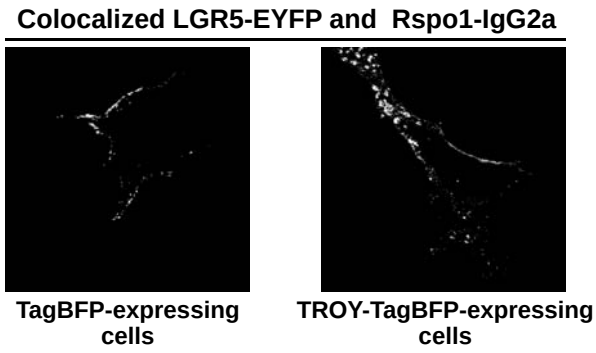


Supplemental Figure S8

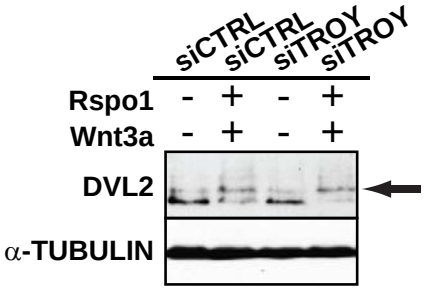
A



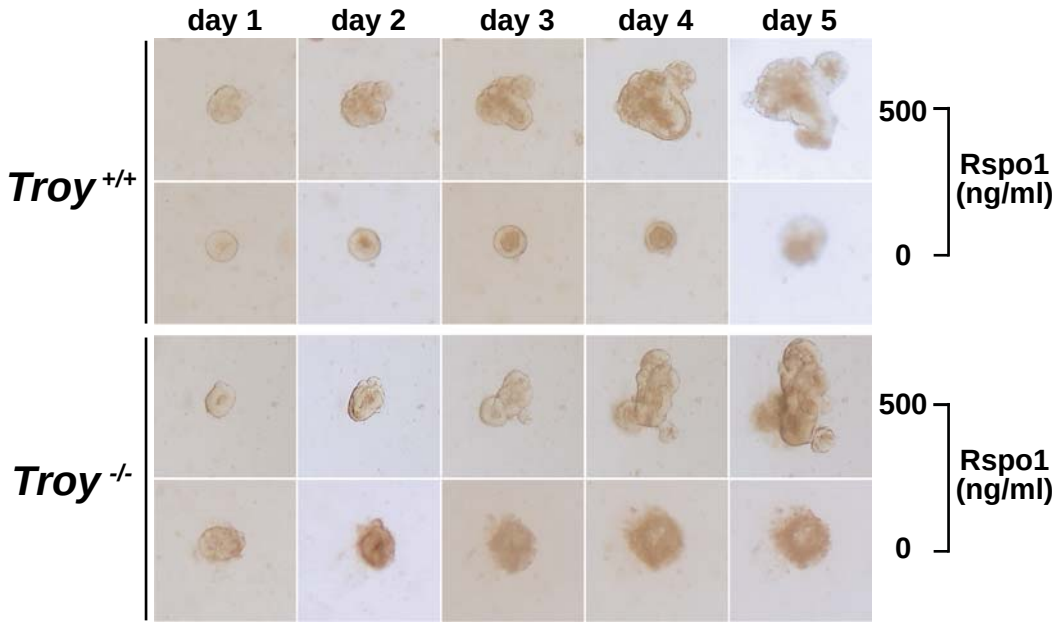
B



C



Supplemental Figure S9



Supplemental Table S1

Gene	Organism	Sequence	Application
β-ACTIN	Human	GGCATCCTCACCCTGAAGTA AGGTGTGGTGCCAGATTTTC	qRT PCR/ChIP
β-Actin	Mouse	GATCTGGCACCACACCTTCT GGGGTGTTGAAGGTCTCAAA	qRT PCR
β-catenin	Human	TTCCAGACACGCTATCATGC AATCCACTGGTGAACCAAGC	qRT PCR
AXIN1	Human	GAAGGTGAGGACGGCGATCCAT AGGCACCTGGCACCTCGGTGC	qRT PCR
Axin1	Mouse	ACCCAGTACCACAGAGGACG CTGCTTCCTCAACCCAGAAG	qRT PCR
AXIN2	Human	CTGGCTTTGGTGAACTGTTG AGTTGCTCACAGCCAAGACA	qRT PCR
Axin2	Mouse	GGGGGAAAACACAGCTTACA TCTTCATTCAAGGTGGGGAG	qRT PCR
Bmi1	Mouse	TGTGTCCTGTGTGGAGGGTA TTGAAAAGCCCTGGGACTAA	qRT PCR
Cre	P1 phage	GCACTGATTTCGACCAGGTT GCTAACCAGCGTTTTCGTTC	qRT PCR/genotyping
c-MYC	Human	CTCCTGGCAAAAGGTCAGAG TCGGTTGTTGCTGATCTGTC	ChIP
Defensin α 20	Mouse	TGGGACCTGCTCAGGACGACT TCATCTGCATGTTCAGTGGCGG	qRT PCR
LGR5	Human	CTCTTCCTCAAACCGTCTGC GATCGGAGGCTAAGCAACTG	qRT PCR
LGR5	Human	GTGAAGGAAAAGGGTGTCCA ATGTGCCTTCCTTCATGTCC	ChIP
Lgr5	Mouse	CCTGTCCAGGCTTTCAGAAG CTGTGGAGTCCATCAAAGCA	qRT PCR
Lysozyme	Mouse	CCTGACTCTGGGACTCCTCCTGCT CTAAACACACCCAGTCGGCCAGGC	qRT PCR
NKD1	Human	CGCCGGGATAGAAAACTACA CTGGAGCTCTGAGACCTTGG	qRT PCR
NKD1	Human	GACCTCCCCAGACAAAACAA TCAGCCAGTCTCTGGGATCT	ChIP
Nkd1	Mouse	AGGACGACTTCCCCCTAGAA TGCAGCAAGCTGGTAATGTC	qRT PCR
SP5	Human	ACTTTGCGCAGTACCAGAGC ACGTCTTCCCGTACACCTTG	qRT PCR
SP5	Human	TCCAGACCAACAAACACACC GCTTCAGGATCACCTCCAAG	ChIP
Sp5	Mouse	ACTCACTGCAGGCCTTCCT TCCAAGGGTGGAAAAGTCTG	qRT PCR
TROY	Human	CTATGGGGAGGATGCACAGT TCTCCACAAGGCACACACTC	qRT PCR
TROY	Human	TTTCATCTCCCTGCTCGTCT TGCGAAAAATGCAGTGAAAG	ChIP
Troy	Mouse	GCTCAGGATGCTCAAAGGAC CCAGACACCAAGACTGCTCA	qRT PCR
Troy locus	Mouse	TTGCATGCTGTGCAGAGACG CACCTCAGTGTGGCATCGAC	qRT PCR/genotyping
UBB	Human	GCTTTGTTGGGTGAGCTTGT TCACGAAGATCTGCATTTTGA	qRT PCR
Ubb	Mouse	ATGTGAAGGCCAAGATCCAG TAATAGCCACCCCTCAGACG	qRT PCR

Supplemental Table S2

Clinical and histopathological features of colorectal cancer patients (*n=20*)	
	Total N (%)
No. of patients	20
Primary tumor duplicity	1 (5)
Total No. of tumors included in the study	21
Gender	
Male/Female	17/3
Age, Years	
Median	64
Range	45-86
≥ 65 years	9 (45)
Primary tumor location	
left-sided	10 (50)
right-sided	10 (50)
Metastatic disease	
Synchronous	8 (40)
Location of metastasis	
Liver	5 (25)
lymph nodes	8 (25)
Other	1 (5)
Histological differentiation level	
G1	2 (10)
G2-3	19 (90)

Supplemental Table S3

Clinical and histopathological features of patients with precancerous lesions (*n=35*)	
	Total N (%)
Total no. of lesions included in the study	35
Gender	
Male/Female	35/0
Age, Years	
Median	66
Range	38-83
≥ 65 years	21 (60)
Colon segment involved	
left-sided	29 (83)
right-sided	6 (17)
Histological examination	
Hyperplasia (H)	7 (20)
Low grade dysplasia (LGD)	12 (34)
High grade dysplasia (HGD)	16 (46)

Supplemental Table S4

Gene-specific primers			
Primer ID	Primer sequence	Product size (nucleotides)	Amplified region
APCex18/1T7	taatacgactcactatagTGTTACTGCATACACATTGTGACC	567	APC, exon 18
APCex18/1RP	tgaaacagctatgaccatgTGACCTATTATCATCATGTCGATTG		c.1959-55bp[2] – c.2433[1]
APCex18/2T7	taatacgactcactatagTCCCAAGGCATCTCATCGTAG	567	APC, exon 18
APCex18/2RP	tgaaacagctatgaccatgTGTATTCTAATTTGGCATAAGGCATAG		c.2340 – c.2869[1]
APCex18/3T7	taatacgactcactatagTGCCCATACACATTCAAACAC	552	APC, exon 18
APCex18/3RP	tgaaacagctatgaccatgCACATTCCTGCTGTCCAAAATG		c.2781 – c.3295[1]
APCex18/4T7	taatacgactcactatagAAAGTGAGCAAAGACAATCAAGG	589	APC, exon 18
APCex18/4RP	tgaaacagctatgaccatgCCTTTTGAGGCTGACCACTTC		c.3185 – c.3736[1]
APCex18/5T7	taatacgactcactatagCCGAACATATGTCTTCAAGCAGTG	545	APC, exon 18
APCex18/5RP	tgaaacagctatgaccatgACATAGTGTTCAGGTGGACTTTTGG		c.3623 - c.4130[1]
APCex18/6T7	taatacgactcactatagATCAGCCAGGCACAAAGC	548	APC, exon 18
APCex18/6RP	tgaaacagctatgaccatgAAATGGCTCATCGAGGCTCAG		c.4035 - c.4545[1]
APCex18/7T7	taatacgactcactatagAGAGGGTCCAGGTTCTTCCAG	552	APC, exon 18
APCex18/7RP	tgaaacagctatgaccatgAGGTGTCCCTTCAACACAATAC		c.4430 - c.4944[1]
CTNNB1ex3T7	taatacgactcactatagTGCTTTTCTTGGCTGTCTTTCAG	571	CTNNB1, exon 3 including intron-exon boundaries;
CTNNB1ex3RP	tgaaacagctatgaccatgTCCACAGTTCAGCATTTACCTAAG		c.1-134bp[3] – c.241+172bp[4]
CTNNB1ex4T7	taatacgactcactatagTTGTGGTGAAGAAAAGAGAGTAATAGC	486	CTNNB1, exon 4 including intron-exon boundaries;
CTNNB1ex4RP	tgaaacagctatgaccatgTGGTATTGGGTAGACATTCTGAAAC		c.242-111bp[5] – c.495+84bp[6]

Supplemental Table S5

Mutation analysis of *APC* in human sporadic colorectal carcinomas							
Stage	**Patient No.**	**Mutation in genomic DNA[1]**	**Change in APC protein**	**Mutation type**	**Mutation in genomic DNA[1]**	**Change in APC protein**	**Mutation type**
0	8	c.4666_4667insA	p.T1556fs*3	Insertion - Frameshift	c.3095C>T	p. S1032L[2]	Substitution - Missense
	10	c.2956_2963delTATTCTGA	p.Y986fs*2	Deletion - Frameshift	c.4474_4475insT	p.A1492fs*22	Insertion - Frameshift
I	12	c.3183_3187delACAAA	p.Q1062fs*1	Deletion - Frameshift	c.4326T>A	p.Pro1442=	Substitution - Silent
	15	c.3910delA	p.I1303fs*1	Deletion - Frameshift	c.4479 A/A (n.a.)[4]	---	---
	20	c.4666_4667insA	p.T1556fs*3	Insertion - Frameshift	c.4479 G/A (wt)[4]	---	---
II	1	c.4926T>A	p.Y1642*	Substitution - Nonsense	c.4479 G/A>A/A (LOH)[4]	---	---
	6	c.3095C>T	p. S1032L[2]	Substitution - Missense	c.4479 A/A (n.a.)[4]	---	---
III	2	n.d.[5]	---	---	c.4479 G/A>A/A (LOH)[4,5]	---	---
	5	c.3340C>T	p. R1114*	Substitution - Nonsense	c.3961A>G	p. S1321G[3]	Substitution - Missense
	18	n.d.[5]	---	---	c.4479 G/A>A/A (LOH)[4,5]	---	---
	14	c.4348C>T	p.R1450*	Substitution - Nonsense	c.4479 G/A (wt)[4]	---	---

Supplemental Table S6

Linear model *ΔCp ~ patient + tissue / (stage * mutation)*					**Wilcoxon's rank-sum test**	
Early stage cancer					***Early stage cances***	
Gene	**ΔΔCp**	**FC**	**mean ΔCp**	**p-value**	**Gene**	**p-value**
APC wt tumor vs. healthy surrounding mucosa						
LGR5	-1.8	3.48	9.36	0.032	*LGR5*	0.09
TROY	0.07	0.95	11.92	0.91	*TROY*	0.82
AXIN2	-0.07	1.05	8.71	0.91	*AXIN2*	0.70
APC mut tumor vs. healthy surrounding mucosa						
LGR5	-4.33	20.05	9.36	< 0.0001	*LGR5*	0.0022
AXIN2	-2.35	5.09	8.71	0.002	*AXIN2*	0.0087
TROY	0.27	0.83	11.92	0.68	*TROY*	0.39
APC mut tumor vs. APC wt tumor						
AXIN2	-2.27	4.83	8.71	0.027	*AXIN2*	0.18
LGR5	-2.53	5.77	9.36	0.032	*LGR5*	0.041
TROY	0.19	0.87	11.92	0.83	*TROY*	0.82
Advanced stage cancer					***Advanced stage cancer***	
Gene	**ΔΔCp**	**□C**	**mean ΔCp**	**p-value**	**Gene**	**p-value**
APC wt tumor vs. healthy surrounding mucosa						
LGR5	-4.13	17.47	9.36	0.00072	*LGR5*	0.029
AXIN2	-1.17	2.26	8.71	0.22	*AXIN2*	0.11
TROY	0.26	0.83	11.92	0.77	*TROY*	0.89
APC mut tumor vs. healthy surrounding mucosa						
LGR5	-3.47	11.05	9.36	0.0049	*LGR5*	0.10
AXIN2	-2.34	5.06	8.71	0.024	*AXIN2*	0.10
TROY	0.76	0.59	11.92	0.41	*TROY*	0.70
APC mut tumor vs. APC wt tumor						
AXIN2	-1.16	2.24	8.71	0.4	*AXIN2*	0.63
LGR5	0.66	0.63	9.36	0.68	*LGR5*	0.11
TROY	0.5	0.71	11.92	0.7	*TROY*	0.63

Supplemental Table S7

Linear model *ΔCp ~ tissue_stage + patient*					Wilcoxon´s rank-sum test	
Precancerous lesions of the colon						
Gene	**ΔΔCp**	**FC**	**mean ΔCp**	**p-value**	**Gene**	**p-value**
Polyp hyperplasia vs. healthy mucosa						
TROY	1.98	0.25	8.58	< 0.0001	*TROY*	0.0012
AXIN2	1.09	0.47	2.75	< 0.0001	*AXIN2*	0.097
LGR5	0.05	0.97	4.60	0.91	*LGR5*	0.71
Polyp low grade dysplasia vs. healthy mucosa						
AXIN2	-2.45	5.47	2.75	< 0.0001	*AXIN2*	0.00058
LGR5	-2.69	6.46	4.60	< 0.0001	*LGR5*	0.0012
TROY	2.31	0.20	8.58	< 0.0001	*TROY*	0.0041
Polyp high grade dysplasia vs. healthy mucosa						
AXIN2	-2.73	6.63	2.75	< 0.0001	*AXIN2*	< 0.0001
LGR5	-3.59	12.00	4.60	< 0.0001	*LGR5*	< 0.0001
TROY	1.60	0.33	8.58	< 0.0001	*TROY*	< 0.0001
Polyp low grade dysplasia vs. polyp hyperplasia						
AXIN2	-3.54	11.62	2.75	< 0.0001	*AXIN2*	0.00058
LGR5	-2.74	6.67	4.60	< 0.0001	*LGR5*	0.0023
TROY	0.33	0.80	8.58	0.50	*TROY*	0.71
Polyp high grade dysplasia vs. polyp hyperplasia						
AXIN2	-3.82	14.10	2.75	< 0.0001	*AXIN2*	< 0.0001
LGR5	-3.63	12.39	4.60	< 0.0001	*LGR5*	< 0.0001
TROY	-0.38	1.30	8.58	0.35	*TROY*	0.33
Polyp high grade dysplasia vs. polyp low grade dysplasia						
LGR5	-0.89	1.86	4.60	0.044	*LGR5*	0.19
TROY	-0.71	1.63	8.58	0.087	*TROY*	0.25
AXIN2	-0.28	1.21	2.75	0.29	*AXIN2*	0.21

Mist1 expressing gastric stem cells maintain the normal and neoplastic gastric epithelium and are supported by a perivascular stem cell niche

Similarly to the identification of SCs in the intestinal epithelium, description of unique markers of gastric epithelial SCs represents one of the main topics in GIT research. Determination of unique markers of gastric SCs enables their monitoring and evaluation of their tumor-originating potential. Direct focusing on GCSCs allows development of advanced "tailored" treatment that can reduce harmful side effects and extends life expectance of patients. Gastric SCs were previously described by various markers depending on their contribution to the pool of corpus or pyloric epithelial cells and proliferation rate. Among them, $Mist1^+$ chief cells were previously described as $Lgr5^+$ cells residing at the bottom of the gastric glands (Nam et al. 2010; Stange et al. 2013). Chief cells alias zymogenic cells producing digestive enzymes are, similarly to acid producing parietal cells, the matured descendants of mucous neck cells secreting mucins. It has been shown that Mist1 is the bHLH transcription factor activating the Mindbomb1 (Mib1) production, that drives gastric epithelial cell to secretory fate (Capoccia et al. 2013). In case of Mist1 loss, gastric epithelium succumbs to atrophy and metaplasia (Ramsey et al. 2007; Bredemeyer et al. 2009; Lennerz et al. 2010). Interestingly, matured $Mist1^+$ chief cell is capable to undergo dedifferentiation and regain its stemness in case of epithelial injury (Nam et al. 2010). Although many studies described characteristics and behavior of $Mist1^+$ gland-bottom-residing chief cells (Ramsey et al. 2007; Nam et al. 2010; Goldenring et al. 2011; Choi et al. 2014), minimal effort was put on investigating the granule-free cells in the isthmus of the stomach corpus, that are also positive for Mist1 (Karam and Leblond 1993).

$Mist1^+$ isthmal cells were not noted for many years probably due to their slow proliferation and infrequency in the isthmus, which was somehow overshadowed by the numerous $Mist1^+$ chief population. Dividing only once in 5 days, $Mist1^+$ isthmal cells are extremely long-lived and able to expand bidirectionally, giving rise to all cell types in the gastric epithelium to colonize whole gland. In our recent publication, we showed that $Mist1^+$ SCs in the isthmus are different from $Lgr5^+$, $Troy^+$ $Mist1^+$ chief cells. Mist1 was described previously also as a marker and indispensable effector in differentiation of plasma cells (Capoccia et al. 2011), pancreatic acinar cells (Direnzo et al. 2012), lactacing mammary epithelial cells and even in Paneth cells (Zhao et al. 2006; King et al. 2013). Finally, Mist1 became a representative of a class of transcription factors named scaling

factors (Pin 2012). These transcription factors are expressed uniquely in differentiated cells, where they enhance rather than initiate existing transcriptional activity. Our notion, that Mist1 is also a marker of quiescent SCs in isthmus of the gastric corpus is strikingly challenging the presumable function of scaling factors.

Mist1$^+$ chief cells were previously depicted as originators of spasmolytic polypeptide-expressing metaplasia (SPEM). In SPEM, they re-express markers of their progenitors, mucous neck cells. SPEM may prograde to gastric dysplasia and carcinoma (Nam et al. 2007; Lennerz et al. 2010). Previous studies, which described Mist1 expression nearly exclusively in chief cells, observed loss of Mist1 in all gastric carcinoma (Lennerz et al. 2010). Discovery of Mist1 as a marker of gastric SCs in the corpus isthmus refuted this postulate. We found Mist1$^+$ isthmal cells as the originators of both IGC and DGC. Development of IGC was simulated by pathological activation of Kras leading to the increased numbers of actively proliferating cells with appearance of dysplastic and metaplastic cells. Crossbreeding of Mist1-Cre mice with mice harboring the conditional APC allele showed no dysplasia. We presumed, that IGC is a Wnt signaling independent event. Indeed, experiments with Mist1$^+$ isthmal organoids showed Wnt3a independency and preference for the Notch ligand Jagged. In our study, DGC in murine Mist1$^+$ cells was initiated by conditional loss of *Cdh1* gene encoding E-cadherin. E-cadherin maintains the stability of epithelial architecture, cell polarity and differentiation (Stemmler 2008; van Roy and Berx 2008). A germ line heterozygous mutation in the *CDH1* gene was found in 30 % cases of hereditary DGC, frequently followed by LOH and methylation or mutation of the second wt allele (Barber et al. 2008; Oliveira et al. 2009). *Cdh1* ablation leads to tumor invasion and progression (Vleminckx et al. 1991; Katoh 2005). We noted, that loss of E-cadherin is not efficient for adenoma development, therefore we introduced chronic inflammatory agent, *H. felis* as a murine variant of human *H. pylori*. *H. pylori* infection facilitates epigenetic alteration of many genes including *Cdh1* (Perri et al. 2007). In condition of permanent inflammation, metaplasia developed in persistent and progressive manner.

Independency of stomach organoids derived from the corpus on Wnt3a implied that the cells produce their own Wnt ligand that participate in the maintenance of the isthmal SC compartment. From 18 investigated Wnt ligands, non-canonical Wnt5a was identified as highly expressed in the corpus isthmus stroma. Wnt5a expression was detected in Cxcr4$^+$ cells in the isthmus adjacent to Mist1$^+$ cells. Subsequent experiments uncovered the

signaling cascade initiated by activation of the BMP pathway by BMPR2. The *BMPR2* gene is expressed in $CD31^+$ endomucin producing endothelial cells which then stimulate $Cxcr4^+$ intraepithelial gastric innate lymphoid cells (ILCs) by chemokine Cxcl12 production. The stimulation of ILCs, heterogenous population of immune cells, by Cxcl12 leads to the Wnt5a production supporting $Mist1^+$ cells in the isthmus. The Cxcl12/Cxcr4 axis was previously described as the activator of signaling pathways related to chemotaxis, proliferation and cell survival (Teicher and Fricker 2010). The pathways are involved in hematopoiesis, SC maintenance and vascularization of GIT during embryonic development (Tachibana et al. 1998; Sugiyama et al. 2006). Additionally, Cxcl12/Cxcr4 axis functions as the main actor in various types of cancers such as breast (Zhou et al. 2009), prostate (Engl et al. 2006), or gastric cancer (Yasumoto et al. 2006) with features of robust tumor progression and invasion (Sun et al. 2010; Wu et al. 2013b). We showed possible contribution of Cxcl12/Cxcr4 signaling to DGC by bone marrow transplantation from mice with ablated Wnt5a in ILCs to DGC affected animal. Wnt5a produced by $Cxcr4^+$ ILCs activated the small GTPase Ras homolog gene family member A (RhoA). This protein was shown to inhibit anoikis in gastric cancer, thus contributing to DGC (Cai et al. 2008; Liu et al. 2013). In other studies, activating mutations in the *RHOA* gene also supports DGC development (Kakiuchi et al. 2014; Wang et al. 2014). RhoA support to in vitro cultured $Mist1^+$ SCs with ablated E-cadherin resulted in longer-lasting viability. We concluded that RhoA and Wnt5a definitely contribute to the onset of DGC.

In our recent work, we postulated the new marker of quiescent SCs in the stomach isthmus, Mist1. The marker was previously described in the bottom of the gastric glands only, directing the descendants of the mucous neck progenitors to secretory chief cells. In the intestine, a differentiating cell is destined to become secretory cell by blocking Notch signaling. The active Notch pathway suppresses *Atoh1*, which functions as the inducer of secretory markers (Ueo et al. 2012). Although *Mist1*, whose product is expressed in stomach chief cells, encodes – similarly to the Notch effectors – a bHLH-type transcription factor, its contribution to the regulation of Notch target genes was not observed. Moreover, in chief cells Mist1 directs *Mib1* transcription leading the secretory cell lineage, even though, in the Notch-independent manner. On the other hand, in the corpus isthmus the increased Notch activity was detected, though SCs there were not previously identified as $Mist1^+$ (Capoccia et al. 2013). Our notions introduces a

hypothesis, that similarly to the intestine, Notch signaling in the stomach maintains stemness of SCs. Additionally, we identified Wnt5a as the regulator of the Mist1 SC niche. Moreover, Wnt5a is produced as the result of BMP and Cxcl12/Cxcr4 signaling. Finally, we elucidated contribution of these pathways to DGC development. Our work therefore ambitiously contributed to questions in the field of gastric SCs and gastric cancer development.

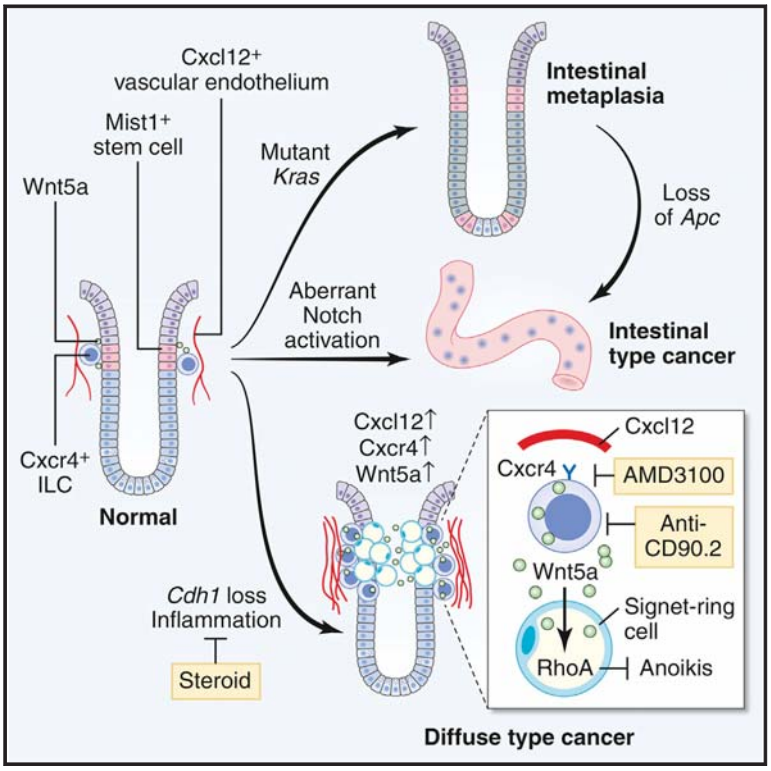
Author´s contribution: mouse - intraperitoneal injections, fixation and paraffin or O.C.T. embedding, tissue sectioning, X-gal staining, immunohistochemistry

Article

Cancer Cell

Mist1 Expressing Gastric Stem Cells Maintain the Normal and Neoplastic Gastric Epithelium and Are Supported by a Perivascular Stem Cell Niche

Graphical Abstract



Highlights

- Quiescent Mist1$^+$ stem cells reside in the corpus isthmus
- Mist1$^+$ stem cells are a cellular origin of gastric cancers
- Cxcl12/Cxcr4 perivascular niche supports isthmus stem cells
- Wnt5a from Cxcr4$^+$ ILCs promotes diffuse cancer development

Authors

Yoku Hayakawa, Hiroshi Ariyama, Jitka Stancikova, ..., Daniel L. Worthley, Vladimir Korinek, Timothy C. Wang

Correspondence

tcw21@columbia.edu

In Brief

Hayakawa et al. show that Cxcl12$^+$ endothelial cells and Cxcr4$^+$ gastric innate lymphoid cells (ILCs) form a perivascular niche to support diffuse-type gastric cancer (DGC) development from Mist1-expressing gastric stem cells through Wnt5a produced by ILCs. Targeting ILCs, Cxcr4, or Wnt5a inhibits DGC development.

Hayakawa et al., 2015, Cancer Cell *28*, 1–15
December 14, 2015 ©2015 Elsevier Inc.
http://dx.doi.org/10.1016/j.ccell.2015.10.003

Please cite this article in press as: Hayakawa et al., Mist1 Expressing Gastric Stem Cells Maintain the Normal and Neoplastic Gastric Epithelium and Are Supported by a Perivascular Stem Cell Niche, Cancer Cell (2015), http://dx.doi.org/10.1016/j.ccell.2015.10.003

Cancer Cell
Article

CellPress

Mist1 Expressing Gastric Stem Cells Maintain the Normal and Neoplastic Gastric Epithelium and Are Supported by a Perivascular Stem Cell Niche

Yoku Hayakawa,[1,12] Hiroshi Ariyama,[1,12] Jitka Stancikova,[2] Kosuke Sakitani,[1] Samuel Asfaha,[1] Bernhard W. Renz,[1,11] Zinaida A. Dubeykovskaya,[1] Wataru Shibata,[1] Hongshan Wang,[1] Christoph B. Westphalen,[1] Xiaowei Chen,[1] Yoshihiro Takemoto,[1] Woosook Kim,[1] Shradha S. Khurana,[1] Yagnesh Tailor,[1] Karan Nagar,[1] Hiroyuki Tomita,[3] Akira Hara,[3] Antonia R. Sepulveda,[4] Wanda Setlik,[5] Michael D. Gershon,[5] Subhrajit Saha,[6] Lei Ding,[7] Zeli Shen,[8] James G. Fox,[8] Richard A. Friedman,[9] Stephen F. Konieczny,[10] Daniel L. Worthley,[1] Vladimir Korinek,[2] and Timothy C. Wang[1,*]

[1]Division of Digestive and Liver Disease, Department of Medicine, Columbia University College of Physicians and Surgeons, New York, NY 10032, USA
[2]Department of Cell and Developmental Biology, Institute of Molecular Genetics, Academy of Sciences of the Czech Republic, Prague 14220, Czech Republic
[3]Department of Tumor Pathology, Gifu University Graduate School of Medicine, Gifu 501-1194, Japan
[4]Division of Clinical Pathology and Cell Biology, Department of Pathology, Columbia University College of Physicians and Surgeons, New York, NY 10032, USA
[5]Department of Pathology and Cell Biology, Columbia University College of Physicians and Surgeons, New York, NY 10032, USA
[6]Department of Radiation Oncology, Albert Einstein College of Medicine, Bronx, NY 10461, USA
[7]Departments of Rehabilitation and Regenerative Medicine and Microbiology and Immunology, Columbia University College of Physicians and Surgeons, New York, NY 10032, USA
[8]Division of Comparative Medicine, Massachusetts Institute of Technology, Cambridge, MA 02139, USA
[9]Herbert Irving Comprehensive Cancer Center Biomedical Informatics Shared Resource and Department of Biomedical Informatics, Columbia University College of Physicians and Surgeons, New York, NY 10032, USA
[10]Department of Biological Sciences and the Purdue Center for Cancer Research, Purdue University, West Lafayette, IN 47907, USA
[11]Department of General, Visceral, Transplantation, Vascular, and Thoracic Surgery, Hospital of the University of Munich, Munich 81377, Germany
[12]Co-first author
*Correspondence: tcw21@columbia.edu
http://dx.doi.org/10.1016/j.ccell.2015.10.003

SUMMARY

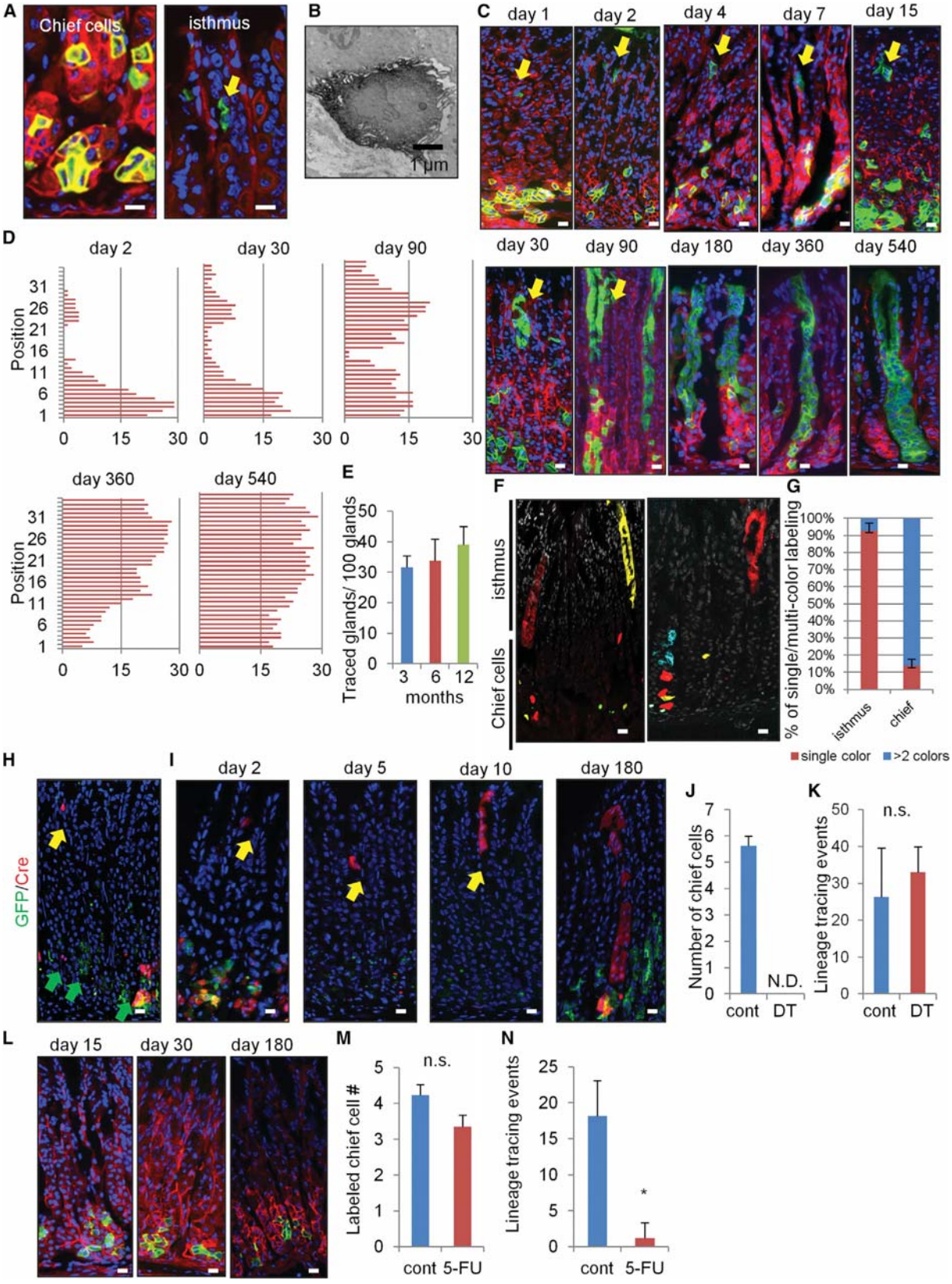
The regulation and stem cell origin of normal and neoplastic gastric glands are uncertain. Here, we show that Mist1 expression marks quiescent stem cells in the gastric corpus isthmus. Mist1$^+$ stem cells serve as a cell-of-origin for intestinal-type cancer with the combination of *Kras* and *Apc* mutation and for diffuse-type cancer with the loss of E-cadherin. Diffuse-type cancer development is dependent on inflammation mediated by Cxcl12$^+$ endothelial cells and Cxcr4$^+$ gastric innate lymphoid cells (ILCs). These cells form the perivascular gastric stem cell niche, and Wnt5a produced from ILCs activates RhoA to inhibit anoikis in the E-cadherin-depleted cells. Targeting Cxcr4, ILCs, or Wnt5a inhibits diffuse-type gastric carcinogenesis, providing targets within the neoplastic gastric stem cell niche.

INTRODUCTION

Gastric cancer is the third most frequent cause of cancer death worldwide. In the gastric corpus within the proximal stomach, the glands contain chief cells that are important for digestion, and parietal cells that are vital for acid production, controlled in part by enterochromaffin-like (ECL) cells. There are also intervening mucous neck cells, above which are the superficial pits that are lined by pit cell epithelium. Despite abundant literature on small intestinal stem cells (ISCs), an infrequent site of human

Significance

We identified a quiescent stem cell in the corpus isthmus, which can give rise to gastric cancer. We also discovered a Cxcl12/Cxcr4 perivascular niche in the stomach, which supports normal and neoplastic stem cells through Wnt5a production.



(legend on next page)

cancer, there have been relatively few studies addressing the stem cells that maintain the normal and neoplastic gastric epithelium.

Tissue stem cells maintain the integrity of rapidly proliferating tissues such as the gastrointestinal epithelium, residing within a stem cell niche. Replicative quiescence and a relatively undifferentiated morphology have generally been considered cardinal properties of adult stem cells (Malam and Cohn, 2014; Mills and Shivdasani, 2011). In the gastric corpus, earlier radiolabeling and electron microscopy studies suggest a single undifferentiated, ''granule free'' cell as the putative stem cell in the isthmus of each gastric unit of the mouse (Karam and Leblond, 1993; Mills and Shivdasani, 2011). Studies suggest that within the corpus isthmus, Sox2$^+$ cells may be long-lived stem cells, while Tff2$^+$ cells are relatively short-lived progenitors (Arnold et al., 2011; Quante et al., 2010). More recently, a ''reserve stem-like cell'' population expressing *Troy* or *Mist1* was postulated to reside at the base of corpus gland (Stange et al., 2013).

Gastric cancer is classified into an intestinal-type and a diffuse-type, and carcinogenesis in the stomach is strongly associated with chronic inflammation. Oncogenic mutations such as *Kras* and *Apc* targeted to gastric stem/progenitor cells led to intestinal-type metaplasia or dysplasia in mice (Barker et al., 2010; Okumura et al., 2010). By contrast, the E-cadherin gene (*CDH1)* is frequently mutated or downregulated in diffuse-type gastric cancer (DGC) (Guilford et al., 1998). In a rodent model, knock out of *Cdh1* was insufficient to initiate gastric tumors, but did predispose to the development of DGC with signet-ring cells following additional genetic events (Shimada et al., 2012). Studies of prophylactic gastrectomy specimens from germline carriers of *CDH1* mutations have revealed that DGC appears to arise in the proximal gastric isthmus (Humar et al., 2007), but the cellular origin of all gastric cancers remains unknown.

Tissue stem cells and cancer development are maintained by their niche. The Wnt signaling pathway plays a central role in the maintenance of ISCs, which are supported by the ISC niche, including both Paneth cells (Sato et al., 2011) and the surrounding mesenchyme (Farin et al., 2012). However, the gastric corpus does not normally depend on the Wnt pathway (Mills and Shivdasani, 2011), and therefore the critical pathway regulating corpus stem cell niche is largely unknown. In the gut mesenchyme, several cell types including pericytes, nerves, or mesothelial cells (Miyoshi et al., 2012; Worthley et al., 2015; Zhao et al., 2014) are reported to maintain tissue stem cells and contribute to cancer development. In the bone marrow, perivascular stromal cells including endothelial cells, Cxcl12-abundant reticular (CAR) cells, and nerves, promote hematopoietic stem cell (HSC) maintenance and neoplastic changes through the production of cytokines or chemokines such as Cxcl12 or SCF (Hanoun et al., 2014; Mendelson and Frenette, 2014; Pitt et al., 2015). However, whether such stromal factors play a role in the normal and neoplastic gut stem cell niche remains unclear.

RESULTS

Mist1 Is a Marker of Quiescent Stem Cells in the Gastric Corpus Isthmus

We utilized *Mist1*-CreERT2 knockin mice, where Cre recombinase is induced by tamoxifen (TAM) in cells expressing a bHLH transcription factor Mist1, and investigated the contribution of Mist1$^+$ reserve stem-like chief cells to gastric carcinogenesis. To clarify the expression pattern of *Mist1* in the normal stomach, we crossed *Mist1*-CreERT2 mice with *R26*-mTmG mice. This reporter features the dichotomous expression of red (without recombination) or green fluorescence (with recombination). Most of the recombined Mist1$^+$ cells were detected in mature chief cells in the lower third of the glands (position 1–14) 1 day after TAM induction (Figure 1A). However, Mist1$^+$ recombined cells were also evident as rare single cells in the isthmus. Recombination in the isthmus was observed in either *R26*-TdTomato or *R26*-LacZ mice, or with low dose TAM (1 mg) (Figure S1A). Endogenous *Mist1* expression in the isthmus was confirmed by in situ hybridization (Figure S1B). Their electron microscopy appearance was similar to the granule free stem cells previously reported (Karam and Leblond, 1993) (Figure 1B).

The GFP$^+$ Mist1 lineage expanded gradually over 540 days (Figures 1C and 1D). In contrast to a previous report (Stange et al., 2013), our detailed time course revealed bi-directional expansion from single Mist1$^+$ cells at position 25–30 in the isthmus, both upward toward the lumen and deeper into the gland, independent of the dose of TAM (Figure S1C). The approximate doubling time of Mist1$^+$ isthmus cells is 120 hr or 5 days (Figure S1D), and these cells first divided into isthmus progenitors with small or spindle appearance (Figure S1E),

Figure 1. Mist1 Is a Marker of Quiescent Stem Cells in the Corpus Isthmus

(A) The corpus of *Mist1*-CreERT2;*R26*-mTmG mice day 1 after 3 mg TAM. The left image shows chief cells and the right image shows isthmus cells (arrow).

(B) Electron microscopy of Mist1$^+$ cells in the isthmus.

(C) Lineage tracing in *Mist1*-CreERT2;*R26*-mTmG mice from day 1–540. The arrow indicates the isthmus cells.

(D) Mist1-traced cell position. The total 50 glands are analyzed at each time point.

(E) The number of traced glands per 100 glands at 3, 6, and 12 months. The total 300 glands from three mice are used at each time point.

(F and G) *Mist1*-CreERT2;*R26*-Confetti mice 8 months after TAM (F). The single color and multi-color clones in the isthmus and chief cells are quantified (G). The total 50 glands are analyzed.

(H and I) *Mist1*-CreERT2;*Lgr5*-DTR-GFP (green);*R26*-TdTomato (red) mouse corpus 24 hr after TAM (H) and 2, 5, 10, and 180 days after TAM + DT ablation (I). The yellow arrows show Mist1$^+$ isthmus cell tracing and the green arrows show Lgr5$^+$ chief cells.

(J and K) The numbers of labeled chief cells per gland (J, day 4) and lineage tracing events per 100 glands (K, day 30) with or without DT ablation.

(L) Lineage tracing in 5-FU-treated *Mist1*-CreERT2;*R26*-mTmG mouse corpus (refer to Figure 1C for control images).

(M and N) The numbers of labeled chief cells per gland 4 days after TAM (cont) or TAM + 5-FU (5-FU) treatments (M) and the number of lineage tracing events per 100 glands on day 30 (N). The total 500 glands from five mice/group are analyzed for (J), (K), (M), and (N). Scale bars represent 1 μm (B) and 10 μm (A, C, F, H, I, and L) (means ± SEM) (*$p < 0.05$).

See also Figure S1.

followed later by the differentiation into surface pit and neck cells and subsequently into parietal cells. Over time, the number of GFP$^+$ cells in the chief cell region declines while the isthmus clone expands (Figure 1D). Lineage tracing persisted beyond 18 months post-induction with whole labeled corpus glands, proving that Mist1$^+$ cells self-renew (Figure 1E). *Mist1*-CreERT2;*R26*-Confetti mice show that single-color clonal expansion is seen predominantly in the isthmus area, while chief cells show scattered multi-color labeling (Figures 1F and 1G). These data indicate that the Mist1$^+$ isthmus cell is the major source of lineage tracing of corpus glands.

In this period, Mist1$^+$ cells gave rise to mucus neck cells (GS-II), parietal cells (H/K-ATPase), surface pit cells (TFF1), tuft cells (Dclk1), and ECL cells (chromogranin A), while initially Mist1$^+$ cells were negative for these markers (Figures S1F and S1G). Mist1$^+$ chief cells at the base of glands are as expected positive for GIF at day 2 after TAM, while the Mist1$^+$ isthmus cells are GIF-negative (Figure S1H). However, the early traced GIF$^+$ chief cells at the base of glands decreased over time with an increase of traced GIF$^-$ isthmus cells (Figures S1I and S1J). Thus, Mist1$^+$ basal chief cells are labeled by initial TAM induction, but these cells turn over and disappear, finally to be renewed from the isthmus-derived Mist1$^+$ stem cell.

Mist1$^+$ Isthmus Cells Are Responsible for Gastric Lineage Tracing

We confirmed no overlap between Mist1$^+$ cells and reported gastric stem cell markers Cckbr$^+$ or Sox2$^+$ (Arnold et al., 2011; Hayakawa et al., 2015) (Figures S1K and S1L). Since chief cells have also been shown to be Lgr5$^+$ (Stange et al., 2013), we generated *Mist1*-CreERT2;*Lgr5*-DTR-GFP;*R26*-Tdtomato mice (Tian et al., 2011). Similar to GIF staining, the vast majority of Mist1$^+$ chief cells at the base are Lgr5$^+$, whereas the Mist1$^+$ isthmus cells are Lgr5$^-$ (Figure 1H). Thus, we ablated Lgr5$^+$ cells, which included Mist1$^+$ chief cells, by administration of diphtheria toxin (DT) (Figure S1M). After giving TAM and DT, 100% of labeled chief cells were ablated (Figures 1I, 1J, and S1N). The expression of *Lgr5* or *Gif* was markedly reduced by DT ablation (Figure S1O). However, the number of isthmus Mist1$^+$ cells was even increased and lineage tracing occurred at the same frequency as the control (non-DT) group, accompanied with faster cell division (Figures 1I, 1K, and S1P–S1S). After 6 months, the isthmus Mist1$^+$ cells gave rise to chief cells. Similarly, ablation of chief cells by the elastase inhibitor DMP-777 (Nomura et al., 2005) did not affect the frequency of lineage tracing (Figures S1T–S1W). In contrast, when we treated mice with 5-Fluorouracil (5-FU) to kill isthmus stem/progenitor cells (Figures S1X and S1Y) (Stange et al., 2013), the mice showed almost no lineage tracing events, but maintained a similar number of labeled chief cells at the gland base for 6 months (Figures 1L–1N). Thus, Mist1$^+$ isthmus cells, and not Mist1$^+$ chief cells, are responsible for lineage tracing in the corpus.

Isthmus Mist1$^+$ Cells Give Rise to Intestinal-type Metaplasia and Cancer

In the isthmus, 1.1% of the Mist1$^+$ cells were Ki67$^+$ (Figure 2A), thus, more than 98% of Mist1$^+$ isthmus stem cells are quiescent. *KRAS* is one of the most commonly mutated proto-oncogenes in a variety of cancers, including gastric cancer. To investigate the effect of *Kras* mutation in gastric stem cells, we crossed *Mist1*-CreERT2 mice to LSL-*Kras*^{G12D} mutant mice. *Kras* mutation in Mist1$^+$ isthmus cells resulted in an increased percentage of Ki67$^+$Mist1$^+$ cells and overall faster cell division (Figures S2A–S2C). These cells formed Ki67$^+$ dysplastic foci in the isthmus, which contained Alcian blue positive metaplastic cells (Figures 2B–2D). The metaplastic/dysplastic foci moved from the isthmus to the bottom of glands with loss of parietal cells and chief cells and eventually replaced the entire glands with intestinal metaplasia (IM) and dysplasia (Figure S2D). We generated *Mist1*-CreERT2;LSL-*Kras*^{G12D};*Lgr5*-DTR mice and ablated isthmus cells and chief cells by giving 5-FU and DT, accordingly, after TAM induction (Figure S2E). Strikingly, 5-FU inhibited the metaplasia development, while DT ablation did not (Figures 2E and 2F), indicating that the Mist1$^+$ isthmus cells, and not the Mist1$^+$ chief cells, are an origin of *Kras*-induced IM and dysplasia.

Aberrant activation of the Wnt signaling pathway by inactivating *Apc* is a common initiating event in many gastrointestinal tumors (Barker et al., 2009, 2010). Thus, we established *Mist1*-CreERT2;*Apc*$^{flox/flox}$ mice. Nuclear accumulation of β-catenin was observed in the Mist1$^+$ lineage (isthmus and chief cells). However, nuclear β-catenin$^+$ cells in corpus Mist1$^+$ cells did not form dysplasia at later time points (up to 8 months) (Figures 2G and 2H), which seems contrary to the phenotype of *Apc* loss in stem cells in the gastric antrum, small intestine, and colon. In fact, whereas Wnt inhibition by Dickkopf-1 (DKK1) overexpression leads to marked decrease in proliferation in the intestine and colon, proliferation in the corpus was not inhibited (Figures S2F and S2G), suggesting that tumor initiation or proliferation in the corpus is likely independent of Wnt/β-catenin signaling.

IM in the stomach is a known risk factor or precursor lesion for intestinal-type gastric cancer (IGC). Thus, we attempted to induce Wnt/β-catenin activation in the presence of IM. We generated *Mist1*-CreERT2;LSL-*Kras*^{G12D};*Apc*$^{flox/flox}$ mice, and this mouse developed intramucosal IGC with the expansion of nuclear β-catenin$^+$ cells in 4 months (Figure 2I). Thus, Mist1$^+$ stem cells can give rise to IGC with loss of *Apc* only when *Kras*-induced IM is also present. Notch signaling is another important pathway regulating gastric proliferation (Kim and Shivdasani, 2011). The Notch inhibitor dibenzazepine (DBZ) reduced the expansion of *Mist1*-lineage tracing as well as proliferation in the isthmus (Figures S2H–S2K), and constitutive activation of Notch signaling in Mist1$^+$ stem cells by generating Mist1-CreERT2;*Eef1a1*-LSL-*Notch1(IC)* mice (Buonamici et al., 2009) resulted in the development of IGC (Figure S2L). Although Mist1 protein expression is decreased in *Kras*/*Apc*-induced IGC, aberrant Notch activation increased the number of Mist1$^+$ cells in the tumor (Figures S1Q and S2M). The dysplastic cells in Notch-induced tumor did not display nuclear β-catenin accumulation, suggesting that in the corpus, Notch signaling is a Wnt-independent oncogenic pathway through which Mist1$^+$ stem cells can progress to IGC.

Mist1$^+$ Isthmus Cells Can Form Corpus Organoids in a Lgr5-Independent Fashion

To evaluate the stem cell properties of Mist1$^+$ cells in vitro, we isolated corpus glands from *Mist1*-CreERT2;*R26*-mTmG mice 1 day following TAM induction. Mist1$^+$ green cells were observed

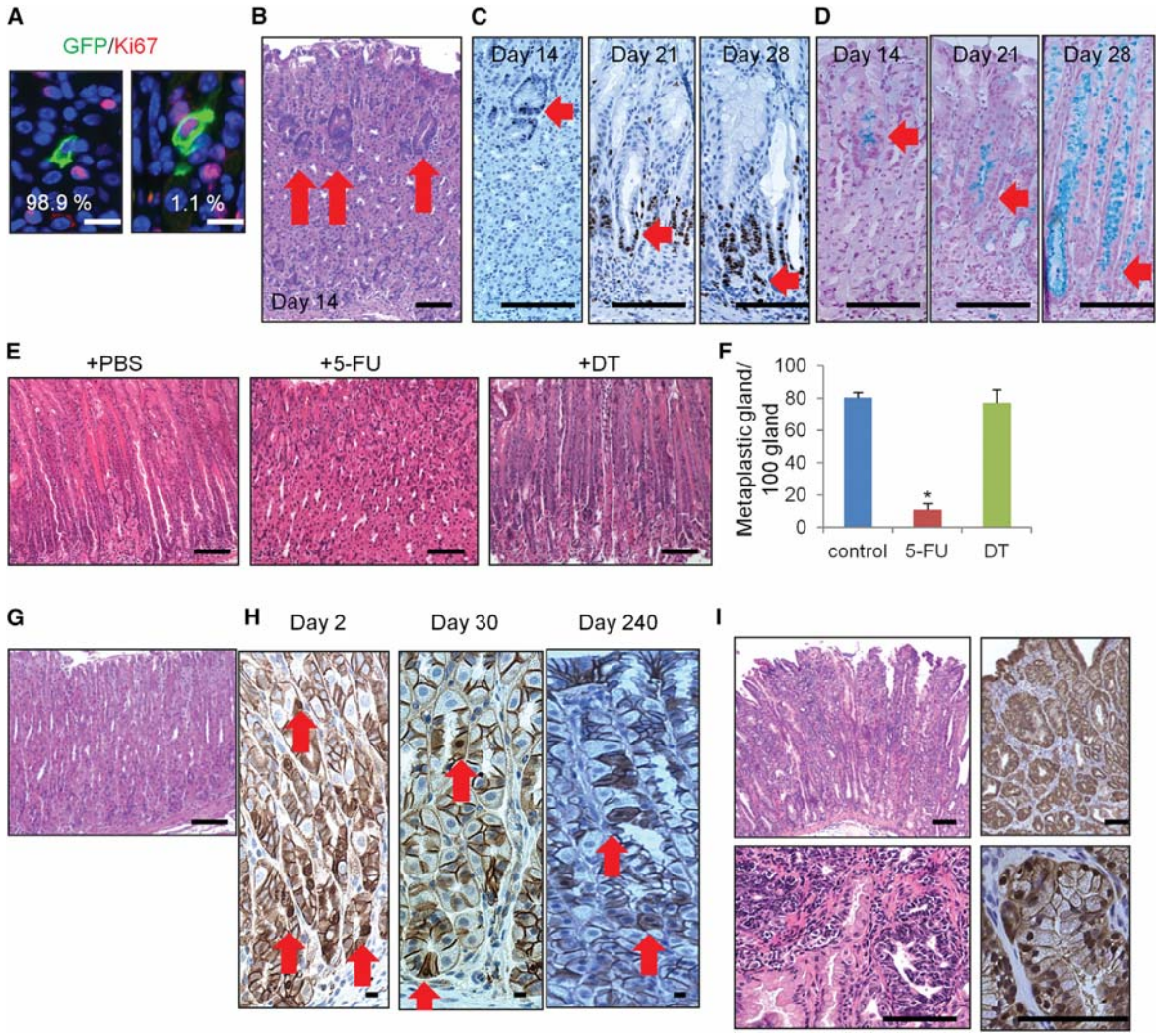


Figure 2. Mist1^{+} Isthmus Cells Give Rise to IM and IGC

(A) Ki67 (red) and GFP staining (green) of *Mist1*-CreERT2;*R26*-mTmG mice at day 2.

(B–D) Hematoxylin and eosin (H&E) (B), Ki67 (C), and Alcian blue (D) staining in *Mist1*-CreERT2;LSL-*Kras*^{G12D} mice on days 14, 21, and 28 after induction. The arrows indicate isthmus-derived dysplastic cells.

(E and F) H&E staining (E) and numbers of metaplastic glands per 100 glands (F) of *Mist1*-CreERT2;LSL-*Kras*^{G12D};*Lgr5*-DTR-GFP mice treated with PBS (left), 5-FU (middle), or DT (right) 30 days after TAM. The total 300 glands from three mice/group are analyzed.

(G and H) H&E (G, day 240) and β-catenin (H) staining in *Mist1*-CreERT2;*Apc*$^{flox/flox}$ mouse. The arrows indicate the nuclear β-catenin^{+} cells.

(I) H&E (left) and β-catenin (right) staining in *Mist1*-CreERT2;LSL-*Kras*^{G12D};*Apc*$^{flox/flox}$ mouse corpus on day 120 post-induction (means ± SEM) (*$p < 0.05$). Scale bars represent 10 μm (A) and 100 μm (B–E and G–I).

See also Figure S2.

in the two distinct positions, and Mist1^{+} isthmus cells expanded to form cystic organoids in the reported culture method (Stange et al., 2013), while Mist1^{+} chief cells remained as single cells and eventually disappeared (Figure 3A). The GFP^{+} Mist1-derived cells survived in vitro for at least 2 months, confirming longevity. Even after ablation of Lgr5^{+} chief cells in *Mist1*-CreERT2;*Lgr5*-DTR;*R26*-TdTomato mice by DT injection, isthmus Mist1^{+} cells continued to lineage trace and give rise to chief cells in cultured organoids (Figures 3B and 3C). We next sorted Mist1^{+} cells after DT or 5-FU treatment to the mice (lacking chief cells and isthmus cells, respectively) (Figures 3D–3F). Colony formation efficiency increased in the DT-treated group and decreased in the 5-FU-treated group, suggesting that isthmus Mist1^{+} cells are the true corpus stem cells, rather than Mist1^{+} chief cells. We compared gene expression patterns between the total Mist1^{+} population (majority of which were chief cells), DT-ablated isthmus Mist1^{+} population, and the differentiated parietal cell population (Figure S3A). *Lgr5* and *Gif* expression are markedly downregulated in isthmus Mist1^{+} cells compared to total Mist1^{+} cells. *Mist1* expression is upregulated in both total and isthmus Mist1^{+} population. The expression of several stem/progenitor markers, such as *Cd44* and *Sox9*, or target genes of Wnt and Notch

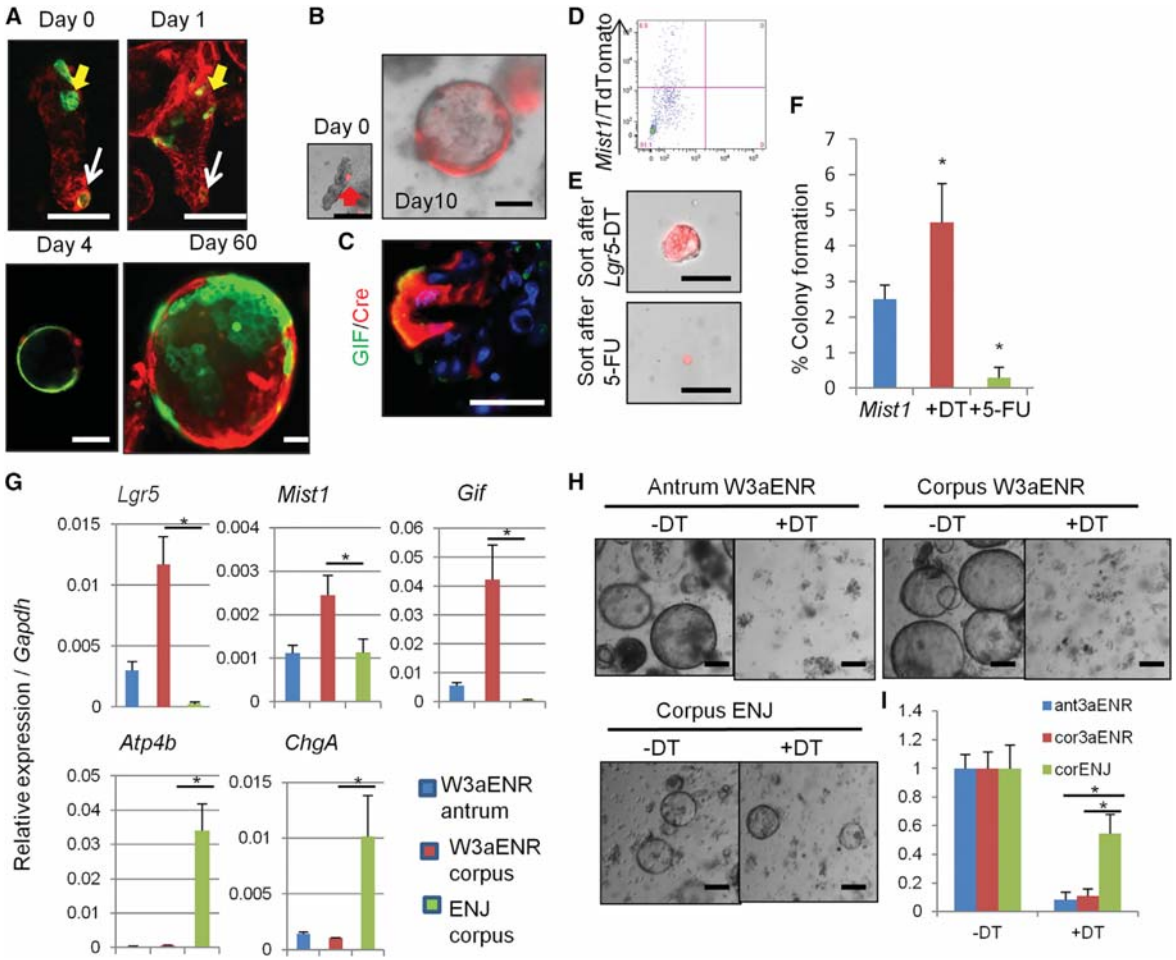


Figure 3. Mist1$^+$ Isthmus Cells Can Form Corpus Organoids in a Lgr5-Independent Fashion

(A) Corpus gland culture of TAM-induced *Mist1*-CreERT2;*R26*-mTmG mice. The yellow arrows show isthmus cells and the white arrows show chief cells.

(B and C) Lineage tracing (B) and GIF staining (C, green) of corpus gland culture from *Mist1*-CreERT2;*Lgr5*-DTR-GFP;*R26*-TdTomato mice treated with DT.

(D–F) TdTomato$^+$ cells were sorted and cultured from DT or 5-FU-treated *Mist1*-CreERT2;*Lgr5*-DTR-GFP;*R26*-TdTomato mice corpus after TAM. The FACS plot (D), images (E), and the colony formation efficiency (F) at day 7 are shown (n = 4/group).

(G) Relative gene expression per *Gapdh* in antral or corpus organoids cultured with the indicated media for 10 days (n = 3/group).

(H and I) Organoid growth of antrum and corpus glands cultured with W3aENR or ENJ media. The day 10 images (H) and the relative numbers of organoids cultured in the indicated media (I) are shown. The numbers in non-DT organoids in each group are set as 1.0 (n = 3/group) (means ± SEM) (*$p < 0.05$). Scale bars represent 50 μm.

See also Figure S3.

signaling, such as *Ccnd1*, *Notch1*, and *Hes1*, remain at higher levels in the isthmus population, suggesting that isthmus Mist1$^+$ cells are Lgr5$^-$, but still exhibit stem cell characteristics.

The Wnt3a/R-spondin1 (W3a/Rspo1)-dependent culture system fails to produce corpus-specific cell lineage such as parietal cells and ECL cells (Stange et al., 2013). Instead, W3aENR media (W3a, EGF, Noggin, and Rspo1) induces marked upregulation of *Lgr5* (three times higher than gastric antrum organoids) (Figure 3G). Compared to standard W3aENR media, culture of corpus glands in ENJ media (where Wnt3a/Rspo1 were replaced by Notch ligand Jagged-1) led to decreased expression of *Lgr5* or *Gif*, suggesting that Wnt3a/Rspo1 lead to expansion of chief cells. In contrast, in ENJ media, we observed greater amounts of parietal cells and ECL cells than in W3aENR media both in RT-PCR and immunostaining assays (Figures 3G and S3B), suggesting that the activation of Notch signaling is more important for preserving mature corpus cell types in culture than canonical Wnt signaling. Addition of a γ-secretase inhibitor blocked corpus organoid growth (Figures S3C and S3D), thus Notch signaling is important for corpus stem cell maintenance and growth. When we cultured *Mist1*-CreERT2;*Lgr5*-DTR;*R26*-TdTomato glands, antral and corpus organoids cultured with W3aENR did not grow and died following DT treatment (Figures 3H and 3I), indicating that organoid growth is highly dependent on Lgr5$^+$ cells in W3aENR media. However, lineage-traced corpus organoids survived with ENJ plus DT media (Figure S3E), proving that a non-Lgr5 stem cell population maintains organoid growth in Wnt3a/Rspo1-independent culture conditions.

Cxcl12$^+$ Endothelium and Cxcr4$^+$ ILCs Contribute to the Corpus Stem Cell Niche through Wnt5a Production

Given our in vitro data suggesting that Wnt3a or canonical Wnt signaling is not a critical niche factor in the corpus, we explored which Wnt ligands are indeed expressed in the stomach and intestine (Figures 4A and S4A). Among known Wnt ligands, *Wnt3a* expression was quite low in the corpus, in contrast to the intestine. Instead, an atypical Wnt ligand, *Wnt5a*, was highly expressed in the corpus. In situ hybridization of *Wnt5a* revealed focal expression in the isthmus stroma (Figure 4B) coincident with the known expression of Cxcr4 (Shibata et al., 2013). In *Cxcr4*-EGFP mice, Cxcr4$^+$ cells were found in the isthmus area as rare single cells, showing almost identical distribution to *Wnt5a* expression (Figure 4C). Cxcr4$^+$ cells and Mist1$^+$ cells represent distinct populations, although they were located in close proximity within the isthmus (Figure 4D).

Immunostaining revealed that Cxcr4$^+$ cells in the corpus are negative for E-cadherin or stromal markers, αSMA, NG2, and S100B, but positive for CD45, suggesting that they are tissue-resident hematopoietic cells recruited to the isthmus (Figures 4E and S4B). About 60% of gastric CD45$^+$Cxcr4$^+$ cells from the whole gastric corpus are CD11b$^+$ myeloid lineages (Figure S4C). CD3$^+$ T cells, CD19$^+$ B cells, and NK1.1$^+$ classical NK cells are Cxcr4$^-$. The remaining 40% of CD45$^+$Cxcr4$^+$ cells are Lineage-negative (CD3$^-$Gr1$^-$CD11b$^-$CD45R$^-$Ter119$^-$) and about half of the Lin$^-$Cxcr4$^+$ population is a CD90.2$^+$CD127$^+$ lymphoid population (Figures 4F and S4C). The other half is predominantly c-kit$^+$FcεRIα$^+$ mast cells. Immunostaining defined the isthmus Cxcr4$^+$ cells as Lin$^-$CD90.2$^+$ intraepithelial gastric innate lymphoid cells (ILCs) (Figures 4E and S4D). *Id2*-GFP mice, which mark all types of ILCs (Hoyler et al., 2012), show a similar distribution pattern as Cxcr4$^+$ cells (Figure S4E). The majority (90%) of gastric Cxcr4$^+$ ILCs are NKp46$^-$CD4$^-$, ScaI$^+$ICOS$^+$KLRG$^+$ ILC2 cells, and a small population (5%) are Rorgt$^+$NKp46$^-$ ILC3 cells (Figures 4F and S4F). In fact, the gastric Cxcr4$^+$ ILC population is enriched with ILC2-specific genes (Figure S4G).

In the sorted Mist1$^+$ cells and Cxcr4$^+$ cells, *Wnt5a* was expressed primarily in the Cxcr4$^+$ cells (Figures S4H and S4I), confirming our in situ hybridization findings. When we treated Cxcr4$^+$ cells with Cxcl12 in vitro, *Wnt5a* expression was upregulated (Figure S4J). We hypothesized that the Cxcr4$^+$ cell might be a niche cell, supporting gastric stem cell function. To test this possibility, we performed a co-culture experiment with "red" Mist1$^+$ cells and "green" Cxcr4$^+$ cells. Co-culture of Mist1$^+$ cells with Cxcr4$^+$ cells significantly enhanced red colony formation ability (Figures 4G and 4H). Treatment with Cxcl12 demonstrated an additive effect on Cxcr4$^+$ cell co-culture, while it had no effect on Mist1$^+$ cell culture alone, indicating that Cxcl12 acts through the Cxcr4$^+$ ILCs. Furthermore, the Cxcr4$^+$ ILC population exhibits the highest expression of *Wnt5a* compared to CD45$^+$Cxcr4$^-$ cells or Cxcr4$^+$ non-ILCs (Figure 4I). The colony formation ability of Mist1$^+$ stem cells is enhanced by Wnt5a or co-culture with Cxcr4$^+$ ILC population. However, *Wnt5a*-deficient ILCs which are sorted from *Cag*-CreERT2;*Wnt5a*$^{flox/flox}$ mouse stomach after TAM induction failed to show the same effect (Figure 4J). Thus, Cxcr4$^+$ILC-derived Wnt5a plays a key role for promoting Mist1$^+$ stem cell colony formation.

We explored the source of Cxcl12 in the stomach. In *Cxcl12*-dsRED mice (Ding and Morrison, 2013), there were frequent dsRED$^+$ cells in the stroma near the isthmus (Figure 4K). Indeed, Cxcr4$^+$ ILCs and Cxcl12$^+$ stromal cells in *Cxcr4*-EGFP;*Cxcl12*-dsRED mice were frequently positioned in close proximity (Figures 4L and 4M). We confirmed that Cxcl12$^+$ cells are CD31$^+$ and endomucin$^+$ endothelial cells (Figures 4N and S4K). We compared RNA expression between dsRED$^+$CD31$^+$ cells (35% of total CD31$^+$ cells) and dsRED$^-$CD31$^+$ cells by quantitative RT-PCR array (Figure S4L; Table S1). Among pathways potentially involved in the regulation of *Cxcl12* expression, we found that Cxcl12$^+$ cells express BMP receptor 2, and BMP2 treatment in vitro upregulates *Cxcl12* expression (Figures S4M and S4N), consistent with previous findings (Yang et al., 2008). Interestingly, *Tie2*-Cre;*Cxcl12*$^{flox/flox}$;*Cxcr4*-EGFP mice, with targeted knock out of *Cxcl12* in endothelial cells, displayed a significant reduction in the number of Cxcr4$^+$ cells in the isthmus compared to control mice (Figures 4O and 4P). Together, endothelial Cxcl12 is important for the recruitment of Wnt5a-producing Cxcr4$^+$ ILCs in the stomach.

E-cadherin Loss in Mist1$^+$ Cells Develops a Diffuse-type Cancer Dependent on Chronic Inflammation

We sought to establish whether Mist1$^+$ stem cells were also a cell of origin for the DGC by knocking out the *Cdh1* gene in Mist1$^+$ cells. *Mist1*-CreERT2;*Cdh1*$^{flox/flox}$ mice (*Cdh1*$^{\Delta Mist1}$) developed the pathognomonic, small mucous-producing atypical cell foci in the isthmus 10 days after TAM, but not in the chief cell region (Figures 5A and 5B). E-cadherin was downregulated in these atypical cells in the isthmus, consistent with early signet-ring cell morphology, recapitulating the earliest events in the pathogenesis of human signet-ring cell carcinoma. Ablation of chief cells and isthmus cells by DT and 5-FU treatment with *Mist1*-CreERT2;*Cdh1*$^{flox/flox}$;*Lgr5*-DTR mice confirmed that the isthmus Mist1$^+$ cells are an origin of signet-ring cells (Figures S5A and S5B). Cxcl12/Cxcr4 niche cells were not affected by 5-FU treatment (data not shown).

Nevertheless, the number of atypical cells gradually declined and disappeared (Figure 5C), suggesting that E-cadherin loss leads to epithelial cell death and is on its own insufficient to initiate DGC. Given that mild inflammation without gastric atrophy is a common feature of DGC (Carneiro et al., 2004), we infected TAM-induced *Cdh1*$^{\Delta Mist1}$ mice with *Helicobacter felis* (*Hf*) to induce chronic inflammation. Surprisingly, in mice with *Hf* infection, atypical foci were preserved and expanded even after 1 year following TAM induction (Figure 5C). Lineage-traced DGC with numerous signet-ring cells was detected at 18 months post *Hf* infection in *Cdh1*$^{\Delta Mist1}$ mice (Figure 5D; seven of nine mice, 78%), along with the increase of Mist1$^+$ cells in DGC (Figures S1Q and S5C). The addition of *Trp53* mutation in this setting led to invasive DGC within 9 months (Figure S5D). Interestingly, administration of dexamethasone to *Hf*-infected *Cdh1*$^{\Delta Mist1}$ mice reduced the number of signet-ring cell foci to the same level as non-infected control mice (Figures 5E–5G). In contrast, another inflammation-associated cancer model, H/K-ATPase-IL-1β transgenic mice (Tu et al., 2008), also showed a dramatic expansion of lineage-traced signet-ring cells when crossed to *Cdh1*$^{\Delta Mist1}$ mice, even without *Hf* infection (Figures 5H–5J). Thus, DGC development from Mist1$^+$ stem cells is dependent

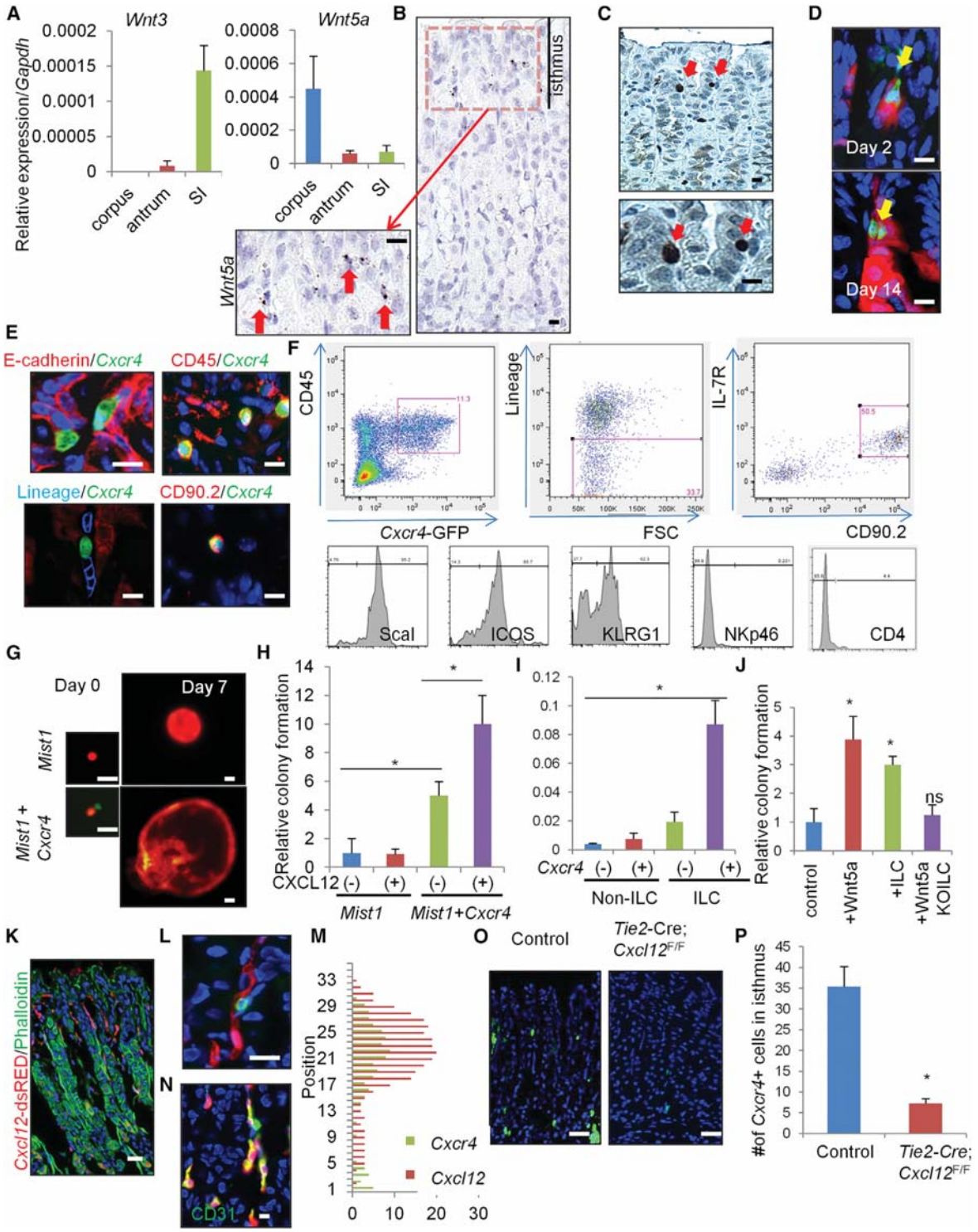


Figure 4. Cxcl12$^+$ Vascular Endothelial and Cxcr4$^+$ ILCs Contribute to Corpus Stem Cell Niche through Wnt5a Production

(A) Relative expression of *Wnt3* and *Wnt5a* in the corpus, antrum, and small intestine (n = 3/group).

(B) In situ hybridization of *Wnt5a* in the corpus. The arrows indicate the *Wnt5a*-expressing cells in the isthmus stroma.

(C) GFP staining in the *Cxcr4*-EGFP mouse corpus gland. The arrows indicate the GFP$^+$ cells in the isthmus.

(D) Lineage tracing in *Mist1*-CreERT2;*Cxcr4*-EGFP;*R26*-TdTomato mice on days 2 and 14. The arrows indicate the GFP$^+$ cells.

(E) E-cadherin (red), CD45 (red), Lineage (blue), and CD90.2 (red) staining of *Cxcr4*-EGFP$^+$ cells.

(legend continued on next page)

on chronic inflammation and anti-inflammatory therapy may be useful for preventing DGC.

Although Troy$^+$ chief cells are reported to act as reserve stem cells (Stange et al., 2013), we observed a rare Troy$^+$ population in the isthmus that could lineage trace and give rise to cancers by examining *Troy*-BAC-CreERT2 mice (Fafilek et al., 2013) (Figures S6A–S6G). Also, while Troy$^+$ chief cells with intact Troy expression do not proliferate and do not lineage trace, loss of *Troy* expression significantly promoted chief cell proliferation and lineage tracing after injury (Figures S6H–S6L), similar in most respects to the previous report, reconciling our findings with those of earlier groups (Stange et al., 2013).

Cxcl12/Cxcr4 Perivascular Niche Regulates DGC Progression through Wnt5a Production

During DGC development under chronic inflammation, corpus stem cell niche factors—Cxcl12$^+$ endothelium and Cxcr4$^+$ ILCs—are markedly expanded or upregulated in the region surrounding the isthmus DGC lesion (Figures 6A–6E), suggesting that these niche factors contribute to DGC development. We tested therapeutic intervention with AMD3100, a specific inhibitor of CXCR4, and an anti-CD90.2 antibody (Ab) for specific depletion of ILCs. Compared with vehicle-injected control mice, AMD3100 and the anti-CD90.2 Ab significantly reduced the number of signet-ring cell foci (Figures 6F–6H). In contrast, overexpression of *Cxcl12* in *Mist1*-CreERT2;H/K-ATPase-*Cxcl12*;*Cdh1*$^{flox/flox}$ mice led to persistence and growth of DGC lesions over 3 months even without *Hf* infection (Figures 6I–6K). *Hf* infection further accelerated DGC progression in this mouse model, while anti-CD90.2 Ab treatment significantly reduced the number of DGC foci in the setting of Cxcl12 overexpression (Figures S6M and S6N). Thus, upregulation of Cxcl12/Cxcr4 signaling through activation of ILCs plays a central role in DGC development.

After *Hf* infection, *Wnt5a* is highly upregulated in the stroma surrounding signet-ring lesions in the isthmus (Figure 6L). In addition, AMD3100 and anti-CD90.2 Ab treatment, or knock out of *Cxcl12* in Tie2-lineage, significantly decreased the number of Cxcr4$^+$ cells in the isthmus and the expression of *Wnt5a*, while Cxcl12-overexpression led to an increase in Cxcr4$^+$ cell number and upregulation of *Wnt5a* (Figures 6M and S6O). Thus, we tested the contribution of Wnt5a in DGC development by transplanting *Cag*-CreERT; *Wnt5a*$^{flox/flox}$ mouse bone marrow cells into *Cdh1*$^{\Delta Mist1}$ mice (Figure 6N). In these chimeric mice, E-cadherin is depleted in the Mist1$^+$ lineage and *Wnt5a* is knocked out in bone-marrow derived ILCs after TAM induction. *Cdh1*$^{\Delta Mist1}$ mice with *Cag*-CreERT;*Wnt5a*$^{flox/flox}$ bone marrow exhibited significantly fewer signet-ring cell foci compared to *Cdh1*$^{\Delta Mist1}$ mice with wild-type (WT) bone marrow cells (Figures 6O and 6P), indicating that Wnt5a in the hematopoietic cells promotes DGC progression. Although there was a significant increase in the number of Cxcr4$^+$ cells in the *Kras*-induced IGC model, AMD3100 failed to block either *Kras* or *Notch*-dependent IGC progression (Figures S6P and S6Q), suggesting the more predominant role of this pathway in DGC development.

RhoA Activation by Wnt5a Plays a Role in DGC Development

Wnt5a is known to activate a small GTPase protein, RhoA, which has a prosurvival effect by inhibiting anoikis in gastric and other cancer cells (Cai et al., 2008; Liu et al., 2013). Thus, we hypothesized that ILC-derived Wnt5a activates RhoA in E-cadherin-depleted cells and prolongs cell survival. We confirmed that Wnt5a activates RhoA in a *CDH1* mutant AGS cells by immunoprecipitation (Figure 7A). In a soft-agar assay, treatment of AGS cells with Wnt5a enhanced sphere formation, indicating that Wnt5a promotes anchorage-independent cell growth. Interestingly, blocking RhoA activation using a Rho inhibitor, Rhosin, diminished Wnt5a-mediated effects (Figures 7B and 7C). Similar results were observed with another DGC cell line, KATO-III. Furthermore, we found that E-cadherin-deficient Mist1$^+$ stem cells, which are normally unable to survive in vitro upon *Cdh1* deletion, displayed prolonged survival in the presence of Wnt5a (Figures 7D and 7E). This prosurvival effect was blocked by Rhosin, suggesting that Wnt5a-mediated RhoA activation is a key event for the survival of *Cdh1*-deleted organoids. However, Wnt5a did not affect the expansion of *Kras* or *Notch*-induced IGC organoids (data not shown).

We compared these murine DGC findings with human DGC samples. Histologically, the DGC lesions in the *Cdh1*$^{\Delta Mist1}$ mice appeared quite similar to early DGC with E-cadherin loss in patient samples (Figure 7F). Importantly, Cxcl12$^+$ cells were found in stromal cells that appeared similar histologically to blood vessels, with KLRG1$^+$ lymphocytes surrounding the signet-ring cancer cells, consistent with a role for these cells in supporting the DGC stem cell niche.

DISCUSSION

In this study, we report four major discoveries regarding gastric stem cell and cancer biology: (1) quiescent Mist1$^+$ gastric stem

(F) FACS plots of gastric Cxcr4$^+$ cells. The top left image shows gating by CD45$^+$ and *Cxcr4*-EGFP$^+$. The top middle image shows gating by Lin$^-$. The top right image shows the ILCs are identified by IL-7R$^+$CD90.2$^+$. The bottom image shows the histograms of the indicated ILC markers.
(G) Single-cell culture of Mist1$^+$ cells (red) with or without Cxcr4$^+$ cell (green) co-culture.
(H) Relative colony forming efficiency of Mist1$^+$ cells with Cxcl12 treatment and Cxcr4$^+$ cell co-culture (n = 4/group). The colony formation efficiency of the control group is set as 1.0 in (H) and (J).
(I) *Wnt5a* gene expression in Cxcr4$^{+/-}$ ILCs and non-ILC CD45$^+$ cells (n = 3/group).
(J) Relative colony forming efficiency of Mist1$^+$ cells with Wnt5a (100 ng/ml), Cxcr4$^+$ ILCs, or *Cag*-CreERT;*Wnt5a*$^{flox/flox}$ ILCs (n = 4/group).
(K) *Cxcl12*-dsRED mouse stomach with phalloidin staining (green).
(L) *Cxcr4*-EGFP;*Cxcl12*-dsRED mouse stomach.
(M) Cell positions of Cxcr4$^+$ cells and Cxcl12$^+$ cells.
(N) Immunostaining (green) of CD31 in Cxcl12$^+$ cells (red).
(O and P) GFP expression (O) and the numbers of GFP$^+$ cells (P) in *Cxcr4*-EGFP and *Tie2*-Cre;*Cxcl12*$^{flox/flox}$;*Cxcr4*-EGFP mouse corpus (n = 30/group) (means ± SEM and *p < 0.05). Scale bars represent 10 μm (B–E, K, and N) and 25 μm (G, L, and O).
See also Figure S4 and Table S1.

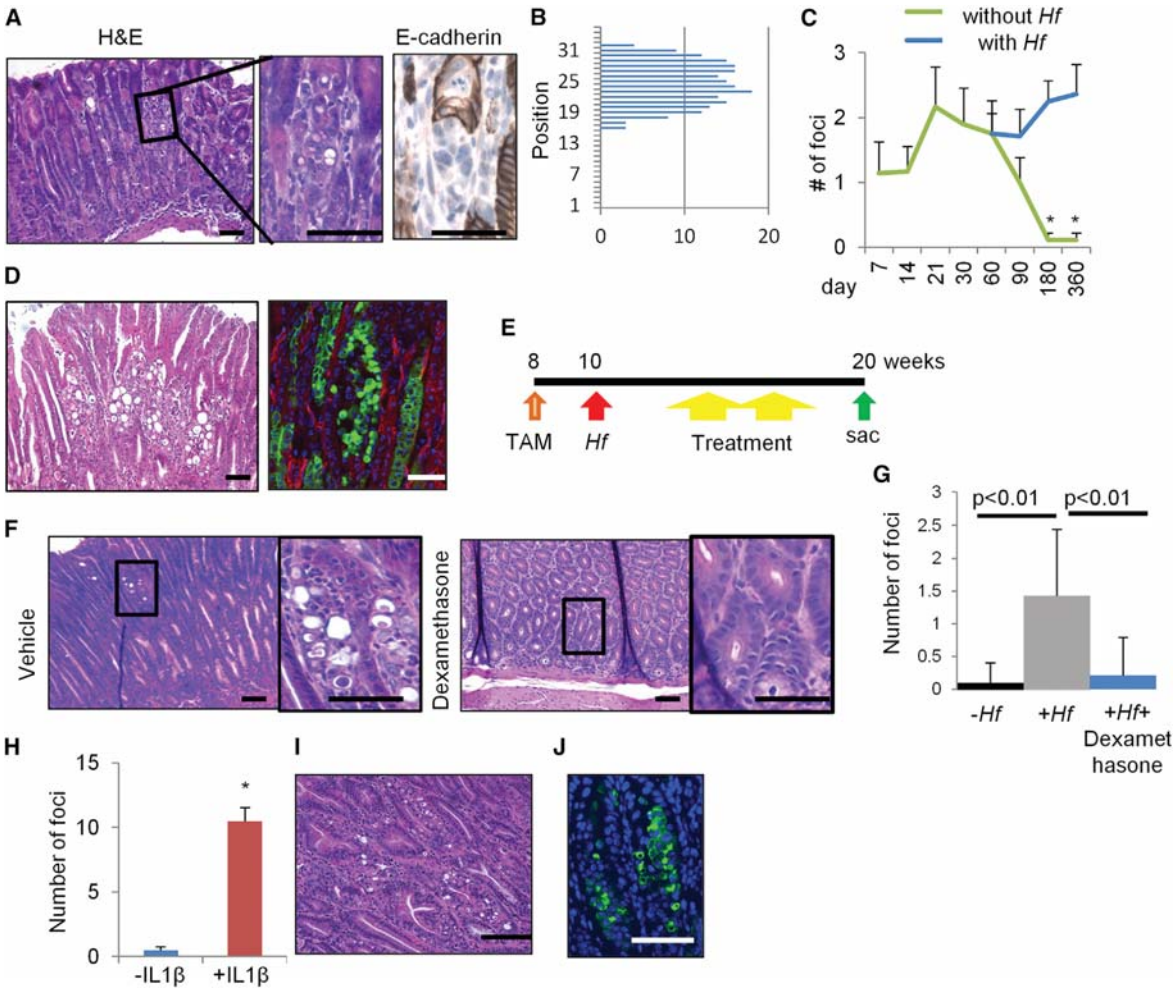


Figure 5. E-cadherin Loss in Mist1$^+$ Cells Develops DGC Dependent on Chronic Inflammation

(A and B) H&E and E-cadherin staining (A) and the location (B) of atypical foci in *Cdh1*$^{\Delta Mist1}$ mice (day 10).

(C) Numbers of atypical foci per section with or without *Hf* infection (n = 3 mice/group at each time point).

(D) H&E staining (left) and GFP expression (right) in *Hf*-infected *Mist1*-CreERT2;*Cdh1*$^{flox/flox}$;*R26*-mTmG mice 18 months after TAM induction.

(E) Protocols for TAM, *Hf*, and therapies (dexamethasone, AMD3100, and anti-CD90.2 Ab).

(F and G) H&E staining (F) and numbers of atypical foci per section (G) in *Hf*-infected *Cdh1*$^{\Delta Mist1}$ mice treated with or without dexamethasone (n = 4 mice/group and four sections/mouse are analyzed).

(H–J) Numbers of atypical foci per section (H), H&E (I), and GFP staining (J) in *Cdh1*$^{\Delta Mist1}$and *Cdh1*$^{\Delta Mist1}$ mice crossed with H/K-ATPase-IL1β mice after 4 months TAM induction (means ± SEM and *$p < 0.05$). Scale bars represent 50 μm.

See also Figure S5.

cells located at the isthmus of the corpus gland are an origin of all epithelial lineages, (2) they can serve as a cellular origin of all histological types of gastric cancer, (3) the Cxcl12/Cxcr4 axis comprising endothelial cells and ILCs regulates the normal and neoplastic gastric stem cell niche, and (4) Wnt5a from Cxcr4$^+$ ILCs promotes diffuse-type cancer growth by activating RhoA. Our data provide a focus for gastric regeneration and cancer prevention and therapy.

In the gastric corpus, the isthmus is the major site of epithelial proliferation and for many years has been thought to contain the granule free stem cell population (Karam and Leblond, 1993). We found that the isthmus Mist1$^+$ cells are these granule free bona fide stem cells in the corpus, which are remarkably quiescent, dividing infrequently (every 5 days), consistent with the original expectations for mammalian adult stem cells (Malam and Cohn, 2014). It has been hypothesized that corpus glands may possess two different stem cell zones, isthmus and chief cells (Nam et al., 2010; Stange et al., 2013). Our ablation experiments using a 5-FU and *Lgr5*-DT system find that only isthmus cells, not chief cells, play a predominant role in maintaining the gastric gland and are an origin of gastric cancer. The gradient of BMP or Shh expression determines the localized expression of *Lgr5* at the gastrointestinal gland base (Shyer et al., 2015) and basal chief cells in the corpus express *Lgr5*. Thus, our model suggests that *Lgr5* expression may not always reflect actual stemness, especially in a Wnt-independent organ.

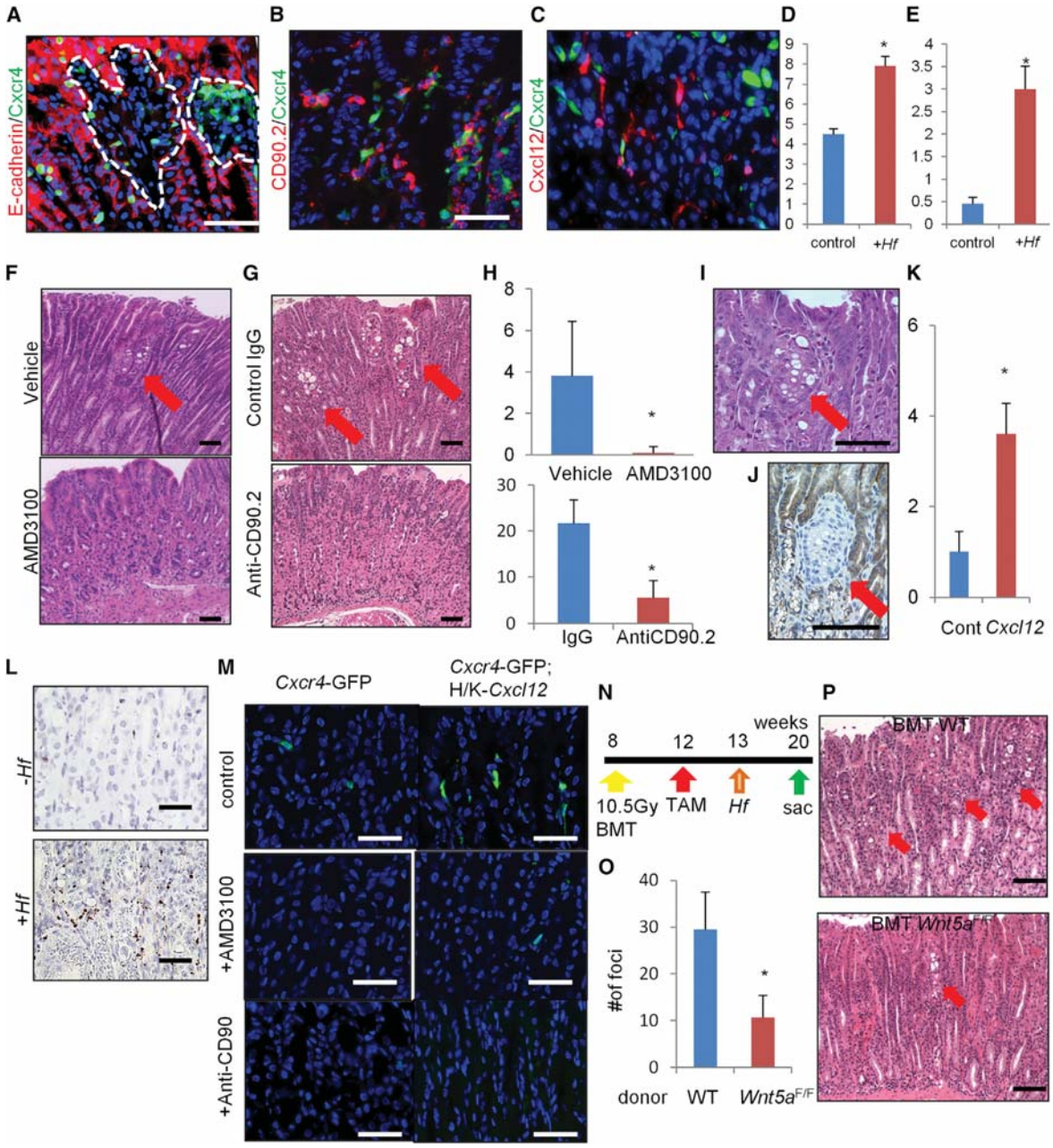


Figure 6. Cxcl12/Cxcr4 Perivascular Niche Regulates DGC Progression through Wnt5a Production

(A–E) E-cadherin (A) and CD90.2 staining (B) (red) of *Mist1*-CreERT2;*Cdh1*$^{flox/flox}$;*Cxcr4*-EGFP (green) mice, and *Mist1*-CreERT2;*Cdh1*$^{flox/flox}$;*Cxcl12*-dsRED (red);*Cxcr4*-EGFP (green) (C) mice treated with TAM and *Hf* (6 months). The numbers of Cxcl12^{+} cells (D) and Cxcr4^{+}CD90.2^{+} cells (E) per gland with or without *Hf* infection are shown. The total 20 glands per group were analyzed.

(F–H) H&E staining of *Hf*-infected *Cdh1*$^{\Delta Mist1}$ mice treated with or without AMD3100 (F) or treated with control IgG Ab or anti-CD90.2 Ab (G). The numbers of atypical foci per section (H) (n = 4 mice/group and four sections/mouse are analyzed) are shown. The arrows indicate the atypical foci.

(I–K) H&E (I) and E-cadherin (J) staining and numbers of atypical foci per section (K) in *Cdh1*$^{\Delta Mist1}$ mice crossed to H/K-ATPase-*Cxcl12* mice 3 months after TAM (n = 3 mice/group and four sections/mouse are analyzed). The arrows indicate the atypical foci.

(L) In situ hybridization of *Wnt5a* in *Cdh1*$^{\Delta Mist1}$ mice with or without *Hf* infection.

(M) *Cxcr4*-EGFP expression in WT and H/K-ATPase-*Cxcl12* mouse stomach treated with control, AMD-3100, or anti-CD90.2 Abs.

(N–P) Control or *Cag*-CreERT;*Wnt5a*$^{flox/flox}$ mouse bone marrow cells were transplanted into *Mist1*-CreERT2;H/K-ATPase-*Cxcl12*;*Cdh1*$^{flox/flox}$ mice after 10.5 Gy whole body irradiation (N). The numbers (O) of atypical foci per section and H&E staining (P) are shown (n = 4 mice/group and four sections/mouse are analyzed). The arrows indicate the atypical foci (means ± SEM and *p < 0.05). Scale bars represent 50 μm (A–C, F, G, L, and M) and 100 μm (I, J, and P).

See also Figure S6.

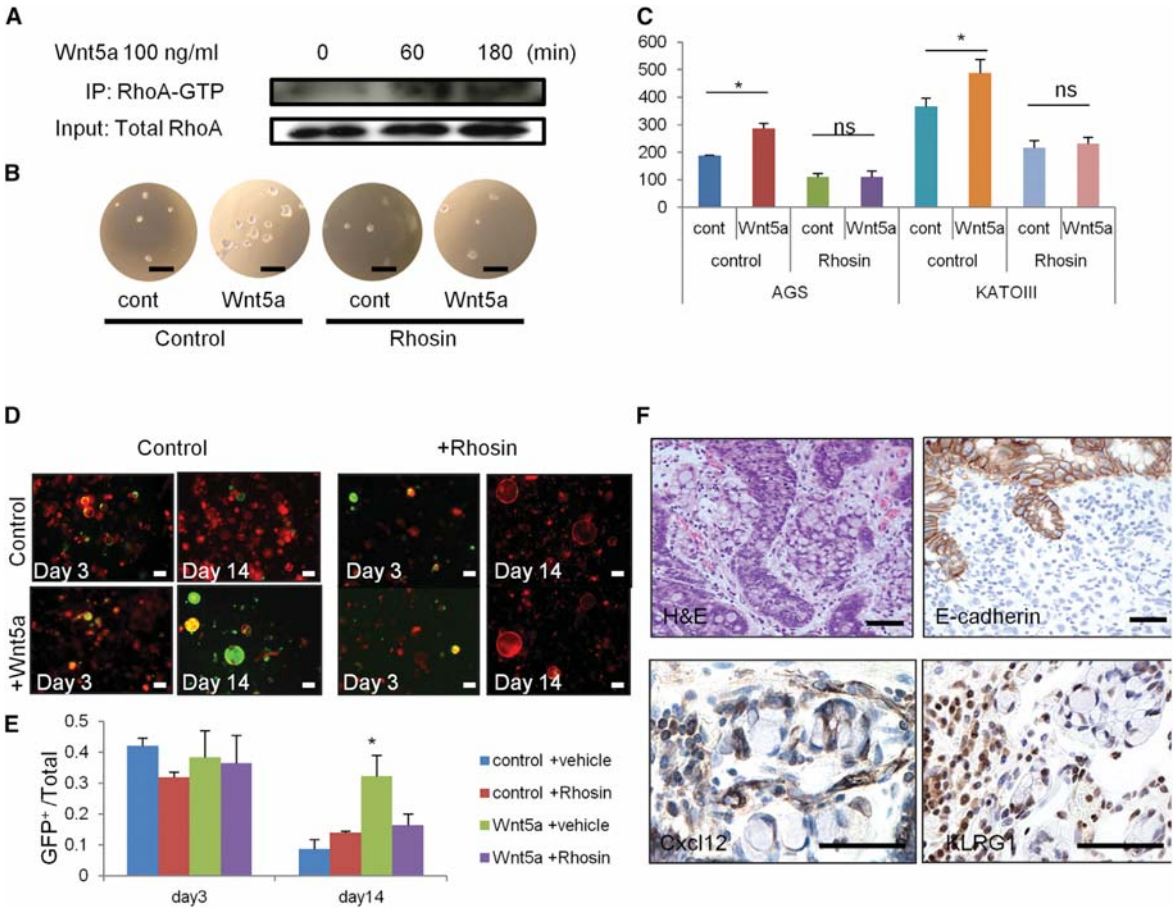


Figure 7. RhoA Activation by Wnt5a Plays a Role in DGC Development

(A) AGS cells were treated with 100 ng/ml Wnt5a for the indicated times. The cell lysates were immunoprecipitated with RhoA-GTP Ab and immunoblotted with total RhoA Ab.

(B and C) Soft-agar sphere forming assay of Wnt5a-treated AGS and KATO-III cells. The cells were treated with vehicle or 30 μM Rhosin. The sphere images (B) and numbers (C) of spheres at day 10 are shown (n = 4/group).

(D and E) Corpus organoids from TAM-treated *Mist1*-CreERT2;*Cdh1*$^{flox/flox}$;*R26*-mTmG mice treated with 100 ng/ml Wnt5a and/or 30 μM Rhosin. The images (D) and numbers (E) of GFP^{+}*Cdh1*$^{-}$ organoids per total organoid number on days 3 and 14 are shown (n = 4/group).

(F) H&E, E-cadherin, Cxcl12, and KLRG1 staining in human DGC. Scale bars represent 100 μm (D) and 50 μm (B and F) (means ± SEM and *p < 0.05).

Lineage-tracing studies have been based largely on TAM-induced Cre activation, but TAM treatment may cause epithelial cell death and influence stem cell activity (Huh et al., 2012; Zhu et al., 2013). Given that *Troy* is known to have an inhibitory effect on Wnt signaling, the knockin *Troy* lineage tracing may be related to a reduction in *Troy* expression in the knockin mice, secondary to haploinsufficiency, resulting in enhanced Wnt signaling activity in those mice. While knockin lines have many potential advantages, disruption of even one copy of the endogenous gene can apparently alter certain phenotypes.

The Cxcl12/Cxcr4 perivascular niche in the bone marrow was previously identified and studied as a major regulator of HSC (Ding and Morrison, 2013; Sugiyama et al., 2006). However, until now the role of the Cxcl12/Cxcr4 stem cell niche axis beyond the bone marrow has been unclear. In addition, Cxcl12 and Cxcr4 modulate the tumor microenvironment and targeting this axis was an effective strategy in certain cancers (Pitt et al., 2015; Quante et al., 2011; Roccaro et al., 2014). Given that human DGCs are in general extremely resistant to current treatment regimens, anti-inflammatory drugs such as steroids or non-steroidal anti-inflammatory drugs (NSAIDs), as well as specific Cxcr4 antagonists, may be useful for chemoprevention of DGC, particularly for hereditary-type DGC prior to gastrectomy, and/or for prevention of recurrent disease.

E-cadherin is essential for epithelial cell survival under normal conditions (Schneider et al., 2010) and loss of E-cadherin causes cell anoikis (Kantak and Kramer, 1998). Previous studies suggest that Cxcr4 and Wnt5a are upregulated in human gastric cancer tissues (Iwasa et al., 2009; Kanzawa et al., 2013). Recent genome-wide analyses revealed in human DGCs the presence of gain-of-function *RHOA* mutations that can inhibit anoikis (Cancer Genome Atlas Research Network, 2014; Kakiuchi et al., 2014; Wang et al., 2014). Thus, the activation of RhoA signaling, either by gene mutation or Wnt5a-mediated effect, may be essential for the development of DGC.

Wnt5a is a representative ligand that activates non-canonical Wnt signaling by binding to Ror2 to regulate cell migration, polarity, proliferation, or invasion. Wnt5a is expressed in gut stroma and contributes to intestinal elongation and colonic regeneration, however, the precise source of stromal Wnt5a has been unclear (Cervantes et al., 2009; Gregorieff et al., 2005; Miyoshi et al., 2012). We propose ILCs as a major source of Wnt5a, at least in the stomach. The function of ILCs has been highlighted in the setting of inflammatory or infectious states, although the possibility has been raised of a role for ILCs in stem cell niche or cancer development (Bando et al., 2015; Hanash et al., 2012; Kirchberger et al., 2013). Our findings would support this model, and given that ILCs are a heterogeneous population of immune cells, further efforts at detailed profiling of the ILC population in stem cell niche and cancer are needed.

EXPERIMENTAL PROCEDURES

Mice

Mist1-CreERT2 mice (Shi et al., 2009), *Cxcl12*-dsRED mice (Ding and Morrison, 2013), *Troy*$^{-/-}$ and *Troy*-BAC-CreERT2 mice (Fafilek et al., 2013), H/K-ATPase-*Cxcl12* mice (Shibata et al., 2013), *Eef1a1*-LSL-*Notch1(IC)* mice (Buonamici et al., 2009), and *Wnt5a*^{flox} mice (Miyoshi et al., 2012) were described previously. *Cxcr4*-EGFP mice were kindly provided by Richard J. Miller (Northwestern University Medical School). LSL-*Kras*^{G12D} and LSL-*Trp53*^{R172H} mice were provided by Dr. Kenneth Olive (Columbia University). *Apc*^{flox} mice were obtained from the National Cancer Institute (NCI). *Lgr5*-DTR-GFP mice were provided by Genentech. *Cdh1*^{flox}, *R26*-mTmG, *R26*-LacZ, *R26*-TdTomato, *R26*-Confetti, *R26*-EYFP, *Cxcl12*^{flox}, *Tie2*-Cre, *Id2*-GFP, and *Cag*-CreERT mice were purchased from the Jackson Laboratory. Cre recombinase was activated by oral administration of TAM (1–5 mg/0.2 ml corn oil, as indicated). All animal studies and procedures were approved by the ethics committees at Columbia University and the Academy of Sciences of the Czech Republic. Human stomach tissue sections were obtained from DGC patients who underwent surgical resection or endoscopic submucosal dissection from 2001 to 2012 at Gifu University Hospital, Gifu, Japan. All study protocols were approved by the ethics committees, and written informed consent was obtained from all patients.

Treatment

5-FU (Sigma) was administered intraperitoneally (i.p.) at a dose of 150 mg/kg. DMP-777 was given as described previously (Nam et al., 2010). DBZ was dissolved in 10% dimethyl sulfoxide and injected i.p. (30 μmol/kg) for 14 days. For Lgr5^{+} cell ablation, DT was administered i.p. at a dose of 20 mg/kg. Mice were treated with 5 mg/kg AMD3100 (Tocris) to inhibit Cxcr4 for 2 weeks, as described previously (Quante et al., 2011). Dexamethasone (Sigma) was administered i.p. at a dose of 5 mg/kg for 2 weeks. CD90.2 mAb (30H12) (BioXCell) was administered i.p. every 2 days at a dose of 250 mg/mouse for 4 weeks. Control groups were treated with appropriate vehicles or control antibodies.

SUPPLEMENTAL INFORMATION

Supplemental Information includes Supplemental Experimental Procedures, six figures, and one table and can be found with this article online at http://dx.doi.org/10.1016/j.ccell.2015.10.003.

AUTHOR CONTRIBUTIONS

Y.H. and H.A. contributed equally to the design of the experiments, performance of the animal experiments and histology, and analysis of the data. J.S., K.S., S.A., H.W., W.S., B.W.R., Y.T., X.C., W.K., S.S.K., Y. Tailor, K.N., H.T., and Z.S. performed various portions of the animal experiments. S.A. and Z.A.D. assisted with the in vitro experiments. H.T. and A.H. collected the human samples and performed the pathological evaluation. A.R.S. conducted the pathological evaluation of mice. W.S. and M.D.G. performed electron microscopy. L.D. and S.F.K. provided the mice. S.S. assisted in situ hybridization and adenovirus injection experiments. Y.H., H.A., S.A., C.B.W., L.D., J.G.F., R.A.F., D.L.W., V.K., and T.C.W. wrote the manuscript and contributed to the study supervision and coordination as well as to the performance of the experiments.

ACKNOWLEDGMENTS

We thank Dr. Anil Rustgi, Dr. Kenneth Olive, Dr. Terry Yamaguchi, Dr. Leonard H. Augenlicht, Dr. Carrie Shawber, and Dr. Richard J. Miller for providing the mice; Ms. Kristie Gordon for assisting in the fluorescence-activated cell sorting (FACS) analysis; Mr. Adam White and Ms. Theresa Swayne for producing the 3D images; Dr. Rani Sellers, Ms. Barbara Cannella, and Ms. Supreet Kainth for assisting with the in situ hybridization; Ms. Ashlesha Muley and Mr. Tao Su for technical assistance; Ms. Wendy Beth Jackelow (Medical & Scientific Illustration) for creating schematic images; and Dr. James R. Goldenring for providing DMP-777.

This research was supported by NIH grants U54CA126513, R01CA093405, R01CA120979, and R01DK052778 and by the Clyde Wu Family Foundation (T.C.W.). Y.H. was supported by Mitsukoshi Health and Welfare Foundation, JSPS Postdoctoral Fellowships for Research Abroad, and the Uehara Memorial Foundation. J.S. and V.K. were supported by the Czech Science Foundation grant numbers P305/11/1780 and 14-33952S.

Received: May 26, 2015
Revised: August 26, 2015
Accepted: October 8, 2015
Published: November 12, 2015

REFERENCES

Arnold, K., Sarkar, A., Yram, M.A., Polo, J.M., Bronson, R., Sengupta, S., Seandel, M., Geijsen, N., and Hochedlinger, K. (2011). Sox2(+) adult stem and progenitor cells are important for tissue regeneration and survival of mice. Cell Stem Cell *9*, 317–329.

Bando, J.K., Liang, H.E., and Locksley, R.M. (2015). Identification and distribution of developing innate lymphoid cells in the fetal mouse intestine. Nat. Immunol. *16*, 153–160.

Barker, N., Ridgway, R.A., van Es, J.H., van de Wetering, M., Begthel, H., van den Born, M., Danenberg, E., Clarke, A.R., Sansom, O.J., and Clevers, H. (2009). Crypt stem cells as the cells-of-origin of intestinal cancer. Nature *457*, 608–611.

Barker, N., Huch, M., Kujala, P., van de Wetering, M., Snippert, H.J., van Es, J.H., Sato, T., Stange, D.E., Begthel, H., van den Born, M., et al. (2010). Lgr5(+ve) stem cells drive self-renewal in the stomach and build long-lived gastric units in vitro. Cell Stem Cell *6*, 25–36.

Buonamici, S., Trimarchi, T., Ruocco, M.G., Reavie, L., Cathelin, S., Mar, B.G., Klinakis, A., Lukyanov, Y., Tseng, J.C., Sen, F., et al. (2009). CCR7 signalling as an essential regulator of CNS infiltration in T-cell leukaemia. Nature *459*, 1000–1004.

Cai, J., Niu, X., Chen, Y., Hu, Q., Shi, G., Wu, H., Wang, J., and Yi, J. (2008). Emodin-induced generation of reactive oxygen species inhibits RhoA activation to sensitize gastric carcinoma cells to anoikis. Neoplasia *10*, 41–51.

Cancer Genome Atlas Research Network (2014). Comprehensive molecular characterization of gastric adenocarcinoma. Nature *513*, 202–209.

Carneiro, F., Huntsman, D.G., Smyrk, T.C., Owen, D.A., Seruca, R., Pharoah, P., Caldas, C., and Sobrinho-Simões, M. (2004). Model of the early development of diffuse gastric cancer in E-cadherin mutation carriers and its implications for patient screening. J. Pathol. *203*, 681–687.

Cervantes, S., Yamaguchi, T.P., and Hebrok, M. (2009). Wnt5a is essential for intestinal elongation in mice. Dev. Biol. *326*, 285–294.

Ding, L., and Morrison, S.J. (2013). Haematopoietic stem cells and early lymphoid progenitors occupy distinct bone marrow niches. Nature *495*, 231–235.

Fafilek, B., Krausova, M., Vojtechova, M., Pospichalova, V., Tumova, L., Sloncova, E., Huranova, M., Stancikova, J., Hlavata, A., Svec, J., et al. (2013). Troy, a tumor necrosis factor receptor family member, interacts with lgr5 to inhibit wnt signaling in intestinal stem cells. Gastroenterology *144*, 381–391.

Farin, H.F., Van Es, J.H., and Clevers, H. (2012). Redundant sources of Wnt regulate intestinal stem cells and promote formation of Paneth cells. Gastroenterology *143*, 1518–1529 e1517.

Gregorieff, A., Pinto, D., Begthel, H., Destrée, O., Kielman, M., and Clevers, H. (2005). Expression pattern of Wnt signaling components in the adult intestine. Gastroenterology *129*, 626–638.

Guilford, P., Hopkins, J., Harraway, J., McLeod, M., McLeod, N., Harawira, P., Taite, H., Scoular, R., Miller, A., and Reeve, A.E. (1998). E-cadherin germline mutations in familial gastric cancer. Nature *392*, 402–405.

Hanash, A.M., Dudakov, J.A., Hua, G., O'Connor, M.H., Young, L.F., Singer, N.V., West, M.L., Jenq, R.R., Holland, A.M., Kappel, L.W., et al. (2012). Interleukin-22 protects intestinal stem cells from immune-mediated tissue damage and regulates sensitivity to graft versus host disease. Immunity *37*, 339–350.

Hanoun, M., Zhang, D., Mizoguchi, T., Pinho, S., Pierce, H., Kunisaki, Y., Lacombe, J., Armstrong, S.A., Dührsen, U., and Frenette, P.S. (2014). Acute myelogenous leukemia-induced sympathetic neuropathy promotes malignancy in an altered hematopoietic stem cell niche. Cell Stem Cell *15*, 365–375.

Hayakawa, Y., Jin, G., Wang, H., Chen, X., Westphalen, C.B., Asfaha, S., Renz, B.W., Ariyama, H., Dubeykovskaya, Z.A., Takemoto, Y., et al. (2015). CCK2R identifies and regulates gastric antral stem cell states and carcinogenesis. Gut *64*, 544–553.

Hoyler, T., Klose, C.S., Souabni, A., Turqueti-Neves, A., Pfeifer, D., Rawlins, E.L., Voehringer, D., Busslinger, M., and Diefenbach, A. (2012). The transcription factor GATA-3 controls cell fate and maintenance of type 2 innate lymphoid cells. Immunity *37*, 634–648.

Huh, W.J., Khurana, S.S., Geahlen, J.H., Kohli, K., Waller, R.A., and Mills, J.C. (2012). Tamoxifen induces rapid, reversible atrophy, and metaplasia in mouse stomach. Gastroenterology *142*, 21–24 e27.

Humar, B., Fukuzawa, R., Blair, V., Dunbier, A., More, H., Charlton, A., Yang, H.K., Kim, W.H., Reeve, A.E., Martin, I., and Guilford, P. (2007). Destabilized adhesion in the gastric proliferative zone and c-Src kinase activation mark the development of early diffuse gastric cancer. Cancer Res. *67*, 2480–2489.

Iwasa, S., Yanagawa, T., Fan, J., and Katoh, R. (2009). Expression of CXCR4 and its ligand SDF-1 in intestinal-type gastric cancer is associated with lymph node and liver metastasis. Anticancer Res. *29*, 4751–4758.

Kakiuchi, M., Nishizawa, T., Ueda, H., Gotoh, K., Tanaka, A., Hayashi, A., Yamamoto, S., Tatsuno, K., Katoh, H., Watanabe, Y., et al. (2014). Recurrent gain-of-function mutations of RHOA in diffuse-type gastric carcinoma. Nat. Genet. *46*, 583–587.

Kantak, S.S., and Kramer, R.H. (1998). E-cadherin regulates anchorage-independent growth and survival in oral squamous cell carcinoma cells. J. Biol. Chem. *273*, 16953–16961.

Kanzawa, M., Semba, S., Hara, S., Itoh, T., and Yokozaki, H. (2013). WNT5A is a key regulator of the epithelial-mesenchymal transition and cancer stem cell properties in human gastric carcinoma cells. Pathobiology *80*, 235–244.

Karam, S.M., and Leblond, C.P. (1993). Dynamics of epithelial cells in the corpus of the mouse stomach. I. Identification of proliferative cell types and pinpointing of the stem cell. Anat. Rec. *236*, 259–279.

Kim, T.H., and Shivdasani, R.A. (2011). Notch signaling in stomach epithelial stem cell homeostasis. J. Exp. Med. *208*, 677–688.

Kirchberger, S., Royston, D.J., Boulard, O., Thornton, E., Franchini, F., Szabady, R.L., Harrison, O., and Powrie, F. (2013). Innate lymphoid cells sustain colon cancer through production of interleukin-22 in a mouse model. J. Exp. Med. *210*, 917–931.

Liu, J., Zhang, Y., Xu, R., Du, J., Hu, Z., Yang, L., Chen, Y., Zhu, Y., and Gu, L. (2013). PI3K/Akt-dependent phosphorylation of GSK3β and activation of RhoA regulate Wnt5a-induced gastric cancer cell migration. Cell. Signal. *25*, 447–456.

Malam, Z., and Cohn, R.D. (2014). Stem cells on alert: priming quiescent stem cells after remote injury. Cell Stem Cell *15*, 7–8.

Mendelson, A., and Frenette, P.S. (2014). Hematopoietic stem cell niche maintenance during homeostasis and regeneration. Nat. Med. *20*, 833–846.

Mills, J.C., and Shivdasani, R.A. (2011). Gastric epithelial stem cells. Gastroenterology *140*, 412–424.

Miyoshi, H., Ajima, R., Luo, C.T., Yamaguchi, T.P., and Stappenbeck, T.S. (2012). Wnt5a potentiates TGF-β signaling to promote colonic crypt regeneration after tissue injury. Science *338*, 108–113.

Nam, K.T., Lee, H.J., Sousa, J.F., Weis, V.G., O'Neal, R.L., Finke, P.E., Romero-Gallo, J., Shi, G., Mills, J.C., Peek, R.M., Jr., et al. (2010). Mature chief cells are cryptic progenitors for metaplasia in the stomach. Gastroenterology *139*, 2028–2037.e9.

Nomura, S., Yamaguchi, H., Ogawa, M., Wang, T.C., Lee, J.R., and Goldenring, J.R. (2005). Alterations in gastric mucosal lineages induced by acute oxyntic atrophy in wild-type and gastrin-deficient mice. Am. J. Physiol. Gastrointest. Liver Physiol. *288*, G362–G375.

Okumura, T., Ericksen, R.E., Takaishi, S., Wang, S.S., Dubeykovskiy, Z., Shibata, W., Betz, K.S., Muthupalani, S., Rogers, A.B., Fox, J.G., et al. (2010). K-ras mutation targeted to gastric tissue progenitor cells results in chronic inflammation, an altered microenvironment, and progression to intraepithelial neoplasia. Cancer Res. *70*, 8435–8445.

Pitt, L.A., Tikhonova, A.N., Hu, H., Trimarchi, T., King, B., Gong, Y., Sanchez-Martin, M., Tsirigos, A., Littman, D.R., Ferrando, A.A., et al. (2015). CXCL12-producing vascular endothelial niches control acute T cell leukemia maintenance. Cancer Cell *27*, 755–768.

Quante, M., Marrache, F., Goldenring, J.R., and Wang, T.C. (2010). TFF2 mRNA transcript expression marks a gland progenitor cell of the gastric oxyntic mucosa. Gastroenterology *139*, 2018–2027.e2012.

Quante, M., Tu, S.P., Tomita, H., Gonda, T., Wang, S.S., Takashi, S., Baik, G.H., Shibata, W., Diprete, B., Betz, K.S., et al. (2011). Bone marrow-derived myofibroblasts contribute to the mesenchymal stem cell niche and promote tumor growth. Cancer Cell *19*, 257–272.

Roccaro, A.M., Sacco, A., Purschke, W.G., Moschetta, M., Buchner, K., Maasch, C., Zboralski, D., Zöllner, S., Vonhoff, S., Mishima, Y., et al. (2014). SDF-1 inhibition targets the bone marrow niche for cancer therapy. Cell Rep. *9*, 118–128.

Sato, T., van Es, J.H., Snippert, H.J., Stange, D.E., Vries, R.G., van den Born, M., Barker, N., Shroyer, N.F., van de Wetering, M., and Clevers, H. (2011). Paneth cells constitute the niche for Lgr5 stem cells in intestinal crypts. Nature *469*, 415–418.

Schneider, M.R., Dahlhoff, M., Horst, D., Hirschi, B., Trülzsch, K., Müller-Höcker, J., Vogelmann, R., Allgäuer, M., Gerhard, M., Steininger, S., et al. (2010). A key role for E-cadherin in intestinal homeostasis and Paneth cell maturation. PLoS ONE *5*, e14325.

Shi, G., Zhu, L., Sun, Y., Bettencourt, R., Damsz, B., Hruban, R.H., and Konieczny, S.F. (2009). Loss of the acinar-restricted transcription factor Mist1 accelerates Kras-induced pancreatic intraepithelial neoplasia. Gastroenterology *136*, 1368–1378.

Shibata, W., Ariyama, H., Westphalen, C.B., Worthley, D.L., Muthupalani, S., Asfaha, S., Dubeykovskaya, Z., Quante, M., Fox, J.G., and Wang, T.C. (2013). Stromal cell-derived factor-1 overexpression induces gastric dysplasia through expansion of stromal myofibroblasts and epithelial progenitors. Gut *62*, 192–200.

Shimada, S., Mimata, A., Sekine, M., Mogushi, K., Akiyama, Y., Fukamachi, H., Jonkers, J., Tanaka, H., Eishi, Y., and Yuasa, Y. (2012). Synergistic tumour suppressor activity of E-cadherin and p53 in a conditional mouse model for metastatic diffuse-type gastric cancer. Gut *61*, 344–353.

Shyer, A.E., Huycke, T.R., Lee, C., Mahadevan, L., and Tabin, C.J. (2015). Bending gradients: how the intestinal stem cell gets its home. Cell *161*, 569–580.

Stange, D.E., Koo, B.K., Huch, M., Sibbel, G., Basak, O., Lyubimova, A., Kujala, P., Bartfeld, S., Koster, J., Geahlen, J.H., et al. (2013). Differentiated

Troy+ chief cells act as reserve stem cells to generate all lineages of the stomach epithelium. Cell *155*, 357–368.

Sugiyama, T., Kohara, H., Noda, M., and Nagasawa, T. (2006). Maintenance of the hematopoietic stem cell pool by CXCL12-CXCR4 chemokine signaling in bone marrow stromal cell niches. Immunity *25*, 977–988.

Tian, H., Biehs, B., Warming, S., Leong, K.G., Rangell, L., Klein, O.D., and de Sauvage, F.J. (2011). A reserve stem cell population in small intestine renders Lgr5-positive cells dispensable. Nature *478*, 255–259.

Tu, S., Bhagat, G., Cui, G., Takaishi, S., Kurt-Jones, E.A., Rickman, B., Betz, K.S., Penz-Oesterreicher, M., Bjorkdahl, O., Fox, J.G., and Wang, T.C. (2008). Overexpression of interleukin-1beta induces gastric inflammation and cancer and mobilizes myeloid-derived suppressor cells in mice. Cancer Cell *14*, 408–419.

Wang, K., Yuen, S.T., Xu, J., Lee, S.P., Yan, H.H., Shi, S.T., Siu, H.C., Deng, S., Chu, K.M., Law, S., et al. (2014). Whole-genome sequencing and comprehensive molecular profiling identify new driver mutations in gastric cancer. Nat. Genet. *46*, 573–582.

Worthley, D.L., Churchill, M., Compton, J.T., Tailor, Y., Rao, M., Si, Y., Levin, D., Schwartz, M.G., Uygur, A., Hayakawa, Y., et al. (2015). Gremlin 1 identifies a skeletal stem cell with bone, cartilage, and reticular stromal potential. Cell *160*, 269–284.

Yang, S., Pham, L.K., Liao, C.P., Frenkel, B., Reddi, A.H., and Roy-Burman, P. (2008). A novel bone morphogenetic protein signaling in heterotypic cell interactions in prostate cancer. Cancer Res. *68*, 198–205.

Zhao, C.M., Hayakawa, Y., Kodama, Y., Muthupalani, S., Westphalen, C.B., Andersen, G.T., Flatberg, A., Johannessen, H., Friedman, R.A., Renz, B.W., et al. (2014). Denervation suppresses gastric tumorigenesis. Sci. Transl. Med. *6*, 250ra115.

Zhu, Y., Huang, Y.F., Kek, C., and Bulavin, D.V. (2013). Apoptosis differently affects lineage tracing of Lgr5 and Bmi1 intestinal stem cell populations. Cell Stem Cell *12*, 298–303.

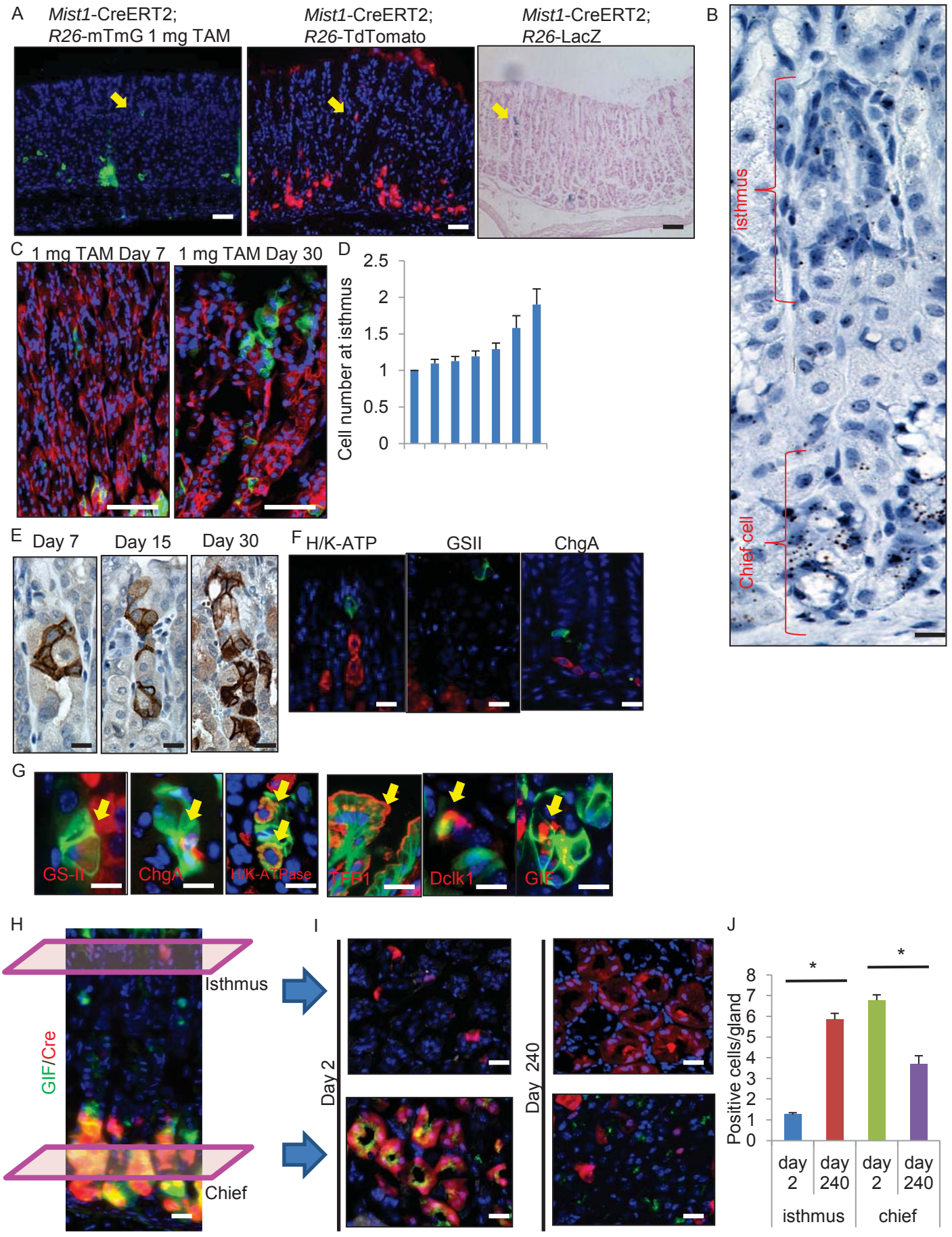
Cancer Cell, Volume *28*

Supplemental Information

Mist1 Expressing Gastric Stem Cells Maintain the Normal and Neoplastic Gastric Epithelium and Are Supported by a Perivascular Stem Cell Niche

Yoku Hayakawa, Hiroshi Ariyama, Jitka Stancikova, Kosuke Sakitani, Samuel Asfaha, Bernhard W. Renz, Zinaida A. Dubeykovskaya, Wataru Shibata, Hongshan Wang, Christoph B. Westphalen, Xiaowei Chen, Yoshihiro Takemoto, Woosook Kim, Shradha S. Khurana, Yagnesh Tailor, Karan Nagar, Hiroyuki Tomita, Akira Hara, Antonia R. Sepulveda, Wanda Setlik, Michael D. Gershon, Subhrajit Saha, Lei Ding, Zeli Shen, James G. Fox, Richard A. Friedman, Stephen F. Konieczny, Daniel L. Worthley, Vladimir Korinek, and Timothy C. Wang

Supplemetal Data



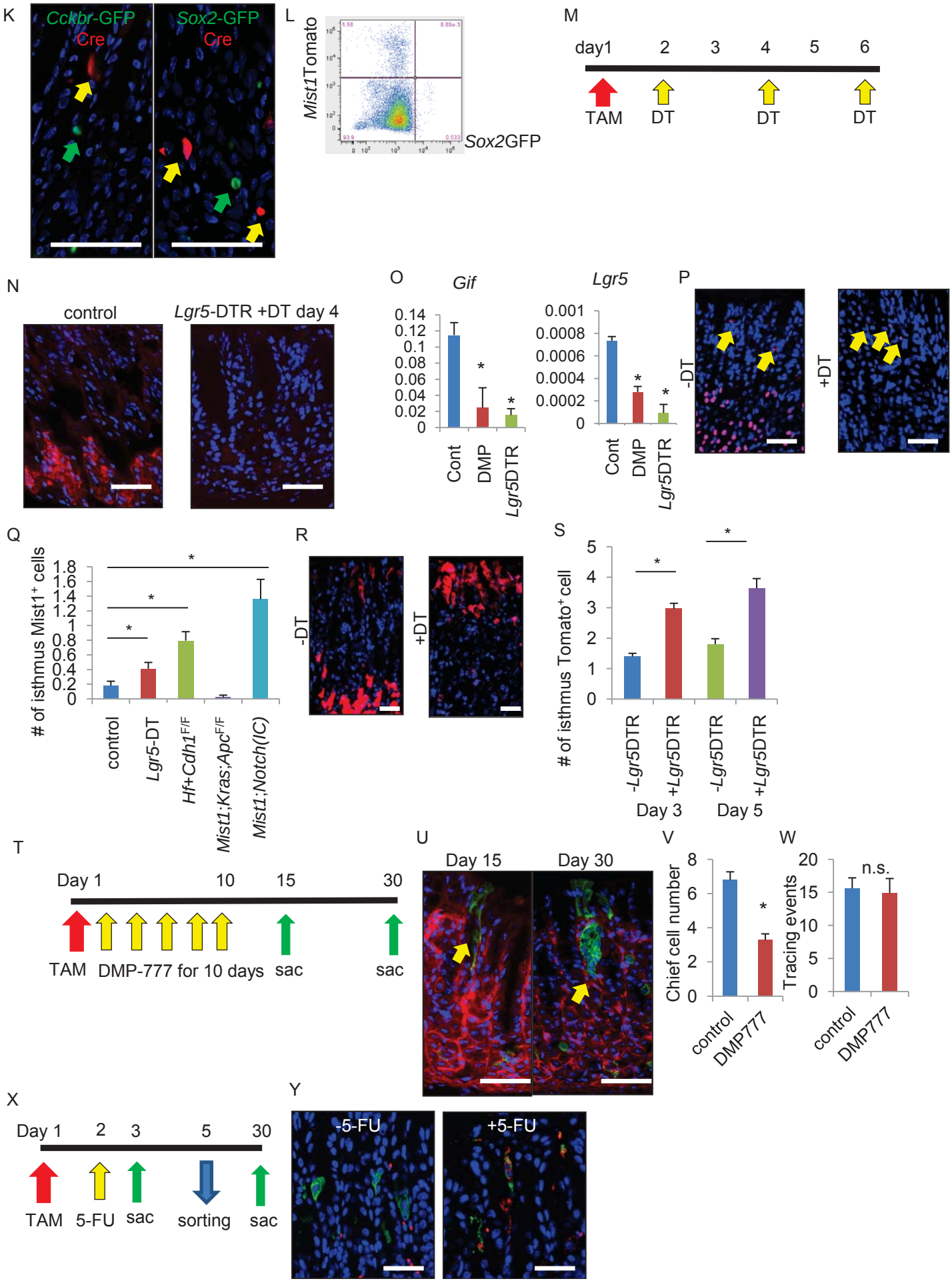

K
Cckbr-GFP
Cre
Sox2-GFP
Cre
L
Mist1Tomato
Sox2GFP
M
day1
2
3
4
5
6
TAM
DT
DT
DT
N
control
Lgr5-DTR +DT day 4
O
Gif
0.14
0.12
0.1
0.08
0.06
0.04
0.02
0
Cont
DMP
Lgr5DTR
Lgr5
0.001
0.0008
0.0006
0.0004
0.0002
0
Cont
DMP
Lgr5DTR
P
-DT
+DT
Q
# of isthmus Mist1+ cells
1.8
1.6
1.4
1.2
1
0.8
0.6
0.4
0.2
0
control
Lgr5-DT
Hf+Cdh1F/F
Mist1;Kras;ApcF/F
Mist1;Notch(IC)
R
-DT
+DT
S
# of isthmus Tomato+ cell
5
4
3
2
1
0
-Lgr5DTR
+Lgr5DTR
-Lgr5DTR
+Lgr5DTR
Day 3
Day 5
T
Day 1
10
15
30
TAM
DMP-777 for 10 days
sac
sac
U
Day 15
Day 30
V
Chief cell number
8
6
4
2
0
control
DMP777
W
Tracing events
20
15
10
5
0
n.s.
control
DMP777
X
Day 1
2
3
5
30
TAM
5-FU
sac
sorting
sac
Y
-5-FU
+5-FU

Figure S1, Related to Figure 1. Mist1^{+} lineage tracing in the corpus isthmus.
(A) Lineage tracing on day 1 in *Mist1*-CreERT2;*R26*-mTmG (1 mg TAM), *R26*-TdTomato, and *R26*-LacZ mice. Arrows indicage Mist1^{+} isthmus cells. (B) In situ hybridization of *Mist1* in the corpus glands. (C) Lineage tracing in *Mist1*-CreERT2;*R26*-mTmG 7 and 30 days after 1 mg TAM induction. (D) Mist1^{+} cell numbers of the isthmus at the indicated time points. Means ± SEM. 30 glands are analyzed at each time point. (E) GFP staining of lineage tracing in *Mist1*-CreERT2;*R26*-mTmG 7, 15, 30 days after TAM induction. (F) H/K-ATPase, GS-II, and Chg-A staining (red) with GFP staining (green) in *Mist1*-CreERT2;*R26*-mTmG mouse corpus on day 1. (G) Immunofluorescence of the indicated markers (red) with GFP staining (green) in *Mist1*-CreERT2;*R26*-mTmG mice 12 months after TAM. Arrows indicate double-positive cells. (H-I) Cross sectional images of *Mist1*-CreERT2;*R26*-Tdtomato mice at day 2 and 240. Sections are stained with GIF (green). (J) The numbers of TdTomato^{+} cells per gland in the cross section at day 2 and 240. 50 glands/group are analyzed at each time point. (K) The corpus images of *Mist1*-CreERT2;*R26*-TdTomato mice crossed to *Cckbr*-GFP and *Sox2*-GFP mice 24 hr after TAM. Yellow arrows indicate Mist1^{+} isthmus cells and green arrows indicate Cckbr^{+} or Sox2^{+} cells. (L) FACS plot of *Mist1*-CreERT;*Sox2*-GFP;*R26*-TdTomato mouse corpus. Mice were sacrificed 24 hr after TAM. (M) Protocol for TAM and DT treatments. (N) GIF staining (red) in control and DT-treated (day 4) *Lgr5*-DTR mouse corpus glands. (O) Relative gene expressions in the corpus glands of control, DMP-777-treated, and DT-treated *Lgr5*-DTR mice. n = 3/group. (P) Mist1 staining (red) in control and DT-treated (day 4) *Lgr5*-DTR mouse corpus glands. Arrows indicate isthmus Mist1^{+} cells. (Q) The numbers of isthmus Mist1^{+} cells in control, DT-treated (day 4) *Lgr5*-DTR mouse, *Hf*-infected *Cdh1*$^{\Delta Mist1}$ (3 months), *Mist1*-CreERT2;LSL-*Kras*^{G12D};*Apc*$^{flox/flox}$, (3 months) and *Mist1*-CreERT2;LSL-*Notch1(IC)* (3 months) mice. Total 50 glands /group were analyzed. (R and S) *Mist1*-CreERT2;*Lgr5*-DTR;*R26*-TdTomato mice were treated with TAM at day1, and given DT at day 2, then sacrificed at day 3 or day 5. Representative tracing (red) at day 3 (R) and the numbers of TdTomato^{+} cells in the isthmus (S) are shown. (T) Protocol for DMP-777 and TAM treatments. (U) Day 15 and 30 lineage tracing of DMP-777-treated *Mist1*-CreERT2;*R26*-mTmG mice. Refer to Fig. 1C for control tracing images. Arrows indicate isthmus cell lineage. (V-W) The number of GFP^{+} chief cells per gland (V) and tracing events per 100 glands (W) in day 30 *Mist1*-CreERT2;*R26*-mTmG mice treated with or without DMP-777. Total 90 glands from 3 mice /group are analyzed for chief cell number, and total 300 glands from 3 mice /group are analyzed for tracing events. (X) Protocol for TAM and 5-FU treatments. (Y) Immunostaining of cleaved caspase 3 (red) and GFP (green) in *Mist1*-CreERT2;*R26*-mTmG mice. Mice were treated with TAM at day 1, and with 5-FU or PBS at day 2, then sacrificed at day 3. Note that Mist1^{+} cells become cleaved caspase 3-positive after 5-FU treatment. Bars=50 μm (A, C, K, N, P, R, U, Y), 10 μm (B, E-I). Means ± SEM. *$p < 0.05$.

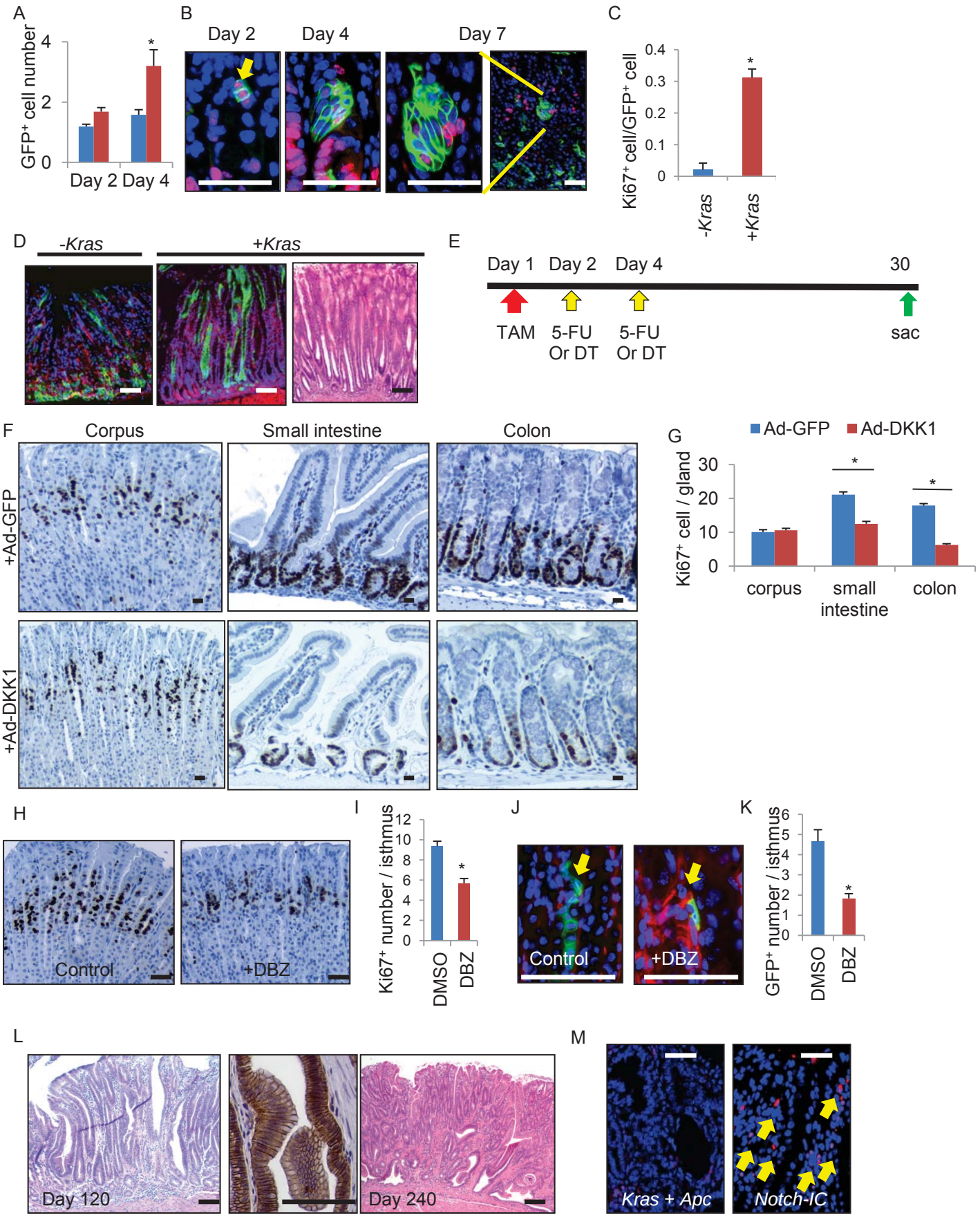

A
GFP+ cell number
Day 2 Day 4
B
Day 2
Day 4
Day 7
C
Ki67+ cell/GFP+ cell
-Kras
+Kras
D
-Kras
+Kras
E
Day 1 Day 2 Day 4 30
TAM
5-FU Or DT
5-FU Or DT
sac
F
Corpus
Small intestine
Colon
+Ad-GFP
+Ad-DKK1
G
Ad-GFP
Ad-DKK1
Ki67+ cell / gland
corpus
small intestine
colon
H
Control
+DBZ
I
Ki67+ number / isthmus
DMSO
DBZ
J
Control
+DBZ
K
GFP+ number / isthmus
DMSO
DBZ
L
Day 120
Day 240
M
Kras + Apc
Notch-IC

Figure. S2, Related to Figure 2. Mist1^{+} lineage tracing with oncogenic mutations.
(A) Numbers of GFP^{+} cells in the corpus gland 2 and 4 days after TAM induction in *Mist1*-CreERT2;*R26*-mTmG mice (blue) and *Mist1*-CreERT2;LSL-*Kras*^{G12D};*R26*-mTmG mice (red). n = 30 glands/group. (B) Lineage tracing and Ki67 staining in *Mist1*-CreERT2;*R26*-mTmG mice with or without LSL-*Kras*^{G12D} mutation. Arrow indicates isthmus stem cell. (C) The numbers of Ki67 and GFP double-positive cells per total number of GFP^{+} cells with or without *Kras* mutation on day 2. Total 100 glands from 5 animals/group are analyzed. (D) Lineage tracing and H&E staining in *Mist1*-CreERT2;*R26*-mTmG mice with or without *Kras* mutation after 3 months. (E) Protocol for TAM and 5-FU or DT treatment. (F) Ki67 staining in the corpus gland, small intestine, and colon of mice 2 days after injection of GFP-expressing (Ad-GFP) and DKK1-expressing adenoviruses (Ad-DKK1). (G) Number of Ki67^{+} cells per gland. n = 30 glands/group. (H and I) Ki67 staining (H) and Ki67^{+} cell numbers (I) in mouse corpus glands treated with or without 14 days DBZ. n = 30 glands/group. (J-K) Lineage tracing images (J) and the number of GFP^{+} cells (K) in *Mist1*-CreERT2;*R26*-mTmG mice with or without DBZ treatment for 14 days. Total 30 glands /group are analyzed. (L) H&E and β-catenin staining in *Mist1*-CreERT2;*Eef1a1*-LSL-*Notch1(IC)* mouse corpus on day 120 and 240 post-induction. (M) Mist1 staining (red) of *Mist1*-CreERT2;LSL-*Kras*^{G12D};*Apc*$^{flox/flox}$ and *Mist1*-CreERT2;LSL-*Notch1(IC)* mice 3 months after TAM. Arrows indicate Mist1^{+} cell. Means ± SEM. *p < 0.05. Bars=50 μm.

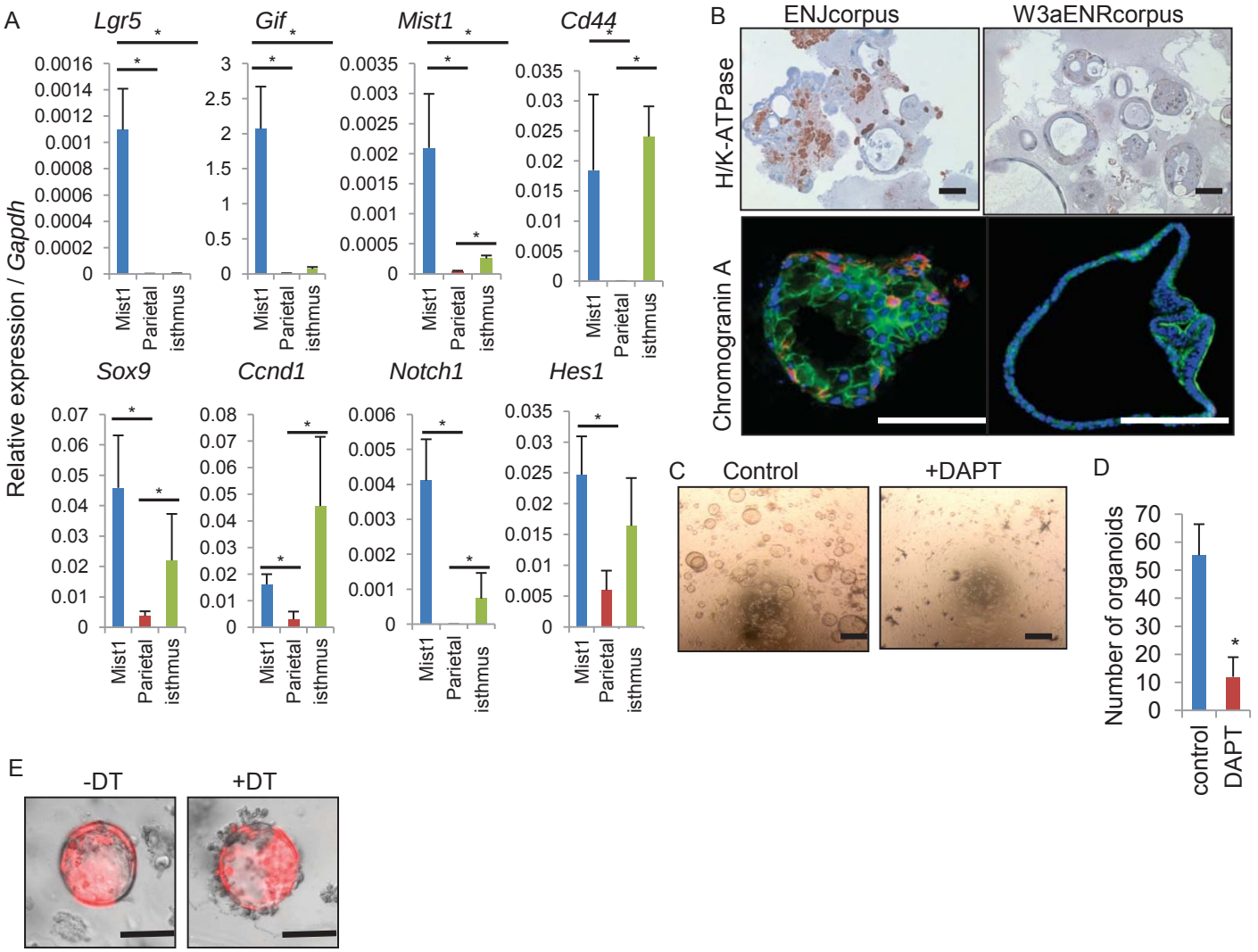
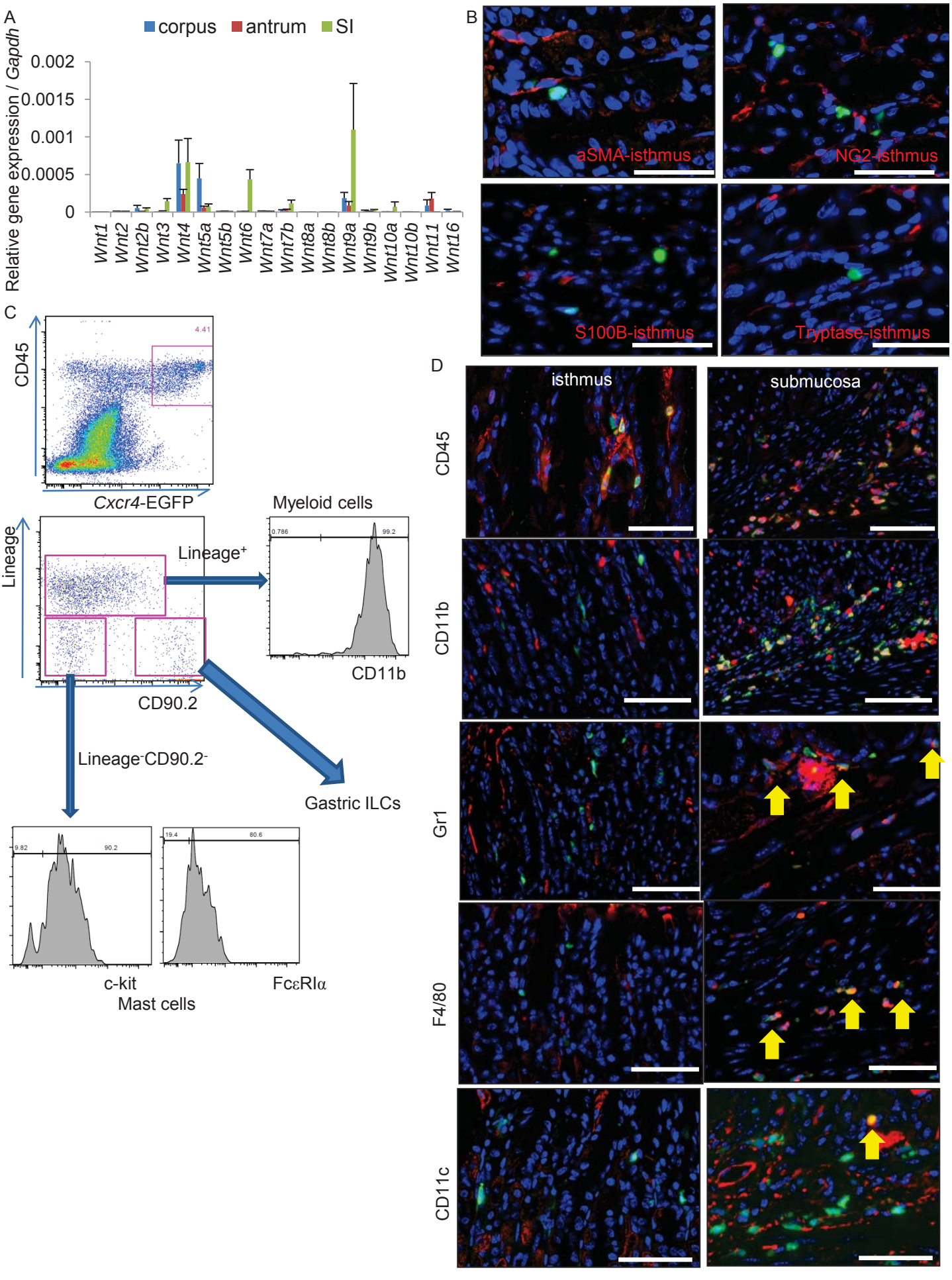


Figure S3, Related to Figure 3. Notch signaling is important for the Mist1⁺ stem cell maintenance.

(A) Relative gene expression per *Gapdh* in sorted total Mist1⁺ population, parietal cell population, and Mist1⁺ isthmus cell population after DT ablation. n = 3/group. (B) H/K-ATPase (brown; counter-stained by hematoxylene) and Chromogranin A (red; counter-stained by DAPI (blue) and phalloidin (green)) staining in the corpus organoids cultured with W3aENR and ENJ media for 20 days. (C and D) Corpus gland cultures in W3aENR media treated with vehicle or DAPT on day 10. Representative images (C) and numbers of organoids per well (D) are shown. n = 3/group. (E) In vitro lineage tracing of *Mist1*-CreERT2;*R26*-TdTomato corpus. Glands were isolated 1 day after tamoxifen and cultured with ENJ media with or without DT. Bars=50 μm (B, C), 100 μm (E). Means ± SEM. *p < 0.05.


A
corpus
antrum
SI
Relative gene expression / Gapdh
0.002
0.0015
0.001
0.0005
0
Wnt1
Wnt2
Wnt2b
Wnt3
Wnt4
Wnt5a
Wnt5b
Wnt6
Wnt7a
Wnt7b
Wnt8a
Wnt8b
Wnt9a
Wnt9b
Wnt10a
Wnt10b
Wnt11
Wnt16
B
aSMA-isthmus
NG2-isthmus
S100B-isthmus
Tryptase-isthmus
C
CD45
Cxcr4-EGFP
Lineage
Lineage+
Myeloid cells
CD11b
CD90.2
Lineage-CD90.2-
Gastric ILCs
c-kit
Mast cells
FcεRIα
D
isthmus
submucosa
CD45
CD11b
Gr1
F4/80
CD11c

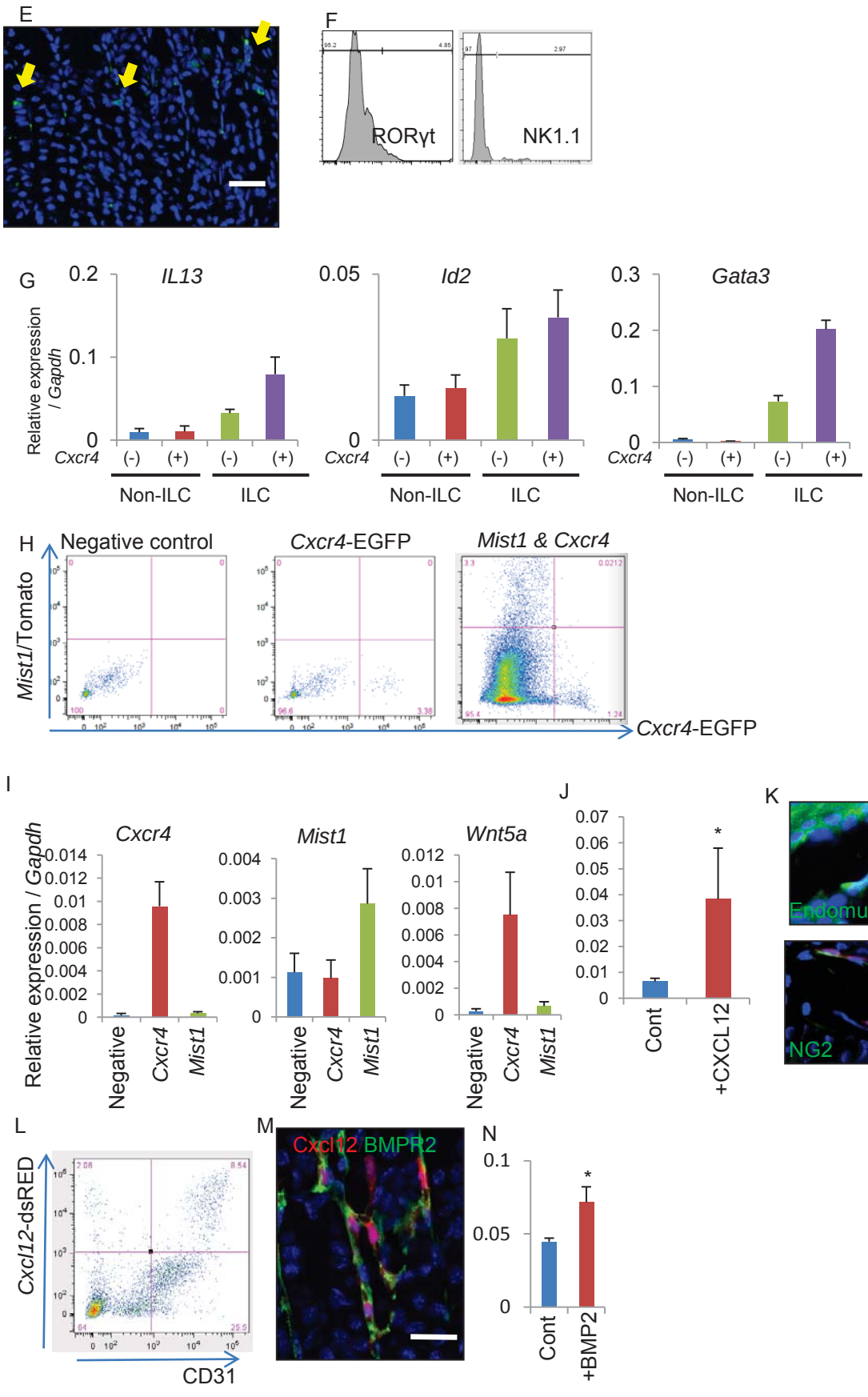

E
F
RORγt
NK1.1
G
IL13
Id2
Gata3
Relative expression / Gapdh
Cxcr4
(-)
(+)
Non-ILC
ILC
H
Negative control
Cxcr4-EGFP
Mist1 & Cxcr4
Mist1/Tomato
Cxcr4-EGFP
I
Cxcr4
Mist1
Wnt5a
Relative expression / Gapdh
Negative
J
Cont
+CXCL12
K
Endomucin
a-SMA
NG2
GAP43
L
Cxcl12-dsRED
CD31
M
Cxcl12 BMPR2
N
Cont
+BMP2

Figure S4, Related to Figure 4. Cxcr4^{+} cell population in the corpus.
(A) Relative Wnt ligand expression per *Gapdh* in mouse corpus, antrum, and small intestine. n = 3/group. Means ± SEM. (B) Negative control image of *Wnt5a* in situ hybridyzation. (C) Immunostaining with the indicated markers (red) of *Cxcr4*-EGFP corpus isthmus. (C) FACS plot with CD11b, c-kit, and FcεRIα. Lineage^{+}Cxcr4^{+} population is CD11b^{+} myeloid cells. Lineage^{-} CD90.2^{-}Cxcr4^{+} population are mast cells. (D) CD45, CD11b, Gr1, F4/80, and CD11c staining (red) in the corpus (isthmus and submucosal area) of *Cxcr4*-EGFP mice. Arrows indicate double positive cells. (E) *Id2*-GFP mouse corpus. Arrows indicate GFP^{+} cells. (F) FACS histogram with RORγt and NK1.1 of CD45^{+}Cxcr4^{+}Lin^{-}CD127^{+} population. (G) Gene expression of type2 ILC markers in Cxcr4$^{+/-}$ ILCs and non-ILCs. n = 3/group. (H-I) FACS plot (H) of WT (negative control), *Cxcr4*-EGFP mice, and *Mist1*-CreERT;*Cxcr4*-EGFP;*R26*-TdTomato mice corpus. Refer to Fig. 3D as TdTomato alone control. Relative gene expression (I) of TdTomato^{+}, GFP^{+}, and double-negative cells sorted from *Mist1*-CreERT2;*Cxcr4*-EGFP;*R26*-TdTomato mice 1 day after TAM induction. n = 3/group. (J) *Wnt5a* gene expression in sorted Cxcr4^{+} cells from the stomach. Cells were treated with Cxcl12 and harvested 24 hr later. n = 3/group. (K) Immunostaining with the indicated markers (green) of *Cxcl12*-dsRED cells. (L) FACS plot of dsRED and CD31 from *Cxcl12*-dsRED mouse stomach. (M) BMPR2 immunostaining (green) of *Cxcl12*-dsRED mouse stomach. (N) *Cxcl12* gene expression in cultured *Cxcl12*-dsRED cells treated with or without BMP2 for 24 hr. n = 3/group. Means ± SEM. *$p < 0.05$ compared to control. Bars=20 μm (K, M), 50 μm (B, D-E).

Table S1, Related to Figure 4. qRT-PCR array comparing gene expression between Cxcl12^{+}CD31^{+} cells and Cxcl12^{-}CD31^{+} cells.

Symbol	Fold Change (Cxcl12^{+}CD31^{+} cells vs Cxcl12^{-}CD31^{+} cells)
Ar	13.6895
Arnt	1.3803
Atf1	0.933
Atf2	1.3947
Atf3	0.4047
Atf4	1.9588
Cebpa	0.0899
Cebpb	0.2269
Cebpg	1.9119
Clasrp	0.8888
Creb1	1.3519
Crebbp	1.2483
Ctnnb1	4.2281
Dr1	0.8827
E2f1	0.3231
E2f6	1.0534
Egr1	1.1329
Esr1	0.2932
Ets1	11.5915
Ets2	1.6586
Fos	0.8066
Foxa2	1.2058
Foxg1	0.9138
Gata1	0.0988
Gata2	1.1933
Gata3	1.0105
Gli1	0.6666
Gtf2b	1.5476
Gtf2f1	0.8011
Hand1	0.3242
Hand2	1.454
Hdac1	1.2269
Hif1a	1.3379

Hnf1a	0.75
Hnf4a	1.3755
Hoxa5	11.0425
Hsf1	1.3149
Id1	1.8856
Irf1	2.8779
Jun	1.5052
Junb	0.7346
Jund	1.1019
Kcnh8	0.3287
Max	1.2924
Mef2a	1.3241
Mef2b	2.0069
Mef2c	7.4643
Myc	0.6902
Myf5	0.8467
Myod1	0.9138
Nanos2	1.8596
Nfat5	2.2815
Nfatc2	0.1811
Nfatc3	1.0389
Nfatc4	0.4665
Nfkb1	0.7765
Nfyb	1.7532
Nr3c1	1.9386
Pax6	0.473
Pou2af1	0.0527
Ppara	0.8827
Pparg	1.676
Rb1	2.166
Rel	0.2154
Rela	1.007
Smad1	1.8088
Smad4	2.395
Smad5	2.0491
Smad9	1.0461
Sp1	1.1487
Sp3	1.834

Stat1	1.3613
Stat2	1.5801
Stat3	1.5263
Stat4	0.2793
Stat5a	0.8409
Stat5b	0.9862
Stat6	1.0718
Tbp	1.1728
Tcf7l2	1.083
Tfap2a	2.114
Tgif1	0.6878
Trp53	0.6329
Yy1	1.2311

* Upregulated genes (> 2 fold) are shown in red, and downregulated genes (< 0.5 fold) are shown in blue.

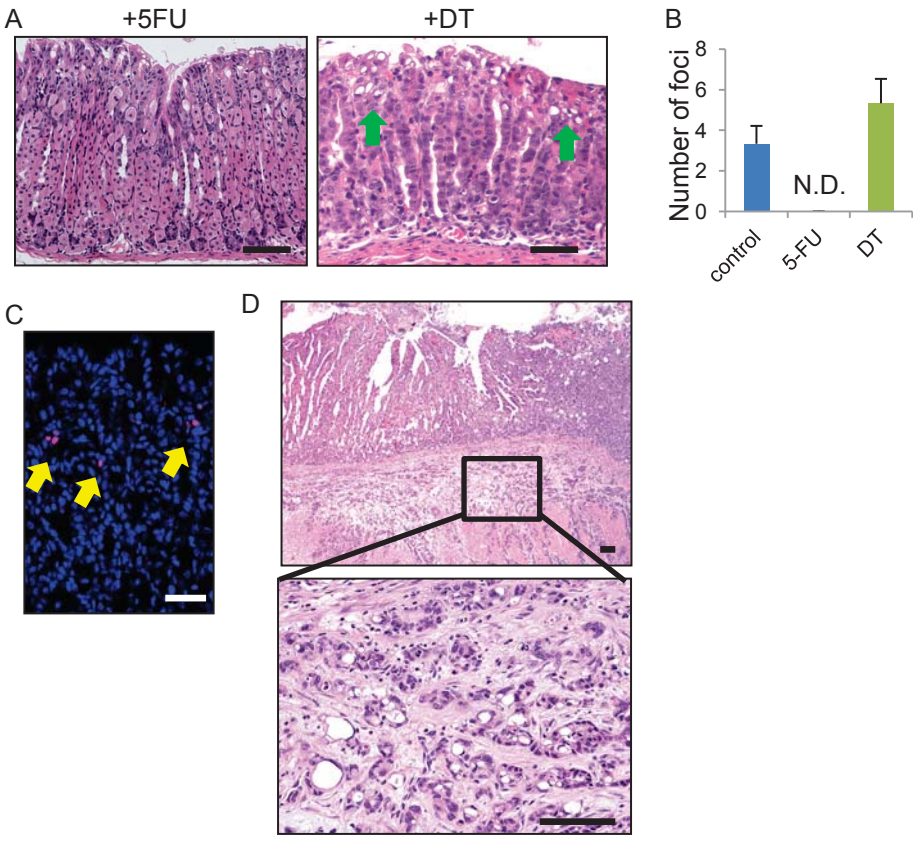
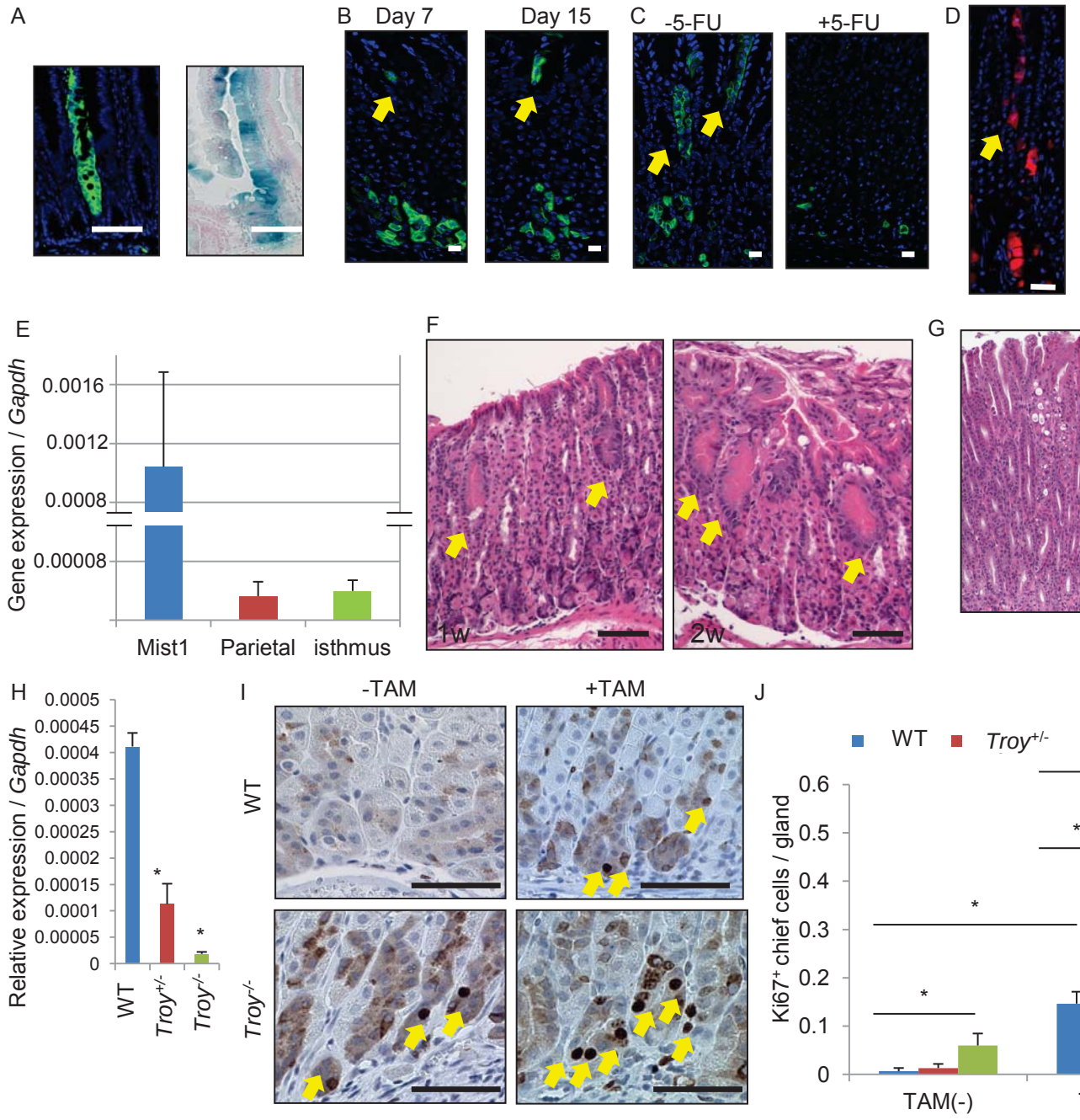


Figure S5, Related to Figure 5. Cxcl12/Cxcr4 perivascular niche in the stomach and DGC development.

(A-B) *Cdh1*$^{\Delta Mist1}$ crossed to *Lgr5*-DTR mice were treated with 5-FU or DT after TAM plus *Hf* treatment. Day 30 H&E images (A) and numbers of atypical foci (B). n = 3 mice/group and 4 sections/mouse are analyzed. Arrows indicate atypical foci in the isthmus. (C) Mist1 staining (red) of *Hf*-infected *Cdh1*$^{\Delta Mist1}$ mice 3 months after TAM. Arrows indicate isthmus Mist1^{+} cells. (D) H&E staining of *Hf*-infected *Cdh1*$^{\Delta Mist1}$ crossed to LSL-*Trp53*^{R172H} mice 9 months after TAM. The lower panel shows higher magnification of box area in the upper panel, showing that signet-ring cancer cells invade into submucosa. Means ± SEM. *p < 0.05 compared to control. Bar=50 μm (C-D), 100 μm (A).


A
B Day 7
Day 15
C -5-FU
+5-FU
D
E
Gene expression / Gapdh
0.0016
0.0012
0.0008
0.00008
Mist1
Parietal
isthmus
F
1w
2w
G
H
Relative expression / Gapdh
0.0005
0.00045
0.0004
0.00035
0.0003
0.00025
0.0002
0.00015
0.0001
0.00005
0
WT
Troy+/-
Troy-/-
I
-TAM
+TAM
WT
Troy-/-
J
WT
Troy+/-
Troy-/-
Ki67+ chief cells / gland
0.6
0.5
0.4
0.3
0.2
0.1
0
TAM(-)
TAM(+)
K
-5-FU
+5-FU
L
25
20
15
10
5
0
N.D.
control
5-FU
control
5-FU
Troy+/+
Troy+/-
M
Control IgG
Anti-CD90.2
N
40
35
30
25
20
15
10
5
0
IgG
Anti CD90.2
O
Relative expression / Gapdh
3
2.5
2
1.5
1
0.5
0
control
HKATP-Cxcl12
control+CD90
Cxcl12+CD90
Tie2-Cre;Cxcl12F/F

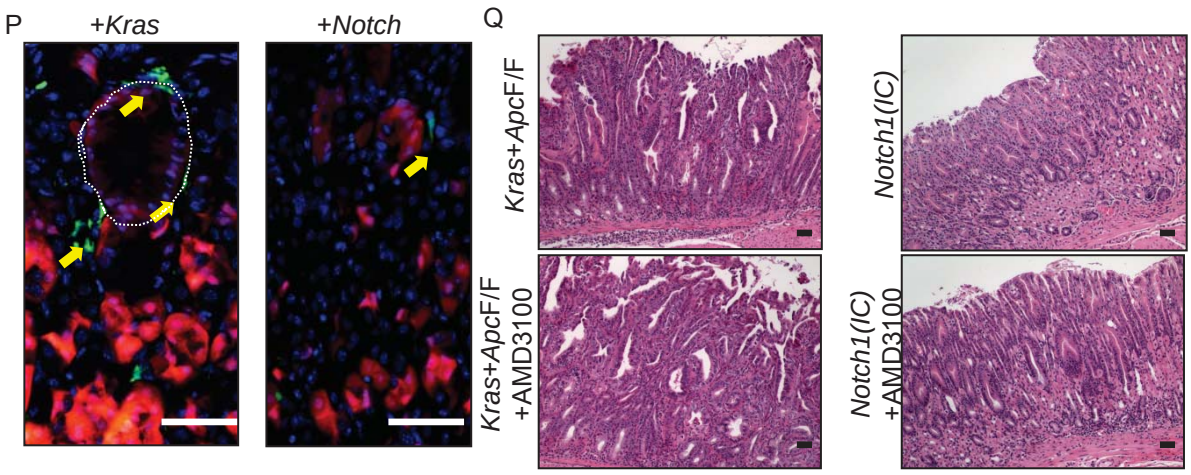


Figure S6, Related to Figure 6. Troy^{+} isthmus stem cells give rise to gastric cancers and loss of *Troy* expression leads to increased proliferation and lineage tracing of chief cells. (A) Lineage tracing in the small intestine of *Troy*-BAC-CreERT2 mice 30 days after TAM induction. (B) Lineage tracing (day 7, 15) in the corpus glands of *Troy*-BAC-CreERT2;*R26*-mTmG mice. Arrows indicate isthmus Troy^{+} cells. (C) Lineage tracing (day 30) in the *Troy*-BAC-CreERT2;*Troy*$^{+/+}$;*R26*-mTmG mice with or without 5-FU. Arrows indicate isthmus Troy^{+} cells. (D) Day 30 lineage tracing of *Troy*-CreERT2;*Lgr5*-DTR;*R26*-TdTomato mice after DT ablation. TAM and DT were given as shown in Fig. S2S. Arrows indicate isthmus Troy^{+} cells. (E) *Troy* gene expression per *Gapdh* in sorted total Mist1^{+} population, parietal cell population, and Mist1^{+} isthmus cell population after DT ablation. n = 3/group. (F) H&E staining of *Troy*-CreERT;LSL-*Kras*^{G12D} mice 1 week and 2 weeks after TAM. Arrows indicate isthmus Troy^{+} cell-derived metaplasia. (G) H&E staining of *Troy*-CreERT;*Cdh1*$^{flox/flox}$ mice treated with *Hf* and TAM (day 30). (H) Relative *Troy* expression in WT, *Troy*$^{+/-}$, and *Troy*$^{-/-}$ mouse corpus glands. n = 3/group. (I-J) WT, *Troy*$^{+/-}$, and *Troy*$^{-/-}$ mice were treated with 5 mg TAM and sacrificed after 4 days. Ki67 staining (I) and the number of Ki67^{+} chief cells per gland (J) are shown. Total 90 glands from 3 mice /group are analyzed. Arrows indicate Ki67^{+} chief cells. (K) Lineage tracing in the*Troy*-BAC-CreERT2;*Troy*$^{+/-}$ mice with or without 5-FU. (L) The numbers of lineage tracing events per 100 glands in *Troy*-BAC-CreERT2;*Troy*$^{+/+}$ or *Troy*-BAC-CreERT2;*Troy*$^{+/-}$ mice with or without 5-FU at day 30. Total 500 glands from 5 mice/group are analyzed. (M and N) H&E staining (M) and the numbers of atypical foci per section (N) of *Hf*-infected *Cdh1*$^{\Delta Mist1}$ crossed to H/K-ATPase-*Cxcl12* mice treated with control or anti-CD90.2 antibodies. n = 4 mice/group and 4 sections/mouse are analyzed. (O) Relative gene expression of *Wnt5a* in WT, H/K-ATPase-*Cxcl12*, or *Tie2*-Cre;*Cxcl12*$^{flox/flox}$ mouse stomach treated with control or anti-CD90.2 antibodies. The expression in control group is set as 1.0. n =3 /group. (P) *Mist1*-CreERT2;LSL-*Kras*^{G12D};*Cxcr4*-EGFP;*R26*-TdTomato and *Mist1*-CreERT2;LSL-*Notch1(IC)*;*Cxcr4*-EGFP;*R26*-TdTomato mouse corpus 30 days after TAM. Note that the number of Cxcr4^{+} cells (arrows) in the isthmus is increased in mutant *Kras* mice (metaplastic area is indicated by white line) but not in *Notch1(IC)* mice. (Q) H&E staining of *Mist1*-CreERT2;LSL-*Kras*^{G12D};*Apc*$^{flox/flox}$ and *Mist1*-CreERT2;LSL-*Notch1(IC)* mice 30 days after TAM. Mice were treated with vehicle or AMD3100 for 2 weeks (day 7 to 21) as shown in Experimental procedures. Histological changes were not improved by AMD3100 in these models. Means ± SEM. *p < 0.05. Bars=10 μm (B-D, K), 50 μm (A, F, M, P-Q), and 100 μm (G, I).

Supplemental Experimental Procedures

Gland isolation and in vitro culture system

The harvested mouse stomachs were opened longitudinally and washed with cold PBS. The tissue was chopped into approximately 5 mm pieces, washed with cold PBS, and incubated in 8 mM EDTA in PBS for 60 min on ice. The tissue fragments were suspended vigorously in cold 10 % FBS using a 10-mL pipette, yielding supernatants enriched in crypts. Gland fractions were centrifuged at 900 rpm for 6 min at 4 °C and diluted with advanced DMEM/F12 (Invitrogen) containing B27, N2, 1 μM n-Acetylcysteine, 10 mM HEPES, penicillin/streptomycin, and Glutamax (all from Invitrogen). Samples were passed through 100-μm filters (BD Biosciences) and centrifuged at 720 rpm for 5 min at 4°C, and single cells were discarded. Glands were embedded in Matrigel (provided from NCI) and 500 glands/well were seeded in a pre-warmed 24-well plate. After the Matrigel solidified, it was overlaid with advanced DMEM/F12 medium containing 50 ng/mL EGF (Invitrogen), 100 ng/mL Noggin (Peprotech), 1 μg/mL R-spondin 1, and 10 μg/mL Wnt3a. Growth factors were added every other day, and all medium contents were changed twice a week. Murine Cxcl12 (Peprotech), Wnt5a (Millipore), and Jagged-1 were added to the culture media in the indicated experiments. Organoids were treated with vehicle (DMSO) or 25 μM DAPT (Stengent) for 10 days in the indicated experiments. For $Lgr5^{+}$ cell ablation, DT was

added to the culture medium at 100 µg/mL. Gastric single cells were isolated and cultured as described previously (van Es et al., 2012). Glands were dissociated using TrypLE express (Invitrogen) including 1 mg/mL DNase I (Roche) for 10 min at 37 °C. Dissociated cells were passed through a 20-µm cell strainer and washed with 2 % FBS/PBS. Parietal cell isolation was performed as described previously (Hinkle et al., 2003). For the isolation of $Cxcr4^+$ cells and $Cxcl12^+$ cells, stomach was chopped into approximately 5 mm pieces, washed with cold HBSS, and incubated in 0.1 mg/ml dispase and 3.5 mg/ml collagenase 4 in HBSS for 30 min at 37 °C. The tissue fragments were suspended vigorously in 10 % FBS using a 10-mL pipette, and the supernatant was centrifuged at 1300 rpm for 5 min, resuspended in 5 ml of 40 % Percoll, and then centrifuged at 2000 g for 10 min, yielding the lymphocytes or endothelial cell fraction. Viable epithelial single cells were gated by forward scatter, side scatter and a pulse-width parameter, and propidium iodide-negative staining. For staining, cell suspensions were incubated with conjugated monoclonal antibodies against CD4 (RM4-5 or GK1.5), CD11b (M1/70), CD11c (N418), CD19 (6D5), CD31 (390), CD45 (30-F11), F4/80 (BM8), FcεRIα (MAR-1), c-kit (2B8), Gr-1 (RB6-8C5), ICOS (C398.4A), IL-7Ra (A7R34), KLRG1 (2F1), NK1.1 (PK136), NKp46 (29A1.4), Sca-1 (D7), CD90.2 (53-2.1), and lineage-cocktail antibodies (purchased from BD Biosciences, BioLegend, eBioscience or R&D Systems). For intracellular staining,

cells were fixed and permeabilized via a Foxp3 staining kit (eBioscience) and stained with an antibody to RORgt (eBioscience). Sorted cells were collected, pelleted and embedded in extracellular matrix, followed by seeding in a 48-well plate (100-3000 singlets per well). The images of gastric organoids were acquired using fluorescent microscopy (Nikon, TE2000-U) and two-photon microscopy (Nikon, A1RMP). $Cxcl12^{+}CD31^{+}$ cells were cultured on collagen-coated plates with mouse endothelial cell medium (Cell biologics).

Histopathologic Analysis

Stomach and other tissues from transgenic and control mice were fixed in either 10 % formalin or 4 % paraformaldehyde, embedded in paraffin or OCT, respectively, and cut into 5 μm sections. Immunohistochemistry and immunofluorescence were performed as described previously (Hayakawa et al., 2015). The primary antibodies used included the following: E-cadherin (1:100, Cell Signaling Technology), Ki67 (1:50, DAKO), TFF1 (1:100, Santa Cruz), lectin GS-II (1:200, Invitrogen), Intrinsic Factor (1:2000, a gift from Dr. D. Alpers, Washington University, USA), H/K-ATPase (1:500, Abcam), Cxcl12 (1:200, R&D), vWF (1:200, Dako), CD31 (1:200, Dako), beta-catenin (1:500, BD laboratories), BrdU (1:500, Dako), GFP (1:400, Invitrogen), GFP (1:400, Abcam), cleaved caspase-3 (1:100, Cell Signaling Technology), F4/80 (1:100, Abcam), αSMA (1:500, Abcam), and Mist1 (1:500, provided by Dr. Konieczny).

Subsequently, the sections were incubated with biotinylated secondary antibodies (Vectastain ABC kit; Vector Laboratories) for 30 min, followed by incubation with avidin-coupled peroxidase (Vector Laboratories) for 30 min. Diaminobenzidine (DAB; Dako) was used as the chromogen, and the slides were counterstained with Mayer's hematoxylin. For immunofluorescence, the slides were incubated with Alexa fluor 488 or 594 secondary antibodies (Invitrogen) and counterstained with 4', 6-diamidino-2-phenylindole (Vector Laboratories). For X-gal staining, a solution containing 4 % paraformaldehyde and 2 % glutaraldehyde in 0.1 M Sorensen's phosphate buffer (pH 7.4) (comprising 2 mM $MgCl_2$ and 5 mM EGTA) was perfused intracardially, the tissues were fixed in 4 % PFA at 4 °C for 2-3 hours and cryopreserved in 30 % sucrose before embedding in OCT compound. Tissues were sectioned on a cryostat for enzyme histochemical analysis. Frozen sections (5 µm) were washed (0.01 % sodium deoxycholate and 0.02 % Nonidet P-40) and incubated overnight at room temperature in a 0.1 % X-gal solution (4 % 4-chloro-5-bromo-3-indolyl-D-galactopyranoside (X-gal) dissolved in dimethylformamide, 5 mM K3Fe(CN)6, 5 mM K4Fe(CN)6.6H_2O). Sections were then counterstained with nuclear fast red and visualized using standard light microscopy. In situ hybridization was performed on paraffin-embedded sections using the

RNAScope 2.0 kit (Advanced Cell Diagnostics). Mouse and human DGC were diagnosed by veteran pathologists (A.R.S., H.T., and A.H.).

Bone marrow transplantation

Bone marrow cell suspensions were prepared from femurs and tibias, filtered, and counted. Recipient mice received a single intravenous injection of 1×10^7 bone marrow cells, after being irradiated with 10.5 Gy x-rays. For 4 weeks following the transplant, drinking water was replaced with water containing neomycin sulfate/polymyxin B sulfate mixture. Genomic DNA was extracted from spleen, and bone marrow chimerism was determined by PCR.

***Hf* infection**

Preparation of the *Helicobacter felis* (*Hf*) strain (ATCC 49179) used in this study has been described previously (Hayakawa et al., 2015). Briefly, the organism was grown for 48 hr at 37 °C under microaerobic conditions on 5 % sheep blood agar supplemented with antibiotics. The bacteria were harvested and aliquoted at a titer of 10^{10} organisms/mL in trypticase soy broth with 10 % glycerol, and the bacterial suspension was stored at -80 °C. Before use, aliquots were thawed, analyzed for motility, and cultured for evidence of aerobic or anaerobic microbial contamination. Mice were infected by oral gavage with *Hf* in 0.2 mL trypticase broth three times per week, achieving a total dose of 100 million colony-forming units (CFU)/mouse.

Adenovirus treatment

Adult (8 weeks old) male WT mice received single i.v. tail vein injection of 2 x 10^9 pfu of the GFP- or DKK1-expressing vectors (Vector Biolabs).

Quantitative RT-PCR (qRT-PCR) of proinflammatory cytokines

Total RNA was extracted from whole stomach samples from each animal using TRIzol reagent (Invitrogen) or the RNAqueous-micro kit (Ambion) and subjected to first-strand complementary DNA synthesis using the Superscript III cDNA Amplification System (Invitrogen) following the manufacturer's instructions. qRT-PCR was performed using a three-step method, an ABI 7300 system and SYBR green (Roche). The qRT-PCR primer sequences are available upon request. The results were expressed as the copy number of each gene relative to that of *Gapdh*. For RT-PCR array, gene expression in gastric *Cxcl12*-dsRED$^+$CD31$^+$ cells and *Cxcl12*-dsRED$^-$CD31$^+$ cells was analyzed by RT^2 Profiler^{TM} PCR Array Mouse Transcriptional Factors. n = 2/group. RT² Profiler™ PCR Array Mouse Transcription Factors (SABiosciences) was performed as manufacturer's instructions.

Electron Microscopy

Murine corpus tissue was fixed by immersion for 3 hr at room temperature (RT) in a solution of 4 % formaldehyde (from paraformaldehyde) and 0.1 % glutaraldehyde in 0.1 M phosphate buffer (pH 7.4) containing 6 % sucrose. Fixed specimens were

embedded in 20 % gelatin and 70 µm sections were cut using a vibratome. The sections were incubated for 30 min at RT in a blocking solution containing 10 % normal goat serum in phosphate buffered saline (PBS) followed by 48 hr at 4 °C with rabbit antibodies targeting dsRED (diluted 1:50) in PBS containing 10 % goat serum. Bound primary antibodies were detected using biotinylated secondary antibodies and avidin coupled to horseradish peroxidase (HRP; Vector ABC elite kit). Peroxidase activity was visualized using 3-3'-diaminobenzine (DAB) and glucose/glucose oxidase to generate the peroxide substrate. Sections were washed with PBS, treated with 1 % OsO_4 for 1 hr at RT, washed again with PBS and maleate buffer (3 x 5 min) and stained en bloc for 1 hr with iced 2 % aqueous uranyl acetate. The treated sections were finally dehydrated through a graded ethanol series, cleared with propylene oxide, and embedded in an epoxy resin (Epon 812; Electron Microscopy Sciences). Thin (silver) sections were cut, placed on copper grids and examined using a JEOL 1200EX electron microscope.

Western blotting and immunoprecipitation

Protein lysates were prepared from cells, separated by sodium dodecyl sulfate-polyacrylamide gel electrophoresis (SDS-PAGE), transferred to polyvinylidene difluoride membranes (Millipore). The membrane was probed with primary antibodies, and then incubated with the secondary antibody.

Immunocomplexes were detected using the enhanced chemiluminescence system (Amersham Biosciences). For immunoprecipitation, samples were lysed in radioimmunoprecipitation assay buffer and immunoprecipitated with RhoA activation detection kit (Abcam). The beads were washed for 3 times with radioimmunoprecipitation buffer and then analyzed by SDS-PAGE.

Cell line culture and soft agar assay

The human cancer cell lines were cultured in Ham's F-12 or IMEM medium supplemented with 10 % fetal bovine serum. Soft agar assay was performed as described previously (Kakiuchi et al., 2014).

Statistical Analysis

The differences between the means were compared using either the Student's *t*-test or the Wilcoxon test. p values < 0.05 were considered to indicate statistical significance.

Supplemental References

Hinkle, K.L., Bane, G.C., Jazayeri, A., and Samuelson, L.C. (2003). Enhanced calcium signaling and acid secretion in parietal cells isolated from gastrin-deficient mice. Am J Physiol Gastrointest Liver Physiol *284*, G145-153.

van Es, J.H., Sato, T., van de Wetering, M., Lyubimova, A., Nee, A.N., Gregorieff, A., Sasaki, N., Zeinstra, L., van den Born, M., Korving, J.*, et al.* (2012). Dll1+ secretory progenitor cells revert to stem cells upon crypt damage. Nat Cell Biol *14*, 1099-1104.

NKD1 marks intestinal and liver tumors linked to aberrant Wnt signaling

In our previous study describing TROY as a novel marker of intestinal SCs, we also detected *NKD1* as a Wnt signaling target gene. The notion was not surprising as NKD1 is known Wnt target and inhibitor of the pathway, functioning in the negative feedback loop (Rousset et al. 2001). In the study, we described expression of *Nkd1* in epithelial cells in the small intestine and, furthermore, its specific production in PC hepatocytes. Additionally, we focused on *Nkd1* expression in mouse and human intestinal tumors and human hepatocellular cancer tissue.

In vertebrates, Nkd1 is primarily located in the cytoplasm nearby the plasma membrane, where it interacts with Dvl (Van Raay et al. 2011). It has been shown that in the presence of the Wnt ligand, Nkd1 is released from Dvl and Dvl is recruited to the multiprotein transmembrane signalosome, which initiates Wnt signaling. Liberated Nkd1 subsequently interacts with β-catenin and prevents its translocation to the nucleus (Larraguibel et al. 2015). In our study, we detected high mRNA level of *Nkd1* in tumors of $Apc^{min/+}$ mice indicating its relation to excessive Wnt signaling. Since the endogenous levels of *Nkd1* in the mouse intestinal epithelium were not detectable, we used transgenic mouse harboring tamoxifen regulated Cre recombinase under control of the *Nkd1* promoter. Lineage tracing experiments unveiled *Nkd1* expression in the lower part of the crypt, containing CBC cells, Paneth cells and progenitors of secretory cells and TA cells. High expression of *Nkd1* in these cell types was confirmed afterwards by cell sorting analysis. In addition, expression of the *Nkd1* gene in PC hepatocytes (Zhang et al. 2007) was also visualized.

We also evaluated Nkd1 expression in cancer tissue. Previous studies described upregulated *Nkd1* and *Wnt3a* expression in CRC (Yan et al. 2001; Caldwell et al. 2008; Guo et al. 2009; Voloshanenko et al. 2013). From other types of cancer, decreased expression of the *NKD1* gene was described in breast invasive ductal carcinoma (Lv et al. 2015). Interestingly, low levels of *Nkd1* are correlated with lower life expectance, and, on the other hand, upregulation of *Nkd1* decreases the invasiveness of breast cancer cells. A similar pattern was described in non-small cell lung cancer (Zhang et al. 2011b). In our study, premalignant intestinal dysplasia of mice with truncated APC exhibited upregulated *Nkd1* mRNA. Controversially, hyperplastic polyps display decreased *Nkd1* expression. In human CRC samples, the *Nkd1* levels were significantly higher than in the

paired healthy tissues, regardless to the presence or absence of mutations in *APC*. Nevertheless, the mutation was inspected only in the "hot spot" locus in exon 19, therefore the mutations in the other regions could be omitted (Norheim Andersen et al. 1999; Fafilek et al. 2013). Additionally, it has to be mentioned that some intestinal neoplasia follow the fate of so-called serrated pathway that is initiated by *BRAF* and *APC* mutations (Mundade et al. 2014). Moreover, in several studies epigenetic silencing of Wnt inhibitors as the cause of tumor growth has been described (Valdora et al. 2013; Saito et al. 2014; Surana et al. 2014). Increased levels of *Nkd1* in CRC samples in our study was compared to the results from The Cancer Genome Atlas (TCGA) database. Upregulation of *NKD1* mRNA expression in 227 samples was in agreement with our investigation. Next, we focused on the mutations in the *NKD1* gene which were previously related to the MSI CRC pathway (Guo et al. 2009). Four specimens from TCGA database were mutated in *NKD1*, although the mutations were not located in sites indispensable for interaction with its protein partners. We therefore concluded that the *NKD1* function is important for tumor maintenance (Lewis et al. 2010; Chandra et al. 2012). Of note, *Nkd1*$^{-/-}$ mice do not develop tumors (Li et al. 2005). Since virtually none mutations in the *NKD1* gene were found, we focused on possible *NKD1* epigenetic silencing by DNA methylation observed not only by *NKD1*, but also by its paralog *NKD2*, in various types of cancer (Dai et al. 2011; Dong et al. 2015; Yoda et al. 2015). In the TCGA CRC samples, CpG island located upstream of the *NKD1* promoter was significantly hypomethylated, whereas the downstream CpG island was heavily methylated. *NKD1* mRNA was upregulated in the CRC specimens with hypomethylated S-shore region (sequence in distance up to 2 kb downstream from the CpG island) in intron 3 of the *NKD1* gene.

Human HCC specimens that we collected included 28 neoplastic liver tissues. Using qRT-PCR analysis, we observed a subgroup of the "Wnt class" samples (Lachenmayer et al. 2012a) with substantially upregulated *NKD1* mRNA expression. Wnt class samples expressed also increased levels of Wnt target genes *AXIN2*, *EPHB2, GS*, *TROY* and *LGR5*, confirming the results of Effendi et al. (Effendi et al. 2014). Mutation analysis of the *CTNNB1* gene uncovered stabilizing mutations in exon 3 in 11 samples, from which 9 belonged to the Wnt class. This result is in agreement with results published previously describing mutated *CTNNB1* in 20 – 40 % of HCC cases. On the contrary to CRC, *APC* is mutated only in 2-3 % of HCC tumors (Kan et al. 2013). The TCGA database contains

197 HCC specimens with the same proportions of different subgroup including the Wnt class as our HCC sample collection. The mutational status of the *CTNNB1* gene reached 26 %, whereas *APC* and *AXIN1* and *AXIN2* were mutated only in a few tumors. Previous findings about *NKD1* expression in human hepatocellular tumors described upregulated *NKD1* mRNA and decreased NKD1 protein levels, probably maintaining equilibrium for tumor survival (Cheng et al. 2011; Zhang et al. 2015). Moreover, the higher mRNA production and lower protein level, the more aggressive metastases and tumor size was observed. Higher expression of *NKD1* in comparison to healthy adjacent tissue was detected in hepatoblastomas, the liver tumors of the young age (Koch et al. 2005).

Nkd1 represents Wnt target gene and regulator of the pathway, which transcription is detectably expressed in Wnt-activated cells. Nevertheless, its impact on the cell fate is rarely substantial. It seems that Nkd1 acts as a passive inhibitor, playing the perceptible role in cell when signaling passes certain threshold, e.g. in various types of cancers (Angonin and Van Raay 2013). *Nkd1* in CRC and HCC is mutated infrequently, however, its impaired expression is linked to tumor growth and could be potentially used as a correlating marker of the cancer severity.

Author´s contribution: mouse - intraperitoneal injections, fixation and paraffin or O.C.T. embedding, tissue sectioning, in situ hybridization, immunohistochemistry, X-gal staining, qRT-PCR, FACS, co-designing the experiments, co-writing the manuscript

Cellular Signalling 27 (2015) 245–256

Contents lists available at ScienceDirect

Cellular Signalling

journal homepage: www.elsevier.com/locate/cellsig

NKD1 marks intestinal and liver tumors linked to aberrant Wnt signaling

Jitka Stancikova [a,d,1,2], Michaela Krausova [a,2], Michal Kolar [a], Bohumil Fafilek [a], Jiri Svec [a,b], Radislav Sedlacek [a], Magdalena Neroldova [c], Jan Dobes [a], Monika Horazna [a], Lucie Janeckova [a], Martina Vojtechova [a], Martin Oliverius [c], Milan Jirsa [c], Vladimir Korinek [a,*]

[a] Institute of Molecular Genetics, Academy of Sciences of the Czech Republic, Videnska 1083142 20 Prague 4, Czech Republic
[b] Second Department of Internal Medicine, Third Faculty of Medicine, Charles University, Prague, Srobarova 50, 100 34 Prague 10, Czech Republic
[c] Institute for Clinical and Experimental Medicine, Videnska 1958/9, 140 21 Prague 4, Czech Republic
[d] Faculty of Science, Charles University in Prague, Albertov 6, 128 43 Praha 2, Czech Republic

ARTICLE INFO

Article history:
Received 17 August 2014
Received in revised form 24 October 2014
Accepted 8 November 2014
Available online 14 November 2014

Keywords:
Wnt signaling
NKD1
Intestine
Liver
Colorectal cancer
Hepatocellular carcinoma

ABSTRACT

The activity of the Wnt pathway undergoes complex regulation to ensure proper functioning of this principal signaling mechanism during development of adult tissues. The regulation may occur at several levels and includes both positive and negative feedback loops. In the present study we employed one of such negative feedback regulators, naked cuticle homolog 1 (Nkd1), to follow the Wnt pathway activity in the intestine and liver and in neoplasia originated in these organs. Using lineage tracing in transgenic mice we localized *Nkd1* mRNA to the bottom parts of the small intestinal crypts and hepatocytes surrounding the central vein of the hepatic lobule. Furthermore, in two mouse models of intestinal tumorigenesis, *Nkd1* expression levels were elevated in tumors when compared to healthy tissue. We utilized a collection of human intestinal polyps and carcinomas to confirm that *NKD1* represents a robust marker of neoplastic growth. In addition, expression analysis of *NKD1* in liver cancer showed that high expression levels of the gene distinguish a subclass of hepatocellular carcinomas related to aberrant Wnt signaling. Finally, our results were confirmed by bioinformatic analysis of large publicly available datasets that included gene expression profiling and high-throughput sequencing data of human colon and liver cancer specimens.

© 2014 The Authors. Published by Elsevier Inc. This is an open access article under the CC BY-NC-ND license (http://creativecommons.org/licenses/by-nc-nd/3.0/).

1. Introduction

The Wnt pathway represents one of the principal signaling mechanisms regulating development and tissue homeostasis in metazoan species. In the adult organism, aberrant Wnt signaling is involved in various diseases including cancer (reviewed in [1]). The central mediator of the best studied so-called canonical Wnt pathway is β-catenin, a protein playing a dual role in cell adhesion and signaling (reviewed in [2]). In the absence of an extracellular Wnt stimulus the β-catenin destruction complex, which is composed of casein kinase 1 alpha (CK1α) and glycogen synthase kinase 3 (GSK3), and scaffolding proteins adenomatous polyposis coli (Apc) and axin/conductin, phosphorylates β-catenin on the N-terminal serine/threonine residues. The phosphorylated protein is ubiquitinylated and subsequently degraded by the proteasome. Consequently, in unstimulated cell, the cytoplasmic levels of β-catenin remain low. Interaction of Wnt ligand with the receptor complex comprised of the Frizzled receptor and low-density lipoprotein receptor-related protein 5/6 (LRP5/6) co-receptor disrupts the function of the destruction complex. Subsequently, β-catenin accumulates in the cytoplasm and in the nucleus, where it associates with transcription factors of the lymphoid enhancer-binding factor/T-cell factor (LEF/TCF) family (further referred to as TCFs). Since β-catenin contains a transactivation domain, the TCF-β-catenin complexes act as bipartite transcriptional activators of the Wnt-responsive genes, such as *Axin2*, *c-Myc*, *CD44* or *cyclin D1* (for more comprehensive survey about the Wnt signaling target genes refer to the Wnt signaling home page: http://web.stanford.edu/group/nusselab/cgi-bin/wnt/target_genes).

Abbreviations: APC, adenomatous polyposis coli; BAC, bacterial artificial chromosome; CBC, crypt base columnar; Cp, crossing point; CRC, colorectal carcinoma; CTNNB1, the *β-CATENIN* gene; Dvl, dishevelled; EGFP, enhanced green fluorescent protein; EphB2, ephrin type-B receptor 2; GI, gastrointestinal; GS, glutamine synthetase; HBV, hepatitis B virus; HCC, hepatocellular carcinoma; HCV, hepatitis C virus; ISC, intestinal stem cell; ISH, *in situ* hybridization; LacZ, β-galactosidase; Lgr5, leucine-rich repeat containing G protein-coupled receptor 5; Min, multiple intestinal neoplasia; Nkd, naked cuticle homolog; Olfm4, olfactomedin 4; PCA, principal component analysis; qRT-PCR, reverse-transcription quantitative polymerase chain reaction; SD, standard deviation; TA, transit amplifying; TCF, T-cell factor; TCGA, The Cancer Genome Atlas.

* Corresponding author at: Institute of Molecular Genetics AS CR, Videnska 1083, 142 20 Prague 4, Czech Republic. Tel.: +420 241063146; fax: +420 244472282.
E-mail address: korinek@img.cas.cz (V. Korinek).

[1] Affiliation to the Faculty of Science is related to the support of the first author from the Grant Agency of Charles University in Prague; none of the results presented in this article were generated, obtained, or analyzed in relation to this affiliation.

[2] These authors contributed equally to this work.

http://dx.doi.org/10.1016/j.cellsig.2014.11.008
0898-6568/© 2014 The Authors. Published by Elsevier Inc. This is an open access article under the CC BY-NC-ND license (http://creativecommons.org/licenses/by-nc-nd/3.0/).

The intestinal epithelium represents one of the most dynamic tissue in mammalian body (reviewed in [3]). The single-layer epithelium of the small intestine is formed by microscopic projections into the intestinal lumen called villi, and invaginations into underlying mesenchyme, so-called crypts of Lieberkühn. Tissue homeostasis is maintained by intestinal stem cells (ISCs) residing in the bottom part of the crypts. ISCs divide asymmetrically, giving rise to fast-cycling transit amplifying (TA) cells located above the stem cell zone. Descendants of TA cells move up along the crypt/villus axis. At the crypt orifice these cells differentiate to generate specialized cell lineages of the gut that mainly include absorptive enterocytes, mucus-secreting goblet cells, and enteroendocrine cells producing hormones. Differentiated cells continue their movement up to the top of the villus, where they are extruded to the intestinal lumen. The process of epithelial self-renewal is completed in 3–5 days. One exception from this scheme are Paneth cells. The life span of these cells is 6–8 weeks. Furthermore, mature Paneth cells do not migrate from the crypt but stay at the crypt bottom, where they produce antibacterial cryptidins, defensins, and lysozyme (reviewed in [4]). The tissue architecture of the colon reminds the small intestine; however, it does not contain Paneth cells and its surface is flat without the extruding villi. ISCs, alternatively named according to their slender appearance and localization in the lower portion of the crypt as crypt base columnar (CBC) cells, can be recognized by expression of leucine-rich repeat containing G protein-coupled receptor 5 (Lgr5) [5]. Recently, several other markers of ISCs were discovered. These include the tumor necrosis factor receptor family member Troy [6], transcription regulator achaete-scute complex homolog 2 (Ascl2), and an extracellular matrix glycoprotein, olfactomedin 4 (Olfm4) [7]. In addition, CBCs produce high levels of transmembrane ephrin type-B receptor 2 (EphB2), whose expression declines in TA cells, and Paneth cells are EphB2 negative [8].

A number of studies established the Wnt pathway as the main constituent of the signaling network regulating ISCs pluripotency and proliferation (reviewed in [9]). For example, the expression of stem cell markers *Ascl2*, *Lgr5* and *Troy* is governed by the canonical Wnt pathway. Moreover, genetic disruption of genes encoding the Wnt pathway effectors *Tcf4* [10,11] or *β-catenin* [12,13] is associated with demise of intestinal crypts. Interestingly, Wnt/β-catenin signaling plays a key role in the metabolic zonation of the liver (reviewed in [14]). To fulfill its metabolic function, the liver tissue is organized into hepatic lobules, hexagonal-shaped functional units of hepatic parenchyma composed of 15–25 cells. The hepatocytes in the center of the lobule are called perivenous, since they surround a hepatic centrilobular vein. The outer row of lobular hepatocytes line the portal space. These periportal cells are in close contact with the so-called portal triad consisting of the hepatic artery, portal vein and bile duct. Consequently, the periportal hepatocytes receive a mixture of blood originating from both vessels. The portocentrovenular axis of the lobule is the basis for the zonation of the metabolic functions in the adult organ. Cells in different areas of the hepatic lobule are not equal, but they express different genes involved in the metabolism of carbohydrates, xenobiotics, bile production, and detoxification of ammonia. The perivenous hepatocytes contain nuclear β-catenin and they display active Wnt signaling. The Wnt pathway regulates genes encoding enzymes of ammonia detoxication and transport. The genes include *glutamine synthetase* (*GS*/*Glul*), *ornithine aminotransferase* (*Oat*), and *leukocyte cell-derived chemotaxin-2* (*Lect2*). In contrast, high Apc protein levels in the periportal hepatocytes suppress the Wnt pathway activity. This leads to production of a different set of enzymes mainly participating in ammonia, urea, and carbohydrate metabolism such as *glutaminase 2* (*Gls2*), *arginase 1*, and *phosphoenolpyruvate carboxykinase 1* (*Pck1*) [15].

Aberrant Wnt signaling is found in a multitude of solid tumors, particularly in carcinoma of the colon and rectum [colorectal carcinoma (CRC) [reviewed in [16]]. It is assumed that in the majority of sporadic CRCs the "driver" mutation providing selective advantage to the prospective cancer cell occurs in the *APC* tumor supressor [17,18]. The mutational changes in *APC* lead to production of truncated APC polypeptide that compromises proper functioning of the β-catenin destruction complex (reviewed in [19]). The Wnt pathway might also be activated by inactivating mutations in *AXIN1* [20] or *AXIN2* [21]. In addition, approximately 5% of CRCs contain oncogenic mutations in the *CTNNB1* gene (this gene encodes β-catenin) that alter regulatory amino acid residues at the β-catenin N-terminus and stabilize the protein [22]. The most common type of liver cancer is hepatocellular carcinoma (HCC). The etiology of the disease is heterogeneous and is frequently linked to hepatitis B virus (HBV) or hepatitis C virus (HCV) chronic infection or to alcoholism-related cirrhosis (reviewed in [23]). Recently, several studies performed gene expression profiling and/or high-throughput DNA sequencing to identify the molecular subclasses of HCC or to detect the driver mutations related to liver carcinogenesis [24,25]. Importantly, approximately one-half of HCCs display elevated expression levels of genes activated by Wnt signaling, and oncogenic mutations in the *CTNNB1* gene are found in 20-30% of all HCCs. Analogically to CRC, high levels of stabilized β-catenin and inappropriate transcriptional activation of the TCF-β-catenin target genes is a hallmark of a significant portion of HCCs (reviewed in [26]).

In our previous study we employed chromatin immunoprecipitation in combination with DNA microarray analysis (so-called ChIP-on-chip) to identify genes activated by aberrant Wnt/β-catenin signaling in human CRC cells. One of the genes bound by the TCF4-β-catenin complexes was *naked cuticle homolog 1* (*NKD1*) [6]. Nkd1 is an evolutionarily conserved feedback inhibitor of the Wnt pathway [27]. It interacts with dishevelled (Dvl1) and mediates degradation of this cytoplasmic Wnt signal transducer [28]. Nkd1 reduces aberrant Wnt signaling; nevertheless, in the absence the excessive Wnt signal, its function is less apparent [29,30]. Simultaneous inactivation of both vertebrate paralogs *Nkd1* and *Nkd2* in the mouse leads to only subtle alterations in the morphology of cranial bones and slightly reduced litter size, but the mice are otherwise normal [31]. Based on these and other results mainly obtained in zebrafish [30], Angonin and Van Raay proposed that Nkd1 functions as a "passive antagonist" that acts only when the Wnt signaling levels exceed some threshold [32].

In the present study, we analyzed the *Nkd1* expression pattern in adult mouse gut and liver tissue. Using lineage tracing approaches in transgenic animals we show that *Nkd1* expression is confined to the areas with active Wnt signaling. Furthermore, *Nkd1* transcription was robustly increased in tumors developed in multiple intestinal neoplasia (Min) of mice or in hyperplastic crypts generated by conditional deletion of the *Apc* gene. Using a panel of sporadic tumors of the colon we confirmed that elevated expression of *NKD1* marks neoplastic tissue. In hepatic neoplasia, high *NKD1* mRNA levels, together with upregulation of *AXIN2*, *EPHB2*, and *GS*, distinguish a class of HCCs with deregulated Wnt signaling.

2. Materials and methods

2.1. Experimental animals

$Apc^{+/Min}$ [33,34], Lgr5-EGFP- IRES-CreERT2 [5], Rosa26R [35], and Rosa26R-EYFP [36] mice were purchased from the Jackson Laboratory (Bar Harbor, ME). $Apc^{cKO/cKO}$ [37] mice were obtained from the Mouse Repository (National Cancer Institute, Frederick, MD). Villin-CreERT2 mice [38] were kindly provided by Sylvia Robine (Institut Curie, Paris, France). Animals were housed and handled according to the guidelines approved by the institutional committee. Tamoxifen (Sigma-Aldrich, St. Louis, MO) administration was done by intraperitoneal injection of 1 mg of the compound dissolved in 0.1 ml of corn oil. DNA from tail clippings was used for genotyping. Tissue samples were digested in Proteinase K solution (Thermo Fisher Scientific, Waltham, MA) and precipitated using ethanol; pellets were dissolved in 20 μl of TE buffer (10 mM Tris-HCl, 1 EDTA, pH 8) and 1 μl was used for PCR performed with DreamTaq PCR Master Mix (Thermo Fisher Scientific, Waltham, MA).

2.2. Generation of Nkd1-CreERT2 transgenic mice

The Nkd1-CreERT2 bacterial artificial chromosome (BAC) transgenic construct was generated using homologous recombination in bacteria according to the previously published protocol [39]. The BAC clone RP23-301 N2 was purchased from imaGenes (Berlin, Germany); a construct containing CreERT2 cDNA was kindly provided by M. Cepko via Addgene. The adapters "a" (5′-TCCTTTCTTTCCGGCTCCCGCCGCCGCCGC CGCGCGCGATGTGCCCGCAGCCatgtccaatttactgaccgtac- 3′; the *Nkd1*-specific sequence is capitalized, the part complementary to the CreERT2 expression cassette is given in lowercase) and "b" (5′-AGAGACCAAGTT CTCCGGAGTAGGGGCTGGCGACTAGAGGAAGGCGCAAGTGGCGGCCGC TCTAGAACTAGTG- 3′) were derived from the sequence of the *Nkd1* second exon. The adapters were employed for PCR amplification, the product was purified from agarose gel and electroporated into the *E. coli* strain EL250 harboring the BAC clone. Bacterial clones containing correctly recombined BACs were verified by PCR. Isolated recombinant BAC DNA was linearized and used for pronuclear injection of fertilized eggs (C57Bl/6 J background). Two Nkd1-CreERT2 transgenic founder lines were produced using the service of the Transgenic Unit of the Institute of Molecular Genetics (IMG). Two lines exhibited a virtually identical pattern of the Cre recombinase activity.

2.3. X-gal staining, immunohistochemistry, antibodies, and periodic acid-Schiff (PAS) staining

Mouse tissues were stained with X-gal (Amresco, Solon, OH) prior to paraffin embedding. Tissue processing and staining was performed as described previously [5]. Slides were immersed in a steam bath (20 min, 10 mM citrate buffer, pH 6) for antigen retrieval. The following rabbit polyclonal antibodies were used for immunohistochemistry: anti-chromogranin A (cat. No. ab15160, Abcam, Cambridge, UK), anti-lysozyme (cat. No. A0099, Dako, Glostrup, DK), anti-glutamine synthetase (cat. No. ab73593, Abcam). PAS (Diapath, Martinengo, IT) staining was performed according to the standard protocol provided by the supplier. Slides were counterstained using either hematoxylin (Penta, Prague, CZ) or nuclear fast red (Diapath, Martinengo, IT).

2.4. RNA probes and in situ hybridization (ISH)

Both sense and antisense RNA probes were derived from the following regions of the analyzed genes: *Axin2* (accession: NM_015732.4), nucleotides (nt) 2069-2938; *Nkd1* (NM_001163660.1), nt 509-944. DNA fragments encompassing the indicated regions were subcloned into pBluescript SK II (Stratagene, La Jolla, CA). The constructs were linearized, and digoxigenin-labeled antisense RNA and control sense probes were generated from the template using the DIG RNA Labeling Kit (Roche Applied Science, Basel, Switzerland). Dissected small intestinal and liver tissue was embedded in O.C.T. medium (Tissue-Tek, Sakura Finetek Europe B.V., The Netherlands). Ten μm sections were cut and mounted on Super Frost Plus slides (Electron Microscopy Sciences, Hatfield, PA). Sections were post-fixed in 4% (w/v) paraformaldehyde in phosphate-buffered saline (PBS; 4 °C, 10 min), acetylated for 10 min (acetic anhydride, 0.25%; Sigma-Aldrich) and hybridized with digoxigenin-labeled probes overnight at 62 °C. ISH was carried out as described previously [40]. Whole-mount ISH was performed according to the protocol of Cepko and Tabin (http://genepath.med.harvard.edu/~cepko/protocol/ctlab/ish.ct.htm).

2.5. Isolation of intestinal crypt cells and hepatocytes, fluorescence-activated cell sorting (FACS)

Crypts from the proximal part of the small intestine of Lgr5-EGFP-IRES-CreERT2 mice were isolated according to the protocol published previously [41]. Single-cell suspension was obtained upon incubation of fresh crypts with dispase I (0.8 mg/ml, 10 min at 37 °C; Sigma-Aldrich) and passing the resulting suspension through 70-μm strainer (Fisher Scientific, Waltham, MA). Cell suspension was stained by biotinylated *Ulex europaeus* agglutinin I (UEA I) (Vector Laboratories, Burlingame, CA) and streptavidin-PE-Cy7 (BD Biosciences, Mississauga, ON). Hepatocytes were isolated from perfused liver of Nkd1-CreERT2^{+}/Rosa26R-EYFP mice as described previously [42]. The animals were injected twice (with 24-hour interval between injections) with tamoxifen (1 mg in 100 μl of corn oil per dose) and utilized the next day upon the second injection.

2.6. RNA isolation and reverse-transcription quantitative polymerase chain reaction (qRT-PCR)

Total RNA was extracted from tissues or sorted cells using RNAeasy MiniKit with DNase treatment (Qiagen, Hilden, Germany) following the manufacturer's instructions and reverse transcribed using MAXIMA reverse transcriptase (Thermo Fisher Scientific, Waltham, MA). The LightCycler 480 apparatus and SYBR Green I Master Mix (Roche Applied Science) were employed for qRT-PCR. Primers are listed in Supplementary Table S1.

2.7. Collection and analysis of human colorectal lesions

The study was approved by the Clinical and Experimental Medicine and the Thomayer University Hospital Research Ethics Committee and the Ethics Committee of the Third Faculty of Medicine, Charles University in Prague. Processing and histopathological evaluation of samples of 35 precancerous and 20 malignant lesions of colorectal tissue were described in full detail previously [6]. Briefly, genomic DNA and total RNA was isolated from tumor segments and matched healthy mucosa. RNA was reverse transcribed and used for qRT-PCR analysis; PCR reactions were run in triplicates with two negative controls (RT reactions in which reverse transcriptase was omitted). Mutational analysis of the *APC* gene was performed with genomic DNA extracted from CRC specimens only. To obtain relative expression levels (-ΔCp) (Cp indicates the crossing point value), individual Cp values were normalized by geometric average of internal housekeeping genes *β-ACTIN* (*ACTB*), *UBIQUITIN B* (*UBB*) and *AXIN1* (premalignant lesions of the colon), or using *ACTB* as a sole reference gene (CRC-derived samples). Differential expression was examined by non-parametric Wilcoxon's rank-sum test. In addition, the individual background of the patients was encompassed in a REML-fitted linear model, described by the formula ΔCp ~ patient + tissue/(stage * *APC* mutation) for CRC specimen and ΔCp ~ patient + tissue_stage in cases of precancerous lesions, respectively. Biopsies of surrounding non-tumor tissue constitute a single group (ΔΔCp) in both collections. In corresponding figures and tables, the number of asterisks represents statistically significant changes with the following P values: *$P < 0.05$, **$P < 0.01$, and ***$P < 0.001$. All analyses were performed in R language. Primer sequences are listed in Supplementary Table S1.

2.8. Collection and analysis of human hepatic lesions

Neoplastic liver tissues were obtained from 28 consecutive patients at the time of surgical resection performed at the Transplant Surgery Department of the Institute for Clinical and Experimental Medicine. Collection of clinical samples was accomplished in concordance with the standards and approved by the Institute for Clinical and Experimental Medicine and Thomayer University Hospital Research Ethics Committee; all study subjects signed the informed consent. The paired, non-tumor tissue specimens were used as controls. Histopathology was scored in hematoxylin and eosin stained sections by two independent pathologists; clinical characteristics are given in Supplementary Table S2. Diagnoses of HCC were predominant within the cohort. Total RNA was purified using the RNeasy Mini kit in automated QIAcube extractor (Qiagen). Reverse transcription was performed with 250 ng of

input RNA using RevertAid H Minus First Strand cDNA Synthesis kit supplied with 25 ng/μl oligo(dT)$_{18}$ primers (Thermo Scientific). PCR reactions were run in triplicates using Light Cycler 480. Relative expression levels (-ΔCp) were obtained upon normalization by geometric average of internal housekeeping genes *ACTB* and *UBB*. To detect differences in expression, we employed Wilcoxon's rank-sum test and, in addition, the linear model (REML) described by the formula ΔCp ~ patient + tissue_fibrosis score. Statistical significance levels were set identically to CRC samples.

2.9. CTNNB1 mutation analysis in HCC

Genomic DNA was purified from snap-frozen samples of tumor and matched surrounding tissue using DNeasy Blood & Tissue Kit (Qiagen). Exon 3 of *CTNNB1*, including intron-exon boundaries, was amplified using gene-specific primers: forward: 5′taatac gactcactatag TGCTTTTCTTGGCT GTCTTTCAG 3′; reverse: 5′tgaaa cagctatgaccatgTCCACAGTTCAGCATTTACCTAAG 3′; overhang sequences corresponding to universal sequencing primers T7 and RP, respectively, are given in lowercase letters. Each fragment was directly sequenced from both sides using the BigDye® Terminator v3.1 cycle sequencing kit and ABI 3130 Genetic Analyzer (Applied Biosystems, Life Technologies, Prague, Czech Republic).

2.10. CRC and HCC datasets obtained from The Cancer Genome Atlas (TCGA)

CRC [TCGA_COADREAD; 154 cases of colon cancer (dataset COAD-TP); 73 cases of rectal cancers, (dataset READ-TP)] [18] and HCC (TCGA_LIHC; 197 cases) datasets were downloaded from the Broad Institute using the utility firehose_get (http://gdac.broadinstitute.org, Broad Institute/Massachusetts Institute of Technology, USA) on July 18, 2014. RNA-seq data were extracted from the archive "gdac.broadinstitute.org_COADREAD.Merge_rnaseqv2__illuminaga_rnaseqv2__unc_edu__Level_3__RSEM_genes_normalized__data.Level_3.2014061400.0.0" (CRC) and "gdac.broadinstitute.org_LIHC.Merge_rnaseqv2__illuminahiseq_rnaseqv2__unc_edu__Level_3__RSEM_genes_normalized__data.Level_3.2014061400.0.0" (HCC). Mutation data were obtained from the archive: "gdac.broadinstitute.org_COADREAD.Mutation_Packager_Calls.Level_3.2014061400.0.0" (CRC) and "gdac.broadinstitute.org_LIHC.Mutation_Packager_Calls.Level_3.2014061400.0.0" (HCC). Clinical data were retrieved from the files: "gdac.broadinstitute.org_COADREAD.Merge_Clinical.Level_1.2014061400.0.0/COADREAD.clin.merged.txt" (CRC) and "gdac.broadinstitute.org_LIHC.Merge_Clinical.Level_1.2014061400.0.0/LIHC.clin.merged.txt" (HCC). No further processing was applied to the data. In CRC datasets only samples classified as colon cancer (COAD) and with a determined mutation status of the *APC* gene (104 cases) are presented. DNA methylation data were retrieved from the file: "gdac.broadinstitute.org_COADREAD.Merge_methylation__humanmethylation450__jhu_usc_edu__Level_3__within_bioassay_data_set_function__data.Level_3.2014061400.0.0". Only those data subsets were analyzed that had both expression and methylation data available (366 cases). Positions of the CpG-islands predicted by the algorithm of Wu and colleagues [43] were obtained from the file: "http://rafalab.jhsph.edu/CGI/model-based-cpg-islands-hg19.txt" (accessed on September 8, 2014). North and south shores (N/S-shores) were defined as chromosomal regions flanking the corresponding CpG island 2 kb upstream or downstream, respectively. North/south shelves (N/S-shelves) were defined as chromosomal regions flanking the shores further 2 kb upstream/downstream [44]. Base 2 logarithm of fold change (logFC) of *NKD1* expression intensity between tumor samples and the median of available normal tissue samples was determined. The CRC samples were clustered according to methylation β-values (methylated/overall intensity) for the probes assigned to the *NKD1* gene (**Infinium Human Methylation** 450 array, Illumina). All analyses were performed in the R environment.

3. Results

3.1. Nkd1 expression marks Apc-deficient intestinal tumors in the mouse

To analyze *Nkd1* expression in mouse tumors we performed ISH using specimens obtained from Min mice. These mice (designated Apc$^{+/Min}$) harbor a nonsense mutation in the coding region of the *Apc* gene and all adult animals develop numerous Apc-deficient polyps that progress to malignancy [34]. *Nkd1* mRNA was clearly detected in the small intestinal tumors; nevertheless, we did not observe any

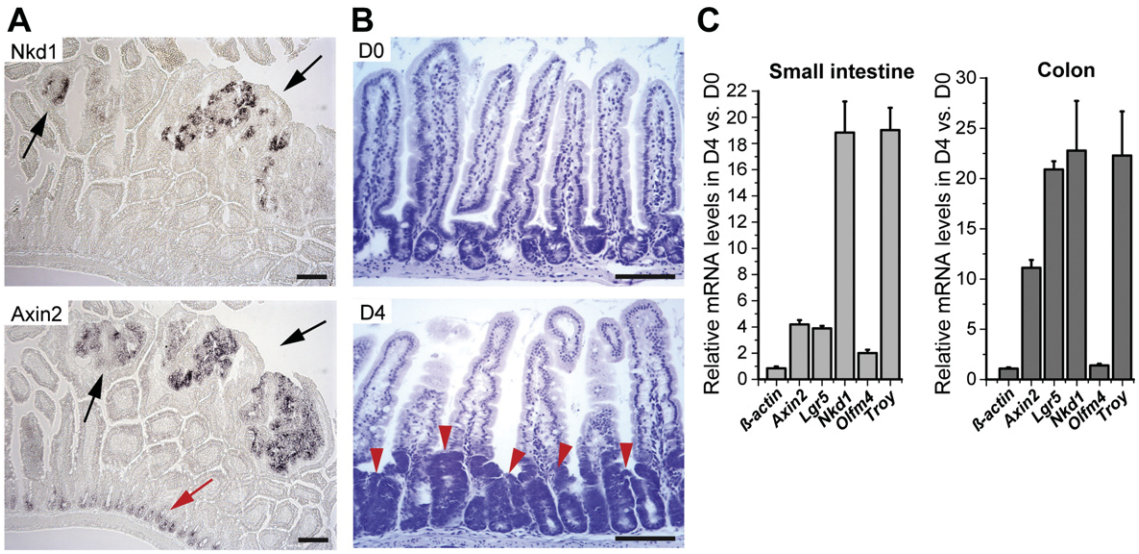


Fig. 1. *Nkd1* mRNA is enriched in mouse intestinal tumors. (A) ISH of *Axin2* and *Nkd1* mRNAs in small intestinal tumors (black arrows) of Apc$^{+/Min}$ mice. In the healthy part of the tissue *Axin2* was also detected in lower parts of the crypts (red arrow). (B) Conditional deletion of the *Apc* allele results in crypt hyperplasia. Hematoxylin-stained sections of the jejunum of Villin-CreERT2^{+}/Apc$^{cKO/cKO}$ mice obtained at day 0 (D0) and day 4 (D4) after tamoxifen administration. Hyperproliferative crypts are indicated by red arrowheads. Scale bar: 0.1 mm. (C) Quantitative RT-PCR analysis of total RNA isolated from crypts at D0 and D4. The results were normalized to *Ubiquitin B* (*Ubb*) mRNA levels; another housekeeping gene, *β-actin*, was also included in the test. The expression level of a given gene in the crypt cells at D0 was arbitrarily set to 1. Error bar: standard deviation (SD).

(specific) *Nkd1* signal in non-neoplastic tissue. This was in contrast to *Axin2*, which was clearly enriched not only in tumors, but also at the bottom of the intestinal crypts (Fig. 1A). To confirm that *Nkd1* expression is directly connected to the loss of *Apc* we employed animals harboring conditional alleles (cKO) of this tumor suppressor. Cre-mediated excision of the floxed exon 14 in $Apc^{cKO/cKO}$ mice results in production of a truncated polypeptide related to nonfunctional Apc protein produced in $Apc^{+/Min}$ mice [37]. The *Apc* gene inactivation was performed in Villin-CreERT2^{+}/$Apc^{cKO/cKO}$ mice expressing tamoxifen-regulated Cre enzyme throughout the epithelia of the gastrointestinal tract [38]. As expected, robust hyperplasia of the small intestinal and colonic crypts was observed several days upon tamoxifen administration (Fig. 1B and data not shown). Quantitative RT-PCR analysis of crypt cells isolated from animals prior and four days after tamoxifen treatment showed more than 18- and 20-fold increase in the *Nkd1* mRNA levels in the Apc-deficient small intestine and colon, respectively. Wnt signaling target genes *Axin2*, *Lgr5*, and *Troy* were also upregulated. In contrast, transcription of *Olfm4*, a marker of small intestinal stem cells which is not driven by active Wnt signaling [7], was slightly elevated in the hyperproliferative crypts isolated from the small intestine and not from the colon (Fig. 1C).

3.2. Nkd1 is produced in the Wnt-responsive areas of the small intestine and liver

Next we analyzed the distribution of Nkd1 in the healthy gut tissue. Since the localization of *Nkd1* mRNA and protein using ISH or immunohistochemical staining was inconclusive, we used transgenesis to follow the expression pattern of the gene. BAC carrying the mouse *Nkd1* locus was employed to generate Nkd1-CreERT2 transgenic mice. In the BAC-based construct, cDNA encoding tamoxifen-inducible Cre enzyme was inserted into the second exon of the *Nkd1* gene. The insertion is in frame with the translation start codon located in the preceding exon (Fig. 2A). The activity of CreERT2 recombinase produced from the Nkd1-CreERT2 BAC transgene was visualized in embryos derived from crossing Nkd1-CreERT2 and Rosa26R mice. Rosa26R animals express bacterial *β-galactosidase* (*LacZ*) mRNA from the ubiquitously active *Rosa26* allele. The mRNA is not translated unless a transcriptional blocker flanked by two loxP sites is excised by Cre [35]. Developing embryos removed from pregnant females one day after tamoxifen injection were used to stain the LacZ-expressing tissue. Importantly, the expression pattern of Nkd1-CreERT2 visualized by the chromogenic X-gal substrate phenocopied the sites of expression of endogenous *Nkd1* mRNA obtained by whole-mount ISH (Fig. 2B). Furthermore, the sites of the CreERT2 activity were in agreement with the previously described *Nkd1* expression pattern [31].

Subsequently, adult Nkd1-CreERT2^{+}/Rosa26R mice were injected with a single dose of tamoxifen and sacrificed at several time points later. In the gastrointestinal (GI) tract, Cre-mediated recombination was the most efficient in the duodenum and jejunum, much less effective in the ileum, and virtually no staining was observed in the colon (Fig. 2C). Since we [6] and others [45] observed that Cre-mediated recombination is less efficient in the distal parts of the GI tract, we supposed that the observed variability in LacZ staining was caused by the inefficient recombination of the floxed blocker rather than heterogeneous expression of *Nkd1*. Therefore, the histological analysis was performed using specimens obtained from the proximal part of the small intestine. One day after the Cre induction, cells producing LacZ were located in the lower parts of the crypts (Fig. 2D). Two distinct staining patterns were observed seven days after the recombination. Some of "blue" cell clones started to extend along the whole crypt axis. However, other clones separated from the crypts and moved as a stripe of cells on the villus, indicating that the recombined cell was possibly a TA cell. Finally, three weeks after recombination, continuous "ribbons" of labelled cells emanating from the crypts and reaching the top of the villi were observed. In addition, blue cells were also found at the bottom of the crypts, i.e. in the positions where mature Paneth cells are localized (green arrow in Fig. 2D). Importantly, Nkd1-CreERT2-expressing cells differentiated into all major cell lineages present in the small intestine (Fig. 2E). The recombined clones persisted in the small intestine for more than two months, confirming that besides Paneth and TA cells some CreERT2-positive cells are indeed ISCs (not shown). To verify that the Nkd1-CreERT2 activity mimics expression of endogenous *Nkd1*, crypt cells obtained from Lgr5-EGFP-IRES-CreERT2 mice were sorted and analyzed using qRT-PCR. Lgr5-IRES-EGFP-CreERT2 animals express enhanced green fluorescent protein (EGFP) from the *Lgr5* locus, and therefore the EGFP protein can be used as a surrogate marker of ISCs [5]. Besides EGFP florescence, cell labeling with UEA I lectin was applied. The lectin binds proteoglycan residues on the surface of secretory cell lineages including Paneth cells and their precursors. Crypts isolated from the jejunum were used for the sorting procedure since this part of the small intestine contains only a minimal count of UEA I-positive goblet cells [46]. The highest *Nkd1* expression (when compared to TA cells negative for UEA and GFP) was detected in mature Paneth cells (phenotype: UEA^{+}GFP^{-}cryptidines^{+}) and Lgr5^{+} ISCs (UEA^{-}GFP^{+-} EphB2^{+}), although expression of cryptidines in the latter population indicated that we did not obtain a homogenous cell population. Interestingly, high levels of *Nkd1* mRNA were also detected in putative progenitors of the Paneth cell lineage that are positive for UEA and GFP, and produce Lgr5 and cryptidins as well [46]. The result was consistent with the frequency of blue cells detected by immunohistochemical staining of crypts in Nkd1-CreERT2^{+}/Rosa26R mice one day after tamoxifen administration (Fig. 2G).

Since previous reports indicated *Nkd1* expression in pericentral hepatocytes [31], we followed the Nkd1-CreERT2 activity in adult liver tissue. One day after tamoxifen administration, X-gal staining was detected in hepatocytes surrounding the putative central vein (Fig. 3A). The identity of LacZ-positive cells was subsequently confirmed by co-staining with an antibody recognizing GS, a robust marker of pericentral hepatocytes (Fig. 3B). Additionally, we intercrossed Nkd1-CreERT2 animals with Rosa26R-EYFP reporter mice that express enhanced yellow fluorescent protein (EYFP) instead of LacZ from the *Rosa26* locus [36]. We performed gene expression profiling of total RNA isolated from EYFP-positive and EYFP-negative hepatocytes sorted from these mice. The analysis confirmed that endogenous *Nkd1* mRNA is robustly enriched in EYFP^{+} cells along with the perivenous hepatocyte-specific genes *GS*, *Lect2*, and *Oat*. In accordance with the literature, these cells also produce increased levels of *Axin2* mRNA [15]. *Apc* and the "housekeeping" gene *glyceraldehyde-3-phosphate dehydrogenase* (*GAPHD*) did not show any differential distribution among the sorted cell populations; however, the periportal *Pck1* gene displayed an inverse expression pattern to the perivenous genes, confirming the quality of the sorting procedure (Fig. 3C).

3.3. Elevated levels of NKD1 mRNA in sporadic premalignant lesions of the colon and in CRC

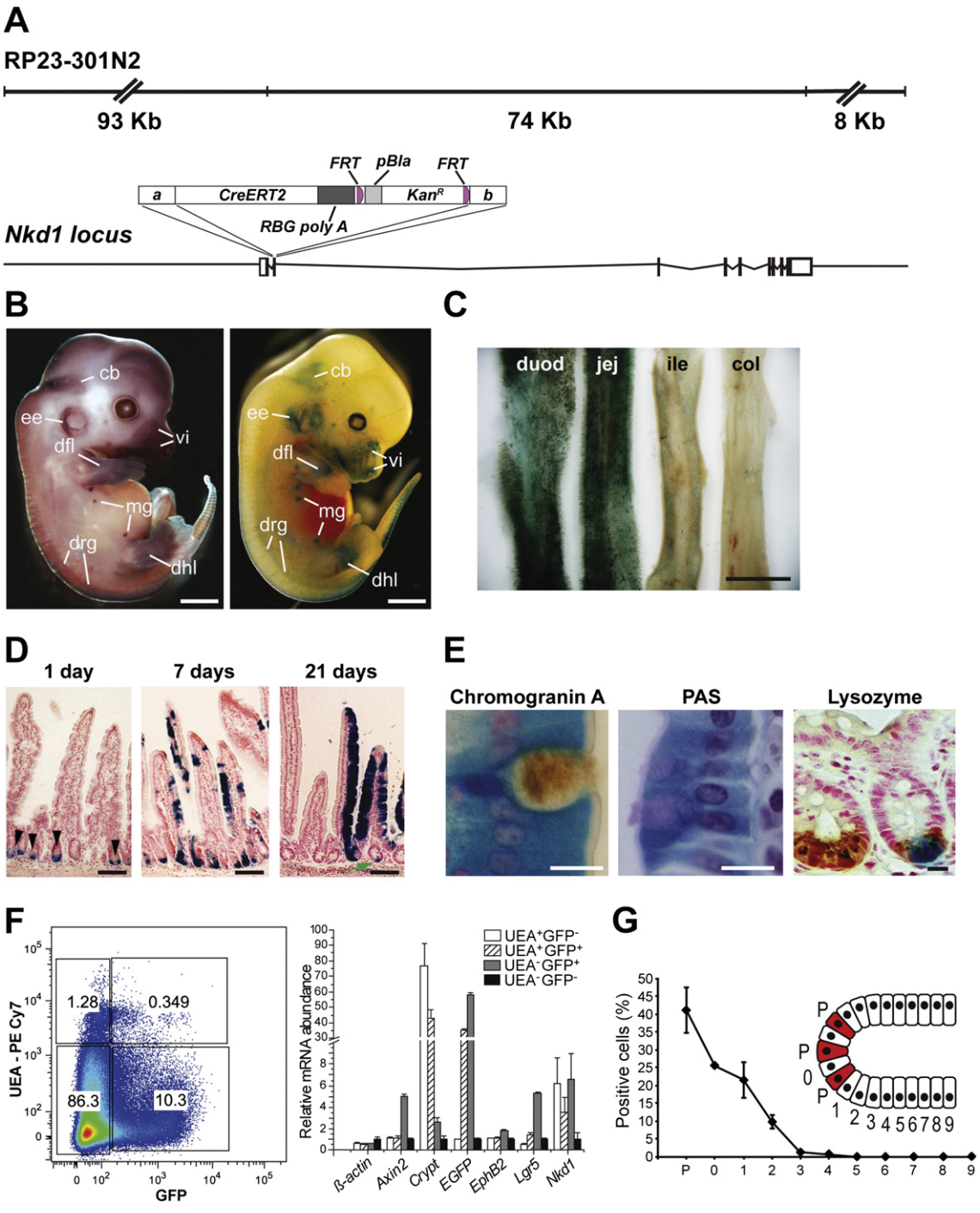
As a next step, we examined the expression pattern of human *NKD1* in tumors arising in the gut. In dysplastic premalignant stages of CRC, we observed robust upregulation of *NKD1* expression. The increase in *NKD1* mRNA abundance showed an ascending tendency as the lesions progressed towards more advanced phenotypes. In contrast, in hyperplastic polyps *NKD1* transcription was significantly decreased when compared to the matched healthy mucosa (Fig. 4A). In CRC the elevated *NKD1* expression occurred irrespective of the *APC* mutational status and hence resembled deregulation of *LGR5* (Fig. 4B) [6].

To explore the alterations in *NKD1* transcription in a larger panel of CRCs, we interrogated relevant datasets from TCGA (227 specimens in total) [18]. The analysis was less straightforward, since the expression data obtained from healthy matched tissue were not accessible from these datasets. Intestinal cancers were stratified according to disease progression, and subsequently, the tumors were further subdivided using the classification system associated with the cellular phenotype

[47] or according to genetic stability [18]. In early-stage tumors *NKD1* mRNA was enriched (similarly to *AXIN2*) in microsatellite stable (MSS) lesions [when compared to lesions displaying low (MSI-L) or high (MSI-H) microsatellite instability (MSI)]. Moreover, in both early and advanced CRCs the *NKD1* transcript was abundant in the progenitor ("TA") type of tumors (Supplementary Fig. S1).

3.4. NKD1 transcription indicates HCC displaying aberrant Wnt signaling

The *NKD1* expression was analyzed in 28 neoplastic liver tissues obtained at the time of surgery. Paired, non-tumor tissue specimens were used as controls. Recently, Lachenmayer and colleagues employed expression data of 642 HCCs to define two classes of HCC displaying dysregulation of the Wnt pathway. The "Wnt class" is characterized by nuclear accumulation of β-catenin and upregulation of liver-specific Wnt signaling target genes. The "Wnt-TGFβ" class is defined by expression of a different set of genes (see further) regulated by Wnt signaling [25]. In the initial analysis we observed a clear separation of a fraction of the HCC samples into the Wnt class that was established by simultaneous upregulation of *AXIN2*, *EPHB2* and *GS*. However, we did not observe any clustering of HCCs to the Wnt-TGFβ class as examined by transcription levels of the *PLAU*, *MMP7*, *SALL1* and *RUNX2* genes (not shown). Thus, we stratified the HCC samples into subgroups defined by the Wnt-signature only. We employed the MCLUST algorithm [48] to group the samples according to their *AXIN2*, *EPBH2*, and *GS* Cp values. The algorithm identified four clusters, three of which showed low and



one (11 samples) exhibited high Wnt-signature "intensity". Due to small cluster sizes, we merged the Wnt signature-negative clusters into a single class and subsequently obtained two classes of HCC designated "HCC" and "HCC_Wnt" (Supplementary Fig. S2). An alternative clustering method, partitioning around medoids (with $k = 2$), resulted in virtually identical grouping (not shown). To further validate the result, we used the algorithm to predict the class of all other samples, i.e. healthy liver parenchyma, precancerous tissues, cholangiocellular carcinoma, and other than HCC liver neoplasia, which we expected to be negative for the Wnt-signature. Indeed, all these samples were correctly classified outside of the HCC_Wnt class (not shown). Finally, we analyzed the *CTNNB1* gene mutation status in genomic DNA obtained from all liver samples. The exon 3 sequence encoding amino acid residues regulating β-catenin protein stability was used for the analysis. Missense mutations in codons for regulatory serines/threonines (or in codons closely adjacent to these residues) were found in 11 HCCs; nine of these tumors were assigned to the HCC_Wnt class (Supplementary Table S3). Consistently, transcription levels of *NKD1* were positively correlated with expression of the genes defining the HCC_Wnt class (*AXIN2*, *EPHB2*, and *GS*), as well as with additional target genes of canonical Wnt/β-catenin signaling *LGR5* and *TROY*. In contrast, transcription of the paralogous *NKD2* gene, which is not regulated by the Wnt pathway, was not elevated in specimens assigned to the HCC_Wnt class (Fig. 5).

Next, we analyzed relevant HCC datasets from TCGA (197 specimens). The expression levels of the Wnt-signature genes *AXIN2*, *EPBH2*, and *GS* and the MCLUST algorithm were employed to group the HCC specimens. The algorithm identified three clusters of HCCs designated HCC_1 (12 samples), HCC_2 (148 samples), and HCC_Wnt (37 samples) (Supplementary Fig. S3). Additionally, we employed genomic DNA sequencing data to determine the *APC*, *AXIN1/2*, and *CTNNB1* mutational status (mutations were classified according to references [49, 50]). In the examined tumors *APC* was compromised in 3%, *AXIN1* in 5%, and *AXIN2* in 2% cases. In contrast, mutations activating *CTNNB1* occurred in 26% of specimens. Consistent with other studies [51], nonsynonymous gene alterations in either the *AXIN1* or *APC* tumor suppressors and *CTNNB1* were mutually exclusive, with only one specimen displaying concurrent oncogenic mutations in the *CTNNB1* exon 3 together with disruption of *AXIN2* (not shown). Since the HCC TCGA dataset contains exome sequencing data, we utilized the mutational status of the *APC*, *CTNNB1*, and *AXIN1/2* genes to divide all specimens to three mutation groups (designated "Wnt_WT", "Wnt_MUT", and "Other"). As expected, HCC_Wnt class-specific genes *AXIN2*, *EPHB2* and *GS* were robustly overexpressed in the Wnt_MUT group (sample count 38) defined by *CTNNB1* (activating) and *APC* (inactivating) mutations (Supplementary Fig. S4). Importantly, in the TCGA HCC1 samples *NKD1* transcription was also positively correlated with *AXIN2*, *EPBH2*, and *GS*, and, furthermore, *NKD1* mRNA was significantly enriched in the Wnt_MUT group (Fig. 6A). Interestingly, in five HCC specimens that were assigned to the HCC_Wnt expression class, no oncogenic mutations in *APC*, *CTNNB1*, and *AXIN1/2* were detected (one sample was assigned to the mutational subgroup "Other" and four other HCCs to the subgroup Wnt_WT) (Supplementary Table S4). Careful scrutiny of genomic DNA from the tumor in the "Other" group revealed that this lesion harbors a missense mutation (c.G417T/p.L139F) in exon 4 of the *CTNNB1* gene that possibly compromises the structural integrity of the first armadillo repeat of β-catenin. Consequently, the alteration might lead – by inhibiting phosphorylations by CK1 – to β-catenin stabilization and inappropriate signaling [52]. We investigated the molecular background of four other samples from the Wnt_WT mutation group. Interestingly, we detected increased levels of *LGR5* in these specimens. In addition, in two tumors, copy-number identified amplification of the *R-spondin 2* (*RSPO2*) gene that encodes the LGR5 ligand and functions as an extracellular Wnt agonist (Fig. 6B; HCCs with *RSPO2* amplification are indicated as orange and violet triangles) [53].

We used data deposited by the TCGA consortium to analyze mutations or genomic rearrangement of the *NKD1* locus in cancer tissue. Previous reports identified the *NKD1* mutations within CRCs displaying MSI [54]. However, the coding region of *NKD1* in the corresponding TCGA dataset showed that the gene was modified only marginally, with one nonsense (p.R294X), one missense (p.P230L), and one silent mutation (p.L142L) detected within CRC samples and one silent mutation (p.C248C) found in rectal cancers, respectively. In addition, TCGA CRC samples were explored using the COSMIC interface (http://cancer.sanger.ac.uk/cancergenome/projects/cosmic/). The open reading frame of *NKD1* was found to be altered by one silent (p.G312G), one missense mutation (p.A374T) and one in-frame deletion (p.K104delK). Of note, neither of the missense mutations affect the NKD1 EFX domain presumably required for the interaction with DVL proteins [27]. Moreover, unlike reported [54], the integrity of the *NKD1* exon 10 poly$(C)_7$ stretch was impaired in a single case. Moreover, the *NKD1* genomic region was never subjected to significant amplification or deletion (data not shown). In line with CRC, mutational inactivation of *NKD1* is rare in HCC, with one p.P349L substitution detected within the HCC TCGA dataset and similarly, two *NKD1* missense mutations (p.R31P and p.K116R) recorded within COSMIC data survey (827 samples).

Finally, the methylation status of the *NKD1* locus in 366 CRC samples from the TCGA dataset

was analyzed and correlated to the *NKD1* transcription level. Whereas the CpG island (and adjacent loci) proximal to the *NKD1* promoter

Fig. 2. Tracking *Nkd1* expression using Nkd1-CreERT2 BAC transgenic mice.(A) Schemes depicting the BAC clone RP23-301N2 harboring the Nkd1 locus and generation of Nkd1-CreERT2 transgenic mice. CreERT2 was inserted into the second coding exon of the *Nkd1* gene of bacteria using homologous recombination. The insertion is in frame with the translation start located in the *Nkd1* first exon. The non-coding or translated regions are indicated by empty and black boxes, respectively. a,b, *Nkd1* sequences employed for homologous recombination; RGB poly A, a poly A signal derived from the rabbit β-globulin gene; KanR, the kanamycin resistance gene; pBla, β-lactamase promoter. Prior to pronuclear injection, the bacterial resistance cassette was excised from recombinant BAC using Flp recombinase and FRT sites (violet semicircles) flanking the cassette. (B) Comparison of the whole-mount hybridization of wild-type mouse embryo at embryonic day (E) 14.5 using an antisense probe against *Nkd1* (left image) with the activity of CreERT2 recombinase produced from the Nkd1-CreERT2 BAC transgene in Nkd1-CreERT2$^+$/Rosa26R embryos obtained at the same developmental stage (right). Tamoxifen was injected intraperitoneally into pregnant females and the animals were sacrificed one day later. cb, cerebral plate; dfl, distal forelimb; dhl, distal hindlimb drg, dorsal root ganglion; ee, ear; ma, maxilla; mg, mammary gland primordium; vi, vibrissae. (C) Stereoscopic images of whole-mount staining of LacZ in different anatomical parts of the intestine of Nkd1-CreERT2$^+$/Rosa26R mice six days after tamoxifen administration. duod, duodenum; jej, jejunum; ile, ileum; col, colon. (D) Lineage tracing in the duodenum of Nkd1-CreERT2$^+$/Rosa26R mice. The LacZ activity was detected in histological specimens at indicated days after tamoxifen administration. The slides were counterstained with nuclear red. One day upon tamoxifen administration the bottom parts of the crypts were labelled (black arrowheads in the left image), whereas three weeks later cellular clones formed blue ribbons extending from the crypts to the villi (right image). In addition, the tissue contains labelled Paneth cells residing at the crypt bottom (green arrow in the left image). (E) Double labeling shows that blue cells express markers of enteroendocrine (visualized by anti-chromogranin A staining), goblet (positive for PAS), and Paneth (anti-lysozyme) cell lineages. (F) Expression of endogenous *Nkd1* in cell populations sorted from the intestinal crypts is confined to the cell types localized at the crypt bottom. Left, diagram of the sorting procedure using crypt cells isolated from the proximal half of the small intestine of three Lgr5-EGFP-IRES-CreERT2 mice. Four cell populations were obtained representing ISCs (GFP$^+$), putative precursors of Paneth and enteroendocrine cell lineages (GFP$^+$UEA$^+$), mature Paneth cells (GFP$^-$UEA$^+$), TA cells (GFP$^-$UEA$^-$). Right, qRT-PCR of sorted crypt cell populations. Cp values were normalized to *Ubb*. Means relative to values obtained in GFP$^-$UEA$^-$ cells are presented with corresponding SDs. *Crypt*, *cryptidins 1/3/6 – 12/14/15*. (G) Distribution of LacZ-positive cells in the crypts of Nkd1-CreERT2$^+$/Rosa26R mice one day after tamoxifen administration. Four hundred crypts in proximal parts of the small intestine in two mice were counted. Results are depicted as means with SDs. The cell positions are indicated in the scheme in the inset: Paneth cells ("P") are depicted in red, CBC stem cells occupy crypt positions "0" and "1", and putative Paneth cell progenitors position "2". Scale bar: 2 mm (B), 5 mm (C), 0.1 mm (D), 5 μM (E).

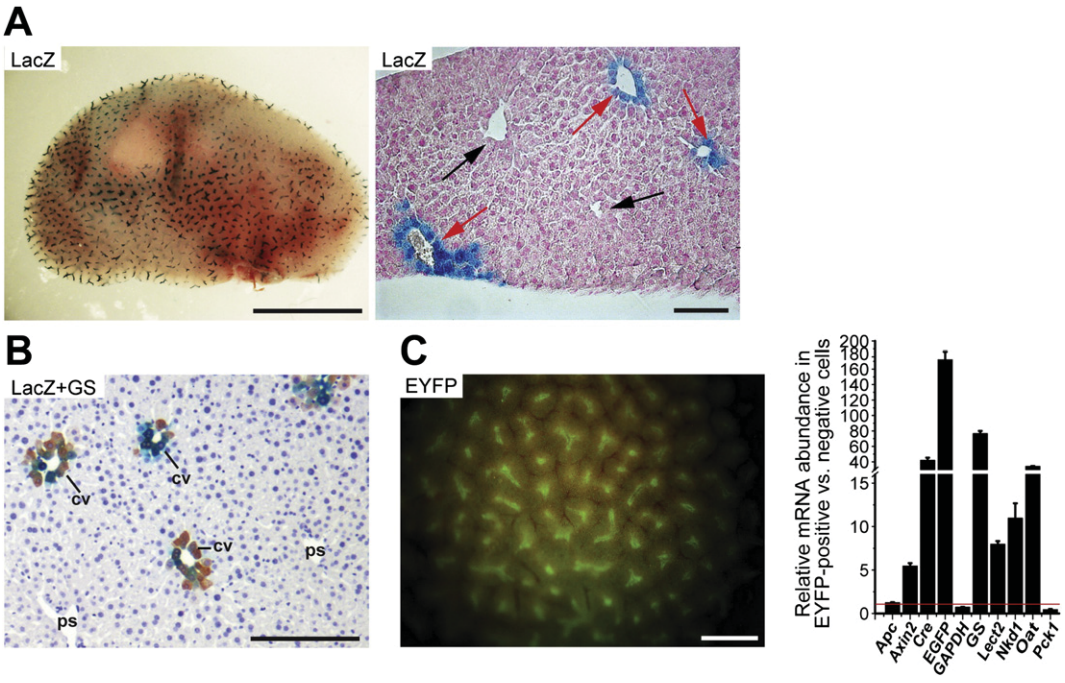


Fig. 3. *Nkd1* transcription is zonated to the perivenous hepatocytes. (A) Left, whole-mount staining of LacZ in the adult liver of Nkd1-CreERT2^{+}/Rosa26R mice one day after tamoxifen administration. Right, histochemical staining detects the LacZ activity in hepatocytes surrounding the putative centrilobular veins [(cv); red arrow]; periportal hepatocytes in close proximity to the portal space [(ps); black arrow] are LacZ negative. The specimen was counterstained with nuclear red. Scale bar: 4 mm (left image), 0.3 mm (right image). (B) Immunohistochemical co-localization of LacZ (blue color) and anti-GS (brown color) staining. The specimen was counterstained with hematoxylin. Scale bar: 0.3 mm. (C) Left, whole-mount fluorescent image of the Nkd1-CreERT2^{+}/Rosa26R-EYFP liver taken four days upon tamoxifen administration. Scale bar: 0.4 mm. Right, qRT-PCR analysis of EYFP^{+} and EYFP^{-} cells sorted from the Nkd1-CreERT2^{+}/Rosa26R-EYFP liver. The results were normalized to *Ubb* mRNA levels. The expression level of a given gene in EYFP^{-} cells was arbitrarily set to 1 (red line). Error bar: SD. Notice the enrichment of *Nkd1* mRNA along with other pericentral hepatocyte genes *Axin2*, *GS*, *Lect2*, and *Oat*. In contrast, *Apc* and *GAPDH* genes are not zonated and portal-specific *Pck1* displays a complementary expression pattern to the perivenous hepatocyte genes.

was hypomethylated in the majority of CRCs, the distal CpG island was heavily methylated. In concordance with previously published data [44] , differential methylation of the CpG island and adjacent "shores" (for terminology see Materials and Methods) situated within 2 kb of the transcription start site was strongly associated with transcription of the *NKD1* gene. Interestingly, the highest *NKD1* mRNA levels were

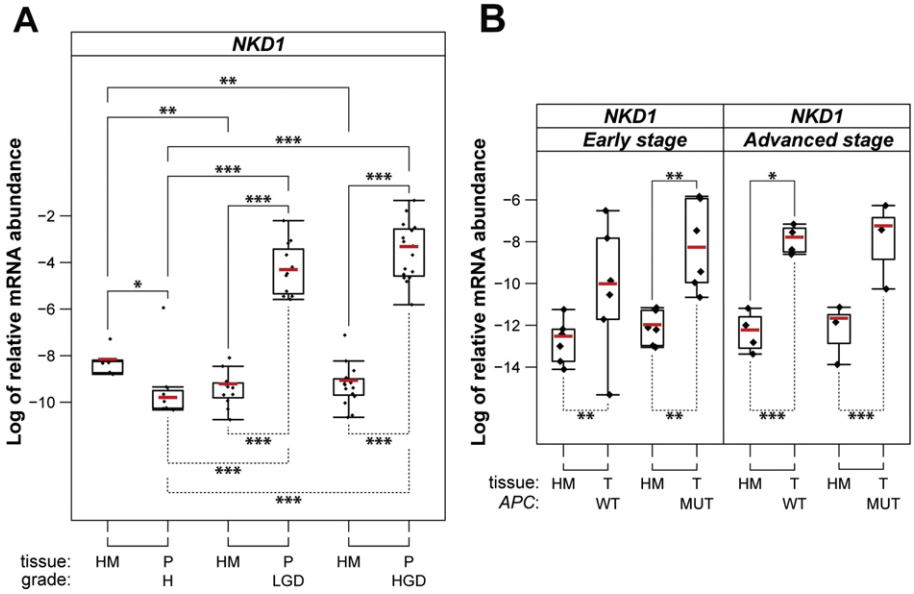


Fig. 4. NKD1 expression is increased during colorectal cancerogenesis. (A) Relative expression levels of *NKD1* in colorectal polyps. Log of relative expression levels (-ΔCp) were obtained following normalization of Cp values by geometric average of internal housekeeping genes *ACTB*, *UBB* and *AXIN1*. Predominant histological appearance stratified the lesions to hyperplasia (H), low-grade dysplasia (LGD) and high-grade dysplasia (HGD) subgroups. (B) Relative levels of *NKD1* transcript in CRCs. Cp values were normalized using *ACTB* as a reference gene to obtain ΔCp's. Malignant lesions were subdivided to distinct subgroups with respect to the *APC* mutation status (WT, wild-type *APC*; MUT, *APC* mutated) and disease progression. Statistical significance of differential expression in the given groups was examined by nonparametric Wilcoxon's rank-sum test (solid line). Moreover, the linear model (REML; dashed line), which accounted for the individual background of the patients, tissue type, histopathology, *APC* mutation status (CRC specimens only), was applied. The boxed areas correspond to the second and third quartiles; the range of the values is given by "whiskers" above and below each box. Median of ΔCp values for individual categories is depicted as the red line. Statistical data accompanying Fig. 4A and B can be found in Supplementary Table S5 and S6, respectively. *P < 0.05, **P < 0.01, and ***P < 0.001. HM, matching healthy mucosa; P, polyp; T, tumor.

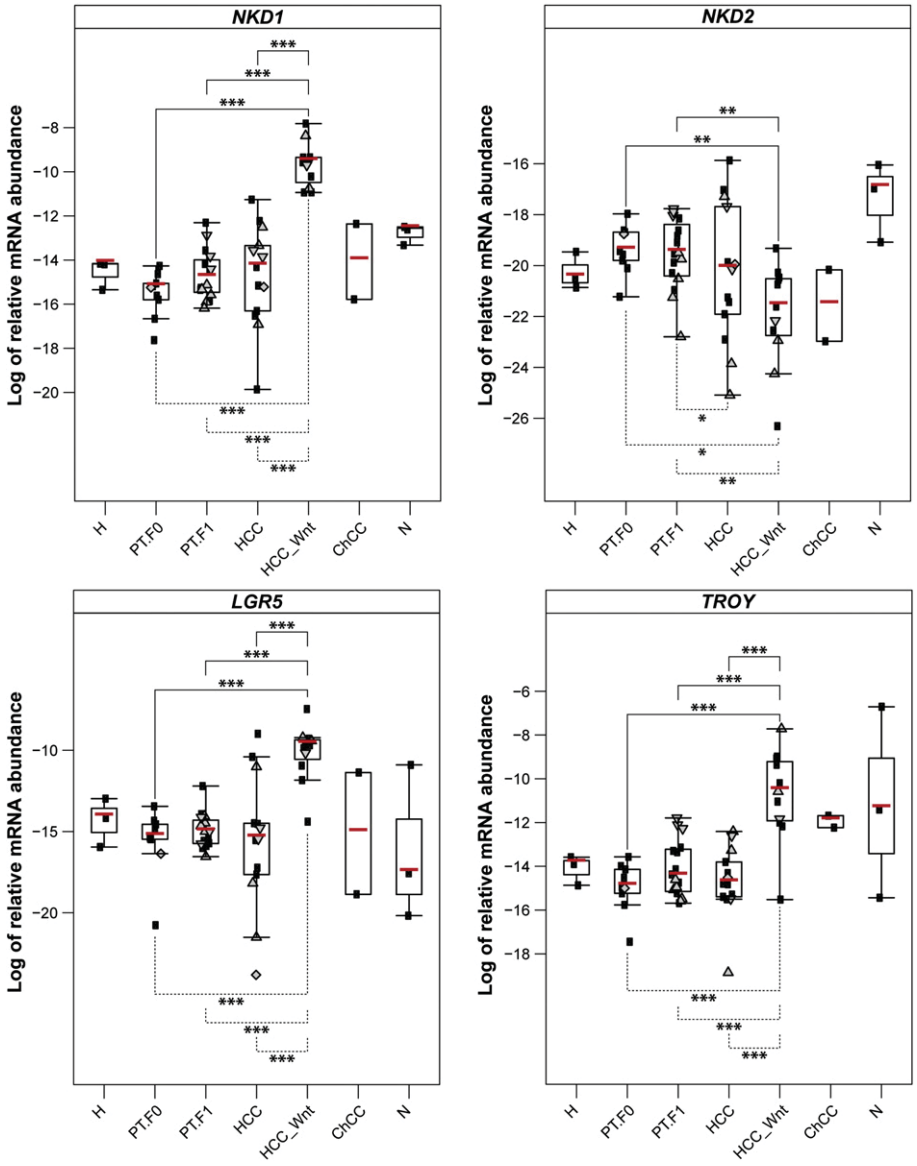


Fig. 5. NKD1 transcription is elevated in the Wnt class of HCCs. Relative mRNA abundance of the indicated genes in liver tumors and matched surrounding tissue. For each gene, Cp values were normalized by geometric average of the housekeeping genes *ACTB* and *UBB* (−ΔCp). The Wnt class (HCC_Wnt) was defined by expression levels of *AXIN2*, *EPBH2*, and *GS* genes (details are given in Supplementary Fig. S2). Two cases of cholangiocellular carcinoma constitute a separate group designated as ChCC. Additional types of liver neoplasia (adenolipoma, focal nodular hyperplasia and metastasis of colorectal carcinoma) were merged to a single group (N). Specimens of matched surrounding parenchyma were assessed according to the degree of fibrosis as healthy (H), precancerous tissue displaying mild to moderate fibrosis (PT.F0), or precancerous tissue exhibiting severe fibrosis to cirrhosis (PT.F1) [73]. Statistical significance of differential expression in the given groups was examined by nonparametric Wilcoxon's rank-sum test (solid line). Moreover, the linear model (REML; dashed line), which accounted for the individual background of the patients, tissue type and fibrosis score, was applied. The presence of viral infection is indicated by graphical symbols [circle: virus not detected; triangle: HBV positive; down-pointing triangle: HCV positive; lozenge: HBV + HCV positive]. Statistical analysis of ChCC samples was omitted from the image due to the small group size. Median of ΔCp values for individual categories is depicted as the red line. Numeric values accompanying this figure are given in Supplementary Table S7. *P < 0.05, **P < 0.01, and ***P < 0.001.

detected in CRC specimens that showed hypomethylation in the intron 3 S-shore region (Supplementary Figure S5).

4. Discussion

The activity of the Wnt pathway undergoes complex regulation to ensure proper functioning of signaling during development and in adult tissue homeostasis. The regulation may occur at several levels and includes both positive and negative feedback loops. In the intestinal crypt, a well-established cellular system depending on Wnt signaling, the pathway up-regulates Lgr5, a receptor for Rspos, and consequently, the Lgr5-Rspo interaction augments the Wnt/β-catenin signaling output [53]. In addition, Axin2 and Troy, two inhibitors of the Wnt pathway, are also induced by Wnt signaling [6,55]. Interestingly, mRNA levels encoding these genes display some variations among different cellular types located in the crypt. Troy appears to be exclusively expressed in ISCs [6,56]. However, Lgr5 – originally sought to be a unique stem cell marker – is also produced in non-dividing progenitors of the Paneth cells lineage [46]. Moreover, Axin2 expression is confined to the majority of cellular types located in the lower part of the crypts, i.e. ISCs, Paneth cells and their progenitors, and TA cells [46]. According to our lineage tracing experiments and expression analysis (Fig. 2), *Nkd1* represents another negative feedback regulator of Wnt signaling displaying relatively broad expression in the mouse crypt. Currently, it is not clear whether the observed differences in expression profiles of these Wnt pathway genes have any functional consequences. It is possible that these differences contribute to the fine-tuning of Wnt signaling. However, since targeted inactivation of any of the genes described above has no obvious phenotype, such explanation seems unlikely. More probably, random fluctuations in gene transcription might account for

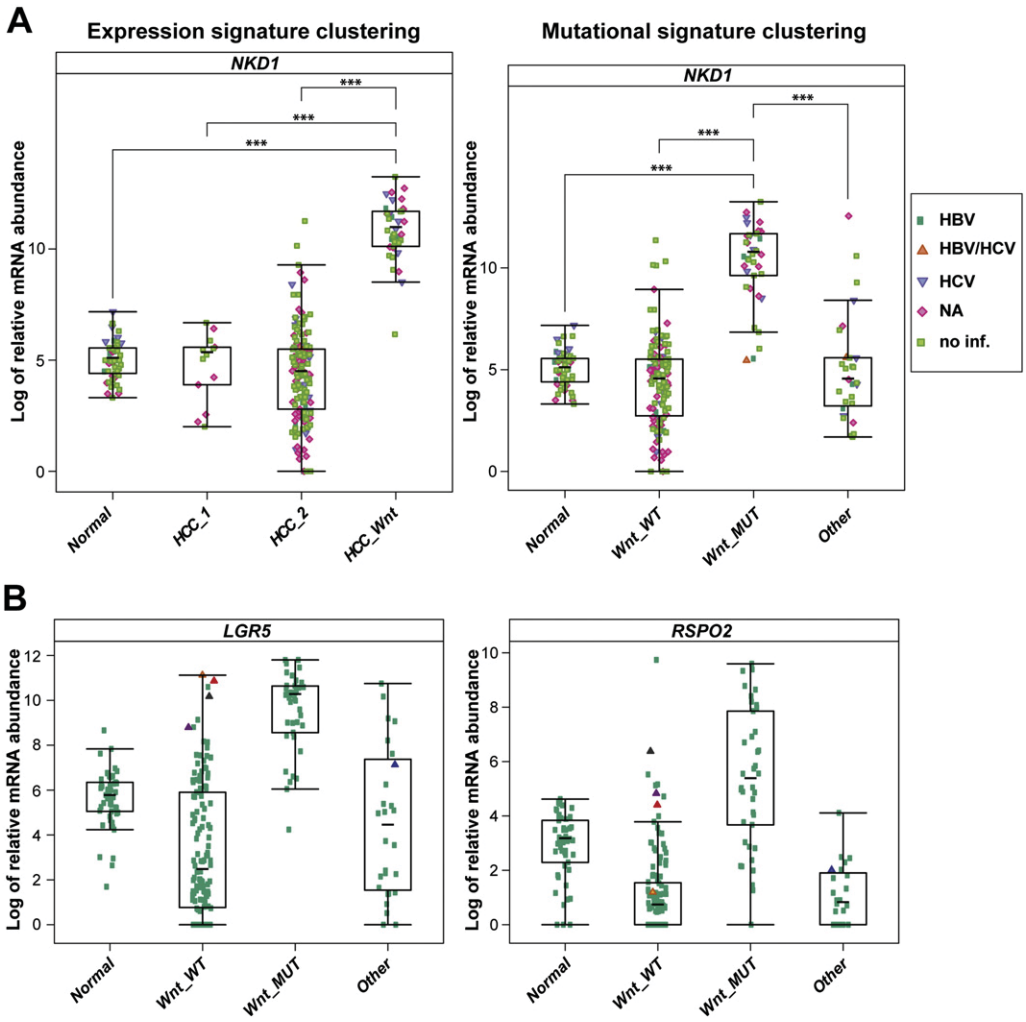


Fig. 6. NKD1 defines HCC displaying aberrant Wnt signaling. (A) Left panel, expression of *NKD1* in three gene expression classes of HCCs. The TCGA HCC specimens were stratified using transcription levels of the *AXIN2*, *EPHB2*, and *GS* (details are given in Supplementary Fig. S3). Right panel, relative expression of *NKD1* in HCC samples assigned to the individual mutation groups. Classification of the TCGA HCC specimens according to mutational changes in *APC*, *AXIN1/2*, and *CNNB1* is given in Supplementary Fig. S4. (B) Expression of *LGR5* and *RSPO2* in the HCC mutation groups. Samples assigned to the HCC_Wnt class that do not fall to the Wnt_MUT group are indicated by triangles of matched color. Black lines indicate median of expression levels for individual categories. Numerical values accompanying this figure are given in Supplementary Tables S7 and S8. *P < 0.05, **P < 0.01, and ***P < 0.001.

the observed variations in mRNA levels of a given gene in crypt cells [57] . In the mouse liver, *Nkd1* represents, together with *Axin2* and *Troy* (BF and VK, unpublished data), a robust marker of perivenous hepatocytes. Although the involvement of Wnt signaling in liver zonation is well established, the liver-specific *Nkd1* function has not been – similarly as in gut tissue – documented.

In a collection of human intestinal neoplasia the *NKD* mRNA levels were upregulated in nearly all of the tumors irrespective of the *APC* status (Fig. 4). This was seemingly surprising, since in mouse hyperplastic crypts *Nkd1* overexpression was directly linked to *Apc* loss. Nevertheless, the mutational status of *APC* in the panel of CRCs was based on sequencing of the exon 19 (NCBI nomenclature) that contains the mutational "hot spot", but it likely does not cover all *APC* mutations [6]. Moreover, recent studies employing massive parallel sequencing of tumor DNA indicated that gene alterations resulting in hyperactive Wnt signaling can be found in more than 90% of CRCs [18]. Therefore, limited knowledge of the status of the Wnt pathway in (our) CRC collection can be attributed to the discrepancy between *Nkd1* expression data obtained in the mouse and in clinical samples. This explanation may interpret the observed decrease in the *NKD1* mRNA levels in hyperplastic polyps (Fig. 4A). According to the recent concept of the "serrated neoplasia pathway", precancerous hyperplasia is linked to the development of a separate subclass of gut tumors [58]. Serrated CRC lesions are predominantly initiated by oncogenic *BRAF* mutations and do not harbor genetic changes that would compromise control over Wnt signaling [59].

Relevant CRC datasets obtained from TCGA did not include paired samples of the healthy mucosa, and thus we could not directly compare the *NKD1* mRNA levels in tumors and normal (matched) tissue. Nevertheless, in APC-deficient CRCs at early stage of progression, *NKD1* transcription was higher in MSS lesions than in tumors displaying increased levels of microsatellite instability. Furthermore, upon subdivision of CRCs according to their expression signature, *NKD1* mRNA was significantly increased in the TA (progenitor) type of the tumors (Supplementary Fig. S1). Whether the extent of *NKD1* upregulation reflects a particular mechanism of tumor initiation or mirrors the variability of *NKD1* expression in the cellular types present in the healthy colon remains to be determined.

Although in the majority of CRCs the aberrant Wnt activity is attributable to mutations affecting intracellular components of the Wnt pathway [18], the signaling output can be augmented by epigenetic silencing of genes encoding secreted Wnt antagonists, such as secreted frizzled-related proteins (SFRPs) and dickkopf WNT signaling pathway inhibitors (DKKs) [60–63]. Thus, integration of genetic and epigenetic changes that affect multiple steps of the Wnt signal transduction likely confers a selective advantage to tumor cells. In line with these "multiple-hit"

concepts and given that methylation of *NKD1* regulatory elements was observed in ovarian and gastric cancer [64,65], we investigated the methylation status in 366 CRC samples of the TCGA dataset and examined its relation to *NKD1* transcription. In contrast to other neoplasia, loci proximal to the *NKD1* promoter were unmethylated. Moreover, *NKD1* mRNA was more abundant in colorectal tumors displaying hypomethylation in the S-shore region located in the third intron of the *NKD1* gene (Supplementary Figure S5). Strikingly, the CRC "methylome" analysis by Irizarry and colleagues identified an identical inverse relationship between intron 3 S-shore methylation and *NKD1* expression [44]. In summary, dysregulation of *NKD1* in tumors is possibly driven by as yet undescribed epigenetic mechanisms.

The etiology of HCC is mainly associated with alcohol abuse and HBV and HCV infection. Consequently, HCC is rather a heterogeneous disease and the link between aberrant Wnt signaling and HCC is less obvious than in the cancer of the colon and rectum. Although there is no generally accepted molecular classification of the disease, several recent studies identified (sub)classes of HCC. Importantly, the Wnt-associated class of HCC (approximately 20–40% of all cases) is predominantly defined by the presence of activating mutations in the *CTNNB1* gene. In contrast, alterations in *APC*, so dominant in CRC, are less frequent in HCC (2–3%) [66]. This is rather peculiar since the *APC* gene represents a substantially larger "target" than the exon 3 in the *CTNNB1* gene. Of note, in hepatoblastoma, the most frequent malignant pediatric tumor of the liver, approximately 50% of neoplastic lesions harbor activating mutation in *CTNNB1* [67] and display elevated expression of *NKD1* [68]. Nevertheless, since *APC* and *CTNNB1* mutations are mutually exclusive, the high frequency of the changes in the latter gene possibly reflects a combination of the locus accessibility and/or presence of liver-specific mutagens rather than any unique β-catenin-dependent role in HCC initiation or progression.

The gene expression signature of three Wnt signaling target genes, *AXIN2*, *EPHB2*, and *GS*, was used to stratify HCCs to the β-catenin-dependent "HCC_Wnt" class. Although we were unable (probably due to the limited number of specimens in our experimental collection) to separate the rest of the samples to other classes as described previously [25], the *NKD1* expression profile fitted well to the "HCC_Wnt" class. In agreement with these results, bioinformatic analysis of the HCC datasets obtained from TCGA confirmed that *AXIN2*, *EPHB2*, *GS*, and *NKD1* represent robust markers of the HCC_Wnt class. Interestingly, not all specimens from this class harbored mutations in the *APC*, *AXIN1/2*, and *CTNNB1* genes. Interestingly, we observed amplification of the *RSPO2* locus in two of the samples (out of four in total). This is in accordance with recent data indicating that the amplification of the *RSPO* genes represents a frequent event in HCC (up to 25%) [51–66]. Increased production of *RSPO* ligands has been observed in CRC as an oncogenic "by-pass" mechanism that circumvents intact *APC* [69]. Collectively, the membranous inputs may contribute to liver tumorigenesis in a manner analogous to signaling circuits described in CRC. Finally, seven samples assigned to the Wnt_MUT group did not display the Wnt-dependent expression signature. Since all these samples carried "likely oncogenic mutations" (LOMs) in exon 3 of the *CTNNB1* (Supplementary Table S4) that do not change the regulatory serine/threonine residue, we presume that these mutations are "passenger" without any effect on the β-catenin stability.

Simultaneous inactivation of *APC* and *AXIN2* or *APC* and *NKD1* occurs in exceptional cases only. Since sustained expression of *AXIN2* and *NKD1* is typical of APC-deficient tumors, we speculate that the function of these Wnt pathway inhibitors might be strongly favored to keep the Wnt pathway activity "optimal" for tumor growth [70,71]. This conclusion is in accordance with recent results of Barrry and colleagues demonstrating that another DVL interacting partner, yes-associated protein 1 (YAP1), limits aberrant Wnt signaling and that YAP1-deficiency leads to highly aggressive undifferentiated CRCs or results in Wnt hypersensitivity during intestinal regeneration [72]. Interestingly, YAP1 restricts Wnt signaling independently of the β-catenin destruction complex by suppressing nuclear translocation of Dvl. Thus, we propose that in concordance with the "passive antagonist" model [32], Nkd1 might directly influence the nuclear Dvl function in cells displaying hyperactive Wnt signaling.

In summary, despite its unclear molecular function, *NKD1* can serve as a reliable marker of intestinal and liver tumors that display aberrant Wnt/β-catenin signaling.

5. Conclusion

Mutations in genes encoding components of the Wnt/β-catenin pathway that result in aberrant activation of the signaling are undoubtedly linked to the onset of intestinal cancer. In contrast, the etiology of liver cancer is heterogeneous and frequently linked to viral infection. Although several recent studies aimed to identify subclasses of HCC, there is no generally accepted molecular classification of the disease. In the present study we employed a negative feedback regulator of Wnt signaling, Nkd1, as a marker of active Wnt signaling in the intestine and liver and in tumors originating from these organs. Our results provide evidence that *NKD1* can be utilized to distinguish a class of HCC linked to aberrant Wnt signaling.

Conflicts of interest

There are no conflicts of interest to disclose.

Acknowledgements

We thank S. Takacova for critically reading the manuscript. We also thank M. Cepko and S. Robine for reagents and Villin-CreERT2 mice. This work was supported by the Grant Agency of the Czech Republic (Grant No. P305/11/1780), institutional grant from the Academy of Sciences of the Czech Republic (RVO 68378050), project BIOCEV – Biotechnology and Biomedicine Centre of the Academy of Sciences and Charles University (CZ.1.05/1.1.00/02.0109) from the European Regional Development Fund to V.K. and R.S., Ministry of Education, Youth and Sports of the Czech Republic (LM2011032) to R.S., Institutional support from the Ministry of Health of the Czech Republic for development of research organization (00023001) to M.O., M.N., and M.J., Grant Agency of Charles University in Prague (1400-243-253470) to J.St., Charles University in Prague Research Project PRVOUK - Oncology P27 to J.Sv.

The results shown here are in part based upon data generated by the TCGA Research (http://cancergenome.nih.gov/). We are deeply grateful to all specimen donors and research groups that have made the data publicly available. We also express our special thanks to the employees of the Transgenic and Archiving Module, the Czech Centre for Phenogenomics, IMG, Prague for their excellent effort in generation of transgenic mice.

Appendix A. Supplementary data

Supplementary data to this article can be found online at http://dx.doi.org/10.1016/j.cellsig.2014.11.008.

References

[1] K.M. Cadigan, Cold Spring Harb. Perspect. Biol. 1 (2009) a002881.
[2] T. Valenta, G. Hausmann, K. Basler, EMBO J. 31 (2012) 2714–2736.
[3] A. Schepers, H. Clevers, Cold Spring Harb. Perspect. Biol. 4 (2012) a007989.
[4] H.C. Clevers, C.L. Bevins, Annu. Rev. Physiol. 75 (2013) 289–311.
[5] N. Barker, J.H. van Es, J. Kuipers, P. Kujala, M. van den Born, M. Cozijnsen, A. Haegebarth, J. Korving, H. Begthel, P.J. Peters, H. Clevers, Nature 449 (2007) 1003–1007.
[6] B. Fafilek, M. Krausova, M. Vojtechova, V. Pospichalova, L. Tumova, E. Sloncova, M. Huranova, J. Stancikova, A. Hlavata, J. Svec, R. Sedlacek, O. Luksan, M. Oliverius, L. Voska, M. Jirsa, J. Paces, M. Kolar, M. Krivjanska, K. Klimesova, H. Tlaskalova-Hogenova, V. Korinek, Gastroenterology 144 (2013) 381–391.

[7] L.G. van der Flier, M.E. van Gijn, P. Hatzis, P. Kujala, A. Haegebarth, D.E. Stange, H. Begthel, M. van den Born, V. Guryev, I. Oving, J.H. van Es, N. Barker, P.J. Peters, M. van de Wetering, H. Clevers, Cell 136 (2009) 903–912.
[8] E. Batlle, J.T. Henderson, H. Beghtel, M.M. van den Born, E. Sancho, G. Huls, J. Meeldijk, J. Robertson, M. van de Wetering, T. Pawson, H. Clevers, Cell 111 (2002) 251–263.
[9] M. Krausova, V. Korinek, Cell. Signal. 26 (2014) 570–579.
[10] V. Korinek, N. Barker, P. Moerer, E. van Donselaar, G. Huls, P.J. Peters, H. Clevers, Nat. Genet. 19 (1998) 379–383.
[11] J.H. van Es, A. Haegebarth, P. Kujala, S. Itzkovitz, B.K. Koo, S.F. Boj, J. Korving, M. van den Born, A. van Oudenaarden, S. Robine, H. Clevers, Mol. Cell. Biol. 32 (2012) 1918–1927.
[12] T. Fevr, S. Robine, D. Louvard, J. Huelsken, Mol. Cell. Biol. 27 (2007) 7551–7559.
[13] H. Ireland, R. Kemp, C. Houghton, L. Howard, A.R. Clarke, O.J. Sansom, D.J. Winton, Gastroenterology 126 (2004) 1236–1246.
[14] S.P. Monga, Gene Expr. 16 (2014) 51–62.
[15] S. Benhamouche, T. Decaens, C. Godard, R. Chambrey, D.S. Rickman, C. Moinard, M. Vasseur-Cognet, C.J. Kuo, A. Kahn, C. Perret, S. Colnot, Dev. Cell 10 (2006) 759–770.
[16] P. Polakis, Cold Spring Harb. Perspect. Biol. 4 (2012).
[17] K.W. Kinzler, B. Vogelstein, Cell 87 (1996) 159–170.
[18] Nature 487 (2012) 330–337.
[19] D.P. Minde, Z. Anvarian, S.G. Rudiger, M.M. Maurice, Mol. Cancer 10 (2011) 101.
[20] Y. Shimizu, S. Ikeda, M. Fujimori, S. Kodama, M. Nakahara, M. Okajima, T. Asahara, Genes Chromosom. Cancer 33 (2002) 73–81.
[21] W. Liu, X. Dong, M. Mai, R.S. Seelan, K. Taniguchi, K.K. Krishnadath, K.C. Halling, J.M. Cunningham, L.A. Boardman, C. Qian, E. Christensen, S.S. Schmidt, P.C. Roche, D.I. Smith, S.N. Thibodeau, Nat. Genet. 26 (2000) 146–147.
[22] P.J. Morin, A.B. Sparks, V. Korinek, N. Barker, H. Clevers, B. Vogelstein, K.W. Kinzler, Science 275 (1997) 1787–1790.
[23] H.B. El-Serag, K.L. Rudolph, Gastroenterology 132 (2007) 2557–2576.
[24] Y. Hoshida, S.M. Nijman, M. Kobayashi, J.A. Chan, J.P. Brunet, D.Y. Chiang, A. Villanueva, P. Newell, K. Ikeda, M. Hashimoto, G. Watanabe, S. Gabriel, S.L. Friedman, H. Kumada, J.M. Llovet, T.R. Golub, Cancer Res. 69 (2009) 7385–7392.
[25] A. Lachenmayer, C. Alsinet, R. Savic, L. Cabellos, S. Toffanin, Y. Hoshida, A. Villanueva, B. Minguez, P. Newell, H.W. Tsai, J. Barretina, S. Thung, S.C. Ward, J. Bruix, V. Mazzaferro, M. Schwartz, S.L. Friedman, J.M. Llovet, Clin. Cancer Res. 18 (2012) 4997–5007.
[26] S. Li, M. Mao, Cancer Lett. 340 (2013) 247–253.
[27] R. Rousset, J.A. Mack, K.A. Wharton Jr., J.D. Axelrod, K.M. Cadigan, M.P. Fish, R. Nusse, M.P. Scott, Genes Dev. 15 (2001) 658–671.
[28] I. Schneider, P.N. Schneider, S.W. Derry, S. Lin, L.J. Barton, T. Westfall, D.C. Slusarski, Dev. Biol. 348 (2010) 22–33.
[29] T.J. Van Raay, R.J. Coffey, L. Solnica-Krezel, Dev. Biol. 309 (2007) 151–168.
[30] T.J. Van Raay, N.J. Fortino, B.W. Miller, H. Ma, G. Lau, C. Li, J.L. Franklin, L. Attisano, L. Solnica-Krezel, R.J. Coffey, PLoS One 6 (2011) e18650.
[31] S. Zhang, T. Cagatay, M. Amanai, M. Zhang, J. Kline, D.H. Castrillon, R. Ashfaq, O.K. Oz, K.A. Wharton Jr., Mol. Cell. Biol. 27 (2007) 4454–4464.
[32] D. Angonin, T.J. Van Raay, PLoS One 8 (2013) e74666.
[33] A.R. Moser, H.C. Pitot, W.F. Dove, Science 247 (1990) 322–324.
[34] L.K. Su, K.W. Kinzler, B. Vogelstein, A.C. Preisinger, A.R. Moser, C. Luongo, K.A. Gould, W.F. Dove, Science 256 (1992) 668–670.
[35] P. Soriano, Nat. Genet. 21 (1999) 70–71.
[36] S. Srinivas, T. Watanabe, C.S. Lin, C.M. William, Y. Tanabe, T.M. Jessell, F. Costantini, BMC Dev. Biol. 1 (4) (2001).
[37] M. Kuraguchi, X.P. Wang, R.T. Bronson, R. Rothenberg, N.Y. Ohene-Baah, J.J. Lund, M. Kucherlapati, R.L. Maas, R. Kucherlapati, PLoS Genet. 2 (2006) e146.
[38] F. el Marjou, K.P. Janssen, B.H. Chang, M. Li, V. Hindie, L. Chan, D. Louvard, P. Chambon, D. Metzger, S. Robine, Genesis 39 (2004) 186–193.
[39] T. Shimosato, M. Tohno, T. Sato, J. Nishimura, Y. Kawai, T. Saito, H. Kitazawa, Anim. Sci. J. 80 (2009) 597–604.
[40] O. Machon, C.J. van den Bout, M. Backman, O. Rosok, X. Caubit, S.H. Fromm, B. Geronimo, S. Krauss, Neuroscience 112 (2002) 951–966.
[41] T. Sato, J.H. van Es, H.J. Snippert, D.E. Stange, R.G. Vries, M. van den Born, N. Barker, N.F. Shroyer, M. van de Wetering, H. Clevers, Nature 469 (2011) 415–418.
[42] Y. Ohashi, S. Kansal, M. Schreiber Jr., Advances in peritoneal dialysis, Conference on peritoneal dialysis282012. 131–133.
[43] H. Wu, B. Caffo, H.A. Jaffee, R.A. Irizarry, A.P. Feinberg, Biostatistics 11 (2010) 499–514.
[44] R.A. Irizarry, C. Ladd-Acosta, B. Wen, Z. Wu, C. Montano, P. Onyango, H. Cui, K. Gabo, M. Rongione, M. Webster, H. Ji, J.B. Potash, S. Sabunciyan, A.P. Feinberg, Nat. Genet. 41 (2009) 178–186.
[45] A.E. Powell, Y. Wang, Y. Li, E.J. Poulin, A.L. Means, M.K. Washington, J.N. Higginbotham, A. Juchheim, N. Prasad, S.E. Levy, Y. Guo, Y. Shyr, B.J. Aronow, K.M. Haigis, J.L. Franklin, R.J. Coffey, Cell 149 (2012) 146–158.
[46] S.J. Buczacki, H.I. Zecchini, A.M. Nicholson, R. Russell, L. Vermeulen, R. Kemp, D.J. Winton, Nature 495 (2013) 65–69.
[47] A. Sadanandam, C.A. Lyssiotis, K. Homicsko, E.A. Collisson, W.J. Gibb, S. Wullschleger, L.C. Ostos, W.A. Lannon, C. Grotzinger, M. Del Rio, B. Lhermitte, A.B. Olshen, B. Wiedenmann, L.C. Cantley, J.W. Gray, D. Hanahan, Nat. Med. 19 (2013) 619–625.
[48] C. Fraley, A.E. Raftery, J. Classif. 20 (2003) 263–286.
[49] O.N. Ikediobi, H. Davies, G. Bignell, S. Edkins, C. Stevens, S. O'Meara, T. Santarius, T. Avis, S. Barthorpe, L. Brackenbury, G. Buck, A. Butler, J. Clements, J. Cole, E. Dicks, S. Forbes, K. Gray, K. Halliday, R. Harrison, K. Hills, J. Hinton, C. Hunter, A. Jenkinson, D. Jones, V. Kosmidou, R. Lugg, A. Menzies, T. Mironenko, A. Parker, J. Perry, K. Raine, D. Richardson, R. Shepherd, A. Small, R. Smith, H. Solomon, P. Stephens, J. Teague, C. Tofts, J. Varian, T. Webb, S. West, S. Widaa, A. Yates, W. Reinhold, J.N. Weinstein, M.R. Stratton, P.A. Futreal, R. Wooster, Mol. Cancer Ther. 5 (2006) 2606–2612.
[50] G.R. Bignell, C.D. Greenman, H. Davies, A.P. Butler, S. Edkins, J.M. Andrews, G. Buck, L. Chen, D. Beare, C. Latimer, S. Widaa, J. Hinton, C. Fahey, B. Fu, S. Swamy, G.L. Dalgliesh, B.T. Teh, P. Deloukas, F. Yang, P.J. Campbell, P.A. Futreal, M.R. Stratton, Nature 463 (2010) 893–898.
[51] C. Guichard, G. Amaddeo, S. Imbeaud, Y. Ladeiro, L. Pelletier, I.B. Maad, J. Calderaro, P. Bioulac-Sage, M. Letexier, F. Degos, B. Clement, C. Balabaud, E. Chevet, A. Laurent, G. Couchy, E. Letouze, F. Calvo, J. Zucman-Rossi, Nat. Genet. 44 (2012) 694–698.
[52] V.H. Bustos, A. Ferrarese, A. Venerando, O. Marin, J.E. Allende, L.A. Pinna, Proc. Natl. Acad. Sci. U. S. A. 103 (2006) 19725–19730.
[53] W. de Lau, N. Barker, T.Y. Low, B.K. Koo, V.S. Li, H. Teunissen, P. Kujala, A. Haegebarth, P.J. Peters, M. van de Wetering, D.E. Stange, J.E. van Es, D. Guardavaccaro, R.B. Schasfoort, Y. Mohri, K. Nishimori, S. Mohammed, A.J. Heck, H. Clevers, Nature 476 (2011) 293–297.
[54] J. Guo, T. Cagatay, G. Zhou, C.C. Chan, S. Blythe, K. Suyama, L. Zheng, K. Pan, C. Qian, R. Hamelin, S.N. Thibodeau, P.S. Klein, K.A. Wharton, W. Liu, PLoS One 4 (2009) e7982.
[55] B. Lustig, B. Jerchow, M. Sachs, S. Weiler, T. Pietsch, U. Karsten, M. van de Wetering, H. Clevers, P.M. Schlag, W. Birchmeier, J. Behrens, Mol. Cell. Biol. 22 (2002) 1184–1193.
[56] D.E. Stange, B.K. Koo, M. Huch, G. Sibbel, O. Basak, A. Lyubimova, P. Kujala, S. Bartfeld, J. Koster, J.H. Geahlen, P.J. Peters, J.H. van Es, M. van de Wetering, J.C. Mills, H. Clevers, Cell 155 (2013) 357–368.
[57] S. Itzkovitz, A. Lyubimova, I.C. Blat, M. Maynard, J. van Es, J. Lees, T. Jacks, H. Clevers, A. van Oudenaarden, Nat. Cell Biol. 14 (2012) 106–114.
[58] E.M.F. De Sousa, X. Wang, M. Jansen, E. Fessler, A. Trinh, L.P. de Rooij, J.H. de Jong, O.J. de Boer, R. van Leersum, M.F. Bijlsma, H. Rodermond, M. van der Heijden, C.J. van Noesel, J.B. Tuynman, E. Dekker, F. Markowetz, J.P. Medema, L. Vermeulen, Nat. Med. 19 (2013) 614–618.
[59] K.S. Boparai, E. Dekker, M.M. Polak, A.R. Musler, S. van Eeden, C.J. van Noesel, Am. J. Pathol. 178 (2011) 2700–2707.
[60] H. Suzuki, E. Gabrielson, W. Chen, R. Anbazhagan, M. van Engeland, M.P. Weijenberg, J.G. Herman, S.B. Baylin, Nat. Genet. 31 (2002) 141–149.
[61] A. Bafico, G. Liu, L. Goldin, V. Harris, S.A. Aaronson, Cancer Cell 6 (2004) 497–506.
[62] H. Suzuki, D.N. Watkins, K.W. Jair, K.E. Schuebel, S.D. Markowitz, W.D. Chen, T.P. Pretlow, B. Yang, Y. Akiyama, M. Van Engeland, M. Toyota, T. Tokino, Y. Hinoda, K. Imai, J.G. Herman, S.B. Baylin, Nat. Genet. 36 (2004) 417–422.
[63] Q.J. Voorham, J. Janssen, M. Tijssen, S. Snellenberg, S. Mongera, N.C. van Grieken, H. Grabsch, M. Kliment, B.J. Rembacken, C.J. Mulder, M. van Engeland, G.A. Meijer, R.D. Steenbergen, B. Carvalho, BMC Cancer 13 (2013) 603.
[64] W. Dai, J.M. Teodoridis, C. Zeller, J. Graham, J. Hersey, J.M. Flanagan, E. Stronach, D.W. Millan, N. Siddiqui, J. Paul, R. Brown, Clin. Cancer Res. 17 (2011) 4052–4062.
[65] Y. Yoda, H. Takeshima, T. Niwa, J.G. Kim, T. Ando, R. Kushima, T. Sugiyama, H. Katai, H. Noshiro, T. Ushijima, Gastric Cancer (2014), http://dx.doi.org/10.1007/s10120-014-0348-0.
[66] Z. Kan, H. Zheng, X. Liu, S. Li, T.D. Barber, Z. Gong, H. Gao, K. Hao, M.D. Willard, J. Xu, R. Hauptschein, P.A. Rejto, J. Fernandez, G. Wang, Q. Zhang, B. Wang, R. Chen, J. Wang, N.P. Lee, W. Zhou, Z. Lin, Z. Peng, K. Yi, S. Chen, L. Li, X. Fan, J. Yang, R. Ye, J. Ju, K. Wang, H. Estrella, S. Deng, P. Wei, M. Qiu, I.H. Wulur, J. Liu, M.E. Ehsani, C. Zhang, A. Loboda, W.K. Sung, A. Aggarwal, R.T. Poon, S.T. Fan, J. Wang, J. Hardwick, C. Reinhard, H. Dai, Y. Li, J.M. Luk, M. Mao, Genome Res. 23 (2013) 1422–1433.
[67] A. Koch, D. Denkhaus, S. Albrecht, I. Leuschner, D. von Schweinitz, T. Pietsch, Cancer Res. 59 (1999) 269–273.
[68] A. Koch, A. Waha, W. Hartmann, A. Hrychyk, U. Schuller, K.A. Wharton Jr., S.Y. Fuchs, D. von Schweinitz, T. Pietsch, Clin. Cancer Res. 11 (2005) 4295–4304.
[69] S. Seshagiri, E.W. Stawiski, S. Durinck, Z. Modrusan, E.E. Storm, C.B. Conboy, S. Chaudhuri, Y. Guan, V. Janakiraman, B.S. Jaiswal, J. Guillory, C. Ha, G.J. Dijkgraaf, J. Stinson, F. Gnad, M.A. Huntley, J.D. Degenhardt, P.M. Haverty, R. Bourgon, W. Wang, H. Koeppen, R. Gentleman, T.K. Starr, Z. Zhang, D.A. Largaespada, T.D. Wu, F.J. de Sauvage, Nature 488 (2012) 660–664.
[70] A. Lewis, S. Segditsas, M. Deheragoda, P. Pollard, R. Jeffery, E. Nye, H. Lockstone, H. Davis, S. Clark, G. Stamp, R. Poulsom, N. Wright, I. Tomlinson, Gut 59 (2010) 1680–1686.
[71] S.H. Chandra, I. Wacker, U.K. Appelt, J. Behrens, J. Schneikert, PLoS One 7 (2012) e34479.
[72] E.R. Barry, T. Morikawa, B.L. Butler, K. Shrestha, R. de la Rosa, K.S. Yan, C.S. Fuchs, S.T. Magness, R. Smits, S. Ogino, C.J. Kuo, F.D. Camargo, Nature 493 (2013) 106–110.
[73] K. Ishak, A. Baptista, L. Bianchi, F. Callea, J. De Groote, F. Gudat, H. Denk, V. Desmet, G. Korb, R.N. MacSween, et al., J. Hepatol. 22 (1995) 696–699.

Supplementary material

Article: NKD1 marks intestinal and liver tumors linked to aberrant Wnt signaling

Authors: Jitka Stancikova, Michaela Krausova, Michal Kolar, Bohumil Fafilek, Jiri Svec, Radislav Sedlacek, Magdalena Neroldova, Jan Dobes, Monika Horazna, Lucie Janeckova, Martina Vojtechova, Martin Oliverius, Milan Jirsa and Vladimir Korinek

Supplementary Figure legends

Supplementary Figure S1. Expression levels of *AXIN2* and *NKD1* in subclasses of CRCs

Intestinal cancers (dataset TCGA COAD) were stratified according to disease progression (early stage: stage I-IIC; advanced stage: stage IIIA-IV). Only *APC*-compromised tumors are displayed. (A) Tumors were assigned according to genetic stability to the microsatellite stable class (MSS), or to the class displaying low (MSI-L) or high (MSI-H) degree of microsatellite instability (adopted from ref. [18]). (B) Subclassification of CRCs based on cellular phenotypes as described in reference [45]. A biological significance criterion was incorporated following Mann-Whitney test – statistical significance is plotted only when the expressional intensity increases at least 2-fold (logFC>1). Numeric values are given in Supplementary Table S8. Median of expression levels for individual categories is indicated by black line. TA, transit amplifying. *P < 0.05, **P < 0.01, and ***P < 0.001.

Supplementary Figure S2. Expression levels of *AXIN2*, *EPHB2* and *GS* define the Wnt class of HCCs

(A) Classification of HCCs as revealed by principal component analysis (PCA) on 24 HCC specimens (letters a-x represent individual lesions). According to *AXIN2*, *EPHB2* and *GS* expression levels the MCLUST algorithm based on the Bayesian Information Criteria (BIC) estimated four non-overlapping clusters of the HCC specimens (HCC_1-4). Samples assigned to the Wnt class were localized to the HCC_2 group. These samples were grouped in panel (B) to the HCC_Wnt class; samples in the groups HCC_1, HCC_3, and HCC_4 were merged to a single class designated “HCC”. Letters representing HCC samples with detected oncogenic *CTNNB1* mutation are underlined. (B) Simultaneous upregulation of *AXIN2*, *EPHB2*, and *GS* transcription stratifies hepatocellular tumors to the HCC_Wnt class. Median of ΔCp values for individual categories is indicated by red line. Numeric values accompanying this figure are given in

Supplementary Table S7. Neoplastic lesions and details of the qRT-PCR procedure are described in Fig. 5 legend. *P < 0.05, **P < 0.01, and ***P < 0.001.

Supplementary Figure S3. Simultaneous upregulation of *AXIN2*, *EPHB2* and *GS* defines the HCC_Wnt class in the TCGA HCC dataset

(A) Stratification of HCC specimens using PCA. The MCLUST algorithm estimated three independent clusters within TCGA HCCs designated HCC_1, HCC_2, and HCC_Wnt. Individual hepatic lesions are represented by letters or symbols. (B) Simultaneous deregulation of *AXIN2*, *EPHB2* and *GS* in the HCC_Wnt class. Median of expression levels for individual categories is indicated by black line. The presence of viral infection is indicated by graphical symbols. Statistical data accompanying this figure are given in Supplementary Table S9. *P < 0.05, **P < 0.01, and ***P < 0.001.

Supplementary Figure S4. Transcriptional upregulation of *AXIN2*, *EPHB2* and *GS* is mainly restricted to lesions driven by mutations in the *CTNNB1*, *AXIN1/2* and *APC* genes

(A) Mutations in genes encoding four essential components of the Wnt pathway *APC*, *AXIN1*, *AXIN2*, and *CTNNB1* were evaluated to achieve subdivision of HCCs to three groups. The diagram represents PCA from Supplementary Fig. S3; however, letters (a-n) represent HCCs with particular combinations of sequence variants found in *APC*, *AXIN1*, *AXIN2*, and *CTNNB1*. Group Wnt_WT: specimens do not carry any genomic alterations in the indicated genes (red letter "c"); group Wnt_MUT (blue letters): the group encompasses tentative oncogenic variants (TOVs) in *APC* (a), or likely oncogenic mutations (LOMs) in exon 3 of the *CTNNB1* gene that were found either alone (i) or in combination with TOV (f) or with synonymous single-nucleotide polymorphisms (sSNPs) in *AXIN2* (m); group "Others" (green letters): lesions carrying gene variants of unknown significance (VUS) in *APC* (b); TOV (d) and VUS (e) in *AXIN1*; TOV (g) and VUS (h) in *AXIN2*; or TOV in *CTNNB1* alone (j) or in combination with sSNP in *APC* (n), and VUS (k) or sSNPs (l) in *CTNNB1*. (B) Relative mRNA levels of the *AXIN2*, *EPHB2* and *GS* in HCCs assigned to the indicated mutation group. Median of expression levels for a given group is depicted by black line. Numerical values accompanying this figure are given in Supplementary Table S10; summary of mutations is given in Supplementary Table S4. *P < 0.05, **P < 0.01, and ***P < 0.001.

Supplementary Figure S5. Hypomethylation of the *NKD1* intron 3 S-shore regions is related to the increased *NKD1* levels in CRC

Correlation between *NKD1* DNA methylation profile and expression in CRC samples. The central panel depicts the *NKD1* methylation status in 366 CRC cases as examined by 26 methylation probes covering the *NKD1* locus. The specimens were arranged according to the extent of methylation plotted as a grey-shaded heatmap of β-values (unmethylated: white; completely methylated: black). Probes are listed horizontally with their identification code (ID) in a successive order according to their target sequence coordinates (the 5´ gene end is shown at the left). A color-based classification of CpG islands and other elements is indicated above the main panel. Rectangles along one horizontal row represent DNA methylation-dependent signals recorded in genomic DNA isolated from one CRC sample. In parallel, differential expression of *NKD1* in the tumor vs. control healthy mucosae was scored in a corresponding vertical bar. The proximal CpG island including adjacent loci (probes cg03214308, cg00503804, cg05238767, cg17804302, cg16208433, cg06812033, cg00083833) or the S-shore in exon 2 (cg16750777) is hypomethylated. Methylation of the *NKD1* intron 3 S-shore region dictates the levels of *NKD1* expression. logFC, base 2 logarithm of fold change of *NKD1* expression in tumor sample vs. normal tissue sample; N, north; S, south.

Supplementary Tables

Supplementary Table S1 List of primers used in the study

Supplementary Table S2 Clinicopathological features of hepatic cancer patients

Supplementary Table S3 Mutation analysis of *CTNNB1* in HCCs

Supplementary Table S4 Mutations detected in the TCGA HCC dataset

Supplementary Table S5 Relative expression levels of *NKD1* in colorectal polyps

Supplementary Table S6 Relative expression levels of *NKD1* in CRCs

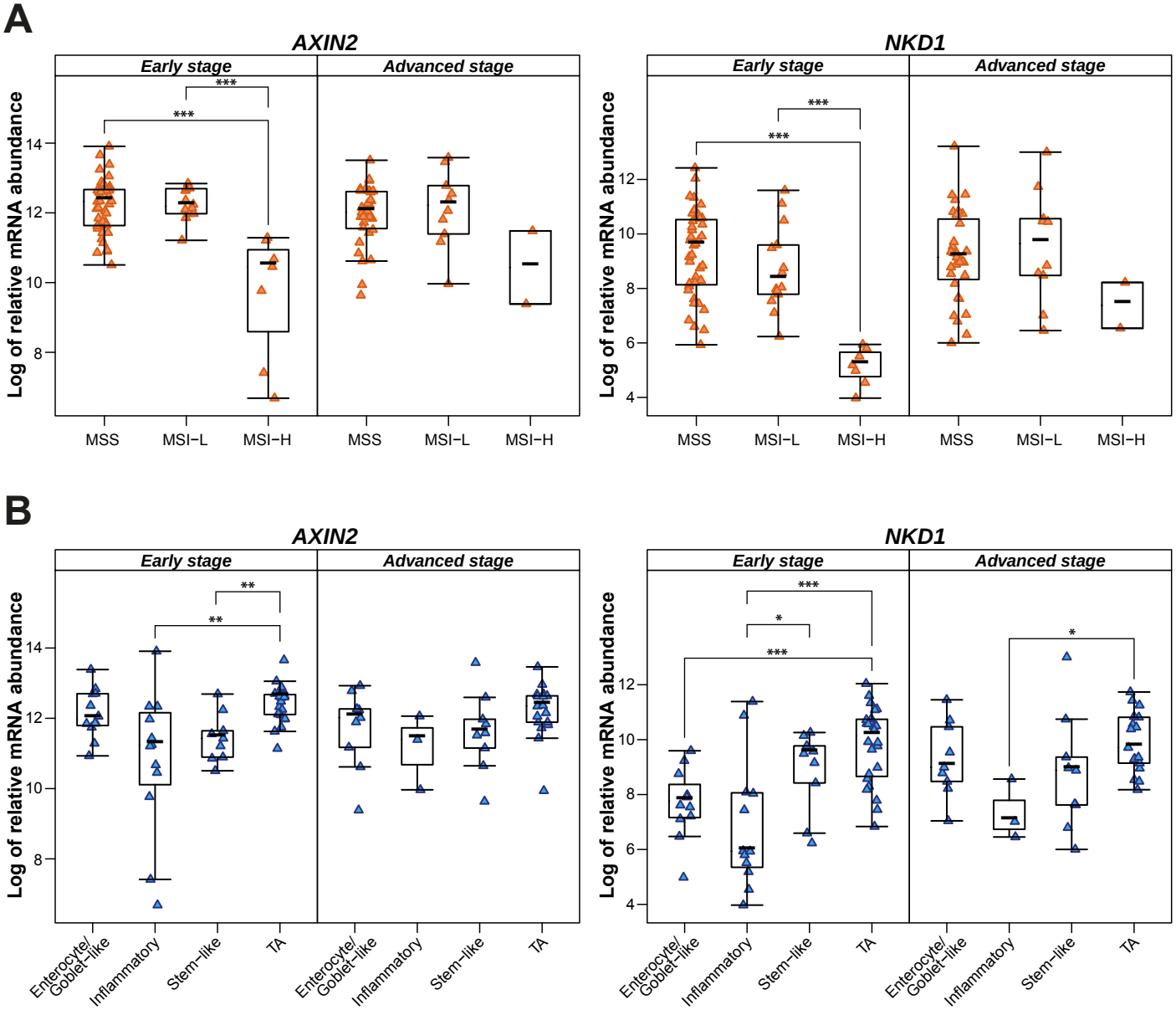
Supplementary Table S7 Gene expression profiles in HCCs

Supplementary Table S8 Expression levels of *AXIN2* and *NKD1* in subclasses of CRCs

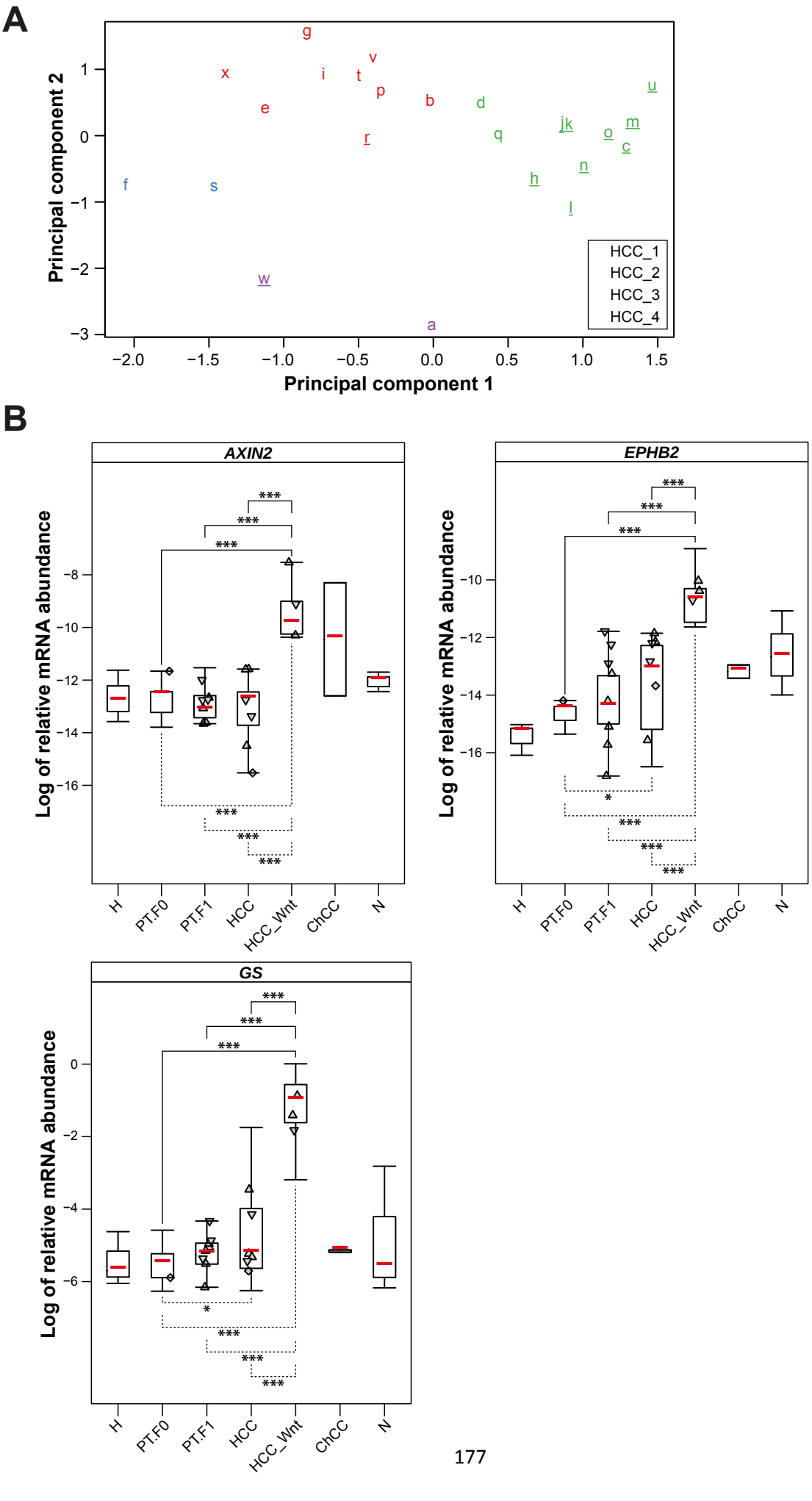
Supplementary Table S9 Gene expression profiles in the TCGA HCC dataset

Supplementary Table S10 Gene expression profiles in three mutational groups of HCC (the TCGA HCC dataset)

Supplementary Figure S1

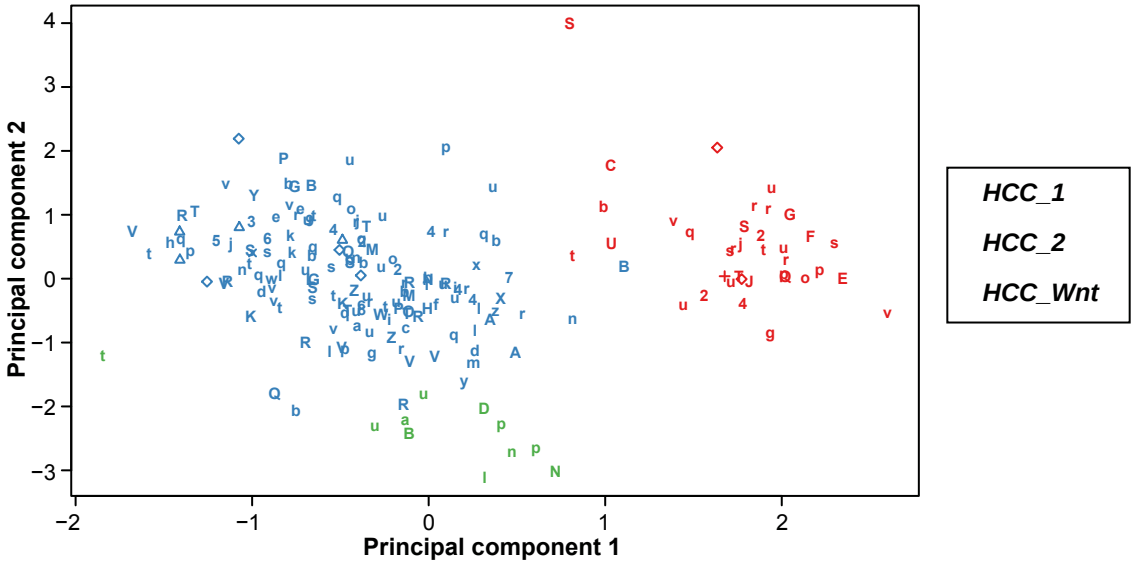


Supplementary Figure S2

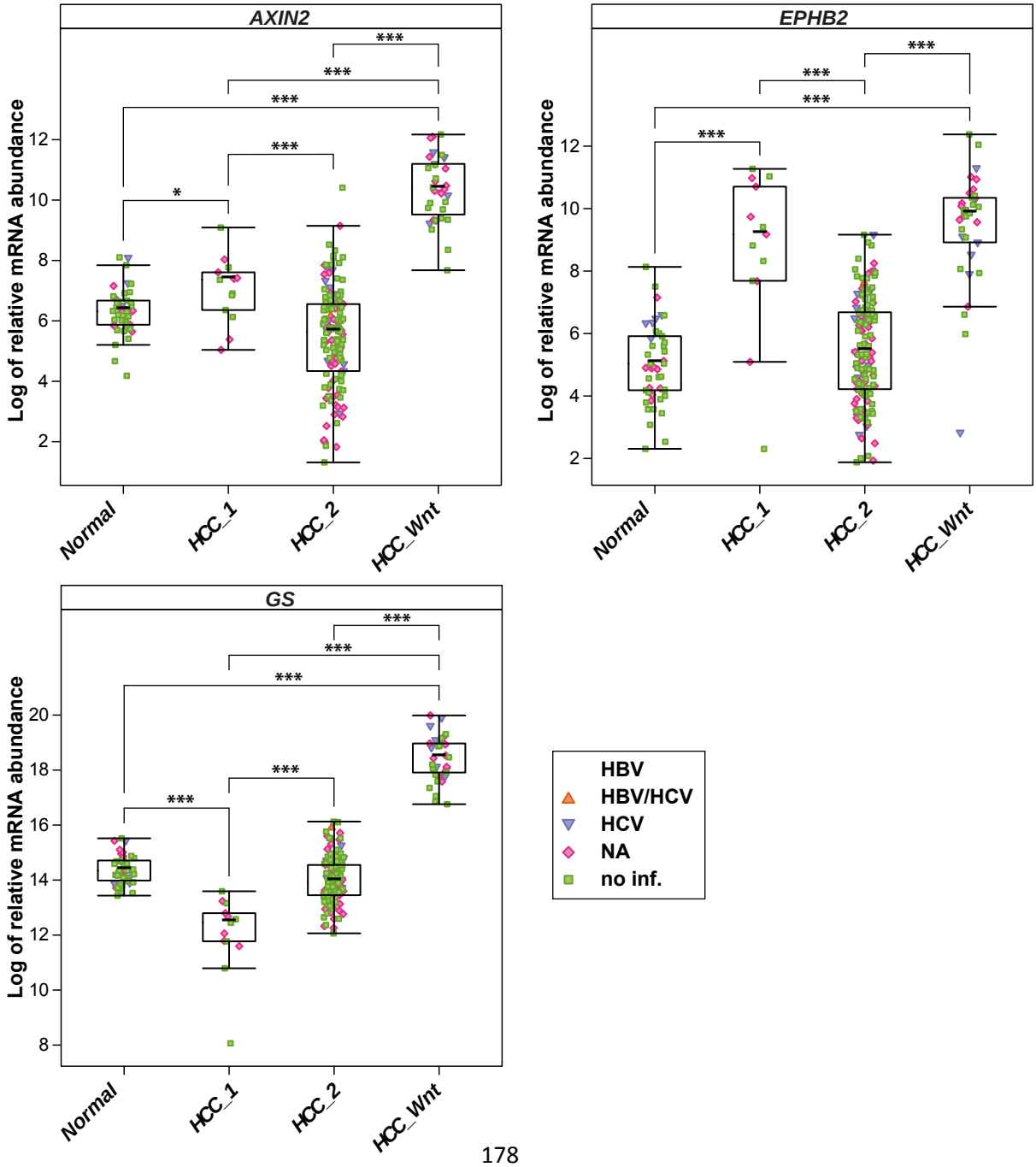


Supplementary Figure S3

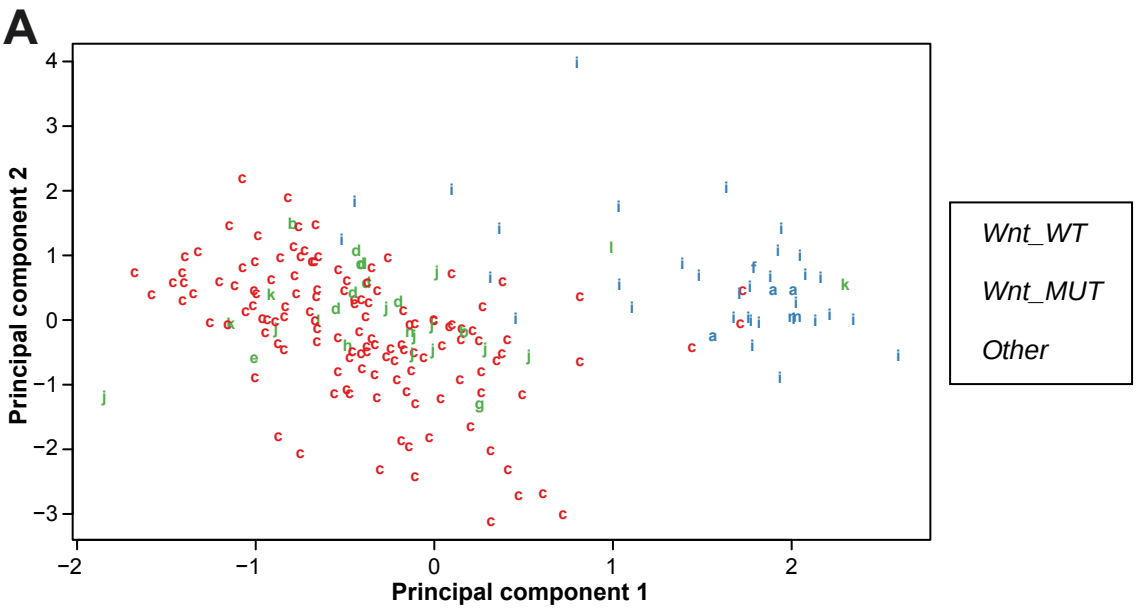
A

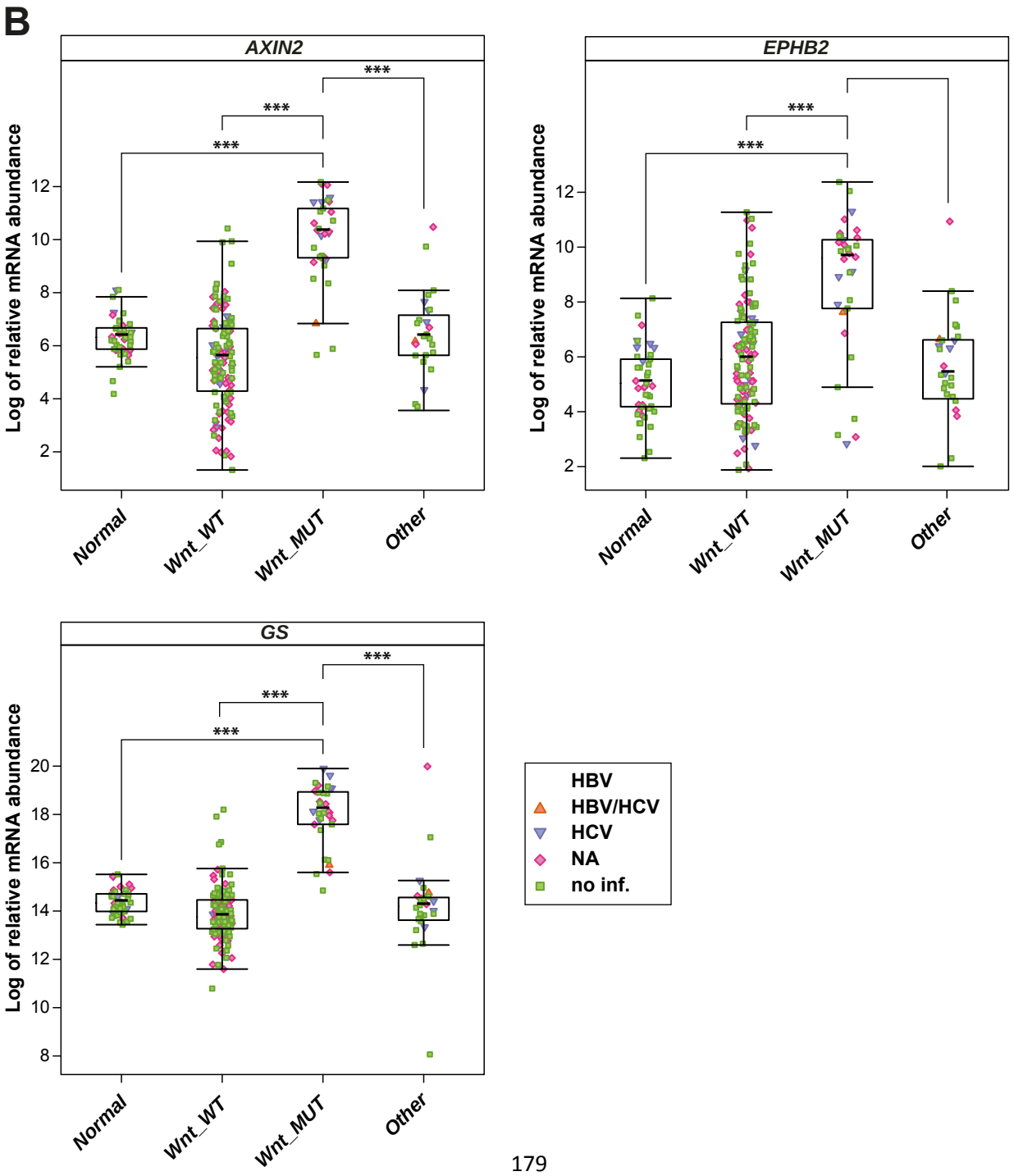


B

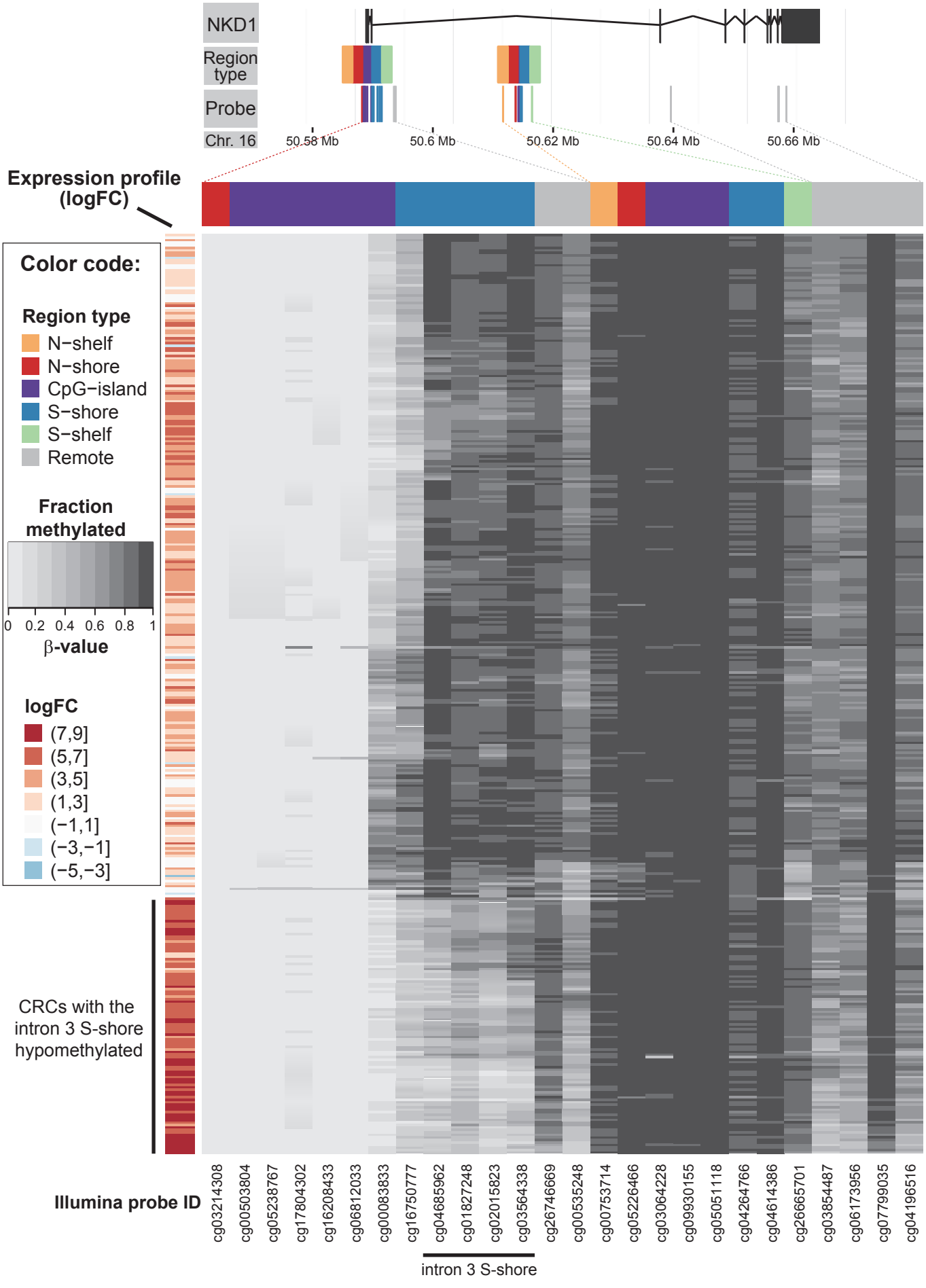


Supplementary Figure S4





Supplementary Figure S5



Supplementary Table S1 List of primers used in the study

Gene	Organism	Sequence (5′ to 3′)	Application
β-Actin (Actb)	Mouse	GATCTGGCACCACACCTTCT GGGGTGTTGAAGGTCTCAAA	qRT-PCR
β-ACTIN (ACTB)	Human	GGCATCCTCACCCTGAAGTA AGGTGTGGTGCCAGATTTTC	qRT-PCR
Apc	Mouse	GCGTGCACAGCGAAGAATAG TCCACACGTGTAGCTGGACT	qRT-PCR
AXIN1	Human	GAAGGTGAGGACGGCGATCCAT AGGCACCTGGCACCTCGGTGC	qRT-PCR
Axin2	Mouse	GGGGGAAAACACAGCTTACA TCTTCATTCAAGGTGGGGAG	qRT-PCR
AXIN2	Human	CTGGCTTTGGTGAACTGTTG AGTTGCTCACAGCCAAGACA	qRT-PCR
Cre	P1 phage	GCACTGATTTCGACCAGGTT GCTAACCAGCGTTTTCGTTC	qRT PCR/genotyping
CTNNB1	Human	ex3T7 taatacgactcactatagTGCTTTTCTTGGCTGTCTTTCAG ex3RP tgaaacagctatgaccatgTCCACAGTTCAGCATTTACCTAAG	sequencing
EGFP	Aequorea victoria	GACGTAAACGGCCACAAGTT GAACTTCAGGGTCAGCTTGC	qRT-PCR
EPHB2	Human	GTTCGCCTCTGTGAACATCA GACCACGACAGGGTAATGCT	qRT-PCR
GS	Mouse	AGCGACATGTACCTCCATCC GCCGTCTGTTCCCATAAGAG	qRT-PCR
GS	Human	GGACAGTGAGCCCAAGTGTG CACCAGCTTGTTAGGGTCCTT	qRT-PCR
Lect2	Mouse	TAGCAGGACCATGGGCTAAC GCCCACTATCTTCCCAGTGA	qRT-PCR
Lgr5	Mouse	CCTGTCCAGGCTTTCAGAAG CTGTGGAGTCCATCAAAGCA	qRT-PCR
LGR5	Human	CTCTTCCTCAAACCGTCTGC GATCGGAGGCTAAGCAACTG	qRT-PCR
MMP7	Human	AAAGAGATCCCCCTGCATTT AGACTGCTACCATCCGTCCA	qRT-PCR
Nkd1	Mouse	AGGACGACTTCCCCCTAGAA TGCAGCAAGCTGGTAATGTC	qRT-PCR
Nkd1 locus	Mouse	ACTTCACTCGAAGCCGGGTC AGGGAGGAGGCAATATACCC	genotyping
NKD1	Human	CGCCGGGATAGAAAACTACA CTGGAGCTCTGAGACCTTGG	qRT-PCR
NKD2	Human	AGACCCTCCGTGTGAAGCTA TGTTCTCGTCCACGCAGTAG	qRT-PCR
Oat	Mouse	ATGTAAGCTCGCTCGTCGTT GAAGGCAGCAACATTTGGAT	qRT-PCR
Olfm4	Mouse	TGGGCAGAAGGTGGGACTGTGT TGTCAGCGGGAAAGGCGGTA	qRT-PCR
Pck1	Mouse	GACAACTGTTGGCTGGCTCT CACATAGGGCGAGTCTGTCA	qRT-PCR
PLAU	Human	TACTGCAGGAACCCAGACAA TCCTGTAGATGGCCGCAAAC	qRT-PCR
RUNX2	Human	TCTGGCCTTCCACTCTCAGT GACTGGCGGGGTGTAAGTAA	qRT-PCR
SALL1	Human	GCAATCTTAAGGTACACATGGGC TGACGGGATTGCCTCCTAGA	qRT-PCR
Troy	Mouse	GCTCAGGATGCTCAAAGGAC CCAGACACCAAGACTGCTCA	qRT-PCR
TROY	Human	CTATGGGGAGGATGCACAGT TCTCCACAAGGCACACACTC	qRT-PCR
Ubb	Mouse	ATGTGAAGGCCAAGATCCAG TAATAGCCACCCCTCAGACG	qRT-PCR
UBB	Human	GCTTTGTTGGGTGAGCTTGT TCACGAAGATCTGCATTTTGA	qRT-PCR

Supplementary Table S2

Clinicopathological features of hepatic cancer patients (*n=28*)	
	Total N (%)
No. of patients	28
Primary tumor recurrence	1 (4)
Total no. of tumors included in the study	29
Gender	
Male/Female	21/7
Age, Years	
median	63
range	25-81
≥ 65 years	14 (50)
Aethiology of underlying disease	
viral (HCV-HBV)	7 (25)
exotoxic (alcohol abuse)	5 (18)
cryptogenic/unknown	16 (58)
Diagnosis	
Hepatocellula carcinoma (HCC)	24 (83)
Cholangiocellular carcinoma (ChCC)	2 (7)
Other diagnosis	3 (10)
adenolipoma	*1 (33)*
focal nodular hyperplasia	*1 (33)*
colorectal carcinoma metastasis	*1 (33)*
TNM stage	
0-II	23 (79)
III-IV	6 (21)
Histological differentiation level	
G1	2 (7)
G2-4	24 (83)
other category	3 (10)
Fibrosis score	
healthy	3 (10)
F0 (mild to moderate fibrosis)	10 (35)
F1 (severe fibrosis to cirrhosis)	16 (55)

Supplementary Table S3 Mutation analysis of *CTNNB1* in HCCs

Patient No.	Assigned letter in Suppl. Fig. S2	Mutation in DNA	Change in beta-catenin protein	Mutation type	COSMIC database linkout	Class	HCV serology	HBsAg
3	l	c.122C>T	p.Thr41Ile	Substitution - Missense	COSM5676	HCC_Wnt	neg	neg
8	w	c.110C>T	p.Ser37Phe	Substitution - Missense	COSM5662	HCC	n.d.*	n.d.*
12	c	c.104T>G	p.Ile35Ser	Substitution - Missense	COSM5674	HCC_Wnt	neg	neg
25	h	c.107A>C	p.His36Pro	Substitution - Missense	COSM5678	HCC_Wnt	neg	neg
27	j	c.121A>G	p.Thr41Ala	Substitution - Missense	COSM13153	HCC_Wnt	poz	neg
29	k	c.101G>A	p.Gly34Glu	Substitution - Missense	COSM5671	HCC_Wnt	n.d.*	n.d.*
30	m	c.109T>G	p.Ser37Ala	Substitution - Missense	COSM5675	HCC_Wnt	neg	poz
31	n	c.122C>T	p.Thr41Ile	Substitution - Missense	COSM5676	HCC_Wnt	n.d.*	n.d.*
32	o	c.97T>C	p.Ser33Pro	Substitution - Missense	COSM5682	HCC_Wnt	n.d.	n.d.
37	r	c.101G>A	p.Gly34Glu	Substitution - Missense	COSM5671	HCC	neg	neg
40	u	c.121A>G	p.Thr41Ala	Substitution - Missense	COSM13153	HCC_Wnt	neg	neg

*) histological detection negative

Supplementary Table S4 **Mutations detected in the TCGA HCC dataset**

	No. of HCC specimen assigned to the HCC expression class			Assignment to the mutation groups			
Mutation status ***APC*** **/** ***AXIN1*** **/** ***AXIN2*** **/** ***CTNNB1***	**HCC_1**	**HCC_2**	**HCC_WNT**	**Mutational group**	**Letter assigned in Supplementary Fig. S4**	**Color code assigned in Supplementary Fig. S4**	**No. of HCC specimen assigned to the mutation group**
WT / WT / WT / WT	11	116	4	Wnt_WT	c	red	131
TOV / WT / WT / WT	0	0	3	Wnt_MUT	a	blue	3
WT / sSNP / WT / LOM	0	0	1	Wnt_MUT	m		1
WT / WT / TOV / LOM	0	0	1	Wnt_MUT	f		1
WT / WT / WT / LOM	0	7	27	Wnt_MUT	i		33
VUS / WT / WT / WT	0	2	0	Other	b	green	2
WT / TOV / WT / WT	0	7	0	Other	d		7
WT / VUS / WT / WT	0	1	0	Other	e		1
WT / WT / TOV / WT	0	1	0	Other	g		1
WT / WT / VUS / WT	0	1	0	Other	h		1
WT / WT / WT / TOV	1	9	0	Other	j		10
WT / WT / WT / VUS	0	2	1	Other	k		3
WT / WT / WT / sSNP	0	1	0	Other	l		2
sSNP / WT / WT / TOV	0	1	0	Other	n		1
total	12	148	37				

Explanatory notes:

WT, wild-type

TOV, tentative oncogenic variant

sSNP, synonymous single-nucleotide polymorphisms

LOM, likely oncogenic mutation

VUS, gene variants of unknown significance

Supplementary Table S5 Relative expression levels of *NKD1* in colorectal polyps

Linear model *ΔCp ~ patient + tissue_stage*					Wilcoxon´s rank-sum test	
Precancerous lesions of the colon						
Gene	**ΔΔCp**	**FC**	**mean ΔCp**	**p value**	**Gene**	**p value**
Polyp hyperplasia vs. healthy surrounding mucosa						
NKD1	0.26	0.83	7.06	0.56	*NKD1*	0.026
Polyp low grade dysplasia vs. healthy surrounding mucosa						
NKD1	-4.85	28.90	7.06	< 0.0001	*NKD1*	< 0.0001
Polyp high grade dysplasia vs. healthy surrounding mucosa						
NKD1	-5.58	47.98	7.06	0	*NKD1*	< 0.0001
Polyp low grade dysplasia vs. polyp hyperplasia						
NKD1	-5.12	34.66	7.06	< 0.0001	*NKD1*	< 0.0001
Polyp high grade dysplasia vs. polyp hyperplasia						
NKD1	-5.85	57.55	7.06	< 0.0001	*NKD1*	< 0.0001
Polyp high grade dysplasia vs. polyp low grade dysplasia						
NKD1	-0.73	1.66	7.06	0.094	*NKD1*	0.20
Healthy mucosa low grade dysplasia vs. healthy mucosa hyperplasia						
NKD1	N/A				*NKD1*	0.0059
Healthy mucosa high grade dysplasia vs. healthy mucosa hyperplasia						
NKD1	N/A				*NKD1*	0.0046

Supplementary Table S6 Relative expression levels of *NKD1* in CRCs

Linear model *ΔCp ~ patient + tissue / (stage * mutation)*						**Wilcoxon´s rank-sum test**	
Early stage cancer						***Early stage cancer***	
Gene	**ΔΔCp**	**FC**	**mean ΔCp**	**p value**		**Gene**	**p value**
APC wt tumor vs. healthy surrounding mucosa							
NKD1	-2.5	5.67	9.96	0.0044		*NKD1*	0.093
APC mut tumor vs. healthy surrounding mucosa							
NKD1	-3.92	15.09	9.96	< 0.0001		*NKD1*	0.0022
APC mut tumor vs. APC wt tumor							
NKD1	-1.41	2.66	9.96	0.22		*NKD1*	0.24
Advanced stage cancer						***Advanced stage cancer***	
Gene	**ΔΔCp**	**FC**	**mean ΔCp**	**p value**		**Gene**	**p value**
APC wt tumor vs. healthy surrounding mucosa							
NKD1	-4.21	18.5	9.96	0.00068		*NKD1*	0.029
APC mut tumor vs. healthy surrounding mucosa							
NKD1	-4.27	19.31	9.96	0.0009		*NKD1*	0.1
APC mut tumor vs. APC wt tumor							
NKD1	-0.06	1.04	9.96	0.97		*NKD1*	0.86

Supplementary Table S7 Gene expression profiles in HCCs

Linear model *ΔCp ~ patient + tissue_fibrosis score*					Wilcoxon´s rank-sum test	
Hepatocellular carcinomas						
Gene	**ΔΔCp**	**FC**	**mean ΔCp**	**p value**	**Gene**	**p value**
Hepatocellular carcinoma vs. precancerous tissue F0						
GS	-0.93	1.90	4.29	0.022	*GS*	0.14
EPHB2	-1.18	2.27	13.34	0.028	*EPHB2*	0.096
NKD2	1.15	0.45	20.37	0.16	*NKD2*	0.26
NKD1	-0.92	1.89	13.68	0.17	*NKD1*	0.209
LGR5	0.95	0.52	14.33	0.36	*LGR5*	0.85
TROY	-0.27	1.20	13.58	0.7	*TROY*	0.70
AXIN2	0.02	0.98	11.98	0.96	*AXIN2*	0.79
Hepatocellular carcinoma Wnt class vs. precancerous tissue F0						
GS	-4.35	20.43	4.29	< 0.0001	*GS*	< 0.0001
NKD1	-5.72	52.53	13.68	< 0.0001	*NKD1*	< 0.0001
EPHB2	-4.08	16.86	13.34	< 0.0001	*EPHB2*	< 0.0001
AXIN2	-3.36	10.24	11.98	< 0.0001	*AXIN2*	< 0.0001
TROY	-4.18	18.18	13.58	< 0.0001	*TROY*	0.00054
LGR5	-5.23	37.62	14.33	< 0.0001	*LGR5*	< 0.0001
NKD2	2.19	0.22	20.37	0.011	*NKD2*	0.0012
Hepatocellular carcinoma vs. precancerous tissue F1						
NKD2	1.35	0.39	20.37	0.048	*NKD2*	0.37
GS	-0.67	1.59	4.29	0.051	*GS*	0.398
EPHB2	-0.77	1.71	13.34	0.076	*EPHB2*	0.308
LGR5	1.13	0.46	14.33	0.19	*LGR5*	0.62
TROY	0.58	0.67	13.58	0.35	*TROY*	0.48
NKD1	-0.22	1.16	13.38	0.69	*NKD1*	0.78
AXIN2	-0.14	1.10	11.98	0.73	*AXIN2*	0.91
Hepatocellular carcinoma Wnt class vs. precancerous tissue F1						
GS	-4.10	17.14	4.29	< 0.0001	*GS*	< 0.0001
NKD1	-5.02	32.36	13.68	< 0.0001	*NKD1*	< 0.0001
EPHB2	-3.67	12.71	13.34	< 0.0001	*EPHB2*	< 0.0001
AXIN2	-3.52	11.50	11.98	< 0.0001	*AXIN2*	< 0.0001
LGR5	-5.05	33.19	14.33	< 0.0001	*LGR5*	< 0.0001
TROY	-3.34	10.13	13.58	< 0.0001	*TROY*	0.00023
NKD2	2.39	0.19	20.37	0.0019	*NKD2*	0.0018
Hepatocellular carcinoma Wnt class vs. hepatocellular carcinoma						
GS	-3.43	10.75	4.29	< 0.0001	*GS*	< 0.0001
NKD1	-4.80	27.79	13.68	< 0.0001	*NKD1*	< 0.0001
AXIN2	-3.38	10.42	11.98	< 0.0001	*AXIN2*	< 0.0001
LGR5	-6.18	72.74	14.33	< 0.0001	*LGR5*	0.00053
EPHB2	-2.89	7.44	13.34	< 0.0001	*EPHB2*	< 0.0001
TROY	-3.92	15.10	13.58	< 0.0001	*TROY*	0.00022
NKD2	1.04	0.48	20.37	0.19	*NKD2*	0.15

Supplementary Table S8

Expression levels of *AXIN2* and *NKD1* in subclasses of CRCs

MSI status
Wilcoxon´s rank-sum test

TCGA Colon carcinomas					
Early stage cancer			***Advanced stage cancer***		
Gene	**p value**	**log FC**	**Gene**	**p value**	**log FC**
MSI-L vs. MSS			***MSI-L vs. MSS***		
AXIN2	0.82	-0.14	*AXIN2*	0.601	0.20
NKD1	0.25	-1.27	*NKD1*	0.8	0.503
MSI-H vs. MSS			***MSI-H vs. MSS***		
AXIN2	< 0.0001	-1.87	*AXIN2*	0.076	-1.58
NKD1	< 0.0001	-4.39	*NKD1*	0.14	-1.76
MSI-H vs. MSI-L			***MSI-H vs. MSI-L***		
AXIN2	< 0.0001	-1.73	*AXIN2*	0.18	-1.78
NKD1	< 0.0001	-3.12	*NKD1*	0.18	-2.27

CRC assigner
Wilcoxon´s rank-sum test

TCGA Colon carcinomas					
Early stage cancer			***Advanced stage cancer***		
Gene	**p value**	**log FC**	**Gene**	**p value**	**log FC**
Inflammatory vs. Enterocyte/Goblet-like			***Inflammatory vs. Enterocyte/Goblet-like***		
AXIN2	0.039	-0.73	*AXIN2*	0.48	-0.62
NKD1	0.242	-1.82	*NKD1*	0.064	-1.98
Stem-like vs. Enterocyte/Goblet-like			***Stem-like vs. Enterocyte/Goblet-like***		
AXIN2	0.023	-0.53	*AXIN2*	0.61	-0.43
NKD1	0.069	1.73	*NKD1*	0.49	-0.11
TA vs. Enterocyte/Goblet-like			***TA vs. Enterocyte/Goblet-like***		
AXIN2	0.24	0.64	*AXIN2*	0.40	0.33
NKD1	0.00017	2.38	*NKD1*	0.29	0.72
Stem-like vs. Inflammatory			***Stem-like vs. Inflammatory***		
AXIN2	0.55	0.2	*AXIN2*	0.73	0.19
NKD1	0.034	3.55	*NKD1*	0.28	1.86
TA vs. Inflammatory			***TA vs. Inflammatory***		
AXIN2	0.0011	1.37	*AXIN2*	0.093	0.95
NKD1	0.00081	4.2	*NKD1*	0.012	2.69
TA vs. Stem-like			***TA vs. Stem-like***		
AXIN2	0.0011	1.17	*AXIN2*	0.075	0.76
NKD1	0.072	0.65	*NKD1*	0.085	0.83

Supplementary Table S9

Gene expression profiles in the TCGA HCC dataset

Wilcoxon´s rank-sum test		
TCGA Hepatocellular carcinomas		
Gene	**p value**	**log FC**
HCC_1 vs. non-tumor liver		
AXIN1	0.00013	0.64
AXIN2	0.018	1.04
EPHB2	< 0.0001	4.14
GS	< 0.0001	-1.89
LGR5	0.0042	-3.04
NKD1	0.95	0.25
NKD2	0.60	1.21
TROY	0.0055	2.58
HCC_2 vs. non-tumor liver		
AXIN1	< 0.0001	0.56
AXIN2	< 0.0001	-0.69
EPHB2	0.092	0.37
GS	0.00086	-0.407
LGR5	< 0.0001	-3.01
NKD1	0.010	-0.601
NKD2	0.13	-0.42
TROY	0.0024	-0.706
HCC_Wnt vs. non-tumor liver		
AXIN1	0.046	0.18
AXIN2	< 0.0001	4.04
EPHB2	< 0.0001	4.77
GS	< 0.0001	4.11
LGR5	< 0.0001	4.65
NKD1	< 0.0001	5.58
NKD2	0.0057	-1.19
TROY	< 0.0001	4.3
HCC_2 vs. HCC_1		
AXIN1	0.46	-0.074
AXIN2	0.00045	-1.73
EPHB2	< 0.0001	-3.77
GS	< 0.0001	1.48
LGR5	0.93	0.0302
NKD1	0.37	-0.85
NKD2	0.38	-1.62
TROY	0.00060	-3.28
HCC_Wnt vs. HCC_1		
AXIN1	0.011	-0.46
AXIN2	< 0.0001	3
EPHB2	0.41	0.63
GS	< 0.0001	6
LGR5	< 0.0001	7.69
NKD1	< 0.0001	5.63
NKD2	0.19	-2.4
TROY	0.00921	1.72
HCC_Wnt vs. HCC_2		
AXIN1	0.0056	-0.39
AXIN2	< 0.0001	4.72
EPHB2	< 0.0001	4.41
GS	< 0.0001	4.52
LGR5	< 0.0001	7.66
NKD1	< 0.0001	6.48
NKD2	0.14	-0.77
TROY	< 0.0001	5.01

Supplementary Table S10

Gene expression profiles in three mutational groups of HCC (TCGA HCC dataset)

Wilcoxon´s rank-sum test		
TCGA Hepatocellular carcinomas		
Gene	**p value**	**log FC**
Wnt_WT vs. non-tumor liver		
AXIN1	< 0.0001	0.61
AXIN2	0.00033	-0.77
EPHB2	0.012	0.87
GS	< 0.0001	-0.58
LGR5	< 0.0001	-3.3
NKD1	0.018	-0.55
NKD2	0.25	-0.40
TROY	0.056	-0.503
Wnt_MUT vs. non-tumor liver		
AXIN1	0.03	0.14
AXIN2	< 0.0001	3.96
EPHB2	< 0.0001	4.56
GS	< 0.0001	3.83
LGR5	< 0.0001	4.5
NKD1	< 0.0001	5.67
NKD2	0.00028	-1.29
TROY	< 0.0001	4.09
Other vs. non-tumor liver		
AXIN1	0.095	0.403
AXIN2	0.94	-0.0075
EPHB2	0.11	0.34
GS	0.16	-0.15
LGR5	0.050	-1.32
NKD1	0.23	-0.56
NKD2	0.27	-0.15
TROY	0.21	-0.64
Wnt_MUT vs. Wnt_WT		
AXIN1	0.007	-0.47
AXIN2	< 0.0001	4.73
EPHB2	< 0.0001	3.69
GS	< 0.0001	4.41
LGR5	< 0.0001	7.8
NKD1	< 0.0001	6.23
NKD2	0.029	-0.89
TROY	< 0.0001	4.59
Other vs. Wnt_WT		
AXIN1	0.1	-0.202
AXIN2	0.012	0.76
EPHB2	0.62	-0.54
GS	0.15	0.43
LGR5	0.063	1.98
NKD1	0.52	-0.0071
NKD2	0.69	0.24
TROY	0.905	-0.14
Other vs. Wnt_MUT		
AXIN1	0.903	0.27
AXIN2	< 0.0001	-3.97
EPHB2	< 0.0001	-4.23
GS	< 0.0001	-3.98
LGR5	< 0.0001	-5.83
NKD1	< 0.0001	-6.23
NKD2	0.15	1.13
TROY	< 0.0001	-4.73

HIC1 tumor suppressor loss potentiates TLR2/NF-kappaB signaling and promotes tissue damage-associated tumorigenesis

In intestine, epithelial SCs divide and differentiate into various types of cells performing the proper function of the digestive system. The differentiation is a result of cooperative or antagonistic effects of multiple signaling pathways. Notch signaling employs Hes to support production of Ascl2, which subsequently has a suppressive effect on *Atoh1*. Atoh1 directs the daughter cells of intestinal progenitors to the secretory lineage (Kim and Shivdasani 2011a; Ueo et al. 2012). The *Atoh* gene contains specific regulatory elements in its promoter sequence called Hic1 responsive elements (HiREs) targeting the gene to Hic1-mediated transcriptional regulation.

The *Hic1* gene codes for transcriptional repressor regulating various target genes acting in cell cycle regulation (e.g. *Cyclin D1*) (Van Rechem et al.), cell differentiation (*Atoh1, Sox9*) (VanDussen and Samuelson 2010; Mohammad et al. 2011), DNA damage response [*sirtulin 1* (*Sirt1*)] (Dehennaut et al. 2013b) and metastatic invasion (*Cxcr7*) (Van Rechem et al. 2009). Apart from direct repression of target genes containing HiRE, Hic1 can also impair gene expression indirectly by sequestrating Tcf4 and β-catenin to so called Hic1 bodies, thus blocking the Wnt signaling pathway (Valenta et al. 2006). Human *HIC1* is a tumor suppressor gene located on the short arm of chromosome 17, distal to the *TP53* gene, i. e. the region frequently methylated or deleted in various types of cancers such as CRC (Pehlivan et al. 2010), prostate cancer (Kilinc et al. 2012), endometrial cancer (Hedberg Oldfors et al. 2015) or other types of malignancies (Fleuriel et al. 2009). In our recent work, we focused on search for novel target genes repressed by Hic1 and their impact on colorectal tumor growth.

Deletion of *Hic1* provokes lethal defects in mouse embryo (Carter et al. 2000). Heterozygous mice are, in contrast, viable, although they develop neoplasia of various tissues, as the wt allele becomes silenced by methylation during the life (Chen et al. 2003). By conditional *Hic1* deletion in MEFs and subsequent expression profiling, we identified six genes potentially suppressed by Hic1. Among them, *TLR2* was confirmed as the HIC1 target gene in human HEK293 and BJ cells. *Tlr2* has never been described as the Hic1 target before. Tlr2 is a representative of pathogen recognizing receptors which, among other functions, activate the NF-κB pathway resulting in increased production of proinflammatory cytokines as well as MAP kinases p35- and JNK-dependent signaling

through myeloid differentiation primary response 88 (MyD88) molecules (Schnare et al. 2001). It has been shown, that Myd88 signaling is indispensable for development of the adaptive immunity (Medzhitov et al. 1998), because it can identify commensal microbiota in the intestine (Rakoff-Nahoum et al. 2004; Menendez et al. 2013). We therefore focused on the NF-κB pathway and its target genes. Strikingly, we observed activation of NF-κB signaling and, moreover, *Tlr2* upregulation as a consequence of *Hic1* ablation in MEFs.

In the intestinal epithelium, Hic1 expression is mostly present in the villus compartment rather than in the crypts. We used mice enabling conditional *Hic1* inactivation in the intestinal epithelium for evaluation of the results obtained *in vitro*. Importantly, upon *Hic1* loss, we detected increased amounts of Tlr2 in the intestine. We also noted upregulation of putative Hic1 target genes as well as NF-κB target genes upon *Hic1* ablation in intestinal organoid cultures. Additionally, we focused on the possible effect of Hic1 on the expression of genes driving the secretory lineages in epithelium. As in cerebellum and osteosarcoma cells, Hic1 repressed *Atoh1* and *Sox9* expression (Briggs et al. 2008; Van Rechem et al. 2009). Atoh1 acts as a main regulator of cell secretory fate and Sox9 is essential for Paneth cell maturity (Gerbe et al. 2011; Kim and Shivdasani 2011a). Our study confirmed such results, and we observed increased number of Paneth cells, goblet cells and chromogranin A positive enteroendocrine cells in Hic1-deficient intestinal epithelium.

The activated NF-κB pathway contributes to intestinal inflammation due to upregulated Tlr2 expression (Hausmann et al. 2002), moreover, direct link between NF-κB signaling and IBD development was established (Frolova et al. 2008). To induce inflammatory conditions, we treated mice with conditionally deleted *Hic1* by DSS. In the regenerative phase after the treatment, we noted more robust hyperproliferative response in mice with compromised *Hic1* than in their wt littermates. Furthermore, it was shown that colon cancer cells exhibit the upregulated NF-κB pathway (Maeda et al. 2011). We treated mice with chemical carcinogen azoxymethane and, subsequently, induced inflammation by DSS. Interestingly, mice with compromised *Hic1* developed larger colorectal tumors when compared to wt animals. In addition, we observed decreased levels of p53 and p21 proteins in the *Hic1*-deficient tumors. Additionally, only a small fraction of cells in chemically induced tumors displayed stabilized p53. This result is in agreement with the notion, that Hic1 suppresses expression of *Sirt1*, blocking the production of p53 (Chen et al. 2005). In contrast, Hic1 directly represses transcription of the p21-encoding gene,

CDKN1A (Dehennaut et al. 2013a). In study of Kumar, p53, p21 and p27 are increased in HIC1 KO glioma cells (Kumar 2014). It seems that in colorectal tumors pro-tumor growth influencing mechanisms induced by activated Tlr2/NF-κB signaling outbalances the p53 tumor suppressive effect.

In conclusion, we identified *Tlr2* as the Hic1-suppressed target gene with high impact on inflammation, particularly in the intestinal epithelium. *Hic1* deletion is a frequently observed concomitant mutation in many types of tumors in humans. Our mice model harboring such mutation, suffers from augmented colorectal tumor growth. Outcomes from our publication may contribute to the research field of CRC-related molecular pathways.

Author´s contribution: MEFs isolation and cultivation

Published OnlineFirst May 1, 2015; DOI: 10.1158/1541-7786.MCR-15-0033

Oncogenes and Tumor Suppressors

Molecular Cancer Research

HIC1 Tumor Suppressor Loss Potentiates TLR2/NF-κB Signaling and Promotes Tissue Damage–Associated Tumorigenesis

Lucie Janeckova[1], Vendula Pospichalova[1], Bohumil Fafilek[1], Martina Vojtechova[1], Jolana Tureckova[1], Jan Dobes[1], Marion Dubuissez[2], Dominique Leprince[2], Nikol Baloghova[1], Monika Horazna[1], Adela Hlavata[1], Jitka Stancikova[1], Eva Sloncova[1], Katerina Galuskova[1], Hynek Strnad[1], and Vladimir Korinek[1]

Abstract

Hypermethylated in cancer 1 (*HIC1*) represents a prototypic tumor suppressor gene frequently inactivated by DNA methylation in many types of solid tumors. The gene encodes a sequence-specific transcriptional repressor controlling expression of several genes involved in cell cycle or stress control. In this study, a *Hic1* allele was conditionally deleted, using a Cre/loxP system, to identify genes influenced by the loss of Hic1. One of the transcripts upregulated upon Hic1 ablation is the *toll-like receptor 2* (*TLR2*). *Tlr2* expression levels increased in Hic1-deficient mouse embryonic fibroblasts (MEF) and cultured intestinal organoids or in human cells upon *HIC1* knockdown. In addition, HIC1 associated with the *TLR2* gene regulatory elements, as detected by chromatin immunoprecipitation, indicating that *Tlr2* indeed represents a direct Hic1 target. The Tlr2 receptor senses "danger" signals of microbial or endogenous origin to trigger multiple signaling pathways, including NF-κB signaling. Interestingly, Hic1 deficiency promoted NF-κB pathway activity not only in cells stimulated with Tlr2 ligand, but also in cells treated with NF-κB activators that stimulate different surface receptors. In the intestine, Hic1 is mainly expressed in differentiated epithelial cells and its ablation leads to increased Tlr2 production. Finally, in a chemical-induced mouse model of carcinogenesis, Hic1 absence resulted in larger Tlr2-positive colonic tumors that showed increased proportion of proliferating cells.

Implications: The tumor-suppressive function of Hic1 in colon is related to its inhibitory action on proproliferative signaling mediated by the Tlr2 receptor present on tumor cells. *Mol Cancer Res; 13(7); 1139–48. ©2015 AACR.*

Introduction

The *HIC1* gene was isolated as a candidate tumor suppressor gene during tumor DNA hypermethylation screen of the chromosome 17 short arm, a chromosomal region which is frequently reduced to homozygosity in human cancers (1). *Hic1*$^{-/-}$ mice die prenatally due to severe developmental defects of craniofacial structures and limbs (2). *Hic1*$^{+/-}$ mice are viable; however, they develop spontaneous malignant tumors that are Hic1 deficient due to the intact *Hic1* allele methylation (3). Hic1 protein functions as an evolutionarily conserved transcription repressor, which cooperates with several partners to regulate expression of multiple target genes (4). The protein is composed of three structural domains. The Broad complex, Tramtrack, Bric à brac/POx viruses, and Zinc finger (BTB/POZ) domain responsible for Hic1 multimerization is situated N-terminally, followed by the central region binding co-repressors such as C-terminal binding protein (CtBP). The C-terminal domain consists of five zinc fingers providing affinity to the specific Hic1-responsive (HiRE) sequence motif in DNA (5). The known Hic1 target genes participate in diverse cellular processes, including cell-cycle regulation, cell differentiation, DNA damage response, and metastatic invasion (reviewed in ref. 4). *Hic1* transcription is positively regulated by p53 protein, a key molecule inducing either cell-cycle arrest or apoptosis upon various cellular stress-inducing insults (6). Conversely, the p53 activity is restrained by a protein deacetylase encoded by the *sirtuin 1* (*Sirt1*) gene, whose expression is blocked by Hic1. *Hic1* inactivation thus leads to functional suppression of p53, allowing damaged cells to escape the p53-mediated response (7). Besides the direct regulation of gene expression, Hic1 attenuates transcription via interaction with other transcription factors. For example, association with Wnt pathway effector T-cell factor 4 (TCF4) sequesters TCF4 (and its transcriptional activator β-catenin) to nuclear speckles called Hic1 bodies. Subsequently, expression of the TCF4/β-catenin-responsive genes is inhibited (8).

The tissue maintenance of the single-layer intestinal epithelium is sustained by intestinal stem cells (ISC) that reside at the bottom

[1]Institute of Molecular Genetics, Academy of Sciences of the Czech Republic, Prague, Czech Republic. [2]CNRS UMR 8161, Institut de Biologie de Lille, Université Lille Nord de France, Institut Pasteur de Lille, Lille Cedex, France.

Note: Supplementary data for this article are available at Molecular Cancer Research Online (http://mcr.aacrjournals.org/).

Current address for V. Pospichalova: Faculty of Science, Masaryk University, Kotlarska 2, 611 37 Brno, Czech Republic.

Corresponding Author: Vladimir Korinek, Institute of Molecular Genetics AS CR, Videnska 1083, 142 20 Prague 4, Czech Republic. Phone: 420-241063146; Fax: 420-244472282; E-mail: korinek@img.cas.cz

doi: 10.1158/1541-7786.MCR-15-0033

©2015 American Association for Cancer Research.

Downloaded from mcr.aacrjournals.org on February 27, 2016. © 2015 American Association for Cancer Research.

Published OnlineFirst May 1, 2015; DOI: 10.1158/1541-7786.MCR-15-0033

of invaginations called intestinal crypts, where ISCs divide regularly and give rise to transit amplifying cells (TA). Rapidly dividing TA cells migrate upward and while exiting the crypt, they differentiate to absorptive enterocytes, mucus-producing goblet cells, and hormone-secreting enteroendocrine cells. In the small intestine, differentiated cells cover finger-like protrusions called villi; the surface of the colon is flat. The intestinal epithelium self-renewing in 3 to 5 days represents one of the most rapidly self-renewing tissues in the mammalian body. One exception from the outlined scheme are Paneth cells that secrete bactericidal cryptidins, defensins, or lysozyme. These relatively long-lived cells are present in the small intestine only. Moreover, during maturation, the Paneth cell does not migrate from the crypt but stays at the crypt bottom, where it persists for 6 to 8 weeks (reviewed in ref. 9). Owing to the dynamic turnover, the intestinal epithelium is at high risk of carcinogenesis. Although aberrant activation of the Wnt pathway initiates the majority of colorectal carcinomas (reviewed in ref. 10), CRC development is a multistep process that entails accumulation not only of genetic, but also of epigenetic changes in epithelial cells (11). The physiologic role of HIC1 in the intestine has not yet been elucidated in detail. However, in the mouse, Hic1 represses *atonal homolog 1* (*Atoh1*) and *SRY-box containing gene 9* (*Sox9*) genes, which are involved in the cell fate determination of secretory cell lineages in the small intestine (12–14).

In the present study, we used a conditional knock-out of the *Hic1* gene (15) to identify genes repressed by Hic1. Expression profiling of mouse embryonic fibroblasts (MEF) revealed six novel Hic1 target genes, including *Tlr2*. Tlr2 functions as a microbial sensor to initiate inflammation and immune responses. In addition, the receptor recognizes endogenous inflammatory mediators released from dead cells (review in ref. 16). Upon ligand binding, Tlr2 triggers several signal transduction pathways, including NF-κB signaling that activates expression of proinflammatory cytokines and enzymes, such as tumor necrosis factor-alpha (TNFα), interleukin 6 (IL6), and cyclooxygenase-2 (Cox2) (17). Solid tumors contain inflammatory infiltrates, and many recent studies have shown association between inflammation and increased risk of cancer development and progression. Furthermore, there is growing evidence that Tlr2 activators released from cancer cells might initiate persistent inflammation found in many tumors (reviewed in ref. 18). However, two recent studies documented an inflammation-independent Tlr2 role in promoting gastric and intestinal cancer (17, 19). Here, we show that *Hic1* depletion in the intestinal epithelium resulted in increased Tlr2 expression that promoted proliferation of colonic tumors induced by chemical carcinogenesis.

Materials and Methods

Experimental mice

Housing of mice and *in vivo* experiments were performed in compliance with the European Communities Council Directive of 24 November 1986 (86/609/EEC) and national and institutional guidelines. Animal care and experimental procedures were approved by the Animal Care Committee of the Institute of Molecular Genetics (Ref. 82/2011). Generation and genotyping of $Hic1^{flox/flox}$ and Hic1 citrine reporter ($Hic1^{cit/+}$) mice was described previously (15). The *Rosa26-CreERT2* [B6.129-Gt (ROSA)26Sor$^{tm1(cre/ERT2)Tyj}$/J] mouse strain was purchased from The Jackson Laboratory and was genotyped as recommended by the provider. *Villin-CreERT2* and *Villin-Cre* transgenic mice (20) were kindly provided by Sylvie Robine (Institut Curie, Centre de Recherche, Paris, France). Animals were housed in specific pathogen-free conditions. Tumors of the colon and rectum were collected from adult $Hic1^{flox/flox}$ $Villin\text{-}Cre^{+}$ mice 5 weeks after a single subcutaneous injection of azoxymethane [(AOM); 10 mg/kg; purchased from Sigma] that was followed by a 5-day dextran sodium sulfate (DSS) treatment in drinking water [2% (w/v) DSS; MW 36–50 kDa; MP Biomedicals]. The mice were euthanized and the intestines were dissected, washed in PBS, and fixed in 4% formaldehyde (v/v) in PBS for 3 days. Fixed intestines were embedded in paraffin, sectioned and stained. The number and size of the neoplastic lesions were quantified using Ellipse software (ViDiTo). Colitis was induced by DSS (2% in the drinking water for 5 days) without AOM treatment. Colons were collected 2, 6, and 9 days upon DSS withdrawal.

Cell and organoid culture, 4-hydroxytamoxifen (4-OHT) treatment

MEFs were isolated from embryos obtained at embryonic day (E) 11 to E14, details of the procedure are given in Supplement. For Cre-mediated recombination, cells were cultured in the presence of 4-OHT at a final concentration of 2 μmol/L (prepared from 1 mmol/L solution in ethanol; Sigma). Control cells were treated with the corresponding amount of ethanol. Small intestinal crypts were isolated and cultured according to the previously published protocol (21). Colonic crypts were isolated using the same procedure, but the culture medium was additionally supplemented with conditioned medium obtained from mouse Wnt3a-producing L cells (L-Wnt3a; ref. 22). L-Wnt3a, HEK293, and BJ-Tert cells were purchased from the ATCC (Cat. No.: CRL-2647, CRL-1573, and CRL-4001, respectively). All cell lines were obtained in 2006 and maintained in DMEM (Sigma) supplemented with 10% FBS (Gibco), penicillin, streptomycin, and gentamicin (Invitrogen). Upon receipt, cells were expanded and aliquots of cells at passage number <10 were stored frozen in liquid nitrogen. Cells from one aliquot were kept in culture for less than 2 months after resuscitation. The cell identity was not authenticated by the authors.

Microarray analysis

Total RNA was isolated from MEFs harvested 24, 48, 72, and 120 hours upon 4-OHT addition using RNeasy Plus Mini Kit (Qiagen). Control cells were grown with the same volume of vehicle (ethanol). The quality of isolated mRNA was checked using Agilent Bioanalyzer 2100; RNAs with RNA integrity number (RIN) above 8 were further processed. Two biologic replicates were used for each time point and treatment. The RNA samples were analyzed using MouseRef-8 v2.0 Expression BeadChip (Illumina). Raw data were processed using the beadarray package of Bioconductor and analyzed as described previously (23). Gene set enrichment analysis (GSEA) was performed using the Enricher gene analysis tool (http://amp.pharm.mssm.edu/Enrichr; ref. 24). Microarray data were deposited in ArrayExpress (http://www.ebi.ac.uk/arrayexpress) under accession number E-MTAB-3486.

Luciferase reporter assay, biochemistry, RNAi

MEFs were electroporated (details are given in Supplement); transfection of HEK293 cells was performed using Lipofectamine 2000 reagent (Invitrogen). Luciferase reporter constructs NF-κB-Luc and pRL-TK were purchased from Promega. To generate Tlr2-Luc reporter plasmid, genomic DNA containing the mouse Tlr2 promoter region encompassing nucleotides −796 to +52 (the

Downloaded from mcr.aacrjournals.org on February 27, 2016. © 2015 American Association for Cancer Research.

Published OnlineFirst May 1, 2015; DOI: 10.1158/1541-7786.MCR-15-0033

transcription start site corresponds to position +1) was amplified by PCR and cloned into the pGL4.26 luciferase reporter vector (Promega). The HIC1 construct was described previously (8). Details of the luciferase assay and NF-κB pathway stimulation are given in Supplement. For RNAi, BJ-Tert fibroblasts were reverse-transfected with Lipofectamine RNAiMax (Invitrogen) according to manufacturer's instructions using 10 nmol/L small interfering RNA (siRNA) targeting *HIC1* (HIC1 siGENOME SMART Pool M-006532-01, Dharmacon) or a scrambled control siRNA (siCtrl; siGENOME RISC free control siRNA, Dharmacon) and harvested 2 days upon transfection.

ChIP and droplet digital PCR

Chromatin immunoprecipitation (ChIP) using chromatin obtained from immortalized BJ-Tert fibroblasts was performed as described previously (25). Occupancy of gene regulatory regions by HIC1 was assayed by ddPCR (QX200, Bio-Rad) using EvaGreen master mix (Bio-Rad). PCR primers are listed in Supplement.

FACS

Paneth cell sorting was performed according to the previously published protocol (26). Antibodies used for flow cytometry: phycoerythrin (PE)-conjugated anti-CD24 (12-0242-81, eBioscience), allophycocyanin (APC)-conjugated anti-EpCam (17-5791-80, eBioscience), FITC-conjugated anti-CD45 (ED7018, ExBio).

IHC

The technique was performed as described previously (27, 28). Hematoxylin and eosin (Sigma) were used for counterstaining. Antibodies are given in Supplement. For visualization of citrine fluorescence, intestines dissected from $Hic1^{cit/+}$ and wild-type (wt) mice were snap frozen in liquid nitrogen and immediately sectioned. Specimens were stained with 4′,6-diamidino-2-phenylindole, dihydrochloride (DAPI; Life Technologies) and the citrine fluorescence signal was evaluated using a laser scanning confocal microscope (Leica TCS SP5).

Western blotting and antibodies

Hic1-specific polyclonal antisera were generated in rabbit or chicken immunized with the recombinant His-tagged fragment of human HIC1 protein (amino acids 154-396). Commercially available antibodies are given in Supplement.

RNA purification and reverse-transcription quantitative PCR

Total RNAs were isolated from cells and tissues using RNeasy Mini Kit (Qiagen) and reversely transcribed and analyzed by qRT-PCR as described previously (29). The primers are listed in Supplementary Table S1.

Statistical analysis of data

Results of the gene reporter assay, Ellipse, and qRT-PCR analysis were evaluated by the Student *t* test. Datasets obtained using DNA microarrays were analyzed in the R environment using the package LIMMA (Linear Models for Microarray Data LIMMA; ref. 30).

Results

Identification of *Tlr2* as a novel target gene repressed by Hic1 in mouse and human cells

To investigate the biologic function of transcription repressor Hic1, we have recently developed the $Hic1^{flox/flox}$ mouse strain that enables conditional inactivation of the *Hic1* gene (15). These mice were crossed to *Rosa26-CreERT2* animals expressing Cre recombinase estrogen receptor T2 fusion protein (CreERT2) from the *Rosa26* locus (31). The fusion protein resides in the cytoplasm until an antagonist of the estrogen receptor, tamoxifen (or its active metabolite 4-OHT), is administered. Subsequently, Cre enzyme is translocated into the nucleus, where it allows excision of DNA sequences flanked, that is, "floxed", by loxP sites (32). MEFs were isolated from embryos, cultured with 4-OHT or vehicle (ethanol) and genotyped by PCR to confirm locus recombination and generation of the $Hic1^{delEx2}$ allele. Simultaneously, the presence of Hic1 protein was detected by immunoblotting (Fig. 1A). Subsequently, total RNA was isolated at four time points after the addition of 4-OHT (or vehicle) into the culture media, and microarray analysis of the expression profile was performed. The analysis revealed genes whose expression was changed significantly ($q < 0.05$) after the *Hic1* locus recombination. Furthermore, six genes were upregulated in at least two time points and more than twice [the binary logarithm of fold change (log FC) > 1; Fig. 1B and Supplementary Fig. S1 and Supplementary Table S2]. These genes were *angiopoietin-like 7* (*Angptl7*), *carbonyl reductase 2* (*Cbr2*), *death-associated protein kinase 2* (*Dapk2*), *HSP, α-crystallin-related, B6* (*Hspb6*), *Tlr2*, and *WAP four-disulfide core domain 2* (*Wfdc2*). In addition, increased expression of previously identified HIC1 target genes *cyclin-dependent kinase inhibitor 1a* (*CDKN1A*; ref. 33), *Sox9* (13), and *Sirt1* (7) was observed, but these genes did not satisfy the significance criteria (not shown). Rather unexpectedly, the GSEA analysis using the Enricher gene library online tool (24) revealed that the inactivation of the *Hic1* gene in MEFs mainly altered expression of genes involved in lipid metabolism (Supplementary Table S3).

As recent evidence supports the role of TLR signaling in inflammation-associated tumorigenesis in the gastrointestinal tract (reviewed in ref. 34), we further investigated the relationship between Hic1 and *Tlr2* expression. First, we generated a Tlr2-Luc reporter by subcloning genomic DNA harboring the *Tlr2* promoter region before the luciferase sequence. Then, we cotransfected the Tlr2-Luc reporter together with the expression construct encoding HIC1 into HEK293 cells and performed the luciferase reporter assay. As expected, increasing amounts of HIC1 resulted in reduced activity of the reporter, whereas cotransfection with a control "empty" plasmid had no significant effect (Fig. 1C). Moreover, we used a HIC1-specific antibody to perform ChIP using chromatin isolated from BJ fibroblasts that express detectable amounts of endogenous HIC1 (25). Droplet digital PCR confirmed the enrichment of genomic DNA encompassing the promoter regions of *TLR2* and *SIRT1* (used as positive control) genes in the precipitate. Importantly, none of these regions was precipitated using a control "irrelevant" antibody and, furthermore, the anti-HIC1 antibody did not pull down the *β-ACTIN* promoter used as negative control. In addition, upregulation of *TLR2* and *SIRT1* was detected upon *HIC1* mRNA knockdown (Fig. 1D and data not shown). The *Tlr2* gene is activated by NF-κB signaling (35); therefore, the luciferase assay was performed in MEFs stimulated with NF-κB pathway activators TNFα, LTα, and with synthetic bacterial lipopeptide Pam3csk4, which functions as the Tlr2 ligand (36). Interestingly, Pam3csk4 appeared to be the most potent enhancer of the Tlr2-Luc activity, especially upon Hic1 deletion; however, the Tlr2-Luc activity was also significantly increased upon stimulation with unrelated LTα. In addition, the luciferase reporter assay clearly showed increased Tlr2-Luc activity

Downloaded from mcr.aacrjournals.org on February 27, 2016. © 2015 American Association for Cancer Research.

Published OnlineFirst May 1, 2015; DOI: 10.1158/1541-7786.MCR-15-0033

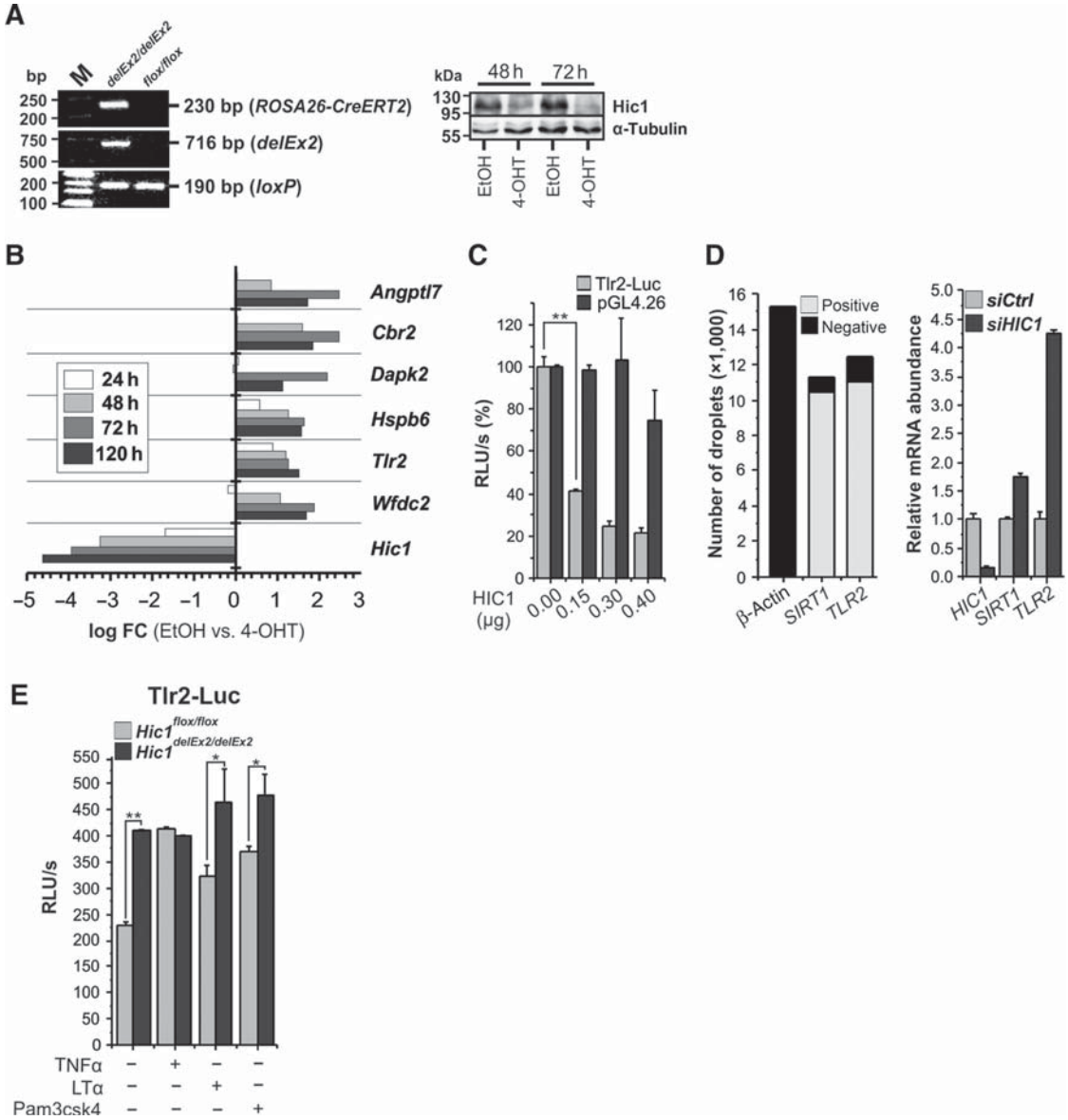


Figure 1.

Tlr2 represents a novel direct target gene of transcriptional repressor Hic1. A, left, PCR genotyping of MEFs isolated from *Hic1*$^{flox/flox}$ *Rosa26*$^{CreERT2/+}$ embryos. Cells were cultured with 4-OHT for 4 days. PCR on the homozygous *flox/flox* and hemizygous *CreERT2* allele produced 190 bp or 230 bp DNA fragments, respectively. Cre-mediated recombination generated the *delEx2* allele lacking the second *Hic1* exon encoding the major part of the protein. The recombination is documented by the presence of the 716-bp PCR product. Right, immunoblotting of *Hic1*$^{flox/flox}$ *Rosa26*$^{CreERT2/+}$ cell lysates obtained from MEFs 48 and 72 hours after adding 4-OHT or solvent [ethanol (EtOH)]. Western blotting with an anti–α-tubulin antibody was used as a loading control. B, expression profile of *Hic1*$^{delEx2/delEx2}$ MEFs compared to *Hic1*$^{flox/flox}$ cells at the indicated time points after adding 4-OHT. The decrease in *Hic1* mRNA levels was accompanied by significant upregulation ($q < 0.05$) of six genes; log FC, binary logarithm of fluorescent intensity of the indicated gene-specific probe upon hybridization with labeled RNA isolated from MEFs treated with 4-OHT versus fluorescent intensity obtained using RNA isolated from cells treated with vehicle only. C, luciferase reporter assays in HEK293 cells cotransfected with the Tlr2-Luc reporter or control vector pGL4, respectively, together with increasing amounts of HIC1-producing plasmid. D, left, ddPCR using genomic DNA obtained from human BJ cells by ChIP with an anti-HIC1 antibody. Although PCR using primers designed from the promoter regions of *SIRT1* and *TLR2* genes, that is, genes directly repressed by HIC1, produced mainly droplets containing a PCR product, PCR with primers designed from the *β-ACTIN* promoter gave droplets without any product. Right, qRT-PCR analysis of BJ cells upon HIC1 knockdown. Expression level of the respective gene in cells treated with non-silencing siRNA (siCtrl) was set to 1. E, luciferase reporter assays in MEFs electroporated with Tlr2-Luc reporter plasmid. Cells were stimulated overnight with TNFα, LTα, or Pam3csk4. The histograms represent average luciferase light units per second (RLU/s) obtained in three independent experiments performed in triplicates. The values were corrected for efficiency of electroporation using *Renilla* luciferase as the internal control. Error bars represent SDs; *, $P < 0.05$; **, $P < 0.01$.

Downloaded from mcr.aacrjournals.org on February 27, 2016. © 2015 American Association for Cancer Research.

Published OnlineFirst May 1, 2015; DOI: 10.1158/1541-7786.MCR-15-0033

in Hic1-deficient MEFs when compared with cells with the intact *Hic1* locus (Fig. 1E). Several studies indicate the NF-κB pathway activation via Tlr2 signaling (37, 38). Thus, we next examined the consequence of *Hic1* deficiency for the NF-κB pathway. Luciferase reporter assay using the NF-κB-Luc reporter showed increased NF-κB signaling even in unstimulated $Hic1^{delEx2/delEx2}$ cells (compared with MEFs before Cre-mediated *Hic1* inactivation). Treatment of cells with Pam3csk4 further potentiated the reporter activity. However, increased NF-κB signaling was also observed upon stimulation with LTα and TNFα, indicating that the NF-κB pathway output was not completely dependent on Tlr2 (over) expression (Fig. 2A). The augmentation of the NF-κB pathway activity in Hic1-deficient MEFs was confirmed by qRT-PCR analysis that showed increased expression of the putative NF-κB target genes *Cox2* and *TNFα* (Fig. 2B). In agreement with these results, immunoblotting revealed increased levels of the phosphorylated transcriptionally active form of the nuclear mediator of NF-κB signaling p65 (Fig. 2C). In summary, all the data supported direct transcriptional repression of *Tlr2* by Hic1 and, moreover, potentiation of the NF-κB pathway activity upon loss of the *Hic1* gene.

Hic1 depletion in the intestinal epithelium results in *Tlr2* upregulation

In the intestinal epithelium, the *Hic1* expression was examined using previously generated Hic1-citrine "reporter" mice. In this mouse strain, the sequence encoding the central and C-terminal portions of Hic1 protein was replaced by cDNA encoding citrine (yellow) fluorescent protein (15). In both the small and large intestine, native citrine fluorescence was observed in epithelial cells (Fig. 3A). Subsequently, production of Hic1 protein in the gut epithelia was confirmed by immunoblotting using cell lysates prepared from crypts and differentiated cells lining the villi in the small intestine or intercrypt regions (ICR) in the colon. The analysis revealed higher amounts of Hic1 in the villus and ICR fractions when compared with the crypts. This result was confirmed by qRT-PCR using total RNA isolated from the same epithelial fractions (Fig. 3B). In order to evaluate the expressional changes of the putative Hic1 target genes in epithelial cells, we established three-dimensional "organoid" cultures (21) from the small intestinal crypts of $Hic1^{flox/flox}$ *Villin-CreERT2*$^{+}$ mice producing tamofixen-regulated Cre enzyme in all intestinal cell lineages (20). Interestingly, Cre-mediated inactivation of the *Hic1* gene increased mRNA levels of all genes identified by the microarray analysis. Furthermore, like in MEFs, Hic1 deficiency resulted in upregulation of the NF-κB-responsive genes *Cox2* and *TNFα* (Fig. 3C). In addition, Tlr2 was analyzed in $Hic1^{flox/flox}$ *Villin-Cre*$^{+}$ mice expressing the constitutively active form of Cre enzyme in the embryonic and adult gut epithelia (20). Although efficient recombination and generation of the $Hic1^{delEx2}$ allele along the rostrocaudal axis of the gastrointestinal tract was confirmed by PCR genotyping (data not shown), these mice—lacking *Hic1* in the intestinal epithelium—were viable, showing no signs of any health problems. However, IHC staining showed increased Tlr2 positivity in the small intestine and colon (Fig. 3D).

Hic1-deficient intestinal epithelium contains increased numbers of secretory cell lineages

As morphology and proliferation of the $Hic1^{loxP/loxP}$*Villin-Cre*$^{+}$ intestinal epithelium appeared to be normal, we performed detailed analysis of all major cellular lineages present in the small intestine. Maturation of Paneth cells is driven by transcription factors *Atoh1* and *Sox9* (14). Interestingly, Hic1 is a transcriptional repressor of *Atoh1* and *SOX9* in the mouse developing cerebellum and in U2OS osteosarcoma cells, respectively (12, 13). Using

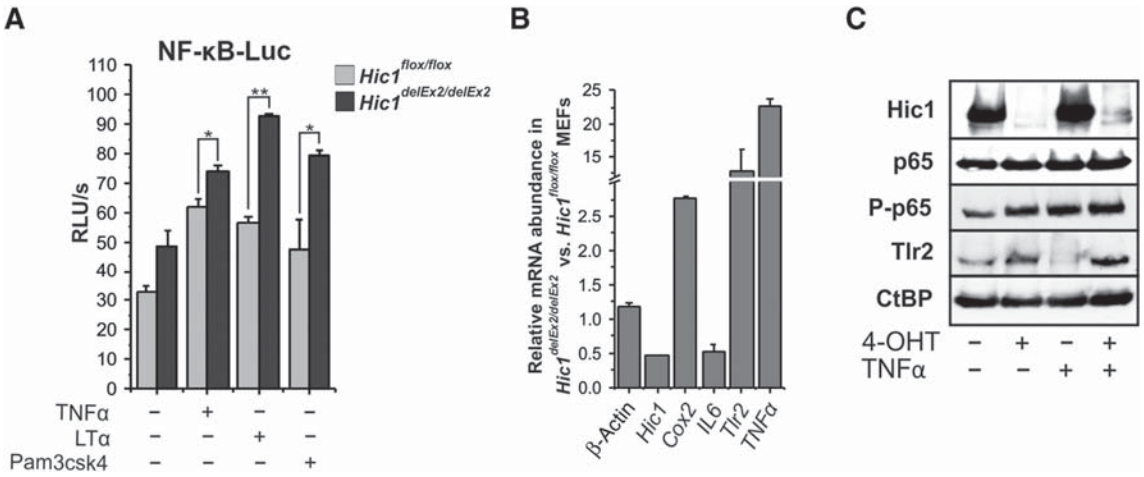


Figure 2.
Hic1-deficient MEFs display upregulated NF-κB signaling. A, luciferase reporter assays in MEFs cultured with 4-OHT or vehicle (ethanol) for 3 days and then electroporated with the NF-κB-Luc reporter. Six hours upon electroporation, TNFα, LTα, or Pam3csk4 was added to the culture medium and the cells were harvested 12 hours later. The assay was performed in triplicates, representative results are shown. *, $P<0.05$; **, $P < 0.01$. B, qRT-PCR analysis of putative target genes of NF-κB signaling *Cox2*, *IL6*, and *TNFα* in *Hic1*-deficient or control vehicle-treated MEFs. Total RNA was isolated from cells cultured with 4-OHT or vehicle for 3 days and then stimulated with the indicated ligand overnight. The results were normalized to the *Ubiquitin B* (*Ubb*) housekeeping gene; the relative expression of another housekeeping gene, *β-actin*, is also shown. The expression level of the respective gene in control vehicle-treated cells was arbitrarily set to 1. The analysis was performed in triplicates; error bars: SDs. C, immunoblotting of lysates prepared from MEFs cultured with 4-OHT or vehicle for 3 days and then stimulated with TNFα for 30 minutes. The experiment was repeated twice, representative blot is presented. CtBP, loading control; P-p65, immunoblotting with an antibody recognizing p65 phosphorylated at S536.

Downloaded from mcr.aacrjournals.org on February 27, 2016. © 2015 American Association for Cancer Research.

Published OnlineFirst May 1, 2015; DOI: 10.1158/1541-7786.MCR-15-0033

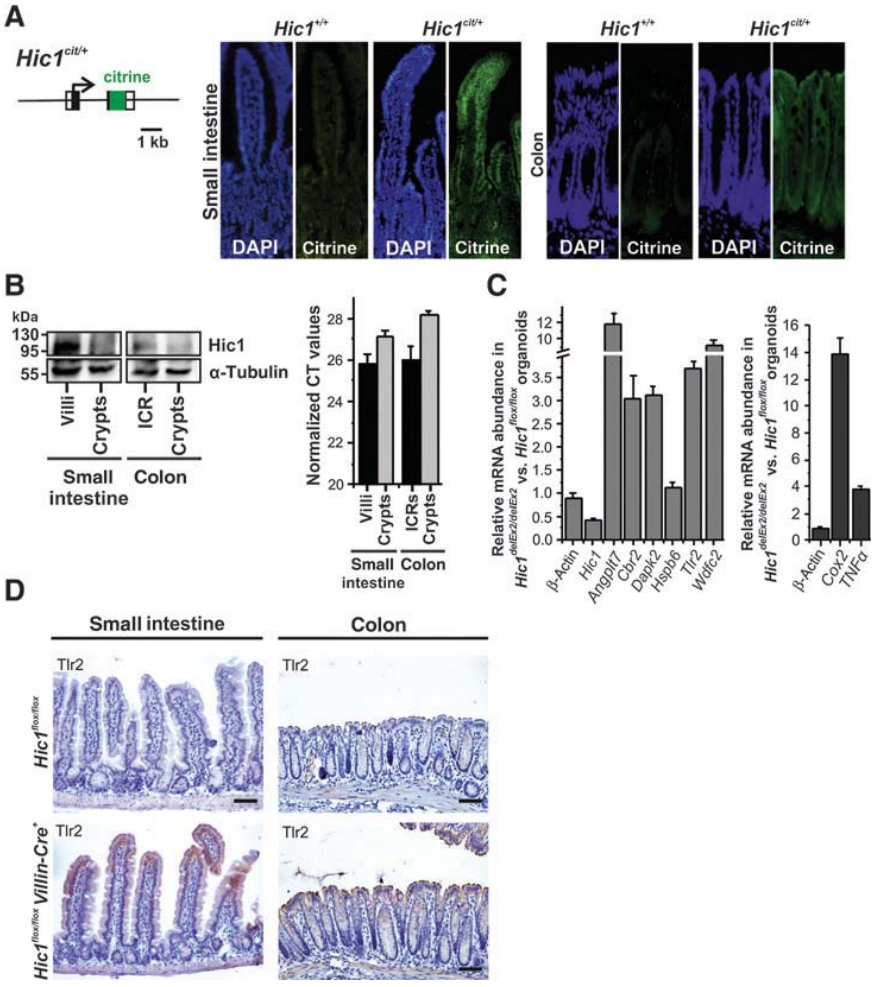


Figure 3.
Increased expression of *Tlr2* in *Hic1*-deficient small intestinal organoids and intestinal epithelia. A, production of Hic1-citrine fusion protein in *Hic1*$^{cit/+}$ mouse is restricted to the epithelium of the small intestine and colon. Left, a scheme of the *Hic1-citrine* reporter allele producing citrine fluorescent protein from the *Hic1* locus. Exons are depicted by boxes; coding sequences are filled, arrow indicates the transcription start site. Right, fluorescent microphotographs of cryosections of the small intestine and colon of *Hic1*$^{+/+}$ and *Hic1*$^{cit/+}$ mouse counterstained with DAPI nuclear stain (blue fluorescence). The right image from each pair was gained in "citrine" (green fluorescence) channel to monitor expression from the *Hic1* locus. No citrine fluorescence was observed in the intestine of control *Hic1*$^{+/+}$ animals. B, left, Western blotting from separated epithelial lining of the wt small intestinal villi and crypts and from the wt intercrypt regions (ICRs) and crypts of the colon; α-tubulin, loading control. Right, qRT-PCR analysis of total RNA isolated from the indicated regions of the intestinal epithelium. Cycle threshold (C_t) values normalized to *Ubb* are shown. C, qRT-PCR analysis of RNA isolated from organoids established from the small intestinal crypts of *Hic1*$^{flox/flox}$ *Villin-CreERT2*$^{+}$ mice. Vehicle (EtOH) or 4-OHT was added to the culture medium third day after the crypt isolation and the organoids were harvested after another 3 days. The expression level of the respective gene in vehicle-treated organoids was arbitrarily set to 1. The scheme represents results obtained in two independent experiments (each) performed in triplicates. Errors bars: SDs. D, IHC staining of Tlr2 [brown 3,3′-Diaminobenzidine (DAB) stain] in *Hic1*$^{flox/flox}$ and *Hic1*$^{flox/flox}$ *Villin-Cre*+ intestines. The specimens were counterstained with hematoxylin (blue nuclear stain). Scale bar: 0.15 mm.

expression profiling of sorted Paneth cells isolated from the *Hic1*$^{flox/flox}$ *Villin-Cre*$^{+}$ and control (*Hic1*$^{flox/flox}$) small intestinal crypts, we observed a significant increase in *Atoh1*, *Sox9*, and *Tlr2* mRNA levels upon loss of Hic1. Moreover, FACS analysis showed a slight increase in Paneth cell counts in *Hic1*$^{flox/flox}$ *Villin-Cre*$^{+}$ animals (Fig. 4A). Increased Paneth cell numbers along the rostrocaudal axis of the small intestine were also recorded using paraffin sections stained with an antibody recognizing Paneth cell-specific marker lysozyme (Fig. 4B). In addition, the numbers of mucin-producing goblet cells and chromogranin A-positive enteroendocrine cells were also elevated. In contrast, the differentiation and number of absorptive enterocytes seemed unchanged in the Hic1-deficient intestine (Supplementary Fig. S2).

Loss of Hic1 promotes colitis-associated tumorigenesis

Recently, Mohammad and colleagues described accelerated formation of tumors upon loss of *Hic1* in the *Apc*$^{Min/+}$ mouse model of intestinal cancer (39). Because inflammation is an important tumor promoter in colorectal neoplasia, the role of Hic1 was examined utilizing colitis-associated tumorigenesis. In

Downloaded from mcr.aacrjournals.org on February 27, 2016. © 2015 American Association for Cancer Research.

Published OnlineFirst May 1, 2015; DOI: 10.1158/1541-7786.MCR-15-0033

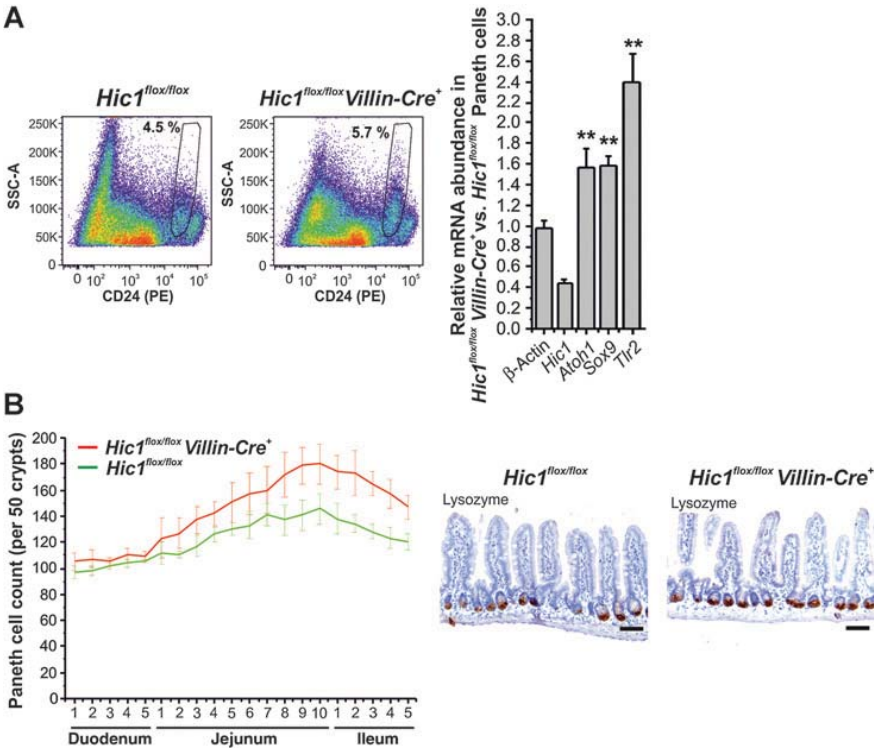


Figure 4.
Loss of the Hic1 function results in increased counts of Paneth cells. A, left, FACS analysis of Paneth cells obtained from the indicated mouse strains. Representative histograms show higher numbers of Paneth cells in the Hic1-deficient small intestine. Four animals per strain were used for the experiment. Right, qRT-PCR of sorted Paneth cells. Decreased *Hic1* expression results in upregulation of Hic1 target genes *Atoh1*, *Sox9*, and *Tlr2*. The expression level of the respective gene in *Hic1* wt cells was arbitrarily set to 1. **, $P < 0.01$. B, Paneth cell distribution in the indicated segments of the small intestine. Specimens obtained from four $Hic1^{flox/flox}$ and four $Hic1^{flox/flox}$ *Villin-Cre*$^{+}$ mice were stained using an anti-lysozyme antibody to visualize Paneth cells (right images). Lysozyme-positive cells were counted in 50 neighboring crypts in several different fields indicated by numbers on the *x*-axis. Scale bar: 0.15 mm; error bars: SDs.

the acute colitis phase – induced by DSS treatment – no differences in the extent of tissue damage were observed in histologic specimens obtained from $Hic1^{flox/flox}$ *Villin-Cre*$^{+}$ and $Hic1^{flox/flox}$ mice. However, $Hic1^{flox/flox}$ *Villin-Cre*$^{+}$ individuals displayed more robust DSS treatment-associated transcriptional response of the *Cox2*, *Tlr2*, and *TNFα* genes, that is, genes upregulated upon *Hic*1 loss. Analysis of the colon during the regenerative phase, that is, 6 and 9 days upon DSS withdrawal, showed a more robust hyperproliferative response of the colonic epithelium of $Hic1^{flox/flox}$ *Villin-Cre*$^{+}$ individuals when compared with their $Hic1^{flox/flox}$ littermates (Fig. 5A). Moreover, a continuous increase of *Cox2*, *Tlr2*, and *TNFα* expression was observed at these time points (Supplementary Fig. S3). Strikingly, upon combined AOM/DSS treatment, Hic1 deficiency significantly increased the size of colonic and rectal tumors (Fig. 5B; average tumor size in $Hic1^{flox/flox}$ mouse = 3.1 mm^2 vs. 8.7 mm^2 in $Hic1^{flox/flox}$ *Villin-Cre*$^{+}$; $P = 0.00862$). IHC examination revealed decreased numbers of p53-positive cells within the tumor mass of *Hic1*-negative mice. Nevertheless, even in $Hic1^{flox/flox}$ mice, cells displaying nuclear p53 staining were rare and scattered throughout the neoplastic tissue. However, expression of the p21 cell-cycle inhibitor, the most prominent in wt cells at the surface area of the tumors, was reduced in *Hic1* knock-outs. Strikingly, proliferating cell nuclear antigen (PCNA) expressing cells were localized in wt mice in areas clearly distinguished from the regions containing p21-positive cells. In contrast, in Hic1-deficient mice, proliferating cells were more abundant and dispersed throughout the neoplastic tissue. Finally, no differences were noted in the numbers of apoptotic cells (Fig. 5C and not shown).

Discussion

In the present study, we used a gene inactivation-based screen to identify genes regulated by the Hic1 tumor suppressor. Interestingly, none of the identified presumptive Hic1 target genes was described previously. As the expression of all tested genes reacted to the Hic1 presence not only in MEFs, but also in intestinal organoids, we can exclude the possibility that the genes represent a small (sub)set of tissue-specific Hic1 targets. More likely, because the majority of previous studies utilized cells (over)producing ectopic HIC1 or cells treated with HIC1-specific siRNA (33), we suggest that (our) genes represent Hic1 target genes whose expression is relieved when the Hic1 steady-state levels are diminishing. On the other hand, the previously identified targets might represent genes efficiently repressed (or activated) immediately upon perturbation of the Hic1 protein levels. We used Hic1-reporter mice, Western blotting, and FACS analysis to demonstrate that in the adult intestine, Hic1 is mainly expressed in the differentiated epithelial cells. The expression of its target gene, *Tlr2*, was documented in ISCs (19). However, in the Hic1-deficient gut, Tlr2 was upregulated in differentiated cells, confirming the inverse Hic1-Tlr2 relationship. Moreover, intestinal ablation of *Hic1* resulted in a moderate increase in Paneth, goblet, and enteroendocrine cell numbers. Such phenotype might be attributed to upregulation of *Atoh1*, the Hic1 target gene functioning as the master regulator of secretory cell lineages in the small intestine (14). Upon ligand binding, Tlr2 triggers several signal transduction pathways, including NF-κB signaling (17). Interestingly, qRT-PCR analysis and luciferase reporter assays revealed that not only

Downloaded from mcr.aacrjournals.org on February 27, 2016. © 2015 American Association for Cancer Research.

Published OnlineFirst May 1, 2015; DOI: 10.1158/1541-7786.MCR-15-0033

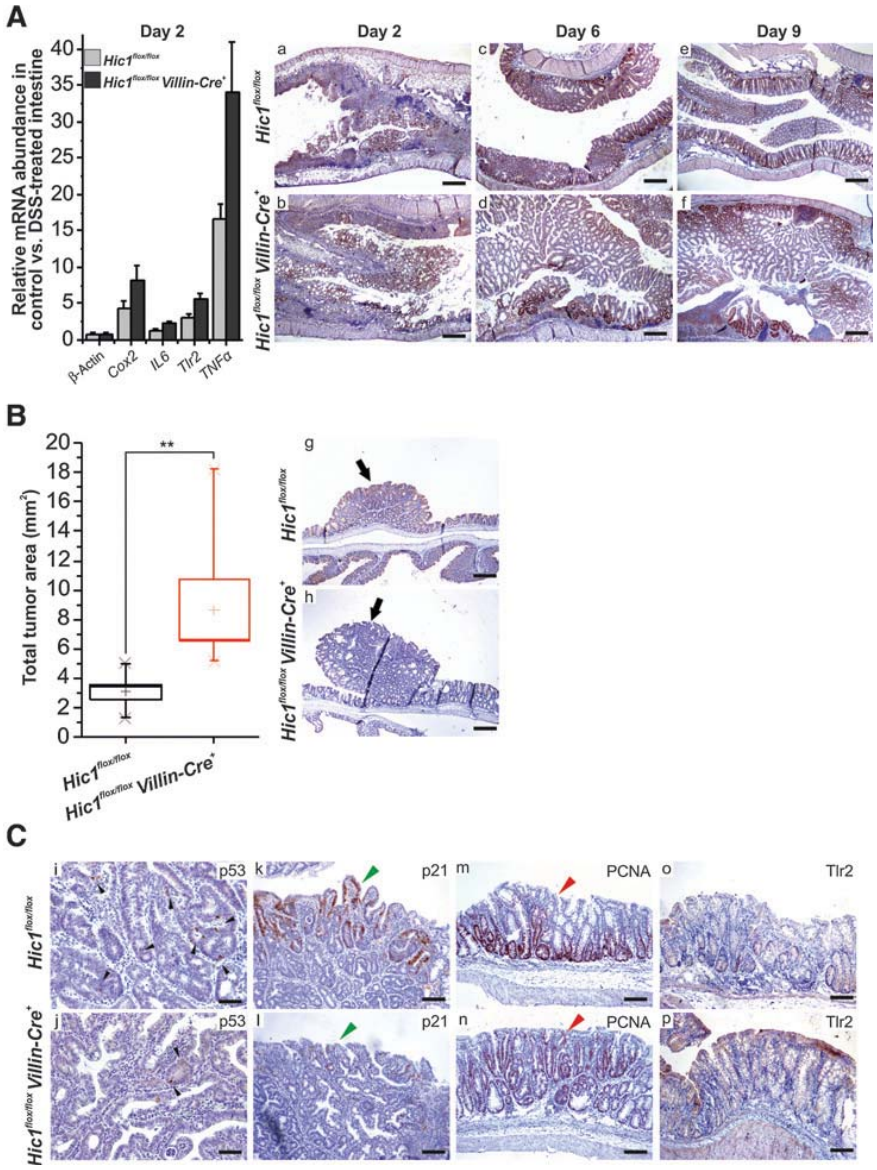


Figure 5.
Hic1 deficiency increased the size of colonic tumors generated upon AOM/DSS treatment. A, acute colitis and regeneration after DSS treatment. Left, DSS-induced transcriptional response in the colon of $Hic1^{flox/flox}$ and $Hic1^{flox/flox}$ *Villin-Cre*$^{+}$ mice 2 days upon DSS withdrawal. The expression level of the corresponding genes in mice without DSS treatment was arbitrarily set to 1. Four animals for each genotype were analyzed. Right, representative microscopic images of the colon two (a, b), six (c, d) and nine (e, f) days upon DSS withdrawal. The specimens were stained using an anti-PCNA antibody to detect proliferative cells (brown nuclear precipitate) and counterstained with hematoxylin (blue nuclear staining). B, tumor size in the colon generated in the indicated mouse strains upon combined AOM/DSS treatment. Intestines dissected from seven animals in each group were analyzed 5 weeks after the AOM/DSS application. Left, quantification of the total tumor area indicating significantly increased tumor burden in the *Hic1*-deficient colon. The total tumor area determined in each individual is indicated in the boxplots. The boxed areas correspond to the second and third quartiles; the spread of the values is given by "whiskers" above and below each box. Median (transverse line) and mean (cross) is marked inside each box. **, $P < 0.01$; error bars: SDs. Right, representative microscopic images of the colon; neoplastic outgrows are indicated by black arrows. The specimens were counterstained with hematoxylin and an anti-β-catenin antibody. C, IHC detection of tumor suppressor p53 [black arrowheads in panel (i) and (j)], cell-cycle inhibitor p21 [green arrowheads in (k) and (l)], PCNA-positive [(m, n); red arrowheads indicate differentially stained tumor surface] and Tlr2-producing (o, p) cells in colonic tumors. Scale bar: 0.75 mm (a–h); 0.15 mm (i, j); 0.3 mm (k-p).

ligand-induced, but also basal levels of the NF-κB signaling are elevated in Hic1-deficient cells (Fig. 2A and B). As the NF-κB pathway activity was more pronounced even in cells stimulated with other NF-κB inducers, the observed NF-κB (hyper)activity cannot be solely attributed to the increase in Tlr2 expression or function. Indeed, Western blotting confirmed that $Hic1^{delEx2/delEx2}$ cells displayed higher amounts of phosphorylated nuclear NF-κB mediator p65 (Fig. 2C). The exact reason(s) why Hic1 deficiency potentiates NF-κB signaling remains to be determined. Nevertheless, since several studies reported interaction between the STAT3 and NF-κB pathways (reviewed in ref. 40), we suggest that the autocrine IL6-STAT3 signaling might also be linked to the observed "boosts" in cellular reactivity to the stimuli activating the NF-κB pathway and to the increase in p65 stability and phosphorylation.

Several studies have demonstrated that *Tlr2* expression is increased during intestinal inflammation (41) or in human patients with ulcerative colitis (42). In addition, Maeda and colleagues showed that conditioned medium obtained from cultured colon cancer cells might activate NF-κB signaling via Tlr2 (43). These data are in accordance with our observation that in damaged tissue, transcription of *Tlr2* and genes linked to active NF-κB signaling is elevated. Importantly, in the *Hic1*-deficient colon, the damage-induced transcriptional response was more robust than in wt mice, supporting the Hic1 repressive role in *Tlr2* expression and NF-κB activation (Fig. 5A and Supplementary Fig. S3). Interestingly, several recent studies reported decreased tumor burden in $Apc^{+/Min}$ mice deficient in Tlr2 or its intracellular adaptor myeloid differentiation primary response protein-88 (Myd88; refs. 19, 44). Furthermore, deletion of *Tlr2* (or *Myd88*) reduced development of

Downloaded from mcr.aacrjournals.org on February 27, 2016. © 2015 American Association for Cancer Research.

Published OnlineFirst May 1, 2015; DOI: 10.1158/1541-7786.MCR-15-0033

colonic tumors in DSS-treated animals. Moreover, functional blocking of TLR2 inhibited *in vitro* growth of cancer cells (19). In another study, epithelial expression of Tlr2 and Tlr2/NF-κB signaling promoted growth and survival of gastric cancer cells (17). In summary, all these results support the cell-autonomous and inflammation-independent role of Tlr2 in cancer.

HIC1 participates in the cellular network regulating the DNA damage response (7). HIC1-mediated repression of deacetylase *SIRT1* gene promotes p53 stability and potentiates transcription of p53-dependent genes such as *p21* (45) and, in a positive regulatory feedback loop, also *HIC1* itself (1, 46). Unexpectedly, only a small fraction of cells in tumors generated by AOM/DSS treatment displayed stabilized p53 (Fig. 5C). Although the portion of p53-positive cells was decreased in $Hic1^{-/-}$ neoplastic tissues, it is unlikely that the increased tumor size observed upon Hic1 deletion is linked to the attenuated p53-mediated response. In human cells, HIC1 directly represses transcription of the *CDKN1A* gene encoding p21 (33). Strikingly, in Hic1-deficient tumors, we observed the opposite effect of Hic1 absence, that is, reduced p21 staining (Fig. 5C). Nevertheless, the observed discrepancy of the results might be explained by the fact that next to p53 and HIC1, p21 levels might be controlled by many other stimuli and also by post-transcriptional mechanisms (reviewed in ref. 47). As we noted increased cell proliferation upon DSS-induced epithelial damage and in Hic1-negative AOM/DSS tumors, we suggest that besides compromising the p53-mediated tumor-suppressive mechanisms the loss of Hic1 might potentiates tumor-promoting proproliferative Tlr2/NF-κB signaling.

Disclosure of Potential Conflicts of Interest

No potential conflicts of interest were disclosed.

Authors' Contributions

Conception and design: L. Janeckova, V. Pospichalova, V. Korinek
Development of methodology: V. Pospichalova, M. Dubuissez, D. Leprince, A. Hlavata, V. Korinek
Acquisition of data (provided animals, acquired and managed patients, provided facilities, etc.): L. Janeckova, V. Pospichalova, M. Vojtechova, J. Tureckova, J. Dobes, M. Dubuissez, D. Leprince, N. Baloghova, M. Horazna, A. Hlavata, J. Stancikova, E. Sloncova
Analysis and interpretation of data (e.g., statistical analysis, biostatistics, computational analysis): L. Janeckova, V. Pospichalova, A. Hlavata, H. Strnad, V. Korinek
Writing, review, and/or revision of the manuscript: L. Janeckova, V. Pospichalova, D. Leprince, V. Korinek
Administrative, technical, or material support (i.e., reporting or organizing data, constructing databases): K. Galuskova
Study supervision: V. Korinek

Acknowledgments

The authors thank S. Robine for Villin-Cre and Villin-CreERT2 mice, and S. Takacova for critically reading the manuscript.

Grant Support

This work was supported by Grant Agency of the Czech Republic Grant No. P305/12/2347, institutional Grant No. RVO 68378050, and project BIOCEV – Biotechnology and Biomedicine Centre of the Academy of Sciences and Charles University (CZ.1.05/1.1.00/02.0109) from the European Regional Development Fund.

The costs of publication of this article were defrayed in part by the payment of page charges. This article must therefore be hereby marked *advertisement* in accordance with 18 U.S.C. Section 1734 solely to indicate this fact.

Received January 19, 2015; revised March 20, 2015; accepted April 1, 2015; published OnlineFirst May 1, 2015.

References

1. Wales MM, Biel MA, el Deiry W, Nelkin BD, Issa JP, Cavenee WK, et al. p53 activates expression of HIC-1, a new candidate tumour suppressor gene on 17p13.3. Nat Med 1995;1:570–7.
2. Carter MG, Johns MA, Zeng X, Zhou L, Zink MC, Mankowski JL, et al. Mice deficient in the candidate tumor suppressor gene Hic1 exhibit developmental defects of structures affected in the Miller-Dieker syndrome. Hum Mol Genet 2000;9:413–9.
3. Chen WY, Zeng X, Carter MG, Morrell CN, Chiu Yen RW, Esteller M, et al. Heterozygous disruption of Hic1 predisposes mice to a gender-dependent spectrum of malignant tumors. Nat Genet 2003;33:197–202.
4. Rood BR, Leprince D. Deciphering HIC1 control pathways to reveal new avenues in cancer therapeutics. Expert Opin Ther Targets 2013; 17:811–27.
5. Pinte S, Stankovic-Valentin N, Deltour S, Rood BR, Guerardel C, Leprince D. The tumor suppressor gene HIC1 (hypermethylated in cancer 1) is a sequence-specific transcriptional repressor: definition of its consensus binding sequence and analysis of its DNA binding and repressive properties. J Biol Chem 2004;279:38313–24.
6. Guerardel C, Deltour S, Pinte S, Monte D, Begue A, Godwin AK, et al. Identification in the human candidate tumor suppressor gene HIC-1 of a new major alternative TATA-less promoter positively regulated by p53. J Biol Chem 2001;276:3078–89.
7. Chen WY, Wang DH, Yen RC, Luo J, Gu W, Baylin SB. Tumor suppressor HIC1 directly regulates SIRT1 to modulate p53-dependent DNA-damage responses. Cell 2005;123:437–48.
8. Valenta T, Lukas J, Doubravska L, Fafilek B, Korinek V. HIC1 attenuates Wnt signaling by recruitment of TCF-4 and beta-catenin to the nuclear bodies. EMBO J 2006;25:2326–37.
9. Clevers HC, Bevins CL. Paneth cells: maestros of the small intestinal crypts. Annu Rev Physiol 2013;75:289–311.
10. Krausova M, Korinek V. Wnt signaling in adult intestinal stem cells and cancer. Cell Signal 2014;26:570–9.
11. De Sousa EMF, Wang X, Jansen M, Fessler E, Trinh A, de Rooij LP, et al. Poor-prognosis colon cancer is defined by a molecularly distinct subtype and develops from serrated precursor lesions. Nat Med 2013;19:614–8.
12. Briggs KJ, Eberhart CG, Watkins DN. Just say no to ATOH: how HIC1 methylation might predispose medulloblastoma to lineage addiction. Cancer Res 2008;68:8654–6.
13. Van Rechem C, Rood BR, Touka M, Pinte S, Jenal M, Guerardel C, et al. Scavenger chemokine (CXC motif) receptor 7 (CXCR7) is a direct target gene of HIC1 (hypermethylated in cancer 1). J Biol Chem 2009;284: 20927–35.
14. Gerbe F, van Es JH, Makrini L, Brulin B, Mellitzer G, Robine S, et al. Distinct ATOH1 and Neurog3 requirements define tuft cells as a new secretory cell type in the intestinal epithelium. J Cell Biol 2011;192: 767–80.
15. Pospichalova V, Tureckova J, Fafilek B, Vojtechova M, Krausova M, Lukas J, et al. Generation of two modified mouse alleles of the Hic1 tumor suppressor gene. Genesis 2011;49:142–51.
16. Kim S, Karin M. Role of TLR2-dependent inflammation in metastatic progression. Ann N Y Acad Sci 2011;1217:191–206.
17. Tye H, Kennedy CL, Najdovska M, McLeod L, McCormack W, Hughes N, et al. STAT3-driven upregulation of TLR2 promotes gastric tumorigenesis independent of tumor inflammation. Cancer Cell 2012;22:466–78.
18. Campana L, Bosurgi L, Rovere-Querini P. HMGB1: a two-headed signal regulating tumor progression and immunity. Curr Opin Immunol 2008; 20:518–23.
19. Scheeren FA, Kuo AH, van Weele LJ, Cai S, Glykofridis I, Sikandar SS, et al. A cell-intrinsic role for TLR2-MYD88 in intestinal and breast epithelia and oncogenesis. Nat Cell Biol 2014;16:1238–48.

Downloaded from mcr.aacrjournals.org on February 27, 2016. © 2015 American Association for Cancer Research.

Published OnlineFirst May 1, 2015; DOI: 10.1158/1541-7786.MCR-15-0033

20. el Marjou F, Janssen KP, Chang BH, Li M, Hindie V, Chan L, et al. Tissue-specific and inducible Cre-mediated recombination in the gut epithelium. Genesis 2004;39:186–93.
21. Sato T, Vries RG, Snippert HJ, van de Wetering M, Barker N, Stange DE, et al. Single Lgr5 stem cells build crypt-villus structures *in vitro* without a mesenchymal niche. Nature 2009;459:262–5.
22. Willert K, Brown JD, Danenberg E, Duncan AW, Weissman IL, Reya T, et al. Wnt proteins are lipid-modified and can act as stem cell growth factors. Nature 2003;423:448–52.
23. Melenovsky V, Benes J, Skaroupkova P, Sedmera D, Strnad H, Kolar M, et al. Metabolic characterization of volume overload heart failure due to aorto-caval fistula in rats. Mol Cell Biochem 2011; 354:83–96.
24. Chen EY, Tan CM, Kou Y, Duan Q, Wang Z, Meirelles GV, et al. Enrichr: interactive and collaborative HTML5 gene list enrichment analysis tool. BMC Bioinformatics 2013;14:128.
25. Dubuissez M, Faiderbe P, Pinte S, Dehennaut V, Rood BR, Leprince D. The Reelin receptors ApoER2 and VLDLR are direct target genes of HIC1 (Hypermethylated In Cancer 1). Biochem Biophys Res Commun 2013; 440:424–30.
26. Fafilek B, Krausova M, Vojtechova M, Pospichalova V, Tumova L, Sloncova E, et al. Troy, a tumor necrosis factor receptor family member, interacts with lgr5 to inhibit wnt signaling in intestinal stem cells. Gastroenterology 2013;144:381–91.
27. Waaler J, Machon O, Tumova L, Dinh H, Korinek V, Wilson SR, et al. A novel tankyrase inhibitor decreases canonical Wnt signaling in colon carcinoma cells and reduces tumor growth in conditional APC mutant mice. Cancer Res 2012;72:2822–32.
28. Doubravska L, Krausova M, Gradl D, Vojtechova M, Tumova L, Lukas J, et al. Fatty acid modification of Wnt1 and Wnt3a at serine is prerequisite for lipidation at cysteine and is essential for Wnt signalling. Cell Signal 2011;23:837–48.
29. Lukas J, Mazna P, Valenta T, Doubravska L, Pospichalova V, Vojtechova M, et al. Dazap2 modulates transcription driven by the Wnt effector TCF-4. Nucleic Acids Res 2009;37:3007–20.
30. Kerr MK. Linear models for microarray data analysis: hidden similarities and differences. J Comput Biol 2003;10:891–901.
31. Ventura A, Kirsch DG, McLaughlin ME, Tuveson DA, Grimm J, Lintault L, et al. Restoration of p53 function leads to tumour regression *in vivo*. Nature 2007;445:661–5.
32. Indra AK, Warot X, Brocard J, Bornert JM, Xiao JH, Chambon P, et al. Temporally-controlled site-specific mutagenesis in the basal layer of the epidermis: comparison of the recombinase activity of the tamoxifen-inducible Cre-ER(T) and Cre-ER(T2) recombinases. Nucleic Acids Res 1999;27:4324–7.
33. Dehennaut V, Loison I, Boulay G, Van Rechem C, Leprince D. Identification of p21 (CIP1/WAF1) as a direct target gene of HIC1 (Hypermethylated In Cancer 1). Biochem Biophys Res Commun 2013;430: 49–53.
34. Slattery ML, Herrick JS, Bondurant KL, Wolff RK. Toll-like receptor genes and their association with colon and rectal cancer development and prognosis. Int J Cancer 2012;130:2974–80.
35. Matsuda A, Suzuki Y, Honda G, Muramatsu S, Matsuzaki O, Nagano Y, et al. Large-scale identification and characterization of human genes that activate NF-kappaB and MAPK signaling pathways. Oncogene 2003; 22:3307–18.
36. Aliprantis AO, Yang RB, Mark MR, Suggett S, Devaux B, Radolf JD, et al. Cell activation and apoptosis by bacterial lipoproteins through toll-like receptor-2. Science 1999;285:736–9.
37. Takeuchi O, Kaufmann A, Grote K, Kawai T, Hoshino K, Morr M, et al. Cutting edge: preferentially the R-stereoisomer of the mycoplasmal lipopeptide macrophage-activating lipopeptide-2 activates immune cells through a toll-like receptor 2- and MyD88-dependent signaling pathway. J Immunol 2000;164:554–7.
38. Faure E, Thomas L, Xu H, Medvedev A, Equils O, Arditi M. Bacterial lipopolysaccharide and IFN-gamma induce Toll-like receptor 2 and Toll-like receptor 4 expression in human endothelial cells: role of NF-kappa B activation. J Immunol 2001;166:2018–24.
39. Mohammad HP, Zhang W, Prevas HS, Leadem BR, Zhang M, Herman JG, et al. Loss of a single Hic1 allele accelerates polyp formation in Apc (Delta716) mice. Oncogene 2011;30:2659–69.
40. Grivennikov SI, Karin M. Dangerous liaisons: STAT3 and NF-kappaB collaboration and crosstalk in cancer. Cytokine Growth Factor Rev 2010; 21:11–9.
41. Hausmann M, Kiessling S, Mestermann S, Webb G, Spottl T, Andus T, et al. Toll-like receptors 2 and 4 are up-regulated during intestinal inflammation. Gastroenterology 2002;122:1987–2000.
42. Frolova L, Drastich P, Rossmann P, Klimesova K, Tlaskalova-Hogenova H. Expression of Toll-like receptor 2 (TLR2), TLR4, and CD14 in biopsy samples of patients with inflammatory bowel diseases: upregulated expression of TLR2 in terminal ileum of patients with ulcerative colitis. J Histochem Cytochem 2008;56:267–74.
43. Maeda S, Hikiba Y, Sakamoto K, Nakagawa H, Hirata Y, Hayakawa Y, et al. Colon cancer-derived factors activate NF-kappaB in myeloid cells via TLR2 to link inflammation and tumorigenesis. Mol Med Rep 2011; 4:1083–8.
44. Rakoff-Nahoum S, Medzhitov R. Regulation of spontaneous intestinal tumorigenesis through the adaptor protein MyD88. Science 2007;317: 124–7.
45. el-Deiry WS, Tokino T, Velculescu VE, Levy DB, Parsons R, Trent JM, et al. WAF1, a potential mediator of p53 tumor suppression. Cell 1993;75:817–25.
46. Britschgi C, Rizzi M, Grob TJ, Tschan MP, Hugli B, Reddy VA, et al. Identification of the p53 family-responsive element in the promoter region of the tumor suppressor gene hypermethylated in cancer 1. Oncogene 2006;25:2030–9.
47. Abbas T, Dutta A. p21 in cancer: intricate networks and multiple activities. Nat Rev Cancer 2009;9:400–14.

Downloaded from mcr.aacrjournals.org on February 27, 2016. © 2015 American Association for Cancer Research.

Published OnlineFirst May 1, 2015; DOI: 10.1158/1541-7786.MCR-15-0033

AACR American Association for Cancer Research

Molecular Cancer Research

HIC1 Tumor Suppressor Loss Potentiates TLR2/NF-κB Signaling and Promotes Tissue Damage–Associated Tumorigenesis

Lucie Janeckova, Vendula Pospichalova, Bohumil Fafilek, et al.

Mol Cancer Res 2015;13:1139-1148. Published OnlineFirst May 1, 2015.

Updated version	Access the most recent version of this article at: doi:10.1158/1541-7786.MCR-15-0033
Supplementary Material	Access the most recent supplemental material at: http://mcr.aacrjournals.org/content/suppl/2015/05/02/1541-7786.MCR-15-0033.DC1.html

Cited articles	This article cites 47 articles, 15 of which you can access for free at: http://mcr.aacrjournals.org/content/13/7/1139.full.html#ref-list-1

E-mail alerts	Sign up to receive free email-alerts related to this article or journal.
Reprints and Subscriptions	To order reprints of this article or to subscribe to the journal, contact the AACR Publications Department at pubs@aacr.org.
Permissions	To request permission to re-use all or part of this article, contact the AACR Publications Department at permissions@aacr.org.

Downloaded from mcr.aacrjournals.org on February 27, 2016. © 2015 American Association for Cancer Research.

Supplementary Material

Supplementary Material and Methods

MEFs preparation and electroporation

Dissected embryos were washed in cold PBS, head and entrails (heart, liver) were excised and used for genotyping. The remaining embryonic tissues were sliced, incubated in Trypsin/EDTA solution (15 min at 37°C; Sigma), further dissociated and cultured in Iscove's Modified Dulbecco's Medium [(IMDM); purchased from Sigma)] supplemented with 10% fetal bovine serum (FBS), penicillin/streptomycin (100 UI), 2 mM L-glutamine and 1× non-essential amino acids (all chemicals were from Gibco). Cells were electroporated in buffer (125 mM KCl, 15 mM NaCl, 3 mM glucose, 25 mM Hepes pH 7.4, 1.2 mM MgCl2) supplemented with 0.66 % (w/v) ethylene glycol (PEG) 4000 in 4 mm gap cuvettes using an ECM 830 electroporator (BTX; settings: 240V, 30 ms).

Luciferase assay and NF-kB pathway activation

The luciferase assay was performed according to the supplier's protocol using Dual-Glo Luciferase Assay System (Promega). To activate the NF-κB pathway, cells were stimulated overnight with 20 ng/ml TNFα (stock 100 μg/ml; Peprotech), 20 ng/ml lymphotoxin α (LTα; stock 10 μg/ml; Invivogen) or 100 ng/ml Pam3csk4 (stock 100 μg/ml, Invivogen).

PCR primers used for ddPCR

The first primer is in forward and the second primer in reverse orientation:

β-ACTIN, 5'- CTAGGCGGACTATGAC-3', 5'- GACTTGGGAGAGGACT-3';

SIRT1, 5'- CTCCAGGCAGATGCCATAAC-3', 5'- TGCCCTTGGTTAAAATTTGG-3';

TLR2, 5'- CCTCCAATCAGGCTTCTCTG-3', 5'- TGGAGGTTCACACACCTCTG-3'.

Antibodies used for IHC and Western blotting

IHC: anti-β-catenin (mouse monoclonal, EM-22, Exbio), anti-chromogranin A (rabbit polyclonal, ab15160, Abcam), anti-lysozyme (rabbit polyclonal, A0099, Dako), anti-p21 (mouse monoclonal, SXM30, BD Pharmingen), anti-p53 (rabbit polyclonal, NCL-p53-CM5p, Novocastra), anti-PCNA (rabbit polyclonal, ab18197, Abcam), anti-Tlr2 (goat polyclonal, sc-16237, Santa Cruz). The activity of brush border enzyme alkaline phosphatase was visualized using Alkaline Phosphatase Magenta™ IHC Substrate Solution (Sigma). Goblet cells were stained with Periodic acid Schiff kit (Hotchkiss-McManus) purchased from DiaPath. Western blotting: anti-α-tubulin (mouse monoclonal, TU-01, Exbio), anti-CtBP (mouse monoclonal, sc-17759, Santa Cruz), anti-p21 (mouse monoclonal, SXM30, BD Pharmingen), anti-p53 (rabbit polyclonal, NCL-p53-CM5p, Novocastra), anti-p65 (rabbit monoclonal, #8242, Cell Signalling), anti-phospho-p65 (detecting phosphorylated Ser536; rabbit monoclonal, #3033, Cell Signaling), anti-Tlr2 (rabbit monoclonal, E1J2W, Cell Signalling).

Supplementary Figure and Table Legends

Supplementary Figure S1. Heatmaps depicting gene expression in *Hic1*$^{flox/flox}$ MEFs treated with 4-OHT when compared to MEFs treated with vehicle (ethanol) only. Genes (299 in total) displaying significantly ($q < 0.05$) changed expression in at least one of the indicated time points are listed. The position of *Hic1* and six genes whose expression was changed more than twice ($|\log FC| > 1$) in at least two time points is highlighted.

Supplementary Figure S2. Loss of Hic1 results in increased counts of goblet and enteroendocrine cells. A,B, goblet (A) and enteroendocrine (B) cell distribution in the indicated segments of the small intestine. Specimens obtained from four *Hic1*$^{flox/flox}$ and four *Hic1*$^{flox/flox}$ *Villin-Cre*$^{+}$ mice were stained using Periodic acid Schiff (PAS) and an anti-chromogranin A antibody to visualize goblet and enteroendocrine cells, respectively. Stained cells (indicated by black arrowheads in the histology images on the right) were in several different fields indicated by numbers on the X axis. C, no changes in enterocytes were noted in the Hic1-deficient small intestine. Left, qRT-PCR analysis of enterocyte-specific markers hairy and enhancer of split-1 (Hes1) and sucrase-isomaltase (SI). The expression level of the respective gene in wt mice (upon normalization to *Ubb*) was arbitrarily set to 1. Right, staining of brush border enzyme alkaline phosphatase (AP) produced by differentiated enterocytes in the small intestine. Scale bar: 0.15 mm; error bars: SDs.

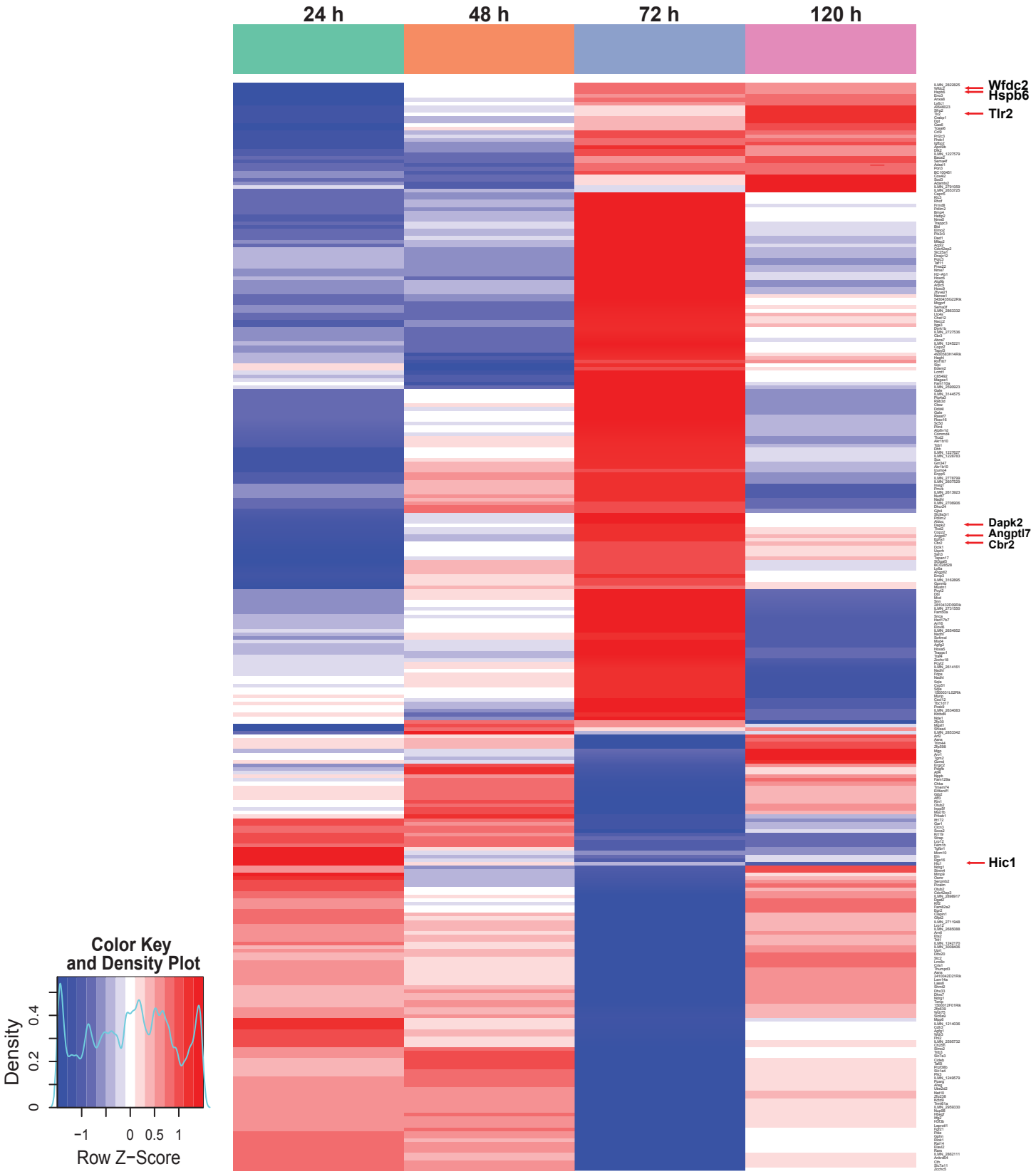
Supplementary Figure S3. DSS-induced transcriptional response in the colon of *Hic1*$^{flox/flox}$ and *Hic1*$^{flox/flox}$ *Villin-Cre*$^{+}$ mice six and nine days after DSS withdrawal. Epithelial lining of the colon obtained from four animals of each genotype was analyzed using qRT-PCR. The results were normalized to the Ubiquitin B (Ubb) housekeeping gene; the relative expression of another housekeeping gene, *β-actin*, is also shown. The expression level of the corresponding gene in mice without DSS treatment was arbitrarily set to 1. Error bars: SDs.

Supplementary Table S1 Primers used for qRT-PCR analysis

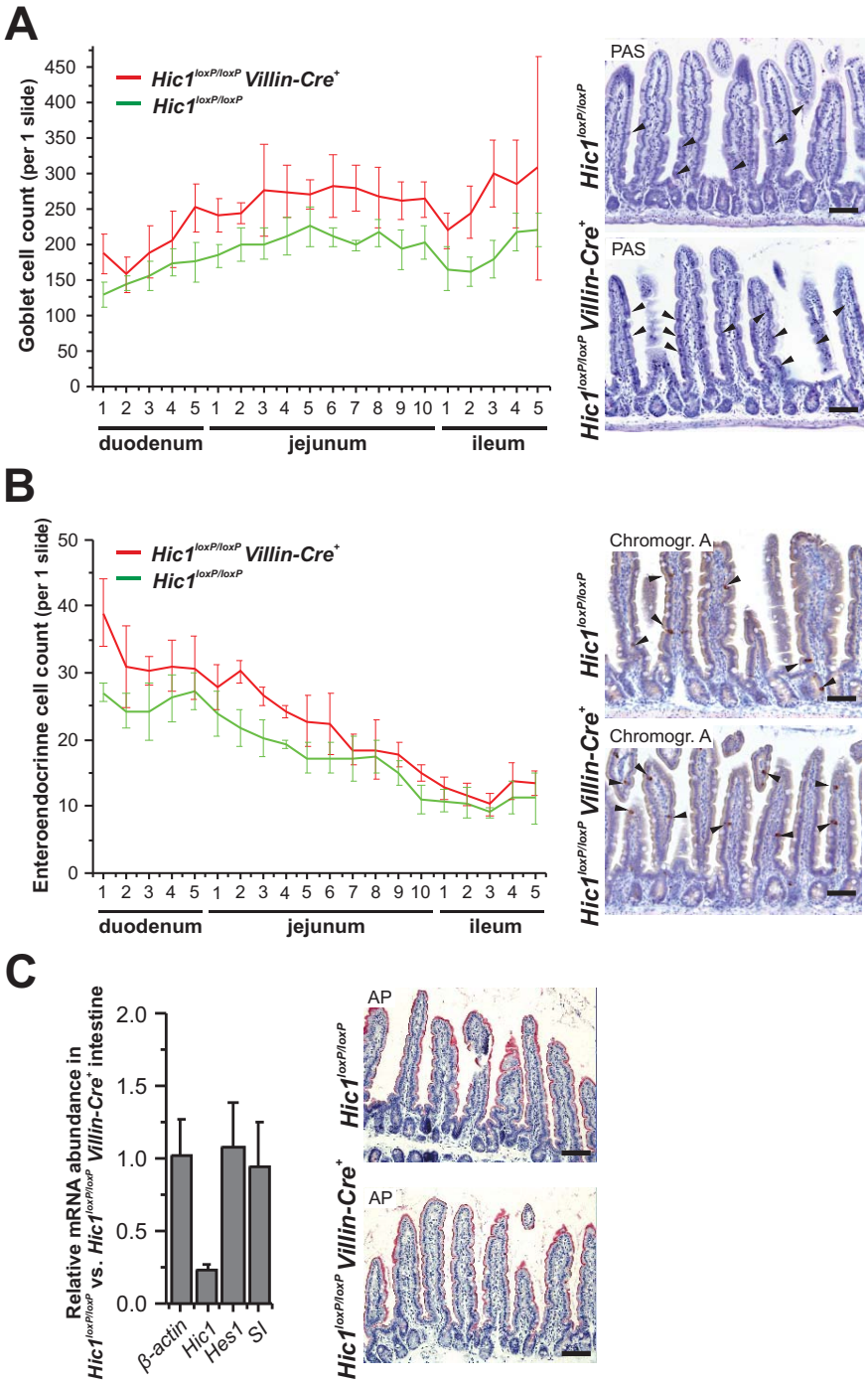
Supplementary Table S2. List of genes differentially expressed in *Hic1*$^{flox/flox}$ MEFs treated with 4-OHT for 48, 72, and 120 hours when compared to control MEFs treated (for the given time periods) with vehicle. Selection criterion: $q < 0.05$. Of note, none of the genes passed the selection criterion for the 24-hour time point.

Supplementary Table S3. The most different 'Gene Ontology Biological Processes' (GO BPs) and WikiPathways categories in expression profiles of *Hic1*$^{flox/flox}$ MEFs 72 hours after addition of 4-OHT when compared to MEFs treated with vehicle only. In total, 268 gene probes passed the significance criterion (q-value < 0.05). Corresponding annotated genes (listed in Supplementary Table S2) were analyzed using the GO BP and WikiPathways 2015 Enricher datasets. The results were sorted according to the p-value; GO BPs and WikiPathways with $p < 0.05$ are listed.

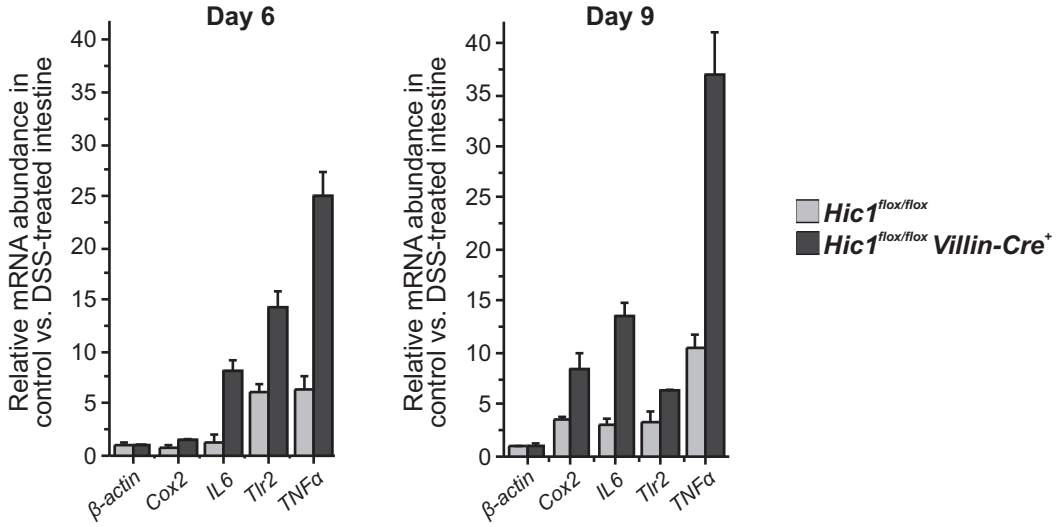
Supplementary Figure S1



Supplementary Figure S2



Supplementary Figure S3



Supplementary Table S1 Primers for qRT-PCR

Gene symbol	Organism	Sequence
Actb	Mouse	Forward: 5'-GATCTGGCACCACACCTTCT-3'
		Reverse: 5'-GGGGTGTTGAAGGTCTCAAA-3'
Atoh1	Mouse	Forward: 5'-GCTGTGCAAGCTGAAGGG-3'
		Reverse: 5'-TCTTGTCGTTGTTGAAGG-3'
Cox2	Mouse	Forward: 5'-CGGAGAGAGTTCATCCCTGA-3'
		Reverse: 5'-ACCTCTCCACCAATGACCTG-3'
Hic1	Mouse	Forward: 5'-GAGGCTGCTGAGGTGGCTGC-3'
		Reverse: 5'-CTCTTGTCGCAGGACGCGCA-3'
Hes1	Mouse	Forward: 5'-GCTCACTTCGGACTCCATGTG-3'
		Reverse: 5'-GCTAGGGACTTTACGGGTAGCA-3'
IL6	Mouse	Forward: 5'-GATGGATGCTACCAAACTGGA-3'
		Reverse: 5'-GGAAATTGGGGTAGGAAGGA-3'
SI	Mouse	Forward: 5'-TTCAAGAAATCACAACATTCAATTTACCTAG-3'
		Reverse: 5'-CTAAAACTTTCTTTGACATTTGAGCAA-3'
Sirt1	Mouse	Forward: 5'-CGGAGGGCCAGAGAGGCAGT-3'
		Reverse: 5'-CTCTTGCGGAGCGGCTCGTC-3'
Sox9	Mouse	Forward: 5'-GTGGCCCCGGTTTCGTTCTCTGT-3'
		Reverse: 5'-CGGCTCTAAACCCGGGGAAGG-3'
Tlr2	Mouse	Forward: 5'-GTTCATCTCTGGAGCATCCG -3'
		Reverse: 5'-ACTCCTGAGCAGAACAGCGT-3'
TNFα	Mouse	Forward: 5'-TCGTAGCAAACCACCAAGTG-3'
		Reverse: 5'- AGATAGCAAATCGGCTGACG-3'
Ubb	Mouse	Forward: 5'-ATGTGAAGGCCAAGATCCAG-3'
		Reverse: 5'-TAATAGCCACCCCTCAGACG-3'

Supplementary Table S2

Genes differentialy expressed in *Hic1*$^{flox/flox}$ MEFs treated with 4-OHT for 48 hours when compared to MEFs treated with vehicle

ENTREZ No.	Symbol	Gene name	log FC	q value
15248	Hic1	hypermethylated in cancer 1	-3.23	0.00039
243912	Hspb6	heat shock protein, alpha-crystallin-related, B6	1.26	0.023
56615	Mgst1	microsomal glutathione S-transferase 1	0.99	0.047

Genes differentialy expressed in *Hic1*$^{flox/flox}$ MEFs treated with 4-OHT for 72 hours when compared to MEFs treated with vehicle

ENTREZ No.	Symbol	Gene name	log FC	q value
27403	Abca7	ATP-binding cassette, sub-family A (ABC1), member 7	0.67	0.038
235534	Acpl2	acid phosphatase-like 2	0.94	0.044
11565	Adssl1	adenylosuccinate synthetase like 1	0.94	0.0033
15463	Agfg1	ArfGAP with FG repeats 1	-0.72	0.019
231801	Agfg2	ArfGAP with FG repeats 2	0.89	0.039
192734	AI646023	expressed sequence AI646023	1	0.027
67861	Akr1b10	aldo-keto reductase family 1, member B10 (aldose reductase)	0.79	0.018
11676	Aldoc	aldolase C, fructose-bisphosphate	1.67	0.0071
26360	Angptl2	angiopoietin-like 2	0.62	0.043
654812	Angptl7	angiopoietin-like 7	2.51	0.013
223690	Ankrd54	ankyrin repeat domain 54	-0.61	0.018
11752	Anxa8	annexin A8	1.12	0.044
71770	Ap2b1	adaptor-related protein complex 2, beta 1 subunit	-0.51	0.046
71898	Apol9b	apolipoprotein L 9b	1.39	0.041
11839	Areg	amphiregulin	-1.83	0.0013
11841	Arf2	ADP-ribosylation factor 2	-0.77	0.044
16801	Arhgef1	Rho guanine nucleotide exchange factor (GEF) 1	-0.92	0.048
70317	Arl16	ADP-ribosylation factor-like 16	0.63	0.038
11865	Arntl	aryl hydrocarbon receptor nuclear translocator-like	-1.39	0.021
67771	Arpc5	actin related protein 2/3 complex, subunit 5	0.58	0.025
68865	Arv1	ARV1 homolog (yeast)	-0.64	0.045
27053	Asns	asparagine synthetase	-0.85	0.019
11910	Atf3	activating transcription factor 3	-2.79	0.021
11911	Atf4	activating transcription factor 4	-0.93	0.021
213948	Atg9b	ATG9 autophagy related 9 homolog B (S. cerevisiae)	0.8	0.044
73834	Atp6v1d	ATPase, H+ transporting, lysosomal V1 subunit D	0.56	0.03
26362	Axl	AXL receptor tyrosine kinase	-0.56	0.047
56175	Bace2	beta-site APP-cleaving enzyme 2	0.88	0.029
12159	Bmp4	bone morphogenetic protein 4	1.35	0.0033
26363	Btd	biotinidase	0.82	0.025
215494	C85492	expressed sequence C85492	0.75	0.044
12337	Capn5	calpain 5	0.96	0.044
12409	Cbr2	carbonyl reductase 2	2.45	0.0013
109857	Cbr3	carbonyl reductase 3	1.3	0.021
20308	Ccl9	chemokine (C-C motif) ligand 9	1.27	0.021
104252	Cdc42ep2	CDC42 effector protein (Rho GTPase binding) 2	1.31	0.0056
260409	Cdc42ep3	CDC42 effector protein (Rho GTPase binding) 3	-0.7	0.042
12560	Cdh3	cadherin 3	-0.79	0.025
12642	Ch25h	cholesterol 25-hydroxylase	-1.63	0.016
12660	Chka	choline kinase alpha	-0.9	0.04
59031	Chst12	carbohydrate sulfotransferase 12	0.84	0.019
109006	Ciapin1	cytokine induced apoptosis inhibitor 1	-0.77	0.025
12684	Cideb	cell death-inducing DNA fragmentation factor, alpha subunit-like effector B	-0.49	0.046
12725	Clcn3	chloride channel 3	-0.9	0.031
66199	Commd4	COMM domain containing 4	0.66	0.04
56358	Copz2	coatomer protein complex, subunit zeta 2	0.52	0.021
84682	Cox4i2	cytochrome c oxidase subunit IV isoform 2	0.75	0.0084
12903	Crabp1	cellular retinoic acid binding protein I	1.01	0.028
171508	Creld1	cysteine-rich with EGF-like domains 1	0.68	0.048
66586	Crls1	cardiolipin synthase 1	-0.91	0.045
107869	Cth	cystathionase (cystathionine gamma-lyase)	-1.6	0.015
13041	Ctsw	cathepsin W	1.18	0.011
20315	Cxcl12	chemokine (C-X-C motif) ligand 12	0.91	0.024
13121	Cyp51	cytochrome P450, family 51	1.2	0.011
13135	Dad1	defender against cell death 1	0.71	0.017
13143	Dapk2	death-associated protein kinase 2	2.18	0.0015
13167	Dbi	diazepam binding inhibitor	0.86	0.021
13175	Dclk1	doublecortin-like kinase 1	0.72	0.043
73284	Ddit4l	DNA-damage-inducible transcript 4-like	1.2	0.011
53975	Ddx20	DEAD (Asp-Glu-Ala-Asp) box polypeptide 20	-0.6	0.043

67800	Dgat2	diacylglycerol O-acyltransferase 2	-0.8	0.034
74754	Dhcr24	24-dehydrocholesterol reductase	1.06	0.034
13363	Dhh	desert hedgehog	0.98	0.029
66375	Dhrs7	dehydrogenase/reductase (SDR family) member 7	-0.95	0.026
216877	Dhx33	DEAH (Asp-Glu-Ala-His) box polypeptide 33	-0.8	0.043
106565	Dlk2	delta-like 2 homolog (Drosophila)	1.54	0.008
30045	Dnajc12	DnaJ (Hsp40) homolog, subfamily C, member 12	0.74	0.043
13549	Dyrk1b	dual-specificity tyrosine-(Y)-phosphorylation regulated kinase 1b	1.2	0.029
108687	Edem2	ER degradation enhancer, mannosidase alpha-like 2	0.75	0.025
13654	Egr2	early growth response 2	-1.12	0.037
74203	Eif4enif1	eukaryotic translation initiation factor 4E nuclear import factor 1	-0.51	0.043
13690	Eif4g2	eukaryotic translation initiation factor 4, gamma 2	-0.84	0.047
15569	Elavl2	ELAV (embryonic lethal, abnormal vision, Drosophila)-like 2 (Hu antigen B)	-0.82	0.027
140579	Elmo2	engulfment and cell motility 2, ced-12 homolog (C. elegans)	0.79	0.018
13717	Eln	elastin	-0.67	0.043
170439	Elovl6	ELOVL family member 6, elongation of long chain fatty acids (yeast)	1.21	0.037
13732	Emp3	epithelial membrane protein 3	0.73	0.011
13808	Eno3	enolase 3, beta muscle	1.12	0.043
83965	Enpp5	ectonucleotide pyrophosphatase/phosphodiesterase 5	0.76	0.017
13849	Ephx1	epoxide hydrolase 1, microsomal	0.92	0.034
67456	Ergic2	ERGIC and golgi 2	-0.51	0.042
23872	Ets2	E26 avian leukemia oncogene 2, 3' domain	-1.56	0.0078
73847	Fam110a	family with sequence similarity 110, member A	0.71	0.031
63913	Fam129a	family with sequence similarity 129, member A	-0.86	0.033
108160	Fam50a	family with sequence similarity 50, member A	0.76	0.032
67809	Fam82a2	family with sequence similarity 82, member A2	-0.67	0.034
50759	Fbxo16	F-box protein 16	0.99	0.013
66822	Fbxo25	F-box protein 25	0.81	0.048
110196	Fdps	farnesyl diphosphate synthetase	1.54	0.019
14155	Fem1b	feminization 1 homolog b (C. elegans)	-0.57	0.045
56636	Fgf21	fibroblast growth factor 21	-1.71	0.038
229474	Fhdc1	FH2 domain containing 1	0.98	0.0033
14200	Fhl2	four and a half LIM domains 2	-1.04	0.025
14205	Figf	c-fos induced growth factor	0.69	0.049
67457	Frmd8	FERM domain containing 8	0.73	0.012
74246	Gale	galactose-4-epimerase, UDP	1.64	0.0051
68147	Gar1	GAR1 ribonucleoprotein homolog (yeast)	-0.71	0.025
14456	Gas6	growth arrest specific 6	0.82	0.019
14584	Gfpt2	glutamine fructose-6-phosphate transaminase 2	-0.77	0.031
14619	Gjb2	gap junction protein, beta 2	-1.28	0.021
14621	Gjb4	gap junction protein, beta 4	1.1	0.028
241289	Gm347	predicted gene 347	0.98	0.01
268566	Gphn	gephyrin	-0.67	0.046
93695	Gpnmb	glycoprotein (transmembrane) nmb	1.38	0.0094
14941	Gzmd	granzyme D	-1.02	0.043
14961	H2-Ab1	histocompatibility 2, class II antigen A, beta 1	0.84	0.018
15081	H3f3b	H3 histone, family 3B	-0.87	0.043
68977	Haghl	hydroxyacylglutathione hydrolase-like	0.83	0.035
15200	Hbegf	heparin-binding EGF-like growth factor	-1.29	0.017
56016	Hebp2	heme binding protein 2	0.58	0.034
15248	Hic1	hypermethylated in cancer 1	-3.92	6.90E-05
15361	Hmga1	high mobility group AT-hook 1	-0.6	0.049
15402	Hoxa5	homeobox A5	0.95	0.024
15425	Hoxc6	homeobox C6	0.81	0.016
15427	Hoxc9	homeobox C9	1.03	0.0082
15490	Hsd17b7	hydroxysteroid (17-beta) dehydrogenase 7	1.54	0.013
243912	Hspb6	heat shock protein, alpha-crystallin-related, B6	1.61	0.0013
15574	Hus1	Hus1 homolog (S. pombe)	-0.65	0.046
68572	Ict1	immature colon carcinoma transcript 1	0.79	0.047
67661	Ift172	intraflagellar transport 172 homolog (Chlamydomonas)	-0.73	0.043
16008	Igfbp2	insulin-like growth factor binding protein 2	0.8	0.037
101490	Inpp5f	inositol polyphosphate-5-phosphatase F	-0.91	0.017
231070	Insig1	insulin induced gene 1	1.33	0.041
101142	Itfg2	integrin alpha FG-GAP repeat containing 2	-1.15	0.015
16400	Itga3	integrin alpha 3	0.99	0.019
71564	Izumo4	IZUMO family member 4	0.62	0.045
72106	Jmjd8	jumonji domain containing 8	0.41	0.048
67136	Kbtbd4	kelch repeat and BTB (POZ) domain containing 4	0.67	0.044
105440	Kctd9	potassium channel tetramerisation domain containing 9	-0.61	0.038
16560	Kif1a	kinesin family member 1A	1.14	0.048
232943	Klc3	kinesin light chain 3	0.59	0.018
16598	Klf2	Kruppel-like factor 2 (lung)	-0.83	0.04
16669	Krt19	keratin 19	-1.08	0.026
241447	Lass6	LAG1 homolog, ceramide synthase 6	-1.13	0.028

30949	Lcmt1	leucine carboxyl methyltransferase 1	0.84	0.0094
68192	Leprotl1	leptin receptor overlapping transcript-like 1	-0.96	0.043
239393	Lrp12	low density lipoprotein-related protein 12	-0.69	0.028
100604	Lrrc8c	leucine rich repeat containing 8 family, member C	-0.85	0.025
67070	Lsm14a	LSM14 homolog A (SCD6, S. cerevisiae)	-0.74	0.016
17001	Ltc4s	leukotriene C4 synthase	0.81	0.018
110454	Ly6a	lymphocyte antigen 6 complex, locus A	1.05	0.019
17067	Ly6c1	lymphocyte antigen 6 complex, locus C1	1.11	0.041
107528	Magee1	melanoma antigen, family E, 1	0.83	0.026
26415	Mapk13	mitogen-activated protein kinase 13	0.73	0.048
70024	Mcm10	minichromosome maintenance deficient 10 (S. cerevisiae)	-0.58	0.025
210529	Mettl14	methyltransferase like 14	-0.98	0.048
17150	Mfap2	microfibrillar-associated protein 2	0.81	0.026
17313	Mgp	matrix Gla protein	-0.53	0.026
56615	Mgst1	microsomal glutathione S-transferase 1	0.73	0.017
17395	Mmp9	matrix metallopeptidase 9	-1.52	0.0045
17427	Mns1	meiosis-specific nuclear structural protein 1	1.1	0.047
56524	Mpp6	membrane protein, palmitoylated 6 (MAGUK p55 subfamily member 6)	-0.61	0.021
211577	Mrgprf	MAS-related GPR, member F	1.87	0.019
66175	Mustn1	musculoskeletal, embryonic nuclear protein 1	1.2	0.0051
192156	Mvd	mevalonate (diphospho) decarboxylase	1.91	0.0013
17122	Mxd4	Max dimerization protein 4	1.06	0.0033
17912	Myo1b	myosin IB	-0.87	0.045
245049	Myrip	myosin VIIA and Rab interacting protein	0.48	0.03
67991	Nacc2	nucleus accumbens associated 2, BEN and BTB (POZ) domain containing	1.32	0.0084
332397	Nanos1	nanos homolog 1 (Drosophila)	1.22	0.0033
98956	Nat10	N-acetyltransferase 10	-0.71	0.031
67203	Nde1	nuclear distribution gene E homolog 1 (A nidulans)	0.65	0.019
17988	Ndrg1	N-myc downstream regulated gene 1	-1.39	0.011
75533	Nme5	non-metastatic cells 5, protein expressed in (nucleoside-diphosphate kinase)	0.89	0.025
171567	Nme7	non-metastatic cells 7, protein expressed in (nucleoside-diphosphate kinase)	0.7	0.016
67963	Npc2	Niemann Pick type C2	0.58	0.046
18158	Nppb	natriuretic peptide type B	-1.21	0.0076
18194	Nsdhl	NAD(P) dependent steroid dehydrogenase-like	1.21	0.0084
67528	Nudt7	nudix (nucleoside diphosphate linked moiety X)-type motif 7	0.55	0.045
269966	Nup98	nucleoporin 98	-0.77	0.025
18414	Osmr	oncostatin M receptor	-0.84	0.036
68149	Otub2	OTU domain, ubiquitin aldehyde binding 2	-1.12	0.0082
100102	Pcsk9	proprotein convertase subtilisin/kexin type 9	1.07	0.018
68671	Pcyt2	phosphate cytidylyltransferase 2, ethanolamine	1.18	0.0033
18591	Pdgfb	platelet derived growth factor, B polypeptide	-0.51	0.043
213019	Pdlim2	PDZ and LIM domain 2	1.28	0.013
233489	Picalm	phosphatidylinositol binding clathrin assembly protein	-0.89	0.044
18710	Pik3r3	phosphatidylinositol 3 kinase, regulatory subunit, polypeptide 3 (p55)	0.96	0.016
57435	Plin4	perilipin 4	0.99	0.021
12795	Plk3	polo-like kinase 3 (Drosophila)	-1.03	0.019
68603	Pmvk	phosphomevalonate kinase	0.82	0.027
18973	Pole	polymerase (DNA directed), epsilon	-1.01	0.016
269823	Pon3	paraoxonase 3	0.54	0.043
19016	Pparg	peroxisome proliferator activated receptor gamma	-1.26	0.0071
17872	Ppp1r15a	protein phosphatase 1, regulatory (inhibitor) subunit 15A	-1.77	0.047
217430	Pqlc3	PQ loop repeat containing	0.85	0.0084
19079	Prkab1	protein kinase, AMP-activated, beta 1 non-catalytic subunit	-0.55	0.029
18812	Prl2c3	prolactin family 2, subfamily c, member 3	1.11	0.011
66921	Prpf38b	PRP38 pre-mRNA processing factor 38 (yeast) domain containing B	-1.2	0.019
70835	Prss22	protease, serine, 22	1.22	0.017
19245	Ptp4a3	protein tyrosine phosphatase 4a3	0.96	0.017
59038	Pxmp4	peroxisomal membrane protein 4	0.79	0.046
19340	Rab3d	RAB3D, member RAS oncogene family	1.13	0.021
75646	Rai14	retinoic acid induced 14	-0.81	0.046
104458	Rars	arginyl-tRNA synthetase	-1.08	0.043
66985	Rassf7	Ras association (RalGDS/AF-6) domain family (N-terminal) member 7	1.13	0.031
19734	Rgs16	regulator of G-protein signaling 16	-1.12	0.037
23912	Rhof	ras homolog gene family, member f	1.05	0.043
225870	Rin1	Ras and Rab interactor 1	-0.83	0.0094
71340	Riok1	RIO kinase 1 (yeast)	-0.66	0.041
70510	Rnf167	ring finger protein 167	0.63	0.023
66234	Sc4mol	sterol-C4-methyl oxidase-like	1.15	0.029
235293	Sc5d	sterol-C5-desaturase (fungal ERG3, delta-5-desaturase) homolog (S. cerevisae)	0.88	0.028
20289	Scx	scleraxis	1.26	0.043
231452	Sdad1	SDA1 domain containing 1	-0.96	0.049
20350	Sema3f	sema domain, immunoglobulin domain (Ig), short basic domain, secreted, (semaphorin) 3F	1.05	0.044
20355	Sema4f	sema domain, immunoglobulin domain (Ig), TM domain, and short cytoplasmic domain	0.9	0.029

18788	Serpinb2	serine (or cysteine) peptidase inhibitor, clade B, member 2	-0.93	0.035
77552	Shisa4	shisa homolog 4 (Xenopus laevis)	0.46	0.038
108037	Shmt2	serine hydroxymethyltransferase 2 (mitochondrial)	-0.84	0.044
98365	Slamf9	SLAM family member 9	-1.35	0.046
55963	Slc1a4	solute carrier family 1 (glutamate/neutral amino acid transporter), member 4	-1.15	0.0084
13358	Slc25a1	solute carrier family 25 (mitochondrial carrier, citrate transporter), member 1	0.83	0.021
14664	Slc6a9	solute carrier family 6 (neurotransmitter transporter, glycine), member 9	-1.62	0.0033
26570	Slc7a11	solute carrier family 7 (cationic amino acid transporter, y+ system), member 11	-1.87	0.026
11989	Slc7a3	solute carrier family 7 (cationic amino acid transporter, y+ system), member 3	-1.6	0.018
224022	Slc7a4	solute carrier family 7 (cationic amino acid transporter, y+ system), member 4	0.66	0.049
26941	Slc9a3r1	solute carrier family 9 (sodium/hydrogen exchanger), member 3 regulator 1	1.4	0.036
66390	Slmo2	slowmo homolog 2 (Drosophila)	-0.54	0.043
20568	Slpi	secretory leukocyte peptidase inhibitor	0.72	0.043
20617	Snca	synuclein, alpha	1.15	0.025
20621	Snn	stannin	0.76	0.043
216233	Socs2	suppressor of cytokine signaling 2	-1.65	0.015
20775	Sqle	squalene epoxidase	1.33	0.0084
245857	Ssh3	slingshot homolog 3 (Drosophila)	0.71	0.03
20454	St3gal5	ST3 beta-galactoside alpha-2,3-sialyltransferase 5	1	0.0084
76630	Stambpl1	STAM binding protein like 1	-1.15	0.049
20856	Stc2	stanniocalcin 2	-1.26	0.026
56471	Stmn4	stathmin-like 4	-0.64	0.0085
20901	Strap	serine/threonine kinase receptor associated protein	-0.5	0.038
68776	Taf11	TAF11 RNA polymerase II, TATA box binding protein (TBP)-associated factor	0.71	0.046
102162	Taf5l	TAF5-like RNA polymerase II, p300/CBP-associated factor (PCAF)-associated factor	-1.03	0.0094
233204	Tbc1d17	TBC1 domain family, member 17	0.42	0.039
66104	Tceal6	transcription elongation factor A (SII)-like 6	0.56	0.029
21812	Tgfbr1	transforming growth factor, beta receptor I	-0.67	0.044
21817	Tgm2	transglutaminase 2, C polypeptide	-0.59	0.028
14911	Thumpd3	THUMP domain containing 3	-0.86	0.023
380712	Tlcd2	TLC domain containing 2	1.14	0.0033
24086	Tlk2	tousled-like kinase 2 (Arabidopsis)	-0.84	0.049
24088	Tlr2	toll-like receptor 2	1.27	0.019
66990	Tmem134	transmembrane protein 134	0.63	0.047
239408	Tmem74	transmembrane protein 74	-0.89	0.028
22057	Tob1	transducer of ErbB-2.1	1.04	0.044
22032	Traf4	TNF receptor associated factor 4	0.56	0.028
245828	Trappc1	trafficking protein particle complex 1	0.72	0.039
27096	Trappc3	trafficking protein particle complex 3	0.84	0.019
228775	Trib3	tribbles homolog 3 (Drosophila)	-1.15	0.035
80985	Trim44	tripartite motif-containing 44	-0.4	0.037
66966	Trit1	tRNA isopentenyltransferase 1	-0.66	0.031
328162	Trmt61a	tRNA methyltransferase 61 homolog A (S. cerevisiae)	-1.02	0.035
74257	Tspan17	tetraspanin 17	0.89	0.021
241732	Tspyl3	TSPY-like 3	0.78	0.029
56338	Txnip	thioredoxin interacting protein	-1.34	0.0014
56550	Ube2d2	ubiquitin-conjugating enzyme E2D 2	-0.72	0.033
21429	Ubtf	upstream binding transcription factor, RNA polymerase I	-0.5	0.047
331487	Uprt	uracil phosphoribosyltransferase (FUR1) homolog (S. cerevisiae)	-0.62	0.021
66576	Uqcrh	ubiquinol-cytochrome c reductase hinge protein	0.72	0.038
22359	Vldlr	very low density lipoprotein receptor	-0.85	0.047
269470	Wdr3	WD repeat domain 3	-0.68	0.037
73674	Wdr75	WD repeat domain 75	-1.2	0.014
67701	Wfdc2	WAP four-disulfide core domain 2	1.85	0.0084
170750	Xpnpep1	X-prolyl aminopeptidase (aminopeptidase P) 1, soluble	0.62	0.047
66995	Zcchc18	zinc finger, CCHC domain containing 18	0.79	0.043
213436	Zcchc5	zinc finger, CCHC domain containing 5	-2.12	0.026
30928	Zfp238	zinc finger protein 238	-1.11	0.029
213753	Zfp598	zinc finger protein 598	-1.08	0.034
67778	Zfp639	zinc finger protein 639	-0.88	0.018
68520	Zfyve21	zinc finger, FYVE domain containing 21	0.75	0.015

Genes differentialy expressed in *Hic1*$^{flox/flox}$ MEFs treated with 4-OHT for 120 hours when compared to MEFs treated with vehicle

ENTREZ No.	Symbol	Gene name	log FC	q value
216725	Adamts2	a disintegrin-like and metallopeptidase (reprolysin type) with thrombospondin type 1 motif, 2	1.25	0.028
11565	Adssl1	adenylosuccinate synthetase like 1	0.92	0.0093
56175	Bace2	beta-site APP-cleaving enzyme 2	1.1	0.039
12409	Cbr2	carbonyl reductase 2	1.8	0.013
84682	Cox4i2	cytochrome c oxidase subunit IV isoform 2	1.54	0.00031
12903	Crabp1	cellular retinoic acid binding protein I	1.51	0.018
106565	Dlk2	delta-like 2 homolog (Drosophila)	1.24	0.039

56429	Dpt	dermatopontin	1.17	0.028
229474	Fhdc1	FH2 domain containing 1	1.01	0.0071
14456	Gas6	growth arrest specific 6	1.05	0.02
15248	Hic1	hypermethylated in cancer 1	-4.64	1.20E-05
243912	Hspb6	heat shock protein, alpha-crystallin-related, B6	1.59	0.0015
66175	Mustn1	musculoskeletal, embryonic nuclear protein 1	0.89	0.039
18812	Prl2c3	prolactin family 2, subfamily c, member 3	0.97	0.047
20355	Sema4f	sema domain, immunoglobulin domain (Ig), TM domain, and short cytoplasmic domain	1.07	0.047
20319	Sfrp2	secreted frizzled-related protein 2	1.33	0.032
77552	Shisa4	shisa homolog 4 (Xenopus laevis)	0.62	0.039
20657	Sod3	superoxide dismutase 3, extracellular	1.08	0.039
66104	Tceal6	transcription elongation factor A (SII)-like 6	0.84	0.018
24088	Tlr2	toll-like receptor 2	1.53	0.028
67701	Wfdc2	WAP four-disulfide core domain 2	1.68	0.029
22693	Zfp30	zinc finger protein 30	-0.63	0.047

Supplementary Table S3

The most significantly changed Gene Ontology Biological Processes (GO BPs) in expression profiles of *Hic1*$^{flox/flox}$ MEFs 72 hours after addition of 4-OHT when compared to MEFs treated with vehicle only

GO BP term	p-value	Gene symbol
sterol biosynthetic process (GO:0016126)	1.10041E-09	FDPS;SQLE;CH25H;NSDHL;INSIG1;PMVK;SC5D;DHCR24;MVD;HSD17B7
cholesterol biosynthetic process (GO:0006695)	6.05213E-09	FDPS;SQLE;NSDHL;INSIG1;PMVK;SC5D;DHCR24;MVD;HSD17B7
cholesterol metabolic process (GO:0008203)	1.16244E-08	FDPS;INSIG1;PCSK9;DHCR24;VLDLR;HSD17B7;SQLE;CH25H;NSDHL;NPC2;PMVK;SC5D;MVD
sterol metabolic process (GO:0016125)	3.6955E-08	FDPS;INSIG1;PCSK9;DHCR24;VLDLR;HSD17B7;SQLE;CH25H;NSDHL;NPC2;PMVK;SC5D;MVD
alcohol biosynthetic process (GO:0046165)	5.72469E-07	FDPS;SQLE;CH25H;NSDHL;CHKA;INSIG1;PMVK;SC5D;DHCR24;MVD;HSD17B7
steroid metabolic process (GO:0008202)	2.79234E-06	FDPS;INSIG1;PCSK9;DHCR24;VLDLR;HSD17B7;SQLE;CH25H;ARV1;NSDHL;AKR1B10;NPC2;PMVK;SC5D;MVD
small molecule biosynthetic process (GO:0044283)	5.0268E-06	FDPS;CHKA;SHMT2;INSIG1;HAGHL;ASNS;ELOVL6;DHCR24;HSD17B7;LTC4S;PRKAB1;SQLE;CH25H;NSDHL;CHST12;CTH;PMVK;S
steroid biosynthetic process (GO:0006694)	5.68446E-06	FDPS;SQLE;CH25H;NSDHL;INSIG1;PMVK;SC5D;DHCR24;MVD;HSD17B7
organic hydroxy compound biosynthetic process (GO:1901617)	7.19194E-06	FDPS;SQLE;CH25H;NSDHL;CHKA;INSIG1;PMVK;SC5D;DHCR24;MVD;HSD17B7;SNCA
alcohol metabolic process (GO:0006066)	1.03213E-05	FDPS;DGAT2;CHKA;INSIG1;PCSK9;DBI;DHCR24;VLDLR;HSD17B7;SQLE;CH25H;NSDHL;AKR1B10;NPC2;PMVK;SC5D;MVD
lipid biosynthetic process (GO:0008610)	2.9994E-05	SLC25A1;FDPS;DGAT2;PCYT2;CHKA;INSIG1;PIK3R3;ELOVL6;DHCR24;HSD17B7;LTC4S;CRLS1;PRKAB1;SQLE;CH25H;NSDHL;PMVK;ST3G
organic hydroxy compound metabolic process (GO:1901615)	6.20635E-05	FDPS;DGAT2;CHKA;INSIG1;PCSK9;DBI;DHCR24;VLDLR;HSD17B7;SQLE;CH25H;ARV1;NSDHL;AKR1B10;NPC2;PMVK;SC5D;MVD
acyl-CoA metabolic process (GO:0006637)	0.000303496	SLC25A1;NUDT7;DGAT2;PMVK;ELOVL6;MVD
thioester metabolic process (GO:0035383)	0.000303496	SLC25A1;NUDT7;DGAT2;PMVK;ELOVL6;MVD
response to oxidative stress (GO:0006979)	0.000323818	PLK3;MGST1;DHCR24;SLC7A11;AREG;KLF2;ARNTL;ANGPTL7;AXL;STC2;TXNIP;SNCA;ATF4
respiratory tube development (GO:0030323)	0.000401715	BMP4;TRAF4;HOXA5
response to peptide (GO:1901652)	0.000466726	EGR2;PDGFB;PCSK9;PIK3R3;AREG;PRKAB1;KLF2;SOCS2;CXCL12;STC2;TRIB3;PPARG;UPRT;ATP6V1D;TLR2
ER-nucleus signaling pathway (GO:0006984)	0.000514598	PPP1R15A;CTH;INSIG1;STC2;ASNS;ATF3;ATF4
neutral lipid metabolic process (GO:0006638)	0.000514598	SLC25A1;DGAT2;INSIG1;PCSK9;DBI;ELOVL6;SNCA
negative regulation of glycoprotein biosynthetic process (GO:0010561)	0.000682158	BACE2;ABCA7;HBEGF
gluconeogenesis (GO:0006094)	0.000689142	SLC25A1;ALDOC;ENO3;ATF3;ATF4
amino acid transmembrane transport (GO:0003333)	0.000689142	SLC7A4;SLC6A9;SLC1A4;SLC7A11;SLC7A3
renal system process (GO:0003014)	0.00069807	NPPB;BMP4;SLC9A3R1;ITGA3;PDGFB;GAS6
phagocytosis (GO:0006909)	0.000823217	AXL;ELMO2;ABCA7;GAS6;TGM2
response to peptide hormone (GO:0043434)	0.000832563	EGR2;PDGFB;PCSK9;PIK3R3;AREG;PRKAB1;SOCS2;CXCL12;STC2;TRIB3;PPARG;UPRT;ATP6V1D;TLR2
hexose biosynthetic process (GO:0019319)	0.000975835	SLC25A1;ALDOC;ENO3;ATF3;ATF4
phospholipid metabolic process (GO:0006644)	0.001012647	FDPS;DGAT2;PCYT2;INPP5F;CHKA;PMVK;PCSK9;PIK3R3;DBI;MVD;CRLS1;SNCA
organ regeneration (GO:0031100)	0.001059576	CXCL12;AXL;PPARG;ALDOC;GAS6
cofactor metabolic process (GO:0051186)	0.001252172	SLC25A1;NUDT7;DGAT2;AKR1B10;BTD;SHMT2;PMVK;ELOVL6;MVD;GPHN;CBR3
negative regulation of glycoprotein metabolic process (GO:1903019)	0.001295255	BACE2;ABCA7;HBEGF
response to endoplasmic reticulum stress (GO:0034976)	0.001342081	PPP1R15A;CTH;STC2;FAM129A;ASNS;TRIB3;ATF3;ATF4
endoplasmic reticulum unfolded protein response (GO:0030968)	0.001491441	PPP1R15A;CTH;STC2;ASNS;ATF3;ATF4
apoptotic cell clearance (GO:0043277)	0.001556795	AXL;GAS6;TGM2
monosaccharide biosynthetic process (GO:0046364)	0.001560479	SLC25A1;ALDOC;ENO3;ATF3;ATF4
organophosphate biosynthetic process (GO:0090407)	0.001609477	FDPS;DGAT2;PCYT2;CHKA;GFPT2;PIK3R3;NME5;CRLS1;GPHN;NPPB;NME7;PMVK;ADSSL1;MVD;UPRT
cellular response to unfolded protein (GO:0034620)	0.001768483	PPP1R15A;CTH;STC2;ASNS;ATF3;ATF4
triglyceride metabolic process (GO:0006641)	0.001868989	SLC25A1;DGAT2;INSIG1;PCSK9;DBI;ELOVL6
coenzyme metabolic process (GO:0006732)	0.00229581	SLC25A1;NUDT7;DGAT2;SHMT2;PMVK;ELOVL6;MVD;GPHN;CBR3
cellular response to topologically incorrect protein (GO:0035967)	0.002437882	PPP1R15A;CTH;STC2;ASNS;ATF3;ATF4
acylglycerol metabolic process (GO:0006639)	0.002565752	SLC25A1;DGAT2;INSIG1;PCSK9;DBI;ELOVL6
response to estrogen (GO:0043627)	0.003003644	SOCS2;KRT19;DHH;IGFBP2;PDGFB;TXNIP;PPARG;AREG
carbohydrate biosynthetic process (GO:0016051)	0.003030062	SLC25A1;CHST12;GFPT2;ALDOC;ENO3;ATF3;ATF4
regulation of lipid metabolic process (GO:0019216)	0.003036847	ARV1;NPC2;DHH;INSIG1;DDX20;PDGFB;PIK3R3;TRIB3;PPARG;SNCA
response to insulin (GO:0032868)	0.003122961	EGR2;PDGFB;PCSK9;PIK3R3;TRIB3;PPARG;UPRT;PRKAB1;ATP6V1D;TLR2
regeneration (GO:0031099)	0.003128169	CXCL12;AXL;PPARG;ALDOC;GAS6;ENO3
acetyl-CoA metabolic process (GO:0006084)	0.003350156	NUDT7;PMVK;MVD
negative regulation of leukocyte apoptotic process (GO:2000107)	0.003454142	BMP4;CXCL12;AXL;GAS6
response to estradiol (GO:0032355)	0.003606857	SOCS2;DHH;IGFBP2;PDGFB;TXNIP;AREG
response to unfolded protein (GO:0006986)	0.003696081	PPP1R15A;CTH;STC2;EDEM2;ASNS;ATF3;ATF4
regulation of receptor biosynthetic process (GO:0010869)	0.003813609	PPARG;HOXA5;FGF21
glycerolipid metabolic process (GO:0046486)	0.003817796	SLC25A1;DGAT2;PCYT2;INPP5F;CHKA;INSIG1;PCSK9;PIK3R3;DBI;ELOVL6;CRLS1
response to topologically incorrect protein (GO:0035966)	0.004986306	PPP1R15A;CTH;STC2;EDEM2;ASNS;ATF3;ATF4

The most significantly changed WikiPathways in expression profiles of *Hic1*$^{flox/flox}$ MEFs 72 hours after addition of 4-OHT when compared to MEFs treated with vehicle only

WikiPathway	p-value	Gene symbol
Cholesterol Biosynthesis (Homo sapiens)	1.0645E-06	FDPS;SQLE;NSDHL;PMVK;SC5D;MVD
Cholesterol Biosynthesis (Mus musculus)	1.0645E-06	FDPS;SQLE;NSDHL;PMVK;SC5D;MVD
SREBP signalling (Homo sapiens)	0.000212448	FDPS;SQLE;INSIG1;DBI;PPARG;MVD;FGF21
One carbon metabolism and related pathways (Mus musculus)	0.009413457	PCYT2;CHKA;SHMT2;CTH
IL1 and megakaryotyces in obesity (Homo sapiens)	0.011103596	MMP9;TLR2;HBEGF
Regulation of Actin Cytoskeleton (Homo sapiens)	0.015872983	RASSF7;PDGFB;PIK3R3;ARHGEF1;ARPC5;SSH3;FGF21
Regulation of Actin Cytoskeleton (Mus musculus)	0.018086038	RASSF7;PDGFB;PIK3R3;ARHGEF1;ARPC5;SSH3;FGF21
Kennedy pathway (Mus musculus)	0.030797066	PCYT2;CHKA
Leptin Insulin Overlap (Mus musculus)	0.03451293	SOCS2;PIK3R3
Hedgehog Signaling Pathway (Homo sapiens)	0.038393353	DHH;ARNTL

Monensin inhibits canonical Wnt signaling in human colorectal cancer cells and suppresses tumor growth in multiple intestinal neoplasia mice

Treatment of CRC is conducted by chemotherapy, therefore great effort is undertaken to develop novel therapeutic substances with less harmful side effects. In cure of FAP or AFAP, chemoprevention seems to be deeply desirable. Some drugs can postpone surgery (colectomy as prevention of CRC), such as sulindac and celecoxib. Unfortunately, the cardiovascular and many other effects of these therapeutics cannot be excluded (Steinbach et al. 2000; Vasen et al. 2008). In recent years, high throughput screenings (HTS) of chemical compound libraries are in focus of many research teams with prospect to identify drug(s) influencing intracellular signaling pathway (Alvin et al. 2014; Nishiya et al. 2014; Robertson et al. 2014; Song et al. 2015). By reporter gene-based HTS we identified a polyether antibiotic from Actinobacteria *Streptomyces cinnamonensis* (Huczynski et al. 2012), monensin, as an inhibitor of proliferation of cells stimulated by Wnt ligand or GSK3 inhibitors.

Monensin has been used in poultry and cattle feed for more than 40 years for its anti-coccidia effect and increasing milk yield and muscle mass (Pressman 1968; Pressman 1976). The antibiotic passes the membrane of cells and organelles multiple times by passive diffusion, therefore its effectivity is achieved even in small amounts (Pressman 1968). Previously, it was found, that monensin induces cell-cycle arrest and apoptosis in renal and colon carcinoma as well as myeloma and lymphoma cells (Park et al. 2002; Park et al. 2003a; Park et al. 2003b; Park et al. 2003c). In head and neck squamous cell carcinoma, monensin enhanced cytotoxicity of EGFR inhibitors (Dayekh et al. 2014). In our HTS analysis, we used three commercially available libraries of small compounds (2,448 small molecules in total) on SuperTOPFLASH (STF) cells (Xu et al. 2004) stimulated by recombinant Wnt3a ligand. From seven compounds with an inhibitory effect on Wnt signaling we selected four without any described link to the Wnt pathway. Among them monensin has been chosen for additional experiments, since it inhibited Wnt signaling at very low concentrations (0.2-5 μmol/L).

Monensin exhibited high levels of specificity for Wnt pathway inhibition. Exposure to monensin induced reduction of β-catenin in the cytoplasm and nucleus and reduced expression of Wnt target genes such as *AXIN2*. As these results seemed promising for the next investigation, we attempted to reveal a component of the pathway that the antibiotic

inhibits. First, we combined monensin treatment with the GSK3 inhibitors BIO (Meijer et al. 2003) and CHIR99021 (Ring et al. 2003). In this case monensin affected the pathway less efficiently than upon Wnt3a stimulation. Therefore we presumed that the antibiotic affects Wnt signaling upstream or at the level of the β-catenin destruction complex. Subsequently, we recognized that Dvl phosphorylation was not impaired. Strikingly, phosphorylation of the internal domain of Lrp6 was blocked by monensin. We asked, whether there is unknown kinase with the ability to phosphorylate Lrp6 and the kinase is affected by monensin. Unfortunately, the activity analysis of various kinases in monensin-treated cells brought no conclusive results. Chen et al. described kinases Src and Fer, phosphorylating the Lrp6 internal domain with an inhibiting effect on Wnt signaling (Chen et al. 2014). However, our list of analyzed kinases did not contain Fer kinase, and, moreover, CK1γ kinase was not included. It was recognized that CK1γ functions as a de-repressor of the Src and Fer suppressive effect, therefore monensin may interfere with the CK1γ effect. Nevertheless, the most likely the monensin effect is not related to any kinase.

One more unsolved question was risen in relation to the monensin effect on CRC cells proliferation and Wnt activation. Whereas in Colo320 and SW480 cells, which are APC deficient, monensin demonstrably suppressed both Wnt signaling and cell division, in HCT116 cells (harboring the stabilizing β-catenin mutation) the antibiotic showed no effect. Controversially, another colorectal cell line LS174T harboring another mutation stabilizing the protein responded to monensin treatment. To resolve this discrepancy, we performed liquid chromatography / tandem mass spectrometry (LS/MS-MS) assay to compare the effect of monensin on β-catenin phosphorylation and acylation in SW480 and HCT116 cells. Regrettably, no difference was found. Although HCT116 cells harbor one wt and one mutated β-catenin allele, which could explain the reduced but still appropriate ability of β-catenin to activate Wnt signaling, the insensitivity to monensin exposure remained unexplained.

Testing monensin efficacy to cancer treatment was performed in two mouse models of intestinal cancer. Six weeks long treatment by monensin in $Apc^{min/+}$ mice resulted in decreased tumor size, even though the number of tumors was equal to mice treated with the vehicle only. Subsequent immunohistochemical staining of p21 in the lesions implicated decreased cell proliferation. Therefore, it is likely that monensin inhibited adenoma progression not initiation. Although the outcome of such experiments appeared

to be promising, it is important to realize that the mouse model has some limits. In $Apc^{min/+}$ mouse, the adenomas develop mainly in the small intestine, whereas humans suffer predominantly from colonic tumors (Gupta et al. 1997; Cheung et al. 2010). Furthermore, the mouse intestinal tumors do not prograde to malignancy (Taketo and Edelmann 2009).

Although we did not define precise mechanisms of monensin action, we believe that the next investigation can lead to the successful application of this beneficial compound in CRC treatment.

Author´s contribution: mouse – intraperitoneal injections, gavage, tissue isolation, fixation and paraffin or O.C.T. embedding, tissue sectioning, immunohistochemistry

Published OnlineFirst February 19, 2014; DOI: 10.1158/1535-7163.MCT-13-0625

Small Molecule Therapeutics

Molecular Cancer Therapeutics

Monensin Inhibits Canonical Wnt Signaling in Human Colorectal Cancer Cells and Suppresses Tumor Growth in Multiple Intestinal Neoplasia Mice

Lucie Tumova[1], Antonio R. Pombinho[2], Martina Vojtechova[1], Jitka Stancikova[1], Dietmar Gradl[5], Michaela Krausova[1], Eva Sloncova[1], Monika Horazna[1], Vitezslav Kriz[1], Olga Machonova[2], Jindrich Jindrich[2,3], Zbynek Zdrahal[4], Petr Bartunek[2], and Vladimir Korinek[1]

Abstract

The Wnt signaling pathway is required during embryonic development and for the maintenance of homeostasis in adult tissues. However, aberrant activation of the pathway is implicated in a number of human disorders, including cancer of the gastrointestinal tract, breast, liver, melanoma, and hematologic malignancies. In this study, we identified monensin, a polyether ionophore antibiotic, as a potent inhibitor of Wnt signaling. The inhibitory effect of monensin on the Wnt/β-catenin signaling cascade was observed in mammalian cells stimulated with Wnt ligands, glycogen synthase kinase-3 inhibitors, and in cells transfected with β-catenin expression constructs. Furthermore, monensin suppressed the Wnt-dependent tail fin regeneration in zebrafish and Wnt- or β-catenin–induced formation of secondary body axis in Xenopus embryos. In Wnt3a-activated HEK293 cells, monensin blocked the phoshorylation of Wnt coreceptor low-density lipoprotein receptor related protein 6 and promoted its degradation. In human colorectal carcinoma cells displaying deregulated Wnt signaling, monensin reduced the intracellular levels of β-catenin. The reduction attenuated the expression of Wnt signaling target genes such as *cyclin D1* and *SP5* and decreased the cell proliferation rate. In multiple intestinal neoplasia (Min) mice, daily administration of monensin suppressed progression of the intestinal tumors without any sign of toxicity on normal mucosa. Our data suggest monensin as a prospective anticancer drug for therapy of neoplasia with deregulated Wnt signaling. *Mol Cancer Ther; 13(4); 812–22. ©2014 AACR.*

Introduction

The Wnt pathway is an evolutionarily conserved signaling mechanism that evolved in metazoans. During embryonic development, the pathway is essential for cell proliferation, differentiation, and migration. In adult organisms, Wnt signaling is involved in somatic tissue homeostasis and tissue regeneration upon injury (reviewed in ref. 1); moreover, deregulation of Wnt signaling is a hallmark of various types of cancer (reviewed in ref. 2). The key component of the canonical the Wnt signaling pathway is β-catenin (reviewed in ref. 3). In unstimulated cells, β-catenin is phosphorylated at the N-terminus by the cytoplasmic "destruction complex" that includes axis inhibition protein (Axin), adenomatous polyposis coli (APC) and serine/threonine kinases casein kinase-1α (CK1α), and glycogen synthase kinase-3 (GSK-3). The phosphorylation promotes ubiquitination and subsequent degradation of the protein keeping the cellular level of the free pool of β-catenin low. Binding of the secreted Wnt ligands to the Frizzled (Fz) receptor and Wnt coreceptor lipoprotein receptor related protein (LRP)-5/6 initiates the CK1ε-dependent phoshorylation of multidomain cytoplasmic transducer Dishevelled (Dvl). In addition, LRP is phosphorylated at its intracellular part by CK1γ and GSK3. The latter event leads to the formation of the LRP–Axin complex and dephosphorylation of Axin. Dephosphorylated Axin constitutes inactive conformation that is unable to interact with LRP and β-catenin. Without the Axin scaffold β-catenin phosphorylation is inhibited and, consequently, the protein accumulates in the cell cytoplasm and nucleus. In the nucleus, β-catenin forms complexes with DNA-binding factors of the lymphoid enhancer factor/T-cell factor (LEF/TCF) family (further referred to as TCFs). The complexes act as

Authors' Affiliations: [1]Department of Cell and Developmental Biology, [2]CZ-OPENSCREEN, Institute of Molecular Genetics AS CR; [3]Department of Organic Chemistry, Faculty of Science, Charles University in Prague, Prague; and [4]Central European Institute of Technology, Masaryk University, Brno, Czech Republic; and [5]Zoologisches Institut II, Universität Karlsruhe, Karlsruhe, Germany

Note: Supplementary data for this article are available at Molecular Cancer Therapeutics Online (http://mct.aacrjournals.org/).

L. Tumova and A.R. Pombinho contributed equally to this work.

Corresponding Authors: Vladimir Korinek, Institute of Molecular Genetics, Videnska 1083, 14220 Prague 4, Czech Republic. Phone: 420-241-063-146; Fax: 420-244-472-282; E-mail: korinek@img.cas.cz; and Petr Bartunek, E-mail: bartunek@img.cas.cz

doi: 10.1158/1535-7163.MCT-13-0625

©2014 American Association for Cancer Research.

Downloaded from mct.aacrjournals.org on August 10, 2015. © 2014 American Association for Cancer Research.

Published OnlineFirst February 19, 2014; DOI: 10.1158/1535-7163.MCT-13-0625

bipartite transcriptional activators of specific Wnt signaling target genes.

Cancer affecting colon and rectum constitutes one of the most commonly diagnosed neoplasia in developed countries (4). Intriguingly, pathogenesis of the colorectal carcinoma is connected with the aberrant activity of the Wnt/β-catenin signaling cascade. Germinal mutations of the *APC* gene underlie the hereditary familial adenomatous polyposis (FAP) syndrome (5). Similarly, about 50% of sporadic colorectal tumors arise upon biallelic loss of *APC* (6). Hyperactive Wnt signaling might also result upon activation mutations in the β-catenin (also designated as *CTNNB1*) gene (7). In either case, stabilized β-catenin mediates inappropriate transcriptional activation of TCF/β-catenin target genes, thus driving pathologic transformation of the gut epithelium (8).

In the present study, we performed a reporter gene-based high-throughput screen (HTS) to identify inhibitors of the Wnt signaling pathway. We identified monensin, an antibiotic isolated from *Streptomyces cinnamonensis* bacteria (9), as a potent blocker of the Wnt-induced transcription in cells stimulated with Wnt ligands or GSK3 inhibitors. The suppressive effect of monensin on Wnt signaling was also observed in the tail fin regeneration assay in zebrafish and Xenopus body axis duplication experiment. In human colorectal carcinoma cells harboring mutations in *APC* or β-*catenin*, the monensin-mediated block of the TCF/β-catenin transcription activity led to slowdown in cell-cycle progression. Finally, monensin treatment reduced the size of the *Apc*-deficient tumors in the mouse model of intestinal cancer.

Materials and Methods

Cell lines and generation of Wnt1-producing cells

SuperTOPFLASH HEK293 (STF) cells (10) harboring the genome-integrated Wnt-responsive luciferase reporter SuperTOPFLASH were a gift of Q. Xu and J. Nathans (Johns Hopkins University, Baltimore, MD). COLO320, HCT116, HEK293, L, LS174T, RKO, and SW480 cell lines were purchased from the American Type Culture Collection. All cell lines were obtained in 2006 and maintained in Dulbecco's modified Eagle medium (Sigma) supplemented with 10% FBS (Gibco), penicillin, streptomycin, and gentamicin (Invitrogen). Upon receipt, cells were expanded and aliquots of cells at passage number <10 were stored frozen in liquid nitrogen. Cells from one aliquot were kept in culture for less than 2 months after resuscitation. The cell identity was not authenticated by the authors. Mouse Wnt1 cDNA (11) was cloned into the lentiviral vector pCDH1 (System Biosciences). Lentiviruses were prepared using the Trans-Lentiviral Packaging System (Open Biosystems). Transduced STF cells were selected without subcloning using puromycin (Alexis; 5 μg/mL).

Compounds, luciferase reporters and assays, transfections, and biochemistry

The small compound collections included the Library of Pharmacologically Active Compounds (LOPAC1280; Sigma-Aldrich), Prestwick Chemical Library (Illkirch, France), and NIH Clinical Trial Collection. Monensin sodium salt, (2′Z,3′E)-6-Bromoindirubin-3′-oxime (BIO) and bafilomycin A1 were purchased from Sigma, and CHIR99021 from Selleckchem. Luciferase reporter constructs, NF-κB-Luc and pRL-TK, were purchased from Promega. The TCF/β-catenin–dependent reporter TOPFLASH and negative control reporter FOPFLASH were described previously (8). The luciferase assays were performed as described previously (11) using the ONE-Glo Luciferase Assay System (Promega) for HTS and Dual-Glo Luciferase Assay System (Promega) for subsequent analysis. Mouse Wnt3a ligand was isolated from the culture medium of Wnt3a-producing L cells as described previously (12). Human recombinant lymphotoxin-α (LTα) was purchased from R&D Systems. Transfections were performed using Lipofectamine 2000 reagent (Invitrogen). RNA purification, quantitative reverse transcription PCR (qRT-PCR), coimmunoprecipitations, and immunoblotting were performed as described previously (11). The primers for qRT-PCR are listed in Supplementary Table S1.

Cell viability, apoptosis, and cell proliferation assays

Cell viability and apoptosis were determined after overnight incubation with respective compounds using the Cell Titer-Blue Cell Viability Assay Kit and Caspase-Glo 3/7 Assay Kit, respectively (Promega). In control experiments, cells were incubated with recombinant TRAIL (kindly provided by L. Andera, Institute of Molecular Genetics, Prague, Czech Republic). Apoptotic cells in the mouse intestine were detected using TumorTACS Detection Kit (RD Systems). Metabolic incorporation of [^{3}H]-thymidine (MP Radiochemicals; final concentration 0.1 mCi/μL) was measured using MicroBeta2 Microplate Counter (PerkinElmer) after overnight incubation at 37°C.

Monitoring cell proliferation and attachment in "real time"

xCELLigence Real-Time Cell Analysis System (Roche Applied Science) was used according to the instructions of the manufacturer. Cells were seeded at the density of 1,500 cells per well. The electronic impedance of sensor electrodes was monitored every 15 minutes. Eighteen hours after seeding, monensin or dimethyl sulfoxide (DMSO) was added to the wells and the measurement continued for additional 24 hours. Cell index was quantified as described previously (13).

Immunocytochemistry and immunohistochemistry

The techniques were performed as described previously (14, 15).

Zebrafish tailfin regeneration assay

Zebrafish (less than 6 months of age) were kept in E3 medium (5 mmol/L NaCl, 0.17 mmol/L KCl, 0.33 mmol/L $CaCl_2$, and 0.33 mmol/L $MgSO_4$ in distilled H_2O) at 28°C. Fishes that were approximately 2.5 cm long were anesthetized with tricaine (Sigma) and tips of their tail fin were

Downloaded from mct.aacrjournals.org on August 10, 2015. © 2014 American Association for Cancer Research.

Published OnlineFirst February 19, 2014; DOI: 10.1158/1535-7163.MCT-13-0625

carefully amputated using scissors. The animals were randomly distributed into aquaria (4–5 fish per tank) containing E3 medium with 2 μmol/L (prepared from stock solution of 20 mmol/L monensin in ethanol) or equivalent volume of ethanol alone. One week later, fishes were anesthetized and photographed. The regenerated area (recognizable by lack of pigmentation) was scored in three independent experiments using ImageJ software.

Xenopus double axis formation assay

The assay was performed as described previously (16). A marginal zone of the ventral blastomeres of 4-cell stage *Xenopus laevis* embryos was injected (4 nL) using 20 or 800 pg of *XWnt8* or β-*CATENIN* mRNA, respectively. Messenger RNA was injected together with monensin (0.04 pmol) or vehicle (DMSO). The developing embryos were kept at 20°C; the duplication of the body axis was scored 36 hours after injection.

Tumor treatment in mice

Multiple intestinal neoplasia (Min) mice (further referred to as the $Apc^{+/Min}$ strain) were purchased from the Jackson Laboratory. Animals were housed and handled in accordance with the approved guidelines. Four-week-old pups were weaned, genotyped, and randomized. The animals were divided into two groups and treated with monensin (10 mg/kg) or vehicle (DMSO). Daily oral applications continued for 6 weeks. In addition, six pairs of $Apc^{+/Min}$ mice ages 7, 10, 13, 16, 19, and 22 weeks were treated with monensin or vehicle for 5 weeks. The mice were sacrificed and the intestines were dissected, washed in PBS, and fixed in 4% formaldehyde (v/v) in PBS for 3 days. Fixed intestines were embedded in paraffin, sectioned and stained. The number and size of the neoplastic lesions were quantified using Ellipse software (ViDiTo).

Statistical analysis

Fisher exact test was used to analyze the statistical significance of the results of the double axis formation assay. Data obtained in the gene reporter and qRT-PCR analyses were evaluated by Student *t* test.

Additional materials and methods, including details of HTS, plasmid constructs, and antibodies, are given in Supplementary Materials and Methods.

Results

HTS for inhibitors of the Wnt signaling pathway

Luciferase reporter gene assay in STF cells was used to search for novel inhibitors of Wnt/β-catenin signaling. The screen included 2,448 compounds from three commercially available collections. STF cells were stimulated with recombinant Wnt3a ligand and, simultaneously, the tested compounds were added to culture medium to 1 μmol/L concentration. The luciferase activity was quantified 18 hours later using bioluminescent signal detection. The primary screen identified seven "small molecules" displaying a profound inhibitory effect on the SuperTOPFLASH activity. These molecules included the previously identified Wnt pathway inhibitors indometacin (17), thapsigargin (18), and harmine (19). In addition, four compounds without any (published) relation to Wnt signaling were discovered. The putative novel Wnt pathway modulators were examined for their effective concentration range, cell toxicity, and direct repressive effect on the luciferase reaction. Moreover, because the zebrafish has the ability to regrow damaged tissues in the process that depends on active Wnt/β-catenin signaling (20), we used the tail fish regeneration assay to validate the action of the identified Wnt pathway inhibitors *in vivo*. Polyether antibiotic monensin, which suppressed the activity of the TCF/β-catenin reporter SuperTOPFLASH at concentrations 0.2 to 5 μmol/L and decreased the tail fish regeneration to 50% (compared with control vehicle-treated animals), was selected for subsequent studies (Fig. 1).

Monensin inhibits the Wnt signaling cascade at multiple levels

To confirm the specificity of the monensin action, reporter gene assays in HEK293 cells were performed using the Wnt-responsive reporter TOPFLASH (8), negative-control reporter FOPFLASH, and the NF-κB pathway luciferase reporter plasmid NF-κB-Luc. Cells transiently transfected with the reporters were stimulated with recombinant Wnt3a or LTα to activate Wnt or NK-κB signaling, respectively. In agreement with the results obtained in STF cells, 1 and 5 μmol/L monensin reduced the TOPFLASH activity to 34% and 32%, respectively (Fig. 2A). Conversely, monensin had no effect on the transcription from the NF-κB-Luc and FOPFLASH reporters (Fig. 2A; data not shown). In addition, we performed qRT-PCR analysis of HEK293 cells. Monensin treatment resulted in downregulation of the previously described Wnt target genes *AXIN2*, *CYCLIN D1*, *LGR5*, *NKD1*, and *SP5* (Fig. 2B). To verify these results in a different cell type, the β-catenin stabilization was visualized in L cells (15). In these mouse fibroblasts, monensin reduced Wnt3a-mediated accumulation of β-catenin in the cytoplasm and nucleus (Fig. 2C). Recently, Morrell and colleagues have reported that some inhibitors of the Wnt pathway antagonize recombinant Wnt3a protein but are ineffective against ectopically expressed Wnt ligands (21). To exclude this possibility, the results of luciferase and qRT-PCR assays were confirmed using Wnt1-transduced STF cells (not shown). In addition, Western blot analysis of Wnt1-producing STF cells showed that monensin treatment decreased the cellular levels of β-catenin, including the presumably transcriptionally active forms of the protein either nonphoshorylated at the N-terminus (non-P-β-CATENIN) or containing the phosphorylated serine residue at position 675 (P-S675-β-CATENIN; ref. 22). Reduction in the production of the AXIN2 protein was also observed, indicating that monensin did not inhibit tankyrase (14). In contrast, monensin had no effect on the cellular levels of nuclear Wnt signaling effector TCF4 (Fig. 2D).

Downloaded from mct.aacrjournals.org on August 10, 2015. © 2014 American Association for Cancer Research.

Published OnlineFirst February 19, 2014; DOI: 10.1158/1535-7163.MCT-13-0625

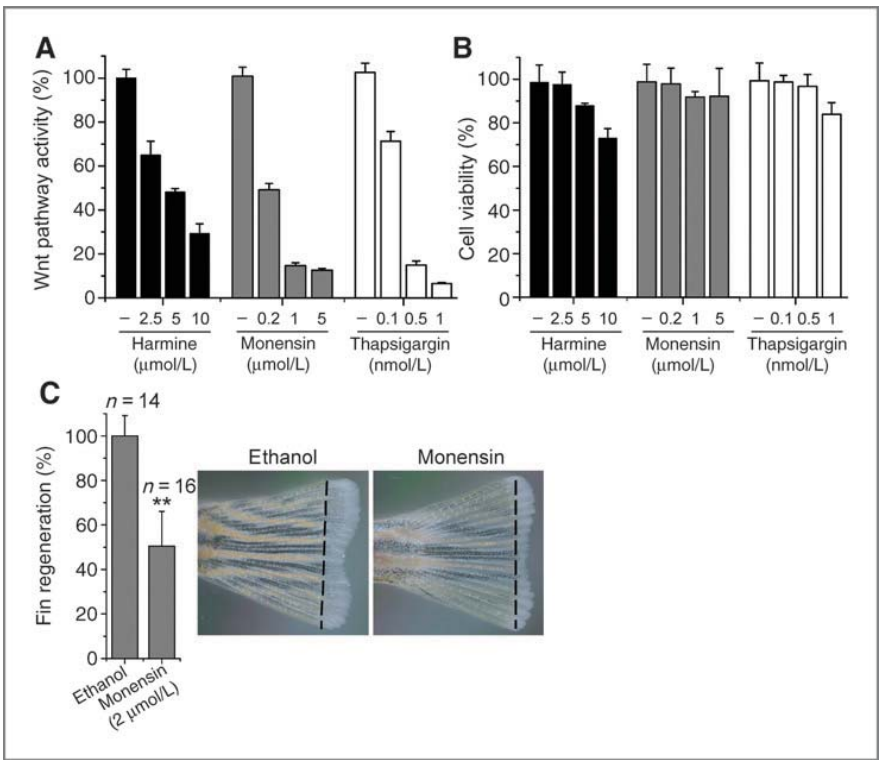


Figure 1. Monensin inhibits the SuperTOPFLASH reporter and suppresses tail fin regeneration. A, luciferase reporter assay in Wnt3a-stimulated STF cells. The reporter activity in cells treated with Wnt3a and vehicle (DMSO) was arbitrarily set to 100%. B, results of the cell viability test. The histograms represent mean values of triplicate experiments; SDs are shown by error bars. C, monensin blocks the zebrafish tail fin regeneration. The amputation plane is indicated by a dashed line. The average area of regrown fins obtained in control experiment was arbitrarily set to 100%; error bars, SD. **, $P < 0.01$ (Student t test); n, number of examined animals.

To identify the molecular mechanism of the monensin action in more detail, we used GSK3 inhibitors BIO (23) and CHIR99021 (24) to trigger Wnt signaling. Monensin suppressed the activity of both compounds in STF and L cells (Fig. 3A and B; data not shown). In HEK293 cells, BIO increased the cellular levels of total and "active" non-P-β-CATENIN. Combined cell treatment with BIO and monensin caused a moderate decrease in all tested β-catenin forms (Fig. 3C and Supplementary Fig. S1). We noted that monensin antagonized GSK3 inhibitors less efficiently than the signaling initiated by Wnt ligands, indicating that monensin "hits" the Wnt pathway upstream and at the level (or downstream) of the β-catenin destruction complex. This conclusion was confirmed in STF cells displaying aberrant Wnt signaling after disruption of the *APC* gene induced by transcription activator-like effector nucleases (Supplementary Fig. S2). One of the proximal events of Wnt signaling is phosphorylation of cytoplasmic protein Dvl followed by phosphorylation of Wnt coreceptor LRP (25). Immunoblotting of HEK293 cells revealed that the phoshorylation of Dvl was not influenced by monensin (Supplementary Fig. S3); however, the compound blocked the phoshorylation of LRP6 and induced its degradation (Fig. 3D). To determine which protein kinase is inhibited by monensin, selectivity profiling was performed. Nevertheless, none of the 50 enzymes representing the main protein kinase families was affected by monensin (Supplementary Table S2).

We next tested whether monensin inhibits Wnt-induced dorsalization of Xenopus embryos. Injection of *XWnt8* with vehicle alone resulted in 65.9% embryos with a duplicated body axis. In contrast, coinjection of *XWnt8* with monensin caused a significant ($P = 0.002$) decrease in the proportion of dorsalized animals to 30.7%. Interestingly, monensin also reduced the secondary body axis formation initiated by β-*catenin* mRNA (Fig. 3E). In agreement with the results obtained in Xenopus embryos, in STF cells monensin suppressed the transcription activity of wild-type (wt) β-catenin. Strikingly, monensin also inhibited stable forms of β-catenin mutated at the N-terminal regulatory residues but had no effect on transcription induced by the Lef1-VP16 fusion protein (Fig. 3F).

Disruption of intracellular pH homeostasis suppresses paracrine Wnt signaling; moreover, inhibition of vacuolar acidification interferes with Wnt secretion (26). Because monensin acts as a ionophore blocking cellular acidification, we compared its effect on Wnt signaling with bafilomycin A, a compound disrupting vacuolar acidification through pharmacologic inhibition of V-ATPase (27). In contrast with monensin, bafilomycin inhibited the signaling activity of the recombinant and ectopically expressed Wnt ligand, but the inhibitor was not effective against signaling stimulated by β-catenin or constitutively active LRP6 (ΔN-LRP6; Supplementary Fig. S4). Taken together, these results provided evidence that monensin

Downloaded from mct.aacrjournals.org on August 10, 2015. © 2014 American Association for Cancer Research.

Published OnlineFirst February 19, 2014; DOI: 10.1158/1535-7163.MCT-13-0625

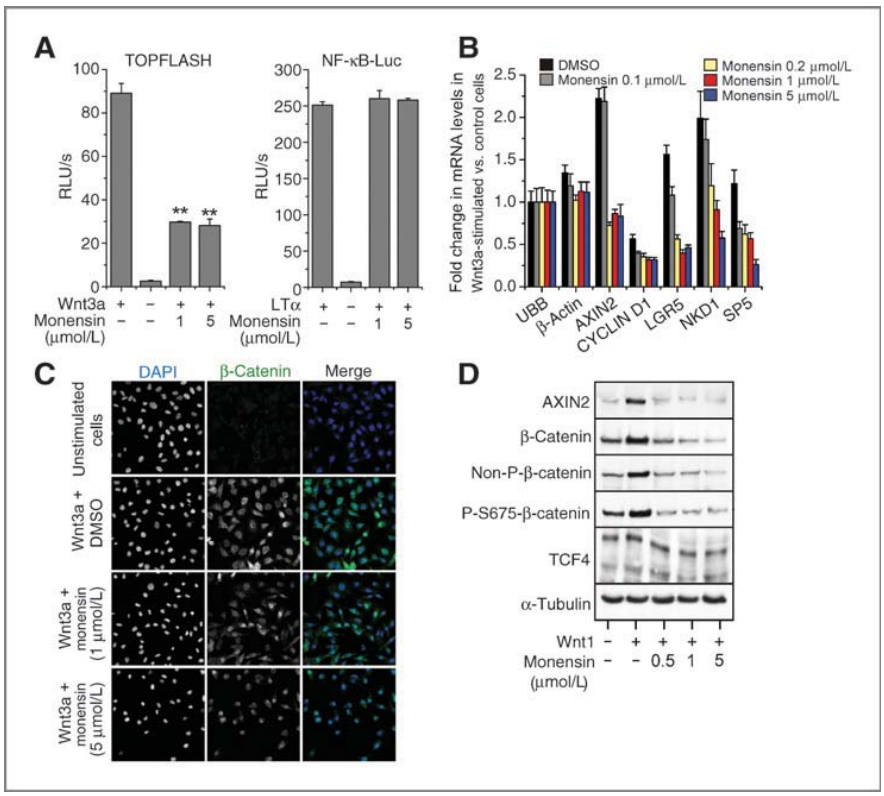


Figure 2. The inhibitory effect of monensin is specific for Wnt signaling. A, luciferase reporter assays in HEK293. Cells transfected with the indicated reporters were stimulated with recombinant Wnt3a or LTα (10 ng/mL), respectively, and grown with vehicle or monensin. The histograms represent average luciferase light units per second (RLU/second) of a triplicate corrected for the efficiency of transfection using *Renilla* luciferase as the internal control; **, $P < 0.01$. B, qRT-PCR analysis. HEK293 cells treated with vehicle or monensin were stimulated with Wnt3a and analyzed 20 hours later. The levels of input cDNAs were normalized to the *UBIQUITIN B* (*UBB*) housekeeping gene. The expression level of the respective gene in unstimulated cells was arbitrarily set to 1. C, monensin suppresses accumulation of β-catenin in mouse L cells. Microscopy images of cells stained with an anti-β-catenin monoclonal antibody (green) or 4′,6-diamidino-2-phenylindole dihydrochloride (DAPI) nuclear stain (blue). Original magnification, ×630. D, immunoblotting analysis of STF cells transduced with Wnt1-expressing lentivirus; cells were grown with vehicle or monensin for 20 hours; non-P-β-CATENIN, β-catenin unphosphorylated at S33, S37, and T41; P-S675-β-CATENIN, β-catenin phosphorylated at S675; α-TUBULIN, loading control. Densitometric analysis of the Western blot analyses is given in Supplementary Fig. S1A.

specifically antagonized the Wnt signaling pathway at the LRP and β-catenin levels.

Monensin attenuates aberrant Wnt signaling in human colorectal carcinoma cells

The effect of monensin was investigated in four colorectal carcinoma-derived cell lines. SW480 and COLO320 cells are *APC* deficient, whereas LS174T and HCT116 cells contain intact APC but produce stabilized S45A and ΔS45 β-catenin proteins, respectively (28). Interestingly, monensin decreased the activity of the TOPFLASH reporter and the expression of Wnt signaling target genes in SW480, COLO320, and LS174T cells but not in HCT116 cells (Fig. 4A and B; Supplementary Table S3; Supplementary Fig. S5A). Microscopy supported this finding, showing reduced anti-β-catenin staining in monensin-treated SW480, COLO320, and LS174T cells. No reduction in the anti-β-catenin signal was observed in HCT116 cells, although the treated cells gained a spindle-like shape (Fig. 4C and Supplementary Fig. S5B). Using immunoblotting, we detected a decrease in all forms of β-catenin in SW480 cells. In the other colorectal carcinoma-derived cells, the decrease in the stability of different β-catenin forms was moderate (COLO32O and HCT116 cells) or negligible (LS174T cells; Fig. 4D and Supplementary Fig. S5C). We noted a discrepancy between clear reduction of the β-catenin signal as documented by microscopy and rather moderate changes in the β-catenin levels obtained by immunoblotting. The phenomenon was not associated with the specificity of the monoclonal antibody because another two anti-β-catenin monoclonal antibodies displayed a similar variation in the β-catenin detection (data not shown). The observed discrepancy possibly reflects differences in the robustness of these two readouts, and monensin to some extent promoted β-catenin degradation in three (SW480, COLO320, and LS174T) out of four colorectal carcinoma cells tested.

Downloaded from mct.aacrjournals.org on August 10, 2015. © 2014 American Association for Cancer Research.

Published OnlineFirst February 19, 2014; DOI: 10.1158/1535-7163.MCT-13-0625

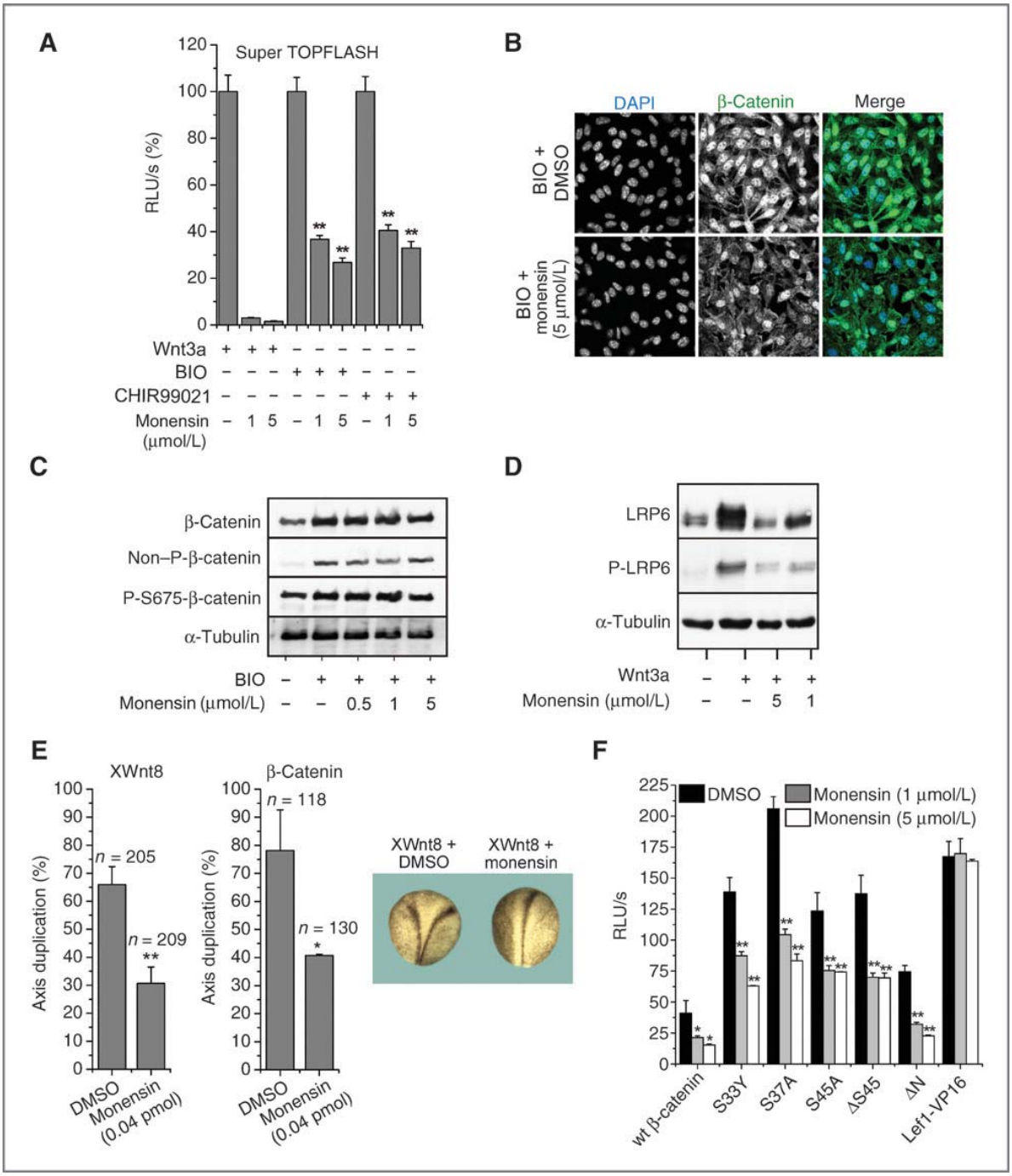


Figure 3. Monensin suppresses Wnt signaling initiated by GSK3 inhibitors and ectopic β-catenin. A, luciferase reporter assays in STF cells stimulated with recombinant Wnt3a or GSK3 inhibitors BIO (1 μmol/L) and CHIR99021 (3 μmol/L); error bars, SDs. B, fluorescent microscopy images of L cells treated overnight with BIO in combination with vehicle or monensin. C, immunoblotting of lysates obtained from STF cells stimulated overnight with BIO in combination with vehicle or monensin. Densitometric analysis of the Western blot analyses is given in Supplementary Fig. S1B. D, monensin reduces the protein level and phosphorylation of the Wnt coreceptor LRP6 in HEK293 cells; P-LRP6, LRP6 phosphorylated at S1490. E, monensin reduces double axis formation in Xenopus embryos; representative images of embryos are shown at the right. *n*, total number of injected embryos; error bars, SEM. F, results of the luciferase reporter assays performed in STF cells transfected with the indicated β-catenin–expressing constructs. S33Y, S37A, S45A, stable β-catenin with the amino acid changes at the serine residue in positions 33, 37, and 45; ΔS45, S45 deleted; ΔN, the N-terminally truncated variant of β-catenin; Lef1-VP16, Lef1 lacking the N-terminal β-catenin–interaction domain fused to the transcription transactivation domain of herpes simplex virus protein VP16; *, $P < 0.05$; **, $P < 0.01$.

Downloaded from mct.aacrjournals.org on August 10, 2015. © 2014 American Association for Cancer Research.

Published OnlineFirst February 19, 2014; DOI: 10.1158/1535-7163.MCT-13-0625

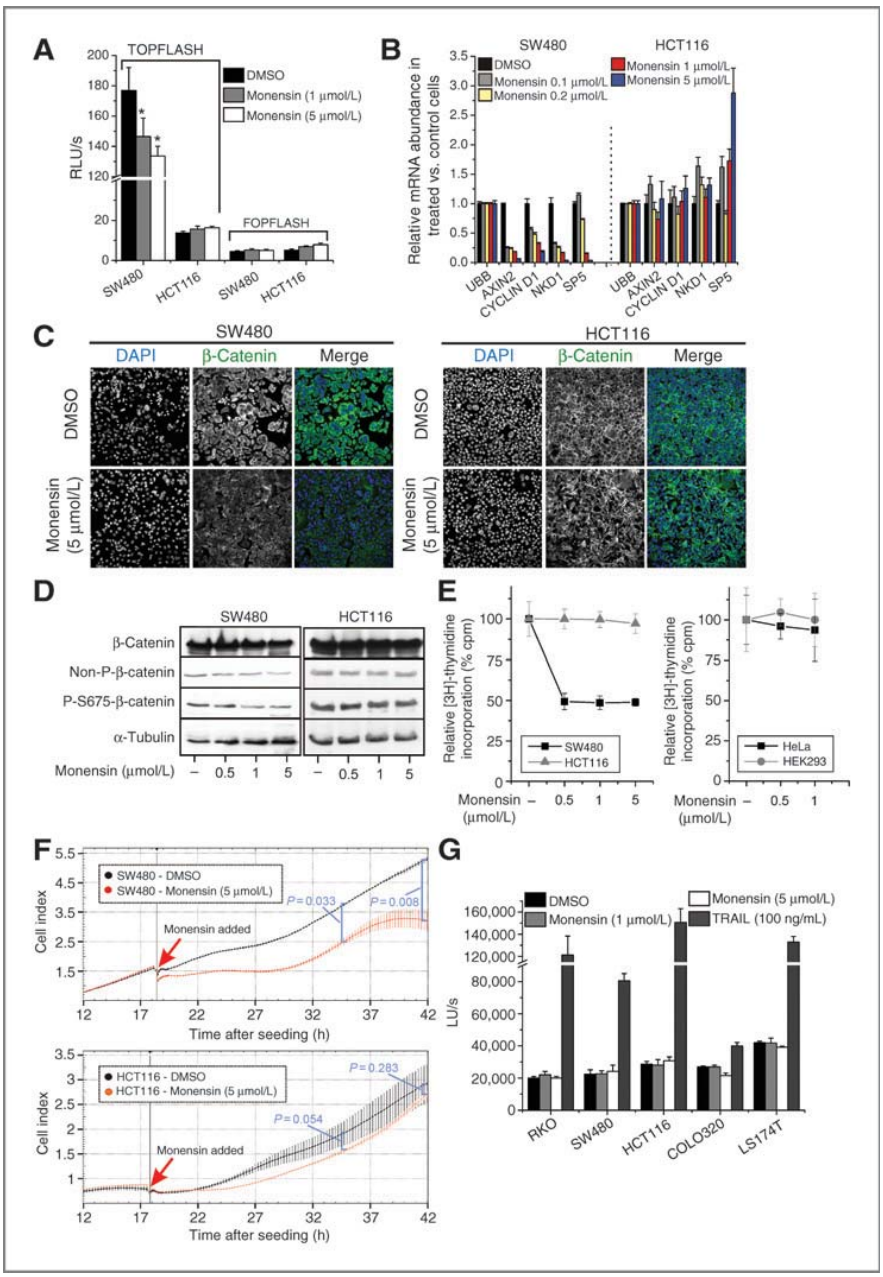


Figure 4. Differential sensitivity of SW480 and HCT116 colorectal carcinoma cells to monensin. A, monensin inhibits the activity of the TOPFLASH reporter in SW480 but not in HCT116 cells. *, $P < 0.05$; error bars, SD. B, qRT-PCR analysis of cells treated with vehicle or monensin for 36 hours before harvesting. The expression level of the respective gene in unstimulated cells was arbitrarily set to 1. C, fluorescent microscopy images of SW480 and HCT116 cells treated with vehicle or monensin for 36 hours; original magnification, ×400. D, immunoblot analyses of SW480 and HCT116 cells incubated for 36 hours with DMSO or monensin. Densitometric analysis of the Western blot analyses is given in Supplementary Fig. S1C. E, cell proliferation assay. The ^{3}H-thymidine counts in cells cultured with vehicle (DMSO) was arbitrarily set to 100%. F, impedance-based measurement of growth and dimensional changes of SW480 and HCT116 cells treated with monensin or vehicle. G, monensin does not induce apoptosis of colorectal carcinoma cells. TRAIL-sensitive RKO colorectal carcinoma cells were also included in the test. The assay was performed in triplicate; the average luminescence units (LU)/second are shown; error bars, SD.

Cell proliferation assays in SW480 and COLO320 cells revealed more than 50% decrease in [^{3}H]-thymidine incorporation in cultures with monensin when compared with controls treated with DMSO alone. The proliferation rate of LS174T cells was affected by monensin to a lesser extent; nevertheless, the antibiotic caused 25% decline in [^{3}H]-thymidine counts. No substantial changes in proliferation of HCT116 and Wnt "signaling inactive" HEK293 and HeLa cells were recorded (Fig. 4E and Supplementary Fig. S5D). Subsequently, cell-cycle analysis showed that monensin reduced the fraction of SW480 cells in S and G_2–M phases. Conversely, the cell fraction in G_1 phase was increased (Supplementary Table S4). In addition, we used the xCELLigence system to gain continuous information about the cell growth, death, and morphological changes of SW480 and HCT116 cells. As shown in Fig. 4F, monensin significantly influenced the cell index (this parameter depends on the number and dimensional changes of attached cells) of SW480 cells. In HCT116, the cell index fluctuations were possibly attributed to the

Downloaded from mct.aacrjournals.org on August 10, 2015. © 2014 American Association for Cancer Research.

Published OnlineFirst February 19, 2014; DOI: 10.1158/1535-7163.MCT-13-0625

changes in cellular shape because monensin did not induce apoptosis in any of the colorectal carcinoma cells tested (Fig. 4G). In prostate cancer cells, monensin treatment reduced the amount of androgen receptor mRNA and elevated oxidative stress (29). However, monensin did not increase the levels of reactive oxygen species (ROS) in HEK293 and SW480 cells (Supplementary Fig. S6); thus, we could exclude that its effect on Wnt signaling was indirectly mediated by changes in the intracellular ROS concentration.

The insensitivity of HCT116 cells to monensin was peculiar as LS174T cells, which also express mutant β-catenin, were sensitive to the antibiotic. Interestingly, HCT116 cells show considerably less TOPFLASH activity than other colorectal carcinoma cells carrying APC truncations or β-catenin mutations (Fig. 4A; ref. 28). Moreover, in HCT116 cells, β-catenin is mainly associated with the cellular membrane (Supplementary Fig. S7). Recently, several studies documented that β-catenin localization or intracellular concentration can be regulated by several kinases, including RAF1, c-*Jun* NH_2-terminal kinase 2, AKT, protein kinase A (PKA), and P21-activated kinase 1 (22, 30–33). We therefore evaluated the effect of monensin on the phosphorylation of β-catenin. The endogenous protein was precipitated from control and monensin-treated SW480 and HCT116 cells, and phosphorylated peptides were determined using liquid chromatography/tandem mass spectrometry (LC/MS–MS). The analysis revealed that β-catenin is indeed phosphorylated at S191 (HCT116 cells only), S552, and S675; however, the observed modifications did not change in monensin-sensitive SW480 cells upon the treatment (Supplementary Table S5). Because acetylation influences β-catenin stability and transcriptional activity (34), the impact of monensin on β-catenin acetylation was also determined. Nevertheless, the extent of β-catenin acetylation did not change in the cells cultured with monensin (Supplementary Fig. S8).

Monensin reduces tumor size in the $APC^{+/Min}$ mouse model of intestinal cancer

The possible antitumor activity of monensin was analyzed in $Apc^{+/Min}$ mice. The mice harbor a truncation mutation in one allele of the *Apc* gene, and all adult animals eventually develop large amounts of intestinal polyps and die of cancer (35). The initial daily oral applications of monensin (dose 10 mg/kg) started at the weaning age. Animals in the control group received vehicle (DMSO) only. No effect on body weight was noticed throughout the experiment and individuals in both groups were steadily gaining weight as they were reaching sexual maturity (not shown). After six weeks, the mice were sacrificed and the dissected intestines were embedded in paraffin and sectioned. Immunohistochemical staining showed elevated production of β-catenin in neoplastic lesions found mainly in the small intestine (Fig. 5A). Stained tumors contrasted with the healthy mucosa enabled quantitative analysis of the tumor size and numbers using the image analysis software Ellipse (14). Although the numbers of tumors did not change substantially, a significant ($P = 0.0144$) reduction in the average size of lesions was observed in monensin-treated $Apc^{+/Min}$ mice when compared with control animals (mean 0.199 mm^2 vs. 0.299 mm^2). Consequently, the total tumor area estimated in one animal was decreased in individuals receiving monensin (mean 10.16 mm^2 vs. 16.46 mm^2; $P = 0.0125$; Fig. 5B). The inhibitory effect of monensin on the tumor growth was also observed in the second experiment, in which the compound (or vehicle) was administered to paired adult animals at various ages (Fig. 5C). Interestingly, the proportion of proliferating cells positive for the Ki-67 or proliferating cell nuclear antigen marker did not change in adenomas exposed to monensin (Fig. 5D, c and d′ and Supplementary Fig. S9). However, monensin treatment increased the numbers of apoptotic cells and cells expressing the p21 cell-cycle inhibitor at the surface area of the neoplastic outgrowths (Fig. 5D, e–h′). This indicated that the smaller size of lesions in monensin-treated $APC^{+/Min}$ mice was related to the cell-cycle arrest and/or cell death at the tumor periphery. Importantly, no changes in the cell proliferation, differentiation, and tissue architecture in the healthy parts of mucosa were noted after exposure to monensin (Fig. 5E, i–l).

Discussion

Monensin belongs to the group of natural carboxylic polyether ionophores (36). The ionophoric antibiotics, the group currently includes more than 100 compounds, are studied mainly for their antibacterial, antifungal, and antiparasitic biologic activity (9). Monensin was approved by the U.S. Food and Drug Administration for use in veterinary practice as a coccidiostat in poultry and growth-promoting agent in cattle (New Animal Drug Application No. 95-735). The antibiotic increased dairy cattle milk production with no negative side effects on the animal health or reproduction (37, 38). Stimulation of growth in ruminants is associated with changes in intestinal microflora that lead to increased amounts of digestible proteins (39). Monensin antibacterial and antiparasitic activity is related to the intracellular changes in pH and sodium–potassium balance that can result in cell death (40). Several recent studies have demonstrated that monensin inhibits growth and induces apoptosis of cells derived from renal, prostate, and colon carcinoma (29, 41, 42). In addition, monensin induced cell-cycle arrest of acute myelogenous leukemia and lymphoma cells (43, 44). In glioma cells, monensin provoked endoplasmic reticulum stress and sensitized these cells to TRAIL-induced apoptosis (45). According to our results, monensin antagonized the Wnt signaling cascade at multiple levels involving LRP6 and β-catenin. Interestingly, a similar "mode of action" was described for other potassium ionophores salinomycin and nigericin in chronic lymphocytic leukemia

Downloaded from mct.aacrjournals.org on August 10, 2015. © 2014 American Association for Cancer Research.

Published OnlineFirst February 19, 2014; DOI: 10.1158/1535-7163.MCT-13-0625

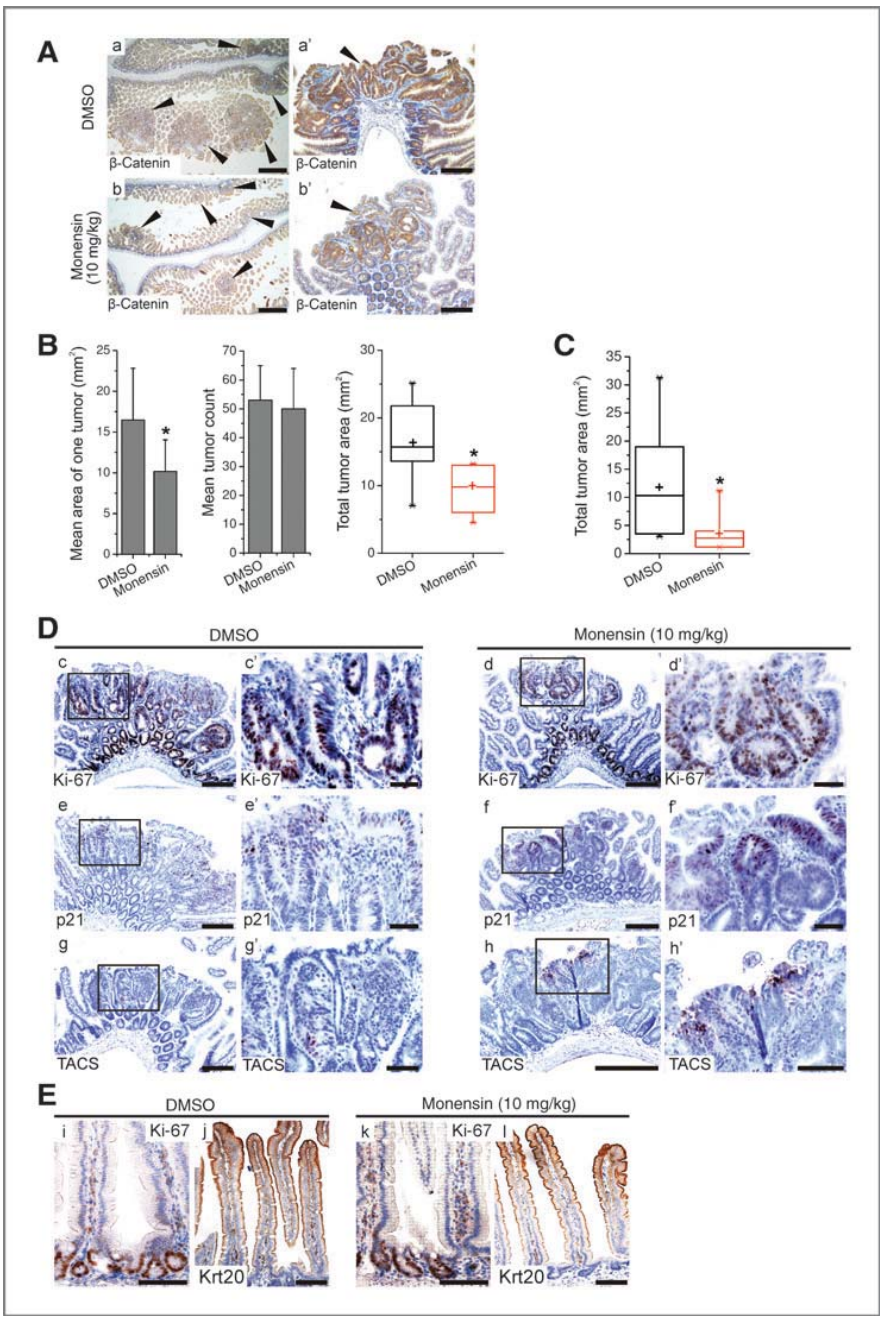


Figure 5. Monensin treatment decreases the size of adenomas in APC$^{+/Min}$ mice. A, hematoxylin and anti-β-catenin–stained sections of the jejunum of APC$^{+/Min}$ mice. Tumors are indicated by black arrowheads. B and C, quantification of the tumor size and count in the ileum of vehicle- and monensin-treated APC$^{+/Min}$ mice; the treatment started either in 4-week-old animals just after weaning (B) or in adult animals 7 to 22 weeks of age (C). The total tumor area determined in each individual is indicated in the boxplots. The boxed areas correspond to the second and third quartiles; the spread of the values is given by "whiskers" above and below each box. Median (transverse line) and mean (cross) is marked inside each box; statistical significance was determined using Student (B) or paired (C) *t* test; *, $P < 0.05$; error bars, SD. D, detection of proliferation marker Ki-67 (c and d), cell-cycle inhibitor p21 (e and f), and apoptotic cells (TACS; g and h) in the small intestinal tumors. Detailed images are shown in panels c′, d′, e′, f′, g′, and h′. E, phenotype of healthy parts of the small intestine is not affected by monensin. The specimens were stained with Ki-67 (i and k) and cytokeratin 20 (Krt20; j and l) to label proliferating cells in the crypts and terminally differentiated epithelial cells on the villi, respectively. Bar, 0.5 mm (a and b), 0.15 mm (a′, b′, c, d, e, f, g, and h), 0.08 mm (i, j, k, and l), 0.05 mm (c′, d′, e′, f′, g′, and h′).

cells (46). However, the detailed inhibitory mechanism of these antibiotics on the Wnt signaling pathway has not been identified.

Protein phosphorylation is the key modification in virtually all signaling cascades. Therefore, we performed kinase selectivity profiling, but no conclusive result was obtained. This would imply that (i) the monensin action is highly specific and monensin-sensitive kinase was not included in the test, (ii) the selected concentrations of the antibiotic were too low to elicit any effect in this particular type of experiment, and (iii) the monensin action is not related to the inhibition of any protein kinase. The last possibility seems to be most likely, at least in relation to β-catenin, because LC/MS-MS analysis did not identify any phosphorylation sites that changed in monensin-sensitive SW480 cells.

Downloaded from mct.aacrjournals.org on August 10, 2015. © 2014 American Association for Cancer Research.

Published OnlineFirst February 19, 2014; DOI: 10.1158/1535-7163.MCT-13-0625

In $APC^{+/Min}$ mice, monensin suppressed tumor growth without any noticeable negative impact on healthy mucosa. In the treated animals, the size of neoplastic lesions was decreased, but the average number of tumors remained unchanged. This result indicated that monensin inhibited tumor progression rather than the tumor initiation process. The conclusion was confirmed by immunohistochemical staining that showed markers of cell-cycle arrest and apoptosis at the surface of neoplastic outgrowths. In colorectal carcinoma cells, this proapoptotic activity of monensin was not observed, presumably due to the genetic alterations impairing cell death-inducing mechanisms (47).

In HCT116 cells, β-catenin displayed clear membrane localization; however, in LS174T cells, the protein was detected not only at the cellular membrane, but also in the cytoplasm and nucleus. As reported previously, the level of aberrant TCF/β-catenin–driven transcription depends on mutations in the genome of colorectal carcinoma cells. Cells expressing "short" APC mutants lacking the nuclear export signals exhibit high activity of the TOPFLASH reporter when compared with cells with wt *APC* but mutant β-*catenin* (28). HCT116 cells harbor one wt and one mutant (ΔS45) allele of β-*catenin*, whereas LS174T are homozygous for *missense* mutations (S45A) in the same triplet of the gene. This implies that subcellular distribution of β-catenin is related to the partially retained ability of HCT116 cells to regulate Wnt/β-catenin signaling. Nevertheless, because both mutant alleles (i.e., ΔS45 and S45A) are inhibited by monensin in reporter gene assays, the reason why HCT116 and LS174T cells display differential sensitivity to monensin is unclear. We suggest that particular cellular "wiring" of various signaling pathways or networks can contribute to the response of the respective cell to monensin.

Despite some prevailing uncertainties about the detailed inhibitory mechanism of monensin, our data imply that the antibiotic might be used as an anticancer drug, especially in neoplasia displaying aberrant Wnt signaling.

Disclosure of Potential Conflicts of Interest

No potential conflicts of interest were disclosed.

Authors' Contributions

Conception and design: P. Bartunek, V. Korinek
Development of methodology: A.R. Pombinho, P. Bartunek, V. Korinek
Acquisition of data (provided animals, acquired and managed patients, provided facilities, etc.): L. Tumova, A.R. Pombinho, M. Vojtechova, J. Stancikova, D. Gradl, M. Krausova, E. Sloncova, M. Horazna, V. Kriz, O. Machonova, Z. Zdrahal, V. Korinek
Analysis and interpretation of data (e.g., statistical analysis, biostatistics, computational analysis): L. Tumova, A.R. Pombinho, D. Gradl, Z. Zdrahal, V. Korinek
Writing, review, and/or revision of the manuscript: L. Tumova, V. Korinek
Administrative, technical, or material support (i.e., reporting or organizing data, constructing databases): J. Jindrich, P. Bartunek
Study supervision: P. Bartunek, V. Korinek

Acknowledgments

The authors thank S. Takacova for critically reading the manuscript, L. Andera, V. Bryja, K. Chalupsky, T. Valenta, and Q. Xu for reagents, and K. Sedova for the LC/MS-MS analysis.

Grant Support

This work was supported by Grant Agency of the Czech Republic Grant No. P305/12/2347 (to V. Korinek), Ministry of Industry and Trade of the Czech Republic Grant No. FR-TI4/802 (to P. Bartunek), Ministry of Education, Youth Sports of the Czech Republic Grants Nos. LM2011022 and LO1220 (to P. Bartunek), institutional Grant No. RVO 68378050 (to V. Korinek), and project CEITEC from the European Regional Development Fund Project No. CZ.1.05/1.1.00/02.0068 (to Z. Zdrahal).

The costs of publication of this article were defrayed in part by the payment of page charges. This article must therefore be hereby marked *advertisement* in accordance with 18 U.S.C. Section 1734 solely to indicate this fact.

Received August 2, 2013; revised December 23, 2013; accepted December 30, 2013; published OnlineFirst February 19, 2014.

References

1. Clevers H, Nusse R. Wnt/beta-catenin signaling and disease. Cell 2012;149:1192–205.
2. Polakis P. Wnt signaling in cancer. Cold Spring Harb Perspect Biol 2012;4.
3. Valenta T, Hausmann G, Basler K. The many faces and functions of beta-catenin. Embo J 2012;31:2714–36.
4. Siegel R, Naishadham D, Jemal A. Cancer statistics, 2012. CA Cancer J Clin 2012;62:10–29.
5. Kinzler KW, Nilbert MC, Su LK, Vogelstein B, Bryan TM, Levy DB, et al. Identification of FAP locus genes from chromosome 5q21. Science 1991;253:661–5.
6. Kinzler KW, Vogelstein B. Lessons from hereditary colorectal cancer. Cell 1996;87:159–70.
7. Morin PJ, Sparks AB, Korinek V, Barker N, Clevers H, Vogelstein B, et al. Activation of beta-catenin-Tcf signaling in colon cancer by mutations in beta-catenin or APC. Science 1997;275:1787–90.
8. Korinek V, Barker N, Morin PJ, van Wichen D, de Weger R, Kinzler KW, et al. Constitutive transcriptional activation by a beta-catenin-Tcf complex in APC−/− colon carcinoma. Science 1997;275:1784–7.
9. Huczynski A, Janczak J, Lowicki D, Brzezinski B. Monensin A acid complexes as a model of electrogenic transport of sodium cation. Biochim Et Biophys Acta 2012;1818:2108–19.
10. Xu Q, Wang Y, Dabdoub A, Smallwood PM, Williams J, Woods C, et al. Vascular development in the retina and inner ear: control by Norrin and Frizzled-4, a high-affinity ligand-receptor pair. Cell 2004;116:883–95.
11. Lukas J, Mazna P, Valenta T, Doubravska L, Pospichalova V, Vojtechova M, et al. Dazap2 modulates transcription driven by the Wnt effector TCF-4. Nucleic Acids Res 2009;37:3007–20.
12. Willert K, Brown JD, Danenberg E, Duncan AW, Weissman IL, Reya T, et al. Wnt proteins are lipid-modified and can act as stem cell growth factors. Nature 2003;423:448–52.
13. Urcan E, Haertel U, Styllou M, Hickel R, Scherthan H, Reichl FX. Real-time xCELLigence impedance analysis of the cytotoxicity of dental composite components on human gingival fibroblasts. Dent Mater 2010;26:51–8.
14. Waaler J, Machon O, Tumova L, Dinh H, Korinek V, Wilson SR, et al. A novel tankyrase inhibitor decreases canonical Wnt signaling in colon carcinoma cells and reduces tumor growth in conditional APC mutant mice. Cancer Res 2012;72:2822–32.
15. Doubravska L, Krausova M, Gradl D, Vojtechova M, Tumova L, Lukas J, et al. Fatty acid modification of Wnt1 and Wnt3a at serine is prerequisite for lipidation at cysteine and is essential for Wnt signalling. Cell Signal 2011;23:837–48.

Downloaded from mct.aacrjournals.org on August 10, 2015. © 2014 American Association for Cancer Research.

Published OnlineFirst February 19, 2014; DOI: 10.1158/1535-7163.MCT-13-0625

16. Gradl D, Kuhl M, Wedlich D. Keeping a close eye on Wnt-1/wg signaling in Xenopus. Mech Dev 1999;86:3–15.
17. Hawcroft G, D'Amico M, Albanese C, Markham AF, Pestell RG, Hull MA. Indomethacin induces differential expression of beta-catenin, gamma-catenin and T-cell factor target genes in human colorectal cancer cells. Carcinogenesis 2002;23:107–14.
18. Lu D, Carson DA. Spiperone enhances intracellular calcium level and inhibits the Wnt signaling pathway. BMC Pharmacol 2009;9:13.
19. Waki H, Park KW, Mitro N, Pei L, Damoiseaux R, Wilpitz DC, et al. The small molecule harmine is an antidiabetic cell-type-specific regulator of PPARgamma expression. Cell Metab 2007;5:357–70.
20. Stoick-Cooper CL, Weidinger G, Riehle KJ, Hubbert C, Major MB, Fausto N, et al. Distinct Wnt signaling pathways have opposing roles in appendage regeneration. Development 2007;134:479–89.
21. Morrell NT, Leucht P, Zhao L, Kim JB, ten Berge D, Ponnusamy K, et al. Liposomal packaging generates Wnt protein with in vivo biological activity. PLoS ONE 2008;3:e2930.
22. Zhu G, Wang Y, Huang B, Liang J, Ding Y, Xu A, et al. A Rac1/PAK1 cascade controls beta-catenin activation in colon cancer cells. Oncogene 2012;31:1001–12.
23. Meijer L, Skaltsounis AL, Magiatis P, Polychronopoulos P, Knockaert M, Leost M, et al. GSK-3-selective inhibitors derived from Tyrian purple indirubins. Chem Biol 2003;10:1255–66.
24. Ring DB, Johnson KW, Henriksen EJ, Nuss JM, Goff D, Kinnick TR, et al. Selective glycogen synthase kinase 3 inhibitors potentiate insulin activation of glucose transport and utilization in vitro and in vivo. Diabetes 2003;52:588–95.
25. Bernatik O, Ganji RS, Dijksterhuis JP, Konik P, Cervenka I, Polonio T, et al. Sequential activation and inactivation of Dishevelled in the Wnt/beta-catenin pathway by casein kinases. J Biol Chem 2011;286:10396–410.
26. Coombs GS, Yu J, Canning CA, Veltri CA, Covey TM, Cheong JK, et al. WLS-dependent secretion of WNT3A requires Ser209 acylation and vacuolar acidification. J Cell Sci 2010;123:3357–67.
27. Cruciat CM, Ohkawara B, Acebron SP, Karaulanov E, Reinhard C, Ingelfinger D, et al. Requirement of prorenin receptor and vacuolar H+-ATPase-mediated acidification for Wnt signaling. Science 2010;327:459–63.
28. Rosin-Arbesfeld R, Cliffe A, Brabletz T, Bienz M. Nuclear export of the APC tumour suppressor controls beta-catenin function in transcription. Embo J 2003;22:1101–13.
29. Ketola K, Vainio P, Fey V, Kallioniemi O, Iljin K. Monensin is a potent inducer of oxidative stress and inhibitor of androgen signaling leading to apoptosis in prostate cancer cells. Mol Cancer Ther 2010;9:3175–85.
30. Phelps RA, Chidester S, Dehghanizadeh S, Phelps J, Sandoval IT, Rai K, et al. A two-step model for colon adenoma initiation and progression caused by APC loss. Cell 2009;137:623–34.
31. Wu X, Tu X, Joeng KS, Hilton MJ, Williams DA, Long F. Rac1 activation controls nuclear localization of beta-catenin during canonical Wnt signaling. Cell 2008;133:340–53.
32. Hino S, Tanji C, Nakayama KI, Kikuchi A. Phosphorylation of beta-catenin by cyclic AMP-dependent protein kinase stabilizes beta-catenin through inhibition of its ubiquitination. Mol Cell Biol 2005;25:9063–72.
33. Fang D, Hawke D, Zheng Y, Xia Y, Meisenhelder J, Nika H, et al. Phosphorylation of beta-catenin by AKT promotes beta-catenin transcriptional activity. J Biol Chem 2007;282:11221–9.
34. Levy L, Wei Y, Labalette C, Wu Y, Renard CA, Buendia MA, et al. Acetylation of beta-catenin by p300 regulates beta-catenin-Tcf4 interaction. Mol Cell Biol 2004;24:3404–14.
35. Su LK, Kinzler KW, Vogelstein B, Preisinger AC, Moser AR, Luongo C, et al. Multiple intestinal neoplasia caused by a mutation in the murine homolog of the APC gene. Science 1992;256:668–70.
36. Kevin Ii DA, Meujo DA, Hamann MT. Polyether ionophores: broad-spectrum and promising biologically active molecules for the control of drug-resistant bacteria and parasites. Expert Opin Drug Discov 2009;4:109–46.
37. Beckett S, Lean I, Dyson R, Tranter W, Wade L. Effects of monensin on the reproduction, health, and milk production of dairy cows. J Dairy Sci 1998;81:1563–73.
38. Duffield T, Bagg R, Kelton D, Dick P, Wilson J. A field study of dietary interactions with monensin on milk fat percentage in lactating dairy cattle. J Dairy Sci 2003;86:4161–6.
39. Goren E, de Jong WA, Doornenbal P, Koopman JP, Kennis HM. Protection of chicks against Salmonella infantis infection induced by strict anaerobically cultured intestinal microflora. Vet Q 1984;6:22–6.
40. Mollenhauer HH, Morre DJ, Rowe LD. Alteration of intracellular traffic by monensin; mechanism, specificity and relationship to toxicity. Biochim Biophys Acta 1990;1031:225–46.
41. Park WH, Kim ES, Jung CW, Kim BK, Lee YY. Monensin-mediated growth inhibition of SNU-C1 colon cancer cells via cell cycle arrest and apoptosis. Int J Oncol 2003;22:377–82.
42. Park WH, Jung CW, Park JO, Kim K, Kim WS, Im YH, et al. Monensin inhibits the growth of renal cell carcinoma cells via cell cycle arrest or apoptosis. Int J Oncol 2003;22:855–60.
43. Park WH, Lee MS, Park K, Kim ES, Kim BK, Lee YY. Monensin-mediated growth inhibition in acute myelogenous leukemia cells via cell cycle arrest and apoptosis. Int J Cancer 2002;101:235–42.
44. Park WH, Seol JG, Kim ES, Kang WK, Im YH, Jung CW, et al. Monensin-mediated growth inhibition in human lymphoma cells through cell cycle arrest and apoptosis. Br J Haematol 2002;119:400–7.
45. Yoon MJ, Kang YJ, Kim IY, Kim EH, Lee JA, Lim JH, et al. Monensin, a polyether ionophore antibiotic, overcomes TRAIL resistance in glioma cells via endoplasmic reticulum stress, DR5 upregulation and c-FLIP downregulation. Carcinogenesis 2013;34:1918–28.
46. Lu D, Choi MY, Yu J, Castro JE, Kipps TJ, Carson DA. Salinomycin inhibits Wnt signaling and selectively induces apoptosis in chronic lymphocytic leukemia cells. Proc Natl Acad Sci U S A 2011;108:13253–7.
47. Vogelstein B, Kinzler KW. Cancer genes and the pathways they control. Nat Med 2004;10:789–99.

Downloaded from mct.aacrjournals.org on August 10, 2015. © 2014 American Association for Cancer Research.

Published OnlineFirst February 19, 2014; DOI: 10.1158/1535-7163.MCT-13-0625

AACR American Association for Cancer Research

Molecular Cancer Therapeutics

Monensin Inhibits Canonical Wnt Signaling in Human Colorectal Cancer Cells and Suppresses Tumor Growth in Multiple Intestinal Neoplasia Mice

Lucie Tumova, Antonio R. Pombinho, Martina Vojtechova, et al.

Mol Cancer Ther 2014;13:812-822. Published OnlineFirst February 19, 2014.

Updated version	Access the most recent version of this article at: doi:10.1158/1535-7163.MCT-13-0625
Supplementary Material	Access the most recent supplemental material at: http://mct.aacrjournals.org/content/suppl/2014/02/19/1535-7163.MCT-13-0625.DC1.html

Cited articles	This article cites 46 articles, 20 of which you can access for free at: http://mct.aacrjournals.org/content/13/4/812.full.html#ref-list-1

E-mail alerts	Sign up to receive free email-alerts related to this article or journal.
Reprints and Subscriptions	To order reprints of this article or to subscribe to the journal, contact the AACR Publications Department at pubs@aacr.org.
Permissions	To request permission to re-use all or part of this article, contact the AACR Publications Department at permissions@aacr.org.

Downloaded from mct.aacrjournals.org on August 10, 2015. © 2014 American Association for Cancer Research.

Supplementary material

Supplementary Materials and Methods

Cell culture and transfections

All cell lines were maintained in Dulbecco's modified Eagle's medium [(DMEM); purchased from Sigma)] supplemented with 10% fetal bovine serum (Gibco), penicillin, streptomycin and gentamicin (Invitrogen). Transfections were performed using Lipofectamine 2000 reagent (Invitrogen).

HTS

STF cells were seeded in 384-well plates (Corning) at 2500 cells/well density using Multidrop Combi dispenser (Thermo Scientific) and cultured overnight. The next day, mouse recombinant Wnt3a was added together with the tested compound (final concentration 1 mM) using pintool (V&P Scientific) coupled to a JANUS Automated Workstation (PerkinElmer). The cells were cultured for additional 24 h, lysed directly in the well, and the luciferase activity was determined.

Reporter gene, cell viability and apoptosis assays

The luciferase assays were performed as described previously (1) using the ONE-Glo Luciferase Assay System (Promega) for HTS and Dual-Glo Luciferase Assay System (Promega) for subsequent analysis. Bioluminescence was measured using EnVision Multilabel Reader (PerkinElmer). Mouse Wnt3a ligand was isolated from the culture medium of Wnt3a-producing L cells as described previously (2). Cell viability and apoptosis was determined after 48 h incubation with respective compounds using the Cell Titer-Blue Cell Viability Assay Kit and Caspase-Glo 3/7 Assay Kit, respectively (Promega). Recombinant human TRAIL was kindly provided by L. Andera. Apoptotic cells in the mouse intestine were detected using TumorTACS Detection Kit (RD Systems).

Plasmid constructs

Constructs encoding FLAG-tagged (N-terminus) human wt β-CATENIN and S45A and ΔS45 variants were generated by PCR and cloned into the pTripleFLAG-C3 mammalian expression vector. Constructs encoding the β-CATENIN variants S33Y, S37A and ΔN (the

N-terminal deletion encompassed amino acids 1-131) generated in expression vectors pCS2 and pcDNA3.1 (Invitrogen) were kindly provided by T. Valenta. The Lef1-VP16 construct encoding the N-terminally truncated mouse Lef1 (an internal Bgl II restriction enzyme recognition site was utilized for cloning) fused to the C-terminal transcription transactivation domain of the herpes simplex virus protein VP16 was generated in the pK-Myc vector (3); HA-CBP was obtained from Addgene (#32908). The expression construct encoding the N-terminally truncated human LRP6 (ΔN-LRP6) was a kind gift from V. Bryja.

Generation of Wnt1-producing cells

Mouse Wnt1 cDNA (1) was cloned into the lentiviral vector pCDH1 (System Biosciences). Lentiviruses were prepared using the Trans-Lentiviral Packaging System (Open Biosystems). Transduced cells were selected without subcloning using puromycin (Alexis; 5 μg/ml).

Immunocytochemistry, immunohistochemistry and antibodies

The techniques were performed as described previously (4, 5). These mouse monoclonal antibodies were used for immunocytochemistry and immunohistochemistry: anti-β-catenin (clone E-5, Santa Cruz; #14, BD Transduction Laboratories; EM-22, Exbio), anti-Ki67 (Mob 237, Diagnostic BioSystems), anti-Krt20 (K_S 20.8, Dako), anti-p21 (SXM30, BD Pharmingen), anti-PCNA (rabbit polyclonal, Abcam). These antibodies were used for immunoblotting: anti-α-tubulin (mouse monoclonal, TU-01, Exbio), anti-β-catenin (mouse monoclonal, EM-22, Exbio), anti-non-phospho-β-catenin/S33/S37/T41 (rabbit polyclonal, Cell Signaling), anti-phospho-β-catenin/Ser675 (rabbit polyclonal, Cell Signaling), anti-acetylated-lysine (rabbit monoclonal, #9814, Cell Signaling), anti-Axin2 (rabbit monoclonal, 76G6, Cell Signaling), anti-Flag (mouse monoclonal, M2, Sigma), anti-HA tag (mouse monoclonal, 12CA5, Abcam), anti-Tcf4 (rabbit monoclonal, C48H11, Cell Signaling), anti-LRP6 (rabbit monoclonal, C5C7, Cell Signaling), anti-phospho-LRP6/Ser1490 (rabbit polyclonal, Cell Signaling).

Densitometric analysis of western blots

Protein levels were quantified using GS-800 Calibrated Densitometer and Quantity One software (Bio-Rad).

Zebrafish tailfin regeneration assay

Zebrafish (less than 6 months of age) were kept in E3 medium (5 mM NaCl, 0.17 mM KCl, 0.33 mM $CaCl_2$ and 0.33 mM $MgSO_4$ in distilled H_2O) at 28°C. Fish that were approximately 2.5 cm long were anesthetized with tricaine (Sigma) and tips of their tail fin were carefully amputated using scissors. The animals were randomly distributed into aquaria (4-5 fish per tank) containing E3 medium with 2 μM (prepared from stock solution of 20 mM monensin in ethanol) or equivalent volume of ethanol alone. One week later, fish were anesthetized and photographed. The regenerated area (recognizable by lack of pigmentation) was scored in three independent experiments using ImageJ software.

Xenopus double axis formation assay

The assay was performed as described previously (6). Capped *XWnt8* and human *β-CATENIN* mRNAs were synthesized from linearized plasmid template using the mMESSAGE mMACHINE kit (Ambion). A marginal zone of the ventral blastomeres of 4-cell stage *Xenopus laevis* embryos was injected (4 nl) using 20 pg or 800 pg of *XWnt8* or *β-CATENIN* mRNA, respectively. mRNA was injected together with monensin (0.04 pmol) or vehicle (DMSO). The developing embryos were kept at 20 °C; the duplication of the body axis was scored 36 h after injection.

Cell proliferation assay

Metabolic incorporation of [^{3}H]-thymidine (MP Radiochemicals; final concentration 0.1 mCi/μl) was measured using MicroBeta2 Microplate Counter (PerkinElmer) after overnight incubation at 37°C.

Cell cycle analysis

SW480 and HCT116 CRC cells were fixed by 70% ethanol and stained using propidium iodide (Sigma; final concentration 20 μg/ml). Cell fluorescence was acquired using LSR II flow cytometer (BD Biosciences). Cells were stained with Hoechst 33342 (Invitrogen) to discriminate G2 cells and cell doublets.

Monitoring cell proliferation and attachment in "real time"

xCELLigence Real-Time Cell Analysis System (Roche Applied Science) was used according to the instructions of the manufacturer. Cells were seeded at density 1,500 cells per well. The electronic impedance of sensor electrodes was monitored every 15 minutes.

Eighteen hours after seeding monensin or DMSO was added to the wells and the measurement continued for additional 24 h. CI was quantified as described previously (7).

Quantification of proliferating cells in tissue sections

Tissue sections obtained from monensin or vehicle treated mice were incubated with an anti-PCNA antibody, washed and stained using the Alexa 488 dye conjugated to a goat anti-rabbit antibody (Molecular Probes) and DAPI (Sigma) nuclear stain. Ten fluorescent microscopy images were taken from five animals in each group. The PCNA and DAPI fluorescent signal in tumors was analyzed using the ImageJ software.

ROS measurement

The carboxy derivative of fluorescein (carboxy-H_2DCFDA; Molecular Probes) was utilized for ROS detection. Cells were seeded at density 20,000 cells/well of black 96-well plate. Cells were incubated with the carboxy-H_2DCFDA probe dissolved in culture medium (final concentration 100 μM) at 37°C for 50 min. Cells were washed twice with PBS and incubated with monensin or vehicle (DMSO). Hydrogen peroxide was used as a positive control. Probe oxidation measurement using started immediately after monensin/DMSO addition and continued every 6 minutes for 2 hours (at 37°C) using EnVision Multilabel Plate Reader. For each type of treatment, average value of the fluorescence and standard deviation was determined from 6 wells.

Disruption of the *APC* gene using TALENs

Constructs encoding one pair of TALENs targeting the human APC gene was purchased from TALEN Library Resources (H1458; Seoul National University, Korea). The TALENs recognition sequences are given in Supplementary Fig. S2. The TALEN constructs were co-transfected with EYFP-producing plasmid (pEYFP-N3; Clontech) into STF cells; the next day single EYFP positive cells were sorted and expanded. Genomic DNA isolated from individual cell clones was used to identify cells harboring modified *APC* alleles. At first, DNA fragment amplified from genomic DNA by primers hAPC TALEN test F 5’ GGCTGCGGTGAAAGCTATGATCATTCC 3’ and hAPC TALEN test R 5’ GATAACAGAAGTTGGTGGCCTTATATCC 3’ (fragment length obtained from the wt APC allele: 684 bp) was digested using Bgl II restriction endonuclease. Subsequently, DNA fragments isolated from six cell clones that were not (clone number: 1, 3, and 5) or partially

cut (2, 4, 6) by the enzyme were cloned into the pGEM-T Easy vector (Promega) and sequenced.

LC-MS/MS and protein kinase selectivity profiling

LC-MS/MS was performed using anti-β-catenin precipitates obtained from monensin-treated (5 μM) or control (DMSO) SW480 and HCT116 cells. After reduction and alkylation, precipitates were subjected to trypsin (Promega) digestion. The aliquot of each sample (1/100) was directly analyzed by LC-MS/MS for protein identification. Another part of sample (1/3) was subjected to phosphopeptide analysis. Phosphopeptides were enriched using TiO_2 kit (Thermo Fisher Scientific). Eluates were concentrated under vacuum and then diluted in 10 μl of 0.1% FA solution before the analysis. LC–MS/MS analysis was performed using reverse phase RSLCnano system (Dionex) on-line coupled with an Orbitrap Elite hybrid spectrometer (Thermo Fisher Scientific). The analysis of the mass spectrometric data files was carried out using the Proteome Discoverer software (version 1.3) with in-house Mascot search engine utility. Mascot MS/MS ion searches were done against NCBI protein database (taxonomy Mammalia). PhoshoRS feature was used for phosphorylation localization (8). Kinase profiling was performed at the International Centre for Protein Kinase Profiling, MRC, Dundee, UK.

Statistical analysis of data

Fisher's exact test was used to analyze the statistical significance of the results of the double axis formation assay. Data obtained in the gene reporter and qRT-PCR analyses were evaluated by Student's t-test.

Supplementary Figure Legends

Supplementary Figure S1. Densitometric analysis of western blots shown in Figs. 2D (A), 3B (C) and 4C (C). The diagrams represent the average optical density (OD) of detected bands. Values obtained in cells treated with vehicle (DMSO) were set to 100%. The level of the individual protein (or the protein form) was normalized to the α-TUBULIN signal. Error bars represent SDs.

Supplementary Figure S2. Monensin suppresses Wnt signaling activated by TALEN-induced disruption of the *APC* gene. A, luciferase reporter assay in parental STF cells and 6 cellular clones with one (clones 2, 4, 6) or both alleles (clones 1, 3, 5) of *APC* disrupted by TALENs. B, immunoblotting of cell lysates obtained from indicated clones illustrate an increase in the total β-catenin level in *APC*-deficient cells. C, DNA (top) and protein (bottom) sequences of the TALEN-targeted region and allelic changes found in clone 1. Numbers indicate the positions in the translated portion of *APC* cDNA or protein. TALEN-mediated cut and subsequent repair of genomic DNA generates 28 and 14 nucleotide deletions in the coding sequence resulting in a premature stop of the translation. Amino acid residues translated upon the frameshift are shown in red; asterisks indicate premature termini of the protein. D, monensin blocks Wnt signaling in *APC*-deficient STF cells. Results of the luciferase reporter assay performed in clone 1 cells treated with monensin or DMSO. The average luciferase units were corrected for the cell viability using Cell Titer Blue fluorescent measurement; error bars, SDs.

Supplementary Figure S3. Monensin does not interfere with Dvl phoshorylation. Immunoblotting of whole-cell extracts prepared from 3T3 cells treated with Wnt3a and monensin as indicated. The putative phosphorylated form of Dvl with changed mobility in the gel is marked by arrow. Cell extract obtained from cells treated with CK1ε inhibitor PF670462 (Sigma) was analyzed in the very right lane.

Supplementary Figure S4. The inhibitory effect of monensin on Wnt signaling is not restricted to the vesicular acidity blockade. The Wnt pathway was activated in STF using recombinant Wnt3a ligand (A), cell transduction with lentivirus expressing Wnt1 (B), transfection with the construct producing the N-terminally truncated Wnt co-receptor LRP6

(ΔN-LRP6) (C) and transient transfection with the construct encoding wt β-CATENIN (D). Luciferase activity was determined after overnight treatment with monensin, endosomal acidification inhibitor bafilomycin A or DMSO. The average RLU/s of a triplicate were corrected for cell viability or transfection efficiency using the Cell Titer-Blue Cell Viability Assay Kit (A) or Renilla luciferase construct (B, C, D). The Wnt pathway activity in cells treated with vehicle was arbitrary se to 100%. Error bars represent SDs.

Supplementary Figure S5. Monensin inhibits aberrant Wnt signaling in CRC cells COLO320 and LS174T. A, *APC*-deficient COLO320 cells and LS174T cells harboring oncogenic mutation in *β-catenin* were treated either with vehicle alone (DMSO) or monensin for 36 h before analysis. The diagrams depict the results of qRT-PCR analysis of the TCF/β-catenin target gene expression. The expression level of the given gene in unstimulated cells was arbitrarily set to 1. The amount of input cDNA was normalized to the *UBB* gene. The experiment was repeated twice in triplicates; error bars indicate SDs. Corresponding CT values are shown in Supplementary Table S4. Notice that the expression level of the Wnt target gene *LGR5* was evaluated in LST174 cells only, since the gene is not produced in other CRC cells. B, fluorescent microscopy images of COLO320 and LS174T cells treated either with DMSO or monensin for 36 h. In the merged images the β-catenin staining is depicted in green, cell nuclei were stained using DAPI stain (blue); original magnification: 400×. C, Western blot analysis of COLO320 and LS174T cells incubated for 36 h with vehicle or monensin. Densitometric analysis of the western blots is given at the right. D, monensin suppresses cell proliferation of COLO320 and LS174T cells. ^{3}H-thymidine incorporation into genomic DNA of cells treated with vehicle or monensin. The diagram depicts the mean values of four biological replicates with error bars indicating SDs; the ^{3}H-thymidine counts in control cells (treated with vehicle only) was arbitrarily set to 100%.

Supplementary Figure S6. ROS concentration is not increased by monensin. HEK293 and SW480 cells were incubated with the carboxy-H_2DCFDA ROS probe and treated with the indicated concentrations of monensin or vehicle (DMSO). Cell treated with hydrogen peroxide were used as a positive control. Florescence of oxidized probe was determined in 6 minute intervals. The diagrams represent average values of fluorescent units (FUs) obtained from six wells; error bars, SDs.

Supplementary Figure S7. Membranous localization of β-catenin in HCT116 cells. Confocal microscopy images of SW480, LS174T and HCT116 cells stained with the indicated anti-β-catenin antibodies.

Supplementary Figure S8. Monensin does not inhibit β-catenin acetylation. HEK293 cells were co-transfected with constructs encoding HA-tagged acetylase CREB binding protein (HA-CBP) and FLAG-tagged β-catenin. Beta-catenin was immunoprecipitated and its acetylation detected on the western blots using an anti-acetyl-lysine antibody. IP, immunoprecipitation; acetylated proteins non-specifically associated with Sepharose beads are indicated by red asterisk.

Supplementary Figure S9. Monensin does not change the fraction of proliferating cells in intestinal tumors. A, hematoxylin and anti-PCNA-stained sections of the jejunum of $APC^{+/Min}$ mice treated with monensin or vehicle (DMSO). B, microscopic images showing the PCNA flurescent signal in green and DAPI signal in blue. C, estimate of cell proliferation in tumors. Diagram represent the ratio of the PCNA to DAPI florescent signal in tumor tissue derived from monensin-treated or control mice; error bars, SDs. Bar: 0.2 mm (a, b); 0.1 mm (c, d, e, f); 0.066 mm (a', b'); 0.05 mm (c', d', e', f').

Supplementary Table Legends

Supplementary Table S1. Sequences of primers used for qRT-PCR analyses. The sequence of the forward primer is given in the upper line with the corresponding reverse primer in the lower line.

Supplementary Table S2. Monensin does not inhibit enzymatic activity of any of the tested protein kinases. The compound was profiled against a panel of 50 different kinases at a concentration of 0.1 and 1 μM; the quantification employed radioactive ^{33}P-ATP filter-binding assay (9). The data is presented as the remaining kinase activity in % at a given concentration of monensin in duplicate assays, and compared with DMSO controls. The profiling revealed that monensin did not inhibit enzymatic activity of any of the tested kinases below 60%, and the result was therefore considered to be negative.

Supplementary Table S3. qRT-PCR analysis of the TCF/β-catenin target gene expression in CRC cells. Cells were treated with DMSO (vehicle) or monensin 36 h before harvesting. The average CT values for the given gene normalized to *UBB* expression (CT value was arbitrarily set to 19) are shown. The experiment was performed in triplicates; corresponding diagrams (including SDs) are shown in Fig. 4B and Supplementary Fig. S5A.

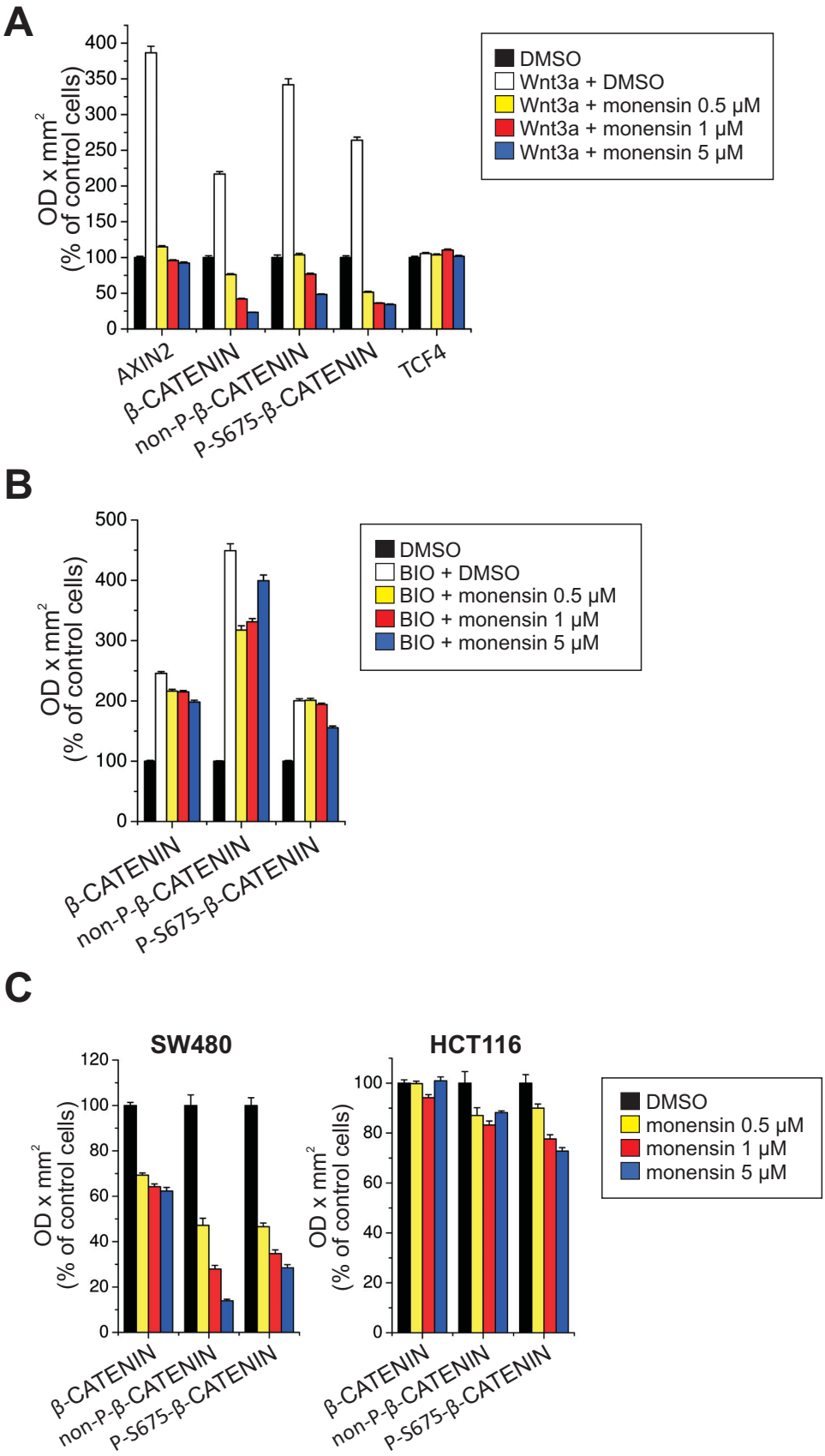
Supplementary Table S4. Cell cycle analysis of SW480 and HCT116 cells. Cells were incubated overnight with monensin, subsequently labeled using propidium iodide (PI) and their DNA content monitored by flow cytometry.

Supplementary Table S5. Analysis of phosphorylated amino acid residues in β-catenin. Beta-catenin precipitated from SW480 and HCT116 was subjected to the LC-MS/MS analysis. Cells were treated overnight with 5 μM monensin or DMSO. The numbers indicate the probability (%) and the ion score for each detected modification. The probability and the ion score was calculated using phoshoRS software and Mascot database search engine, respectively. Phoshorylation with the ion score ≥43 were considered as significant; n.d., not detected.

Supplementary References

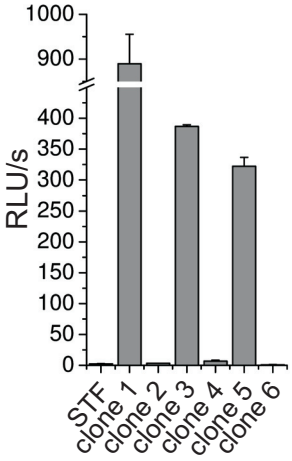
1. Lukas J, Mazna P, Valenta T, Doubravska L, Pospichalova V, Vojtechova M, et al. Dazap2 modulates transcription driven by the Wnt effector TCF-4. Nucleic Acids Res. 2009;37:3007-20.
2. Willert K, Brown JD, Danenberg E, Duncan AW, Weissman IL, Reya T, et al. Wnt proteins are lipid-modified and can act as stem cell growth factors. Nature. 2003;423:448-52.
3. Valenta T, Lukas J, Korinek V. HMG box transcription factor TCF-4's interaction with CtBP1 controls the expression of the Wnt target Axin2/Conductin in human embryonic kidney cells. Nucleic Acids Res. 2003;31:2369-80.
4. Waaler J, Machon O, Tumova L, Dinh H, Korinek V, Wilson SR, et al. A novel tankyrase inhibitor decreases canonical Wnt signaling in colon carcinoma cells and reduces tumor growth in conditional APC mutant mice. Cancer Res. 2012;72:2822-32.
5. Doubravska L, Krausova M, Gradl D, Vojtechova M, Tumova L, Lukas J, et al. Fatty acid modification of Wnt1 and Wnt3a at serine is prerequisite for lipidation at cysteine and is essential for Wnt signalling. Cell Signal. 2011;23:837-48.
6. Gradl D, Kuhl M, Wedlich D. Keeping a close eye on Wnt-1/wg signaling in Xenopus. Mech Dev. 1999;86:3-15.
7. Urcan E, Haertel U, Styllou M, Hickel R, Scherthan H, Reichl FX. Real-time xCELLigence impedance analysis of the cytotoxicity of dental composite components on human gingival fibroblasts. Dental materials : official publication of the Academy of Dental Materials. 2010;26:51-8.
8. Taus T, Kocher T, Pichler P, Paschke C, Schmidt A, Henrich C, et al. Universal and confident phosphorylation site localization using phosphoRS. J Proteome Res. 2011;10:5354-62.
9. Park YW, Cummings RT, Wu L, Zheng S, Cameron PM, Woods A, et al. Homogeneous proximity tyrosine kinase assays: scintillation proximity assay versus homogeneous time-resolved fluorescence. Anal Biochem. 1999;269:94-104.

Supplementary Figure S1

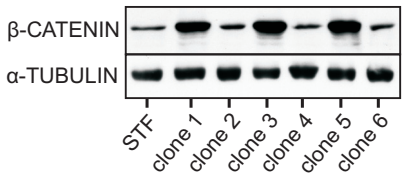


Suplementary Figure S2

A



B



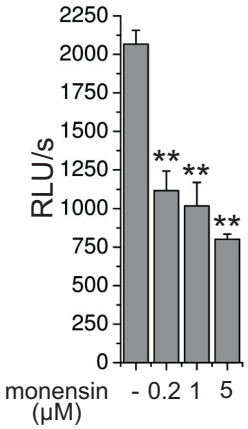
C

TALEN left recognition site — TALEN right recognition site

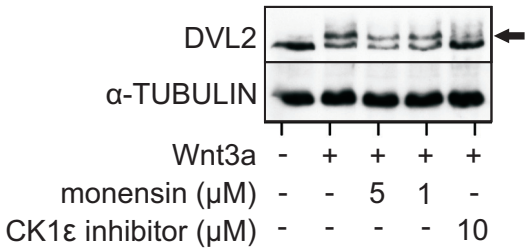
wt APC cDNA	1397	GTGCCAGCTCCTGTTGAACATC**AGATCT**GTCCTGCTGTGTGTGTTCTAATGAAACTTTCATTTGATGAAGAGCATAGACATGCAATGAAT	1487
targeted allele 1		GTGCCAGCTCCTGTTGAACATC----------GAAACTTTCATTTGATGAAGAGCATAGACATGCAATGA	
targeted allele 2		GTGCCAGCTCCT----------CTGTCCTGCTGTGTGTGTTCTAATGAAACTTTCATTTGA	

wt APC protein	367	VPAPVEHQICPAVCVLMKLSFDEEHRHAMN	396
truncated protein 1		VPAPVEHRNFHLMKSIDMQ*	
truncated protein 2		VPAPLSCCVCSNETFI*	

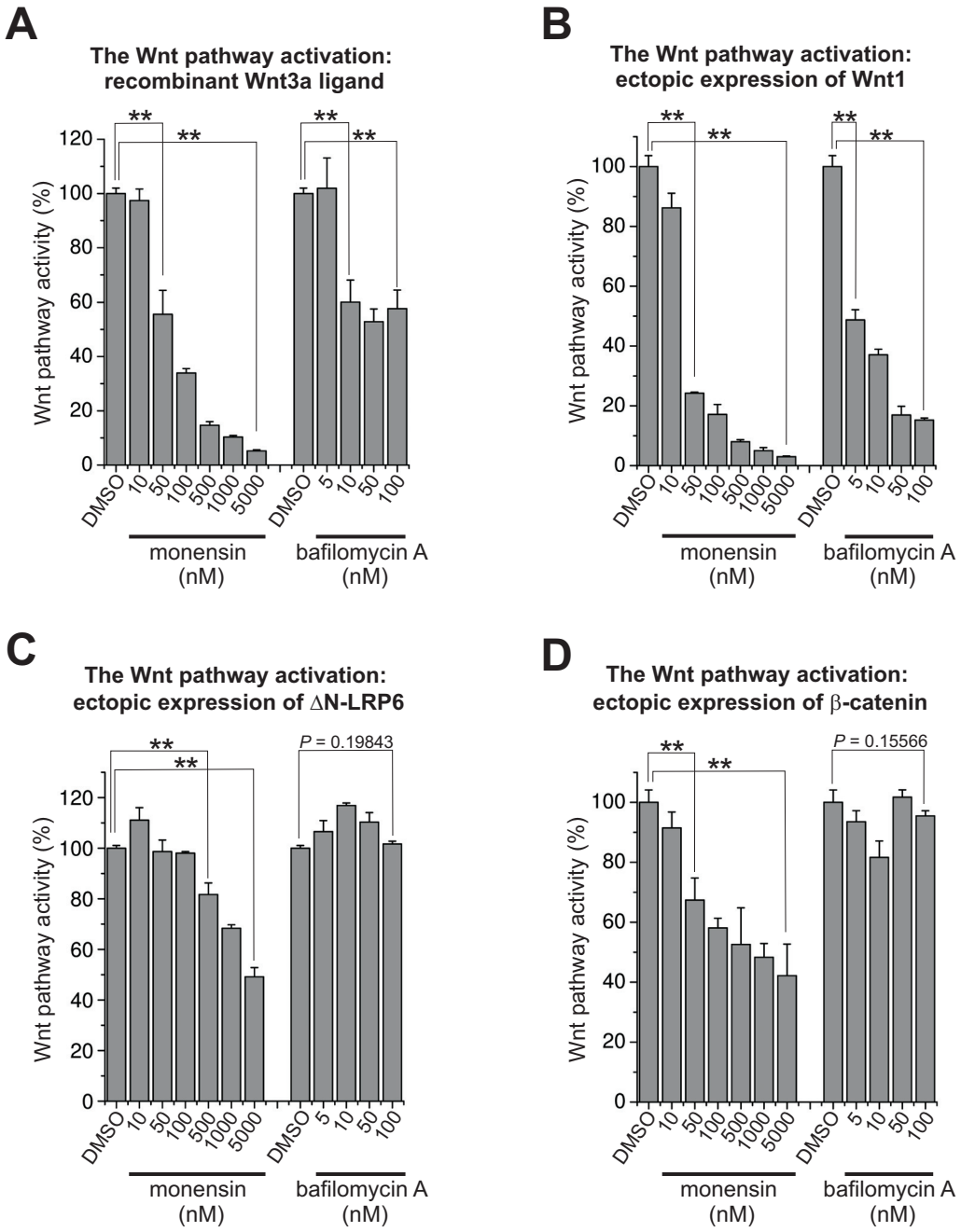
D



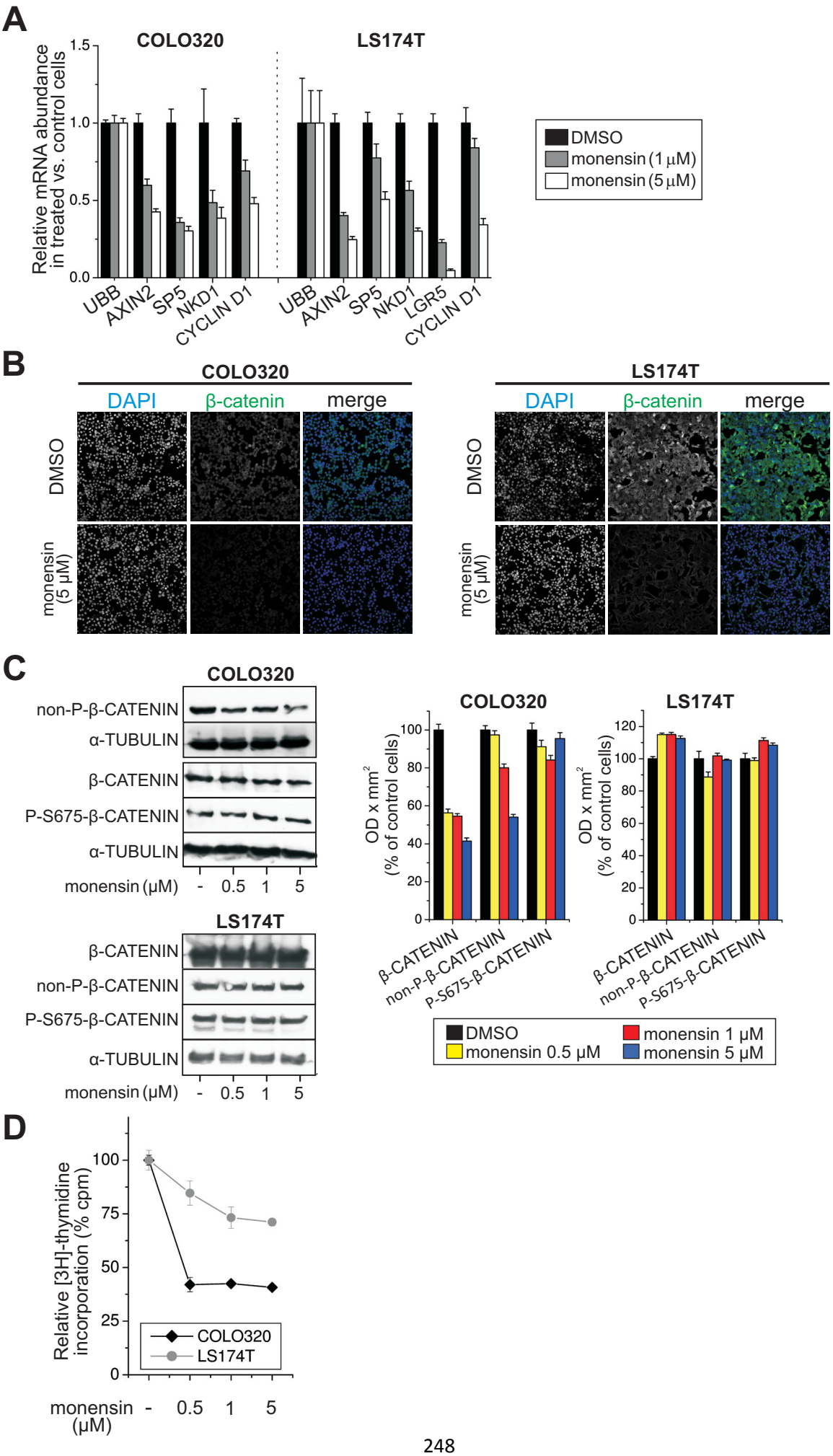
Supplementary Figure S3



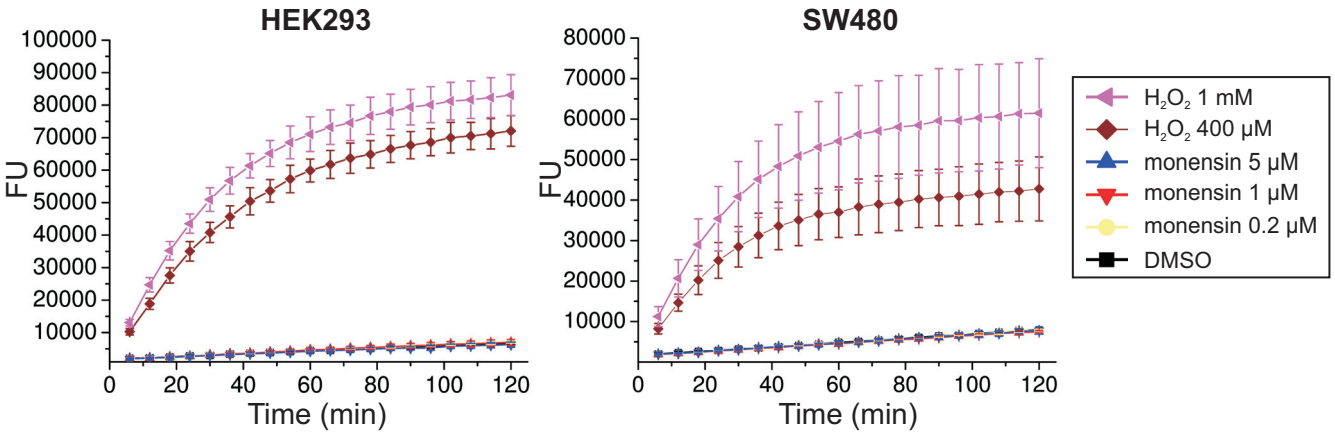
Supplementary Figure S4



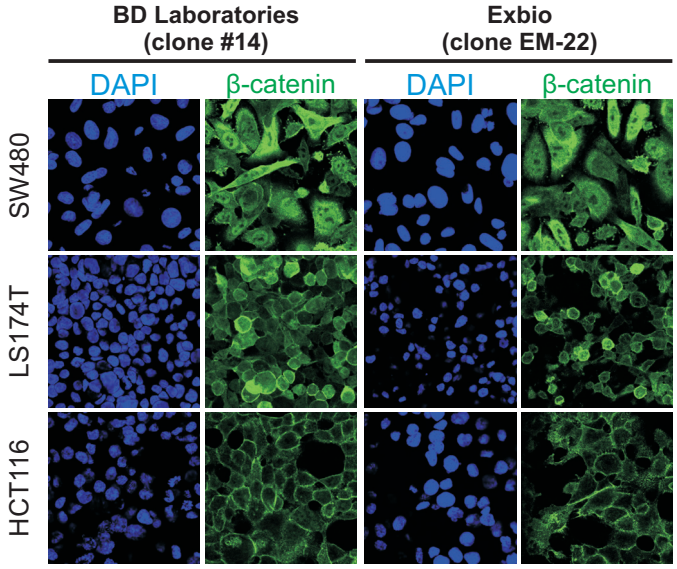
Supplementary Figure S5



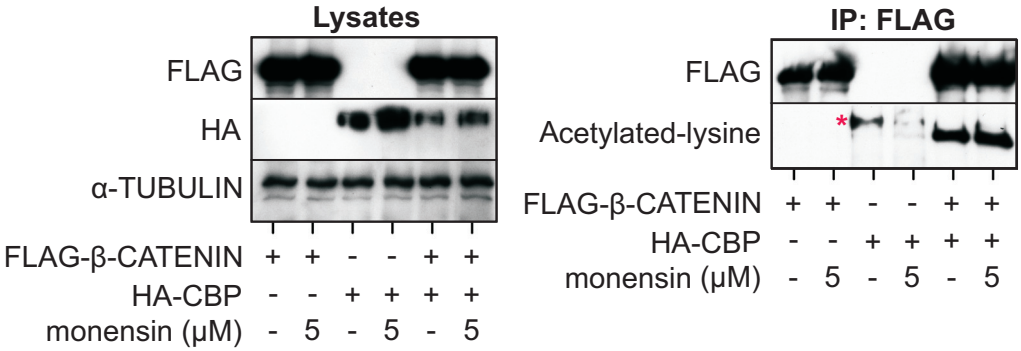
Supplementary Figure S6



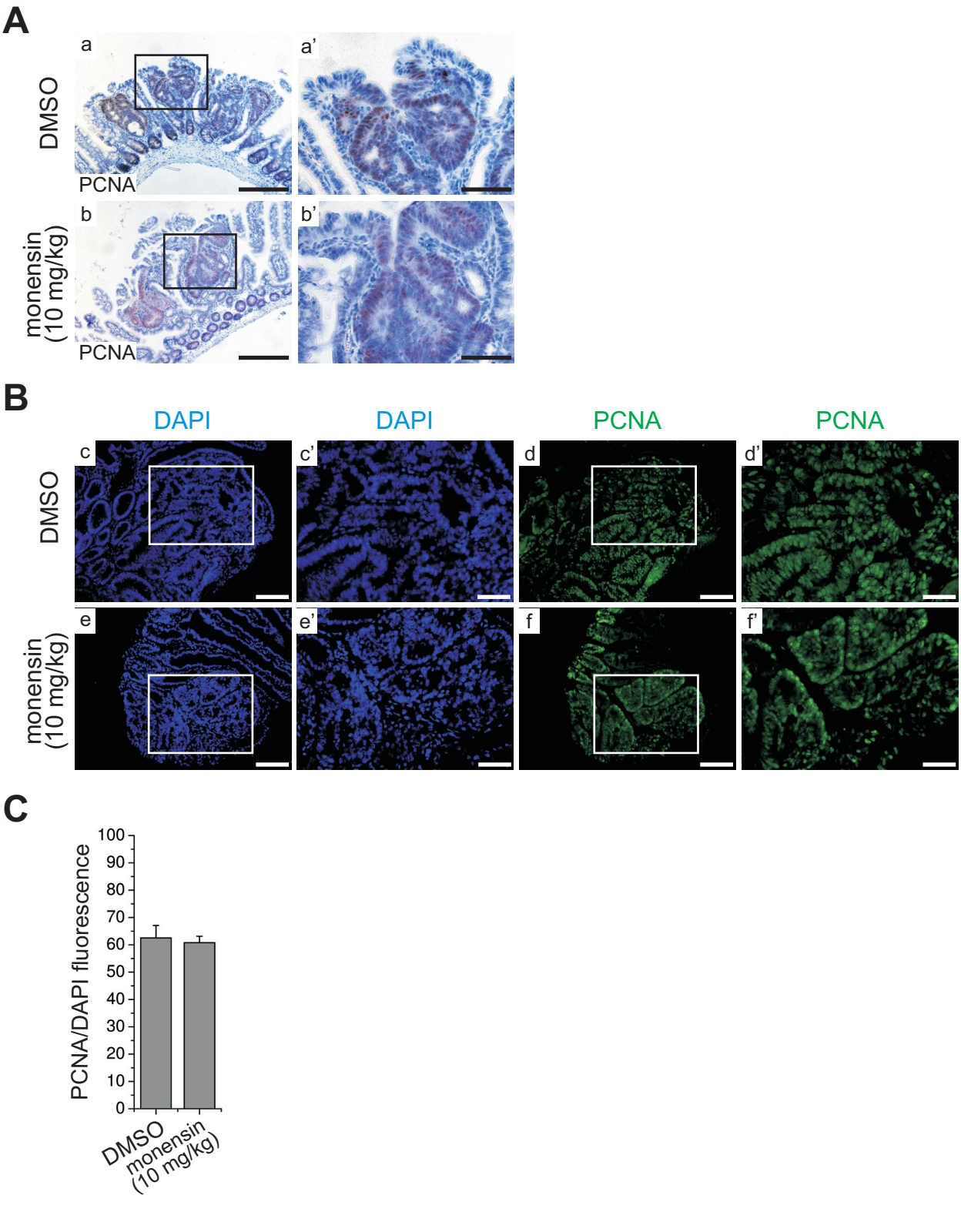
Supplementary Figure S7



Supplementary Figure S8



Supplementary Figure S9



Supplementary Table S1

gene	primer sequence
β-ACTIN	5'-GGCATCCTCACCCTGAAGTA-3'
	5'-AGGTGTGGTGCCAGATTTTC-3'
AXIN2	5'-CTGGCTTTGGTGAACTGTTG-3'
	5'-AGTTGCTCACAGCCAAGACA-3'
CYCLIN D1	5'-CCATCCAGTGGAGGTTTGTC-3'
	5'-AGCGTATCGTAGGAGTGGGA-3'
LGR5	5'-CTCTTCCTCAAACCGTCTGC-3'
	5'-GATCGGAGGCTAAGCAACTG-3'
NKD1	5'-CGCCGGGATAGAAAACTACA-3'
	5'-CTGGAGCTCTGAGACCTTGG-3'
SP5	5'-ACTTTGCGCAGTACCAGAGC-3'
	5'-ACGTCTTCCCGTACACCTTG-3'
UBB	5'-GCTTTGTTGGGTGAGCTTGT-3'
	5'-TCACGAAGATCTGCATTTTGA-3'

Supplementary Table S2

kinase	**monensin 1 µM**		**monensin 0.1 µM**	
	activity (%)	deviation	**activity (%)**	deviation
MKK1	**81**	3	**85**	11
JNK1	**76**	4	**80**	12
p38a MAPK	**87**	0	**90**	2
RSK1	**89**	5	**94**	1
PDK1	**94**	1	**96**	3
PKBa	**97**	13	**105**	11
SGK1	**91**	27	**97**	7
S6K1	**103**	10	**91**	5
PKA	**105**	6	**103**	6
ROCK 2	**88**	5	**78**	4
PRK2	**81**	12	**83**	5
PKCa	**112**	21	**113**	19
PKD1	**82**	5	**92**	5
MSK1	**114**	8	**106**	11
CAMKKb	**85**	5	**97**	8
CAMK1	**82**	8	**101**	9
SmMLCK	**91**	2	**88**	8
CHK2	**101**	2	**94**	12
GSK3b	**87**	9	**98**	12
PLK1	**86**	2	**101**	15
Aurora B	**80**	4	**77**	0
LKB1	**92**	3	**97**	2
AMPK (hum)	**84**	0	**98**	7
MARK3	**82**	5	**78**	4
CK1δ	**78**	0	**92**	8
CK2	**87**	13	**95**	8
DYRK1A	**103**	8	**100**	15
NEK6	**85**	5	**80**	15
TBK1	**90**	4	**92**	17
PIM1	**130**	4	**124**	12
SRPK1	**88**	7	**87**	7
EF2K	**94**	5	**92**	4
HIPK2	**97**	11	**93**	8
PAK4	**93**	2	**84**	4
MST2	**89**	5	**91**	9
MLK3	**78**	2	**76**	3
TAK1	**91**	3	**90**	3
IRAK4	**97**	13	**105**	5

RIPK2	**90**	13	**76**	1
TTK	**100**	3	**88**	40
Src	**89**	9	**93**	8
Lck	**96**	3	**100**	17
BTK	**99**	2	**96**	22
JAK2	**80**	4	**94**	10
SYK	**109**	8	**109**	12
EPH-A2	**99**	14	**103**	8
HER4	**116**	28	**108**	6
IGF-1R	**87**	4	**98**	7
TrkA	**99**	14	**98**	22
VEG-FR	**80**	8	**88**	19

Supplementary Table S3

cell line	**SW480**					**COLO320**		
treatment	DMSO	monensin 0.1 μM	monensin 0.2 μM	monensin 1 μM	monensin 5 μM	DMSO	monensin 1 μM	monensin 5 μM
β-ACTIN	15.74	16.06	16.36	16.20	16.86	16.60	16.53	16.41
AXIN2	22.42	24.43	24.51	24.85	26.34	20.07	20.85	21.30
CYCLIN D1	22.74	23.56	23.81	24.38	25.22	27.78	28.37	28.85
NKD1	21.63	23.26	23.60	24.23	26.29	21.37	22.30	22.59
SP5	26.54	26.34	27.00	29.25	31.25	29.91	31.45	31.75

cell line	**LS174T**			**HCT116**				
treatment	DMSO	monensin 1 μM	monensin 5 μM	DMSO	monensin 0.1 μM	monensin 0.2 μM	monensin 1 μM	monensin 5 μM
β-ACTIN	17.01	16.73	16.73	15.70	15.80	15.74	15.97	15.90
AXIN2	21.45	22.71	23.47	29.95	29.54	30.10	30.39	29.83
CYCLIN D1	22.74	22.99	24.29	23.37	23.22	23.65	23.32	23.04
NKD1	22.03	22.79	23.75	28.04	27.33	27.64	27.89	27.65
SP5	29.15	29.57	30.13	34.15	33.45	34.42	33.36	32.62

Supplementary Table S4

cell line	**SW480**			**HCT116**		
treatment	DMSO	monensin 1 μM	monensin 5 μM	DMSO	monensin 1 μM	monensin 5 μM
G_1	44.4	53.0	59.2	28.8	29.6	28.5
S	43.3	38.0	33.8	50.8	50.4	58.4
G_2/M	11.3	8.2	5.2	18.5	17.2	11.9

Supplementary Table S5

LC-MS/MS analysis				
cell line	**HCT116**		**SW480**	
treatment	**DMSO**	**monensin 5 µM**	**DMSO**	**monensin 5 µM**
Phosphorylated amino acid residue	Probability/Score	Probability/Score	Probability/Score	Probability/Score
S191	100/32	n.d.	n.d.	n.d.
S552	99/57	50/43	99/56	99/57
S675	100/44	100/50	100/47	100/46

Unique gene expression signatures in the intestinal mucosa of germ-free and monoassociated gnotobiotic mice

In many studies from the last years the topic related the gut microbiota has been intensively investigated (Littman and Pamer 2011; Faith et al. 2013; Palm et al. 2015). It was proved, that proper and balanced microbiome composition contributes to development and maintenance of the immune system (Sommer and Backhed 2013) and intestinal epithelium architecture (Johansson and Hansson 2011; Johansson et al. 2011). Moreover, dysbiosis, the pathological disruption of microbiome and host body relationship, could result in autoimmune disease outbreaks and in cancer development (Rao et al. 2006; Poutahidis et al. 2013). It is also evident, that gut microbiome influences various signaling pathways. To uncover some of them, we performed expression profiling of CR and GF mice as well as GF mice monoassociated with pathologic *E. coli* strain O6K13 (Dahlgren et al. 1990) and non-pathogenic probiotic strain Nissle 1917 (Jacobi and Malfertheiner 2011; Behnsen et al. 2013).

In our investigation, we used samples of scraped mucosa from the middle and distal segments of the small intestine and colon. Specimens were evaluated by cDNA microarrays. Subsequently, the Enrichr gene library online tool classed the genes selected by twice fold change to Gene Ontology Biological Process (GO BP) categories. Some of the genes were investigated also at the protein level using immunohistochemistry. At first, we compared the three gut segments of CR and GF animals. In the small intestine, different gene expression was found mainly in GO BPs related to the adaptive or innate immune response. This notion is consistent with results from studies linking poor immune system development in GF mice (Sommer and Backhed 2013; El Aidy et al. 2015). In the colon, the situation appeared quite similar exhibiting downregulated genes connected to the immune system function such as *histocompatibility 2, class II antigen A, beta 1* (*H2-Ab1*), *H2-DMb1* and *class II transactivator* (*Ciita*), although the group of differentially expressed genes was smaller than in the small intestine. Additionally, we noted downregulated genes encoding pancreatic enzymes connected to lipid metabolism. Low adipocyte counts and decreased lipogenesis and levels of triglycerides were previously described in GF mice (Backhed and Crawford 2010).

Next, we focused on comparison of GF together with monoassociated mice strains and CR mice. The results suggested that monoassociation of GF animals did not restore the mucosal immune system as the mentioned immune-related and lipogenesis-related gene

expression is still downregulated in both GF and monoassociated mice. We then compared GF animals with CR and monoassociated mice to uncover genes, which are differently expressed in microbe-free organism. Among others, decreased expression of genes related to IBD (Taggart et al. 2005; Franke et al. 2008; Yamazaki et al. 2009), epithelial cell differentiation [reviewed in (Krausova and Korinek 2012)] and inflammation defense (Baughman et al. 1997), such as *insulin receptor substrate 2* (*Irs2*), *NK2 transcription factor related, locus 3* (*Nkx2-3*), *transforming growth factor, beta receptor II* (*Tgfbr2*), *secretory leukocyte peptidase inhibitor* (*Slpi*) and *FK506 binding protein 5* (*Fkbp5*) were downregulated in small intestine. Genes uniquely upregulated in the small intestine of GF mice were involved in EMT (*Foxq1*) (Qiao et al. 2011; Feng et al. 2012) and IBD [*endothelin 1* (*Edn1*)] (Yu et al. 2010). In the colon, GF mice exhibited decreased levels of *regenerating islet-derived family, member 4* (*Reg4*), an anti-apoptotic factor employed in carcinogenesis and tissue regeneration (Rafa et al. 2010; Numata and Oshima 2012). Additionally, upregulated level of *aldehyde dehydrogenase family 1, subfamily A1* (*Aldh1a1*) previously described as a marker of cancer SCs (Ginestier et al. 2007; Li et al. 2010b) was observed.

Finally, we asked, which genes are differentially expressed in the small intestine and colon associated solely by probiotic Nissle bacteria in comparison to pathogenic *E. coli* O6K13. Many genes scoring in the colon were mostly related to adipose tissue, adipocyte metabolism and lipid metabolism. Moreover, upregulated *Fgf10*, *calbindin 2* (*Calb2*) and *vasoactive intestinal polypeptide* (*Vip*) were detected. *Calb2* is suggested to be expressed in colorectal tumors (Gotzos et al. 1999) and mesothelioma cells (Doglioni et al. 1996). *Vip* is related to colonic relaxation and antiinflammatory defense (Chandrasekharan et al. 2013).

In summary, we described the expression profile in intestine of mice depending on the microbiota composition. We confirmed previous results, that the microbiota composition modulates the organismal immunity development. Furthermore, we deduced that the monoassociation did not restore the natural organismal defense. We believe, that our recent work should be promising for future studies concerning microbial-organismal symbiosis.

Author´s contribution: mouse tissue isolation, fixation and paraffin or O.C.T. embedding, RNA isolation and purification, qRT-PCR, co-design of experiments, co-writing the manuscript

Unique gene expression signatures in the intestinal mucosa of germ-free and monoassociated gnotobiotic mice

Lucie Janeckova[1*], Jitka Stancikova[1*], Hynek Strnad[1], Tomas Hudcovic[2], Jolana Tureckova[1], Monika Horazna[1], Nikol Baloghova[1], Eva Sloncova[1], Katerina Galuskova[1], Helena Tlaskalova-Hogenova[2] and Vladimir Korinek[1#]

Authors' affiliations:

[1] *Institute of Molecular Genetics, Academy of Sciences of the Czech Republic, Videnska 1083, 142 20 Prague 4, Czech Republic*

[2] *Institute of Microbiology, Academy of Sciences of the Czech Republic, Videnska 1083, 142 20 Prague 4, Czech Republic*

*****_These authors contributed equally to this work._

[#] **Corresponding author:**

Vladimir Korinek

Institute of Molecular Genetics AS CR

Videnska 1083

142 20 Prague 4, Czech Republic

Tel: (+420) 241063146

FAX: (+420) 244472282

e-mail: korinek@img.cas.cz

Running title: Gene expression profiling of germ-free and gnotobiotic mice

Key words: expression profiling, Enricher tool, gnotobionts, gut microbiota, monoassociation, transcriptional analysis

Abstract

Mammalian gut is colonized by a vast number of microbiota that are essential for proper functioning of the organ. Commensal microbiota contribute to gut homeostasis by inducing region-dependent mucosal transcription. In this study, we determined the expression profiles of mucosa isolated from the small intestine and colon of germ-free (GF) mice and animals monoassociated with a single bacterial strain. We showed that the complete absence of microbiota in the intestine mainly affected the mucosal immune cells, adipose tissue, and lipid metabolism. The expression signature of small intestinal mucosa of mice monoassociated with two different *E. coli* strains was almost identical. However, in the colon monoassociated with probiotic *E. coli* strain Nissle 1917, more than 60 genes were upregulated in comparison to mice colonized with the *E. coli* uropathogenic strain O6K13. The genes differentially expressed in Nissle 1917-monocolonized mice mainly encoded secreted proteins or enzymes involved in the lipid metabolism, structural proteins of muscle cells and/or factors that influence muscle contractility. In addition, the expression levels of genes coding for proteins mediating cell-to-cell or cell-to-extracellular matrix interactions were increased. The expression data also showed that monoassociation does not fully restore the mucosal immune system.

Introduction

Mammalian gut is a complex organ consisting of cells and tissues intrinsic for the organism and, in addition, containing vast amounts of bacteria. The bacterial population in the gut, so-called microbiota (microbiome), outnumbers the amount of cells in the human body in ratio 10:1[1]. The presence of the commensal microbes is required for proper digestion, vitamin production, and acquisition of nutrients that cannot otherwise be processed. Gut colonization by microbiota is crucial for the development and function of the intestinal immune system [reviewed in[2,3]). The colonization takes place at delivery, while the newborn is passing through the birth canal, and during breast-feeding from the already colonized mother. In case that the colonization occurs at later age, the immune response to various stimuli is decreased and never recovers the levels observed in animals kept in standard conditions[4]. The composition of microbial populations is influenced during the lifetime by the host's diet, antibiotics usage, and genetic background of the host (reviewed in[5]). Interestingly, a single gene polymorphism may impact the bacterial population diversity in the intestine[6]. Furthermore, oral tolerance to various bacterial and food antigens develops in mice during the neonatal period and cannot be fully restored in adult originally GF animals upon bacterial colonization[7]. The absence of immune tolerance in GF animals resulted in allergies and inflammations or metabolic disorders such as diabetes (reviewed in[8]). The link between the gut colonization and diverse disorders including autoimmune diseases has been observed in humans (reviewed in[9]). Moreover, several recent studies documented microbiome changes during intestinal cancerogenesis or involvement of intestinal dysbiosis in cancer development[10-12]. Deciphering the impact of commensal microbiota on the biological processes in the gut provides an important insight into the function of this organ in homeostatic or pathological conditions.

Expression profiles of gut tissue obtained from conventionally reared (CR) or GF mice documented a profound effect of the microbiota on gene expression[4,13,14]. Additionally, colonization of GF animals by the microbiota provokes dynamic alterations in gene expression prior to reaching homeostasis[13,15].

In this study, we employed GF and gnotobiotic mice monocolonized either with *Escherichia coli* (*E. coli*) Nissle 1917 or O6K13 strain to study mucosal gene expression upon exposure to a single bacterial type. The *E.coli* O6K13 strain belongs to antigen K13-producing uropathogenic bacteria[16]. The *E. coli* Nissle 1917 strain represents a striking example of bacterial evolution. Although its serotype is typical of uropathogenic *E. coli* strains, the strain is not pathogenic. It produces neither pathogenic adhesion factors nor enterotoxins or cytotoxins and its beneficial probiotic effects were documented in numerous studies. However, the molecular mechanisms related to its probiotic effects are mostly unclear. It was suggested that the bacteria protect the intestine indirectly by preventing colonization by mucosal pathogens. Additionally, the strain exerts an immune function by suppressing inflammation or it enhances the epithelial defense and barrier functions (reviewed in[17,18]). To reveal which biological processes or cell types are affected by the absence or low complexity of commensal microbiota in the mouse intestine, the expression profiles of mucosa isolated from the small intestine and colon of GF mice and animals monoassociated with the single *E. coli* strains was determined. The results were compared to the expression data obtained in conventionally bred mice harboring a complete microbiome. The obtained datasets were evaluated using the Enricher gene library online tool (http://amp.pharm.mssm.edu/Enrichr/). The analysis revealed that the complete absence of intestinal microbiota mainly affected the mucosal immune system, which was not restored upon monoassociation. Furthermore, the expression changes mainly observed in the colon indicated alterations in adipose tissue and lipid metabolism. Comparison of monoassociated mice showed additional genes encoding extracellular signaling molecules, genes expressed in muscle cells or genes encoding proteins mediating cell-to-cell or cell-to-extracellular matrix interactions.

Results and Discussion

The absence of commensal microbiota in the intestine mainly affects the mucosal immune system

Expression profiling was performed using total RNA isolated from scraped mucosal lining of the middle and distal parts of the small intestine (further indicated as SI-middle, SI-distal, respectively) and from the colon. Of note, RNA obtained from the proximal small intestine was partially degraded, and was excluded from the analysis. The tissues were obtained from GF and CR mice and mice monoassociated with the *E. coli* Nissle 1917 or O6K13 strain[19], further referred to as 'N' and 'O' mice, respectively. RNA isolated from at least four littermates per each group was analyzed using cDNA microarrays. Initial evaluation was focused on genes whose expression had changed significantly (expression intensity of the given gene changed more than twice between samples and $q < 0.05$) in the comparison of CR and GF mice. The analysis revealed that 89, 195, and 94 genes were differentially expressed in the SI-middle, SI-distal, and colonic segments, respectively (Supplementary Table S1). We used the Enricher gene analysis tool to assign the genes to the 'Gene Ontology Biological Process' (GO BP) categories. Enricher provided an optimized algorithm for Gene Set Enrichment Analysis (GSEA)[20] with unique evaluation of statistical significance using the deviation from the expected rank method[21]. As expected, in the small intestine the majority of GO BPs were associated with the adaptive or innate immune response. Nevertheless, 'positive regulation of smooth muscle cell migration' GO BP was on the top of the GO BP list when the SI-middle gene set was analyzed. Thus, we utilized the BioGPS gene annotation portal (http://biogps.org/) to investigate tissue- and cell-specific expression of genes assigned to this GO BP [*allograft inflammatory factor 1* (*Aif1*); *chemokine (C-C motif) ligand 5* (*Ccl5*); *pyrimidinergic receptor P2Y, G-protein coupled, 6* (*P2RY6*)] in more detail. Interestingly, all these genes are highly expressed in various immune cells. Therefore, we extended the analysis and assigned the obtained gene sets to the 'Cell Types/Mouse Gene Atlas' (CT/MGA) category of the Enricher tool. This confirmed that indeed, in the small intestinal mucosa, the majority of genes with the most significantly altered expression encode proteins produced in hematopoietic cells or tissue (Fig. 1). Moreover, since the expression level of these genes

was mainly reduced in GF mice, this was consistent with the previously published observation that gut microbiota are indispensable for establishment and maintenance of the mucosal immune system (reviewed in[3,22]). In contrast, only a limited number of genes were upregulated in the small intestine of GF mice. Microbiota extract energy and various metabolites from partially digested food. Additionally, gut microbiota modulate the proliferation and differentiation of epithelial cells (reviewed in[23]). In accord with these metabolic and trophic functions, the absence of microbiota influenced expression of genes involved in the transport and metabolism of nutrients or various intracellular signaling cascades. Additional upregulated genes in the distal part of the GF small intestine were *endothelin 1* (*Edn1*) encoding a vasoconstrictive peptide[24], *opioid receptor, kappa 1* (*Oprk1*), which is mainly expressed in the nervous system and functions in pain perception[25], and angiopoietin-like 4 [(Angptl4); alternative name fasting-induced adipocyte factor (Fiaf)], a secreted protein with multiple physiological roles in the organisms (reviewed in[26]). Angptl4 blocks lipoprotein lipase-mediated storage of triglycerides in adipocytes and its expression in the small intestine is decreased upon re-colonization of GF mice[27-30]. Additionally, Angptl4 is required for functional partitioning of postnatal intestinal lymphatic and blood vessels and, moreover, it also promotes survival of endothelial cells[31] or inhibits proliferation and migration of endothelial cells[32]. Another gene found upregulated in both SI-middle and SI-distal datasets was *solute carrier family 7, member 8* (*Slc7a8*), a gene encoding a membrane amino acid transporter[33]. *Slc7a8* is specifically produced in mast cells (refer to the http://biogps.org/#goto=genereport&id=50934 web page), possibly indicating increased counts of this specific cell type in the mucosa of germ-free animals. Additionally, the pro-apoptotic *Bcl2-like 11* (*Bcl2l11*) gene upregulated in the SI-middle segment of GF mice is mainly produced in peripheral macrophages (http://biogps.org/#goto=genereport&id=12125). These results indicated that the gene expression changes might be caused either by variation in the numbers of a particular cell type(s) producing the given mRNA or by direct alteration in the expressional level of the given gene in mucosal cells. However, without additional experiments (e.g. immunohistochemical staining or cell sorting) distinguishing these mutually nonexclusive alternatives will be impossible.

The situation in the colon seemed to be more complex and none of the GO BP category contained more than two genes (Fig. 1). However, a significant decrease in the expression of immune

cell-specific genes [e.g. *histocompatibility 2, class II antigen A, beta 1* (*H2-Ab1*) and *H2-DMb1*, *CD74*, *class II transactivator* (*Ciita*)] possibly indicated reduced numbers of immune cells in the GF mice. Many other genes encoded enzymes or enzymatic modulators expressed in several "metabolic" organs including the pancreas, intestine, stomach, and liver. For example, reduced expression was noted for the *pancreatic lipase related protein 1/2* (*Pnliprp1/2*) gene that encodes triglyceride lipase; *colipase* (*Clps*) encoding a cofactor of pancreatic lipase essential for efficient lipid hydrolysis[34], and *phospholipase A2, group IIA* (*Pla2g2a*) that encodes extracellular enzyme hydrolyzing phosphoglycerides. Consequently, the corresponding GO BP and CT/MGA categories were top ranked in the Enricher tool results (Fig. 1, Supplementary Fig. S1). This was in concordance with previous studies showing decreased adipocyte counts and lipogenesis accompanied with low levels of triglycerides in microbiota-free mice (reviewed in[35]). Of note, some of these genes (including *Clps* and *Pnliprp2*) were already discovered in the pioneering study of Hooper and colleagues analyzing expression changes in the ileum of GF mice upon monocolonization with *Bacteroides thetaiotaomicron*[36]. Interestingly, production of several mRNAs encoding signaling molecules were upregulated in the GF colon including *bone morphogenic protein 3* (*Bmp3*) and hormones *somatostatin* and *glucagon*. The increased levels of *glucagon* mRNA possibly reflect changes in the number or composition of colonic enteroendocrine cells[37]. In addition, the level of *Angptl4* gene mRNA was also increased in the GF colon, although according to the previous reports (see the citations above) the gene should be specifically expressed in the small intestine. The observed discrepancies related to the site of expression of a particular gene might be explained by the fact that in the majority of studies, expression analysis was performed with tissue samples prepared during (or several weeks after) monocolonization (or "conventionalization") of originally GF mice. Moreover, total RNA was obtained either from the whole gut segments or from isolated epithelial cells. This was in contrast to our methodology utilizing mucosal samples obtained from the second generation of monoassociated or CR mice. Consequently, although many of the mentioned genes were present in our datasets in the "correct place", they did not pass - possibly due to the differences in experimental setup - the selection criteria.

Monoassociation does not restore the mucosal immune system

Subsequently, we identified genes that distinguish the mucosa of GF, N, and O mice from the mucosa of CR animals. In the small intestinal samples, the majority of transcripts underrepresented in all three (i.e. GF, N, O) tissues encoded proteins related to the immune response or proteins expressed in immune cells (Fig. 2AB and Supplementary Table S2), indicating that colonization with a single *E.coli* strain is not sufficient to (fully) restore the mucosa-associated immune system. In addition, expression of the microbiota-responsive *fibroblast growth factor 15* (*Fgf15*) gene[38] was decreased in GF/monoassociated animals when compared to CR mice. Only a limited number of genes were upregulated in the GF/N/O small intestine, including previously mentioned *Bcl2l11* (in SI-middle) and *Angptl4* (in SI-distal). In the colon, the genes with the most decreased expression were linked to the lipid metabolism (e.g. *Pnliprp2*, *Pla2g2a*, *Pla2g4ac*) and reduced numbers of immune cells, as estimated from decreased expression of the *Cd74*, *H2-Ab1*, *H2-Eb1*, *lymphocyte antigen 6 complex, locus E* (*Ly6e*), and *NLR family, CARD domain containing 5* (*Nlrc5*) genes. Interestingly, the absence or low complexity of commensal microbiota resulted in decreased expression of *angiogenin, ribonuclease A family, member 4* (*Ang4*) mRNA encoding Paneth or goblet cell-derived peptide with anti-microbial properties[39]. *Ang4* expression was induced in the small intestine upon monoassociation with *Bacteroides thetaiotaomicron*[36]; however, *Ang4* mRNA was also detected in the colon of CR mice[40]. This might be related – as mentioned above - to the different experimental approach, or more interestingly, it could indicate functional differences between monoassociation with different bacterial strains. A very small number of genes (nine in total) were enriched in the GF/N/O colon, including *somatostatin* and *Bmp1*. Of note, only the *zinc finger protein 326* (*Zfp326*) gene encoding a nuclear protein with unknown function was expressed inversely in the GF (upregulated in comparison to C mice) and N/O (downregulated) colon (Supplementary Table S2).

Genes uniquely expressed in the intestine of GF mice

Next, we selected genes whose expression had changed significantly in GF mice when compared to animals harboring (any) gut microbiota, i.e. CR, N, and O mice. In the small intestinal mucosa, 11 and 9 gene probes were identified in the SI-middle and SI-distal segment, respectively,

representing 12 different genes (Fig. 3A, Supplementary Table S3). Subsequent qRT-PCR analysis confirmed the results of microarray hybridization with the exception of *insulin receptor substrate 2* (*Irs2*) (Fig. 3B). Since immunohistochemical staining (Fig. 3C) revealed that Irs2 is – besides epithelial cells – highly expressed in the intestinal muscle layer, the inconsistency of the results might be explained by contamination of (some) mucosal samples with muscle cells. In this particular contrast, the genes downregulated in the GF small intestine encoded secreted metalloproteinases ADAM-like, decysin 1 (Adamdec1) and matrix metallopeptidase 10 (Mmp10/stromelysin-2), apolipoprotein E (ApoE) essential for the catabolism of triglyceride-rich lipoproteins, and stem cell antigen-1/lymphocyte antigen 6 complex, locus A (Sca-1/Ly6a). Additional genes downregulated in the GF small intestine were *plasmalemma vesicle associated protein* (*Plvap*) encoding an endothelial cell-specific protein[41], *ankyrin repeat and SOCS box-containing 2* (*Asb2*) encoding E3 ubiquitin ligase highly expressed in immature dendritic cells[42], *biglycan* (*Bgn*) encoding pericellular matrix proteoglycan produced in macrophages[43], and *NK2 transcription factor related, locus 3 (Nkx2-3*). Interestingly, the homeodomain-containing transcription factor Nkx2-3 has been linked to inflammatory bowel disease (IBD)[44,45]. Additionally, GF tissue produced less *transforming growth factor, beta receptor II* (*Tgfbr2*) known for its involvement in epithelial cell differentiation [reviewed in[46]] and *secretory leukocyte peptidase inhibitor* (*Slpi*). Slpi functions as a secreted inhibitor of serine proteases protecting the intestinal epithelium[47]. In addition, Slpi possesses antibiotic activity and its expression is induced by microbial products[48] or is increased in the inflamed mucosa in ulcerative colitis patients[49]. Only the *FK506 binding protein 5* (*Fkbp5*) gene encoding anti-inflammatory immunophilin with peptidyprolyl isomerase activity[50] was expressed inversely in the C (downregulated) and N/O (upregulated in comparison to GF mice) small intestine (Fig. 3BC; Supplementary Table S3). Interestingly, in experimental piglets, *Fkbp5* expressional changes are dependent on the composition of gut microbiota[51]. Finally, three genes were upregulated in the GF small intestine, *forkhead box Q1* (*Foxq1*) encoding transcription factor FOXQ1 that regulates epithelial-mesenchymal transition (EMT) in various carcinomas[52,53] and, additionally, the already mentioned *Oprk1* and *Edn1*. Strikingly, Yu and colleagues observed *EDN1* gene repression by NKX2-

3 in human intestinal endothelial cells[54]. Furthermore, inverse expression (i.e. *NKX2-3* upregulation and *EDN1* downregulation) was found in IBD patients[55].

In the colonic mucosa, 17 gene probes were identified representing 12 differentially expressed transcripts as validated by qRT-PCR (Fig. 4AB, Supplementary Table S3). Of five genes with decreased expression in GF mice four were (functionally) linked to immune cells [*Cd74*, *glucosaminyl (N-acetyl) transferase 1, core* (*Gcnt1*), *2H2-Ab1*, *H2-Ea-ps*]. The fifth gene, *regenerating islet-derived family, member 4* (*Reg4*), encodes a small secreted lectin that is expressed in the gastrointestinal tract, especially in enteroendocrine cells[56]. It was suggested that REG4 is an anti-apoptotic factor[57]. In addition, REG4 possibly participates in carcinogenesis and tissue regeneration and, moreover, its expression is upregulated in IBD and in gastrointestinal neoplasia (reviewed[58]). Additionally, it was shown that *Reg4* and another two members of the Reg family, *Reg3β* and *Reg3γ*, are upregulated during postnatal mouse development by gut-colonizing microbiota[14,59]. Genes significantly upregulated in GF animals included cytochrome P450 family member *Cyp2d26*, sodium/phosphate co-transporter *solute carrier family 17, member 4* (*Slc17a4*), *Zfp326*, and *aldehyde dehydrogenase family 1, subfamily A1* (*Aldh1a1*), which encodes the cytosolic enzyme involved in alcohol metabolism. It has been suggested that human ALDH1A1 represents one of the markers of so-called cancer stem cells[60,61]. However, in the mouse colon, Aldh1a1 was detected in differentiated epithelial cells at the surface of the tissue (and not in the crypts where intestinal stem cells reside). Aldh1a1 staining was remarkably increased in GF mice, confirming the result of mRNA expression profiling (Fig. 4C). Additionally, we observed upregulation of the *FBJ osteosarcoma oncogene B* (*Fosb*), and *transducin-like enhancer of split 4* (*Tle4*), and *cholecystokinin* (*Cck*), genes. The transcription factor Fosb and co-repressor Tle4 are two nuclear proteins with no direct link to the gut physiology; however, *Cck* encodes a gut hormone functioning as the satiation signal in response to absorbed fatty acids upon luminal lipid hydrolysis (reviewed in[62]). Neuropeptides such as glucagon-like peptide-1/2 and peptide YY are produced from enteroendocrine cells that come into contact with bacterial by(products) (reviewed in[63]). In the mouse, *Cck* is predominantly secreted from enteroendocrine cells located in the proximal small intestine[64]. Thus, its increased expression in the colon of GF mice is rather unexpected.

Different expressional signatures in the colon of monoassociated mice

Finally, we compared the expression profiles of RNA isolated from the mucosa colonized with two different *E. coli* strains. The concentration of bacteria increases along the rostrocaudal axis of the gut from 10^4 cells/g in the duodenum to 10^{12} cells/g in the colon (reviewed in[65]). In relation to this fact, only three and no genes displayed significant expression changes in the SI-middle and SI-distal segment of the small intestine, respectively. The genes – showing reduced expression in N mice – were sodium-dependent phosphate transporter *solute carrier family 34, member 2* (*Slc34a2*), putative heme transporter *major facilitator superfamily domain containing 7C* (*Mfsd7c*), and *steroid 5 alpha-reductase 1* (*Srd5a1*) enzyme catalyzing conversion of testosterone into dihydrotestosterone. In contrast, expression of 69 genes was changed (all genes were upregulated) in the colonic mucosa of N mice when compared to O mice (Fig. 5A, Supplementary Table S4). The majority of the genes were related to adipose tissue, adipocyte differentiation, and lipid metabolism [e.g. *adipogenin* (*Adig*), *adiponectin* (*Adipoq*), *cell death-inducing DFFA-like effector c* (*Cidec*), *growth differentiation factor 10* (*Gdf10/Bmp3b*), *Pnliprp2*, *perilipin 4* (*Plin4*), *leptin* (*Lep*)], or encoded structural (cytoskeletal) proteins of muscle cells and/or factors that influence muscle contractility [*desmin* (*Des*), *gastrin releasing peptide* (*Grp*), *myosin, light polypeptide 1* (*Myl1*), *myosin, light polypeptide kinase* (*Mylk*), *smoothelin* (*Smtn*), *synemin* (*Snm*), *tropomyosin 2, beta* (*Tpm2*), *vasoactive intestinal polypeptide* (*Vip*)]. Additionally, some of the genes encoded proteins involved in the cell-to-cell or cell-to-extracellular matrix interactions [*LIM and senescent cell antigen like domains 2* (*Lims2*), *thrombospondin 2* (*Thbs2*)]. Finally, we detected increased expression of *Fgf10*, a factor critical for development of various regions of the mouse gastrointestinal tract including the colon[66]. Interestingly, assignment of the genes to the 'GO Cellular Component' (GO CC) category revealed that a substantial portion of the differentially expressed genes encode secreted or junctional proteins (Fig. 5A). The expression levels of 16 most upregulated genes in the colon of N mice were evaluated using quantitative reverse transcription polymerase chain reaction (qRT-PCR) analysis. The analysis – with the exception of the *Clps* gene – confirmed the results of microarray-based RNA profiling (Fig. 5B). Additionally, we attempted to perform immunohistochemical detection of the corresponding proteins using commercially available antibodies. We succeeded in detecting Vip and calbindin 2 (Calb2), an

intracellular calcium-binding protein. Although Calb2 is mainly expressed in various neuronal populations including sensory neurons and granule cells (reviewed in[67]), its upregulation has also been found in colorectal tumors[68] and mesothelioma cells[69]. Calb2-positive cells were found in the *lamina propria* of the colon in both N and O mice. Interestingly, differentiated cells in N mice produced increased amounts of Calb2. Neuropeptide Vip is produced in neurons and immune cells and affects many different cell types as a neurotransmitter, vasodilator, and immune response modulator (reviewed in[70]). Vip induces colonic relaxation and displays potent anti-inflammatory effects by downregulation of pro-inflammatory cytokines and molecules such as tumor necrosis factor (TNF), interleukin 6 (IL6), and nitric oxide (reviewed in[71]). Vip-positive cells were noted in the colonic connective tissue and in the intestinal muscle layer in both groups of monoassociated animals. However, in agreement with mRNA profiling data, differentiated enterocytes of N mice displayed higher amounts of the Vip protein (Fig. 5C). As reported previously, monoassociation with the *E. coli* O6K13 strain promoted colonic inflammation in both the acute and chronic inflammation model[72]. However, from the differentially produced transcripts, no signs of increased inflammation or immune cell infiltration in the O intestine could be deduced. Thus, the observed differences in the colonic gene expression upon monoassociation might indicate (together with the effect of specific bacteria on mucosal transcription) the overall experimental animal's fitness. However, the particular contribution of the Nissle or O6K13 strain to the observed gene profiles remains to be elucidated.

Materials and Methods

Experimental animals, ethics statement

Housing of mice and *in vivo* experiments were performed in compliance with the European Communities Council Directive of 24 November 1986 (86/609/EEC) and national and institutional guidelines. Animal care and experimental procedures were approved by the Animal Care Committee of the Institute of Molecular Genetics (Ref. 180/2010). The experiments were performed using adult mice (average age 13 weeks) of the BALB/c strain reared in GF or conventional conditions. Generation and housing of GF and monoassociated mice were described previously[72]. Second generation mice upon monocolonization were used.

Microarray and qRT-PCR analysis

Six animals from each group of mice were euthanized by cervical dislocation, and the small intestines and colons were removed. The small intestine was divided into three pieces representing the proximal, middle, and distal parts; the colon was processed in one piece. The intestinal segments were opened longitudinally and washed in cold phosphate-buffered saline (PBS). The intestinal mucosa was scraped from the inner intestinal surface using a lancet. The tissue was immediately homogenized in RNA Blue (Top-Bio) and total RNA was isolated according to the manufacturer's instructions. The quality of isolated mRNA was checked using Agilent Bioanalyzer 2100; RNAs with RNA integrity number (RIN) above 8 were further processed. The RNA samples were analyzed by MouseRef-8 v2.0 Expression BeadChip (Illumina). Raw data were processed using the beadarray package of the Bioconductor and analyzed as described previously[73]. Two RNA samples from each group were further reverse transcribed by RevertAid Reverse Transcriptase (Thermo Fisher Scientific) and qRT-PCR was performed using the LightCycler 480 apparatus and SYBR Green I Master Mix (Roche Applied Science). Primers used for qRT-PCR are listed in Supplementary Table S5. The expression levels were normalized to the *Ubiquitin B* (*Ubb*) housekeeping gene, and the expression of two other housekeeping genes *β-actin (Actb)* and *Glyceraldehyde 3-phosphate dehydrogenase (Gapdh)* were also included as controls.

Gene enrichment analysis

The Enricher gene profiling web tool (http://amp.pharm.mssm.edu/Enrichr) was used to analyze differentially expressed genes[21].

Immunohistochemistry and antibodies

The techniques were performed as described previously[74,75]. Antibodies used for immunohistochemistry: anti-Aldh1a1 (rabbit monoclonal, ab52492, Abcam), anti-Calb2 (rabbit polyclonal, sc-50453, Santa Cruz), anti-Fkbp5 (goat polyclonal, AF4094, R&D Systems), anti-Irs2 (rabbit monoclonal, ab134101, Abcam), anti-Vip (rabbit polyclonal, ab78536, Abcam).

Acknowledgements

We thank S. Takacova for critically reading the manuscript. We also thank the members of the Genomics and Bioinformatics laboratory for cDNA microarray hybridization. This work was supported by the Grant Agency of the Czech Republic Grants Nos. P304/11/1252 and P303/12/0535, and institutional Grants Nos. RVO 68378050 and RVO 61388971.

Contributions

L.J., J.S., H.T.-H., and V.K. conceived and designed the experiments; H.S. performed microarray data analysis including Enricher profiling; L.J., J.S., J.T., M.H., and N.B. performed tissue isolation, qRT-PCR analysis and immunohistochemical staining; T.H. performed monoassociation and produced all mice, E.S. and K.G. provided technical support; L.J., J.S., H.T.-H., and V.K. wrote the manuscript.

Competing interests

The authors declare that they have no competing interests.

References

1 Xu, J. & Gordon, J. I. Honor thy symbionts. *Proc Natl Acad Sci U S A* **100**, 10452-10459, doi:10.1073/pnas.1734063100 (2003).

2 Hooper, L. V., Littman, D. R. & Macpherson, A. J. Interactions between the microbiota and the immune system. *Science* **336**, 1268-1273, doi:10.1126/science.1223490 (2012).

3 Sommer, F. & Backhed, F. The gut microbiota--masters of host development and physiology. *Nature reviews. Microbiology* **11**, 227-238, doi:10.1038/nrmicro2974 (2013).

4 Yamamoto, M. *et al.* A microarray analysis of gnotobiotic mice indicating that microbial exposure during the neonatal period plays an essential role in immune system development. *BMC Genomics* **13**, 335, doi:10.1186/1471-2164-13-335 (2012).

5 Nicholson, J. K. *et al.* Host-gut microbiota metabolic interactions. *Science* **336**, 1262-1267, doi:10.1126/science.1223813 (2012).

6 Khachatryan, Z. A. *et al.* Predominant role of host genetics in controlling the composition of gut microbiota. *PLoS One* **3**, e3064, doi:10.1371/journal.pone.0003064 (2008).

7 Sudo, N. *et al.* The requirement of intestinal bacterial flora for the development of an IgE production system fully susceptible to oral tolerance induction. *J Immunol* **159**, 1739-1745 (1997).

8 Tlaskalova-Hogenova, H. *et al.* The role of gut microbiota (commensal bacteria) and the mucosal barrier in the pathogenesis of inflammatory and autoimmune diseases and cancer: contribution of germ-free and gnotobiotic animal models of human diseases. *Cell Mol Immunol* **8**, 110-120, doi:10.1038/cmi.2010.67 (2011).

9 Vieira, S. M., Pagovich, O. E. & Kriegel, M. A. Diet, microbiota and autoimmune diseases. *Lupus* **23**, 518-526, doi:10.1177/0961203313501401 (2014).

10 Sobhani, I. *et al.* Microbial dysbiosis in colorectal cancer (CRC) patients. *PLoS One* **6**, e16393, doi:10.1371/journal.pone.0016393 (2011).

11 Klimesova, K. *et al.* Altered gut microbiota promotes colitis-associated cancer in IL-1 receptor-associated kinase M-deficient mice. *Inflamm Bowel Dis* **19**, 1266-1277, doi:10.1097/MIB.0b013e318281330a (2013).

12 Schulz, M. D. *et al.* High-fat-diet-mediated dysbiosis promotes intestinal carcinogenesis independently of obesity. *Nature* **514**, 508-512, doi:10.1038/nature13398 (2014).

13 El Aidy, S. *et al.* Temporal and spatial interplay of microbiota and intestinal mucosa drive establishment of immune homeostasis in conventionalized mice. *Mucosal immunology* **5**, 567-579, doi:10.1038/mi.2012.32 (2012).

14 Larsson, E. *et al.* Analysis of gut microbial regulation of host gene expression along the length of the gut and regulation of gut microbial ecology through MyD88. *Gut* **61**, 1124-1131, doi:10.1136/gutjnl-2011-301104 (2012).

15 El Aidy, S. *et al.* Gut bacteria-host metabolic interplay during conventionalisation of the mouse germfree colon. *ISME J* **7**, 743-755, doi:10.1038/ismej.2012.142 (2013).

16 Dahlgren, U. I., Wold, A. E., Hanson, L. A. & Midtvedt, T. The secretory antibody response in milk and bile against fimbriae and LPS in rats monocolonized or immunized in the Peyer's patches with Escherichia coli. *Immunology* **71**, 295-300 (1990).

17 Jacobi, C. A. & Malfertheiner, P. Escherichia coli Nissle 1917 (Mutaflor): new insights into an old probiotic bacterium. *Digestive diseases* **29**, 600-607, doi:10.1159/000333307 (2011).

18 Behnsen, J., Deriu, E., Sassone-Corsi, M. & Raffatellu, M. Probiotics: properties, examples, and specific applications. *Cold Spring Harb Perspect Med* **3**, a010074, doi:10.1101/cshperspect.a010074 (2013).

19 Hudcovic, T. *et al.* Monocolonization with Bacteroides ovatus protects immunodeficient SCID mice from mortality in chronic intestinal inflammation caused by long-lasting dextran sodium sulfate treatment. *Physiol Res* **58**, 101-110 (2009).

20 Subramanian, A. *et al.* Gene set enrichment analysis: a knowledge-based approach for interpreting genome-wide expression profiles. *Proc Natl Acad Sci U S A* **102**, 15545-15550, doi:10.1073/pnas.0506580102 (2005).
21 Chen, E. Y. *et al.* Enrichr: interactive and collaborative HTML5 gene list enrichment analysis tool. *BMC Bioinformatics* **14**, 128, doi:10.1186/1471-2105-14-128 (2013).
22 El Aidy, S., Dinan, T. G. & Cryan, J. F. Gut Microbiota: The Conductor in the Orchestra of Immune-Neuroendocrine Communication. *Clin Ther* **37**, 954-967, doi:10.1016/j.clinthera.2015.03.002 (2015).
23 Villanueva-Millan, M. J., Perez-Matute, P. & Oteo, J. A. Gut microbiota: a key player in health and disease. A review focused on obesity. *J Physiol Biochem* **71**, 509-525, doi:10.1007/s13105-015-0390-3 (2015).
24 Yanagisawa, M. *et al.* A novel potent vasoconstrictor peptide produced by vascular endothelial cells. *Nature* **332**, 411-415, doi:10.1038/332411a0 (1988).
25 Simonin, F. *et al.* Disruption of the kappa-opioid receptor gene in mice enhances sensitivity to chemical visceral pain, impairs pharmacological actions of the selective kappa-agonist U-50,488H and attenuates morphine withdrawal. *EMBO J* **17**, 886-897, doi:10.1093/emboj/17.4.886 (1998).
26 Kadomatsu, T., Tabata, M. & Oike, Y. Angiopoietin-like proteins: emerging targets for treatment of obesity and related metabolic diseases. *FEBS J* **278**, 559-564, doi:10.1111/j.1742-4658.2010.07979.x (2011).
27 Backhed, F. *et al.* The gut microbiota as an environmental factor that regulates fat storage. *Proc Natl Acad Sci U S A* **101**, 15718-15723, doi:10.1073/pnas.0407076101 (2004).
28 Koster, A. *et al.* Transgenic angiopoietin-like (angptl)4 overexpression and targeted disruption of angptl4 and angptl3: regulation of triglyceride metabolism. *Endocrinology* **146**, 4943-4950, doi:10.1210/en.2005-0476 (2005).
29 Mandard, S. *et al.* The fasting-induced adipose factor/angiopoietin-like protein 4 is physically associated with lipoproteins and governs plasma lipid levels and adiposity. *J Biol Chem* **281**, 934-944, doi:10.1074/jbc.M506519200 (2006).
30 Backhed, F., Manchester, J. K., Semenkovich, C. F. & Gordon, J. I. Mechanisms underlying the resistance to diet-induced obesity in germ-free mice. *Proc Natl Acad Sci U S A* **104**, 979-984, doi:10.1073/pnas.0605374104 (2007).
31 Crawford, P. A. & Gordon, J. I. Microbial regulation of intestinal radiosensitivity. *Proc Natl Acad Sci U S A* **102**, 13254-13259, doi:10.1073/pnas.0504830102 (2005).
32 Cazes, A. *et al.* Extracellular matrix-bound angiopoietin-like 4 inhibits endothelial cell adhesion, migration, and sprouting and alters actin cytoskeleton. *Circ Res* **99**, 1207-1215, doi:10.1161/01.RES.0000250758.63358.91 (2006).
33 Pineda, M. *et al.* Identification of a membrane protein, LAT-2, that Co-expresses with 4F2 heavy chain, an L-type amino acid transport activity with broad specificity for small and large zwitterionic amino acids. *J Biol Chem* **274**, 19738-19744 (1999).
34 D'Agostino, D. & Lowe, M. E. Pancreatic lipase-related protein 2 is the major colipase-dependent pancreatic lipase in suckling mice. *The Journal of nutrition* **134**, 132-134 (2004).
35 Backhed, F. & Crawford, P. A. Coordinated regulation of the metabolome and lipidome at the host-microbial interface. *Biochim Biophys Acta* **1801**, 240-245, doi:10.1016/j.bbalip.2009.09.009 (2010).
36 Hooper, L. V. *et al.* Molecular analysis of commensal host-microbial relationships in the intestine. *Science* **291**, 881-884, doi:10.1126/science.291.5505.881 (2001).
37 Arantes, R. M. & Nogueira, A. M. Increased intracellular content of enteroglucagon in proximal colon is related to intestinal adaptation to germ-free status. *Cell Tissue Res* **303**, 447-450 (2001).
38 Sayin, S. I. *et al.* Gut microbiota regulates bile acid metabolism by reducing the levels of tauro-beta-muricholic acid, a naturally occurring FXR antagonist. *Cell Metab* **17**, 225-235, doi:10.1016/j.cmet.2013.01.003 (2013).

39 Forman, R. A. *et al.* The goblet cell is the cellular source of the anti-microbial angiogenin 4 in the large intestine post Trichuris muris infection. *PLoS One* **7**, e42248, doi:10.1371/journal.pone.0042248 (2012).
40 Hooper, L. V., Stappenbeck, T. S., Hong, C. V. & Gordon, J. I. Angiogenins: a new class of microbicidal proteins involved in innate immunity. *Nat Immunol* **4**, 269-273, doi:10.1038/ni888 (2003).
41 Deharvengt, S. J. *et al.* PV1 down-regulation via shRNA inhibits the growth of pancreatic adenocarcinoma xenografts. *Journal of cellular and molecular medicine* **16**, 2690-2700, doi:10.1111/j.1582-4934.2012.01587.x (2012).
42 Lamsoul, I. *et al.* ASB2alpha regulates migration of immature dendritic cells. *Blood* **122**, 533-541, doi:10.1182/blood-2012-11-466649 (2013).
43 Schaefer, L. *et al.* The matrix component biglycan is proinflammatory and signals through Toll-like receptors 4 and 2 in macrophages. *J Clin Invest* **115**, 2223-2233, doi:10.1172/JCI23755 (2005).
44 Franke, A. *et al.* Replication of signals from recent studies of Crohn's disease identifies previously unknown disease loci for ulcerative colitis. *Nat Genet* **40**, 713-715, doi:10.1038/ng.148 (2008).
45 Yamazaki, K. *et al.* Positive association of genetic variants in the upstream region of NKX2-3 with Crohn's disease in Japanese patients. *Gut* **58**, 228-232, doi:10.1136/gut.2007.140764 (2009).
46 Krausova, M. & Korinek, V. Signal transduction pathways participating in homeostasis and malignant transformation of the intestinal tissue. *Neoplasma* **59**, 708-718, doi:10.4149/neo_2012_090 (2012).
47 Si-Tahar, M., Merlin, D., Sitaraman, S. & Madara, J. L. Constitutive and regulated secretion of secretory leukocyte proteinase inhibitor by human intestinal epithelial cells. *Gastroenterology* **118**, 1061-1071 (2000).
48 Taggart, C. C. *et al.* Secretory leucoprotease inhibitor binds to NF-kappaB binding sites in monocytes and inhibits p65 binding. *The Journal of experimental medicine* **202**, 1659-1668, doi:10.1084/jem.20050768 (2005).
49 Schmid, M. *et al.* Attenuated induction of epithelial and leukocyte serine antiproteases elafin and secretory leukocyte protease inhibitor in Crohn's disease. *Journal of leukocyte biology* **81**, 907-915 (2007).
50 Baughman, G., Wiederrecht, G. J., Chang, F., Martin, M. M. & Bourgeois, S. Tissue distribution and abundance of human FKBP51, and FK506-binding protein that can mediate calcineurin inhibition. *Biochem Biophys Res Commun* **232**, 437-443 (1997).
51 Mulder, I. E. *et al.* Environmentally-acquired bacteria influence microbial diversity and natural innate immune responses at gut surfaces. *BMC Biol* **7**, 79, doi:10.1186/1741-7007-7-79 (2009).
52 Feng, J. *et al.* FoxQ1 overexpression influences poor prognosis in non-small cell lung cancer, associates with the phenomenon of EMT. *PLoS One* **7**, e39937, doi:10.1371/journal.pone.0039937 (2012).
53 Qiao, Y. *et al.* FOXQ1 regulates epithelial-mesenchymal transition in human cancers. *Cancer Res* **71**, 3076-3086, doi:10.1158/0008-5472.CAN-10-2787 (2011).
54 Yu, W. *et al.* NKX2-3 transcriptional regulation of endothelin-1 and VEGF signaling in human intestinal microvascular endothelial cells. *PLoS One* **6**, e20454, doi:10.1371/journal.pone.0020454 (2011).
55 Yu, W. *et al.* Genes regulated by Nkx2-3 in siRNA-mediated knockdown B cells: implication of endothelin-1 in inflammatory bowel disease. *Molecular genetics and metabolism* **100**, 88-95, doi:10.1016/j.ymgme.2010.02.001 (2010).
56 Heiskala, K. & Andersson, L. C. Reg IV is differently expressed in enteroendocrine cells of human small intestine and colon. *Regul Pept* **183**, 27-34, doi:10.1016/j.regpep.2013.03.007 (2013).

57 Rafa, L. *et al.* REG4 acts as a mitogenic, motility and pro-invasive factor for colon cancer cells. *Int J Oncol* **36**, 689-698 (2010).
58 Numata, M. & Oshima, T. Significance of regenerating islet-derived type IV gene expression in gastroenterological cancers. *World J Gastroenterol* **18**, 3502-3510, doi:10.3748/wjg.v18.i27.3502 (2012).
59 Rakoff-Nahoum, S. *et al.* Analysis of gene-environment interactions in postnatal development of the mammalian intestine. *Proc Natl Acad Sci U S A* **112**, 1929-1936, doi:10.1073/pnas.1424886112 (2015).
60 Ginestier, C. *et al.* ALDH1 is a marker of normal and malignant human mammary stem cells and a predictor of poor clinical outcome. *Cell Stem Cell* **1**, 555-567, doi:10.1016/j.stem.2007.08.014 (2007).
61 Li, T. *et al.* ALDH1A1 is a marker for malignant prostate stem cells and predictor of prostate cancer patients' outcome. *Lab Invest* **90**, 234-244, doi:10.1038/labinvest.2009.127 (2010).
62 Cote, C. D., Zadeh-Tahmasebi, M., Rasmussen, B. A., Duca, F. A. & Lam, T. K. Hormonal signaling in the gut. *J Biol Chem* **289**, 11642-11649, doi:10.1074/jbc.O114.556068 (2014).
63 Furness, J. B., Rivera, L. R., Cho, H. J., Bravo, D. M. & Callaghan, B. The gut as a sensory organ. *Nat Rev Gastroenterol Hepatol* **10**, 729-740, doi:10.1038/nrgastro.2013.180 (2013).
64 Aiken, K. D., Kisslinger, J. A. & Roth, K. A. Immunohistochemical studies indicate multiple enteroendocrine cell differentiation pathways in the mouse proximal small intestine. *Dev Dyn* **201**, 63-70, doi:10.1002/aja.1002010107 (1994).
65 Kleerebezem, M. & Vaughan, E. E. Probiotic and gut lactobacilli and bifidobacteria: molecular approaches to study diversity and activity. *Annu Rev Microbiol* **63**, 269-290, doi:10.1146/annurev.micro.091208.073341 (2009).
66 Sala, F. G. *et al.* Fibroblast growth factor 10 is required for survival and proliferation but not differentiation of intestinal epithelial progenitor cells during murine colon development. *Dev Biol* **299**, 373-385, doi:10.1016/j.ydbio.2006.08.001 (2006).
67 Camp, A. J. & Wijesinghe, R. Calretinin: modulator of neuronal excitability. *Int J Biochem Cell Biol* **41**, 2118-2121, doi:10.1016/j.biocel.2009.05.007 (2009).
68 Gotzos, V., Wintergerst, E. S., Musy, J. P., Spichtin, H. P. & Genton, C. Y. Selective distribution of calretinin in adenocarcinomas of the human colon and adjacent tissues. *The American journal of surgical pathology* **23**, 701-711 (1999).
69 Doglioni, C. *et al.* Calretinin: a novel immunocytochemical marker for mesothelioma. *The American journal of surgical pathology* **20**, 1037-1046 (1996).
70 Delgado, M. & Ganea, D. Vasoactive intestinal peptide: a neuropeptide with pleiotropic immune functions. *Amino acids* **45**, 25-39, doi:10.1007/s00726-011-1184-8 (2013).
71 Chandrasekharan, B., Nezami, B. G. & Srinivasan, S. Emerging neuropeptide targets in inflammation: NPY and VIP. *Am J Physiol Gastrointest Liver Physiol* **304**, G949-957, doi:10.1152/ajpgi.00493.2012 (2013).
72 Hudcovic, T., Stepankova, R., Kozakova, H., Hrncir, T. & Tlaskalova-Hogenova, H. Effects of monocolonization with Escherichia coli strains O6K13 and Nissle 1917 on the development of experimentally induced acute and chronic intestinal inflammation in germ-free immunocompetent and immunodeficient mice. *Folia microbiologica* **52**, 618-626 (2007).
73 Melenovsky, V. *et al.* Metabolic characterization of volume overload heart failure due to aorto-caval fistula in rats. *Mol Cell Biochem* **354**, 83-96, doi:10.1007/s11010-011-0808-3 (2011).
74 Waaler, J. *et al.* A novel tankyrase inhibitor decreases canonical Wnt signaling in colon carcinoma cells and reduces tumor growth in conditional APC mutant mice. *Cancer Res* **72**, 2822-2832, doi:10.1158/0008-5472.CAN-11-3336 (2012).
75 Doubravska, L. *et al.* Fatty acid modification of Wnt1 and Wnt3a at serine is prerequisite for lipidation at cysteine and is essential for Wnt signalling. *Cell Signal* **23**, 837-848, doi:10.1016/j.cellsig.2011.01.007 (2011).

Figure Legends

Figure 1: The most different 'Gene Ontology Biological Processes' (GO BPs) and 'Cell Types/Mouse Gene Atlas' (CT/MGA) categories in expression profiles of the mucosa obtained from conventionally reared (CR) and germ-free (GF) animals. In total, 103, 217, and 115 gene probes passed the significance criterion (q-value < 0.05; |log FC| ≥ 1) in the middle (SI-middle) and distal (SI-distal) parts of the small intestine and in the colon, respectively. Corresponding annotated genes (listed in Supplementary Table S1) were analyzed using the GO BP and CT/MGA Enricher datasets. The results were sorted according to the combined score (CS; CS is computed by multiplying the log of p-value obtained from the Fisher's exact test by the z-score of the deviation from the expected rank). Maximum of 10 GO BPs and CT/MGA categories containing at least two differentially expressed genes and with CS ≥ 1 is shown. The number of genes in the particular category is indicated by the number before the parenthesis. |log FC|, absolute value of the binary logarithm of relative expression intensity.

Figure 2: The immune system is not reconstituted upon monoassociation with a single *E. coli* strain. (A) Venn diagrams indicating numbers of gene probes differentially expressed in the indicated intestinal segments of the analyzed group of mice (significance criterion: q < 0.05; |log FC| ≥ 1). The genes are listed in Supplementary Table S2. (B) The Enricher analysis of genes expressed differentially in GF, N, and O animals when compared to CR mice. The analysis was performed as described in the Fig. 1 legend.

Figure 3: A limited number of genes are uniquely expressed in the GF small intestine. (A) Venn diagrams comparing gene expression profiles in small intestinal segments of CR, N, and O animals when contrasted with the gene expression profile obtained in GF mice. Eleven gene probes (representing 10 annotated genes) and 9 gene probes (representing 8 annotated genes) were differentially expressed in the SI-middle or SI-distal segment, respectively (selection criterion: |log FC| ≥ 1; p < 0.05 in at least two of three comparisons). The genes are listed in Supplementary Table

S3. (B) Validation of cDNA microarray by qRT-PCR. Diagrams depict expression analysis of the indicated genes performed by cDNA microarray hybridization (left) or by qRT-PCR (right). Normalized fluorescence signal obtained in the respective gene probe upon hybridization with RNA isolated from GF mice was set to 1. Results of qRT-PCR were normalized to Ubb; the expression level of the respective gene in the mucosa of GF mice was set to 1. Two mice from each group were analyzed. Error bars represent SDs. (C) Immunohistochemical detection of Fkbp5 and Irs2 using 3,3'-diaminobenzidine (DAB) staining (brownish precipitate) in the SI-middle part using specimens obtained from animals of the indicated experimental group. Both proteins are mainly produced in epithelial cells (black arrows). In addition, prominent Irs2 staining was also observed in the smooth muscle layer (green arrows). Representative images of specimens counterstained with hematoxylin are shown. Scale bar: 0.15 mm.

Figure 4: Aldh1a1 represents a robust marker of the GF colon. (A) A Venn diagram comparing gene expression profiles of the colonic mucosa of CR, N, and O animals when contrasted with the gene expression profile obtained in GF mice. According to the selection criterion ($|\log FC| \geq 1$; $p < 0.05$), 17 gene probes representing 12 annotated genes were identified. The genes are listed in Supplementary Table S3. (B) Validation of cDNA microarray by qRT-PCR. Comparison of expression analysis of the indicated genes performed by cDNA microarray hybridization (left) or by qRT-PCR (right). Samples were analyzed as described in Fig. 3B. (C) Immunohistochemical detection showing increased production of Aldh1a1 in differentiated epithelial cells (black arrows) of the colon of GF mice. Representative images of specimens counterstained with hematoxylin are shown. Scale bar: 0.15 mm.

Figure 5: Analysis of differentially expressed genes in the colon of monoassociated mice. (A), the most different GO BPs, CT/MGA, and 'GO Cellular Component' (GO CC) categories in expression profiles of the colonic mucosa obtained from monoassociated mice. The significance criterion (q-value < 0.05; $|\log FC| \geq 1$) was passed by 72 gene probes (representing 69 annotated genes) that were analyzed as described in the Fig. 1 legend. The genes are listed in Supplementary Table S4. (B)

Expression analysis of 16 most significantly changed (|log FC| ≥ 2) genes between the N and O colon. Left diagram shows the results of cDNA microarray hybridization; normalized fluorescence signal of the respective gene probe upon hybridization with RNA isolated from the C mice was set to 1. Right, qRT-PCR analysis of total RNA isolated from the colonic mucosa of N and O mice. Results were normalized to *Ubb*; the expression level of the respective gene in the O mucosa was set to 1. Two mice from each group were analyzed. Error bars represent SDs. (C) Immunohistochemical detection of Calb2 and Vip protein in the colon. Both proteins are produced in differentiated epithelial cells (black arrows) with increased positivity in the N colon. In addition, Calb2 is also produced in *lamina propria*; however, the staining intensity is similar between N and O animals (red arrows). Staining of the smooth muscle layer (green arrows) possibly results from non-specific adhesion of primary antibodies. The specimens were counterstained with hematoxylin (blue nuclear stain). Scale bar: 0.15 m.

Figure 1

SI-middle; CR vs. GF

GO BP	
positive regulation of smooth muscle cell migration (GO:0014911)	4 (CS 21.06)
positive regulation of locomotion (GO:0040017)	10 (CS 19.26)
regulation of leukocyte migration (GO:0002685)	7 (CS 18.17)
positive regulation of lymphocyte migration (GO:2000403)	4 (CS 17.97)
positive regulation of lymphocyte proliferation (GO:0050671)	7 (CS 17.60)
positive regulation of mononuclear cell proliferation (GO:0032946)	7 (CS 17.57)
positive regulation of leukocyte proliferation (GO:0070665)	7 (CS 17.48)
positive regulation of T cell activation (GO:0050870)	8 (CS 17.17)
positive regulation of cellular component movement (GO:0051272)	9 (CS 17.00)
positive regulation of cell migration (GO:0030335)	9 (CS 16.97)

CT/MGA	
follicular B-cells	20 (CS 41.59)
T-cells CD8+	7 (CS 9.72)
dendritic plasmacytoid B220+	5 (CS 9.41)
T-cells CD4+	4 (CS 6.62)
spleen	4 (CS 4.78)
lymph nodes	7 (CS 4.27)
macrophage peri LPS thio 1hrs	6 (CS 4.23)
mammary gland lactating	3 (CS 3.28)
macrophage bone marrow 0hrs	3 (CS 1.88)
NK cells	6 (CS 1.80)

SI-distal; CR vs. GF

GO BP	
regulation of lymphocyte activation (GO:0051249)	29 (CS 78.59)
regulation of cell activation (GO:0050865)	31 (CS 78.50)
regulation of leukocyte activation (GO:0002694)	30 (CS 78.44)
leukocyte activation (GO:0045321)	31 (CS 74.71)
regulation of T cell activation (GO:0050863)	25 (CS 73.28)
positive regulation of lymphocyte activation (GO:0051251)	23 (CS 65.31)
positive regulation of leukocyte activation (GO:0002696)	23 (CS 62.11)
positive regulation of cell activation (GO:0050867)	23 (CS 60.79)
positive regulation of T cell activation (GO:0050870)	20 (CS 58.13)
immune response-regulating cell surface receptor signaling (GO:0002768)	23 (CS 58.00)

CT/MGA	
follicular B-cells	45 (CS 98.82)
spleen	13 (CS 9.88)
lymph nodes	13 (CS 8.78)
mast cells	16 (CS 6.17)
T-cells CD8+	10 (CS 5.45)
macrophage peri LPS thio 7hrs	16 (CS 1.87)
thymocyte SP CD8+	6 (CS 1.54)

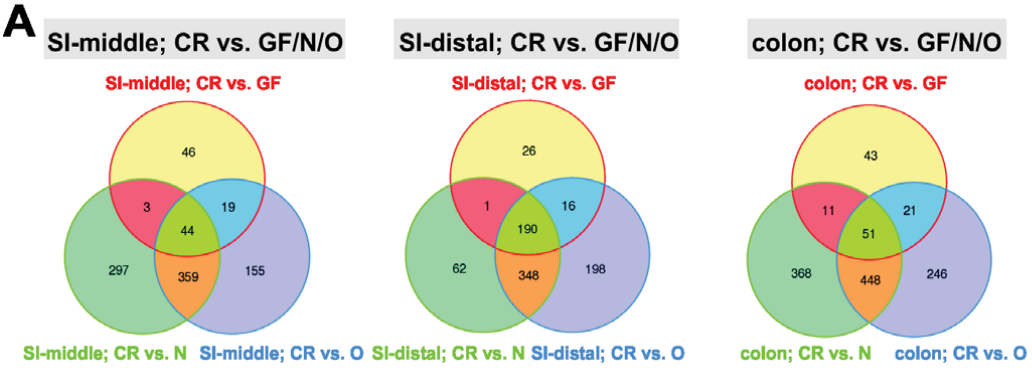
colon; CR vs. GF

GO BP	
negative regulation of lipase activity (GO:0060192)	2 (CS 3.07)
regulation of MHC class I biosynthetic process (GO:0045343)	2 (CS 3.05)
positive regulation of protein oligomerization (GO:0032461)	2 (CS 3.05)
phosphatidylinositol acyl-chain remodeling (GO:0036149)	2 (CS 2.94)
phosphatidylethanolamine acyl-chain remodeling (GO:0036152)	2 (CS 2.86)
phospholipid catabolic processes (GO:0009395)	2 (CS 2.85)
macromolecular complex remodeling (GO:0034367)	2 (CS 2.81)
protein-lipid complex remodeling (GO:0034368)	2 (CS 2.80)

CT/MGA	
pancreas	11 (CS 12.13)
intestine small	8 (CS 7.40)
stomach	6 (CS 6.80)
MEF	5 (CS 4.36)
liver	10 (CS 3.66)
umbilical cord	3 (CS 3.36)
follicular B-cells	7 (CS 2.92)
intestine large	5 (CS 2.91)
mammary gland lact	2 (CS 1.78)
iris	2 (CS 1.78)

Figure 2

A



B

SI-middle; CR vs. GF/N/O

GO BP	
AMP metabolic process (GO:0046033)	2 (CS 9.13)
adenosine metabolic process (GO:0046085)	2 (CS 8.77)
cellular response to electrical stimulus (GO:0071257)	2 (CS 8.33)
regulation of B cell apoptotic process (GO:0002902)	2 (CS 8.28)
negative regulation of B cell apoptotic process (GO:0002903)	2 (CS 8.02)
purine nucleobase metabolic process (GO:0006144)	3 (CS 7.91)
humoral immune response (GO:0006959)	3 (CS 7.76)
negative regulation of lymphocyte apoptotic process (GO:0070229)	2 (CS 7.51)
focal adhesion assembly (GO:0048041)	2 (CS 7.33)
cell-substrate adherens junction assembly (GO:0007045)	2 (CS 7.31)

CT/MGA	
follicular B-cells	13 (CS 36.45)
spleen	3 (CS 5.70)
lymph nodes	4 (CS 2.27)
T-cells CD4+	2 (CS 2.09)

SI-distal; CR vs. GF/N/O

GO BP	
immune response-activating cell surface receptor signaling pathway (GO:0002429)	18 (CS 64.71)
immune response-regulating cell surface receptor signaling pathway (GO:0002768)	21 (CS 64.22)
regulation of leukocyte activation (GO:0002694)	23 (CS 59.11)
regulation of lymphocyte activation (GO:0051249)	22 (CS 58.57)
regulation of cell activation (GO:0050865)	23 (CS 56.66)
positive regulation of lymphocyte activation (GO:0051251)	19 (CS 56.60)
leukocyte activation (GO:0045321)	23 (CS 56.14)
regulation of T cell activation (GO:0050863)	19 (CS 55.04)
positive regulation of leukocyte activation (GO:0002696)	19 (CS 54.62)
antigen receptor-mediated signaling pathway (GO:0050851)	16 (CS 54.01)

CT/MGA	
follicular B-cells	38 (CS 87.87)
T-cells CD8+	10 (CS 7.39)
mast cells	13 (CS 6.40)
lymph nodes	10 (CS 6.13)
spleen	8 (CS 4.71)
thymocyte SP CD8+	5 (CS 2.60)
macrophage peri LPS thio 7hrs	12 (CS 1.16)
T-cells CD4+	6 (CS 1.15)

colon; CR vs. GF/N/O

GO BP	
regulation of MHC class I biosynthetic process (GO:0045343)	2 (CS 8.80)
phosphatidylinositol acyl-chain remodeling (GO:0036149)	2 (CS 8.40)
phosphatidylcholine acyl-chain remodeling (GO:0036151)	2 (CS 8.27)
phosphatidylethanolamine acyl-chain remodeling (GO:0036152)	2 (CS 8.21)
phospholipid catabolic process (GO:0009395)	2 (CS 8.18)
macromolecular complex remodeling (GO:0034367)	2 (CS 8.08)
plasma lipoprotein particle remodeling (GO:0034369)	2 (CS 8.05)
protein-lipid complex remodeling (GO:0034368)	2 (CS 8.05)
neutral amino acid transport (GO:0015804)	2 (CS 7.65)
positive regulation of response to cytokine stimulus (GO:0060760)	2 (CS 7.63)

CT/MGA	
follicular B-cells	6 (CS 4.55)
intestine small	5 (CS 4.24)
pancreas	5 (CS 2.32)
epidermis	3 (CS 1.74)
umbilical cord	2 (CS 1.22)

Figure 3

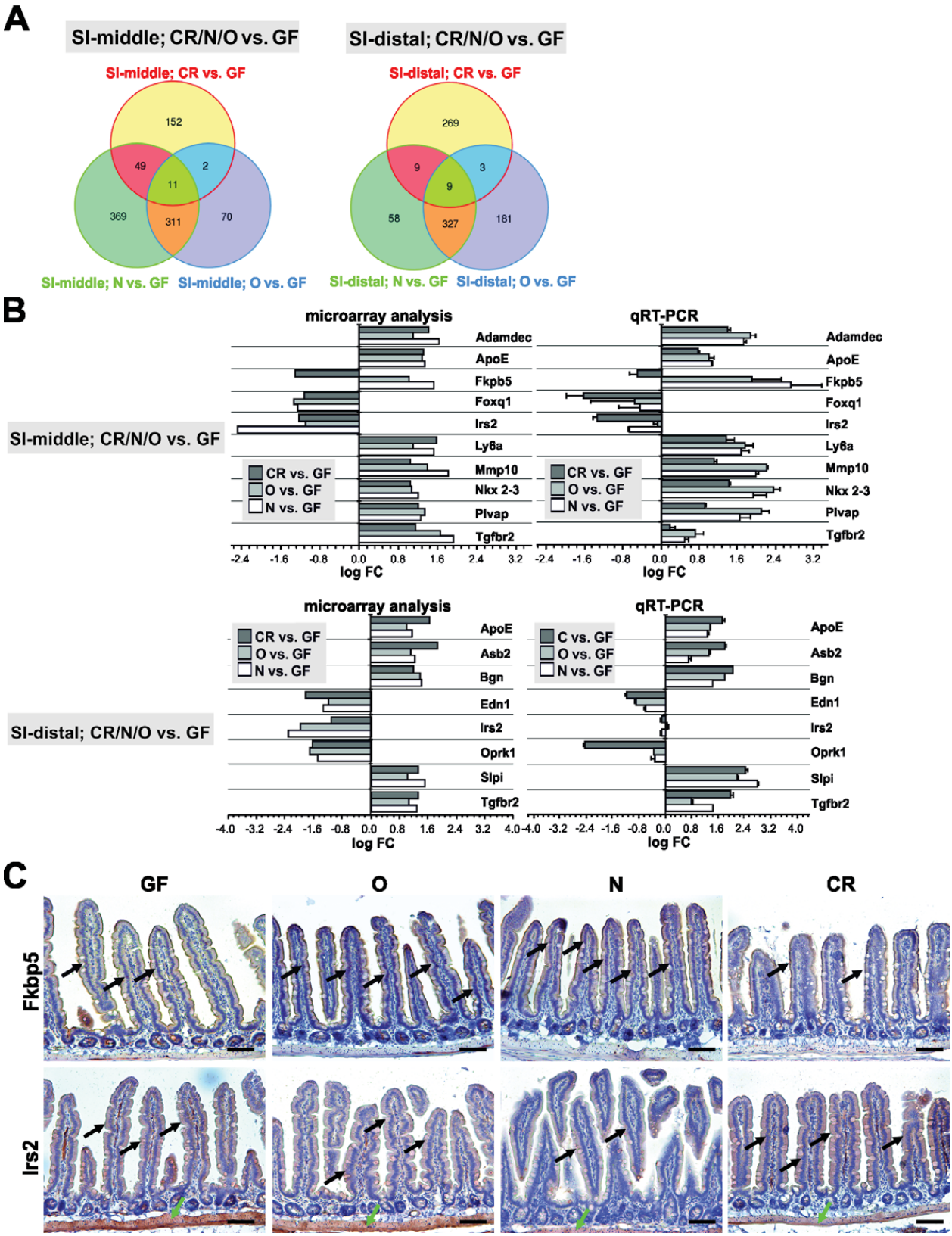

A
SI-middle; CR/N/O vs. GF
SI-middle; CR vs. GF
152
49
2
11
369
311
70
SI-middle; N vs. GF
SI-middle; O vs. GF
SI-distal; CR/N/O vs. GF
SI-distal; CR vs. GF
269
9
3
9
58
327
181
SI-distal; N vs. GF
SI-distal; O vs. GF
B
SI-middle; CR/N/O vs. GF
microarray analysis
qRT-PCR
Adamdec
ApoE
Fkpb5
Foxq1
Irs2
Ly6a
Mmp10
Nkx 2-3
Plvap
Tgfbr2
CR vs. GF
O vs. GF
N vs. GF
-2.4 -1.6 -0.8 0.0 0.8 1.6 2.4 3.2
log FC
SI-distal; CR/N/O vs. GF
microarray analysis
qRT-PCR
ApoE
Asb2
Bgn
Edn1
Irs2
Oprk1
Slpi
Tgfbr2
CR vs. GF
O vs. GF
N vs. GF
C vs. GF
-4.0 -3.2 -2.4 -1.6 -0.8 0.0 0.8 1.6 2.4 3.2 4.0
log FC
C
GF
O
N
CR
Fkbp5
Irs2

Figure 4

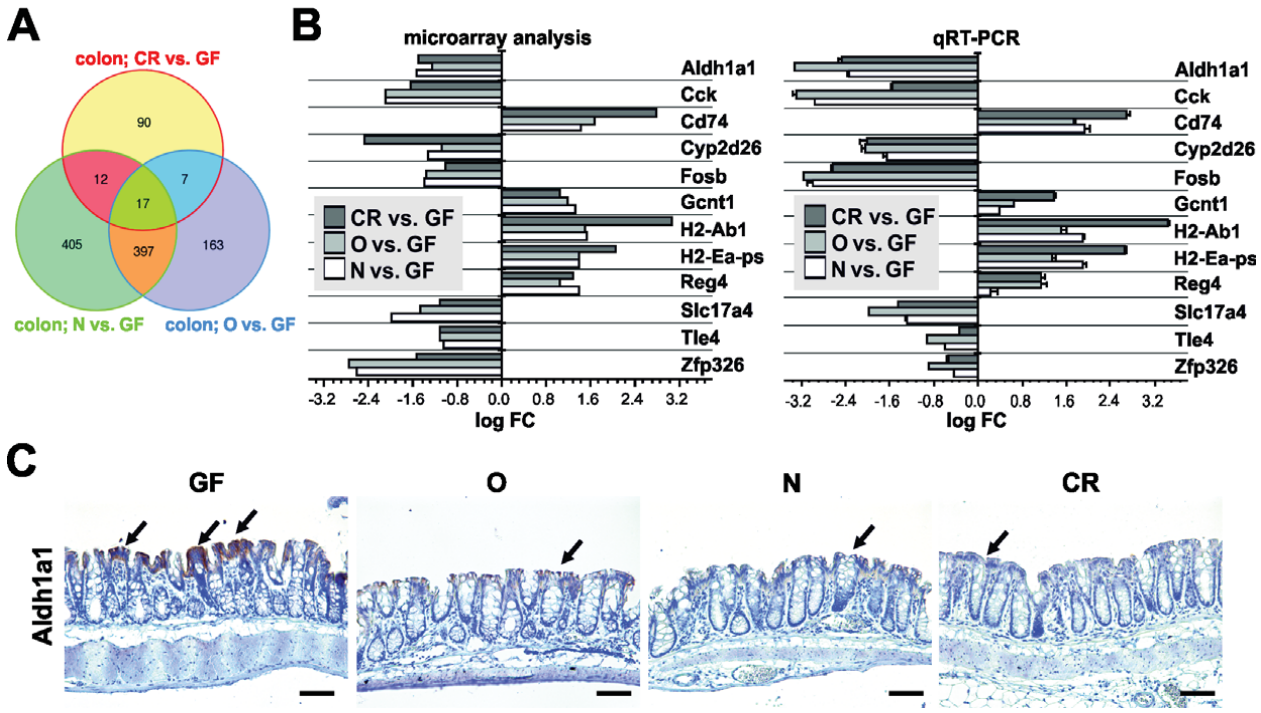

A
colon; CR vs. GF
90
12
7
17
405
397
163
colon; N vs. GF
colon; O vs. GF
B
microarray analysis
qRT-PCR
Aldh1a1
Cck
Cd74
Cyp2d26
Fosb
Gcnt1
H2-Ab1
H2-Ea-ps
Reg4
Slc17a4
Tle4
Zfp326
CR vs. GF
O vs. GF
N vs. GF
-3.2 -2.4 -1.6 -0.8 0.0 0.8 1.6 2.4 3.2
log FC
C
GF
O
N
CR
Aldh1a1

Figure 5

A

GO BP

brown fat cell differentiation (GO:0050873)	4 (CS 13.34)
fat cell differentiation (GO:0045444)	6 (CS 11.90)
muscle contraction (GO:0006936)	7 (CS 11.47)
muscle system process (GO:0003012)	7 (CS 9.49)
muscle filament sliding (GO:0030049)	3 (CS 5.49)
actin-myosin filament sliding (GO:0033275)	3 (CS 5.48)
cellular response to vitamin (GO:0071295)	2 (CS 5.47)
bone mineralization (GO:0030282)	3 (CS 5.41)
regulation of system process (GO:0044057)	7 (CS 5.26)
white fat cell differentiation (GO:0050872)	2 (CS 5.04)

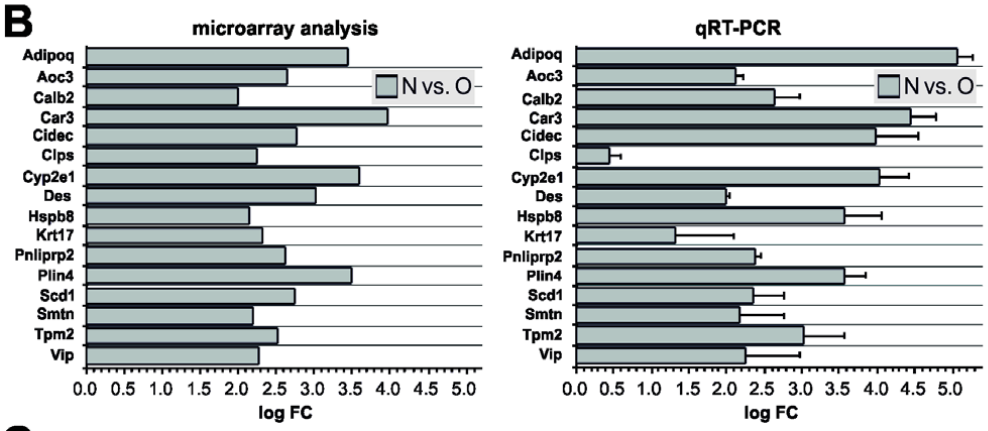
CT/MGA

adipose brown	15 (CS 29.69)
adipose white	10 (CS 12.03)
hypothalamus	6 (CS 10.52)
mammary gland non-lactating	7 (CS 9.36)
skeletal muscle	10 (CS 6.03)
dorsal root ganglia	7 (CS 4.05)
cerebral cortex prefrontal	5 (CS 2.88)
pancreas	4 (CS 2.66)
cerebellum	4 (CS 2.20)

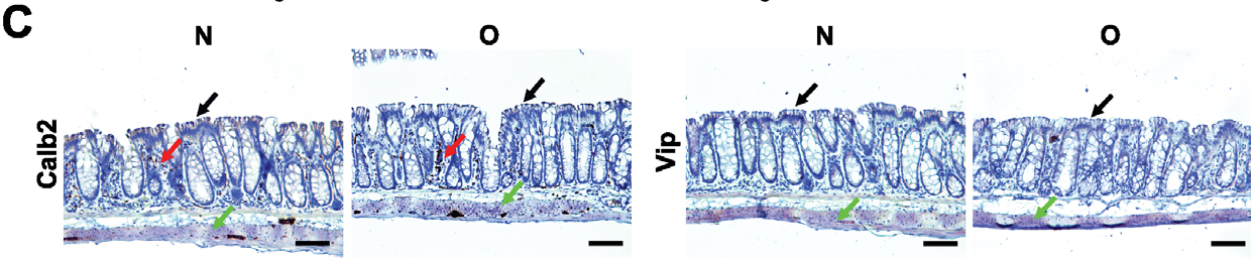
GO CC

extracellular space (GO:0005615)	15 (CS 12.18)
adherens junction (GO:0005912)	7 (CS 8.16)
anchoring junction (GO:0070161)	7 (CS 7.97)
neuronal cell body (GO:0043025)	6 (CS 7.92)
cell body (GO:0044297)	6 (CS 7.57)
stress fiber (GO:0001725)	3 (CS 7.53)
actin filament bundle (GO:0032432)	3 (CS 7.47)
actomyosin (GO:0042641)	3 (CS 7.02)
contractile fiber part (GO:0044449)	4 (CS 5.88)
extracellular region (GO:0005576)	13 (CS 5.36)

B



C



Supplementary Material

Supplementary Table S1: Comparison of CR and GF mice.

Supplementary Table. S2: List of genes differentially expressed in GF, N, and O animals when compared to CR mice.

Supplementary Table S3: List of genes differentially in CR, N, and O animals when compared with GF mice.

Supplementary Table S4: Comparison of monoassociated mice.

Supplementary Table S5: List of primers used for qRT-PCR.

Supplementary Table S1

Differentially expressed genes in the mucosa of the middle part of the small intestine of conventionally reared (CR) vs. germ-free (GF) mice (contrast: CR_GF)

ENTREZ No.	Symbol	Gene name	Log FC	q-value
93695	Gpnmb	glycoprotein (transmembrane) nmb	3.10	0.000000
14961	H2-Ab1	histocompatibility 2, class II antigen A, beta 1	2.99	0.000012
20568	Slpi	secretory leukocyte peptidase inhibitor	2.86	0.004600
69169	Faim3	Fas apoptotic inhibitory molecule 3	2.82	0.038000
14999	H2-DMb1	histocompatibility 2, class II, locus Mb1	2.74	0.000009
16149	Cd74	CD74 antigen (invariant polypeptide of major histocompatibility complex, class II antigen-associated)	2.70	0.000066
55985	Cxcl13	chemokine (C-X-C motif) ligand 13	2.46	0.010000
14969	H2-Eb1	histocompatibility 2, class II antigen E beta	2.40	0.000330
15985	Cd79b	CD79B antigen	2.23	0.015000
11472	Actn2	actinin alpha 2	2.12	0.000000
17067	Ly6c1	lymphocyte antigen 6 complex, locus C1	2.00	0.004600
21838	Thy1	thymus cell antigen 1, theta	1.97	0.000790
74096	Hvcn1	hydrogen voltage-gated channel 1	1.90	0.033000
12511	Cd6	CD6 antigen	1.87	0.005900
20440	St6gal1	beta galactoside alpha 2,6 sialyltransferase 1	1.81	0.000007
14968	H2-Ea-ps	histocompatibility 2, class II antigen E alpha, pseudogene	1.80	0.008300
17110	Lyz1	lysozyme 1	1.79	0.039000
12265	Ciita	class II transactivator	1.76	0.004600
22364	Vpreb3	pre-B lymphocyte gene 3	1.73	0.011000
12721	Coro1a	coronin, actin binding protein 1A	1.61	0.042000
21807	Tsc22d1	TSC22 domain family, member 1	1.61	0.000002
20303	Ccl4	chemokine (C-C motif) ligand 4	1.58	0.002900
12526	Cd8b1	CD8 antigen, beta chain 1	1.57	0.009500
24108	Ubd	ubiquitin D	1.57	0.017000
22379	Fmnl3	formin-like 3	1.52	0.015000
17896	Myl4	myosin, light polypeptide 4	1.40	0.039000
217169	Tns4	tensin 4	1.40	0.000020
11629	Aif1	allograft inflammatory factor 1	1.37	0.003200
74191	P2ry13	purinergic receptor P2Y, G-protein coupled 13	1.36	0.011000
20304	Ccl5	chemokine (C-C motif) ligand 5	1.31	0.020000
67876	Coq10b	coenzyme Q10 homolog B (S. cerevisiae)	1.30	0.006200
231932	Gimap7	GTPase, IMAP family member 7	1.30	0.018000
69772	Bdh2	3-hydroxybutyrate dehydrogenase, type 2	1.29	0.030000
215653	Rassf2	Ras association (RalGDS/AF-6) domain family member 2	1.29	0.010000
107321	Lpxn	leupaxin	1.28	0.036000
381524	AI427809	expressed sequence AI427809	1.27	0.007800
11486	Ada	adenosine deaminase	1.26	0.009400
23959	Nt5e	5' nucleotidase, ecto	1.26	0.038000
11565	Adssl1	adenylosuccinate synthetase like 1	1.24	0.005100
103149	Upb1	ureidopropionase, beta	1.24	0.003500
16421	Itgb7	integrin beta 7	1.23	0.025000
16909	Lmo2	LIM domain only 2	1.23	0.038000
12259	C1qa	complement component 1, q subcomponent, alpha polypeptide	1.20	0.006700
12448	Ccne2	cyclin E2	1.19	0.000005
102595	Plekho2	pleckstrin homology domain containing, family O member 2	1.19	0.005800
320484	Rasal3	RAS protein activator like 3	1.19	0.044000
12458	Ccr6	chemokine (C-C motif) receptor 6	1.17	0.023000
110168	Gpr18	G protein-coupled receptor 18	1.17	0.033000
108956	Apol7c	apolipoprotein L 7c	1.16	0.000063
13036	Ctsh	cathepsin H	1.16	0.000820
11872	Art2b	ADP-ribosyltransferase 2b	1.14	0.036000
268567	Tmem229b	transmembrane protein 229B	1.14	0.001500
74015	Fcho1	FCH domain only 1	1.13	0.009700
56743	Lat2	linker for activation of T cells family, member 2	1.13	0.019000
70785	Dennd1c	DENN/MADD domain containing 1C	1.12	0.030000
233571	P2ry6	pyrimidinergic receptor P2Y, G-protein coupled, 6	1.11	0.006000

20345	Selplg	selectin, platelet (p-selectin) ligand	1.11	0.011000
13057	Cyba	cytochrome b-245, alpha polypeptide	1.10	0.005100
19245	Ptp4a3	protein tyrosine phosphatase 4a3	1.10	0.046000
13041	Ctsw	cathepsin W	1.07	0.024000
72310	Nkg7	natural killer cell group 7 sequence	1.06	0.042000
74131	Sash3	SAM and SH3 domain containing 3	1.05	0.012000
22637	Zap70	zeta-chain (TCR) associated protein kinase	1.05	0.000790
12766	Cxcr3	chemokine (C-X-C motif) receptor 3	1.03	0.000009
15163	Hcls1	hematopoietic cell specific Lyn substrate 1	1.03	0.019000
102545	Cmtm7	CKLF-like MARVEL transmembrane domain containing 7	1.01	0.011000
78416	Rnase6	ribonuclease, RNase A family, 6	1.01	0.042000
76527	Il34	interleukin 34	1.00	0.011000
67603	Dusp6	dual specificity phosphatase 6	-1.02	0.002900
12660	Chka	choline kinase alpha	-1.03	0.000054
67603	Dusp6	dual specificity phosphatase 6	-1.03	0.001600
26897	Acot1	acyl-CoA thioesterase 1	-1.04	0.025000
66270	Fam134b	family with sequence similarity 134, member B	-1.04	0.043000
84112	Sucnr1	succinate receptor 1	-1.04	0.004000
212398	Frat2	frequently rearranged in advanced T-cell lymphomas 2	-1.06	0.000094
224023	Klhl22	kelch-like 22 (Drosophila)	-1.09	0.031000
234788	Slc38a8	solute carrier family 38, member 8	-1.10	0.005200
13131	Dab1	disabled homolog 1 (Drosophila)	-1.18	0.000003
12125	Bcl2l11	BCL2-like 11 (apoptosis facilitator)	-1.19	0.000270
17195	Mbl2	mannose-binding lectin (protein C) 2	-1.22	0.000001
74155	Errfi1	ERBB receptor feedback inhibitor 1	-1.23	0.000430
50490	Nox4	NADPH oxidase 4	-1.23	0.023000
14377	G6pc	glucose-6-phosphatase, catalytic	-1.35	0.038000
17748	Mt1	metallothionein 1	-1.35	0.000009
17750	Mt2	metallothionein 2	-1.35	0.015000
217721	Mfsd7c	major facilitator superfamily domain containing 7C	-1.42	0.000027
11865	Arntl	aryl hydrocarbon receptor nuclear translocator-like	-1.46	0.002900
57875	Angptl4	angiopoietin-like 4	-1.90	0.011000
20531	Slc34a2	solute carrier family 34 (sodium phosphate), member 2	-1.98	0.008300

Differentially expressed genes in the mucosa of the distal part of the small intestine of CR vs. GF mice (contrast: CR_GF)

ENTREZ No.	Symbol	Gene name	Log FC	q-value
14961	H2-Ab1	histocompatibility 2, class II antigen A, beta 1	5.03	0.000000
14999	H2-DMb1	histocompatibility 2, class II, locus Mb1	4.69	0.000000
16149	Cd74	CD74 antigen (invariant polypeptide of major histocompatibility complex, class II antigen-associated)	4.35	0.000000
14969	H2-Eb1	histocompatibility 2, class II antigen E beta	4.11	0.000000
14968	H2-Ea-ps	histocompatibility 2, class II antigen E alpha, pseudogene	3.55	0.000000
20304	Ccl5	chemokine (C-C motif) ligand 5	3.45	0.000000
12501	Cd3e	CD3 antigen, epsilon polypeptide	3.06	0.000000
24108	Ubd	ubiquitin D	3.01	0.000001
12511	Cd6	CD6 antigen	2.98	0.000002
12502	Cd3g	CD3 antigen, gamma polypeptide	2.84	0.000000
14170	Fgf15	fibroblast growth factor 15	2.77	0.000190
12265	Ciita	class II transactivator	2.66	0.000002
16792	Laptm5	lysosomal-associated protein transmembrane 5	2.63	0.000130
12500	Cd3d	CD3 antigen, delta polypeptide	2.53	0.000001
12721	Coro1a	coronin, actin binding protein 1A	2.49	0.000310
239743	Klhl6	kelch-like 6 (Drosophila)	2.49	0.002000
12526	Cd8b1	CD8 antigen, beta chain 1	2.48	0.000007
17105	Lyz2	lysozyme 2	2.46	0.002500
23833	Cd52	CD52 antigen	2.41	0.004300
17329	Cxcl9	chemokine (C-X-C motif) ligand 9	2.38	0.000650
110168	Gpr18	G protein-coupled receptor 18	2.34	0.000001
16407	Itgae	integrin alpha E, epithelial-associated	2.34	0.000000
11857	Arhgdib	Rho, GDP dissociation inhibitor (GDI) beta	2.34	0.001500
17110	Lyz1	lysozyme 1	2.32	0.002700
13041	Ctsw	cathepsin W	2.31	0.000000
21838	Thy1	thymus cell antigen 1, theta	2.27	0.000038
231932	Gimap7	GTPase, IMAP family member 7	2.21	0.000008
18985	Pou2af1	POU domain, class 2, associating factor 1	2.20	0.017000
15985	Cd79b	CD79B antigen	2.19	0.013000
16913	Psmb8	proteasome (prosome, macropain) subunit, beta type 8 (large multifunctional peptidase 7)	2.16	0.000067
72310	Nkg7	natural killer cell group 7 sequence	2.15	0.000002
18301	Fxyd5	FXYD domain-containing ion transport regulator 5	2.14	0.000270
16985	Lsp1	lymphocyte specific 1	2.12	0.000940
14468	Gbp1	guanylate binding protein 1	2.11	0.000750
16421	Itgb7	integrin beta 7	2.06	0.000021
55985	Cxcl13	chemokine (C-X-C motif) ligand 13	2.04	0.036000
20303	Ccl4	chemokine (C-C motif) ligand 4	2.02	0.000032
11872	Art2b	ADP-ribosyltransferase 2b	2.01	0.000020
107321	Lpxn	leupaxin	2.00	0.000170
19419	Rasgrp1	RAS guanyl releasing protein 1	2.00	0.001000
105855	Nckap1l	NCK associated protein 1 like	1.98	0.000440
27371	Sh2d2a	SH2 domain protein 2A	1.98	0.000110
14469	Gbp2	guanylate binding protein 2	1.97	0.002400
68891	Cd177	CD177 antigen	1.96	0.000045
17304	Mfge8	milk fat globule-EGF factor 8 protein	1.96	0.002700
16145	Igtp	interferon gamma induced GTPase	1.94	0.044000
16994	Ltb	lymphotoxin B	1.94	0.005100
22637	Zap70	zeta-chain (TCR) associated protein kinase	1.94	0.000001
20230	Satb1	special AT-rich sequence binding protein 1	1.92	0.003900
17304	Mfge8	milk fat globule-EGF factor 8 protein	1.90	0.004300
65256	Asb2	ankyrin repeat and SOCS box-containing 2	1.89	0.021000
27261	Dok3	docking protein 3	1.89	0.031000
14204	Il4i1	interleukin 4 induced 1	1.89	0.044000
231931	Gimap6	GTPase, IMAP family member 6	1.85	0.006500
15953	Ifi47	interferon gamma inducible protein 47	1.85	0.007600
20715	Serpina3g	serine (or cysteine) peptidase inhibitor, clade A, member 3G	1.85	0.006500

16818	Lck	lymphocyte protein tyrosine kinase	1.82	0.000110
320484	Rasal3	RAS protein activator like 3	1.78	0.000600
11472	Actn2	actinin alpha 2	1.77	0.000000
546546	Serpina3h	serine (or cysteine) peptidase inhibitor, clade A, member 3H	1.77	0.022000
20491	Sla	src-like adaptor	1.77	0.009200
21940	Cd27	CD27 antigen	1.75	0.000170
16909	Lmo2	LIM domain only 2	1.75	0.000800
16498	Kcnab2	potassium voltage-gated channel, shaker-related subfamily, beta member 2	1.75	0.002700
93695	Gpnmb	glycoprotein (transmembrane) nmb	1.69	0.000230
246177	Myo1g	myosin IG	1.69	0.000270
17084	Ly86	lymphocyte antigen 86	1.68	0.012000
16170	Il16	interleukin 16	1.67	0.001100
11816	Apoe	apolipoprotein E	1.66	0.036000
13537	Dusp2	dual specificity phosphatase 2	1.66	0.003600
18826	Lcp1	lymphocyte cytosolic protein 1	1.65	0.000810
12143	Blk	B lymphoid kinase	1.64	0.013000
17972	Ncf4	neutrophil cytosolic factor 4	1.64	0.002200
22271	Upp1	uridine phosphorylase 1	1.64	0.017000
53376	Usp2	ubiquitin specific peptidase 2	1.60	0.000160
20345	Selplg	selectin, platelet (p-selectin) ligand	1.58	0.000070
54215	Cd160	CD160 antigen	1.57	0.000150
12262	C1qc	complement component 1, q subcomponent, C chain	1.56	0.044000
23871	Ets1	E26 avian leukemia oncogene 1, 5' domain	1.56	0.013000
434341	Nlrc5	NLR family, CARD domain containing 5	1.56	0.000052
12493	Cd37	CD37 antigen	1.55	0.006300
17067	Ly6c1	lymphocyte antigen 6 complex, locus C1	1.55	0.029000
22329	Vcam1	vascular cell adhesion molecule 1	1.55	0.009700
30948	Bin1	bridging integrator 1	1.54	0.004500
15000	H2-DMb2	histocompatibility 2, class II, locus Mb2	1.53	0.025000
17698	Msn	moesin	1.53	0.004700
18751	Prkcb	protein kinase C, beta	1.53	0.007700
22379	Fmnl3	formin-like 3	1.52	0.010000
58194	Sh3kbp1	SH3-domain kinase binding protein 1	1.52	0.000130
12515	Cd69	CD69 antigen	1.50	0.001700
19354	Rac2	RAS-related C3 botulinum substrate 2	1.50	0.000680
74015	Fcho1	FCH domain only 1	1.48	0.000190
229323	Gpr171	G protein-coupled receptor 171	1.46	0.000170
18718	Pip4k2a	phosphatidylinositol-5-phosphate 4-kinase, type II, alpha	1.46	0.018000
215653	Rassf2	Ras association (RalGDS/AF-6) domain family member 2	1.45	0.001800
16428	Itk	IL2-inducible T-cell kinase	1.44	0.000001
54354	Rassf5	Ras association (RalGDS/AF-6) domain family member 5	1.44	0.011000
14007	Celf2	CUGBP, Elav-like family member 2	1.43	0.023000
70785	Dennd1c	DENN/MADD domain containing 1C	1.43	0.001900
226594	Rcsd1	RCSD domain containing 1	1.42	0.023000
66995	Zcchc18	zinc finger, CCHC domain containing 18	1.42	0.029000
22376	Was	Wiskott-Aldrich syndrome homolog (human)	1.41	0.006800
15930	Ido1	indoleamine 2,3-dioxygenase 1	1.40	0.016000
16643	Klrd1	killer cell lectin-like receptor, subfamily D, member 1	1.40	0.001200
12522	Cd83	CD83 antigen	1.38	0.012000
13713	Elk3	ELK3, member of ETS oncogene family	1.38	0.004700
16797	Lat	linker for activation of T cells	1.37	0.000034
12145	Cxcr5	chemokine (C-X-C motif) receptor 5	1.36	0.032000
15163	Hcls1	hematopoietic cell specific Lyn substrate 1	1.35	0.000650
67742	Samsn1	SAM domain, SH3 domain and nuclear localization signals, 1	1.35	0.049000
21813	Tgfbr2	transforming growth factor, beta receptor II	1.34	0.049000
16598	Klf2	Kruppel-like factor 2 (lung)	1.33	0.041000
17069	Ly6e	lymphocyte antigen 6 complex, locus E	1.33	0.049000
16541	Napsa	napsin A aspartic peptidase	1.33	0.001500
17896	Myl4	myosin, light polypeptide 4	1.32	0.049000
74131	Sash3	SAM and SH3 domain containing 3	1.32	0.000620
243374	Gimap8	GTPase, IMAP family member 8	1.30	0.019000
232201	Arhgap25	Rho GTPase activating protein 25	1.30	0.026000
18636	Cfp	complement factor properdin	1.29	0.025000

13170	Dbp	D site albumin promoter binding protein	1.29	0.025000
14281	Fos	FBJ osteosarcoma oncogene	1.29	0.003600
70719	Hmha1	histocompatibility (minor) HA-1	1.29	0.034000
15001	H2-Oa	histocompatibility 2, O region alpha locus	1.29	0.012000
13449	Dok2	docking protein 2	1.28	0.003100
321019	Gpr183	G protein-coupled receptor 183	1.28	0.002300
15277	Hk2	hexokinase 2	1.28	0.000550
24099	Tnfsf13b	tumor necrosis factor (ligand) superfamily, member 13b	1.28	0.000017
13057	Cyba	cytochrome b-245, alpha polypeptide	1.27	0.000380
12458	Ccr6	chemokine (C-C motif) receptor 6	1.26	0.008500
224109	Lrrc33	leucine rich repeat containing 33	1.26	0.000970
14960	H2-Aa	histocompatibility 2, class II antigen A, alpha	1.25	0.000008
56743	Lat2	linker for activation of T cells family, member 2	1.24	0.005500
226652	Arhgap30	Rho GTPase activating protein 30	1.24	0.016000
22324	Vav1	vav 1 oncogene	1.24	0.000310
13421	Dnase1l3	deoxyribonuclease 1-like 3	1.22	0.025000
259277	Klk8	kallikrein related-peptidase 8	1.22	0.000550
12508	Cd53	CD53 antigen	1.21	0.017000
21354	Tap1	transporter 1, ATP-binding cassette, sub-family B (MDR/TAP)	1.21	0.037000
238377	Gpr68	G protein-coupled receptor 68	1.19	0.000002
68682	Slc44a2	solute carrier family 44, member 2	1.19	0.000009
12483	Cd22	CD22 antigen	1.18	0.012000
14130	Fcgr2b	Fc receptor, IgG, low affinity IIb	1.18	0.012000
67905	Ppm1m	protein phosphatase 1M	1.17	0.005100
17085	Ly9	lymphocyte antigen 9	1.16	0.000310
19265	Ptprcap	protein tyrosine phosphatase, receptor type, C polypeptide-associated protein	1.16	0.002300
98752	Fcrla	Fc receptor-like A	1.14	0.001200
100182	Akna	AT-hook transcription factor	1.13	0.000360
15894	Icam1	intercellular adhesion molecule 1	1.13	0.017000
19245	Ptp4a3	protein tyrosine phosphatase 4a3	1.13	0.034000
78416	Rnase6	ribonuclease, RNase A family, 6	1.12	0.016000
67102	D16Ertd472e	DNA segment, Chr 16, ERATO Doi 472, expressed	1.11	0.030000
15900	Irf8	interferon regulatory factor 8	1.11	0.000830
239827	Pigz	phosphatidylinositol glycan anchor biosynthesis, class Z	1.11	0.000000
76438	Rftn1	raftlin lipid raft linker 1	1.11	0.028000
216445	Arhgap9	Rho GTPase activating protein 9	1.11	0.022000
102545	Cmtm7	CKLF-like MARVEL transmembrane domain containing 7	1.10	0.001300
74191	P2ry13	purinergic receptor P2Y, G-protein coupled 13	1.10	0.043000
12263	C2	complement component 2 (within H-2S)	1.09	0.049000
14357	Dtx1	deltex 1 homolog (Drosophila)	1.09	0.000002
17259	Mef2b	myocyte enhancer factor 2B	1.09	0.001400
227659	Slc2a6	solute carrier family 2 (facilitated glucose transporter), member 6	1.09	0.019000
12524	Cd86	CD86 antigen	1.08	0.002100
241732	Tspyl3	TSPY-like 3	1.08	0.002000
21939	Cd40	CD40 antigen	1.07	0.004600
22778	Ikzf1	IKAROS family zinc finger 1	1.07	0.015000
18707	Pik3cd	phosphatidylinositol 3-kinase catalytic delta polypeptide	1.07	0.001400
73341	Arhgef6	Rac/Cdc42 guanine nucleotide exchange factor (GEF) 6	1.07	0.000950
232984	B3gnt8	UDP-GlcNAc:betaGal beta-1,3-N-acetylglucosaminyltransferase 8	1.07	0.017000
268857	Nlrc3	NLR family, CARD domain containing 3	1.06	0.002900
108101	Fermt3	fermitin family homolog 3 (Drosophila)	1.04	0.003500
16176	Il1b	interleukin 1 beta	1.04	0.031000
243910	Nfkbid	nuclear factor of kappa light polypeptide gene enhancer in B-cells inhibitor, delta	1.04	0.000100
12443	Ccnd1	cyclin D1	1.03	0.001800
16197	Il7r	interleukin 7 receptor	1.02	0.046000
14667	Gm2a	GM2 ganglioside activator protein	1.00	0.007600
16154	Il10ra	interleukin 10 receptor, alpha	1.00	0.014000
16453	Jak3	Janus kinase 3	1.00	0.002500
18126	Nos2	nitric oxide synthase 2, inducible	1.00	0.000240
68344	Tmem174	transmembrane protein 174	-1.01	0.000004
12408	Cbr1	carbonyl reductase 1	-1.02	0.031000
218454	Lhfpl2	lipoma HMGIC fusion partner-like 2	-1.04	0.011000

18143	Npas2	neuronal PAS domain protein 2	-1.05	0.003700
71733	Susd2	sushi domain containing 2	-1.05	0.009700
11828	Aqp3	aquaporin 3	-1.10	0.001200
50934	Slc7a8	solute carrier family 7 (cationic amino acid transporter, y+ system), member 8	-1.14	0.002000
70113	Odf3b	outer dense fiber of sperm tails 3B	-1.15	0.000270
71904	Paqr7	progestin and adipoQ receptor family member VII	-1.17	0.000850
234788	Slc38a8	solute carrier family 38, member 8	-1.41	0.000089
18387	Oprk1	opioid receptor, kappa 1	-1.64	0.000000
64454	Slc5a4b	solute carrier family 5 (neutral amino acid transporters, system A), member 4b	-1.77	0.000250
13614	Edn1	endothelin 1	-1.83	0.000170
71898	Apol9b	apolipoprotein L 9b	-1.85	0.003500
14377	G6pc	glucose-6-phosphatase, catalytic	-1.98	0.000550
27273	Pdk4	pyruvate dehydrogenase kinase, isoenzyme 4	-2.04	0.001200
57875	Angptl4	angiopoietin-like 4	-3.06	0.000006

Differentially expressed genes in the mucosa of the large intestine of CR vs. GF mice (contrast: CR_GF)

ENTREZ No.	Symbol	Gene name	Log FC	q-value
18947	Pnliprp2	pancreatic lipase-related protein 2	5.16	0.000004
18946	Pnliprp1	pancreatic lipase related protein 1	4.46	0.005400
109791	Clps	colipase, pancreatic	3.73	0.000960
232889	Pla2g4c	phospholipase A2, group IVC (cytosolic, calcium-independent)	3.61	0.006200
16429	Itln1	intelectin 1 (galactofuranose binding)	3.29	0.000230
18780	Pla2g2a	phospholipase A2, group IIA (platelets, synovial fluid)	3.20	0.000042
14999	H2-DMb1	histocompatibility 2, class II, locus Mb1	3.08	0.000001
14961	H2-Ab1	histocompatibility 2, class II antigen A, beta 1	3.07	0.000011
16149	Cd74	CD74 antigen (invariant polypeptide of major histocompatibility complex, class II antigen-associated)	2.90	0.000024
14969	H2-Eb1	histocompatibility 2, class II antigen E beta	2.37	0.000400
219033	Ang4	angiogenin, ribonuclease A family, member 4	2.29	0.040000
57263	Retnlb	resistin like beta	2.28	0.047000
68468	Ly6g6c	lymphocyte antigen 6 complex, locus G6C	2.25	0.002900
15430	Hoxd10	homeobox D10	2.12	0.004500
14968	H2-Ea-ps	histocompatibility 2, class II antigen E alpha, pseudogene	2.06	0.002000
12265	Ciita	class II transactivator	1.93	0.001300
69065	Chac1	ChaC, cation transport regulator-like 1 (E. coli)	1.88	0.001200
110454	Ly6a	lymphocyte antigen 6 complex, locus A	1.82	0.028000
17341	Bhlha15	basic helix-loop-helix family, member a15	1.80	0.001000
15953	Ifi47	interferon gamma inducible protein 47	1.80	0.014000
19367	Rad9	RAD9 homolog (S. pombe)	1.73	0.000640
17069	Ly6e	lymphocyte antigen 6 complex, locus E	1.71	0.008300
67198	Spats2l	spermatogenesis associated, serine-rich 2-like	1.68	0.003100
68891	Cd177	CD177 antigen	1.66	0.000000
66120	Fkbp11	FK506 binding protein 11	1.59	0.000210
23797	Akt3	thymoma viral proto-oncogene 3	1.59	0.000059
26366	Ceacam10	carcinoembryonic antigen-related cell adhesion molecule 10	1.58	0.000000
12332	Capg	capping protein (actin filament), gelsolin-like	1.53	0.000120
23882	Gadd45g	growth arrest and DNA-damage-inducible 45 gamma	1.52	0.007500
233038	Nccrp1	non-specific cytotoxic cell receptor protein 1 homolog (zebrafish)	1.52	0.000290
434341	Nlrc5	NLR family, CARD domain containing 5	1.48	0.000270
13105	Cyp2d9	cytochrome P450, family 2, subfamily d, polypeptide 9	1.47	0.003400
234577	Cpne2	copine II	1.46	0.000026
384009	Glipr2	GLI pathogenesis-related 2	1.40	0.003700
229933	Clca5	chloride channel calcium activated 5	1.37	0.000960
216188	Aldh1l2	aldehyde dehydrogenase 1 family, member L2	1.32	0.000180
67709	Reg4	regenerating islet-derived family, member 4	1.31	0.004700
11872	Art2b	ADP-ribosyltransferase 2b	1.29	0.014000
80859	Nfkbiz	nuclear factor of kappa light polypeptide gene enhancer in B-cells inhibitor, zeta	1.29	0.022000
209588	Sectm1a	secreted and transmembrane 1A	1.24	0.000550
12124	Bik	BCL2-interacting killer	1.23	0.000000
16913	Psmb8	proteasome (prosome, macropain) subunit, beta type 8 (large multifunctional peptidase 7)	1.22	0.047000
103149	Upb1	ureidopropionase, beta	1.22	0.001100
67475	Ero1lb	ERO1-like beta (S. cerevisiae)	1.21	0.002000
104601	Mycbpap	MYCBP associated protein	1.20	0.014000
21818	Tgm3	transglutaminase 3, E polypeptide	1.20	0.000120
74015	Fcho1	FCH domain only 1	1.18	0.006500
27356	Insl6	insulin-like 6	1.14	0.000024
20731	Spink4	serine peptidase inhibitor, Kazal type 4	1.12	0.029000
12409	Cbr2	carbonyl reductase 2	1.11	0.002500
12263	C2	complement component 2 (within H-2S)	1.11	0.049000
216456	Gls2	glutaminase 2 (liver, mitochondrial)	1.10	0.017000
70536	Qpct	glutaminyl-peptide cyclotransferase (glutaminyl cyclase)	1.09	0.000099
317652	Klk15	kallikrein related-peptidase 15	1.09	0.011000
56045	Samhd1	SAM domain and HD domain, 1	1.07	0.000500
100041194	Ahnak2	AHNAK nucleoprotein 2	1.05	0.001600

53376	Usp2	ubiquitin specific peptidase 2	1.05	0.028000
76267	Fads1	fatty acid desaturase 1	1.04	0.044000
14537	Gcnt1	glucosaminyl (N-acetyl) transferase 1, core 2	1.04	0.001500
16402	Itga5	integrin alpha 5 (fibronectin receptor alpha)	1.04	0.004600
16622	Klk1b5	kallikrein 1-related peptidase b5	1.02	0.007300
56773	Chst5	carbohydrate (N-acetylglucosamine 6-O) sulfotransferase 5	1.00	0.022000
15432	Hoxd12	homeobox D12	1.00	0.005200
214897	Csnk1g1	casein kinase 1, gamma 1	-1.00	0.025000
18789	Papola	poly (A) polymerase alpha	-1.00	0.049000
76722	Ckmt2	creatine kinase, mitochondrial 2	-1.02	0.000017
14282	Fosb	FBJ osteosarcoma oncogene B	-1.02	0.005400
22051	Trip6	thyroid hormone receptor interactor 6	-1.06	0.000071
16939	Lor	loricrin	-1.09	0.000570
21888	Tle4	transducin-like enhancer of split 4, homolog of Drosophila E(spl)	-1.10	0.015000
14526	Gcg	glucagon	-1.12	0.007800
56365	Clcnkb	chloride channel Kb	-1.13	0.000750
319848	Slc17a4	solute carrier family 17 (sodium phosphate), member 4	-1.13	0.004000
230163	Aldob	aldolase B, fructose-bisphosphate	-1.17	0.000230
19252	Dusp1	dual specificity phosphatase 1	-1.17	0.003800
11812	Apoc1	apolipoprotein C-I	-1.19	0.024000
258458	Olfr165	olfactory receptor 165	-1.22	0.001800
22239	Ugt8a	UDP galactosyltransferase 8A	-1.33	0.044000
54367	Zfp326	zinc finger protein 326	-1.40	0.001400
13829	Epb4.9	erythrocyte protein band 4.9	-1.47	0.000024
11668	Aldh1a1	aldehyde dehydrogenase family 1, subfamily A1	-1.49	0.018000
12153	Bmp1	bone morphogenetic protein 1	-1.50	0.005700
68404	Nrn1	neuritin 1	-1.57	0.002900
235674	Acaa1b	acetyl-Coenzyme A acyltransferase 1B	-1.58	0.026000
66184	Rps4y2	ribosomal protein S4, Y-linked 2	-1.59	0.007100
17829	Muc1	mucin 1, transmembrane	-1.62	0.000028
12424	Cck	cholecystokinin	-1.64	0.002700
57875	Angptl4	angiopoietin-like 4	-1.79	0.018000
110075	Bmp3	bone morphogenetic protein 3	-1.88	0.000012
74338	Slc6a19	solute carrier family 6 (neurotransmitter transporter), member 19	-1.88	0.000000
20604	Sst	somatostatin	-1.94	0.000001
381204	Naaladl1	N-acetylated alpha-linked acidic dipeptidase-like 1	-2.05	0.000210
30962	Slc7a9	solute carrier family 7 (cationic amino acid transporter, y+ system), member 9	-2.20	0.000001
76279	Cyp2d26	cytochrome P450, family 2, subfamily d, polypeptide 26	-2.49	0.000000

Supplementary Table S2

Differentialy expressed genes in the mucosa of the middle part of the small intestine of conventionally reared (CR) vs. germ-free (GF) and monoassociated (N or O) mice (contrast: CR_GF/N/O)

ENTREZ No.	Symbol	Gene name	Change
11472	Actn2	actinin alpha 2	up
11486	Ada	adenosine deaminase	up
11565	Adssl1	adenylosuccinate synthetase like 1	up
12125	Bcl2l11	BCL2-like 11 (apoptosis facilitator)	down
12448	Ccne2	cyclin E2	up
12458	Ccr6	chemokine (C-C motif) receptor 6	up
12511	Cd6	CD6 antigen	up
16149	Cd74	CD74 antigen (invariant polypeptide of major histocompatibility complex, class II antigen-associated)	up
15985	Cd79b	CD79B antigen	up
12265	Ciita	class II transactivator	up
55985	Cxcl13	chemokine (C-X-C motif) ligand 13	up
69169	Faim3	Fas apoptotic inhibitory molecule 3	up
74015	Fcho1	FCH domain only 1	up
231932	Gimap7	GTPase, IMAP family member 7	up
93695	Gpnmb	glycoprotein (transmembrane) nmb	up
14961	H2-Ab1	histocompatibility 2, class II antigen A, beta 1	up
14999	H2-DMb1	histocompatibility 2, class II, locus Mb1	up
14969	H2-Eb1	histocompatibility 2, class II antigen E beta	up
16421	Itgb7	integrin beta 7	up
17195	Mbl2	mannose-binding lectin (protein C) 2	down
17750	Mt2	metallothionein 2	down
17896	Myl4	myosin, light polypeptide 4	up
23959	Nt5e	5' nucleotidase, ecto	up
215653	Rassf2	Ras association (RalGDS/AF-6) domain family member 2	up
20568	Slpi	secretory leukocyte peptidase inhibitor	up
20440	St6gal1	beta galactoside alpha 2,6 sialyltransferase 1	up
21838	Thy1	thymus cell antigen 1, theta	up
21807	Tsc22d1	TSC22 domain family, member 1	up
24108	Ubd	ubiquitin D	up
22364	Vpreb3	pre-B lymphocyte gene 3	up

Differentialy expressed genes in the mucosa of the distal part of the small intestine of CR vs. GF and monoassociated (N or O) mice (contrast: CR_GF/N/O)

ENTREZ No.	Symbol	Gene name	Change
11472	Actn2	actinin alpha 2	up
57875	Angptl4	angiopoietin-like 4	down
71898	Apol9b	apolipoprotein L 9b	down
11828	Aqp3	aquaporin 3	down
232201	Arhgap25	Rho GTPase activating protein 25	up
226652	Arhgap30	Rho GTPase activating protein 30	up
216445	Arhgap9	Rho GTPase activating protein 9	up
11857	Arhgdib	Rho, GDP dissociation inhibitor (GDI) beta	up
11872	Art2b	ADP-ribosyltransferase 2b	up
232984	B3gnt8	UDP-GlcNAc:betaGal beta-1,3-N-acetylglucosaminyltransferase 8	up
30948	Bin1	bridging integrator 1	up
12143	Blk	B lymphoid kinase	up
12408	Cbr1	carbonyl reductase 1	down
20303	Ccl4	chemokine (C-C motif) ligand 4	up
20304	Ccl5	chemokine (C-C motif) ligand 5	up
12458	Ccr6	chemokine (C-C motif) receptor 6	up
54215	Cd160	CD160 antigen	up
68891	Cd177	CD177 antigen	up
21940	Cd27	CD27 antigen	up
12493	Cd37	CD37 antigen	up
12500	Cd3d	CD3 antigen, delta polypeptide	up
12501	Cd3e	CD3 antigen, epsilon polypeptide	up
12502	Cd3g	CD3 antigen, gamma polypeptide	up
21939	Cd40	CD40 antigen	up
23833	Cd52	CD52 antigen	up
12508	Cd53	CD53 antigen	up
12511	Cd6	CD6 antigen	up
12515	Cd69	CD69 antigen	up
16149	Cd74	CD74 antigen (invariant polypeptide of major histocompatibility complex, class II antigen-associated)	up
15985	Cd79b	CD79B antigen	up
12524	Cd86	CD86 antigen	up
12526	Cd8b1	CD8 antigen, beta chain 1	up
18636	Cfp	complement factor properdin	up
12265	Ciita	class II transactivator	up
102545	Cmtm7	CKLF-like MARVEL transmembrane domain containing 7	up
12721	Coro1a	coronin, actin binding protein 1A	up
13041	Ctsw	cathepsin W	up
55985	Cxcl13	chemokine (C-X-C motif) ligand 13	up
17329	Cxcl9	chemokine (C-X-C motif) ligand 9	up
12145	Cxcr5	chemokine (C-X-C motif) receptor 5	up
13057	Cyba	cytochrome b-245, alpha polypeptide	up
67102	D16Ertd472e	DNA segment, Chr 16, ERATO Doi 472, expressed	up
70785	Dennd1c	DENN/MADD domain containing 1C	up
13449	Dok2	docking protein 2	up
27261	Dok3	docking protein 3	up
13537	Dusp2	dual specificity phosphatase 2	up
13713	Elk3	ELK3, member of ETS oncogene family	up
23871	Ets1	E26 avian leukemia oncogene 1, 5' domain	up
14130	Fcgr2b	Fc receptor, IgG, low affinity IIb	up
74015	Fcho1	FCH domain only 1	up
98752	Fcrla	Fc receptor-like A	up

108101	Fermt3	fermitin family homolog 3 (Drosophila)	up
14170	Fgf15	fibroblast growth factor 15	up
22379	Fmnl3	formin-like 3	up
18301	Fxyd5	FXYD domain-containing ion transport regulator 5	up
14377	G6pc	glucose-6-phosphatase, catalytic	down
14468	Gbp1	guanylate binding protein 1	up
14469	Gbp2	guanylate binding protein 2	up
231931	Gimap6	GTPase, IMAP family member 6	up
231932	Gimap7	GTPase, IMAP family member 7	up
243374	Gimap8	GTPase, IMAP family member 8	up
93695	Gpnmb	glycoprotein (transmembrane) nmb	up
229323	Gpr171	G protein-coupled receptor 171	up
110168	Gpr18	G protein-coupled receptor 18	up
321019	Gpr183	G protein-coupled receptor 183	up
238377	Gpr68	G protein-coupled receptor 68	up
14961	H2-Ab1	histocompatibility 2, class II antigen A, beta 1	up
14999	H2-DMb1	histocompatibility 2, class II, locus Mb1	up
15000	H2-DMb2	histocompatibility 2, class II, locus Mb2	up
14968	H2-Ea-ps	histocompatibility 2, class II antigen E alpha, pseudogene	up
14969	H2-Eb1	histocompatibility 2, class II antigen E beta	up
15001	H2-Oa	histocompatibility 2, O region alpha locus	up
15163	Hcls1	hematopoietic cell specific Lyn substrate 1	up
15277	Hk2	hexokinase 2	up
70719	Hmha1	histocompatibility (minor) HA-1	up
15930	Ido1	indoleamine 2,3-dioxygenase 1	up
15953	Ifi47	interferon gamma inducible protein 47	up
22778	Ikzf1	IKAROS family zinc finger 1	up
16154	Il10ra	interleukin 10 receptor, alpha	up
16170	Il16	interleukin 16	up
16407	Itgae	integrin alpha E, epithelial-associated	up
16421	Itgb7	integrin beta 7	up
16428	Itk	IL2-inducible T-cell kinase	up
16498	Kcnab2	potassium voltage-gated channel, shaker-related subfamily, beta member 2	up
239743	Klhl6	kelch-like 6 (Drosophila)	up
259277	Klk8	kallikrein related-peptidase 8	up
16643	Klrd1	killer cell lectin-like receptor, subfamily D, member 1	up
16792	Laptm5	lysosomal-associated protein transmembrane 5	up
16797	Lat	linker for activation of T cells	up
56743	Lat2	linker for activation of T cells family, member 2	up
16818	Lck	lymphocyte protein tyrosine kinase	up
18826	Lcp1	lymphocyte cytosolic protein 1	up
107321	Lpxn	leupaxin	up
16985	Lsp1	lymphocyte specific 1	up
16994	Ltb	lymphotoxin B	up
17084	Ly86	lymphocyte antigen 86	up
17085	Ly9	lymphocyte antigen 9	up
17110	Lyz1	lysozyme 1	up
17105	Lyz2	lysozyme 2	up
17259	Mef2b	myocyte enhancer factor 2B	up
17304	Mfge8	milk fat globule-EGF factor 8 protein	up
17698	Msn	moesin	up
246177	Myo1g	myosin IG	up
16541	Napsa	napsin A aspartic peptidase	up
17972	Ncf4	neutrophil cytosolic factor 4	up
105855	Nckap1l	NCK associated protein 1 like	up
243910	Nfkbid	nuclear factor of kappa light polypeptide gene enhancer in B-cells inhibitor, delta	up

72310	Nkg7	natural killer cell group 7 sequence	up
434341	Nlrc5	NLR family, CARD domain containing 5	up
70113	Odf3b	outer dense fiber of sperm tails 3B	down
74191	P2ry13	purinergic receptor P2Y, G-protein coupled 13	up
239827	Pigz	phosphatidylinositol glycan anchor biosynthesis, class Z	up
18985	Pou2af1	POU domain, class 2, associating factor 1	up
67905	Ppm1m	protein phosphatase 1M	up
18751	Prkcb	protein kinase C, beta	up
16913	Psmb8	proteasome (prosome, macropain) subunit, beta type 8 (large multifunctional peptidase 7)	up
19245	Ptp4a3	protein tyrosine phosphatase 4a3	up
19265	Ptprcap	protein tyrosine phosphatase, receptor type, C polypeptide-associated protein	up
19354	Rac2	RAS-related C3 botulinum substrate 2	up
320484	Rasal3	RAS protein activator like 3	up
19419	Rasgrp1	RAS guanyl releasing protein 1	up
215653	Rassf2	Ras association (RalGDS/AF-6) domain family member 2	up
54354	Rassf5	Ras association (RalGDS/AF-6) domain family member 5	up
76438	Rftn1	raftlin lipid raft linker 1	up
78416	Rnase6	ribonuclease, RNase A family, 6	up
74131	Sash3	SAM and SH3 domain containing 3	up
20230	Satb1	special AT-rich sequence binding protein 1	up
20345	Selplg	selectin, platelet (p-selectin) ligand	up
20715	Serpina3g	serine (or cysteine) peptidase inhibitor, clade A, member 3G	up
546546	Serpina3h	serine (or cysteine) peptidase inhibitor, clade A, member 3H	up
27371	Sh2d2a	SH2 domain protein 2A	up
58194	Sh3kbp1	SH3-domain kinase binding protein 1	up
20491	Sla	src-like adaptor	up
227659	Slc2a6	solute carrier family 2 (facilitated glucose transporter), member 6	up
68682	Slc44a2	solute carrier family 44, member 2	up
64454	Slc5a4b	solute carrier family 5 (neutral amino acid transporters, system A), member 4b	down
50934	Slc7a8	solute carrier family 7 (cationic amino acid transporter, y+ system), member 8	down
71733	Susd2	sushi domain containing 2	down
21354	Tap1	transporter 1, ATP-binding cassette, sub-family B (MDR/TAP)	up
21838	Thy1	thymus cell antigen 1, theta	up
24099	Tnfsf13b	tumor necrosis factor (ligand) superfamily, member 13b	up
241732	Tspyl3	TSPY-like 3	up
24108	Ubd	ubiquitin D	up
22271	Upp1	uridine phosphorylase 1	up
22324	Vav1	vav 1 oncogene	up
22329	Vcam1	vascular cell adhesion molecule 1	up
22376	Was	Wiskott-Aldrich syndrome homolog (human)	up
22637	Zap70	zeta-chain (TCR) associated protein kinase	up

Differentialy expressed genes in the colonic mucosa of conventional CR vs. GF and monoassociated (N or O) mice (contrast: C_GF/N/O)

ENTREZ No.	Symbol	Gene name	Change
216188	Aldh1l2	aldehyde dehydrogenase 1 family, member L2	up
219033	Ang4	angiogenin, ribonuclease A family, member 4	up
11812	Apoc1	apolipoprotein C-I	down
11872	Art2b	ADP-ribosyltransferase 2b	up
17341	Bhlha15	basic helix-loop-helix family, member a15	up
12153	Bmp1	bone morphogenetic protein 1	down
12332	Capg	capping protein (actin filament), gelsolin-like	up
12409	Cbr2	carbonyl reductase 2	up
68891	Cd177	CD177 antigen	up
16149	Cd74	en (invariant polypeptide of major histocompatibility complex, class II antigen	up
69065	Chac1	ChaC, cation transport regulator-like 1 (E. coli)	up
12265	Ciita	class II transactivator	up
229933	Clca5	chloride channel calcium activated 5	up
76279	Cyp2d26	cytochrome P450, family 2, subfamily d, polypeptide 26	down
13829	Epb4.9	erythrocyte protein band 4.9	down
66120	Fkbp11	FK506 binding protein 11	up
23882	Gadd45g	growth arrest and DNA-damage-inducible 45 gamma	up
216456	Gls2	glutaminase 2 (liver, mitochondrial)	up
14961	H2-Ab1	histocompatibility 2, class II antigen A, beta 1	up
14999	H2-DMb1	histocompatibility 2, class II, locus Mb1	up
14969	H2-Eb1	histocompatibility 2, class II antigen E beta	up
15953	Ifi47	interferon gamma inducible protein 47	up
16429	Itln1	intelectin 1 (galactofuranose binding)	up
16939	Lor	loricrin	down
17069	Ly6e	lymphocyte antigen 6 complex, locus E	up
68468	Ly6g6c	lymphocyte antigen 6 complex, locus G6C	up
434341	Nlrc5	NLR family, CARD domain containing 5	up
18780	Pla2g2a	phospholipase A2, group IIA (platelets, synovial fluid)	up
232889	Pla2g4c	phospholipase A2, group IVC (cytosolic, calcium-independent)	up
18947	Pnliprp2	pancreatic lipase-related protein 2	up
70536	Qpct	glutaminyl-peptide cyclotransferase (glutaminyl cyclase)	up
19367	Rad9	RAD9 homolog (S. pombe)	up
66184	Rps4y2	ribosomal protein S4, Y-linked 2	down
74338	Slc6a19	solute carrier family 6 (neurotransmitter transporter), member 19	down
30962	Slc7a9	solute carrier family 7 (cationic amino acid transporter, y+ system), member 9	down
20604	Sst	somatostatin	down
54367	Zfp326	zinc finger protein 326	C_G: down C_N/O: up

Supplementary Table S3

Differentialy expressed genes in the mucosa of the middle part of the small intestine of conventionally reared (CR) and monoassociated (N or O) vs. germ-free (GF) mice (contrast: CR/N/O_GF)

ENTREZ No.	Symbol	Gene name	Change
58860	Adamdec1	ADAM-like, decysin 1	up
11816	Apoe	apolipoprotein E	up
14229	Fkbp5*	FK506 binding protein 5	C_GF: down N/O_GF: up
15220	Foxq1	forkhead box Q1	down
384783	Irs2*	insulin receptor substrate 2	down
110454	Ly6a	lymphocyte antigen 6 complex, locus A	up
17384	Mmp10	matrix metallopeptidase 10	up
18089	Nkx2-3	NK2 transcription factor related, locus 3 (Drosophila)	up
84094	Plvap	plasmalemma vesicle associated protein	up
21813	Tgfbr2	transforming growth factor, beta receptor II	up

*) these gene did not pass the significance criterion ($p < 0.05$) in the comparison O vs. GF; by other genes the p value was < 0.05 in all three contrasts (i.e. CR vs. GF; N v.s. GF; O vs. GF)

Differentialy expressed genes in the mucosa of the distal part of the small intestine of CR vs. GF and monoassociated (N or O) mice (contrast: CR_GF/N/O)

ENTREZ No.	Symbol	Gene name	Change
11472	Actn2	actinin alpha 2	up
57875	Angptl4	angiopoietin-like 4	down
71898	Apol9b	apolipoprotein L 9b	down
11828	Aqp3	aquaporin 3	down
232201	Arhgap25	Rho GTPase activating protein 25	up
226652	Arhgap30	Rho GTPase activating protein 30	up
216445	Arhgap9	Rho GTPase activating protein 9	up
11857	Arhgdib	Rho, GDP dissociation inhibitor (GDI) beta	up
11872	Art2b	ADP-ribosyltransferase 2b	up
232984	B3gnt8	UDP-GlcNAc:betaGal beta-1,3-N-acetylglucosaminyltransferase 8	up
30948	Bin1	bridging integrator 1	up
12143	Blk	B lymphoid kinase	up
12408	Cbr1	carbonyl reductase 1	down
20303	Ccl4	chemokine (C-C motif) ligand 4	up
20304	Ccl5	chemokine (C-C motif) ligand 5	up
12458	Ccr6	chemokine (C-C motif) receptor 6	up
54215	Cd160	CD160 antigen	up
68891	Cd177	CD177 antigen	up
21940	Cd27	CD27 antigen	up
12493	Cd37	CD37 antigen	up
12500	Cd3d	CD3 antigen, delta polypeptide	up
12501	Cd3e	CD3 antigen, epsilon polypeptide	up
12502	Cd3g	CD3 antigen, gamma polypeptide	up
21939	Cd40	CD40 antigen	up
23833	Cd52	CD52 antigen	up
12508	Cd53	CD53 antigen	up
12511	Cd6	CD6 antigen	up
12515	Cd69	CD69 antigen	up
16149	Cd74	CD74 antigen (invariant polypeptide of major histocompatibility complex, class II antigen-associated)	up
15985	Cd79b	CD79B antigen	up
12524	Cd86	CD86 antigen	up
12526	Cd8b1	CD8 antigen, beta chain 1	up
18636	Cfp	complement factor properdin	up
12265	Ciita	class II transactivator	up
102545	Cmtm7	CKLF-like MARVEL transmembrane domain containing 7	up
12721	Coro1a	coronin, actin binding protein 1A	up
13041	Ctsw	cathepsin W	up
55985	Cxcl13	chemokine (C-X-C motif) ligand 13	up
17329	Cxcl9	chemokine (C-X-C motif) ligand 9	up
12145	Cxcr5	chemokine (C-X-C motif) receptor 5	up
13057	Cyba	cytochrome b-245, alpha polypeptide	up
67102	D16Ertd472e	DNA segment, Chr 16, ERATO Doi 472, expressed	up
70785	Dennd1c	DENN/MADD domain containing 1C	up
13449	Dok2	docking protein 2	up
27261	Dok3	docking protein 3	up
13537	Dusp2	dual specificity phosphatase 2	up
13713	Elk3	ELK3, member of ETS oncogene family	up
23871	Ets1	E26 avian leukemia oncogene 1, 5' domain	up
14130	Fcgr2b	Fc receptor, IgG, low affinity IIb	up
74015	Fcho1	FCH domain only 1	up
98752	Fcrla	Fc receptor-like A	up

108101	Fermt3	fermitin family homolog 3 (Drosophila)	up
14170	Fgf15	fibroblast growth factor 15	up
22379	Fmnl3	formin-like 3	up
18301	Fxyd5	FXYD domain-containing ion transport regulator 5	up
14377	G6pc	glucose-6-phosphatase, catalytic	down
14468	Gbp1	guanylate binding protein 1	up
14469	Gbp2	guanylate binding protein 2	up
231931	Gimap6	GTPase, IMAP family member 6	up
231932	Gimap7	GTPase, IMAP family member 7	up
243374	Gimap8	GTPase, IMAP family member 8	up
93695	Gpnmb	glycoprotein (transmembrane) nmb	up
229323	Gpr171	G protein-coupled receptor 171	up
110168	Gpr18	G protein-coupled receptor 18	up
321019	Gpr183	G protein-coupled receptor 183	up
238377	Gpr68	G protein-coupled receptor 68	up
14961	H2-Ab1	histocompatibility 2, class II antigen A, beta 1	up
14999	H2-DMb1	histocompatibility 2, class II, locus Mb1	up
15000	H2-DMb2	histocompatibility 2, class II, locus Mb2	up
14968	H2-Ea-ps	histocompatibility 2, class II antigen E alpha, pseudogene	up
14969	H2-Eb1	histocompatibility 2, class II antigen E beta	up
15001	H2-Oa	histocompatibility 2, O region alpha locus	up
15163	Hcls1	hematopoietic cell specific Lyn substrate 1	up
15277	Hk2	hexokinase 2	up
70719	Hmha1	histocompatibility (minor) HA-1	up
15930	Ido1	indoleamine 2,3-dioxygenase 1	up
15953	Ifi47	interferon gamma inducible protein 47	up
22778	Ikzf1	IKAROS family zinc finger 1	up
16154	Il10ra	interleukin 10 receptor, alpha	up
16170	Il16	interleukin 16	up
16407	Itgae	integrin alpha E, epithelial-associated	up
16421	Itgb7	integrin beta 7	up
16428	Itk	IL2-inducible T-cell kinase	up
16498	Kcnab2	potassium voltage-gated channel, shaker-related subfamily, beta member 2	up
239743	Klhl6	kelch-like 6 (Drosophila)	up
259277	Klk8	kallikrein related-peptidase 8	up
16643	Klrd1	killer cell lectin-like receptor, subfamily D, member 1	up
16792	Laptm5	lysosomal-associated protein transmembrane 5	up
16797	Lat	linker for activation of T cells	up
56743	Lat2	linker for activation of T cells family, member 2	up
16818	Lck	lymphocyte protein tyrosine kinase	up
18826	Lcp1	lymphocyte cytosolic protein 1	up
107321	Lpxn	leupaxin	up
16985	Lsp1	lymphocyte specific 1	up
16994	Ltb	lymphotoxin B	up
17084	Ly86	lymphocyte antigen 86	up
17085	Ly9	lymphocyte antigen 9	up
17110	Lyz1	lysozyme 1	up
17105	Lyz2	lysozyme 2	up
17259	Mef2b	myocyte enhancer factor 2B	up
17304	Mfge8	milk fat globule-EGF factor 8 protein	up
17698	Msn	moesin	up
246177	Myo1g	myosin IG	up
16541	Napsa	napsin A aspartic peptidase	up
17972	Ncf4	neutrophil cytosolic factor 4	up
105855	Nckap1l	NCK associated protein 1 like	up
243910	Nfkbid	nuclear factor of kappa light polypeptide gene enhancer in B-cells inhibitor, delta	up

72310	Nkg7	natural killer cell group 7 sequence	up
434341	Nlrc5	NLR family, CARD domain containing 5	up
70113	Odf3b	outer dense fiber of sperm tails 3B	down
74191	P2ry13	purinergic receptor P2Y, G-protein coupled 13	up
239827	Pigz	phosphatidylinositol glycan anchor biosynthesis, class Z	up
18985	Pou2af1	POU domain, class 2, associating factor 1	up
67905	Ppm1m	protein phosphatase 1M	up
18751	Prkcb	protein kinase C, beta	up
16913	Psmb8	proteasome (prosome, macropain) subunit, beta type 8 (large multifunctional peptidase 7)	up
19245	Ptp4a3	protein tyrosine phosphatase 4a3	up
19265	Ptprcap	protein tyrosine phosphatase, receptor type, C polypeptide-associated protein	up
19354	Rac2	RAS-related C3 botulinum substrate 2	up
320484	Rasal3	RAS protein activator like 3	up
19419	Rasgrp1	RAS guanyl releasing protein 1	up
215653	Rassf2	Ras association (RalGDS/AF-6) domain family member 2	up
54354	Rassf5	Ras association (RalGDS/AF-6) domain family member 5	up
76438	Rftn1	raftlin lipid raft linker 1	up
78416	Rnase6	ribonuclease, RNase A family, 6	up
74131	Sash3	SAM and SH3 domain containing 3	up
20230	Satb1	special AT-rich sequence binding protein 1	up
20345	Selplg	selectin, platelet (p-selectin) ligand	up
20715	Serpina3g	serine (or cysteine) peptidase inhibitor, clade A, member 3G	up
546546	Serpina3h	serine (or cysteine) peptidase inhibitor, clade A, member 3H	up
27371	Sh2d2a	SH2 domain protein 2A	up
58194	Sh3kbp1	SH3-domain kinase binding protein 1	up
20491	Sla	src-like adaptor	up
227659	Slc2a6	solute carrier family 2 (facilitated glucose transporter), member 6	up
68682	Slc44a2	solute carrier family 44, member 2	up
64454	Slc5a4b	solute carrier family 5 (neutral amino acid transporters, system A), member 4b	down
50934	Slc7a8	solute carrier family 7 (cationic amino acid transporter, y+ system), member 8	down
71733	Susd2	sushi domain containing 2	down
21354	Tap1	transporter 1, ATP-binding cassette, sub-family B (MDR/TAP)	up
21838	Thy1	thymus cell antigen 1, theta	up
24099	Tnfsf13b	tumor necrosis factor (ligand) superfamily, member 13b	up
241732	Tspyl3	TSPY-like 3	up
24108	Ubd	ubiquitin D	up
22271	Upp1	uridine phosphorylase 1	up
22324	Vav1	vav 1 oncogene	up
22329	Vcam1	vascular cell adhesion molecule 1	up
22376	Was	Wiskott-Aldrich syndrome homolog (human)	up
22637	Zap70	zeta-chain (TCR) associated protein kinase	up

Differentialy expressed genes in the colonic mucosa of conventional CR vs. GF and monoassociated (N or O) mice (contrast: C_GF/N/O)

ENTREZ No.	Symbol	Gene name	Change
216188	Aldh1l2	aldehyde dehydrogenase 1 family, member L2	up
219033	Ang4	angiogenin, ribonuclease A family, member 4	up
11812	Apoc1	apolipoprotein C-I	down
11872	Art2b	ADP-ribosyltransferase 2b	up
17341	Bhlha15	basic helix-loop-helix family, member a15	up
12153	Bmp1	bone morphogenetic protein 1	down
12332	Capg	capping protein (actin filament), gelsolin-like	up
12409	Cbr2	carbonyl reductase 2	up
68891	Cd177	CD177 antigen	up
16149	Cd74	en (invariant polypeptide of major histocompatibility complex, class II antigen	up
69065	Chac1	ChaC, cation transport regulator-like 1 (E. coli)	up
12265	Ciita	class II transactivator	up
229933	Clca5	chloride channel calcium activated 5	up
76279	Cyp2d26	cytochrome P450, family 2, subfamily d, polypeptide 26	down
13829	Epb4.9	erythrocyte protein band 4.9	down
66120	Fkbp11	FK506 binding protein 11	up
23882	Gadd45g	growth arrest and DNA-damage-inducible 45 gamma	up
216456	Gls2	glutaminase 2 (liver, mitochondrial)	up
14961	H2-Ab1	histocompatibility 2, class II antigen A, beta 1	up
14999	H2-DMb1	histocompatibility 2, class II, locus Mb1	up
14969	H2-Eb1	histocompatibility 2, class II antigen E beta	up
15953	Ifi47	interferon gamma inducible protein 47	up
16429	Itln1	intelectin 1 (galactofuranose binding)	up
16939	Lor	loricrin	down
17069	Ly6e	lymphocyte antigen 6 complex, locus E	up
68468	Ly6g6c	lymphocyte antigen 6 complex, locus G6C	up
434341	Nlrc5	NLR family, CARD domain containing 5	up
18780	Pla2g2a	phospholipase A2, group IIA (platelets, synovial fluid)	up
232889	Pla2g4c	phospholipase A2, group IVC (cytosolic, calcium-independent)	up
18947	Pnliprp2	pancreatic lipase-related protein 2	up
70536	Qpct	glutaminyl-peptide cyclotransferase (glutaminyl cyclase)	up
19367	Rad9	RAD9 homolog (S. pombe)	up
66184	Rps4y2	ribosomal protein S4, Y-linked 2	down
74338	Slc6a19	solute carrier family 6 (neurotransmitter transporter), member 19	down
30962	Slc7a9	solute carrier family 7 (cationic amino acid transporter, y+ system), member 9	down
20604	Sst	somatostatin	down
54367	Zfp326	zinc finger protein 326	C_G: down C_N/O: up

Supplementary Table S4

Differentialy expressed genes in the mucosa of the middle part of the small intestine in monoassociated mice (contrast: N_O)

ENTREZ No.	Symbol	Gene name	Log FC	q-value
78925	Srd5a1	steroid 5 alpha-reductase 1	-1.13	0.003600
217721	Mfsd7c	major facilitator superfamily domain containing 7C	-1.37	0.000067
20531	Slc34a2	solute carrier family 34 (sodium phosphate), member 2	-2.29	0.003600

Differentialy expressed genes in the colonic mucosa in monoassociated mice (contrast: N_O)

ENTREZ No.	Symbol	Gene name	Log FC	q-value
12350	Car3	carbonic anhydrase 3	3.97	0.036000
13106	Cyp2e1	cytochrome P450, family 2, subfamily e, polypeptide 1	3.59	0.027000
57435	Plin4	perilipin 4	3.48	0.013000
11450	Adipoq	adiponectin, C1Q and collagen domain containing	3.45	0.039000
13346	Des	desmin	3.02	0.028000
18947	Pnliprp2	pancreatic lipase-related protein 2	2.97	0.006100
14311	Cidec	cell death-inducing DFFA-like effector c	2.78	0.000410
20249	Scd1	stearoyl-Coenzyme A desaturase 1	2.75	0.028000
11754	Aoc3	amine oxidase, copper containing 3	2.64	0.045000
22004	Tpm2	tropomyosin 2, beta	2.53	0.042000
109791	Clps	colipase, pancreatic	2.43	0.019000
16667	Krt17	keratin 17	2.31	0.001200
22353	Vip	vasoactive intestinal polypeptide	2.26	0.021000
29856	Smtn	smoothelin	2.19	0.006400
80888	Hspb8	heat shock protein 8	2.14	0.005300
12308	Calb2	calbindin 2	2.01	0.015000
12509	Cd59a	CD59a antigen	1.97	0.014000
17901	Myl1	myosin, light polypeptide 1	1.97	0.021000
233335	Synm	synemin, intermediate filament protein	1.93	0.009800
225341	Lims2	LIM and senescent cell antigen like domains 2	1.92	0.028000
21826	Thbs2	thrombospondin 2	1.84	0.011000
107589	Mylk	myosin, light polypeptide kinase	1.83	0.005100
17984	Ndn	necdin	1.81	0.045000
57262	Retnla	resistin like alpha	1.81	0.001700
246747	Adig	adipogenin	1.79	0.005300
15439	Hp	haptoglobin	1.77	0.028000
16846	Lep	leptin	1.76	0.021000
19242	Ptn	pleiotrophin	1.76	0.005200
18405	Orm1	orosomucoid 1	1.73	0.021000
13007	Csrp1	cysteine and glycine-rich protein 1	1.71	0.027000
14560	Gdf10	growth differentiation factor 10	1.67	0.027000
74116	Pi16	peptidase inhibitor 16	1.60	0.011000
29859	Sult4a1	sulfotransferase family 4A, member 1	1.58	0.011000
59095	Fxyd6	FXYD domain-containing ion transport regulator 6	1.56	0.045000
67896	Ccdc80	coiled-coil domain containing 80	1.55	0.019000
18113	Nnmt	nicotinamide N-methyltransferase	1.53	0.019000
13640	Efna5	ephrin A5	1.52	0.030000
93689	Lmod1	leiomodin 1 (smooth muscle)	1.52	0.007900
654812	Angptl7	angiopoietin-like 7	1.50	0.004100
77037	Mrap	melanocortin 2 receptor accessory protein	1.50	0.030000
70784	Rasl12	RAS-like, family 12	1.47	0.009800
13807	Eno2	enolase 2, gamma neuronal	1.43	0.018000
21835	Thrsp	thyroid hormone responsive SPOT14 homolog (Rattus)	1.42	0.030000
76905	Lrg1	leucine-rich alpha-2-glycoprotein 1	1.39	0.012000
20618	Sncg	synuclein, gamma	1.37	0.027000
20257	Stmn2	stathmin-like 2	1.36	0.019000
12889	Cplx1	complexin 1	1.34	0.006100
67399	Pdlim7	PDZ and LIM domain 7	1.33	0.021000
243912	Hspb6	heat shock protein, alpha-crystallin-related, B6	1.32	0.040000
13628	Eef1a2	eukaryotic translation elongation factor 1 alpha 2	1.31	0.011000
99326	Garnl3	GTPase activating RANGAP domain-like 3	1.29	0.003200
14261	Fmo1	flavin containing monooxygenase 1	1.24	0.001700
225642	Grp	gastrin releasing peptide	1.22	0.002400
244058	Rgma	RGM domain family, member A	1.20	0.024000
23948	Mmp17	matrix metallopeptidase 17	1.18	0.011000
53376	Usp2	ubiquitin specific peptidase 2	1.18	0.005200
68939	Rasl11b	RAS-like, family 11, member B	1.17	0.012000
52906	Ahi1	Abelson helper integration site 1	1.15	0.002200
20411	Sorbs1	sorbin and SH3 domain containing 1	1.13	0.006500
22223	Uchl1	ubiquitin carboxy-terminal hydrolase L1	1.13	0.019000

73712	Dmkn	dermokine	1.11	0.000840
20254	Scg2	secretogranin II	1.11	0.021000
268534	Sntg2	syntrophin, gamma 2	1.11	0.047000
14165	Fgf10	fibroblast growth factor 10	1.10	0.021000
83767	Wasf1	WASP family 1	1.09	0.019000
244757	Glb1l2	galactosidase, beta 1-like 2	1.07	0.028000
27276	Plekhb1	pleckstrin homology domain containing, family B (evectins) member 1	1.05	0.030000
19762	Rit2	Ras-like without CAAX 2	1.01	0.005100
12096	Bglap	bone gamma carboxyglutamate protein	1.00	0.003000

Supplementary Table S5 List of primers used for qRT-PCR

Gene symbol	Primer sequence
Actb	Forward: 5'-GATCTGGCACCACACCTTCT-3'
	Reverse: 5'-GGGGTGTTGAAGGTCTCAAA-3'
Adamdec1	Forward: 5'-GTCCTGGATGTGGGAGAAGA-3'
	Reverse: 5'-TGTGATGTGGTTGGATGCTT-3'
Aldh1a1	Forward: 5'-ACTGGAGTGTGGTGGAGGAC-3'
	Reverse: 5'-CACAGTGATGGCCTTATCCA-3'
Apoe	Forward: 5'-CAGAGCTCCCAAGTCACACA-3'
	Reverse: 5'-AGTCGGTTGCGTAGATCCTC-3'
Asb2	Forward: 5'-AGTCTGTCTCCCGCAATGAC-3'
	Reverse: 5'-ATTCTTGCTGGCCTCGTAGA-3'
Bgn	Forward: 5'-GACAACCGTATCCGCAAAGT-3'
	Reverse: 5'-GTGGTCCAGGTGAAGTTCGT-3'
Cck	Forward: 5'-TACATCCAGCAGGTCCGCAAAG-3'
	Reverse: 5'-CGATGGGTATTCGTAGTCCTCGG-3'
Cd74	Forward: 5'-CACCGAGGCTCCACCTAAAG-3'
	Reverse: 5'-GGGAACACACACCAGCAGTA-3'
Cfd	Forward: 5'-ATGACGACTCTGTGCAGGTG-3'
	Reverse: 5'-ATTGCAAGGGTAGGGGTCTC-3'
Cyp2d26	Forward: 5'-GTGATCGCCTCCCTCATTTA-3'
	Reverse: 5'-GGCTTTATCAGGCAAACCAG-3'
Edn1	Forward: 5'-ACTTCTGCCACCTGGACATC-3'
	Reverse: 5'-GGTGAGCGCACTGACATCTA-3'
Fkbp5	Forward: 5'-GGTTATCAAAGCCTGGGACA-3'
	Reverse: 5'-CGCCTTTCCGTTTGATTCTA-3'
Foxq1	Forward: 5'-CAAGCCCCCATACTCCTACA-3'
	Reverse: 5'-TGACGAAACAGTCGTTGAGC-3'
Fosb	Forward: 5'-TGTCTTCGGTGGACTCCTTC-3'
	Reverse: 5'-GATCCTGGCTGGTTGTGATT-3'
Gapdh	Forward: 5'-AACTTTGGCATTGTGGAAGG-3'
	Reverse: 5'-ATCCACAGTCTTCTGGGTGG-3'
Gcnt1	Forward: 5'-CCGATTGGAGAGTGTGGTTT-3'
	Reverse: 5'-TCCGTTTCCAGGTTGTTTTC-3'
H2-Ab1	Forward: 5'-GTCCTGGTCATGCTGGAGAT-3'
	Reverse: 5'-CTGACTCCTGTGACGGATGA-3'
H2-Ea-ps	Forward: 5'-CTGCCCTCCACAGATGATTT-3'

	Reverse: 5'-GATAATCCCCACAACGATGC-3'
Irs2	Forward: 5'-ACAACCTATCGTGGCACCTC-3'
	Reverse: 5'-GACGGTGGTGGTAGAGGAAA-3'
Ly6a	Forward: 5'-TCTTGTGGCCCTACTGTGTG-3'
	Reverse: 5'-GGCAGATGGGTAAGCAAAGA-3'
Mmp10	Forward: 5'-CAGGTGTGGTGTTCCTGATG-3'
	Reverse: 5'-GGAGAAAGTGAGTGGGGTCA-3'
Nkx2-3	Forward: 5'-GATTCGGGTCTCTGTCCTCA-3'
	Reverse: 5'-AGACCTGAGCTTGCGAGAAG-3'
Oprk1	Forward: 5'-AAGCTTTGGACTTCCGAACA-3'
	Reverse: 5'-GGAAACTGCAAGGAGCATTC-3'
Plvap	Forward: 5'-CATCCTGAGCGAGAAGCAGT-3'
	Reverse: 5'-AGCAGGCTCTCCTTGTCCTT-3'
Reg4	Forward: 5'-GAAACCTGCCTGTGTGGATT-3'
	Reverse: 5'-GCCTGGCTTCACTCTTTGTC-3'
Slc17a4	Forward: 5'-TCCCACTAACTCCCAGGATG-3'
	Reverse: 5'-TTAACAAGCCCAGACCAACC-3'
Slpi	Forward: 5'-CACAATGCCGTACTGACTGG-3'
	Reverse: 5'-GACATTGGGAGGGTTAAGCA-3'
Tgfbr2	Forward: 5'-GGCTTCACTCTGGAAGATGC-3'
	Reverse: 5'-TGACACCCGTCACTTGGATA-3'
Tle4	Forward: 5'-GAGAATGGCCTGGACAAGAC-3'
	Reverse: 5'-GGGTAGGTGCATCAGTTCGT-3'
Ubb	Forward: 5'-ATGTGAAGGCCAAGATCCAG-3'
	Reverse: 5'-TAATAGCCACCCCTCAGACG-3'
Zfp326	Forward: 5'-AACGCCTGCTTATCCTGAAA-3'
	Reverse: 5'-ATCGTCACATTGGCAGGTTT-3'

Conclusions

This dissertation thesis was dedicated to description of the molecular mechanisms employed in gastrointestinal tissues renewal and maintenance, particularly in the intestine, stomach and liver. Points of conclusion can be summarized as follows:

1. We identified Troy as a novel marker of SCs in the intestinal epithelium. We proved that *Troy* is a Wnt target gene and its product inhibits Wnt signaling and its expression is increased in mouse intestinal tumors.

   We described Mist1 as a marker of quiescent SCs in the isthmus of glands in the gastric corpus. Moreover, we uncovered the Mist1 role in gastric epithelium maintenance via the Cxcl12/Cxcr4 signaling axis and involvement of Mist1 in development of IGC and DGC.
2. We found that the *Nkd1* gene is specifically expressed in the intestinal crypt compartment and PC hepatocytes. We established *Nkd1* as a gene with impaired expression in both CRC and HCC tumors.
3. We showed that *Tlr2* is a novel Hic1 target gene. Our experiments gave evidence that ablation of *Hic1* induces *Tlr2* expression and proinflammatory pathway stimulation, which can contribute to exacerbation of colorectal tumor growth.
4. In our study, monensin was identified as a promising small compound that specifically inhibits the Wnt signaling pathway. Monensin blocks Wnt signaling in some human CRC cells. Furthermore, mouse intestinal tumors exhibit reduction in tumor size after monensin treatment.
5. We performed expression profiling of GF mice intestinal epithelium and uncovered differences in profiles between GF, CR, and monoassociated mice. The microarray data confirmed impaired development of the immune system of GF mice. Moreover, monoassociation did not restore immune system formation.

List of figures

Figure 1: Scheme of β-catenin with phosphorylated and binding sites. 24
Figure 2: The canonical Wnt signaling pathway. 28
Figure 3: Architecture of the intestinal epithelium and types of intestinal cells. 36
Figure 4: Stomach anatomy and epithelial architecture. 41
Figure 5: The stomach epithelial cell types, their origin and residence. 41
Figure 6: Architecture of the small intestinal epithelium and signaling pathways involved in its self-renewal. 50
Figure 7: Genetic pathways involved in CRC pathogenesis. 53
Figure 8: Liver lobule unit zonation. 63

References

Al-Tassan N, Chmiel NH, Maynard J, Fleming N, Livingston AL, Williams GT, Hodges AK, Davies DR, David SS, Sampson JR et al. 2002. Inherited variants of MYH associated with somatic G:C-->T:A mutations in colorectal tumors. *Nat Genet* **30**: 227-232.

Alani E. 1996. The Saccharomyces cerevisiae Msh2 and Msh6 proteins form a complex that specifically binds to duplex oligonucleotides containing mismatched DNA base pairs. *Mol Cell Biol* **16**: 5604-5615.

Alessi DR, James SR, Downes CP, Holmes AB, Gaffney PR, Reese CB, Cohen P. 1997. Characterization of a 3-phosphoinositide-dependent protein kinase which phosphorylates and activates protein kinase Balpha. *Curr Biol* **7**: 261-269.

Alison MR. 2005. Liver stem cells: implications for hepatocarcinogenesis. *Stem cell reviews* **1**: 253-260.

Almond A. 2007. Hyaluronan. *Cell Mol Life Sci* **64**: 1591-1596.

Alvin A, Miller KI, Neilan BA. 2014. Exploring the potential of endophytes from medicinal plants as sources of antimycobacterial compounds. *Microbiol Res* **169**: 483-495.

Amaddeo G, Guichard C, Imbeaud S, Zucman-Rossi J. 2012. Next-generation sequencing identified new oncogenes and tumor suppressor genes in human hepatic tumors. *Oncoimmunology* **1**: 1612-1613.

Andersson ER, Sandberg R, Lendahl U. 2011. Notch signaling: simplicity in design, versatility in function. *Development* **138**: 3593-3612.

Angers S, Thorpe CJ, Biechele TL, Goldenberg SJ, Zheng N, MacCoss MJ, Moon RT. 2006. The KLHL12-Cullin-3 ubiquitin ligase negatively regulates the Wnt-beta-catenin pathway by targeting Dishevelled for degradation. *Nat Cell Biol* **8**: 348-357.

Angonin D, Van Raay TJ. 2013. Nkd1 functions as a passive antagonist of Wnt signaling. *PLoS One* **8**: e74666.

Arce L, Pate KT, Waterman ML. 2009. Groucho binds two conserved regions of LEF-1 for HDAC-dependent repression. *BMC Cancer* **9**: 159.

Arnold K, Sarkar A, Yram MA, Polo JM, Bronson R, Sengupta S, Seandel M, Geijsen N, Hochedlinger K. 2011. Sox2(+) adult stem and progenitor cells are important for tissue regeneration and survival of mice. *Cell Stem Cell* **9**: 317-329.

Aruffo A, Stamenkovic I, Melnick M, Underhill CB, Seed B. 1990. CD44 is the principal cell surface receptor for hyaluronate. *Cell* **61**: 1303-1313.

Ascierto PA, Kirkwood JM, Grob JJ, Simeone E, Grimaldi AM, Maio M, Palmieri G, Testori A, Marincola FM, Mozzillo N. 2012. The role of BRAF V600 mutation in melanoma. *J Transl Med* **10**: 85.

Asfaha S, Hayakawa Y, Muley A, Stokes S, Graham TA, Ericksen RE, Westphalen CB, von Burstin J, Mastracci TL, Worthley DL et al. 2015. Krt19(+)/Lgr5(-) Cells Are Radioresistant Cancer-Initiating Stem Cells in the Colon and Intestine. *Cell Stem Cell* **16**: 627-638.

Avruch J, Khokhlatchev A, Kyriakis JM, Luo Z, Tzivion G, Vavvas D, Zhang XF. 2001. Ras activation of the Raf kinase: tyrosine kinase recruitment of the MAP kinase cascade. *Recent progress in hormone research* **56**: 127-155.

Azzolin L, Panciera T, Soligo S, Enzo E, Bicciato S, Dupont S, Bresolin S, Frasson C, Basso G, Guzzardo V et al. 2014. YAP/TAZ incorporation in the beta-catenin destruction complex orchestrates the Wnt response. *Cell* **158**: 157-170.

Baccaro LF, Conde DM, Costa-Paiva L, de Souza Santos Machado V, Pinto-Neto AM. 2015. Cancer in Women over 50 Years of Age: A Focus on Smoking. *Cancers (Basel)* **7**: 450-459.

Backhed F, Crawford PA. 2010. Coordinated regulation of the metabolome and lipidome at the host-microbial interface. *Biochim Biophys Acta* **1801**: 240-245.

Bafico A, Liu G, Yaniv A, Gazit A, Aaronson SA. 2001. Novel mechanism of Wnt signalling inhibition mediated by Dickkopf-1 interaction with LRP6/Arrow. *Nat Cell Biol* **3**: 683-686.

Baker AM, Graham TA, Elia G, Wright NA, Rodriguez-Justo M. 2015. Characterization of LGR5 stem cells in colorectal adenomas and carcinomas. *Scientific reports* **5**: 8654.

Barber M, Murrell A, Ito Y, Maia AT, Hyland S, Oliveira C, Save V, Carneiro F, Paterson AL, Grehan N et al. 2008. Mechanisms and sequelae of E-cadherin silencing in hereditary diffuse gastric cancer. *J Pathol* **216**: 295-306.

Barker N, Bartfeld S, Clevers H. 2010a. Tissue-resident adult stem cell populations of rapidly self-renewing organs. *Cell Stem Cell* **7**: 656-670.

Barker N, Huch M, Kujala P, van de Wetering M, Snippert HJ, van Es JH, Sato T, Stange DE, Begthel H, van den Born M et al. 2010b. Lgr5(+ve) stem cells drive self-renewal in the stomach and build long-lived gastric units in vitro. *Cell Stem Cell* **6**: 25-36.

Barker N, Ridgway RA, van Es JH, van de Wetering M, Begthel H, van den Born M, Danenberg E, Clarke AR, Sansom OJ, Clevers H. 2009. Crypt stem cells as the cells-of-origin of intestinal cancer. *Nature* **457**: 608-611.

Barker N, van Es JH, Kuipers J, Kujala P, van den Born M, Cozijnsen M, Haegebarth A, Korving J, Begthel H, Peters PJ et al. 2007. Identification of stem cells in small intestine and colon by marker gene Lgr5. *Nature* **449**: 1003-1007.

Bates S, Vousden KH. 1996. p53 in signaling checkpoint arrest or apoptosis. *Current opinion in genetics & development* **6**: 12-18.

Batlle E, Henderson JT, Beghtel H, van den Born MM, Sancho E, Huls G, Meeldijk J, Robertson J, van de Wetering M, Pawson T et al. 2002. Beta-catenin and TCF mediate cell positioning in the intestinal epithelium by controlling the expression of EphB/ephrinB. *Cell* **111**: 251-263.

Battaglia S, Maguire O, Campbell MJ. 2010. Transcription factor co-repressors in cancer biology: roles and targeting. *Int J Cancer* **126**: 2511-2519.

Bauer A, Chauvet S, Huber O, Usseglio F, Rothbacher U, Aragnol D, Kemler R, Pradel J. 2000. Pontin52 and reptin52 function as antagonistic regulators of beta- catenin signalling activity. *Embo J* **19**: 6121-6130.

Baughman G, Wiederrecht GJ, Chang F, Martin MM, Bourgeois S. 1997. Tissue distribution and abundance of human FKBP51, and FK506-binding protein that can mediate calcineurin inhibition. *Biochem Biophys Res Commun* **232**: 437-443.

Beauchamp A, Lively MO, Mintz A, Gibo D, Wykosky J, Debinski W. 2012. EphrinA1 is released in three forms from cancer cells by matrix metalloproteases. *Mol Cell Biol* **32**: 3253-3264.

Behari J. 2010. The Wnt/beta-catenin signaling pathway in liver biology and disease. *Expert Rev Gastroenterol Hepatol* **4**: 745-756.

Behari J, Yeh TH, Krauland L, Otruba W, Cieply B, Hauth B, Apte U, Wu T, Evans R, Monga SP. 2010. Liver-specific beta-catenin knockout mice exhibit defective bile acid and cholesterol homeostasis and increased susceptibility to diet-induced steatohepatitis. *Am J Pathol* **176**: 744-753.

Behnsen J, Deriu E, Sassone-Corsi M, Raffatellu M. 2013. Probiotics: properties, examples, and specific applications. *Cold Spring Harbor perspectives in medicine* **3**: a010074.

Behrens J, von Kries JP, Kuhl M, Bruhn L, Wedlich D, Grosschedl R, Birchmeier W. 1996. Functional interaction of beta-catenin with the transcription factor LEF-1. *Nature* **382**: 638-642.

Bellizzi AM, Frankel WL. 2009. Colorectal cancer due to deficiency in DNA mismatch repair function: a review. *Advances in anatomic pathology* **16**: 405-417.

Benhamouche S, Decaens T, Godard C, Chambrey R, Rickman DS, Moinard C, Vasseur-Cognet M, Kuo CJ, Kahn A, Perret C et al. 2006. Apc tumor suppressor gene is the "zonation-keeper" of mouse liver. *Dev Cell* **10**: 759-770.

Bernatik O, Sedova K, Schille C, Ganji RS, Cervenka I, Trantirek L, Schambony A, Zdrahal Z, Bryja V. 2014. Functional analysis of dishevelled-3 phosphorylation identifies distinct mechanisms driven by casein kinase 1 and frizzled5. *J Biol Chem* **289**: 23520-23533.

Bettington M, Walker N, Clouston A, Brown I, Leggett B, Whitehall V. 2013. The serrated pathway to colorectal carcinoma: current concepts and challenges. *Histopathology* **62**: 367-386.

Bioulac-Sage P, Rebouissou S, Thomas C, Blanc JF, Saric J, Sa Cunha A, Rullier A, Cubel G, Couchy G, Imbeaud S et al. 2007. Hepatocellular adenoma subtype classification using molecular markers and immunohistochemistry. *Hepatology* **46**: 740-748.

Blanpain C, Horsley V, Fuchs E. 2007. Epithelial stem cells: turning over new leaves. *Cell* **128**: 445-458.

Boquet P, Ricci V. 2012. Intoxication strategy of Helicobacter pylori VacA toxin. *Trends in microbiology* **20**: 165-174.

Bosch FX, Ribes J, Cleries R, Diaz M. 2005. Epidemiology of hepatocellular carcinoma. *Clinics in liver disease* **9**: 191-211, v.

Brandt WD, Matsui W, Rosenberg JE, He X, Ling S, Schaeffer EM, Berman DM. 2009. Urothelial carcinoma: stem cells on the edge. *Cancer metastasis reviews* **28**: 291-304.

Bredemeyer AJ, Geahlen JH, Weis VG, Huh WJ, Zinselmeyer BH, Srivatsan S, Miller MJ, Shaw AS, Mills JC. 2009. The gastric epithelial progenitor cell niche and differentiation of the zymogenic (chief) cell lineage. *Dev Biol* **325**: 211-224.

Briggs KJ, Eberhart CG, Watkins DN. 2008. Just say no to ATOH: how HIC1 methylation might predispose medulloblastoma to lineage addiction. *Cancer Res* **68**: 8654-8656.

Buczacki SJ, Zecchini HI, Nicholson AM, Russell R, Vermeulen L, Kemp R, Winton DJ. 2013. Intestinal label-retaining cells are secretory precursors expressing Lgr5. *Nature* **495**: 65-69.

Buttitta L, Tanaka TS, Chen AE, Ko MS, Fan CM. 2003. Microarray analysis of somitogenesis reveals novel targets of different WNT signaling pathways in the somitic mesoderm. *Dev Biol* **258**: 91-104.

Cadigan KM, Nusse R. 1997. Wnt signaling: a common theme in animal development. *Genes Dev* **11**: 3286-3305.

Cadoret A, Ovejero C, Terris B, Souil E, Levy L, Lamers WH, Kitajewski J, Kahn A, Perret C. 2002. New targets of beta-catenin signaling in the liver are involved in the glutamine metabolism. *Oncogene* **21**: 8293-8301.

Cai J, Niu X, Chen Y, Hu Q, Shi G, Wu H, Wang J, Yi J. 2008. Emodin-induced generation of reactive oxygen species inhibits RhoA activation to sensitize gastric carcinoma cells to anoikis. *Neoplasia* **10**: 41-51.

Caldwell GM, Jones CE, Soon Y, Warrack R, Morton DG, Matthews GM. 2008. Reorganisation of Wnt-response pathways in colorectal tumorigenesis. *Br J Cancer* **98**: 1437-1442.

Callow MG, Tran H, Phu L, Lau T, Lee J, Sandoval WN, Liu PS, Bheddah S, Tao J, Lill JR et al. 2011. Ubiquitin ligase RNF146 regulates tankyrase and Axin to promote Wnt signaling. *PLoS One* **6**: e22595.

Cancer Genome Atlas N. 2012. Comprehensive molecular characterization of human colon and rectal cancer. *Nature* **487**: 330-337.

Canfield V, West AB, Goldenring JR, Levenson R. 1996. Genetic ablation of parietal cells in transgenic mice: a new model for analyzing cell lineage relationships in the gastric mucosa. *Proc Natl Acad Sci U S A* **93**: 2431-2435.

Capoccia BJ, Jin RU, Kong YY, Peek RM, Jr., Fassan M, Rugge M, Mills JC. 2013. The ubiquitin ligase Mindbomb 1 coordinates gastrointestinal secretory cell maturation. *J Clin Invest* **123**: 1475-1491.

Capoccia BJ, Lennerz JK, Bredemeyer AJ, Klco JM, Frater JL, Mills JC. 2011. Transcription factor MIST1 in terminal differentiation of mouse and human plasma cells. *Physiol Genomics* **43**: 174-186.

Cargnello M, Roux PP. 2011. Activation and function of the MAPKs and their substrates, the MAPK-activated protein kinases. *Microbiology and molecular biology reviews : MMBR* **75**: 50-83.

Carmon KS, Gong X, Lin Q, Thomas A, Liu Q. 2011. R-spondins function as ligands of the orphan receptors LGR4 and LGR5 to regulate Wnt/beta-catenin signaling. *Proc Natl Acad Sci U S A* **108**: 11452-11457.

Carracedo A, Pandolfi PP. 2008. The PTEN-PI3K pathway: of feedbacks and cross-talks. *Oncogene* **27**: 5527-5541.

Carter MG, Johns MA, Zeng X, Zhou L, Zink MC, Mankowski JL, Donovan DM, Baylin SB. 2000. Mice deficient in the candidate tumor suppressor gene Hic1 exhibit developmental defects of structures affected in the Miller-Dieker syndrome. *Hum Mol Genet* **9**: 413-419.

Caspi M, Zilberberg A, Eldar-Finkelman H, Rosin-Arbesfeld R. 2008. Nuclear GSK-3beta inhibits the canonical Wnt signalling pathway in a beta-catenin phosphorylation-independent manner. *Oncogene* **27**: 3546-3555.

Clevers HC, Bevins CL. 2013. Paneth cells: maestros of the small intestinal crypts. *Annu Rev Physiol* **75**: 289-311.

Colletti M, Cicchini C, Conigliaro A, Santangelo L, Alonzi T, Pasquini E, Tripodi M, Amicone L. 2009. Convergence of Wnt signaling on the HNF4alpha-driven transcription in controlling liver zonation. *Gastroenterology* **137**: 660-672.

Cong F, Schweizer L, Varmus H. 2004. Wnt signals across the plasma membrane to activate the beta-catenin pathway by forming oligomers containing its receptors, Frizzled and LRP. *Development* **131**: 5103-5115.

Cong F, Varmus H. 2004. Nuclear-cytoplasmic shuttling of Axin regulates subcellular localization of beta-catenin. *Proc Natl Acad Sci U S A* **101**: 2882-2887.

Corbit KC, Aanstad P, Singla V, Norman AR, Stainier DY, Reiter JF. 2005. Vertebrate Smoothened functions at the primary cilium. *Nature* **437**: 1018-1021.

Correa P. 1988. A human model of gastric carcinogenesis. *Cancer Res* **48**: 3554-3560.

Corthesy B. 2013. Multi-faceted functions of secretory IgA at mucosal surfaces. *Frontiers in immunology* **4**: 185.

Cover TL, Blanke SR. 2005. Helicobacter pylori VacA, a paradigm for toxin multifunctionality. *Nature reviews Microbiology* **3**: 320-332.

Crosnier C, Stamataki D, Lewis J. 2006. Organizing cell renewal in the intestine: stem cells, signals and combinatorial control. *Nat Rev Genet* **7**: 349-359.

Culi J, Mann RS. 2003. Boca, an endoplasmic reticulum protein required for wingless signaling and trafficking of LDL receptor family members in Drosophila. *Cell* **112**: 343-354.

Dahlgren UI, Wold AE, Hanson LA, Midtvedt T. 1990. The secretory antibody response in milk and bile against fimbriae and LPS in rats monocolonized or immunized in the Peyer's patches with Escherichia coli. *Immunology* **71**: 295-300.

Dai W, Teodoridis JM, Zeller C, Graham J, Hersey J, Flanagan JM, Stronach E, Millan DW, Siddiqui N, Paul J et al. 2011. Systematic CpG islands methylation profiling of genes in the wnt pathway in epithelial ovarian cancer identifies biomarkers of progression-free survival. *Clin Cancer Res* **17**: 4052-4062.

Dalerba P, Dylla SJ, Park IK, Liu R, Wang X, Cho RW, Hoey T, Gurney A, Huang EH, Simeone DM et al. 2007. Phenotypic characterization of human colorectal cancer stem cells. *Proc Natl Acad Sci U S A* **104**: 10158-10163.

Daniels DL, Weis WI. 2002. ICAT inhibits beta-catenin binding to Tcf/Lef-family transcription factors and the general coactivator p300 using independent structural modules. *Mol Cell* **10**: 573-584.

Dayekh K, Johnson-Obaseki S, Corsten M, Villeneuve PJ, Sekhon HS, Weberpals JI, Dimitroulakos J. 2014. Monensin inhibits epidermal growth factor receptor trafficking and activation: synergistic cytotoxicity in combination with EGFR inhibitors. *Molecular cancer therapeutics* **13**: 2559-2571.

de La Coste A, Romagnolo B, Billuart P, Renard CA, Buendia MA, Soubrane O, Fabre M, Chelly J, Beldjord C, Kahn A et al. 1998. Somatic mutations of the beta-catenin gene are frequent in mouse and human hepatocellular carcinomas. *Proc Natl Acad Sci U S A* **95**: 8847-8851.

de la Roche M, Bienz M. 2007. Wingless-independent association of Pygopus with dTCF target genes. *Curr Biol* **17**: 556-561.

de Lau W, Barker N, Low TY, Koo BK, Li VS, Teunissen H, Kujala P, Haegebarth A, Peters PJ, van de Wetering M et al. 2011. Lgr5 homologues associate with Wnt receptors and mediate R-spondin signalling. *Nature* **476**: 293-297.

de Lau W, Peng WC, Gros P, Clevers H. 2014. The R-spondin/Lgr5/Rnf43 module: regulator of Wnt signal strength. *Genes Dev* **28**: 305-316.
Dehennaut V, Loison I, Boulay G, Van Rechem C, Leprince D. 2013a. Identification of p21 (CIP1/WAF1) as a direct target gene of HIC1 (Hypermethylated In Cancer 1). *Biochem Biophys Res Commun* **430**: 49-53.
Dehennaut V, Loison I, Dubuissez M, Nassour J, Abbadie C, Leprince D. 2013b. DNA double-strand breaks lead to activation of hypermethylated in cancer 1 (HIC1) by SUMOylation to regulate DNA repair. *J Biol Chem* **288**: 10254-10264.
Del Vecchio Blanco G, Paoluzi OA, Sileri P, Rossi P, Sica G, Pallone F. 2015. Familial colorectal cancer screening: When and what to do? *World J Gastroenterol* **21**: 7944-7953.
Derynck R, Zhang YE. 2003. Smad-dependent and Smad-independent pathways in TGF-beta family signalling. *Nature* **425**: 577-584.
Deschner EE, Lipkin M. 1975. Proliferative patterns in colonic mucosa in familial polyposis. *Cancer* **35**: 413-418.
Deschner EE, Winawer SJ, Katz S, Katzka I, Kahn E. 1983. Proliferative defects in ulcerative colitis patients. *Cancer investigation* **1**: 41-47.
Deuring R, Fanti L, Armstrong JA, Sarte M, Papoulas O, Prestel M, Daubresse G, Verardo M, Moseley SL, Berloco M et al. 2000. The ISWI chromatin-remodeling protein is required for gene expression and the maintenance of higher order chromatin structure in vivo. *Mol Cell* **5**: 355-365.
Ding VW, Chen RH, McCormick F. 2000. Differential regulation of glycogen synthase kinase 3beta by insulin and Wnt signaling. *J Biol Chem* **275**: 32475-32481.
Direnzo D, Hess DA, Damsz B, Hallett JE, Marshall B, Goswami C, Liu Y, Deering T, Macdonald RJ, Konieczny SF. 2012. Induced Mist1 expression promotes remodeling of mouse pancreatic acinar cells. *Gastroenterology* **143**: 469-480.
Doglioni C, Dei Tos AP, Laurino L, Iuzzolino P, Chiarelli C, Celio MR, Viale G. 1996. Calretinin: a novel immunocytochemical marker for mesothelioma. *The American journal of surgical pathology* **20**: 1037-1046.
Dong Y, Cao B, Zhang M, Han W, Herman JG, Fuks F, Zhao Y, Guo M. 2015. Epigenetic silencing of NKD2, a major component of Wnt signaling, promotes breast cancer growth. *Oncotarget*.
Doubravska L, Krausova M, Gradl D, Vojtechova M, Tumova L, Lukas J, Valenta T, Pospichalova V, Fafilek B, Plachy J et al. 2011. Fatty acid modification of Wnt1 and Wnt3a at serine is prerequisite for lipidation at cysteine and is essential for Wnt signalling. *Cell Signal* **23**: 837-848.
Drummond JT, Li GM, Longley MJ, Modrich P. 1995. Isolation of an hMSH2-p160 heterodimer that restores DNA mismatch repair to tumor cells. *Science* **268**: 1909-1912.
Du K, Montminy M. 1998. CREB is a regulatory target for the protein kinase Akt/PKB. *J Biol Chem* **273**: 32377-32379.
Dufresne M, Seva C, Fourmy D. 2006. Cholecystokinin and gastrin receptors. *Physiol Rev* **86**: 805-847.
Eby MT, Jasmin A, Kumar A, Sharma K, Chaudhary PM. 2000. TAJ, a novel member of the tumor necrosis factor receptor family, activates the c-Jun N-terminal kinase pathway and mediates caspase-independent cell death. *J Biol Chem* **275**: 15336-15342.
Effendi K, Yamazaki K, Fukuma M, Sakamoto M. 2014. Overexpression of Leucine-Rich Repeat-Containing G Protein-Coupled Receptor 5 (LGR5) Represents a Typical Wnt/beta-Catenin Pathway-Activated Hepatocellular Carcinoma. *Liver cancer* **3**: 451-457.
Ekataksin W, Kaneda K. 1999. Liver microvascular architecture: an insight into the pathophysiology of portal hypertension. *Seminars in liver disease* **19**: 359-382.
el-Serag HB. 2001. Epidemiology of hepatocellular carcinoma. *Clinics in liver disease* **5**: 87-107, vi.
El Aidy S, Dinan TG, Cryan JF. 2015. Gut Microbiota: The Conductor in the Orchestra of Immune-Neuroendocrine Communication. *Clinical therapeutics* **37**: 954-967.

Elinav E, Strowig T, Kau AL, Henao-Mejia J, Thaiss CA, Booth CJ, Peaper DR, Bertin J, Eisenbarth SC, Gordon JI et al. 2011. NLRP6 inflammasome regulates colonic microbial ecology and risk for colitis. *Cell* **145**: 745-757.
Elliott KL, Catimel B, Church NL, Coates JL, Burgess AW, Layton MJ, Faux MC. 2013. Immunopurification of adenomatous polyposis coli (APC) proteins. *BMC Res Notes* **6**: 429.
Engl T, Relja B, Marian D, Blumenberg C, Muller I, Beecken WD, Jones J, Ringel EM, Bereiter-Hahn J, Jonas D et al. 2006. CXCR4 chemokine receptor mediates prostate tumor cell adhesion through alpha5 and beta3 integrins. *Neoplasia* **8**: 290-301.
Erdman SE, Poutahidis T. 2010. Roles for inflammation and regulatory T cells in colon cancer. *Toxicol Pathol* **38**: 76-87.
Esteve P, Sandonis A, Ibanez C, Shimono A, Guerrero I, Bovolenta P. 2011. Secreted frizzled-related proteins are required for Wnt/beta-catenin signalling activation in the vertebrate optic cup. *Development* **138**: 4179-4184.
Fafilek B, Krausova M, Vojtechova M, Pospichalova V, Tumova L, Sloncova E, Huranova M, Stancikova J, Hlavata A, Svec J et al. 2013. Troy, a tumor necrosis factor receptor family member, interacts with lgr5 to inhibit wnt signaling in intestinal stem cells. *Gastroenterology* **144**: 381-391.
Faith JJ, Guruge JL, Charbonneau M, Subramanian S, Seedorf H, Goodman AL, Clemente JC, Knight R, Heath AC, Leibel RL et al. 2013. The long-term stability of the human gut microbiota. *Science* **341**: 1237439.
Fang D, Hawke D, Zheng Y, Xia Y, Meisenhelder J, Nika H, Mills GB, Kobayashi R, Hunter T, Lu Z. 2007a. Phosphorylation of beta-catenin by AKT promotes beta-catenin transcriptional activity. *J Biol Chem* **282**: 11221-11229.
-. 2007b. Phosphorylation of beta-catenin by AKT promotes beta-catenin transcriptional activity. *J Biol Chem* **282**: 11221-11229.
Fang X, Yu SX, Lu Y, Bast RC, Jr., Woodgett JR, Mills GB. 2000. Phosphorylation and inactivation of glycogen synthase kinase 3 by protein kinase A. *Proc Natl Acad Sci U S A* **97**: 11960-11965.
Fang Z, Xiong Y, Li J, Liu L, Zhang W, Zhang C, Wan J. 2012. APC gene deletions in gastric adenocarcinomas in a Chinese population: a correlation with tumour progression. *Clin Transl Oncol* **14**: 60-65.
Farin HF, Van Es JH, Clevers H. 2012. Redundant Sources of Wnt Regulate Intestinal Stem Cells and Promote Formation of Paneth Cells. *Gastroenterology*.
Fearnhead NS, Britton MP, Bodmer WF. 2001. The ABC of APC. *Hum Mol Genet* **10**: 721-733.
Fei T, Xia K, Li Z, Zhou B, Zhu S, Chen H, Zhang J, Chen Z, Xiao H, Han JD et al. 2010. Genome-wide mapping of SMAD target genes reveals the role of BMP signaling in embryonic stem cell fate determination. *Genome Res* **20**: 36-44.
Fender AW, Nutter JM, Bertrand FE, Sigounas G. 2015. Notch-1 Promotes Stemness and Epithelial to Mesenchymal Transition in Colorectal Cancer. *J Cell Biochem*.
Feng J, Zhang X, Zhu H, Wang X, Ni S, Huang J. 2012. FoxQ1 overexpression influences poor prognosis in non-small cell lung cancer, associates with the phenomenon of EMT. *PLoS One* **7**: e39937.
Ferlay J, Shin HR, Bray F, Forman D, Mathers C, Parkin DM. 2010. Estimates of worldwide burden of cancer in 2008: GLOBOCAN 2008. *Int J Cancer* **127**: 2893-2917.
Fleuriel C, Touka M, Boulay G, Guerardel C, Rood BR, Leprince D. 2009. HIC1 (Hypermethylated in Cancer 1) epigenetic silencing in tumors. *Int J Biochem Cell Biol* **41**: 26-33.
Fox JG, Wang TC. 2007. Inflammation, atrophy, and gastric cancer. *J Clin Invest* **117**: 60-69.
Franca-Koh J, Yeo M, Fraser E, Young N, Dale TC. 2002. The regulation of glycogen synthase kinase-3 nuclear export by Frat/GBP. *J Biol Chem* **277**: 43844-43848.
Franke A, Balschun T, Karlsen TH, Hedderich J, May S, Lu T, Schuldt D, Nikolaus S, Rosenstiel P, Krawczak M et al. 2008. Replication of signals from recent studies of Crohn's disease identifies previously unknown disease loci for ulcerative colitis. *Nat Genet* **40**: 713-715.

Frolova L, Drastich P, Rossmann P, Klimesova K, Tlaskalova-Hogenova H. 2008. Expression of Toll-like receptor 2 (TLR2), TLR4, and CD14 in biopsy samples of patients with inflammatory bowel diseases: upregulated expression of TLR2 in terminal ileum of patients with ulcerative colitis. *J Histochem Cytochem* **56**: 267-274.

Galli LM, Barnes TL, Secrest SS, Kadowaki T, Burrus LW. 2007. Porcupine-mediated lipid-modification regulates the activity and distribution of Wnt proteins in the chick neural tube. *Development* **134**: 3339-3348.

Gallo RL, Hooper LV. 2012. Epithelial antimicrobial defence of the skin and intestine. *Nat Rev Immunol* **12**: 503-516.

Gan XQ, Wang JY, Xi Y, Wu ZL, Li YP, Li L. 2008. Nuclear Dvl, c-Jun, beta-catenin, and TCF form a complex leading to stabilization of beta-catenin-TCF interaction. *J Cell Biol* **180**: 1087-1100.

Gao D, Vahdat LT, Wong S, Chang JC, Mittal V. 2012. Microenvironmental regulation of epithelial-mesenchymal transitions in cancer. *Cancer Res* **72**: 4883-4889.

Gao W, Chen L, Ma Z, Du Z, Zhao Z, Hu Z, Li Q. 2013. Isolation and phenotypic characterization of colorectal cancer stem cells with organ-specific metastatic potential. *Gastroenterology* **145**: 636-646 e635.

Garcia MI, Ghiani M, Lefort A, Libert F, Strollo S, Vassart G. 2009. LGR5 deficiency deregulates Wnt signaling and leads to precocious Paneth cell differentiation in the fetal intestine. *Dev Biol* **331**: 58-67.

Gebhardt R, Baldysiak-Figiel A, Krugel V, Ueberham E, Gaunitz F. 2007. Hepatocellular expression of glutamine synthetase: an indicator of morphogen actions as master regulators of zonation in adult liver. *Progress in histochemistry and cytochemistry* **41**: 201-266.

Gedaly R, Galuppo R, Daily MF, Shah M, Maynard E, Chen C, Zhang X, Esser KA, Cohen DA, Evers BM et al. 2014. Targeting the Wnt/beta-catenin signaling pathway in liver cancer stem cells and hepatocellular carcinoma cell lines with FH535. *PLoS One* **9**: e99272.

Gerbe F, van Es JH, Makrini L, Brulin B, Mellitzer G, Robine S, Romagnolo B, Shroyer NF, Bourgaux JF, Pignodel C et al. 2011. Distinct ATOH1 and Neurog3 requirements define tuft cells as a new secretory cell type in the intestinal epithelium. *J Cell Biol* **192**: 767-780.

Gerlinger M, Rowan AJ, Horswell S, Larkin J, Endesfelder D, Gronroos E, Martinez P, Matthews N, Stewart A, Tarpey P et al. 2012. Intratumor heterogeneity and branched evolution revealed by multiregion sequencing. *N Engl J Med* **366**: 883-892.

Geuking MB, Cahenzli J, Lawson MA, Ng DC, Slack E, Hapfelmeier S, McCoy KD, Macpherson AJ. 2011. Intestinal bacterial colonization induces mutualistic regulatory T cell responses. *Immunity* **34**: 794-806.

Ghaffarzadehgan K, Jafarzadeh M, Raziee HR, Sima HR, Esmaili-Shandiz E, Hosseinnezhad H, Taghizadeh-Kermani A, Moaven O, Bahrani M. 2008. Expression of cell adhesion molecule CD44 in gastric adenocarcinoma and its prognostic importance. *World J Gastroenterol* **14**: 6376-6381.

Giannakis M, Stappenbeck TS, Mills JC, Leip DG, Lovett M, Clifton SW, Ippolito JE, Glasscock JI, Arumugam M, Brent MR et al. 2006. Molecular properties of adult mouse gastric and intestinal epithelial progenitors in their niches. *J Biol Chem*.

Giera S, Braeuning A, Kohle C, Bursch W, Metzger U, Buchmann A, Schwarz M. 2010. Wnt/beta-catenin signaling activates and determines hepatic zonal expression of glutathione S-transferases in mouse liver. *Toxicol Sci* **115**: 22-33.

Ginestier C, Hur MH, Charafe-Jauffret E, Monville F, Dutcher J, Brown M, Jacquemier J, Viens P, Kleer CG, Liu S et al. 2007. ALDH1 is a marker of normal and malignant human mammary stem cells and a predictor of poor clinical outcome. *Cell Stem Cell* **1**: 555-567.

Glinka A, Dolde C, Kirsch N, Huang YL, Kazanskaya O, Ingelfinger D, Boutros M, Cruciat CM, Niehrs C. 2011. LGR4 and LGR5 are R-spondin receptors mediating Wnt/beta-catenin and Wnt/PCP signalling. *EMBO Rep* **12**: 1055-1061.

Goldenring JR, Nam KT, Mills JC. 2011. The origin of pre-neoplastic metaplasia in the stomach: chief cells emerge from the Mist. *Exp Cell Res* **317**: 2759-2764.
Gotzos V, Wintergerst ES, Musy JP, Spichtin HP, Genton CY. 1999. Selective distribution of calretinin in adenocarcinomas of the human colon and adjacent tissues. *The American journal of surgical pathology* **23**: 701-711.
Gracz AD, Ramalingam S, Magness ST. 2010. Sox9 expression marks a subset of CD24-expressing small intestine epithelial stem cells that form organoids in vitro. *Am J Physiol Gastrointest Liver Physiol* **298**: G590-600.
Graham TA, Weaver C, Mao F, Kimelman D, Xu W. 2000. Crystal structure of a beta-catenin/Tcf complex. *Cell* **103**: 885-896.
Gray H, Standring S, Ellis H, Berkovitz BKB. 2005. *Gray's anatomy : the anatomical basis of clinical practice*. Elsevier Churchill Livingstone, Edinburgh ; New York.
Gregorieff A, Pinto D, Begthel H, Destree O, Kielman M, Clevers H. 2005. Expression pattern of Wnt signaling components in the adult intestine. *Gastroenterology* **129**: 626-638.
Griffin CT, Curtis CD, Davis RB, Muthukumar V, Magnuson T. 2011. The chromatin-remodeling enzyme BRG1 modulates vascular Wnt signaling at two levels. *Proc Natl Acad Sci U S A* **108**: 2282-2287.
Grover S, Kastrinos F, Steyerberg EW, Cook EF, Dewanwala A, Burbidge LA, Wenstrup RJ, Syngal S. 2012. Prevalence and phenotypes of APC and MUTYH mutations in patients with multiple colorectal adenomas. *JAMA* **308**: 485-492.
Guarner F, Malagelada JR. 2003. Gut flora in health and disease. *Lancet* **361**: 512-519.
Guidato S, Itasaki N. 2007. Wise retained in the endoplasmic reticulum inhibits Wnt signaling by reducing cell surface LRP6. *Dev Biol* **310**: 250-263.
Guilford P, Hopkins J, Harraway J, McLeod M, McLeod N, Harawira P, Taite H, Scoular R, Miller A, Reeve AE. 1998. E-cadherin germline mutations in familial gastric cancer. *Nature* **392**: 402-405.
Guo J, Cagatay T, Zhou G, Chan CC, Blythe S, Suyama K, Zheng L, Pan K, Qian C, Hamelin R et al. 2009. Mutations in the human naked cuticle homolog NKD1 found in colorectal cancer alter Wnt/Dvl/beta-catenin signaling. *PLoS One* **4**: e7982.
Gupta PK, Sahota A, Boyadjiev SA, Bye S, Shao C, O'Neill JP, Hunter TC, Albertini RJ, Stambrook PJ, Tischfield JA. 1997. High frequency in vivo loss of heterozygosity is primarily a consequence of mitotic recombination. *Cancer Res* **57**: 1188-1193.
Hao HX, Xie Y, Zhang Y, Charlat O, Oster E, Avello M, Lei H, Mickanin C, Liu D, Ruffner H et al. 2012. ZNRF3 promotes Wnt receptor turnover in an R-spondin-sensitive manner. *Nature* **485**: 195-200.
Harada N, Oshima H, Katoh M, Tamai Y, Oshima M, Taketo MM. 2004. Hepatocarcinogenesis in mice with beta-catenin and Ha-ras gene mutations. *Cancer Res* **64**: 48-54.
Harada N, Tamai Y, Ishikawa T, Sauer B, Takaku K, Oshima M, Taketo MM. 1999. Intestinal polyposis in mice with a dominant stable mutation of the beta-catenin gene. *Embo J* **18**: 5931-5942.
Haramis AP, Begthel H, van den Born M, van Es J, Jonkheer S, Offerhaus GJ, Clevers H. 2004. De novo crypt formation and juvenile polyposis on BMP inhibition in mouse intestine. *Science* **303**: 1684-1686.
Hardwick JC, Van Den Brink GR, Bleuming SA, Ballester I, Van Den Brande JM, Keller JJ, Offerhaus GJ, Van Deventer SJ, Peppelenbosch MP. 2004. Bone morphogenetic protein 2 is expressed by, and acts upon, mature epithelial cells in the colon. *Gastroenterology* **126**: 111-121.
Harterink M, Korswagen HC. 2012. Dissecting the Wnt secretion pathway: key questions on the modification and intracellular trafficking of Wnt proteins. *Acta Physiol (Oxf)* **204**: 8-16.
Hashimoto K, Aoyagi K, Isobe T, Kouhuji K, Shirouzu K. 2014. Expression of CD133 in the cytoplasm is associated with cancer progression and poor prognosis in gastric cancer. *Gastric Cancer* **17**: 97-106.
Hashimoto T, Schlessinger D, Cui CY. 2008. Troy binding to lymphotoxin-alpha activates NF kappa B mediated transcription. *Cell Cycle* **7**: 106-111.

Hausmann M, Kiessling S, Mestermann S, Webb G, Spottl T, Andus T, Scholmerich J, Herfarth H, Ray K, Falk W et al. 2002. Toll-like receptors 2 and 4 are up-regulated during intestinal inflammation. *Gastroenterology* **122**: 1987-2000.

Hayakawa Y, Ariyama H, Stancikova J, Sakitani K, Asfaha S, Renz BW, Dubeykovskaya ZA, Shibata W, Wang H, Westphalen CB et al. 2015a. Mist1 Expressing Gastric Stem Cells Maintain the Normal and Neoplastic Gastric Epithelium and Are Supported by a Perivascular Stem Cell Niche. *Cancer Cell*.

Hayakawa Y, Jin G, Wang H, Chen X, Westphalen CB, Asfaha S, Renz BW, Ariyama H, Dubeykovskaya ZA, Takemoto Y et al. 2015b. CCK2R identifies and regulates gastric antral stem cell states and carcinogenesis. *Gut* **64**: 544-553.

He TC, Sparks AB, Rago C, Hermeking H, Zawel L, da Costa LT, Morin PJ, Vogelstein B, Kinzler KW. 1998. Identification of c-MYC as a target of the APC pathway. *Science* **281**: 1509-1512.

He XC, Yin T, Grindley JC, Tian Q, Sato T, Tao WA, Dirisina R, Porter-Westpfahl KS, Hembree M, Johnson T et al. 2007. PTEN-deficient intestinal stem cells initiate intestinal polyposis. *Nat Genet* **39**: 189-198.

He XC, Zhang J, Tong WG, Tawfik O, Ross J, Scoville DH, Tian Q, Zeng X, He X, Wiedemann LM et al. 2004. BMP signaling inhibits intestinal stem cell self-renewal through suppression of Wnt-beta-catenin signaling. *Nat Genet* **36**: 1117-1121.

Hedberg Oldfors C, Dios DG, Linder A, Visuttijai K, Samuelson E, Karlsson S, Nilsson S, Behboudi A. 2015. Analysis of an independent tumor suppressor locus telomeric to Tp53 suggested Inpp5k and Myo1c as novel tumor suppressor gene candidates in this region. *BMC genetics* **16**: 80.

Hecht A, Vleminckx K, Stemmler MP, van Roy F, Kemler R. 2000. The p300/CBP acetyltransferases function as transcriptional coactivators of beta-catenin in vertebrates. *Embo J* **19**: 1839-1850.

Herr P, Basler K. 2012. Porcupine-mediated lipidation is required for Wnt recognition by Wls. *Dev Biol* **361**: 392-402.

Herr P, Hausmann G, Basler K. 2012. WNT secretion and signalling in human disease. *Trends Mol Med* **18**: 483-493.

Heuberger J, Kosel F, Qi J, Grossmann KS, Rajewsky K, Birchmeier W. 2014. Shp2/MAPK signaling controls goblet/paneth cell fate decisions in the intestine. *Proc Natl Acad Sci U S A* **111**: 3472-3477.

Himanen JP, Chumley MJ, Lackmann M, Li C, Barton WA, Jeffrey PD, Vearing C, Geleick D, Feldheim DA, Boyd AW et al. 2004. Repelling class discrimination: ephrin-A5 binds to and activates EphB2 receptor signaling. *Nat Neurosci* **7**: 501-509.

Hisaoka T, Morikawa Y, Kitamura T, Senba E. 2003. Expression of a member of tumor necrosis factor receptor superfamily, TROY, in the developing mouse brain. *Brain Res Dev Brain Res* **143**: 105-109.

Hoffmann W. 2008. Regeneration of the gastric mucosa and its glands from stem cells. *Current medicinal chemistry* **15**: 3133-3144.

Hohenberger P, Gretschel S. 2003. Gastric cancer. *Lancet* **362**: 305-315.

Hooper LV, Gordon JI. 2001. Commensal host-bacterial relationships in the gut. *Science* **292**: 1115-1118.

Horii A, Nakatsuru S, Miyoshi Y, Ichii S, Nagase H, Kato Y, Yanagisawa A, Nakamura Y. 1992. The APC gene, responsible for familial adenomatous polyposis, is mutated in human gastric cancer. *Cancer Res* **52**: 3231-3233.

Horst D, Kriegl L, Engel J, Kirchner T, Jung A. 2009. Prognostic significance of the cancer stem cell markers CD133, CD44, and CD166 in colorectal cancer. *Cancer investigation* **27**: 844-850.

Hoshida Y, Nijman SM, Kobayashi M, Chan JA, Brunet JP, Chiang DY, Villanueva A, Newell P, Ikeda K, Hashimoto M et al. 2009. Integrative transcriptome analysis reveals common molecular subclasses of human hepatocellular carcinoma. *Cancer Res* **69**: 7385-7392.

Houghton J, Stoicov C, Nomura S, Rogers AB, Carlson J, Li H, Cai X, Fox JG, Goldenring JR, Wang TC. 2004. Gastric cancer originating from bone marrow-derived cells. *Science* **306**: 1568-1571.

Hsieh JC, Lee L, Zhang L, Wefer S, Brown K, DeRossi C, Wines ME, Rosenquist T, Holdener BC. 2003. Mesd encodes an LRP5/6 chaperone essential for specification of mouse embryonic polarity. *Cell* **112**: 355-367.

Hsu SY, Kudo M, Chen T, Nakabayashi K, Bhalla A, van der Spek PJ, van Duin M, Hsueh AJ. 2000. The three subfamilies of leucine-rich repeat-containing G protein-coupled receptors (LGR): identification of LGR6 and LGR7 and the signaling mechanism for LGR7. *Mol Endocrinol* **14**: 1257-1271.

Hsu SY, Liang SG, Hsueh AJ. 1998. Characterization of two LGR genes homologous to gonadotropin and thyrotropin receptors with extracellular leucine-rich repeats and a G protein-coupled, seven-transmembrane region. *Mol Endocrinol* **12**: 1830-1845.

Hu B, Elinav E, Huber S, Strowig T, Hao L, Hafemann A, Jin C, Wunderlich C, Wunderlich T, Eisenbarth SC et al. 2013. Microbiota-induced activation of epithelial IL-6 signaling links inflammasome-driven inflammation with transmissible cancer. *Proc Natl Acad Sci U S A* **110**: 9862-9867.

Huang EH, Hynes MJ, Zhang T, Ginestier C, Dontu G, Appelman H, Fields JZ, Wicha MS, Boman BM. 2009. Aldehyde dehydrogenase 1 is a marker for normal and malignant human colonic stem cells (SC) and tracks SC overpopulation during colon tumorigenesis. *Cancer Res* **69**: 3382-3389.

Huber AH, Nelson WJ, Weis WI. 1997. Three-dimensional structure of the armadillo repeat region of beta- catenin. *Cell* **90**: 871-882.

Huczynski A, Janczak J, Lowicki D, Brzezinski B. 2012. Monensin A acid complexes as a model of electrogenic transport of sodium cation. *Biochim Biophys Acta* **1818**: 2108-2119.

Hunter T. 2000. Signaling--2000 and beyond. *Cell* **100**: 113-127.

Chan DW, Chan CY, Yam JW, Ching YP, Ng IO. 2006. Prickle-1 negatively regulates Wnt/beta-catenin pathway by promoting Dishevelled ubiquitination/degradation in liver cancer. *Gastroenterology* **131**: 1218-1227.

Chan SW, Lim CJ, Chen L, Chong YF, Huang C, Song H, Hong W. 2011. The Hippo pathway in biological control and cancer development. *J Cell Physiol* **226**: 928-939.

Chandra SH, Wacker I, Appelt UK, Behrens J, Schneikert J. 2012. A common role for various human truncated adenomatous polyposis coli isoforms in the control of beta-catenin activity and cell proliferation. *PLoS One* **7**: e34479.

Chandrasekharan B, Nezami BG, Srinivasan S. 2013. Emerging neuropeptide targets in inflammation: NPY and VIP. *Am J Physiol Gastrointest Liver Physiol* **304**: G949-957.

Chen D, Zhao CM, Al-Haider W, Hakanson R, Rehfeld JF, Kopin AS. 2002. Differentiation of gastric ECL cells is altered in CCK(2) receptor-deficient mice. *Gastroenterology* **123**: 577-585.

Chen Q, Su Y, Wesslowski J, Hagemann AI, Ramialison M, Wittbrodt J, Scholpp S, Davidson G. 2014. Tyrosine phosphorylation of LRP6 by Src and Fer inhibits Wnt/beta-catenin signalling. *EMBO Rep* **15**: 1254-1267.

Chen S, Song X, Chen Z, Li X, Li M, Liu H, Li J. 2013. CD133 expression and the prognosis of colorectal cancer: a systematic review and meta-analysis. *PLoS One* **8**: e56380.

Chen T, Yang K, Yu J, Meng W, Yuan D, Bi F, Liu F, Liu J, Dai B, Chen X et al. 2012. Identification and expansion of cancer stem cells in tumor tissues and peripheral blood derived from gastric adenocarcinoma patients. *Cell Res* **22**: 248-258.

Chen WY, Wang DH, Yen RC, Luo J, Gu W, Baylin SB. 2005. Tumor suppressor HIC1 directly regulates SIRT1 to modulate p53-dependent DNA-damage responses. *Cell* **123**: 437-448.

Chen WY, Zeng X, Carter MG, Morrell CN, Chiu Yen RW, Esteller M, Watkins DN, Herman JG, Mankowski JL, Baylin SB. 2003. Heterozygous disruption of Hic1 predisposes mice to a gender-dependent spectrum of malignant tumors. *Nat Genet* **33**: 197-202.

Cheng AS, Lau SS, Chen Y, Kondo Y, Li MS, Feng H, Ching AK, Cheung KF, Wong HK, Tong JH et al. 2011. EZH2-mediated concordant repression of Wnt antagonists promotes beta-catenin-dependent hepatocarcinogenesis. *Cancer Res* **71**: 4028-4039.
Cheng H, Leblond CP. 1974. Origin, differentiation and renewal of the four main epithelial cell types in the mouse small intestine. V. Unitarian Theory of the origin of the four epithelial cell types. *The American journal of anatomy* **141**: 537-561.
Cheng XX, Wang ZC, Chen XY, Sun Y, Kong QY, Liu J, Li H. 2005. Correlation of Wnt-2 expression and beta-catenin intracellular accumulation in Chinese gastric cancers: relevance with tumour dissemination. *Cancer Lett* **223**: 339-347.
Cheng YY, Yu J, Wong YP, Man EP, To KF, Jin VX, Li J, Tao Q, Sung JJ, Chan FK et al. 2007. Frequent epigenetic inactivation of secreted frizzled-related protein 2 (SFRP2) by promoter methylation in human gastric cancer. *Br J Cancer* **97**: 895-901.
Cherciu I, Barbalan A, Pirici D, Margaritescu C, Saftoiu A. 2014. Stem cells, colorectal cancer and cancer stem cell markers correlations. *Current health sciences journal* **40**: 153-161.
Cheung AF, Carter AM, Kostova KK, Woodruff JF, Crowley D, Bronson RT, Haigis KM, Jacks T. 2010. Complete deletion of Apc results in severe polyposis in mice. *Oncogene* **29**: 1857-1864.
Chi XZ, Yang JO, Lee KY, Ito K, Sakakura C, Li QL, Kim HR, Cha EJ, Lee YH, Kaneda A et al. 2005. RUNX3 suppresses gastric epithelial cell growth by inducing p21(WAF1/Cip1) expression in cooperation with transforming growth factor {beta}-activated SMAD. *Mol Cell Biol* **25**: 8097-8107.
Choi E, Roland JT, Barlow BJ, O'Neal R, Rich AE, Nam KT, Shi C, Goldenring JR. 2014. Cell lineage distribution atlas of the human stomach reveals heterogeneous gland populations in the gastric antrum. *Gut* **63**: 1711-1720.
Ihara M, Yamamoto H, Kikuchi A. 2005. SUMO-1 modification of PIASy, an E3 ligase, is necessary for PIASy-dependent activation of Tcf-4. *Mol Cell Biol* **25**: 3506-3518.
Ingham PW, McMahon AP. 2001. Hedgehog signaling in animal development: paradigms and principles. *Genes Dev* **15**: 3059-3087.
Ishii M, Nakajima T, Ogawa K. 2011. Complementary expression of EphB receptors and ephrin-B ligand in the pyloric and duodenal epithelium of adult mice. *Histochemistry and cell biology* **136**: 345-356.
Ishizaki Y, Ikeda S, Fujimori M, Shimizu Y, Kurihara T, Itamoto T, Kikuchi A, Okajima M, Asahara T. 2004. Immunohistochemical analysis and mutational analyses of beta-catenin, Axin family and APC genes in hepatocellular carcinomas. *Int J Oncol* **24**: 1077-1083.
Itasaki N, Jones CM, Mercurio S, Rowe A, Domingos PM, Smith JC, Krumlauf R. 2003. Wise, a context-dependent activator and inhibitor of Wnt signalling. *Development* **130**: 4295-4305.
Ito K, Chuang LS, Ito T, Chang TL, Fukamachi H, Salto-Tellez M, Ito Y. 2011. Loss of Runx3 is a key event in inducing precancerous state of the stomach. *Gastroenterology* **140**: 1536-1546 e1538.
Ito K, Lim AC, Salto-Tellez M, Motoda L, Osato M, Chuang LS, Lee CW, Voon DC, Koo JK, Wang H et al. 2008. RUNX3 attenuates beta-catenin/T cell factors in intestinal tumorigenesis. *Cancer Cell* **14**: 226-237.
Itzkovitz S, Lyubimova A, Blat IC, Maynard M, van Es J, Lees J, Jacks T, Clevers H, van Oudenaarden A. 2012. Single-molecule transcript counting of stem-cell markers in the mouse intestine. *Nat Cell Biol* **14**: 106-114.
Iwao K, Nakamori S, Kameyama M, Imaoka S, Kinoshita M, Fukui T, Ishiguro S, Nakamura Y, Miyoshi Y. 1998. Activation of the beta-catenin gene by interstitial deletions involving exon 3 in primary colorectal carcinomas without adenomatous polyposis coli mutations. *Cancer Res* **58**: 1021-1026.
Iyer RR, Pluciennik A, Burdett V, Modrich PL. 2006. DNA mismatch repair: functions and mechanisms. *Chemical reviews* **106**: 302-323.
Jacobi CA, Malfertheiner P. 2011. Escherichia coli Nissle 1917 (Mutaflor): new insights into an old probiotic bacterium. *Digestive diseases* **29**: 600-607.

Jemal A, Bray F, Center MM, Ferlay J, Ward E, Forman D. 2011. Global cancer statistics. *CA: a cancer journal for clinicians* **61**: 69-90.
Jenkins MA, Croitoru ME, Monga N, Cleary SP, Cotterchio M, Hopper JL, Gallinger S. 2006. Risk of colorectal cancer in monoallelic and biallelic carriers of MYH mutations: a population-based case-family study. *Cancer Epidemiol Biomarkers Prev* **15**: 312-314.
Jensen J, Pedersen EE, Galante P, Hald J, Heller RS, Ishibashi M, Kageyama R, Guillemot F, Serup P, Madsen OD. 2000. Control of endodermal endocrine development by Hes-1. *Nat Genet* **24**: 36-44.
Jessen S, Gu B, Dai X. 2008. Pygopus and the Wnt signaling pathway: a diverse set of connections. *BioEssays : news and reviews in molecular, cellular and developmental biology* **30**: 448-456.
Jho E, Lomvardas S, Costantini F. 1999. A GSK3beta phosphorylation site in axin modulates interaction with beta- catenin and Tcf-mediated gene expression. *Biochem Biophys Res Commun* **266**: 28-35.
Jiang X, Charlat O, Zamponi R, Yang Y, Cong F. 2015. Dishevelled Promotes Wnt Receptor Degradation through Recruitment of ZNRF3/RNF43 E3 Ubiquitin Ligases. *Mol Cell* **58**: 522-533.
Jiang Y, Jahagirdar BN, Reinhardt RL, Schwartz RE, Keene CD, Ortiz-Gonzalez XR, Reyes M, Lenvik T, Lund T, Blackstad M et al. 2002. Pluripotency of mesenchymal stem cells derived from adult marrow. *Nature* **418**: 41-49.
Johansson ME, Hansson GC. 2011. Microbiology. Keeping bacteria at a distance. *Science* **334**: 182-183.
Johansson ME, Larsson JM, Hansson GC. 2011. The two mucus layers of colon are organized by the MUC2 mucin, whereas the outer layer is a legislator of host-microbial interactions. *Proc Natl Acad Sci U S A* **108 Suppl 1**: 4659-4665.
Jung H, Kim BG, Han WH, Lee JH, Cho JY, Park WS, Maurice MM, Han JK, Lee MJ, Finley D et al. 2013. Deubiquitination of Dishevelled by Usp14 is required for Wnt signaling. *Oncogenesis* **2**: e64.
Jung P, Sato T, Merlos-Suarez A, Barriga FM, Iglesias M, Rossell D, Auer H, Gallardo M, Blasco MA, Sancho E et al. 2011. Isolation and in vitro expansion of human colonic stem cells. *Nat Med* **17**: 1225-1227.
Kakiuchi M, Nishizawa T, Ueda H, Gotoh K, Tanaka A, Hayashi A, Yamamoto S, Tatsuno K, Katoh H, Watanabe Y et al. 2014. Recurrent gain-of-function mutations of RHOA in diffuse-type gastric carcinoma. *Nat Genet* **46**: 583-587.
Kalani AD, Jack A, Montenegro G, Degliuomini J, Wallack MK. 2008. Immunotherapy as an adjuvant therapy in the management of advanced, surgically resected, melanoma. *Giornale italiano di dermatologia e venereologia : organo ufficiale, Societa italiana di dermatologia e sifilografia* **143**: 59-70.
Kan Z, Zheng H, Liu X, Li S, Barber TD, Gong Z, Gao H, Hao K, Willard MD, Xu J et al. 2013. Whole-genome sequencing identifies recurrent mutations in hepatocellular carcinoma. *Genome Res* **23**: 1422-1433.
Kandasamy K, Srivastava RK. 2002. Role of the phosphatidylinositol 3'-kinase/PTEN/Akt kinase pathway in tumor necrosis factor-related apoptosis-inducing ligand-induced apoptosis in non-small cell lung cancer cells. *Cancer Res* **62**: 4929-4937.
Kang DH, Han ME, Song MH, Lee YS, Kim EH, Kim HJ, Kim GH, Kim DH, Yoon S, Baek SY et al. 2009. The role of hedgehog signaling during gastric regeneration. *J Gastroenterol* **44**: 372-379.
Karam SM, Leblond CP. 1993. Dynamics of epithelial cells in the corpus of the mouse stomach. I. Identification of proliferative cell types and pinpointing of the stem cell. *The Anatomical record* **236**: 259-279.
Kato LM, Kawamoto S, Maruya M, Fagarasan S. 2014. The role of the adaptive immune system in regulation of gut microbiota. *Immunol Rev* **260**: 67-75.
Katoh M. 2005. Epithelial-mesenchymal transition in gastric cancer (Review). *Int J Oncol* **27**: 1677-1683.

-. 2007a. Dysregulation of stem cell signaling network due to germline mutation, SNP, Helicobacter pylori infection, epigenetic change and genetic alteration in gastric cancer. *Cancer Biol Ther* **6**: 832-839.
-. 2007b. WNT signaling pathway and stem cell signaling network. *Clin Cancer Res* **13**: 4042-4045.
Katoh M, Kirikoshi H, Terasaki H, Shiokawa K. 2001. WNT2B2 mRNA, up-regulated in primary gastric cancer, is a positive regulator of the WNT- beta-catenin-TCF signaling pathway. *Biochem Biophys Res Commun* **289**: 1093-1098.
Katz NR. 1992. Metabolic heterogeneity of hepatocytes across the liver acinus. *The Journal of nutrition* **122**: 843-849.
Kavanagh DP, Kalia N. 2011. Hematopoietic stem cell homing to injured tissues. *Stem cell reviews* **7**: 672-682.
Kawada N, Imanaka K, Kawaguchi T, Tamai C, Ishihara R, Matsunaga T, Gotoh K, Yamada T, Tomita Y. 2009. Hepatocellular carcinoma arising from non-cirrhotic nonalcoholic steatohepatitis. *J Gastroenterol* **44**: 1190-1194.
Kawamoto S, Maruya M, Kato LM, Suda W, Atarashi K, Doi Y, Tsutsui Y, Qin H, Honda K, Okada T et al. 2014. Foxp3(+) T cells regulate immunoglobulin a selection and facilitate diversification of bacterial species responsible for immune homeostasis. *Immunity* **41**: 152-165.
Kemper K, Prasetyanti PR, De Lau W, Rodermond H, Clevers H, Medema JP. 2012. Monoclonal antibodies against Lgr5 identify human colorectal cancer stem cells. *Stem Cells* **30**: 2378-2386.
Kilinc D, Ozdemir O, Ozdemir S, Korgali E, Koksal B, Uslu A, Gultekin YE. 2012. Alterations in promoter methylation status of tumor suppressor HIC1, SFRP2, and DAPK1 genes in prostate carcinomas. *DNA Cell Biol* **31**: 826-832.
Killoran RC, Fan J, Yang D, Shilton BH, Choy WY. 2015. Structural Analysis of the 14-3-3zeta/Chibby Interaction Involved in Wnt/beta-Catenin Signaling. *PLoS One* **10**: e0123934.
Kim CJ, Song JH, Cho YG, Kim YS, Kim SY, Nam SW, Yoo NJ, Lee JY, Park WS. 2007. Somatic mutations of the beta-TrCP gene in gastric cancer. *APMIS : acta pathologica, microbiologica, et immunologica Scandinavica* **115**: 127-133.
Kim GH, Han JK. 2005. JNK and ROKalpha function in the noncanonical Wnt/RhoA signaling pathway to regulate Xenopus convergent extension movements. *Dev Dyn* **232**: 958-968.
Kim KA, Kakitani M, Zhao J, Oshima T, Tang T, Binnerts M, Liu Y, Boyle B, Park E, Emtage P et al. 2005. Mitogenic influence of human R-spondin1 on the intestinal epithelium. *Science* **309**: 1256-1259.
Kim MJ, Chia IV, Costantini F. 2008. SUMOylation target sites at the C terminus protect Axin from ubiquitination and confer protein stability. *FASEB J* **22**: 3785-3794.
Kim MS, Kim SS, Ahn CH, Yoo NJ, Lee SH. 2009. Frameshift mutations of Wnt pathway genes AXIN2 and TCF7L2 in gastric carcinomas with high microsatellite instability. *Hum Pathol* **40**: 58-64.
Kim S, Jho EH. 2010. The protein stability of Axin, a negative regulator of Wnt signaling, is regulated by Smad ubiquitination regulatory factor 2 (Smurf2). *J Biol Chem* **285**: 36420-36426.
Kim SE, Huang H, Zhao M, Zhang X, Zhang A, Semonov MV, MacDonald BT, Zhang X, Garcia Abreu J, Peng L et al. 2013. Wnt stabilization of beta-catenin reveals principles for morphogen receptor-scaffold assemblies. *Science* **340**: 867-870.
Kim SE, Paik HY, Yoon H, Lee JE, Kim N, Sung MK. 2015. Sex- and gender-specific disparities in colorectal cancer risk. *World J Gastroenterol* **21**: 5167-5175.
Kim TH, Shivdasani RA. 2011a. Genetic evidence that intestinal Notch functions vary regionally and operate through a common mechanism of Math1 repression. *J Biol Chem* **286**: 11427-11433.
-. 2011b. Notch signaling in stomach epithelial stem cell homeostasis. *The Journal of experimental medicine* **208**: 677-688.

King SL, Mohiuddin JJ, Dekaney CM. 2013. Paneth cells expand from newly created and preexisting cells during repair after doxorubicin-induced damage. *Am J Physiol Gastrointest Liver Physiol* **305**: G151-162.
Kinzel B, Pikiolek M, Orsini V, Sprunger J, Isken A, Zietzling S, Desplanches M, Dubost V, Breustedt D, Valdez R et al. 2014. Functional roles of Lgr4 and Lgr5 in embryonic gut, kidney and skin development in mice. *Dev Biol* **390**: 181-190.
Kinzler KW, Nilbert MC, Su LK, Vogelstein B, Bryan TM, Levy DB, Smith KJ, Preisinger AC, Hedge P, McKechnie D et al. 1991. Identification of FAP locus genes from chromosome 5q21. *Science* **253**: 661-665.
Kitisin K, Shetty K, Mishra L, Johnson LB. 2007. Hepatocellular stem cells. *Cancer biomarkers : section A of Disease markers* **3**: 251-262.
Klein D, Demory A, Peyre F, Kroll J, Augustin HG, Helfrich W, Kzhyshkowska J, Schledzewski K, Arnold B, Goerdt S. 2008. Wnt2 acts as a cell type-specific, autocrine growth factor in rat hepatic sinusoidal endothelial cells cross-stimulating the VEGF pathway. *Hepatology* **47**: 1018-1031.
Kohn AD, Moon RT. 2005. Wnt and calcium signaling: beta-catenin-independent pathways. *Cell calcium* **38**: 439-446.
Koch A, Denkhaus D, Albrecht S, Leuschner I, von Schweinitz D, Pietsch T. 1999. Childhood hepatoblastomas frequently carry a mutated degradation targeting box of the beta-catenin gene. *Cancer Res* **59**: 269-273.
Koch A, Waha A, Hartmann W, Hrychyk A, Schuller U, Wharton KA, Jr., Fuchs SY, von Schweinitz D, Pietsch T. 2005. Elevated expression of Wnt antagonists is a common event in hepatoblastomas. *Clin Cancer Res* **11**: 4295-4304.
Kojima T, Morikawa Y, Copeland NG, Gilbert DJ, Jenkins NA, Senba E, Kitamura T. 2000. TROY, a newly identified member of the tumor necrosis factor receptor superfamily, exhibits a homology with Edar and is expressed in embryonic skin and hair follicles. *J Biol Chem* **275**: 20742-20747.
Komekado H, Yamamoto H, Chiba T, Kikuchi A. 2007. Glycosylation and palmitoylation of Wnt-3a are coupled to produce an active form of Wnt-3a. *Genes Cells* **12**: 521-534.
Kondo Y, Kanai Y, Sakamoto M, Genda T, Mizokami M, Ueda R, Hirohashi S. 1999. Beta-catenin accumulation and mutation of exon 3 of the beta-catenin gene in hepatocellular carcinoma. *Jpn J Cancer Res* **90**: 1301-1309.
Koo BK, Spit M, Jordens I, Low TY, Stange DE, van de Wetering M, van Es JH, Mohammed S, Heck AJ, Maurice MM et al. 2012. Tumour suppressor RNF43 is a stem-cell E3 ligase that induces endocytosis of Wnt receptors. *Nature* **488**: 665-669.
Korinek V, Barker N, Moerer P, van Donselaar E, Huls G, Peters PJ, Clevers H. 1998. Depletion of epithelial stem-cell compartments in the small intestine of mice lacking Tcf-4. *Nat Genet* **19**: 379-383.
Kosinski C, Li VS, Chan AS, Zhang J, Ho C, Tsui WY, Chan TL, Mifflin RC, Powell DW, Yuen ST et al. 2007. Gene expression patterns of human colon tops and basal crypts and BMP antagonists as intestinal stem cell niche factors. *P Natl Acad Sci USA* **104**: 15418-15423.
Kramps T, Peter O, Brunner E, Nellen D, Froesch B, Chatterjee S, Murone M, Zullig S, Basler K. 2002. Wnt/wingless signaling requires BCL9/legless-mediated recruitment of pygopus to the nuclear beta-catenin-TCF complex. *Cell* **109**: 47-60.
Krause C, Korchynskyi O, de Rooij K, Weidauer SE, de Gorter DJ, van Bezooijen RL, Hatsell S, Economides AN, Mueller TD, Lowik CW et al. 2010. Distinct modes of inhibition by sclerostin on bone morphogenetic protein and Wnt signaling pathways. *J Biol Chem* **285**: 41614-41626.
Krausova M, Korinek V. 2012. Signal transduction pathways participating in homeostasis and malignant transformation of the intestinal tissue. *Neoplasma* **59**: 708-718.
-. 2014. Wnt signaling in adult intestinal stem cells and cancer. *Cell Signal* **26**: 570-579.
Kreso A, Dick JE. 2014. Evolution of the cancer stem cell model. *Cell Stem Cell* **14**: 275-291.
Krieghoff E, Behrens J, Mayr B. 2006. Nucleo-cytoplasmic distribution of beta-catenin is regulated by retention. *J Cell Sci* **119**: 1453-1463.

Kryczek I, Lin Y, Nagarsheth N, Peng D, Zhao L, Zhao E, Vatan L, Szeliga W, Dou Y, Owens S et al. 2014. IL-22(+)CD4(+) T cells promote colorectal cancer stemness via STAT3 transcription factor activation and induction of the methyltransferase DOT1L. *Immunity* **40**: 772-784.

Kudo M, Chen T, Nakabayashi K, Hsu SY, Hsueh AJ. 2000. The nematode leucine-rich repeat-containing, G protein-coupled receptor (LGR) protein homologous to vertebrate gonadotropin and thyrotropin receptors is constitutively active in mammalian cells. *Mol Endocrinol* **14**: 272-284.

Kullberg MC, Jankovic D, Gorelick PL, Caspar P, Letterio JJ, Cheever AW, Sher A. 2002. Bacteria-triggered CD4(+) T regulatory cells suppress Helicobacter hepaticus-induced colitis. *The Journal of experimental medicine* **196**: 505-515.

Kumar S. 2014. P53 induction accompanying G2/M arrest upon knockdown of tumor suppressor HIC1 in U87MG glioma cells. *Mol Cell Biochem* **395**: 281-290.

Kurayoshi M, Oue N, Yamamoto H, Kishida M, Inoue A, Asahara T, Yasui W, Kikuchi A. 2006. Expression of Wnt-5a is correlated with aggressiveness of gastric cancer by stimulating cell migration and invasion. *Cancer Res* **66**: 10439-10448.

Kurayoshi M, Yamamoto H, Izumi S, Kikuchi A. 2007. Post-translational palmitoylation and glycosylation of Wnt-5a are necessary for its signalling. *Biochem J* **402**: 515-523.

Lachenmayer A, Alsinet C, Savic R, Cabellos L, Toffanin S, Hoshida Y, Villanueva A, Minguez B, Newell P, Tsai HW et al. 2012a. Wnt-pathway activation in two molecular classes of hepatocellular carcinoma and experimental modulation by sorafenib. *Clin Cancer Res* **18**: 4997-5007.

Lachenmayer A, Toffanin S, Cabellos L, Alsinet C, Hoshida Y, Villanueva A, Minguez B, Tsai HW, Ward SC, Thung S et al. 2012b. Combination therapy for hepatocellular carcinoma: Additive preclinical efficacy of the HDAC inhibitor panobinostat with sorafenib. *J Hepatol*.

Lakritz JR, Poutahidis T, Mirabal S, Varian BJ, Levkovich T, Ibrahim YM, Ward JM, Teng EC, Fisher B, Parry N et al. 2015. Gut bacteria require neutrophils to promote mammary tumorigenesis. *Oncotarget* **6**: 9387-9396.

Langhans N, Rindi G, Chiu M, Rehfeld JF, Ardman B, Beinborn M, Kopin AS. 1997. Abnormal gastric histology and decreased acid production in cholecystokinin-B/gastrin receptor-deficient mice. *Gastroenterology* **112**: 280-286.

Larraguibel J, Weiss AR, Pasula DJ, Dhaliwal RS, Kondra R, Van Raay TJ. 2015. Wnt ligand-dependent activation of the negative feedback regulator Nkd1. *Mol Biol Cell* **26**: 2375-2384.

Larsson E, Tremaroli V, Lee YS, Koren O, Nookaew I, Fricker A, Nielsen J, Ley RE, Backhed F. 2012. Analysis of gut microbial regulation of host gene expression along the length of the gut and regulation of gut microbial ecology through MyD88. *Gut* **61**: 1124-1131.

Lasorella A, Benezra R, Iavarone A. 2014. The ID proteins: master regulators of cancer stem cells and tumour aggressiveness. *Nat Rev Cancer* **14**: 77-91.

Laurent-Puig P, Legoix P, Bluteau O, Belghiti J, Franco D, Binot F, Monges G, Thomas G, Bioulac-Sage P, Zucman-Rossi J. 2001. Genetic alterations associated with hepatocellular carcinomas define distinct pathways of hepatocarcinogenesis. *Gastroenterology* **120**: 1763-1773.

Lee E, Salic A, Kruger R, Heinrich R, Kirschner MW. 2003. The roles of APC and Axin derived from experimental and theoretical analysis of the Wnt pathway. *PLoS Biol* **1**: E10.

Lee HH, Seo KJ, An CH, Kim JS, Jeon HM. 2012. CD133 expression is correlated with chemoresistance and early recurrence of gastric cancer. *Journal of surgical oncology* **106**: 999-1004.

Lee JM, Yang J, Newell P, Singh S, Parwani A, Friedman SL, Nejak-Bowen KN, Monga SP. 2014. beta-Catenin signaling in hepatocellular cancer: Implications in inflammation, fibrosis, and proliferation. *Cancer Lett* **343**: 90-97.

Lee SH, Park YK, Cho SM, Kang JK, Lee DJ. 2015. Technical skills and training of upper gastrointestinal endoscopy for new beginners. *World J Gastroenterol* **21**: 759-785.

Lee SJ, Leoni G, Neumann PA, Chun J, Nusrat A, Yun CC. 2013. Distinct phospholipase C-beta isozymes mediate lysophosphatidic acid receptor 1 effects on intestinal epithelial homeostasis and wound closure. *Mol Cell Biol* **33**: 2016-2028.
Lee YN, Gao Y, Wang HY. 2008. Differential mediation of the Wnt canonical pathway by mammalian Dishevelleds-1, -2, and -3. *Cell Signal* **20**: 443-452.
Lemaigre FP. 2009. Mechanisms of liver development: concepts for understanding liver disorders and design of novel therapies. *Gastroenterology* **137**: 62-79.
Lengauer C, Kinzler KW, Vogelstein B. 1998. Genetic instabilities in human cancers. *Nature* **396**: 643-649.
Lennerz JK, Kim SH, Oates EL, Huh WJ, Doherty JM, Tian X, Bredemeyer AJ, Goldenring JR, Lauwers GY, Shin YK et al. 2010. The transcription factor MIST1 is a novel human gastric chief cell marker whose expression is lost in metaplasia, dysplasia, and carcinoma. *Am J Pathol* **177**: 1514-1533.
Leoz ML, Carballal S, Moreira L, Ocana T, Balaguer F. 2015. The genetic basis of familial adenomatous polyposis and its implications for clinical practice and risk management. *The application of clinical genetics* **8**: 95-107.
Lerner UH, Ohlsson C. 2015. The WNT system: background and its role in bone. *J Intern Med*.
Leung WK, Kim JJ, Wu L, Sepulveda JL, Sepulveda AR. 2000. Identification of a second MutL DNA mismatch repair complex (hPMS1 and hMLH1) in human epithelial cells. *J Biol Chem* **275**: 15728-15732.
Lewis A, Segditsas S, Deheragoda M, Pollard P, Jeffery R, Nye E, Lockstone H, Davis H, Clark S, Stamp G et al. 2010. Severe polyposis in Apc(1322T) mice is associated with submaximal Wnt signalling and increased expression of the stem cell marker Lgr5. *Gut* **59**: 1680-1686.
Li FQ, Mofunanya A, Fischer V, Hall J, Takemaru K. 2010a. Nuclear-cytoplasmic shuttling of Chibby controls beta-catenin signaling. *Mol Biol Cell* **21**: 311-322.
Li FQ, Mofunanya A, Harris K, Takemaru K. 2008. Chibby cooperates with 14-3-3 to regulate beta-catenin subcellular distribution and signaling activity. *J Cell Biol* **181**: 1141-1154.
Li HJ, Johnston B, Aiello D, Caffrey DR, Giel-Moloney M, Rindi G, Leiter AB. 2014a. Distinct cellular origins for serotonin-expressing and enterochromaffin-like cells in the gastric corpus. *Gastroenterology* **146**: 754-764 e753.
Li HJ, Reinhardt F, Herschman HR, Weinberg RA. 2012. Cancer-stimulated mesenchymal stem cells create a carcinoma stem cell niche via prostaglandin E2 signaling. *Cancer discovery* **2**: 840-855.
Li K, Dan Z, Nie YQ. 2014b. Gastric cancer stem cells in gastric carcinogenesis, progression, prevention and treatment. *World J Gastroenterol* **20**: 5420-5426.
Li Q, Ishikawa TO, Miyoshi H, Oshima M, Taketo MM. 2005. A targeted mutation of Nkd1 impairs mouse spermatogenesis. *J Biol Chem* **280**: 2831-2839.
Li Q, Karam SM, Gordon JI. 1996. Diphtheria toxin-mediated ablation of parietal cells in the stomach of transgenic mice. *J Biol Chem* **271**: 3671-3676.
Li QL, Ito K, Sakakura C, Fukamachi H, Inoue K, Chi XZ, Lee KY, Nomura S, Lee CW, Han SB et al. 2002. Causal relationship between the loss of RUNX3 expression and gastric cancer. *Cell* **109**: 113-124.
Li R, Grimm SA, Chrysovergis K, Kosak J, Wang X, Du Y, Burkholder A, Janardhan K, Mav D, Shah R et al. 2014c. Obesity, rather than diet, drives epigenomic alterations in colonic epithelium resembling cancer progression. *Cell Metab* **19**: 702-711.
Li SJ, Yen TY, Endo Y, Klauzinska M, Baljinnyam B, Macher B, Callahan R, Rubin JS. 2009. Loss-of-function point mutations and two-furin domain derivatives provide insights about R-spondin2 structure and function. *Cell Signal* **21**: 916-925.
Li T, Su Y, Mei Y, Leng Q, Leng B, Liu Z, Stass SA, Jiang F. 2010b. ALDH1A1 is a marker for malignant prostate stem cells and predictor of prostate cancer patients' outcome. *Lab Invest* **90**: 234-244.
Liang J, Zubovitz J, Petrocelli T, Kotchetkov R, Connor MK, Han K, Lee JH, Ciarallo S, Catzavelos C, Beniston R et al. 2002. PKB/Akt phosphorylates p27, impairs nuclear import of p27 and opposes p27-mediated G1 arrest. *Nat Med* **8**: 1153-1160.

Lim X, Nusse R. 2013. Wnt signaling in skin development, homeostasis, and disease. *Cold Spring Harb Perspect Biol* **5**.
Lin K, Wang S, Julius MA, Kitajewski J, Moos M, Jr., Luyten FP. 1997. The cysteine-rich frizzled domain of Frzb-1 is required and sufficient for modulation of Wnt signaling. *Proc Natl Acad Sci U S A* **94**: 11196-11200.
Littman DR, Pamer EG. 2011. Role of the commensal microbiota in normal and pathogenic host immune responses. *Cell Host Microbe* **10**: 311-323.
Liu C, Li Y, Semenov M, Han C, Baeg GH, Tan Y, Zhang Z, Lin X, He X. 2002. Control of beta-catenin phosphorylation/degradation by a dual-kinase mechanism. *Cell* **108**: 837-847.
Liu J, Fukunaga-Kalabis M, Li L, Herlyn M. 2014. Developmental pathways activated in melanocytes and melanoma. *Arch Biochem Biophys* **563**: 13-21.
Liu J, Zhang Y, Xu R, Du J, Hu Z, Yang L, Chen Y, Zhu Y, Gu L. 2013. PI3K/Akt-dependent phosphorylation of GSK3beta and activation of RhoA regulate Wnt5a-induced gastric cancer cell migration. *Cell Signal* **25**: 447-456.
Loeppen S, Schneider D, Gaunitz F, Gebhardt R, Kurek R, Buchmann A, Schwarz M. 2002. Overexpression of glutamine synthetase is associated with beta-catenin-mutations in mouse liver tumors during promotion of hepatocarcinogenesis by phenobarbital. *Cancer Res* **62**: 5685-5688.
Lu J, Ye X, Fan F, Xia L, Bhattacharya R, Bellister S, Tozzi F, Sceusi E, Zhou Y, Tachibana I et al. 2013. Endothelial cells promote the colorectal cancer stem cell phenotype through a soluble form of Jagged-1. *Cancer Cell* **23**: 171-185.
Lui TT, Lacroix C, Ahmed SM, Goldenberg SJ, Leach CA, Daulat AM, Angers S. 2011. The ubiquitin-specific protease USP34 regulates axin stability and Wnt/beta-catenin signaling. *Mol Cell Biol* **31**: 2053-2065.
Lum L, Beachy PA. 2004. The Hedgehog response network: sensors, switches, and routers. *Science* **304**: 1755-1759.
Luo W, Peterson A, Garcia BA, Coombs G, Kofahl B, Heinrich R, Shabanowitz J, Hunt DF, Yost HJ, Virshup DM. 2007. Protein phosphatase 1 regulates assembly and function of the beta-catenin degradation complex. *Embo J* **26**: 1511-1521.
Lv ZD, Zhang L, Liu XP, Jin LY, Dong Q, Li FN, Wang HB, Kong B. 2015. NKD1 down-regulation is associated with poor prognosis in breast invasive ductal carcinoma. *Int J Clin Exp Pathol* **8**: 4015-4021.
Macpherson AJ, McCoy KD. 2015. Standardised animal models of host microbial mutualism. *Mucosal immunology* **8**: 476-486.
Madison BB, Braunstein K, Kuizon E, Portman K, Qiao XT, Gumucio DL. 2005. Epithelial hedgehog signals pattern the intestinal crypt-villus axis. *Development* **132**: 279-289.
Maeda S, Hikiba Y, Sakamoto K, Nakagawa H, Hirata Y, Hayakawa Y, Akanuma M. 2011. Colon cancer-derived factors activate NF-kappaB in myeloid cells via TLR2 to link inflammation and tumorigenesis. *Molecular medicine reports* **4**: 1083-1088.
Maetzel D, Denzel S, Mack B, Canis M, Went P, Benk M, Kieu C, Papior P, Baeuerle PA, Munz M et al. 2009. Nuclear signalling by tumour-associated antigen EpCAM. *Nat Cell Biol* **11**: 162-171.
Mahmoudi T, Li VS, Ng SS, Taouatas N, Vries RG, Mohammed S, Heck AJ, Clevers H. 2009. The kinase TNIK is an essential activator of Wnt target genes. *Embo J* **28**: 3329-3340.
Malinauskas T, Jones EY. 2014. Extracellular modulators of Wnt signalling. *Current opinion in structural biology* **29**: 77-84.
Mani SA, Guo W, Liao MJ, Eaton EN, Ayyanan A, Zhou AY, Brooks M, Reinhard F, Zhang CC, Shipitsin M et al. 2008. The epithelial-mesenchymal transition generates cells with properties of stem cells. *Cell* **133**: 704-715.
Manning BD, Cantley LC. 2007. AKT/PKB signaling: navigating downstream. *Cell* **129**: 1261-1274.
Mao B, Wu W, Davidson G, Marhold J, Li M, Mechler BM, Delius H, Hoppe D, Stannek P, Walter C et al. 2002. Kremen proteins are Dickkopf receptors that regulate Wnt/beta-catenin signalling. *Nature* **417**: 664-667.

Mao CD, Byers SW. 2011. Cell-context dependent TCF/LEF expression and function: alternative tales of repression, de-repression and activation potentials. *Critical reviews in eukaryotic gene expression* **21**: 207-236.
Martinez JA, Williams CS, Amann JM, Ellis TC, Moreno-Miralles I, Washington MK, Gregoli P, Hiebert SW. 2006. Deletion of Mtgr1 sensitizes the colonic epithelium to dextran sodium sulfate-induced colitis. *Gastroenterology* **131**: 579-588.
Martins M, McCarthy A, Baxendale R, Guichard S, Magno L, Kessaris N, El-Bahrawy M, Yu P, Katan M. 2014. Tumor suppressor role of phospholipase C epsilon in Ras-triggered cancers. *Proc Natl Acad Sci U S A* **111**: 4239-4244.
Matton N, Simonetti J, Williams K. 2000. Identification of mismatch repair protein complexes in HeLa nuclear extracts and their interaction with heteroduplex DNA. *J Biol Chem* **275**: 17808-17813.
McCain J. 2013. The MAPK (ERK) Pathway: Investigational Combinations for the Treatment Of BRAF-Mutated Metastatic Melanoma. *P & T : a peer-reviewed journal for formulary management* **38**: 96-108.
McEwen DG, Peifer M. 2001. Wnt signaling: the naked truth? *Curr Biol* **11**: R524-526.
McMahon AP. 2000. More surprises in the Hedgehog signaling pathway. *Cell* **100**: 185-188.
McMillan R, Matsui W. 2012. Molecular pathways: the hedgehog signaling pathway in cancer. *Clin Cancer Res* **18**: 4883-4888.
McNamara D, El-Omar E. 2008. Helicobacter pylori infection and the pathogenesis of gastric cancer: a paradigm for host-bacterial interactions. *Dig Liver Dis* **40**: 504-509.
Medzhitov R, Preston-Hurlburt P, Kopp E, Stadlen A, Chen C, Ghosh S, Janeway CA, Jr. 1998. MyD88 is an adaptor protein in the hToll/IL-1 receptor family signaling pathways. *Mol Cell* **2**: 253-258.
Meijer L, Skaltsounis AL, Magiatis P, Polychronopoulos P, Knockaert M, Leost M, Ryan XP, Vonica CA, Brivanlou A, Dajani R et al. 2003. GSK-3-selective inhibitors derived from Tyrian purple indirubins. *Chemistry & biology* **10**: 1255-1266.
Menendez A, Willing BP, Montero M, Wlodarska M, So CC, Bhinder G, Vallance BA, Finlay BB. 2013. Bacterial stimulation of the TLR-MyD88 pathway modulates the homeostatic expression of ileal Paneth cell alpha-defensins. *Journal of innate immunity* **5**: 39-49.
Meng RD, Shelton CC, Li YM, Qin LX, Notterman D, Paty PB, Schwartz GK. 2009. gamma-Secretase inhibitors abrogate oxaliplatin-induced activation of the Notch-1 signaling pathway in colon cancer cells resulting in enhanced chemosensitivity. *Cancer Res* **69**: 573-582.
Metcalfe C, Kljavin NM, Ybarra R, de Sauvage FJ. 2014. Lgr5+ stem cells are indispensable for radiation-induced intestinal regeneration. *Cell Stem Cell* **14**: 149-159.
Mi K, Dolan PJ, Johnson GV. 2006. The low density lipoprotein receptor-related protein 6 interacts with glycogen synthase kinase 3 and attenuates activity. *J Biol Chem* **281**: 4787-4794.
Michalopoulos GK. 2007. Liver regeneration. *J Cell Physiol* **213**: 286-300.
Mills JC, Shivdasani RA. 2011. Gastric epithelial stem cells. *Gastroenterology* **140**: 412-424.
Miura H, Miyazaki T, Kuroda M, Oka T, Machinami R, Kodama T, Shibuya M, Makuuchi M, Yazaki Y, Ohnishi S. 1997. Increased expression of vascular endothelial growth factor in human hepatocellular carcinoma. *J Hepatol* **27**: 854-861.
Miyazaki K, Fujita T, Ozaki T, Kato C, Kurose Y, Sakamoto M, Kato S, Goto T, Itoyama Y, Aoki M et al. 2004. NEDL1, a novel ubiquitin-protein isopeptide ligase for dishevelled-1, targets mutant superoxide dismutase-1. *J Biol Chem* **279**: 11327-11335.
Miyazono K. 2000. TGF-beta signaling by Smad proteins. *Cytokine Growth Factor Rev* **11**: 15-22.
Mo ML, Li MR, Chen Z, Liu XW, Sheng Q, Zhou HM. 2013. Inhibition of the Wnt palmitoyltransferase porcupine suppresses cell growth and downregulates the Wnt/beta-catenin pathway in gastric cancer. *Oncology letters* **5**: 1719-1723.

Mohammad HP, Zhang W, Prevas HS, Leadem BR, Zhang M, Herman JG, Hooker CM, Watkins DN, Karim B, Huso DL et al. 2011. Loss of a single Hic1 allele accelerates polyp formation in Apc(Delta716) mice. *Oncogene* **30**: 2659-2669.

Monga SP. 2015. beta-Catenin Signaling and Roles in Liver Homeostasis, Injury, and Tumorigenesis. *Gastroenterology* **148**: 1294-1310.

Monga SP, Mars WM, Pediaditakis P, Bell A, Mule K, Bowen WC, Wang X, Zarnegar R, Michalopoulos GK. 2002. Hepatocyte growth factor induces Wnt-independent nuclear translocation of beta-catenin after Met-beta-catenin dissociation in hepatocytes. *Cancer Res* **62**: 2064-2071.

Moore AC, Amann JM, Williams CS, Tahinci E, Farmer TE, Martinez JA, Yang G, Luce KS, Lee E, Hiebert SW. 2008. Myeloid translocation gene family members associate with T-cell factors (TCFs) and influence TCF-dependent transcription. *Mol Cell Biol* **28**: 977-987.

Morin PJ, Sparks AB, Korinek V, Barker N, Clevers H, Vogelstein B, Kinzler KW. 1997. Activation of beta-catenin-Tcf signaling in colon cancer by mutations in beta-catenin or APC [see comments]. *Science* **275**: 1787-1790.

Morita H, Mazerbourg S, Bouley DM, Luo CW, Kawamura K, Kuwabara Y, Baribault H, Tian H, Hsueh AJ. 2004. Neonatal lethality of LGR5 null mice is associated with ankyloglossia and gastrointestinal distension. *Mol Cell Biol* **24**: 9736-9743.

Mosimann C, Hausmann G, Basler K. 2006. Parafibromin/Hyrax activates Wnt/Wg target gene transcription by direct association with beta-catenin/Armadillo. *Cell* **125**: 327-341.

-. 2009. Beta-catenin hits chromatin: regulation of Wnt target gene activation. *Nat Rev Mol Cell Biol* **10**: 276-286.

Muncan V, Faro A, Haramis AP, Hurlstone AF, Wienholds E, van Es J, Korving J, Begthel H, Zivkovic D, Clevers H. 2007. T-cell factor 4 (Tcf7l2) maintains proliferative compartments in zebrafish intestine. *EMBO Rep* **8**: 966-973.

Mundade R, Imperiale TF, Prabhu L, Loehrer PJ, Lu T. 2014. Genetic pathways, prevention, and treatment of sporadic colorectal cancer. *Oncoscience* **1**: 400-406.

Munoz J, Stange DE, Schepers AG, van de Wetering M, Koo BK, Itzkovitz S, Volckmann R, Kung KS, Koster J, Radulescu S et al. 2012. The Lgr5 intestinal stem cell signature: robust expression of proposed quiescent '+4' cell markers. *Embo J* **31**: 3079-3091.

Nakatsuru S, Yanagisawa A, Furukawa Y, Ichii S, Kato Y, Nakamura Y, Horii A. 1993. Somatic mutations of the APC gene in precancerous lesion of the stomach. *Hum Mol Genet* **2**: 1463-1465.

Nam KT, Lee HJ, Sousa JF, Weis VG, O'Neal RL, Finke PE, Romero-Gallo J, Shi G, Mills JC, Peek RM, Jr. et al. 2010. Mature chief cells are cryptic progenitors for metaplasia in the stomach. *Gastroenterology* **139**: 2028-2037 e2029.

Nam KT, Varro A, Coffey RJ, Goldenring JR. 2007. Potentiation of oxyntic atrophy-induced gastric metaplasia in amphiregulin-deficient mice. *Gastroenterology* **132**: 1804-1819.

Nejak-Bowen K, Monga SP. 2008. Wnt/beta-catenin signaling in hepatic organogenesis. *Organogenesis* **4**: 92-99.

Nejak-Bowen KN, Thompson MD, Singh S, Bowen WC, Jr., Dar MJ, Khillan J, Dai C, Monga SP. 2010. Accelerated liver regeneration and hepatocarcinogenesis in mice overexpressing serine-45 mutant beta-catenin. *Hepatology* **51**: 1603-1613.

Nejak-Bowen KN, Zeng G, Tan X, Cieply B, Monga SP. 2009. Beta-catenin regulates vitamin C biosynthesis and cell survival in murine liver. *J Biol Chem* **284**: 28115-28127.

Ness RB, Cauley JA. 2004. Antibiotics and breast cancer--what's the meaning of this? *JAMA* **291**: 880-881.

Neufeld KL, Nix DA, Bogerd H, Kang Y, Beckerle MC, Cullen BR, White RL. 2000a. Adenomatous polyposis coli protein contains two nuclear export signals and shuttles between the nucleus and cytoplasm. *Proc Natl Acad Sci U S A* **97**: 12085-12090.

Neufeld KL, Zhang F, Cullen BR, White RL. 2000b. APC-mediated downregulation of beta-catenin activity involves nuclear sequestration and nuclear export. *EMBO Rep* **1**: 519-523.

Ni J, Cozzi P, Hao J, Duan W, Graham P, Kearsley J, Li Y. 2014. Cancer stem cells in prostate cancer chemoresistance. *Current cancer drug targets* **14**: 225-240.
Nielsen M, Morreau H, Vasen HF, Hes FJ. 2011. MUTYH-associated polyposis (MAP). *Critical reviews in oncology/hematology* **79**: 1-16.
Niers LE, Timmerman HM, Rijkers GT, van Bleek GM, van Uden NO, Knol EF, Kapsenberg ML, Kimpen JL, Hoekstra MO. 2005. Identification of strong interleukin-10 inducing lactic acid bacteria which down-regulate T helper type 2 cytokines. *Clin Exp Allergy* **35**: 1481-1489.
Nievergall E, Lackmann M, Janes PW. 2012. Eph-dependent cell-cell adhesion and segregation in development and cancer. *Cell Mol Life Sci* **69**: 1813-1842.
Nigam A. 2013. Breast cancer stem cells, pathways and therapeutic perspectives 2011. *The Indian journal of surgery* **75**: 170-180.
Nishi S, Hsu SY, Zell K, Hsueh AJ. 2000. Characterization of two fly LGR (leucine-rich repeat-containing, G protein-coupled receptor) proteins homologous to vertebrate glycoprotein hormone receptors: constitutive activation of wild-type fly LGR1 but not LGR2 in transfected mammalian cells. *Endocrinology* **141**: 4081-4090.
Nishisho I, Nakamura Y, Miyoshi Y, Miki Y, Ando H, Horii A, Koyama K, Utsunomiya J, Baba S, Hedge P. 1991. Mutations of chromosome 5q21 genes in FAP and colorectal cancer patients. *Science* **253**: 665-669.
Nishiya N, Oku Y, Kumagai Y, Sato Y, Yamaguchi E, Sasaki A, Shoji M, Ohnishi Y, Okamoto H, Uehara Y. 2014. A zebrafish chemical suppressor screening identifies small molecule inhibitors of the Wnt/beta-catenin pathway. *Chemistry & biology* **21**: 530-540.
Norheim Andersen S, Lovig T, Fausa O, Rognum TO. 1999. Germline and somatic mutations in exon 15 of the APC gene and K-ras mutations in duodenal adenomas in patients with familial adenomatous polyposis. *Scand J Gastroenterol* **34**: 611-617.
Numata M, Oshima T. 2012. Significance of regenerating islet-derived type IV gene expression in gastroenterological cancers. *World J Gastroenterol* **18**: 3502-3510.
Nusse R, Varmus HE. 1982. Many tumors induced by the mouse mammary tumor virus contain a provirus integrated in the same region of the host genome. *Cell* **31**: 99-109.
-. 1992. Wnt genes. *Cell* **69**: 1073-1087.
O'Brien CA, Pollett A, Gallinger S, Dick JE. 2007. A human colon cancer cell capable of initiating tumour growth in immunodeficient mice. *Nature* **445**: 106-110.
Ogawa K, Takemoto N, Ishii M, Pasquale EB, Nakajima T. 2011. Complementary expression and repulsive signaling suggest that EphB receptors and ephrin-B ligands control cell positioning in the gastric epithelium. *Histochemistry and cell biology* **136**: 617-636.
Ohtsubo T, Nishioka K, Imaiso Y, Iwai S, Shimokawa H, Oda H, Fujiwara T, Nakabeppu Y. 2000. Identification of human MutY homolog (hMYH) as a repair enzyme for 2-hydroxyadenine in DNA and detection of multiple forms of hMYH located in nuclei and mitochondria. *Nucleic Acids Res* **28**: 1355-1364.
Oishi N, Wang XW. 2011. Novel therapeutic strategies for targeting liver cancer stem cells. *International journal of biological sciences* **7**: 517-535.
Okumura T, Ericksen RE, Takaishi S, Wang SS, Dubeykovskiy Z, Shibata W, Betz KS, Muthupalani S, Rogers AB, Fox JG et al. 2010. K-ras mutation targeted to gastric tissue progenitor cells results in chronic inflammation, an altered microenvironment, and progression to intraepithelial neoplasia. *Cancer Res* **70**: 8435-8445.
Oliveira C, Sousa S, Pinheiro H, Karam R, Bordeira-Carrico R, Senz J, Kaurah P, Carvalho J, Pereira R, Gusmao L et al. 2009. Quantification of epigenetic and genetic 2nd hits in CDH1 during hereditary diffuse gastric cancer syndrome progression. *Gastroenterology* **136**: 2137-2148.
Ooi CH, Ivanova T, Wu J, Lee M, Tan IB, Tao J, Ward L, Koo JH, Gopalakrishnan V, Zhu Y et al. 2009. Oncogenic pathway combinations predict clinical prognosis in gastric cancer. *PLoS Genet* **5**: e1000676.
Ootani A, Li X, Sangiorgi E, Ho QT, Ueno H, Toda S, Sugihara H, Fujimoto K, Weissman IL, Capecchi MR et al. 2009. Sustained in vitro intestinal epithelial culture within a Wnt-dependent stem cell niche. *Nature medicine* **15**: 701-706.

Ormanns S, Neumann J, Horst D, Kirchner T, Jung A. 2014. WNT signaling and distant metastasis in colon cancer through transcriptional activity of nuclear beta-Catenin depend on active PI3K signaling. *Oncotarget* **5**: 2999-3011.

Ostman S, Rask C, Wold AE, Hultkrantz S, Telemo E. 2006. Impaired regulatory T cell function in germ-free mice. *European journal of immunology* **36**: 2336-2346.

Ovejero C, Cavard C, Perianin A, Hakvoort T, Vermeulen J, Godard C, Fabre M, Chafey P, Suzuki K, Romagnolo B et al. 2004. Identification of the leukocyte cell-derived chemotaxin 2 as a direct target gene of beta-catenin in the liver. *Hepatology* **40**: 167-176.

Ozawa M, Baribault H, Kemler R. 1989. The cytoplasmic domain of the cell adhesion molecule uvomorulin associates with three independent proteins structurally related in different species. *EMBO J* **8**: 1711-1717.

Palm NW, de Zoete MR, Flavell RA. 2015. Immune-microbiota interactions in health and disease. *Clinical immunology*.

Paluszczak J, Sarbak J, Kostrzewska-Poczekaj M, Kiwerska K, Jarmuz-Szymczak M, Grenman R, Mielcarek-Kuchta D, Baer-Dubowska W. 2015. The negative regulators of Wnt pathway-DACH1, DKK1, and WIF1 are methylated in oral and oropharyngeal cancer and WIF1 methylation predicts shorter survival. *Tumour biology : the journal of the International Society for Oncodevelopmental Biology and Medicine* **36**: 2855-2861.

Pan D. 2010. The hippo signaling pathway in development and cancer. *Dev Cell* **19**: 491-505.

Pan WJ, Pang SZ, Huang T, Guo HY, Wu D, Li L. 2004. Characterization of function of three domains in dishevelled-1: DEP domain is responsible for membrane translocation of dishevelled-1. *Cell Res* **14**: 324-330.

Pang R, Law WL, Chu AC, Poon JT, Lam CS, Chow AK, Ng L, Cheung LW, Lan XR, Lan HY et al. 2010. A subpopulation of CD26+ cancer stem cells with metastatic capacity in human colorectal cancer. *Cell Stem Cell* **6**: 603-615.

Park WH, Jung CW, Park JO, Kim K, Kim WS, Im YH, Lee MH, Kang WK, Park K. 2003a. Monensin inhibits the growth of renal cell carcinoma cells via cell cycle arrest or apoptosis. *Int J Oncol* **22**: 855-860.

Park WH, Kim ES, Jung CW, Kim BK, Lee YY. 2003b. Monensin-mediated growth inhibition of SNU-C1 colon cancer cells via cell cycle arrest and apoptosis. *Int J Oncol* **22**: 377-382.

Park WH, Kim ES, Kim BK, Lee YY. 2003c. Monensin-mediated growth inhibition in NCI-H929 myeloma cells via cell cycle arrest and apoptosis. *Int J Oncol* **23**: 197-204.

Park WH, Seol JG, Kim ES, Kang WK, Im YH, Jung CW, Kim BK, Lee YY. 2002. Monensin-mediated growth inhibition in human lymphoma cells through cell cycle arrest and apoptosis. *Br J Haematol* **119**: 400-407.

Park WS, Oh RR, Park JY, Lee SH, Shin MS, Kim YS, Kim SY, Lee HK, Kim PJ, Oh ST et al. 1999. Frequent somatic mutations of the beta-catenin gene in intestinal-type gastric cancer. *Cancer Res* **59**: 4257-4260.

Paulino VM, Yang Z, Kloss J, Ennis MJ, Armstrong BA, Loftus JC, Tran NL. 2010. TROY (TNFRSF19) is overexpressed in advanced glial tumors and promotes glioblastoma cell invasion via Pyk2-Rac1 signaling. *Mol Cancer Res* **8**: 1558-1567.

Pehlivan S, Artac M, Sever T, Bozcuk H, Kilincarslan C, Pehlivan M. 2010. Gene methylation of SFRP2, P16, DAPK1, HIC1, and MGMT and KRAS mutations in sporadic colorectal cancer. *Cancer Genet Cytogenet* **201**: 128-132.

Pellegrinet L, Rodilla V, Liu Z, Chen S, Koch U, Espinosa L, Kaestner KH, Kopan R, Lewis J, Radtke F. 2011. Dll1- and dll4-mediated notch signaling are required for homeostasis of intestinal stem cells. *Gastroenterology* **140**: 1230-1240 e1231-1237.

Perez White BE, Getsios S. 2014. Eph receptor and ephrin function in breast, gut, and skin epithelia. *Cell adhesion & migration* **8**: 327-338.

Perri F, Cotugno R, Piepoli A, Merla A, Quitadamo M, Gentile A, Pilotto A, Annese V, Andriulli A. 2007. Aberrant DNA methylation in non-neoplastic gastric mucosa of H. Pylori infected patients and effect of eradication. *Am J Gastroenterol* **102**: 1361-1371.

Perrimon N. 1994. The genetic basis of patterned baldness in Drosophila. *Cell* **76**: 781-784.

Peterson DA, McNulty NP, Guruge JL, Gordon JI. 2007. IgA response to symbiotic bacteria as a mediator of gut homeostasis. *Cell Host Microbe* **2**: 328-339.
Philpott A, Winton DJ. 2014. Lineage selection and plasticity in the intestinal crypt. *Curr Opin Cell Biol* **31**: 39-45.
Piao S, Lee SH, Kim H, Yum S, Stamos JL, Xu Y, Lee SJ, Lee J, Oh S, Han JK et al. 2008. Direct inhibition of GSK3beta by the phosphorylated cytoplasmic domain of LRP6 in Wnt/beta-catenin signaling. *PLoS One* **3**: e4046.
Piazzi G, Fini L, Selgrad M, Garcia M, Daoud Y, Wex T, Malfertheiner P, Gasbarrini A, Romano M, Meyer RL et al. 2011. Epigenetic regulation of Delta-Like1 controls Notch1 activation in gastric cancer. *Oncotarget* **2**: 1291-1301.
Pin C. 2012. A new class of transcription factors? *BioEssays : news and reviews in molecular, cellular and developmental biology* **34**: 6.
Pispa J, Mikkola ML, Mustonen T, Thesleff I. 2003. Ectodysplasin, Edar and TNFRSF19 are expressed in complementary and overlapping patterns during mouse embryogenesis. *Gene expression patterns* **3**: 675-679.
Pispa J, Pummila M, Barker PA, Thesleff I, Mikkola ML. 2008. Edar and Troy signalling pathways act redundantly to regulate initiation of hair follicle development. *Hum Mol Genet* **17**: 3380-3391.
Port F, Basler K. 2010. Wnt trafficking: new insights into Wnt maturation, secretion and spreading. *Traffic* **11**: 1265-1271.
Potten CS. 1998. Stem cells in gastrointestinal epithelium: numbers, characteristics and death. *Philos Trans R Soc Lond B Biol Sci* **353**: 821-830.
Potten CS, Kovacs L, Hamilton E. 1974. Continuous labelling studies on mouse skin and intestine. *Cell and tissue kinetics* **7**: 271-283.
Poutahidis T, Cappelle K, Levkovich T, Lee CW, Doulberis M, Ge Z, Fox JG, Horwitz BH, Erdman SE. 2013. Pathogenic intestinal bacteria enhance prostate cancer development via systemic activation of immune cells in mice. *PLoS One* **8**: e73933.
Poutahidis T, Haigis KM, Rao VP, Nambiar PR, Taylor CL, Ge Z, Watanabe K, Davidson A, Horwitz BH, Fox JG et al. 2007. Rapid reversal of interleukin-6-dependent epithelial invasion in a mouse model of microbially induced colon carcinoma. *Carcinogenesis* **28**: 2614-2623.
Powell AE, Wang Y, Li Y, Poulin EJ, Means AL, Washington MK, Higginbotham JN, Juchheim A, Prasad N, Levy SE et al. 2012. The Pan-ErbB Negative Regulator Lrig1 Is an Intestinal Stem Cell Marker that Functions as a Tumor Suppressor. *Cell* **149**: 146-158.
Pressman BC. 1968. Ionophorous antibiotics as models for biological transport. *Federation proceedings* **27**: 1283-1288.
-. 1976. Biological applications of ionophores. *Annual review of biochemistry* **45**: 501-530.
Price MA. 2006. CKI, there's more than one: casein kinase I family members in Wnt and Hedgehog signaling. *Genes Dev* **20**: 399-410.
Qi J, Zhu YQ, Luo J, Tao WH. 2006. Hypermethylation and expression regulation of secreted frizzled-related protein genes in colorectal tumor. *World J Gastroenterol* **12**: 7113-7117.
Qiao XT, Ziel JW, McKimpson W, Madison BB, Todisco A, Merchant JL, Samuelson LC, Gumucio DL. 2007. Prospective identification of a multilineage progenitor in murine stomach epithelium. *Gastroenterology* **133**: 1989-1998.
Qiao Y, Jiang X, Lee ST, Karuturi RK, Hooi SC, Yu Q. 2011. FOXQ1 regulates epithelial-mesenchymal transition in human cancers. *Cancer Res* **71**: 3076-3086.
Qiu W, Hu Y, Andersen TE, Jafari A, Li N, Chen W, Kassem M. 2010. Tumor necrosis factor receptor superfamily member 19 (TNFRSF19) regulates differentiation fate of human mesenchymal (stromal) stem cells through canonical Wnt signaling and C/EBP. *J Biol Chem* **285**: 14438-14449.
Quante M, Marrache F, Goldenring JR, Wang TC. 2010. TFF2 mRNA transcript expression marks a gland progenitor cell of the gastric oxyntic mucosa. *Gastroenterology* **139**: 2018-2027 e2012.

Rafa L, Dessein AF, Devisme L, Buob D, Truant S, Porchet N, Huet G, Buisine MP, Lesuffleur T. 2010. REG4 acts as a mitogenic, motility and pro-invasive factor for colon cancer cells. *Int J Oncol* **36**: 689-698.

Rakoff-Nahoum S, Paglino J, Eslami-Varzaneh F, Edberg S, Medzhitov R. 2004. Recognition of commensal microflora by toll-like receptors is required for intestinal homeostasis. *Cell* **118**: 229-241.

Ramsey VG, Doherty JM, Chen CC, Stappenbeck TS, Konieczny SF, Mills JC. 2007. The maturation of mucus-secreting gastric epithelial progenitors into digestive-enzyme secreting zymogenic cells requires Mist1. *Development* **134**: 211-222.

Rao VP, Poutahidis T, Ge Z, Nambiar PR, Boussahmain C, Wang YY, Horwitz BH, Fox JG, Erdman SE. 2006. Innate immune inflammatory response against enteric bacteria Helicobacter hepaticus induces mammary adenocarcinoma in mice. *Cancer Res* **66**: 7395-7400.

Rashid S, Pilecka I, Torun A, Olchowik M, Bielinska B, Miaczynska M. 2009. Endosomal adaptor proteins APPL1 and APPL2 are novel activators of beta-catenin/TCF-mediated transcription. *J Biol Chem* **284**: 18115-18128.

Rattner A, Hsieh JC, Smallwood PM, Gilbert DJ, Copeland NG, Jenkins NA, Nathans J. 1997. A family of secreted proteins contains homology to the cysteine-rich ligand-binding domain of frizzled receptors. *Proc Natl Acad Sci U S A* **94**: 2859-2863.

Ravindranath AJ, Cadigan KM. 2014. Structure-function analysis of the C-clamp of TCF/Pangolin in Wnt/ss-catenin signaling. *PLoS One* **9**: e86180.

Reedijk M, Odorcic S, Zhang H, Chetty R, Tennert C, Dickson BC, Lockwood G, Gallinger S, Egan SE. 2008. Activation of Notch signaling in human colon adenocarcinoma. *Int J Oncol* **33**: 1223-1229.

Rehfeld JF, Friis-Hansen L, Goetze JP, Hansen TV. 2007. The biology of cholecystokinin and gastrin peptides. *Curr Top Med Chem* **7**: 1154-1165.

Rennoll SA, Konsavage WM, Jr., Yochum GS. 2014. Nuclear AXIN2 represses MYC gene expression. *Biochem Biophys Res Commun* **443**: 217-222.

Resende C, Thiel A, Machado JC, Ristimaki A. 2011. Gastric cancer: basic aspects. *Helicobacter* **16 Suppl 1**: 38-44.

Rhyu MG, Park WS, Jung YJ, Choi SW, Meltzer SJ. 1994. Allelic deletions of MCC/APC and p53 are frequent late events in human gastric carcinogenesis. *Gastroenterology* **106**: 1584-1588.

Ricci-Vitiani L, Lombardi DG, Pilozzi E, Biffoni M, Todaro M, Peschle C, De Maria R. 2007. Identification and expansion of human colon-cancer-initiating cells. *Nature* **445**: 111-115.

Ring DB, Johnson KW, Henriksen EJ, Nuss JM, Goff D, Kinnick TR, Ma ST, Reeder JW, Samuels I, Slabiak T et al. 2003. Selective glycogen synthase kinase 3 inhibitors potentiate insulin activation of glucose transport and utilization in vitro and in vivo. *Diabetes* **52**: 588-595.

Ritsma L, Ellenbroek SI, Zomer A, Snippert HJ, de Sauvage FJ, Simons BD, Clevers H, van Rheenen J. 2014. Intestinal crypt homeostasis revealed at single-stem-cell level by in vivo live imaging. *Nature* **507**: 362-365.

Robertson JK, Danzmann K, Charles S, Blake K, Olivares A, Bamikole S, Olson M, Van Raay TJ. 2014. Targeting the Wnt pathway in zebrafish as a screening method to identify novel therapeutic compounds. *Exp Biol Med (Maywood)* **239**: 169-176.

Romero-Lanman EE, Pavlovic S, Amlani B, Chin Y, Benezra R. 2012. Id1 maintains embryonic stem cell self-renewal by up-regulation of Nanog and repression of Brachyury expression. *Stem Cells Dev* **21**: 384-393.

Roncucci L, Ponz de Leon M, Scalmati A, Malagoli G, Pratissoli S, Perini M, Chahin NJ. 1988. The influence of age on colonic epithelial cell proliferation. *Cancer* **62**: 2373-2377.

Rook GA, Dalgleish A. 2011. Infection, immunoregulation, and cancer. *Immunol Rev* **240**: 141-159.

Rossig L, Jadidi AS, Urbich C, Badorff C, Zeiher AM, Dimmeler S. 2001. Akt-dependent phosphorylation of p21(Cip1) regulates PCNA binding and proliferation of endothelial cells. *Mol Cell Biol* **21**: 5644-5657.

Rothenberg ME, Nusse Y, Kalisky T, Lee JJ, Dalerba P, Scheeren F, Lobo N, Kulkarni S, Sim S, Qian D et al. 2012. Identification of a cKit(+) Colonic Crypt Base Secretory Cell That Supports Lgr5(+) Stem Cells in Mice. *Gastroenterology*.

Round JL, Mazmanian SK. 2010. Inducible Foxp3+ regulatory T-cell development by a commensal bacterium of the intestinal microbiota. *Proc Natl Acad Sci U S A* **107**: 12204-12209.

Rousset R, Mack JA, Wharton KA, Jr., Axelrod JD, Cadigan KM, Fish MP, Nusse R, Scott MP. 2001. Naked cuticle targets dishevelled to antagonize Wnt signal transduction. *Genes Dev* **15**: 658-671.

Rubin LL, de Sauvage FJ. 2006. Targeting the Hedgehog pathway in cancer. *Nat Rev Drug Discov* **5**: 1026-1033.

Rubinfeld B, Robbins P, El-Gamil M, Albert I, Porfiri E, Polakis P. 1997. Stabilization of beta-catenin by genetic defects in melanoma cell lines. *Science* **275**: 1790-1792.

Rubinfeld B, Souza B, Albert I, Muller O, Chamberlain SH, Masiarz FR, Munemitsu S, Polakis P. 1993. Association of the APC gene product with beta-catenin. *Science* **262**: 1731-1734.

Ruffner H, Sprunger J, Charlat O, Leighton-Davies J, Grosshans B, Salathe A, Zietzling S, Beck V, Therier M, Isken A et al. 2012. R-Spondin potentiates Wnt/beta-catenin signaling through orphan receptors LGR4 and LGR5. *PLoS One* **7**: e40976.

Rustgi AK. 2013. BRAF: a driver of the serrated pathway in colon cancer. *Cancer Cell* **24**: 1-2.

Saeki H, Tanaka S, Tokunaga E, Kawaguchi H, Ikeda Y, Maehara Y, Sugimachi K. 2001. Genetic alterations in the human Tcf-4 gene in Japanese patients with sporadic gastrointestinal cancers with microsatellite instability. *Oncology* **61**: 156-161.

Sachdev S, Bruhn L, Sieber H, Pichler A, Melchior F, Grosschedl R. 2001. PIASy, a nuclear matrix-associated SUMO E3 ligase, represses LEF1 activity by sequestration into nuclear bodies. *Genes Dev* **15**: 3088-3103.

Saikawa Y, Fukuda K, Takahashi T, Nakamura R, Takeuchi H, Kitagawa Y. 2010. Gastric carcinogenesis and the cancer stem cell hypothesis. *Gastric Cancer* **13**: 11-24.

Saito T, Mitomi H, Imamhasan A, Hayashi T, Mitani K, Takahashi M, Kajiyama Y, Yao T. 2014. Downregulation of sFRP-2 by epigenetic silencing activates the beta-catenin/Wnt signaling pathway in esophageal basaloid squamous cell carcinoma. *Virchows Arch* **464**: 135-143.

Sangiorgi E, Capecchi MR. 2008. Bmi1 is expressed in vivo in intestinal stem cells. *Nature genetics* **40**: 915-920.

Sato T, van Es JH, Snippert HJ, Stange DE, Vries RG, van den Born M, Barker N, Shroyer NF, van de Wetering M, Clevers H. 2011. Paneth cells constitute the niche for Lgr5 stem cells in intestinal crypts. *Nature* **469**: 415-418.

Sato T, Vries RG, Snippert HJ, van de Wetering M, Barker N, Stange DE, van Es JH, Abo A, Kujala P, Peters PJ et al. 2009. Single Lgr5 stem cells build crypt-villus structures in vitro without a mesenchymal niche. *Nature* **459**: 262-265.

Satow R, Hirano T, Batori R, Nakamura T, Murayama Y, Fukami K. 2014. Phospholipase Cdelta1 induces E-cadherin expression and suppresses malignancy in colorectal cancer cells. *Proc Natl Acad Sci U S A* **111**: 13505-13510.

Sekine A, Akiyama Y, Yanagihara K, Yuasa Y. 2006a. Hath1 up-regulates gastric mucin gene expression in gastric cells. *Biochem Biophys Res Commun* **344**: 1166-1171.

Sekine S, Lan BY, Bedolli M, Feng S, Hebrok M. 2006b. Liver-specific loss of beta-catenin blocks glutamine synthesis pathway activity and cytochrome p450 expression in mice. *Hepatology* **43**: 817-825.

Sekiya T, Zaret KS. 2007. Repression by Groucho/TLE/Grg proteins: genomic site recruitment generates compacted chromatin in vitro and impairs activator binding in vivo. *Mol Cell* **28**: 291-303.

Semenov MV, Tamai K, Brott BK, Kuhl M, Sokol S, He X. 2001. Head inducer Dickkopf-1 is a ligand for Wnt coreceptor LRP6. *Curr Biol* **11**: 951-961.
Shao Z, Browning JL, Lee X, Scott ML, Shulga-Morskaya S, Allaire N, Thill G, Levesque M, Sah D, McCoy JM et al. 2005. TAJ/TROY, an orphan TNF receptor family member, binds Nogo-66 receptor 1 and regulates axonal regeneration. *Neuron* **45**: 353-359.
Sharma M, Jamieson C, Johnson M, Molloy MP, Henderson BR. 2012. Specific armadillo repeat sequences facilitate beta-catenin nuclear transport in live cells via direct binding to nucleoporins Nup62, Nup153, and RanBP2/Nup358. *J Biol Chem* **287**: 819-831.
Sharma M, Jamieson C, Lui C, Henderson BR. 2014. The hydrophobic rich N- and C-terminal tails of beta-catenin facilitate nuclear import of beta-catenin. *J Biol Chem*.
Sharma RP, Chopra VL. 1976. Effect of the Wingless (wg1) mutation on wing and haltere development in Drosophila melanogaster. *Dev Biol* **48**: 461-465.
Sherman AE, Zavros Y. 2011. Role of Sonic Hedgehog signaling during progression from inflammation to cancer in the stomach. *World journal of gastrointestinal pathophysiology* **2**: 103-108.
Shinohara M, Mao M, Keeley TM, El-Zaatari M, Lee HJ, Eaton KA, Samuelson LC, Merchant JL, Goldenring JR, Todisco A. 2010. Bone morphogenetic protein signaling regulates gastric epithelial cell development and proliferation in mice. *Gastroenterology* **139**: 2050-2060 e2052.
Shiota S, Suzuki R, Yamaoka Y. 2013. The significance of virulence factors in Helicobacter pylori. *Journal of digestive diseases* **14**: 341-349.
Shitashige M, Satow R, Honda K, Ono M, Hirohashi S, Yamada T. 2008. Regulation of Wnt signaling by the nuclear pore complex. *Gastroenterology* **134**: 1961-1971, 1971 e1961-1964.
Shitashige M, Satow R, Jigami T, Aoki K, Honda K, Shibata T, Ono M, Hirohashi S, Yamada T. 2010. Traf2- and Nck-interacting kinase is essential for Wnt signaling and colorectal cancer growth. *Cancer Res* **70**: 5024-5033.
Schepers A, Clevers H. 2012. Wnt signaling, stem cells, and cancer of the gastrointestinal tract. *Cold Spring Harb Perspect Biol* **4**: a007989.
Schnare M, Barton GM, Holt AC, Takeda K, Akira S, Medzhitov R. 2001. Toll-like receptors control activation of adaptive immune responses. *Nat Immunol* **2**: 947-950.
Schon S, Flierman I, Ofner A, Stahringer A, Holdt LM, Kolligs FT, Herbst A. 2014. beta-catenin regulates NF-kappaB activity via TNFRSF19 in colorectal cancer cells. *Int J Cancer* **135**: 1800-1811.
Schulte G, Bryja V. 2007. The Frizzled family of unconventional G-protein-coupled receptors. *Trends in pharmacological sciences* **28**: 518-525.
Schulze WX, Deng L, Mann M. 2005. Phosphotyrosine interactome of the ErbB-receptor kinase family. *Molecular systems biology* **1**: 2005 0008.
Schwab KR, Patterson LT, Hartman HA, Song N, Lang RA, Lin X, Potter SS. 2007. Pygo1 and Pygo2 roles in Wnt signaling in mammalian kidney development. *BMC Biol* **5**: 15.
Schwarz-Romond T, Fiedler M, Shibata N, Butler PJ, Kikuchi A, Higuchi Y, Bienz M. 2007. The DIX domain of Dishevelled confers Wnt signaling by dynamic polymerization. *Nat Struct Mol Biol* **14**: 484-492.
Schweizer L, Varmus H. 2003. Wnt/Wingless signaling through beta-catenin requires the function of both LRP/Arrow and frizzled classes of receptors. *BMC cell biology* **4**: 4.
Schwitalla S, Fingerle AA, Cammareri P, Nebelsiek T, Goktuna SI, Ziegler PK, Canli O, Heijmans J, Huels DJ, Moreaux G et al. 2013. Intestinal tumorigenesis initiated by dedifferentiation and acquisition of stem-cell-like properties. *Cell* **152**: 25-38.
Sikandar SS, Pate KT, Anderson S, Dizon D, Edwards RA, Waterman ML, Lipkin SM. 2010. NOTCH signaling is required for formation and self-renewal of tumor-initiating cells and for repression of secretory cell differentiation in colon cancer. *Cancer Res* **70**: 1469-1478.
Silva AL, Dawson SN, Arends MJ, Guttula K, Hall N, Cameron EA, Huang TH, Brenton JD, Tavare S, Bienz M et al. 2014. Boosting Wnt activity during colorectal cancer

progression through selective hypermethylation of Wnt signaling antagonists. *BMC Cancer* **14**: 891.
Simmini S, Bialecka M, Huch M, Kester L, van de Wetering M, Sato T, Beck F, van Oudenaarden A, Clevers H, Deschamps J. 2014. Transformation of intestinal stem cells into gastric stem cells on loss of transcription factor Cdx2. *Nat Commun* **5**: 5728.
Slattery ML. 2000. Diet, lifestyle, and colon cancer. *Seminars in gastrointestinal disease* **11**: 142-146.
Smith K, McCoy KD, Macpherson AJ. 2007. Use of axenic animals in studying the adaptation of mammals to their commensal intestinal microbiota. *Seminars in immunology* **19**: 59-69.
Snippert HJ, Haegebarth A, Kasper M, Jaks V, van Es JH, Barker N, van de Wetering M, van den Born M, Begthel H, Vries RG et al. 2010. Lgr6 marks stem cells in the hair follicle that generate all cell lineages of the skin. *Science* **327**: 1385-1389.
Solanas G, Cortina C, Sevillano M, Batlle E. 2011. Cleavage of E-cadherin by ADAM10 mediates epithelial cell sorting downstream of EphB signalling. *Nat Cell Biol* **13**: 1100-1107.
Sommer F, Backhed F. 2013. The gut microbiota--masters of host development and physiology. *Nature reviews Microbiology* **11**: 227-238.
Song L, Li Y, He B, Gong Y. 2015. Development of Small Molecules Targeting the Wnt Signaling Pathway in Cancer Stem Cells for the Treatment of Colorectal Cancer. *Clinical colorectal cancer*.
Song N, Schwab KR, Patterson LT, Yamaguchi T, Lin X, Potter SS, Lang RA. 2007. pygopus 2 has a crucial, Wnt pathway-independent function in lens induction. *Development* **134**: 1873-1885.
Song Z, Yue W, Wei B, Wang N, Li T, Guan L, Shi S, Zeng Q, Pei X, Chen L. 2011. Sonic hedgehog pathway is essential for maintenance of cancer stem-like cells in human gastric cancer. *PLoS One* **6**: e17687.
Spanjaard RA, Whren KM, Graves C, Bhawan J. 2007. Tumor necrosis factor receptor superfamily member TROY is a novel melanoma biomarker and potential therapeutic target. *International journal of cancer* **120**: 1304-1310.
Stamataki D, Holder M, Hodgetts C, Jeffery R, Nye E, Spencer-Dene B, Winton DJ, Lewis J. 2011. Delta1 expression, cell cycle exit, and commitment to a specific secretory fate coincide within a few hours in the mouse intestinal stem cell system. *PLoS One* **6**: e24484.
Stamataki D, Ulloa F, Tsoni SV, Mynett A, Briscoe J. 2005. A gradient of Gli activity mediates graded Sonic Hedgehog signaling in the neural tube. *Genes Dev* **19**: 626-641.
Stange DE, Koo BK, Huch M, Sibbel G, Basak O, Lyubimova A, Kujala P, Bartfeld S, Koster J, Geahlen JH et al. 2013. Differentiated Troy+ chief cells act as reserve stem cells to generate all lineages of the stomach epithelium. *Cell* **155**: 357-368.
Steinbach G, Lynch PM, Phillips RK, Wallace MH, Hawk E, Gordon GB, Wakabayashi N, Saunders B, Shen Y, Fujimura T et al. 2000. The effect of celecoxib, a cyclooxygenase-2 inhibitor, in familial adenomatous polyposis. *N Engl J Med* **342**: 1946-1952.
Stemmler MP. 2008. Cadherins in development and cancer. *Mol Biosyst* **4**: 835-850.
Stepan V, Ramamoorthy S, Nitsche H, Zavros Y, Merchant JL, Todisco A. 2005. Regulation and function of the sonic hedgehog signal transduction pathway in isolated gastric parietal cells. *J Biol Chem* **280**: 15700-15708.
Stracci F, Zorzi M, Grazzini G. 2014. Colorectal cancer screening: tests, strategies, and perspectives. *Frontiers in public health* **2**: 210.
Su LK, Vogelstein B, Kinzler KW. 1993. Association of the APC tumor suppressor protein with catenins. *Science* **262**: 1734-1737.
Sugimura H, Wang JD, Mori H, Tsuboi M, Nagura K, Igarashi H, Tao H, Nakamura R, Natsume H, Kahyo T et al. 2010. EPH-EPHRIN in human gastrointestinal cancers. *World journal of gastrointestinal oncology* **2**: 421-428.

Sugiyama T, Kohara H, Noda M, Nagasawa T. 2006. Maintenance of the hematopoietic stem cell pool by CXCL12-CXCR4 chemokine signaling in bone marrow stromal cell niches. *Immunity* **25**: 977-988.

Sun X, Cheng G, Hao M, Zheng J, Zhou X, Zhang J, Taichman RS, Pienta KJ, Wang J. 2010. CXCL12 / CXCR4 / CXCR7 chemokine axis and cancer progression. *Cancer metastasis reviews* **29**: 709-722.

Surana R, Sikka S, Cai W, Shin EM, Warrier SR, Tan HJ, Arfuso F, Fox SA, Dharmarajan AM, Kumar AP. 2014. Secreted frizzled related proteins: Implications in cancers. *Biochim Biophys Acta* **1845**: 53-65.

Suzuki A, Sekiya S, Gunshima E, Fujii S, Taniguchi H. 2010. EGF signaling activates proliferation and blocks apoptosis of mouse and human intestinal stem/progenitor cells in long-term monolayer cell culture. *Lab Invest* **90**: 1425-1436.

Suzuki T, Yano H, Nakashima Y, Nakashima O, Kojiro M. 2002. Beta-catenin expression in hepatocellular carcinoma: a possible participation of beta-catenin in the dedifferentiation process. *J Gastroenterol Hepatol* **17**: 994-1000.

Taggart CC, Cryan SA, Weldon S, Gibbons A, Greene CM, Kelly E, Low TB, O'Neill S J, McElvaney NG. 2005. Secretory leucoprotease inhibitor binds to NF-kappaB binding sites in monocytes and inhibits p65 binding. *The Journal of experimental medicine* **202**: 1659-1668.

Tachibana K, Hirota S, Iizasa H, Yoshida H, Kawabata K, Kataoka Y, Kitamura Y, Matsushima K, Yoshida N, Nishikawa S et al. 1998. The chemokine receptor CXCR4 is essential for vascularization of the gastrointestinal tract. *Nature* **393**: 591-594.

Taipale J, Beachy PA. 2001. The Hedgehog and Wnt signalling pathways in cancer. *Nature* **411**: 349-354.

Takaishi S, Okumura T, Tu S, Wang SS, Shibata W, Vigneshwaran R, Gordon SA, Shimada Y, Wang TC. 2009. Identification of gastric cancer stem cells using the cell surface marker CD44. *Stem Cells* **27**: 1006-1020.

Takaishi S, Okumura T, Wang TC. 2008. Gastric cancer stem cells. *J Clin Oncol* **26**: 2876-2882.

Takao M, Zhang QM, Yonei S, Yasui A. 1999. Differential subcellular localization of human MutY homolog (hMYH) and the functional activity of adenine:8-oxoguanine DNA glycosylase. *Nucleic Acids Res* **27**: 3638-3644.

Takayama T, Miyanishi K, Hayashi T, Sato Y, Niitsu Y. 2006. Colorectal cancer: genetics of development and metastasis. *J Gastroenterol* **41**: 185-192.

Takemaru KI, Moon RT. 2000. The transcriptional coactivator CBP interacts with beta-catenin to activate gene expression. *J Cell Biol* **149**: 249-254.

Taketo MM, Edelmann W. 2009. Mouse models of colon cancer. *Gastroenterology* **136**: 780-798.

Tan X, Apte U, Micsenyi A, Kotsagrelos E, Luo JH, Ranganathan S, Monga DK, Bell A, Michalopoulos GK, Monga SP. 2005. Epidermal growth factor receptor: a novel target of the Wnt/beta-catenin pathway in liver. *Gastroenterology* **129**: 285-302.

Tan X, Behari J, Cieply B, Michalopoulos GK, Monga SP. 2006. Conditional deletion of beta-catenin reveals its role in liver growth and regeneration. *Gastroenterology* **131**: 1561-1572.

Tanaka T. 2009. Colorectal carcinogenesis: Review of human and experimental animal studies. *Journal of carcinogenesis* **8**: 5.

Taniguchi K, Roberts LR, Aderca IN, Dong X, Qian C, Murphy LM, Nagorney DM, Burgart LJ, Roche PC, Smith DI et al. 2002. Mutational spectrum of beta-catenin, AXIN1, and AXIN2 in hepatocellular carcinomas and hepatoblastomas. *Oncogene* **21**: 4863-4871.

Taylor DP, Burt RW, Williams MS, Haug PJ, Cannon-Albright LA. 2010. Population-based family history-specific risks for colorectal cancer: a constellation approach. *Gastroenterology* **138**: 877-885.

Tegtmeyer N, Wessler S, Backert S. 2011. Role of the cag-pathogenicity island encoded type IV secretion system in Helicobacter pylori pathogenesis. *FEBS J* **278**: 1190-1202.

Teicher BA, Fricker SP. 2010. CXCL12 (SDF-1)/CXCR4 pathway in cancer. *Clin Cancer Res* **16**: 2927-2931.

Tian H, Biehs B, Warming S, Leong KG, Rangell L, Klein OD, de Sauvage FJ. 2011. A reserve stem cell population in small intestine renders Lgr5-positive cells dispensable. *Nature* **478**: 255-259.

To KF, Chan MW, Leung WK, Yu J, Tong JH, Lee TL, Chan FK, Sung JJ. 2001. Alterations of frizzled (FzE3) and secreted frizzled related protein (hsFRP) expression in gastric cancer. *Life Sci* **70**: 483-489.

Todaro M, Alea MP, Di Stefano AB, Cammareri P, Vermeulen L, Iovino F, Tripodo C, Russo A, Gulotta G, Medema JP et al. 2007. Colon cancer stem cells dictate tumor growth and resist cell death by production of interleukin-4. *Cell Stem Cell* **1**: 389-402.

Todaro M, Gaggianesi M, Catalano V, Benfante A, Iovino F, Biffoni M, Apuzzo T, Sperduti I, Volpe S, Cocorullo G et al. 2014. CD44v6 is a marker of constitutive and reprogrammed cancer stem cells driving colon cancer metastasis. *Cell Stem Cell* **14**: 342-356.

Tolwinski NS, Wehrli M, Rives A, Erdeniz N, DiNardo S, Wieschaus E. 2003. Wg/Wnt signal can be transmitted through arrow/LRP5,6 and Axin independently of Zw3/Gsk3beta activity. *Dev Cell* **4**: 407-418.

Tovar V, Alsinet C, Villanueva A, Hoshida Y, Chiang DY, Sole M, Thung S, Moyano S, Toffanin S, Minguez B et al. 2010. IGF activation in a molecular subclass of hepatocellular carcinoma and pre-clinical efficacy of IGF-1R blockage. *J Hepatol* **52**: 550-559.

Ueo T, Imayoshi I, Kobayashi T, Ohtsuka T, Seno H, Nakase H, Chiba T, Kageyama R. 2012. The role of Hes genes in intestinal development, homeostasis and tumor formation. *Development* **139**: 1071-1082.

Uchiyama S, Saeki N, Ogawa K. 2015. Aberrant EphB/ephrin-B expression in experimental gastric lesions and tumor cells. *World J Gastroenterol* **21**: 453-464.

Valdora F, Banelli B, Stigliani S, Pfister SM, Moretti S, Kool M, Remke M, Bai AH, Brigati C, Hielscher T et al. 2013. Epigenetic Silencing of DKK3 in Medulloblastoma. *International journal of molecular sciences* **14**: 7492-7505.

Valenta T, Lukas J, Doubravska L, Fafilek B, Korinek V. 2006. HIC1 attenuates Wnt signaling by recruitment of TCF-4 and beta-catenin to the nuclear bodies. *Embo J* **25**: 2326-2337.

van de Wetering M, Cavallo R, Dooijes D, van Beest M, van Es J, Loureiro J, Ypma A, Hursh D, Jones T, Bejsovec A et al. 1997. Armadillo coactivates transcription driven by the product of the Drosophila segment polarity gene dTCF. *Cell* **88**: 789-799.

van den Brink GR. 2007. Hedgehog signaling in development and homeostasis of the gastrointestinal tract. *Physiol Rev* **87**: 1343-1375.

van den Brink GR, Hardwick JC, Tytgat GN, Brink MA, Ten Kate FJ, Van Deventer SJ, Peppelenbosch MP. 2001. Sonic hedgehog regulates gastric gland morphogenesis in man and mouse. *Gastroenterology* **121**: 317-328.

van der Flier LG, Haegebarth A, Stange DE, van de Wetering M, Clevers H. 2009a. OLFM4 is a robust marker for stem cells in human intestine and marks a subset of colorectal cancer cells. *Gastroenterology* **137**: 15-17.

Van der Flier LG, Sabates-Bellver J, Oving I, Haegebarth A, De Palo M, Anti M, Van Gijn ME, Suijkerbuijk S, Van de Wetering M, Marra G et al. 2007. The Intestinal Wnt/TCF Signature. *Gastroenterology* **132**: 628-632.

van der Flier LG, van Gijn ME, Hatzis P, Kujala P, Haegebarth A, Stange DE, Begthel H, van den Born M, Guryev V, Oving I et al. 2009b. Transcription factor achaete scute-like 2 controls intestinal stem cell fate. *Cell* **136**: 903-912.

van Dop WA, Uhmann A, Wijgerde M, Sleddens-Linkels E, Heijmans J, Offerhaus GJ, van den Bergh Weerman MA, Boeckxstaens GE, Hommes DW, Hardwick JC et al. 2009. Depletion of the colonic epithelial precursor cell compartment upon conditional activation of the hedgehog pathway. *Gastroenterology* **136**: 2195-2203 e2191-2197.

van Es JH, Jay P, Gregorieff A, van Gijn ME, Jonkheer S, Hatzis P, Thiele A, van den Born M, Begthel H, Brabletz T et al. 2005a. Wnt signalling induces maturation of Paneth cells in intestinal crypts. *Nat Cell Biol* **7**: 381-386.

van Es JH, Sato T, van de Wetering M, Lyubimova A, Nee AN, Gregorieff A, Sasaki N, Zeinstra L, van den Born M, Korving J et al. 2012. Dll1+ secretory progenitor cells revert to stem cells upon crypt damage. *Nat Cell Biol* **14**: 1099-1104.

van Es JH, van Gijn ME, Riccio O, van den Born M, Vooijs M, Begthel H, Cozijnsen M, Robine S, Winton DJ, Radtke F et al. 2005b. Notch/gamma-secretase inhibition turns proliferative cells in intestinal crypts and adenomas into goblet cells. *Nature* **435**: 959-963.

Van Raay TJ, Fortino NJ, Miller BW, Ma H, Lau G, Li C, Franklin JL, Attisano L, Solnica-Krezel L, Coffey RJ. 2011. Naked1 antagonizes Wnt signaling by preventing nuclear accumulation of beta-catenin. *PLoS One* **6**: e18650.

Van Rechem C, Boulay G, Pinte S, Stankovic-Valentin N, Guerardel C, Leprince D. Differential regulation of HIC1 target genes by CtBP and NuRD, via an acetylation/SUMOylation switch, in quiescent versus proliferating cells. *Mol Cell Biol* **30**: 4045-4059.

Van Rechem C, Rood BR, Touka M, Pinte S, Jenal M, Guerardel C, Ramsey K, Monte D, Begue A, Tschan MP et al. 2009. Scavenger chemokine (CXC motif) receptor 7 (CXCR7) is a direct target gene of HIC1 (hypermethylated in cancer 1). *J Biol Chem* **284**: 20927-20935.

van Roy F, Berx G. 2008. The cell-cell adhesion molecule E-cadherin. *Cell Mol Life Sci* **65**: 3756-3788.

VanDussen KL, Samuelson LC. 2010. Mouse atonal homolog 1 directs intestinal progenitors to secretory cell rather than absorptive cell fate. *Dev Biol* **346**: 215-223.

Vanhaesebroeck B, Alessi DR. 2000. The PI3K-PDK1 connection: more than just a road to PKB. *Biochem J* **346 Pt 3**: 561-576.

Varon C, Dubus P, Mazurier F, Asencio C, Chambonnier L, Ferrand J, Giese A, Senant-Dugot N, Carlotti M, Megraud F. 2012. Helicobacter pylori infection recruits bone marrow-derived cells that participate in gastric preneoplasia in mice. *Gastroenterology* **142**: 281-291.

Vasen HF, Moslein G, Alonso A, Aretz S, Bernstein I, Bertario L, Blanco I, Bulow S, Burn J, Capella G et al. 2008. Guidelines for the clinical management of familial adenomatous polyposis (FAP). *Gut* **57**: 704-713.

Verheyen EM, Gottardi CJ. 2010. Regulation of Wnt/beta-catenin signaling by protein kinases. *Dev Dyn* **239**: 34-44.

Vermeulen L, De Sousa EMF, van der Heijden M, Cameron K, de Jong JH, Borovski T, Tuynman JB, Todaro M, Merz C, Rodermond H et al. 2010. Wnt activity defines colon cancer stem cells and is regulated by the microenvironment. *Nat Cell Biol* **12**: 468-476.

Villavicencio EH, Walterhouse DO, Iannaccone PM. 2000. The sonic hedgehog-patched-gli pathway in human development and disease. *Am J Hum Genet* **67**: 1047-1054.

Vleminckx K, Vakaet L, Jr., Mareel M, Fiers W, van Roy F. 1991. Genetic manipulation of E-cadherin expression by epithelial tumor cells reveals an invasion suppressor role. *Cell* **66**: 107-119.

Voloshanenko O, Erdmann G, Dubash TD, Augustin I, Metzig M, Moffa G, Hundsrucker C, Kerr G, Sandmann T, Anchang B et al. 2013. Wnt secretion is required to maintain high levels of Wnt activity in colon cancer cells. *Nat Commun* **4**: 2610.

Voon DC, Wang H, Koo JK, Nguyen TA, Hor YT, Chu YS, Ito K, Fukamachi H, Chan SL, Thiery JP et al. 2012. Runx3 protects gastric epithelial cells against epithelial-mesenchymal transition-induced cellular plasticity and tumorigenicity. *Stem Cells* **30**: 2088-2099.

Walsh JH. 1990. Role of gastrin as a trophic hormone. *Digestion* **47 Suppl 1**: 11-16; discussion 49-52.

Wang K, Degerny C, Xu M, Yang XJ. 2009. YAP, TAZ, and Yorkie: a conserved family of signal-responsive transcriptional coregulators in animal development and human disease. *Biochemistry and cell biology = Biochimie et biologie cellulaire* **87**: 77-91.
Wang K, Yuen ST, Xu J, Lee SP, Yan HH, Shi ST, Siu HC, Deng S, Chu KM, Law S et al. 2014. Whole-genome sequencing and comprehensive molecular profiling identify new driver mutations in gastric cancer. *Nat Genet* **46**: 573-582.
Wang T, Ong CW, Shi J, Srivastava S, Yan B, Cheng CL, Yong WP, Chan SL, Yeoh KG, Iacopetta B et al. 2011. Sequential expression of putative stem cell markers in gastric carcinogenesis. *Br J Cancer* **105**: 658-665.
Wang W, Li X, Lee M, Jun S, Aziz KE, Feng L, Tran MK, Li N, McCrea PD, Park JI et al. 2015. FOXKs promote Wnt/beta-catenin signaling by translocating DVL into the nucleus. *Dev Cell* **32**: 707-718.
Wang Y, Li X, Wang L, Ding P, Zhang Y, Han W, Ma D. 2004. An alternative form of paraptosis-like cell death, triggered by TAJ/TROY and enhanced by PDCD5 overexpression. *J Cell Sci* **117**: 1525-1532.
Watanabe K, Dai X. 2011. A WNTer revisit: new faces of beta-catenin and TCFs in pluripotency. *Science signaling* **4**: pe41.
Wei C, Peng B, Han Y, Chen WV, Rother J, Tomlinson GE, Boland CR, Chaussabel M, Frazier ML, Amos CI. 2015. Mutations of HNRNPA0 and WIF1 predispose members of a large family to multiple cancers. *Familial cancer*.
Weiss L. 1984. *Modern concepts of gastrointestinal histology*. Elsevier, New York.
Wen L, Chen XZ, Yang K, Chen ZX, Zhang B, Chen JP, Zhou ZG, Mo XM, Hu JK. 2013. Prognostic value of cancer stem cell marker CD133 expression in gastric cancer: a systematic review. *PLoS One* **8**: e59154.
Wen L, Ley RE, Volchkov PY, Stranges PB, Avanesyan L, Stonebraker AC, Hu C, Wong FS, Szot GL, Bluestone JA et al. 2008. Innate immunity and intestinal microbiota in the development of Type 1 diabetes. *Nature* **455**: 1109-1113.
Westphalen CB, Asfaha S, Hayakawa Y, Takemoto Y, Lukin DJ, Nuber AH, Brandtner A, Setlik W, Remotti H, Muley A et al. 2014. Long-lived intestinal tuft cells serve as colon cancer-initiating cells. *J Clin Invest* **124**: 1283-1295.
Wharton KA, Jr., Zimmermann G, Rousset R, Scott MP. 2001. Vertebrate proteins related to Drosophila Naked Cuticle bind Dishevelled and antagonize Wnt signaling. *Dev Biol* **234**: 93-106.
Whissell G, Montagni E, Martinelli P, Hernando-Momblona X, Sevillano M, Jung P, Cortina C, Calon A, Abuli A, Castells A et al. 2014. The transcription factor GATA6 enables self-renewal of colon adenoma stem cells by repressing BMP gene expression. *Nat Cell Biol* **16**: 695-707.
Willert K, Brown JD, Danenberg E, Duncan AW, Weissman IL, Reya T, Yates JR, 3rd, Nusse R. 2003. Wnt proteins are lipid-modified and can act as stem cell growth factors. *Nature* **423**: 448-452.
Wong CM, Fan ST, Ng IO. 2001. beta-Catenin mutation and overexpression in hepatocellular carcinoma: clinicopathologic and prognostic significance. *Cancer* **92**: 136-145.
Wong HC, Bourdelas A, Krauss A, Lee HJ, Shao Y, Wu D, Mlodzik M, Shi DL, Zheng J. 2003. Direct binding of the PDZ domain of Dishevelled to a conserved internal sequence in the C-terminal region of Frizzled. *Mol Cell* **12**: 1251-1260.
Wong VW, Stange DE, Page ME, Buczacki S, Wabik A, Itami S, van de Wetering M, Poulsom R, Wright NA, Trotter MW et al. 2012. Lrig1 controls intestinal stem-cell homeostasis by negative regulation of ErbB signalling. *Nat Cell Biol*.
Woo DK, Kim HS, Lee HS, Kang YH, Yang HK, Kim WH. 2001. Altered expression and mutation of beta-catenin gene in gastric carcinomas and cell lines. *Int J Cancer* **95**: 108-113.
Wright JB, Brown SJ, Cole MD. 2010. Upregulation of c-MYC in cis through a large chromatin loop linked to a cancer risk-associated single-nucleotide polymorphism in colorectal cancer cells. *Mol Cell Biol* **30**: 1411-1420.

Wu C, Xie Y, Gao F, Wang Y, Guo Y, Tian H, Li Y, Fan W. 2013a. Lgr5 expression as stem cell marker in human gastric gland and its relatedness with other putative cancer stem cell markers. *Gene* **525**: 18-25.
Wu PF, Lu ZP, Cai BB, Tian L, Zou C, Jiang KR, Miao Y. 2013b. Role of CXCL12/CXCR4 signaling axis in pancreatic cancer. *Chin Med J (Engl)* **126**: 3371-3374.
Wu WK, Cho CH, Lee CW, Fan D, Wu K, Yu J, Sung JJ. 2010. Dysregulation of cellular signaling in gastric cancer. *Cancer Lett* **295**: 144-153.
Xi Y, Chen Y. 2014. Wnt signaling pathway: implications for therapy in lung cancer and bone metastasis. *Cancer Lett* **353**: 8-16.
Xiao C, Ogle SA, Schumacher MA, Orr-Asman MA, Miller ML, Lertkowit N, Varro A, Hollande F, Zavros Y. 2010. Loss of parietal cell expression of Sonic hedgehog induces hypergastrinemia and hyperproliferation of surface mucous cells. *Gastroenterology* **138**: 550-561, 561 e551-558.
Xing Y, Takemaru K, Liu J, Berndt JD, Zheng JJ, Moon RT, Xu W. 2008. Crystal structure of a full-length beta-catenin. *Structure* **16**: 478-487.
Xu Q, Wang Y, Dabdoub A, Smallwood PM, Williams J, Woods C, Kelley MW, Jiang L, Tasman W, Zhang K et al. 2004. Vascular development in the retina and inner ear: control by Norrin and Frizzled-4, a high-affinity ligand-receptor pair. *Cell* **116**: 883-895.
Yamaguchi S, Ogata H, Katsumata D, Nakajima M, Fujii T, Tsutsumi S, Asao T, Sasaki K, Kuwano H, Kato H. 2014. MUTYH-associated colorectal cancer and adenomatous polyposis. *Surg Today* **44**: 593-600.
Yamamoto H, Kishida S, Kishida M, Ikeda S, Takada S, Kikuchi A. 1999. Phosphorylation of axin, a Wnt signal negative regulator, by glycogen synthase kinase-3beta regulates its stability. *J Biol Chem* **274**: 10681-10684.
Yamashita T, Honda M, Nakamoto Y, Baba M, Nio K, Hara Y, Zeng SS, Hayashi T, Kondo M, Takatori H et al. 2013. Discrete nature of EpCAM+ and CD90+ cancer stem cells in human hepatocellular carcinoma. *Hepatology* **57**: 1484-1497.
Yamazaki K, Takahashi A, Takazoe M, Kubo M, Onouchi Y, Fujino A, Kamatani N, Nakamura Y, Hata A. 2009. Positive association of genetic variants in the upstream region of NKX2-3 with Crohn's disease in Japanese patients. *Gut* **58**: 228-232.
Yan D, Wallingford JB, Sun TQ, Nelson AM, Sakanaka C, Reinhard C, Harland RM, Fantl WJ, Williams LT. 2001. Cell autonomous regulation of multiple Dishevelled-dependent pathways by mammalian Nkd. *Proc Natl Acad Sci U S A* **98**: 3802-3807.
Yan KS, Chia LA, Li X, Ootani A, Su J, Lee JY, Su N, Luo Y, Heilshorn SC, Amieva MR et al. 2012. The intestinal stem cell markers Bmi1 and Lgr5 identify two functionally distinct populations. *Proc Natl Acad Sci U S A* **109**: 466-471.
Yang J, Weinberg RA. 2008. Epithelial-mesenchymal transition: at the crossroads of development and tumor metastasis. *Dev Cell* **14**: 818-829.
Yang Q, Bermingham NA, Finegold MJ, Zoghbi HY. 2001. Requirement of Math1 for secretory cell lineage commitment in the mouse intestine. *Science* **294**: 2155-2158.
Yang YR, Follo MY, Cocco L, Suh PG. 2013. The physiological roles of primary phospholipase C. *Advances in biological regulation* **53**: 232-241.
Yano T, Ito K, Fukamachi H, Chi XZ, Wee HJ, Inoue K, Ida H, Bouillet P, Strasser A, Bae SC et al. 2006. The RUNX3 tumor suppressor upregulates Bim in gastric epithelial cells undergoing transforming growth factor beta-induced apoptosis. *Mol Cell Biol* **26**: 4474-4488.
Yasumoto K, Koizumi K, Kawashima A, Saitoh Y, Arita Y, Shinohara K, Minami T, Nakayama T, Sakurai H, Takahashi Y et al. 2006. Role of the CXCL12/CXCR4 axis in peritoneal carcinomatosis of gastric cancer. *Cancer Res* **66**: 2181-2187.
Yin C, Lin Y, Zhang X, Chen YX, Zeng X, Yue HY, Hou JL, Deng X, Zhang JP, Han ZG et al. 2008. Differentiation therapy of hepatocellular carcinoma in mice with recombinant adenovirus carrying hepatocyte nuclear factor-4alpha gene. *Hepatology* **48**: 1528-1539.

Ying QL, Nichols J, Chambers I, Smith A. 2003. BMP induction of Id proteins suppresses differentiation and sustains embryonic stem cell self-renewal in collaboration with STAT3. *Cell* **115**: 281-292.

Yoda Y, Takeshima H, Niwa T, Kim JG, Ando T, Kushima R, Sugiyama T, Katai H, Noshiro H, Ushijima T. 2015. Integrated analysis of cancer-related pathways affected by genetic and epigenetic alterations in gastric cancer. *Gastric Cancer* **18**: 65-76.

Yokoyama N, Markova NG, Wang HY, Malbon CC. 2012. Assembly of Dishevelled 3-based supermolecular complexes via phosphorylation and Axin. *J Mol Signal* **7**: 8.

Yu W, Lin Z, Hegarty JP, John G, Chen X, Faber PW, Kelly AA, Wang Y, Poritz LS, Schreiber S et al. 2010. Genes regulated by Nkx2-3 in siRNA-mediated knockdown B cells: implication of endothelin-1 in inflammatory bowel disease. *Molecular genetics and metabolism* **100**: 88-95.

Yuzugullu H, Benhaj K, Ozturk N, Senturk S, Celik E, Toylu A, Tasdemir N, Yilmaz M, Erdal E, Akcali KC et al. 2009. Canonical Wnt signaling is antagonized by noncanonical Wnt5a in hepatocellular carcinoma cells. *Mol Cancer* **8**: 90.

Zamolodchikova TS, Scherbakov IT, Khrennikov BN, Svirshchevskaya EV. 2013. Expression of duodenase-like protein in epitheliocytes of Brunner's glands in human duodenal mucosa. *Biochemistry Biokhimiia* **78**: 954-957.

Zarich N, Oliva JL, Martinez N, Jorge R, Ballester A, Gutierrez-Eisman S, Garcia-Vargas S, Rojas JM. 2006. Grb2 is a negative modulator of the intrinsic Ras-GEF activity of hSos1. *Mol Biol Cell* **17**: 3591-3597.

Zeng G, Apte U, Micsenyi A, Bell A, Monga SP. 2006. Tyrosine residues 654 and 670 in beta-catenin are crucial in regulation of Met-beta-catenin interactions. *Exp Cell Res* **312**: 3620-3630.

Zeng G, Awan F, Otruba W, Muller P, Apte U, Tan X, Gandhi C, Demetris AJ, Monga SP. 2007. Wnt'er in liver: expression of Wnt and frizzled genes in mouse. *Hepatology* **45**: 195-204.

Zeng W, Wharton KA, Jr., Mack JA, Wang K, Gadbaw M, Suyama K, Klein PS, Scott MP. 2000. naked cuticle encodes an inducible antagonist of Wnt signalling. *Nature* **403**: 789-795.

Zeng X, Tamai K, Doble B, Li S, Huang H, Habas R, Okamura H, Woodgett J, He X. 2005. A dual-kinase mechanism for Wnt co-receptor phosphorylation and activation. *Nature* **438**: 873-877.

Zeuner A, Todaro M, Stassi G, De Maria R. 2014. Colorectal cancer stem cells: from the crypt to the clinic. *Cell Stem Cell* **15**: 692-705.

Zhang H, Xue Y. 2008. Wnt pathway is involved in advanced gastric carcinoma. *Hepatogastroenterology* **55**: 1126-1130.

Zhang L, Gao X, Wen J, Ning Y, Chen YG. 2006. Dapper 1 antagonizes Wnt signaling by promoting dishevelled degradation. *J Biol Chem* **281**: 8607-8612.

Zhang N, Wei P, Gong A, Chiu WT, Lee HT, Colman H, Huang H, Xue J, Liu M, Wang Y et al. 2011a. FoxM1 promotes beta-catenin nuclear localization and controls Wnt target-gene expression and glioma tumorigenesis. *Cancer Cell* **20**: 427-442.

Zhang N, Yantiss RK, Nam HS, Chin Y, Zhou XK, Scherl EJ, Bosworth BP, Subbaramaiah K, Dannenberg AJ, Benezra R. 2014. ID1 is a functional marker for intestinal stem and progenitor cells required for normal response to injury. *Stem cell reports* **3**: 716-724.

Zhang S, Cagatay T, Amanai M, Zhang M, Kline J, Castrillon DH, Ashfaq R, Oz OK, Wharton KA, Jr. 2007. Viable mice with compound mutations in the Wnt/Dvl pathway antagonists nkd1 and nkd2. *Mol Cell Biol* **27**: 4454-4464.

Zhang S, Li J, Yin ZY, Liu PG, Zhao WX, Xie CR, Zhao BX, Wang XM. 2015. Expression pattern and clinicopathologic significance of NKD1 in human primary hepatocellular carcinoma. *APMIS : acta pathologica, microbiologica, et immunologica Scandinavica* **123**: 315-320.

Zhang S, Wang Y, Dai SD, Wang EH. 2011b. Down-regulation of NKD1 increases the invasive potential of non-small-cell lung cancer and correlates with a poor prognosis. *BMC Cancer* **11**: 186.

Zhang W, Yang J, Liu Y, Chen X, Yu T, Jia J, Liu C. 2009. PR55 alpha, a regulatory subunit of PP2A, specifically regulates PP2A-mediated beta-catenin dephosphorylation. *J Biol Chem* **284**: 22649-22656.

Zhang X, Gaspard JP, Chung DC. 2001. Regulation of vascular endothelial growth factor by the Wnt and K-ras pathways in colonic neoplasia. *Cancer Res* **61**: 6050-6054.

Zhao P, Li Y, Lu Y. 2010. Aberrant expression of CD133 protein correlates with Ki-67 expression and is a prognostic marker in gastric adenocarcinoma. *BMC Cancer* **10**: 218.

Zhao Y, Johansson C, Tran T, Bettencourt R, Itahana Y, Desprez PY, Konieczny SF. 2006. Identification of a basic helix-loop-helix transcription factor expressed in mammary gland alveolar cells and required for maintenance of the differentiated state. *Mol Endocrinol* **20**: 2187-2198.

Zhou W, Jiang Z, Liu N, Xu F, Wen P, Liu Y, Zhong W, Song X, Chang X, Zhang X et al. 2009. Down-regulation of CXCL12 mRNA expression by promoter hypermethylation and its association with metastatic progression in human breast carcinomas. *J Cancer Res Clin Oncol* **135**: 91-102.

Zhu Y, Huang YF, Kek C, Bulavin DV. 2013. Apoptosis differently affects lineage tracing of Lgr5 and Bmi1 intestinal stem cell populations. *Cell Stem Cell* **12**: 298-303.

Ziegler S, Rohrs S, Tickenbrock L, Moroy T, Klein-Hitpass L, Vetter IR, Muller O. 2005. Novel target genes of the Wnt pathway and statistical insights into Wnt target promoter regulation. *FEBS J* **272**: 1600-1615.

Ziskin JL, Dunlap D, Yaylaoglu M, Fodor IK, Forrest WF, Patel R, Ge N, Hutchins GG, Pine JK, Quirke P et al. 2012. In situ validation of an intestinal stem cell signature in colorectal cancer. *Gut*.